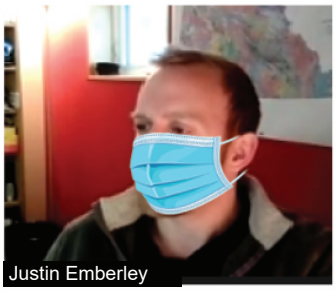


Yukon
Exploration & Geology
2021


Julie Minor


Carolyn Relf


Leyla Weston


Justin Emberley


Panya Lipovsky


Kristen Kennedy


Patrick Sack


Maurice Colpron


Tyler Ambrose


David Moynihan


Diane Skipton


Sarah Sternbergh


Rosie Cobbett


Derek Cronmiller


Sydney van Loon


Derek Torgerson


Scott Casselman


Karen MacFarlane


Jeffery Bond


Warwick Bullen


Brett Elliot


Lara Lewis


Bailey Staffen

Yukon

Yukon Exploration & Geology 2021

Edited by
K.E. MacFarlane

Yukon Geological Survey
Energy, Mines and Resources
Government of Yukon

Published under the authority of the Department of Energy, Mines and Resources, Government of Yukon, https://yukon.ca.

Printed in Whitehorse, Yukon, 2022.

Publié avec l'autorisation du Ministères de l'Énergie, des Mines et des Ressources du gouvernement du Yukon, https://yukon.ca.

Imprimé à Whitehorse (Yukon) en 2022.

©Department of Energy, Mines and Resources, Government of Yukon

ISSN 1718-8326 (online version)

Yukon Geological Survey publications can be obtained from:
Yukon Geological Survey
102-300 Main Street
Box 2703 (K-102)
Whitehorse, Yukon, Canada Y1A 2C6

email geology@yukon.ca

Yukon Geological Survey website https://yukon.ca/en/science-and-natural-resources/geology.

In referring to this publication, please use the following citation:
Yukon Geological Survey, 2022. Yukon Exploration and Geology 2021, K.E. MacFarlane (ed.), 2022. Yukon Geological Survey, 265 p.

Front cover photograph: Looking west, up to the headwaters of Britnell Creek. J. Charlton is measuring the foliation in the Rabbitkettle Formation.

Back cover photograph: Galena, Logan and Mary Ann Roots seated on the commemorative bench installed for the late Charlie Roots.

Preface

Yukon Exploration and Geology (YEG) papers and the Yukon Exploration and Geology Overview are two of the main publications of the Yukon Geological Survey (Energy, Mines and Resources, Government of Yukon). Individual YEG papers, with colour images, are available in digital format and can be downloaded from our website. The YEG Overview is available in digital format and in a limited colour print run.

YEG 2021 contains up-to-date information on mining and mineral exploration activity, studies by industry, and results of recent geological field studies. Information in this volume comes from prospectors, exploration and government geologists, mining companies, and students, all of whom are willing to contribute to public geoscience for the benefit of the scientific community, general public and mineral industries of Yukon. Their work is appreciated.

In this last revolution of Earth around the sun, not much seems to have changed. Okay, so we can say the Yukon experienced above average amounts of precipitation during the cold months that resulted in above normal water levels in many lakes and rivers during the summer. And, maybe we can also say that our summer seemed a little warmer and drier compared to previous years. But, what didn't change was the continued efforts of my colleagues at the Yukon Geological Survey to provide geoscience information and support to our clients. Although YEG season may seem like a love-hate relationship to many, I do appreciate the work of all those who have authored and/or reviewed papers in this year's volume. Thank you all.

Input or suggestions that you may have to improve future YEG publications are welcomed. Please contact us at (867) 667-8519, or by email at geology@yukon.ca.



Karen MacFarlane

In Memoriam

Edward Balon
1946–2022



Ed was born and raised on pioneer family homestead in central Saskatchewan. He graduated from high school 1963 in the small village of Yellow Creek and spent the following five years travelling and working various jobs in Western Canada, in an attempt to find "a path" for the future. These jobs included a short stint as a mill operator at Saskatchewan's very first potash mine – K1, Esterhazy. More importantly, hiking in the mountains of northwestern BC during a longer stint as surveyor's assistant on construction of the Stewart-Cassiar Hwy initiated his interest in geology and exploration.

This interest resulted in his attending Northern College – Haileybury School of Mines, Ontario from 1968 to 1970 where he graduated with top honours from the mining technology program which embraced a broad curriculum including exploration, mining and metallurgy. Ed won several awards/prizes including the Honour Student Gold Medal, but declined scholarships to carry on in academia for the opportunity to become a prospector through field experience - "apprenticeship with the old boys"!

Ed was immediately hired by Cordilleran Engineering Ltd. as a geochem-geological technician and prospector, primarily on large scale regional exploration programs throughout BC, Yukon, western NWT. During this period, under the leadership of John Stollery, Bert Reeve (both Haileybury graduates) and several other great mentors like Pat Duquette and Mike Hamilton, he was fortunate to participate in the discovery of several significant deposits, including: Gayna River, NWT (Zn-Pb), Logan, YT (Zn-Ag-Sn); Midway (Silvertip), BC (Ag-Pb-Zn); and Elk (Siwash) high grade Au veins in southern BC. These discoveries in large measure contributed to John Stollery's receipt of the Spud Huestis Award in 1990.

In 1995, Cordilleran Engineering Ltd. was folded into Fairfield Minerals Ltd., a junior public company founded by John Stollery and associates, and was later taken over by and merged, in 2001, with Almaden Resources Corp. to form Almaden Minerals Ltd. where Ed was engaged in regional and property-scale gold exploration-evaluation programs in BC, Yukon, Alaska and Mexico. Ed recognized the VMS potential of the "southern Yukon Tanana Terrane". He collected many thousands of stream sediment samples in the 70s on the Wolf Lake map sheet area and came up with the idea that the Finlayson belt was offset by the Tintina fault. He used the stream geochem data to target the Morley River VMS belt which resulted in a new drill discovery on the MOR prospect in August, 2004.

From 2002 to 2008 Ed was employed directly by Almaden Minerals Ltd. and worked primarily on southern BC regional and property-scale gold exploration programs. His prospecting efforts resulted in the recognition of the low sulphidation epithermal Spences Bridge Gold Belt including important showings on the PV/NIC, SAM (Skoonka Creek), MERIT, NICOAMEN RIVER (Zak) and SHOVELNOSE properties. These discoveries initiated the largest staking rush in BC history as other exploration groups recognized the potential of the area.

Though officially retired in 2009, Ed continued to take contracts with Archer Cathro and Associates and others to prospect in the Yukon, BC and South America. He also became a technical advisor to Westhaven Ventures in 2010 where he applied his vast experience to the exploration of the Spences Bridge Gold Belt, focusing on the Shovelnose property.

He enjoyed his free time travelling extensively to Antarctica, Turkey, Eastern Europe, Spain, Chile, Peru, Namibia, South Africa and Mongolia. Ed also took great pleasure mentoring many UBC geology and MDRU students where he was considered Prospector Emeritus by sharing his enthusiasm and knowledge with the next generation of explorationists.

Ed was an active member of AME, particularly in his role with the award committee. Ed was awarded AME BC's Spud Huestis award in 2005 for his significant contributions to the mineral resources of BC and Yukon, he was inducted into the Yukon Prospector's Hall of Fame in 2014, and was the recipient of AME BC's Gold Pan award in 2019 for his dedication and contributions to the association.

Ed was diagnosed with ALS in 2020 and died in January 2022. His humility, integrity, generosity and perseverance have left a legacy for the next generation to emulate. He is sorely missed.

Wojtek Jakubowski
February 2022



Yukon Exploration and Geology 2021

Table of Contents

Updates to the Yukon Geological Survey's mineral potential mapping methodology
W. Bullen 1

Update on the bedrock geology of the Rusty Mountain and Bonnet Plume Pass (west half) areas
T. Ambrose 13

Yukon Permafrost Database: A new baseline data resource
P.S. Lipovsky, J.K. Humphries, E.T. Stewart-Jones and D.C. Cronmiller 37

Placer gold settings within an alpine glaciated environment, Granite Creek, Yukon (NTS 105M/14)
J.L. Steinke, J.D. Bond and B.C. Ward 51

Preliminary results and structural interpretations from drone lidar surveys over the Eastern Denali fault, Yukon
T. Finley, G. Salomon, R. Stephen, E. Nissen, J. Cassidy and B. Menounos 83

Surficial geochemical setting of the southern Carmacks-Minto copper belt
K. Kennedy, P.J. Sack and H. Clarke 107

Geology of the Carpenter Creek and McKay Hill areas (NTS 106D/6, 11), central Yukon
R. Cobbett 125

The Yukon Digital Bedrock Geology compilation
M. Colpron 143

Updated bedrock geology of the southern Nash Creek area in central Yukon (parts of NTS 106D/2, 3, 6 and 7)
D. Skipton 161

Geology and U-Pb zircon geochronology and Pb isotope geochemistry of mid-Cretaceous plutonic rocks in the Mount Nansen map area (NTS 115I/3 and part of 115I/2)
P.J. Sack, J.L. Crowley, V. Bennett and J. Gabites 185

Preliminary observations on the geology of the southern Big Salmon Range, south-central Yukon (parts of NTS 105C/13,14, 105F/4 and 105E/1)
D. Moynihan and J.L. Crowley 217

Updates to the Yukon Geological Survey's mineral potential mapping methodology

W. Bullen*
Yukon Geological Survey

Bullen, W., 2022. Updates to the Yukon Geological Survey's mineral potential mapping methodology. *In:* Yukon Exploration and Geology 2022, K.E. MacFarlane (ed.), Yukon Geological Survey, p. 1–12.

Abstract

This paper serves as an update to an earlier paper published by the Yukon Geological Survey: *New mineral potential mapping methodology for Yukon: case studies from the Beaver River and Dawson regional land use planning areas* (Bullen, 2020). Since the release of the earlier paper, a number of the methods have been modified, and new techniques introduced. These are incorporated into this update paper — the reader is referred to the earlier paper for details of the method itself.

Mineral potential maps have thus far been completed for the Beaver River watershed, and the Dawson, Teslin, Na-Cho Nyäk Dun, and Ross River regions.

There have been significant updates made to the mineral potential mapping method:

1. Modifications to buffer distance and factors (these are an important fuzzy logic (*i.e.*, non-Boolean) component of the mineral potential mapping process) to enhance mapping outcomes.
2. The introduction of an in-house generated, machine learning algorithm (unsupervised, clustering-type) to classify mineral potential in order to remove the potential for human bias. The method replaces the statistical, areas-under-the-curve approach used previously.
3. A new method for delineating anomalous stream sediment data based on the lithological makeup of each watershed basin. The method computes and compares expected assay values to actual assay values, with values exceeding a certain threshold taken as anomalous. The previous method did not take lithology into account, relying on simple percentile methods only, and was considered insufficiently robust.
4. A new method for categorizing mineral potential confidence. Mineral potential maps produced by the Geological Survey contain measures of bedrock mapping confidence to facilitate land use planning. The updated method is significantly more robust than that used previously.
5. Revisions to the map legend to account for the new, machine learning-based mineral potential categorization methodology.
6. Revisions to the map colour scheme to make them colour blind-safe.

* Warwick.Bullen@yukon.ca

Introduction

In December 2019, the Yukon Geological Survey (YGS) published a paper entitled: *New mineral potential mapping methodology for Yukon: case studies from the Beaver River and Dawson regional land use planning areas* (Bullen, 2020). Since then, some of the methods have been modified and new techniques introduced, with the aim of enhancing the quality and robustness of mineral potential maps produced by the YGS. This paper serves as an update to the earlier paper.

The reader is referred to the earlier paper for an explanation of the mineral potential mapping methodology used by the YGS, along with its development and implementation in land use planning activities in Yukon.[1]

Updates and New Techniques

Mineral potential maps using YGS's original methodology were completed for the Beaver River watershed and Dawson region land use planning exercises. Mineral potential maps have also been completed for the Teslin Tlingit Council Traditional Area, Traditional Territory of the Na-Cho Nyäk Dun First Nation and the Ross River Dena Council Traditional Area (Fig. 1); these three will be updated in line with the new techniques noted below prior to the initiation of land use planning exercises in these areas.

As detailed in Bullen (2020), the mineral potential mapping procedure uses a generalized minerals systems approach and utilizes block modeling techniques where each block (unit cell) is assigned a prospectivity score and, separately, a confidence score. Scores are calculated based on the presence or absence of categorical features within unit cells and represent the posterior favourability of each unit cell relative to other unit cells. The posterior favourability refers to mineral potential and confidence scores after all evidence has been taken into account. Evidential layers are weighted according to buffer distance and/or through the application of knowledge-based factors. Lithology classes are an exception – these features are factored using a multiclass weights of evidence (WofE) approach with known mineral occurrences used as training points.[2]

The process thus differs to pure data-driven mineral prospectivity mapping, being a hybrid between a classic data-driven probabilistic WofE approach (which uses a binary value assessment, *i.e.*, 0/1) and an expert-driven fuzzy logic[3] approach, the latter providing the advantage of allowing the user to assign a membership value anywhere between 0 and 1 (*i.e.*, 0, 0.01, 0.02,...0.98, 0.99, 1) for any predictive input parameter.

Factors and buffers are an important fuzzy logic (*i.e.*, non-Boolean) component of the mineral potential mapping process. The choice of buffer distance in the case of point, line (and less commonly polygonal) data, and the selection of weighting factors in the case of polygonal data, is critical to a successful outcome. Expert input is key in this respect.

Table 1 shows the modified buffer distances and factors implemented subsequent to the Beaver River watershed and Dawson region mineral potential mapping exercises.

Mineral Potential Categorization

Prior to 2020, the mineral potential of areas in Yukon was categorized as highly prospective, significantly prospective and moderately prospective based on defined standard deviations (Bullen, 2020). The method involved transforming the data (if significantly skewed), converting the transformed data to a standardized normal distribution (with a mean of 0 and a standard

[1] *In Yukon (and elsewhere), land use planning refers to the process whereby land use (e.g., hunting, fishing, mining, agriculture, forestry) is codified. Protected areas such as parks are another outcome of land use planning. The process is overseen by government (territorial and First Nation) appointees who make recommendations based on feedback from land use planners, who rely, in turn, on input from government, non-governmental agencies, and the general public.*

[2] *In weights of evidence prospectivity mapping, a categorical feature/evidential layer is a spatial theme (i.e., a data layer such as bedrock geology, faults, etc.) used as evidence for the occurrence of training points. Each categorical feature occupies a defined area. Training points are the set of spatial point objects whose locations are to be predicted. In mineral exploration, these are the sites of known mineral deposits or occurrences, with the points being either present or absent.*

[3] *Fuzzy logic is an approach to computing based on "degrees of truth" rather than the usual "true or false" (1 or 0) Boolean logic on which the modern computer is based (https://searchenterpriseai.techtarget.com/definition/fuzzy-logic). The concept, first put forward by Lotfi Zadeh in the 1960s, has wide application in today's world – e.g., gear selection in vehicles, cycle selection in dishwashers, copy machines. An example of Boolean logic versus fuzzy logic (taken from techtarget, 2021) is the response to the question "is it hot"? Boolean logic calls for a "no/yes" (0, 1) response whereas a fuzzy logic response might be "somewhat", "moderately", "fairly so" (0.25, 0.50, 0.75), etc.*

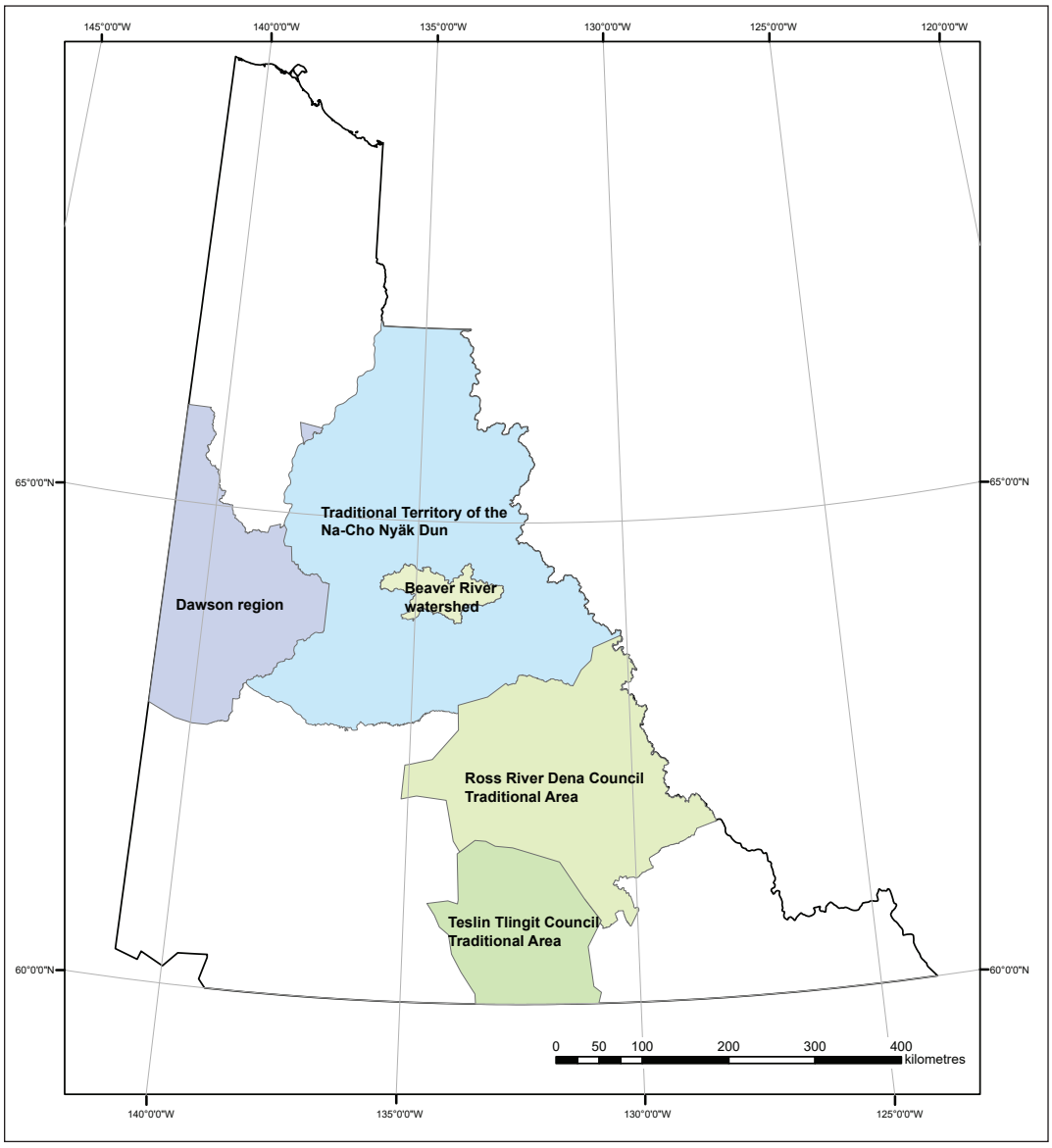


Figure 1. *Mineral potential mapping coverage in Yukon using the Yukon Geological Survey's new mineral potential mapping methodology. The Dawson region and Beaver River watershed mineral potential maps are in the public domain – the remainder are internal working documents at this time.*

deviation of 1), and then assigning values of 1, 2 or 3 to the normalized scores as follows:

1. Scores falling below a StDev of –1 (encompassing approximately 16% of the data) were assigned a value of 1 and were designated "Moderately prospective";
2. Scores falling between a StDev of –1 and +0.5 (approximately 53% of the data) were assigned a value of 2 and were designated "Significantly prospective"; and
3. Scores falling above a StDev of +0.5 (approximately 31% of the data) were assigned a value of 3 and were designated "Highly prospective" (Fig. 2).

The method worked well, and the outcomes were readily accepted by land use planning bodies and other stakeholders. However, the process was command-based, and the mineral potential category boundaries were (somewhat) arbitrarily defined with the potential for human bias. The outcomes were therefore, at least in principle, difficult to defend. Consequently, the author elected to move towards a purely data-driven classification scheme based on data distributions and patterns. To this end, a machine learning algorithm (unsupervised, clustering-type) suitable for mineral potential classification was developed, with the key goal being the removal of subjective input.

Table 1. *Updated factors and buffers used in mineral potential mapping post the Beaver River watershed and Dawson region mapping exercises.*

Bedrock geology weighting factors (YGS, 2021a).

Technique	Polygonal data	Method	Factors applied
Multiclass weights of evidence (see Bullen (2020) for details)	Rock subclass	Contrast values generated using weights of evidence, mineral occurrences used as training data, contrast values scaled from 0 to 1, square root transformation applied to reduce skewness, values converted to a standardized normal distribution and factored	StDev > 2.0 = 1.5
			1.5 < StDev ≤ 2.0 = 1.4
			1.0 < StDev ≤ 1.5 = 1.3
			0.5 < StDev ≤ 1.0 = 1.2
			0.0 < StDev ≤ 0.5 = 1.1
			-0.5 < StDev ≤ 0.0 = 0.9
			-1.0 < StDev ≤ -0.5 = 0.8
			-1.5 < StDev ≤ -1.0 = 0.7
			-2.0 < StDev ≤ -1.5 = 0.6
			-2.0 > StDev = 0.5

Plutonic rocks (YGS, 2021a).

Lithology	Buffer	Factor	Rationale
Felsic to intermediate igneous pluton rocks of Jurassic age and younger	2000 m	None	Estimate of potential influence of intrusion away from contact, must be supported by aeromagnetic data, aeromagnetic “haloes” must be unrelated to bedrock geology

Mineral occurrence data (YGS, 2021b).

Deposit type	Buffer	Factor	Rationale
Past producer/producer	2000 m	None	Relative importance of categorical feature
Deposit	1000 m		
Anomaly/drilled prospect/prospect	500 m		
Showing	250 m		
Unknown	100 m		

Fault data (YGS, 2021a).

Fault category	Ring buffers	Factors	Rationale
Major faults	2000 m, 1000 m, 500 m	1, 1.5 and 2, respectively	Relationship between structure and sites of potential mineralization, influence of categorical feature decreases away from feature
Other faults	1000 m, 500 m	1 and 1.5, respectively	

Fold data (YG, 2021a).

Fold category	Buffer	Factors	Rationale
All folds	500 m, 250 m	1 and 1.25, respectively	Relationship between structure and sites of potential mineralization, influence of categorical feature decreases away from feature

Table 1 *continued.*

Stream sediment geochemistry (YGS, 2021c).

Commodities	Method	Rationale
Primary commodities covering deposit types of interest	Method involves calculating expected stream sediment values and comparing these to the actual values obtained	Lithological makeup of drainage basins the key factor in understanding and identifying anomalies – see below for detailed explanation

Placer claims (YG, 2021b).

Claim category	Buffer	Factor	Rationale
Historic Placer claims	None	0.5	Relatively low factor given that historic and current placer claims potentially overlap, and in which case are additive
Current Placer claims and leases		1.5	Potential economic importance high relative to spatial extent of claims, higher factors allocated
Current Placer claims – Class 3		2	
Current Placer claims – Class 4		2.5	

Quartz claims (YG, 2021c).

Claim category	Buffer	Factor	Rationale
Historic Quartz claims	None	0.5	Relatively low factor given that historic and current quartz claims potentially overlap, and in which case are additive
Current Quartz claims and leases		1	Includes Class 1
Current Quartz claims – Class 2		1.25	Considered to be prospective
Current Quartz claims – Class 3		1.5	Considered to be significantly prospective
Current Quartz claims – Class 4		1.75	Considered to be highly prospective
Current Quartz claims – Class 5		2	Potentially economic

Assessment reports (YGS, 2021d).

Assessment reports	Buffer	Factor	Rationale
Assessment report footprints	None	Varies from 1 to 3 depending on degree and extent of overlap (calculated using ArcMap routines)	Assessment work carried out over the same area more than once (in some cases numerous times) – depends on the perceived prospectivity of the area

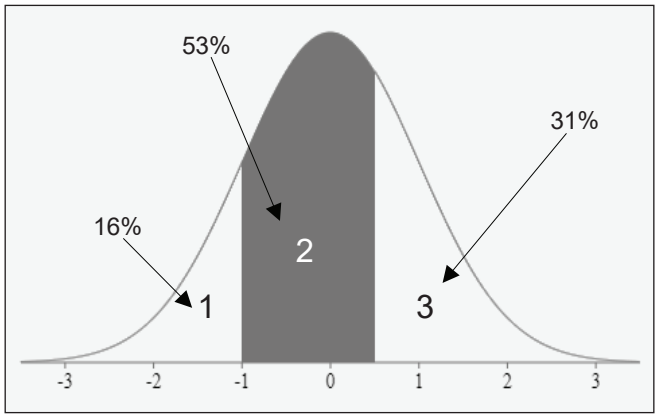


Figure 2. *Normally distributed data showing the areas-under-the-curve method used previously by the Yukon Geological Survey to classify mineral potential. In practice, the normalized scores did not align to a perfect normal distribution, so the mineral potential area percentages varied to a small degree.*

The machine learning algorithm developed by the Yukon Geological Survey uses an iterative, value-optimization approach. To achieve this, the concept of value was introduced into the machine learning process (Bullen, 2021). The resultant machine learning decision model is both intuitive and defendable, and has other applications beyond mineral potential domaining — for example, determining the opportunity cost of land withdrawal alternatives stemming from a land use planning exercise, and value-add multiple mapping (these are beyond the scope of this paper and are not discussed further).

An in-depth description of the machine learning algorithm is given in Bullen (2021), and the reader is referred to this article for further details.

The machine learning decision model delineates four clustered, value-optimized land parcels of decreasing mineral potential. The land parcels are denoted Optimally prospective – Level 1; Optimally prospective – Level 2; Significantly prospective; and Moderately prospective. To delineate the area categorized as Optimally prospective – Level 2, cells falling within the area designated Optimally prospective – Level 1 are removed from the model and algorithm is run without these cells. To delineate the area categorized as Significantly prospective, cells falling within the Optimally prospective – Level 1 and 2 domains are removed and the algorithm rerun, and so on. In all cases the procedure is the same. Clearly, an infinitely large number of mineral potential categories could be derived but this is impractical, as the four categories noted above more than adequately capture variations in mineral potential (Fig. 3). Figure 4 shows the mineral potential map for the Dawson region (excluding, for clarity, measures of confidence – see Bullen, 2020). Cell boundaries are clearly evident in Figure 4 (*i.e.*, no smoothing has been applied) – each cell contains a unique mineral potential score which has been colour-coded according to the value-optimization machine learning prospectivity categories noted in Figure 3.

Processing Stream Sediment Data

Stream sediment anomalies in the Beaver River watershed and Dawson region were previously identified using simple standard deviation and percentile methods (Bullen, 2020). These methods are regarded as insufficiently robust as they do not take lithology, which plays a key role in anomalous value determination, into account. Work by Mackie et al. (2015) on stream sediment data in Yukon showed that lithological variation exhibited a significant control on the distribution of a number of important commodity and pathfinder elements. Consequently, stream sediment data used for mineral potential mapping are now assessed after taking the lithological makeup of each watershed basin into account.

The method involves calculating the expected stream sediment assay values at each drainage sample collection point (located at the outflow point of each defined watershed basin). Built into the method is the understanding that watershed basins of differing orders are superimposed on each other. For example, basins sampling first order streams are superimposed on basins sampling second order streams and so on, with each basin having a unique stream sediment geochemistry (and a unique sample attached to it). From a mineral potential mapping point of view, anomalous basins are additive in the sense that the mineral potential of a first order basin is added to the mineral potential of a second order basin (and so on), if both are anomalous (otherwise they are not additive but are treated, rather, as distinct entities). This is the desired outcome in terms of the mineral potential mapping methodology.

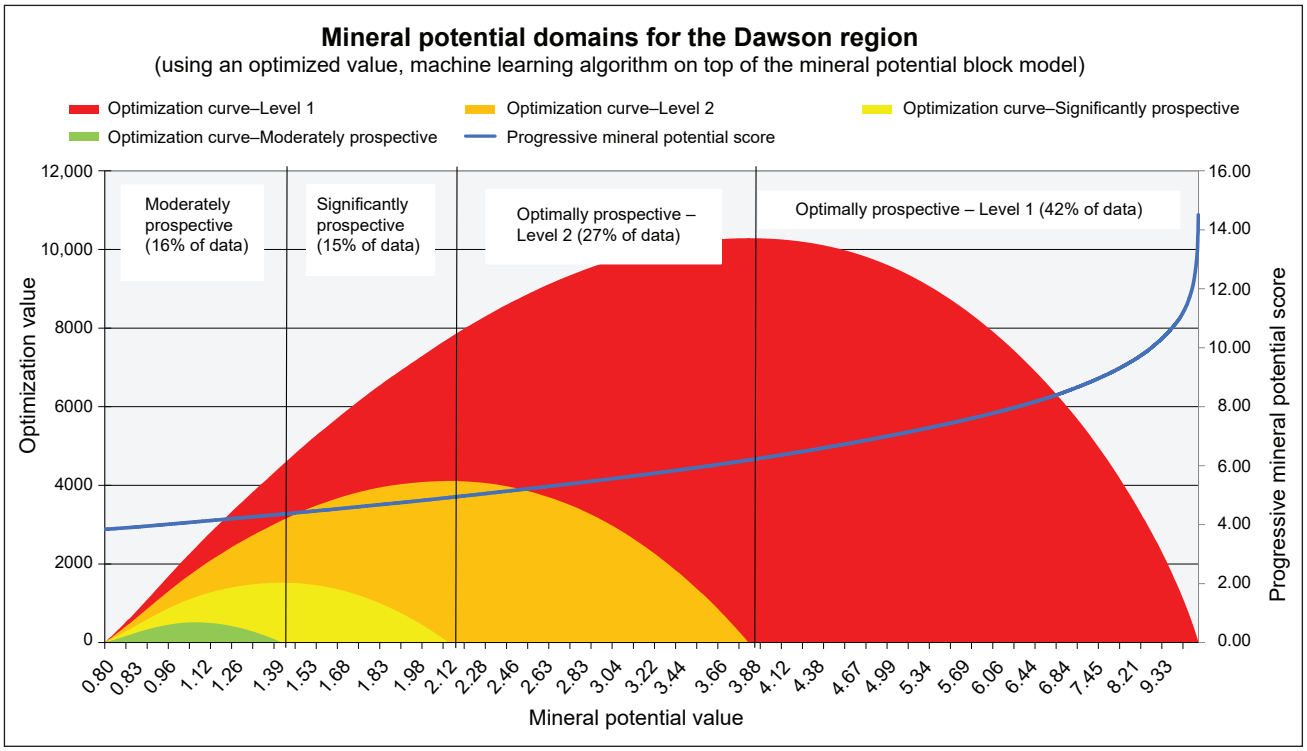


Figure 3. *The machine learning decision model showing mineral potential domains for the Dawson region. The percentage area covered by each domain is shown. The value-optimization measures the total value-add at any point along each of the four curves, which initially increases but then decreases as cells continue to be removed – i.e., after the remaining area drops below a certain threshold. Removal of any cell within a mineral potential category results in a drop in the optimized value. See Bullen (2021) for further details.*

Anomalous stream sediment values are calculated by comparing the expected, lithology-dependent, stream sediment values with the actual values obtained. Each watershed basin is examined separately. Once the expected values are known, anomalous values are taken as those exceeding the 97th percentile.

The process is carried out in ArcMap and is noted below in simplified form:

1. Separate tables for each commodity element of interest are prepared – each table contains the sample ID and assay value fields;
2. The watershed basin and bedrock geology layers are intersected, with the output layer constrained to lithology (at the 250K scale);
3. The spatial extent of each watershed basin, and of each lithological unit within each watershed basin, is calculated;
4. The expected commodity element "grade" of each lithological unit in each drainage basin is calculated using the drainage sample values for each basin split proportionally between the units. The assumption is that each lithological unit in each watershed basin contributes to the stream sediment load in proportion to the area they occupy;[4]
5. The expected average "grade" for each lithological unit within the area of interest as a whole is calculated by averaging the "grade" of each lithological unit within each drainage basin;

4. While this assumption may at first appear to have some limitations – given that rock units weather at different rates, and are chemically distinct from each other – the process of anomaly determination is dependent on both the lithological makeup of individual basins and the lithological makeup of the area as a whole. Expected values are calculated on the back of numerous different lithology combinations of widely differing proportions, so that differing rates of weathering are effectively captured (through a process of averaging, or smoothing), and subsequently applied to individual watersheds for determination of anomalous values.

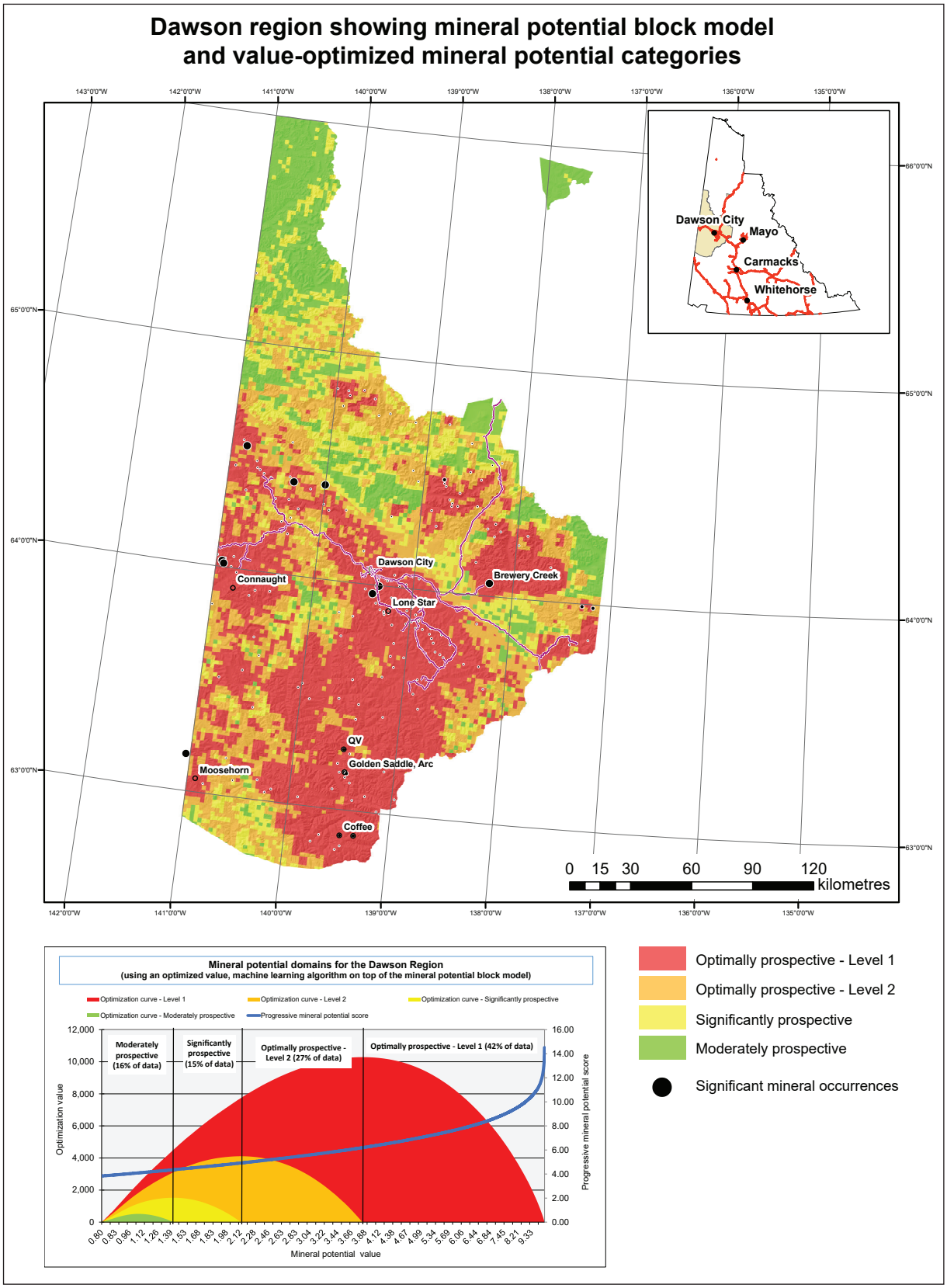


Figure 4. *The value-optimization mineral potential map for the Dawson region. Measures of confidence are excluded for clarity, no smoothing of cell boundaries has been effected.*

6. The expected contribution of each lithological unit in each basin to the drainage sample assay values is calculated using the average lithological "grade" for the area as a whole;
7. The expected sample values for each watershed basin (for the elements of interest) are then calculated;
8. The expected sample values are compared to the actual assay values obtained for each watershed basin; then
9. Anomalous watershed basins at the >97th percentile are identified and separated out.

Categorizing Mineral Potential Confidence

In addition to mineral potential per se, mineral potential maps produced by the Yukon Geological Survey contain measures of bedrock mapping confidence to facilitate land use planning decisions. The confidence metrics distinguish between well-mapped areas that might be deemed highly prospective and poorly mapped areas that might also be rated as highly prospective; or highlight tracts classified as having lower mineral potential due solely to a lack of geological data.

On the Beaver River watershed and Dawson region maps, measures of confidence for non-plutonic rocks were based on the amount of mapping completed (Bullen, 2020), without taking other factors into account, such as the quality and date of the mapping, whether the maps were compiled from a number of earlier unrelated maps or the result of dedicated mapping exercises, scale of mapping, etc. For plutonic rocks, the confidence measures were based on the dating method utilized, and whether whole rock geochemical analyses had been carried out. The confidence measures were deemed to be adequate for land use planning purposes, yet imperfect.

Consequently, a new, more robust, bedrock mapping confidence scheme was devised in the second half of 2020, in close collaboration with Yukon Geological Survey's bedrock mapping group. The scheme has been applied to mineral potential maps since January 2021. The procedure is described below.

1. The bedrock map for Yukon was broken down into individual map components.
2. For each map component, the following four attributes were determined:
   a. Original scale of mapping;
   b. The year the map was produced;
   c. Whether the map was produced as a dedicated product intended for standalone publication, or was compiled from a series of unrelated map products; and
   d. The confidence in the mapping.

   The first three are data-driven attributes, whereas the last is knowledge-based.

Each attribute is ascribed a factor as shown in Table 2.

Table 2. *Attribute factors for bedrock confidence mapping.*

Attribute	Range	Factor	Rationale
Scale of mapping	1:50 000 to 1:1000	1.50	Large-scale maps provide more mapping detail than smaller-scale maps
	1:150 000 to 1:63,000	1.00	
	1:500 000 to 1:250 000	0.50	
Year of mapping	Post-2000	1.50	Mapping methods and technologies improve over time, as does access
	Between 1980 and 2000	1.00	
	Pre-1980	0.50	
Compilation vs standalone publication	Standalone map	1.00	Maps produced as standalone products are superior to those compiled from maps produced during unrelated mapping exercises
	Compilation	0.25	
Confidence in mapping	3	1.50	A knowledge-based factor which rates the quality of the mapping
	2	1.00	
	1	0.50	

The four factors are summed to give each map component an overall confidence score. The scores for each rock unit within the area of interest are then incorporated into the fishnet grid as described in Bullen (2020). The confidence scores derived using the method described above result in a robust metric against which to assess bedrock confidence.

Miscellaneous Updates

Additional updates to the Yukon Geological Survey's mineral potential mapping methodology include:

1. Revisions to the map legend to account for the new mineral potential categorization methodology described above. The 3 × 3 mineral potential/confidence square has been replaced by a 4 × 3 rectangle to account for the four machine learning-derived mineral potential categories (Fig. 5); and

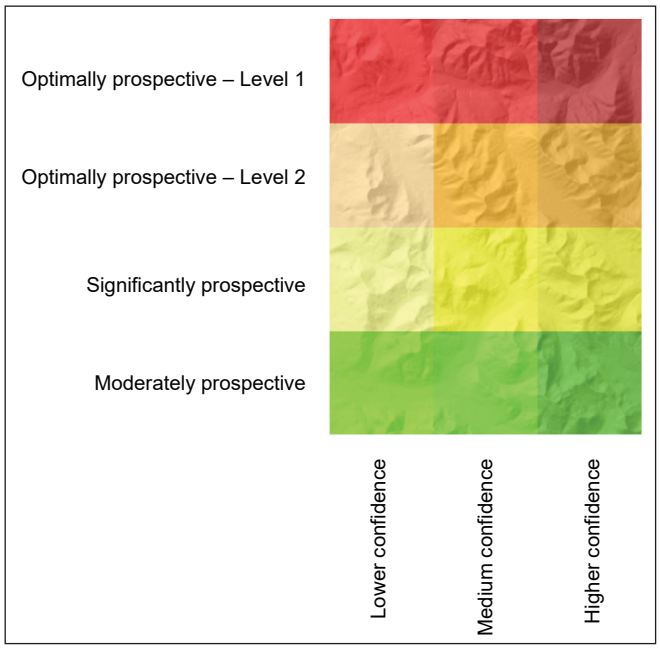


Figure 5. *The mineral potential/confidence graphic from the Teslin mineral potential map revised to incorporate the four machine learning mineral potential categories (the Teslin mineral potential map is not yet in the public domain). In addition, a hillshading underlay has been included to provide a more realistic feel and align with the map itself.*

2. More recently, the map colours have been revised to a multi-hued schema, rather than the red/yellow/green layout used previously. This allows for the production of colour blind-safe maps and also results in output more pleasing to the eye (Fig. 6).

Final Statement

The Yukon Geological Survey has implemented a number of enhancements to the mineral potential mapping process improving the map outputs. These include, *inter alia*, the application of an in-house-derived machine learning algorithm to generate mineral potential categories free of human bias, enhancements to the stream sediment anomaly identification process, a more robust bedrock mapping confidence schema, and improved visual representation. While the mineral potential maps for the Beaver River watershed and Dawson region remain valid in all respects, maps produced in the future will include the new modifications and will resonate better as a result.

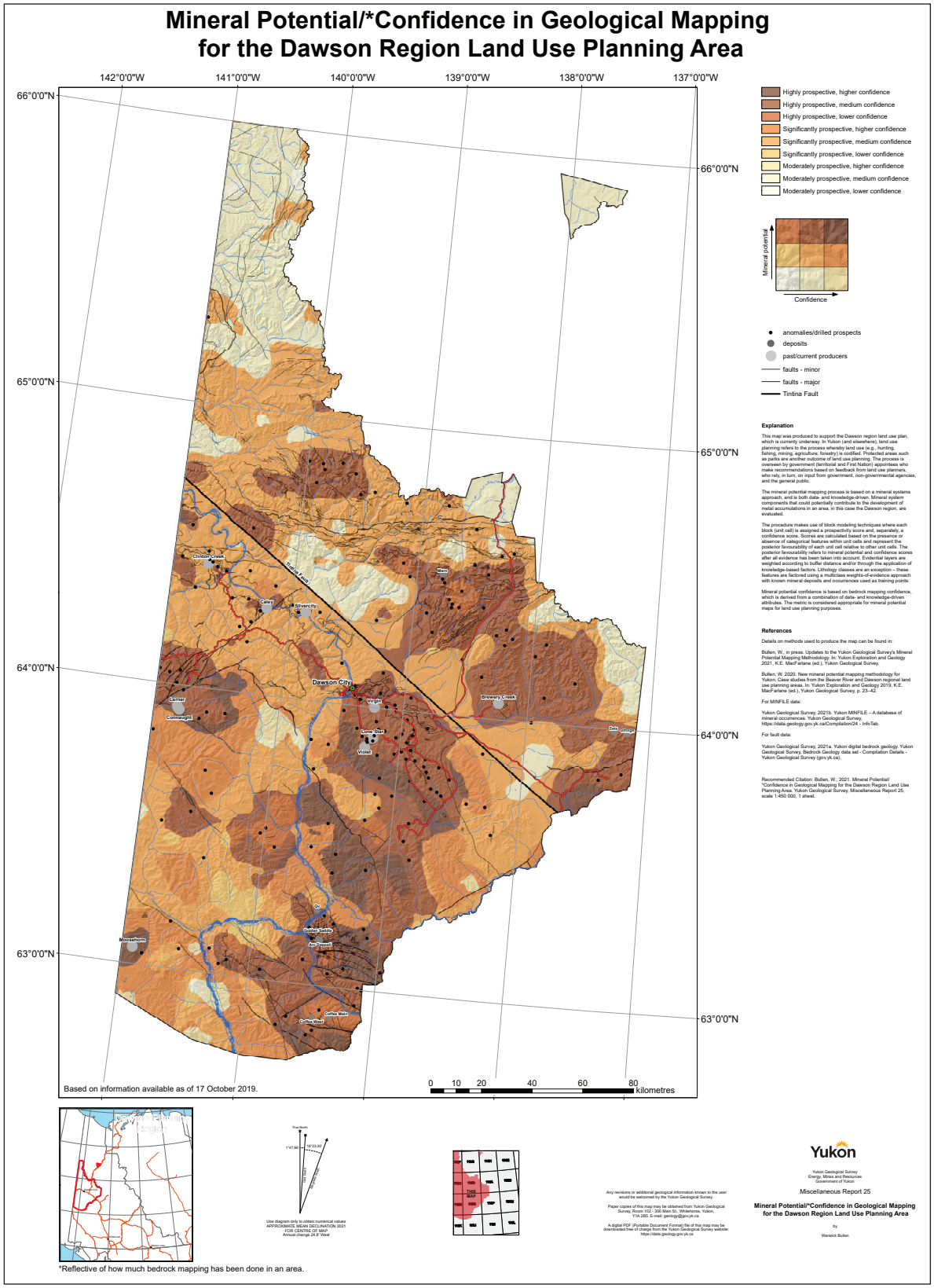


Figure 6. *The mineral potential map for the Dawson land use planning region showing the new multi-hued, colour blind-safe schema.*

References

Bullen, W., 2020. New mineral potential mapping methodology for Yukon: Case studies from the Beaver River and Dawson regional land use planning areas. *In:* Yukon Exploration and Geology 2019, K.E. MacFarlane (ed.), Yukon Geological Survey, p. 23–42.

Bullen, W., 2021. Using machine learning to categorize mineral potential and quantify the opportunity cost of land withdrawal alternatives. Geological Association of Canada – Mineral Deposits Division May 2021 Newsletter.

Mackie, R.A., Arne, D.C. and Brown, O., 2015. Enhanced interpretation of regional geochemical stream sediment data from Yukon: catchment basin analysis and weighted sums modeling. Yukon Geological Survey, Open File 2015-10, 9 p.

Yukon Geological Survey, 2021a. Yukon digital bedrock geology. Yukon Geological Survey, https://data.geology.gov.yk.ca/Compilation/3#InfoTab.

Yukon Geological Survey, 2021b. Yukon MINFILE – A database of mineral occurrences. Yukon Geological Survey, https://data.geology.gov.yk.ca/Compilation/24#InfoTab.

Yukon Geological Survey, 2021c. Regional geochemical surveys (RGS) – A compilation of Yukon regional stream sediment analysis. Yukon Geological Survey, https://data.geology.gov.yk.ca/Compilation/21#InfoTab.

Yukon Geological Survey, 2021d. Yukon Assessment Report Footprints. Yukon Geological Survey, https://data.geology.gov.yk.ca/Compilation/25#InfoTab.

Government of Yukon, 2021a. GeoYukon – Geological Folds (250k). Government of Yukon, map-data.service.yukon.ca/GeoYukon/Geological/Folds_250k/.

Government of Yukon, 2021b. GeoYukon – Placer Claims (50k). Government of Yukon, map-data.service.yukon.ca/GeoYukon/Mining/Placer_Claims_50k/.

Government of Yukon, 2021c. GeoYukon – Quartz Claims (50k). Government of Yukon, map-data.service.yukon.ca/GeoYukon/Mining/Quartz_Claims_50k/.

Update on the bedrock geology of the Rusty Mountain and Bonnet Plume Pass (west half) areas

Tyler Ambrose
Yukon Geological Survey

Ambrose, T., 2022. Update on the bedrock geology of the Rusty Mountain and Bonnet Plume Pass (west half) areas. *In:* Yukon Exploration and Geology 2021, K.E. MacFarlane (ed.), Yukon Geological Survey, p. 13–36.

Abstract

The Rusty Mountain and Bonnet Plume Pass areas are underlain by sedimentary strata of the Paleoproterozoic Gillespie Lake Group, Mesoproterozoic Pinguicula Group, Neoproterozoic Hematite Creek Group and Windermere Supergroup, and Paleozoic Bouvette Formation. Gabbro and diorite of the ca. 1.38 Ga Hart River sills intrude the Gillespie Lake Group. A swarm of east-west striking, mafic dikes intrude strata as young as the Tonian Hematite Creek Group. The main structures in the area include a steeply dipping axial-planar cleavage and upright, gently plunging folds. The northwestern part of the map area is dominated by northeast-southwest oriented structures that affected the ca. 1 Ga Hematite Creek Group, but predate deposition of the ca. 780 Ma Callison Lake Formation (Windermere Supergroup). In the southern and northeastern parts of the map area, the structures are parallel to and likely related to younger Mesozoic–Cenozoic structures.

* Tyler.Ambrose@yukon.ca

Introduction

Paleo and Mesoproterozoic rocks in the northern Cordillera are exposed in a series of erosional inliers surrounded by younger Neoproterozoic and Paleozoic rocks. The inliers are located along the southern margin of the Yukon stable block, a triangular region of isostatically independent and relatively thick lithosphere bounded by the Dawson fault to the south, the Yukon fault to the north, and the Richardson fault array to the east (Jeletsky, 1962; Abbott, 1997; Norris, 1997; Estève *et al*., 2020; Colpron *et al*., 2016).

This paper presents an update on the bedrock geology of the Rusty Mountain (106C/5) and Bonnet Plume Pass (106C/6; west half) areas as well as parts of adjacent map sheets 106C/3, 4, 11, 12 and 106D/1, 8. This report is a companion to the open file geological map of Ambrose (2022). The area is located at the southeast margin of the Wernecke inlier, the largest and farthest east of several inliers that span from Alaska to eastern Yukon (Fig. 1). Strata exposed in the area includes rocks as old as the Paleoproterozoic Gillespie Lake Group and as young as the Cambrian–Devonian Bouvette Formation (Figs. 2 and 3). The goal of this project is to refine structural and stratigraphic relationships and to provide geological context for mineral occurrences in the area. The new map expands to the north and east of the area previously mapped by Ambrose (2020). A summary of previous work in the area is provided by Ambrose and Bowie (2020) and Ambrose (2021). The interpretations presented here revise and supersede the reports of Ambrose and Bowie (2020) and Ambrose (2021), and the map of Ambrose (2020).

Stratigraphy

Gillespie Lake Group

The Gillespie Lake Group (Delaney, 1981) is the uppermost unit of the Paleoproterozoic Wernecke Supergroup and the oldest unit exposed in the map area (Fig. 3). It is dominated by orange, red, buff and grey weathering, thin to thick-bedded, variably silty, resistant (cliff-forming) dolostone (Fig. 4a–c). Microbial laminations are common, and stromatolites are locally abundant (Ambrose, 2021). Silicification is pervasive, particularly in the coarse-grained beds (Fig 4a). Common sedimentary structures include wavy cross-lamination (Fig. 4b) and desiccation cracks. Some beds contain evidence for soft-sediment deformation structures, most commonly intraformational breccias and slump folds. Medium to thickly bedded nodular dolostone and limestone form intervals up to 100 m thick. Beds of silicified oolitic grainstone and less commonly chert are locally found.

In addition to the typical cliff-forming dolostone, the Gillespie Lake Group also includes fine-grained siliciclastic rocks. Resistant intervals up to ~100 m thick of blue, green and grey weathering, variably calcareous/dolomitic siltstone and fine-grained sandstone are well exposed in cliff faces (see Fig. 9 in Ambrose, 2021). Recessive packages of mixed siliciclastic and carbonate rocks up to ~2 km thick occur throughout the Gillespie Lake Group (Figs. 3 and 4d,e). These intervals include both carbonate and siliciclastic dominated sections that are gradational with one another. The carbonate is primarily grey, tan, brown and orange weathering, laminated to thinly bedded, variably silty dolostone. Planar, wavy, and cross-laminations are common. Stromatolites and microbial laminations occur locally in some thicker dolostone beds. Though less abundant, the proportion of limestone in these intervals is higher than typical of Gillespie Lake Group. Siliciclastic rocks consist of laminated to medium-bedded, variably dolomitic-calcareous and carbonaceous, grey, black and orange weathering shale, mudstone, siltstone and fine-grained sandstone (Fig. 4d). A thick siliciclastic-dominated package is commonly present immediately beneath the sub-Pinguicula unconformity (Fig. 2).

Ambrose (2021) incorrectly interpreted the transition from recessive siliciclastic to carbonate rocks to be the gradational contact between the Quartet and Gillespie Lake groups, which required that the stratigraphy was repeated by northwest verging thrust faults. This implies that the Gillespie Lake Group is considerably thicker in the area than the >2 km and ~1.2 km estimates of Ambrose (2020) and Mustard *et al.* (1990), respectively. The revised thickness estimate for the map area is >5 km, which is more consistent with the >4 km estimate of Delaney (1981) and 4.7 km thick estimate of Thorkelson (2000) to the north.

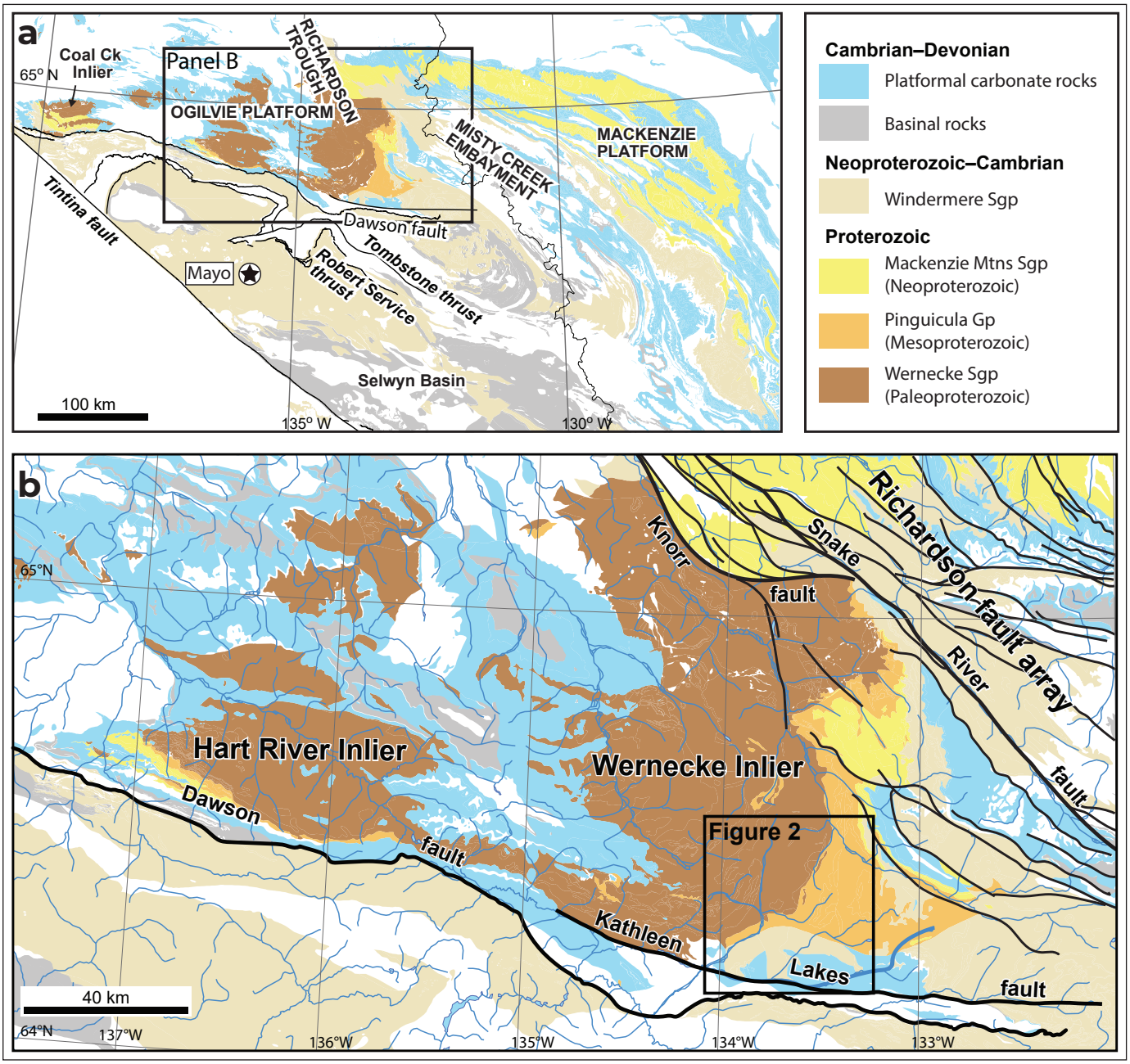


Figure 1. (a) *Simplified geological maps showing the distribution of Proterozoic strata in Yukon and Northwest Territories (after Moynihan et al., 2019).* ***(b)*** *Simplified geological map (extent outlined in (**a**)) of the Hart River and Wernecke Inliers. The study area (extent outlined in b) is located at the southeast margin of the Wernecke inlier, the largest and farthest east of several erosional windows that expose Paleo and Mesoproterozoic strata. Same legend is used for both figures. White areas are Late Devonian and younger rocks. Geology from Yukon Geological Survey (2021).*

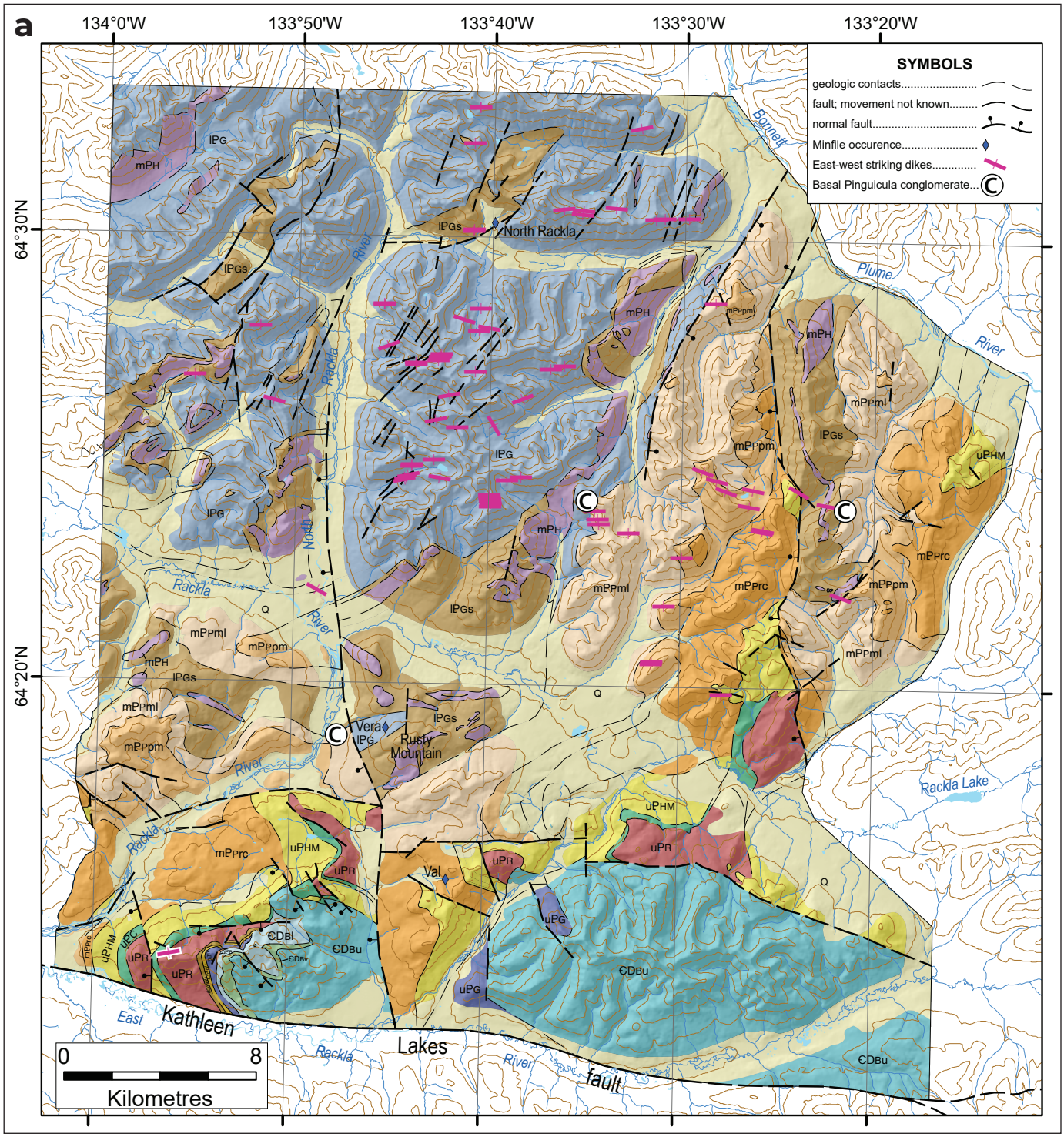


Figure 2. (a) *Simplified geological map of the study area after Ambrose (2022). Three localities where basal Pinguicula sandstone/conglomerate were observed are indicated. Legend (Fig. 2b) on facing page.*

b

QUATERNARY

Q — unconsolidated alluvial, colluvial, fluvial, and glacial deposits

CAMBRIAN TO DEVONIAN

BOUVETTE FORMATION

€DBu — UPPER MEMBER: light to medium grey weathering dolostone; commonly thickly bedded; locally fossiliferous

€DBv — VOLCANICLASTIC MEMBER: grey, green and orange weathering volcaniclastic sandstone and conglomerate; locally fossiliferous

€DBl — LOWER MEMBER: light to medium grey weathering sugary dolostone

EDIACARAN

RACKLA GROUP

uPB — BLUEFLOWER FORMATION: brown weathering shale and siltstone

uPG — GAMETRAIL FORMATION: Well bedded and laminated grey, buff, maroon, yellow-orange, and green weathering silty lime and dolo-mudstone

CRYOGENIAN–EDIACARAN

HAY CREEK GROUP

uPHCr — RAVENSTHROAT FORMATION: grey and cream weathering dolostone, grey and black chert; local chaotic bedding and tepee structures

uPHCp — MOUNT PROFEIT DOLOSTONE/ICE BROOK FORMATION: grey and cream weathering dolostone; light-grey weathered carbonate-clast diamictite

CRYOGENIAN

RAPITAN GROUP

uPR — orange, maroon, and brown weathering clast to matrix-supported diamictite; maroon and green weathering shale, siltstone and sandstone intervals

TONIAN

CALLISON LAKE FORMATION

uPC — light to medium grey weathering dolostone with irregular chert layers; commonly laminated; locally silica replaced oolitic grainstone; locally hematite-cement conglomerate

NEOPROTEROZOIC

HEMATITE CREEK GROUP

uPHM — laminated, medium to very thickly bedded grey, purple, and orange weathering sandstone, with subordinate shale, siltstone, limestone, red-weathering stromatolitic dolostone, and orange-weathering dolostone and dolomitic siltstone

MESOPROTEROZOIC

PINGUICULA GROUP

mPPrc — RUBBLE CREEK FORMATION: dark and light grey laminated dolostone with local zebra textures

mPPpm — PASS MOUNTAIN FORMATION: well bedded, laminated, grey and orange weathering dolomitic limestone; commonly cross-laminated; minor dolomitic/calcareous shale at base

mPPml — MOUNT LANDREVILLE FORMATION: blue, brown and green-grey weathering shale, mudstone, siltstone and fine-grained sandstone; locally interbedded sandstone and conglomerate at base

HART RIVER SILLS

mPH — grey weathering, fine to medium-grained, greenish-grey gabbro sills and dikes

PALEOPROTEROZOIC

GILLESPIE LAKE GROUP

lPG — resistant, thin to thick bedded, orange, red, and grey weathering variably silty dolostone; minor intervals of recessive cream, orange, and grey weathering siltstone, dolomitic silstone, silty dolostone, and lime mudstone; intervals of resistant, grey, orange and brown weathering, variably dolomitic siltstone and fine-grained sandstone

lPGs — grey, brown, black, and terracotta-weathered shale, siltstone and fine-grained sandstone; locally phyllitic and slatey; minor thin to medium bedded carbonate

Figure 2. (b) *Simplified legend.*

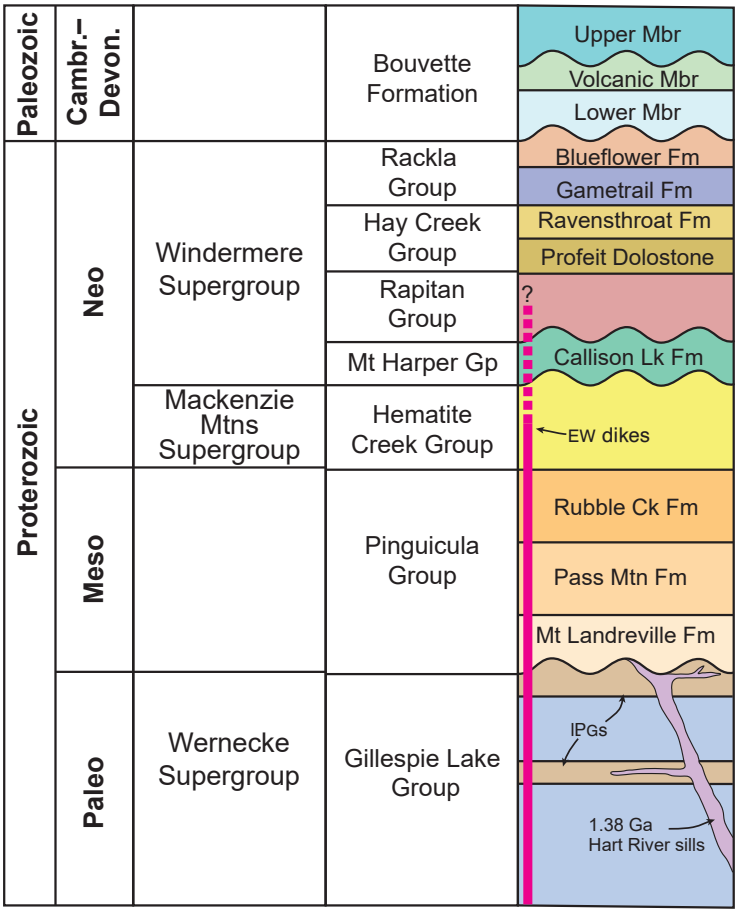


Figure 3. *Schematic lithostratigraphic column of units exposed in the map area. The east-west striking dikes intrude strata at least as young as the Tonian Hematite Creek Group; a single mafic dike in the southwestern part of the map area intrudes the Rapitan Group and suggests this suite may be younger than Cryogenian. Mbr: Member, Fm: Formation, Gp: Group,* lPGs*: fine-grained siliciclastic strata.*

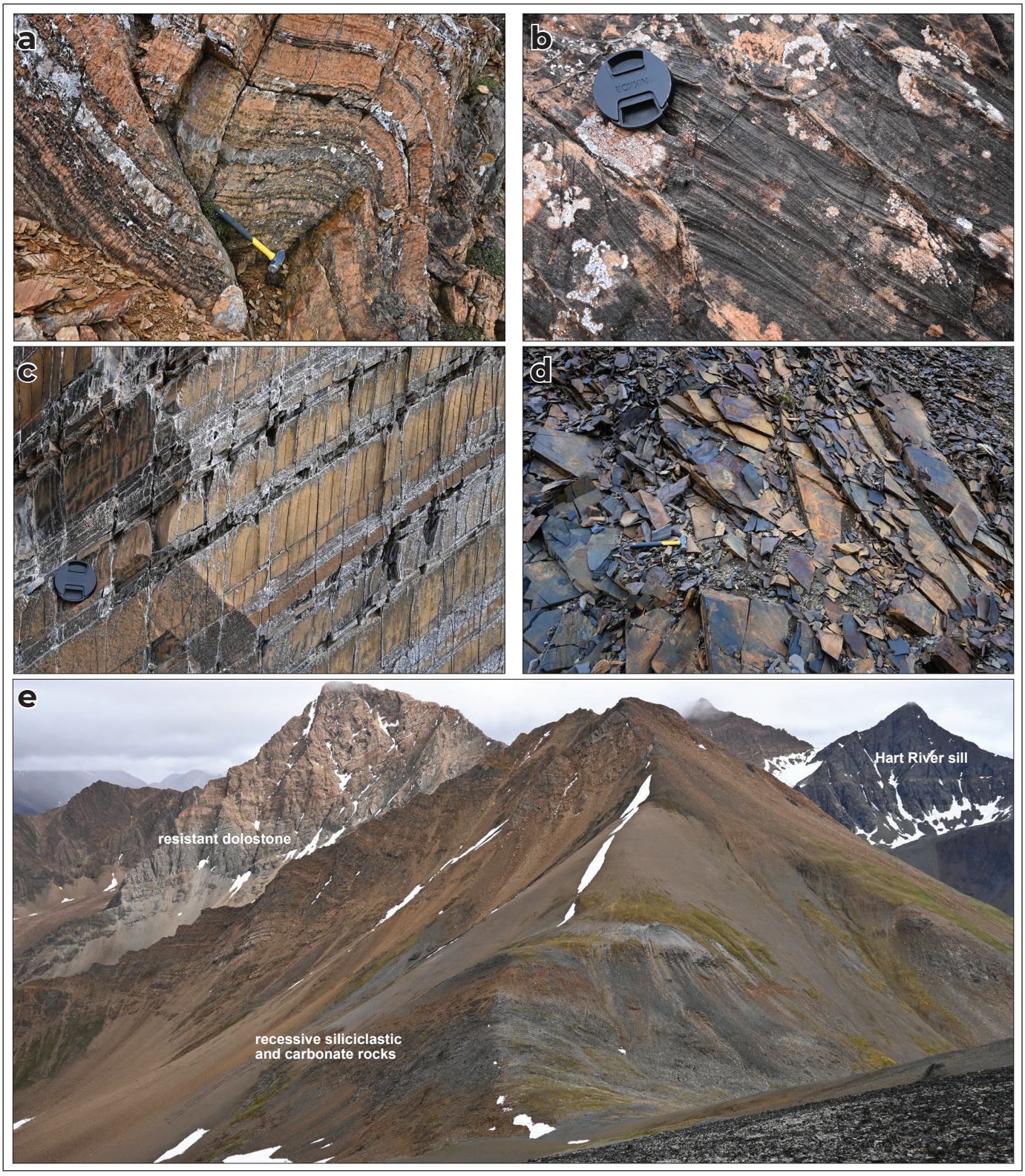


Figure 4. *Field photographs of the Gillespie Lake Group.* ***(a)*** *Minor fold in silicified dolostone. View to northeast.* ***(b)*** *Cross-laminated dolograinstone.* ***(c)*** *Vertical cleavage in dolograinstone-mudstone. View to north.* ***(d)*** *Rusty weathering carbonaceous siltstone and fine-grained sandstone from a siliciclastic interval.* ***(e)*** *Recessive, brown weathering dolomudstone and grey weathering siltstone interval (~100 m thick) below red weathering dolostone cliffs.*

Pinguicula Group

Mount Landreville Formation

The Mount Landreville Formation (Medig et *al.*, 2016; Pinguicula A of Eisbacher, 1978, 1981) is the lowermost unit of the Mesoproterozoic Pinguicula Group and overlies the Gillespie Lake Group and Hart River sills with angular unconformity (Figs. 2, 3 and 5a,b). It consists primarily of laminated to medium-bedded, grey, brown, blue, and green weathering mudstone, shale, siltstone and fine-grained sandstone (Fig. 5b). Planar parallel laminations are common (Fig. 5b). Wavy and cross-laminations are rare. A pencil cleavage is locally developed.

An interval of interbedded sandstone and conglomerate up to ~50 m thick locally marks the base of the unit (Figs. 2 and 5d,e). The sandstone is grey to brown weathering, thin to medium bedded, and fine to medium grained. The conglomerate is matrix to clast supported with granule to pebble-sized clasts of siltstone, sandstone, chert and carbonate. Where the basal conglomerate is absent, the Mount Landreville Formation can be difficult to distinguish from fine-grained siliciclastic rocks of the Gillespie Lake Group. The presence (or lack) of Hart River sills, which intrude the Gillespie Lake Group but not the Pinguicula Group, help to discriminate between the two units.

The appearance of interbedded brown and grey weathering carbonate rocks and increasingly calcareous siliciclastic rocks near the top of the Mount Landreville Formation indicate transition to the overlying Pass Mountain Formation. This upper section can resemble the recessive mixed siliciclastic-carbonate packages of the Gillespie Lake Group. The Mount Landreville Formation is up to ~2 km thick in the map area, which is considerably thicker than the ~300 m thickness measured at the type section by Medig et *al.* (2016) 40 km to the north. The monotonous nature, lack of marker horizons, and structural complexity, however, make it difficult to reliably estimate the thickness.

Pass Mountain Formation

The Pass Mountain Formation (Medig et *al.*, 2016; Pinguicula B of Eisbacher, 1978, 1981) is the middle unit of the Mesoproterozoic Pinguicula Group and gradationally overlies the Mount Landreville Formation (Figs. 3 and 6a; Medig et *al.* 2016). The basal ~50 m of the unit consists of thinly interbedded brown weathering carbonate rocks and calcareous–dolomitic siltstone (Fig. 6b). Following the definition of Medig et *al.* (2016), the basal contact is placed where carbonate rocks become dominant (*i.e.*, >50%). The proportion of siliciclastic minerals decreases upsection and the remaining ~500 m of the unit consist of thin to medium-bedded, bright orange to grey weathering, dolomitic limestone and calcareous dolostone (Fig. 6c–e). Parallel planar to wavy laminations and cross-laminations (including hummocky and swaley in places) are common (Fig. 6e). Intraformational breccia and slump folds are evidence of soft-sediment deformation in some beds. The total thickness of the Pass Mountain Formation is ~550 m in the study area. The type section, located ~15 km to the north of the map area, is estimated to be >500 m thick (Medig et *al.*, 2016). Twenty-five kilometres northeast of the type section, the unit is estimated to be only 150 m thick.

Rubble Creek Formation

The Rubble Creek Formation (Medig et *al.*, 2016; Pinguicula C of Eisbacher, 1978, 1981) is the uppermost unit of the Mesoproterozoic Pinguicula Group (Fig. 4; Medig et *al.*, 2016). The contact with the underlying Pass Mountain Formation is abrupt. The base of the unit typically consists of several tens of metres of thinly bedded to massive, light to medium grey weathering, dark grey lime mudstone with abundant white calcite veins. This passes upsection into thin to medium-bedded, light and dark grey pinstriped, locally fetid, dark grey to black dolostone (Fig. 7a,b). Trough cross-laminations are rare.

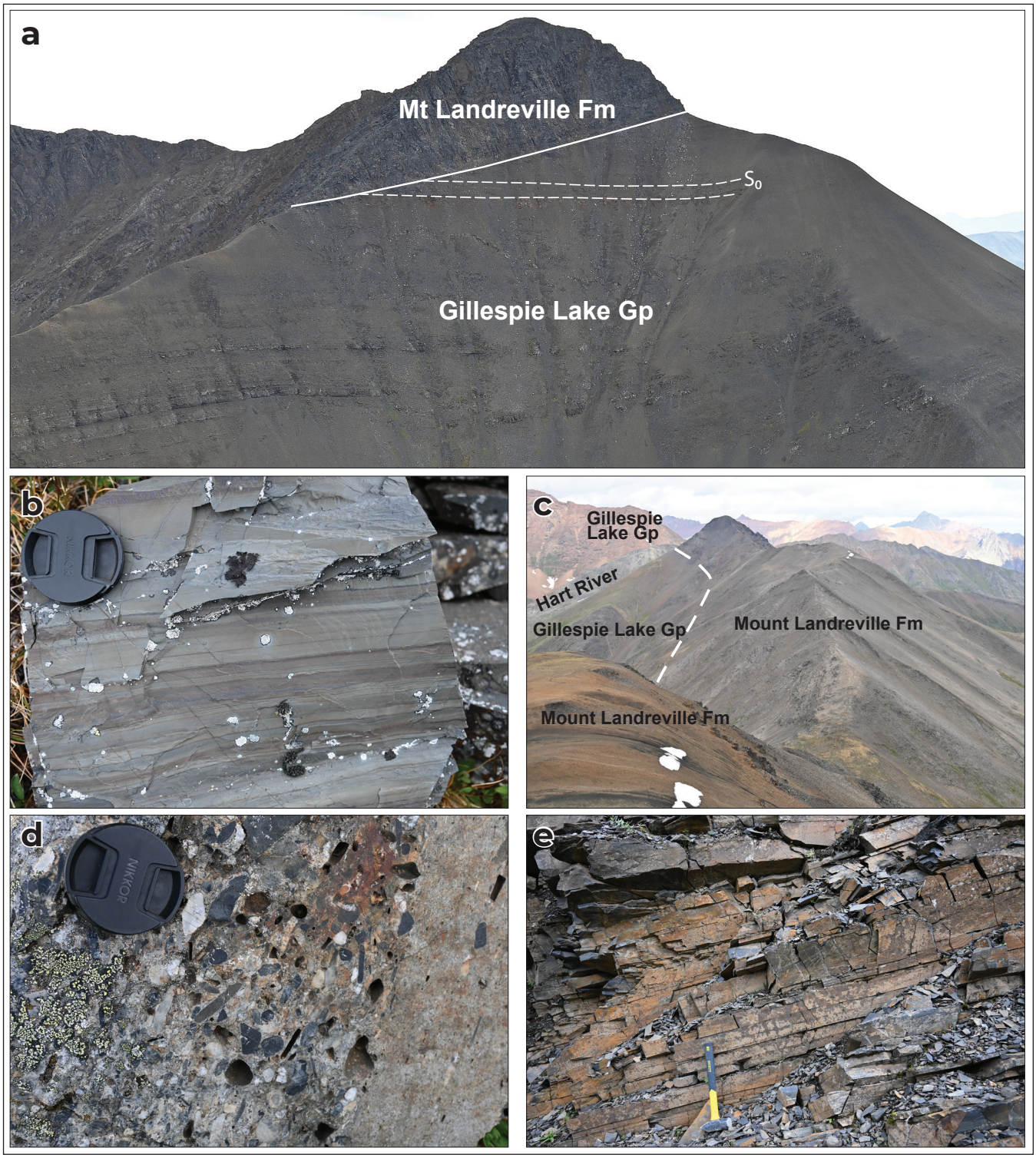


Figure 5. *Field photographs of the Mount Landreville Formation, Pinguicula Group.* ***(a)*** *Angular unconformity between siliciclastic strata of the Mount Landreville Formation and recessive silty dolostone and dolomitic/calcareous siltstone of the Gillespie Lake Group. Bottom ~50 m of Mount Landreville formation consists of interbedded sandstone and conglomerate.* ***(b)*** *Green-grey weathering laminated siltstone.* ***(c)*** *Orange and grey weathering shale, siltstone and fine-grained sandstone of the Mount Landreville Formation overlying recessive, silty dolostone of the Gillespie Lake Group. In top left of photo is red dolostone of the Gillespie Lake Group intruded by grey Hart River gabbro.* ***(d)*** *Basal conglomerate with clasts of chert and siltstone.* ***(e)*** *Basal, thin to medium-bedded sandstone.*

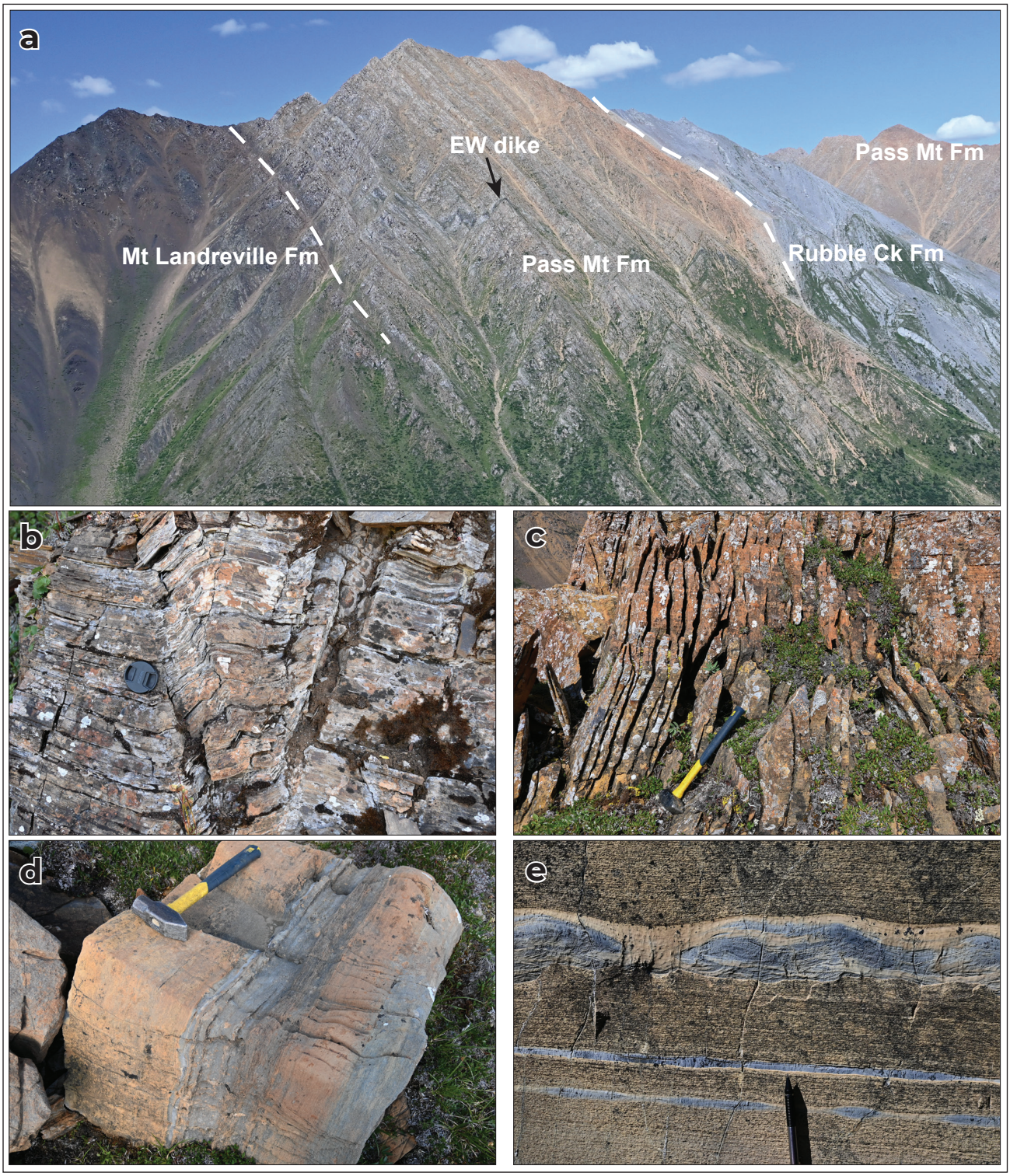


Figure 6. *Field photographs of the Pass Mountain Formation, Pinguicula Group.* ***(a)*** *A complete section of the Pass Mountain formation exposed on the flank of a syncline cored by the Rubble Creek Formation. View to north. Horizontal distance between upper and lower contacts is ~700 m.* ***(b)*** *Thinly bedded silty dolostone near the contact with the underlying Mount Landreville Formation. Fold plunges shallowly to the northeast. Located near the western boundary of the northeastern structural domain. View to northeast.* ***(c)*** *Steeply dipping cleavage in dolomitic limestone of the Pass Mountain Formation in the northeastern structural domain. View to north-northwest.* ***(d)*** *Interbedded orange-weathering dolomitic limestone and grey-weathering limestone.* ***(e)*** *Orange and grey weathering, planar and hummocky-swaley cross-laminated, dolomitic limestone.*

The dolostone is commonly replaced by millimetre to centimetre-scale bands of white and orange weathering sparry dolomite that occur as parallel to *en échelon* arrays described as zebra texture (Ambrose and Bowie, 2020). Brecciation, with a sparry dolomite matrix, and carbonate veining is locally extensive (Fig. 7c). In the northeastern part of the map area, the Rubble Creek Formation contains a discontinuous interval up to several hundred metres thick of recessive, grey and brown weathering limestone with interbedded dark weathering shale and siltstone (Fig. 7d,e). This interval also includes some beds of pinstriped dolostone with zebra texture more characteristic of Rubble Creek Formation. Microbial laminations are present in some beds.

The uppermost ~50 m of the Rubble Creek Formation consists of tan, orange and pink weathering laminated dolostone with sparse dark grey to black chert nodules. Intraformational brecciation (Fig. 7f), along with the anomalous weathering, may reflect subaerial exposure and karst development. The recognition of a karst surface to the north of the map area prompted Thorkelson (2000) to separate the Hematite Creek Group (Pinguicula D–F of Eisbacher, 1978, 1981) from the Pinguicula Group.

The Rubble Creek Formation is up to ~1500 m thick in the map area, but its thickness is regionally variable. At its type section, located 30 km northeast of the map area, the Rubble Creek Formation is 590 m thick (Medig *et al.*, 2016). However, 5 km north of the type section, Thorkelson (2000) estimated a thickness of more than the 1800 m.

Hematite Creek Group

The Rubble Creek Formation is overlain by carbonate and siliciclastic rocks of the Tonian Hematite Creek Group (Figs. 2, 3 and 8; Thorkelson, 2000; Turner, 2011). The basal contact appears sharp in places but gradational elsewhere. Locally, grey weathering pinstriped dolostone that resembles the Rubble Creek Formation occurs interbedded with orange dolostone near the base of the unit. The orientation of bedding across the contact is parallel and throughout the map area the Hematite Creek Group always overlies the Rubble Creek Formation. However, in places the contact appears abrupt, consistent with evidence for subaerial exposure of the uppermost Rubble Creek Formation.

The Hematite Creek Group is stratigraphically complex in the map area. In the northeastern part of the map area, where it is well exposed, the basal section of the unit consists of ~200 m of interlayered orange weathering, variably silty dolostone, dark grey to black shale and siltstone, and grey to orange weathering sandstone (Fig. 8a,b). This transitions upsection into variable proportions of: 1) thin to medium-bedded tan, cream, orange and grey weathering, variably silty, laminated dolostone with locally abundant dark grey chert nodules (Fig. 8c), 2) very thin to medium-bedded, grey weathering, laminated limestone (Fig. 8d,e), 3) grey, and less commonly orange and purplish/pinkish weathering sandstone (Fig. 8b) and 4) grey and maroon weathering siltstone and shale with rare beds of conspicuous red weathering stromatolitic dolostone (Fig. 8f). Sandstone, which is characteristic of the unit, is more abundant in the southwestern part of the map area where it forms intervals up to several hundred metres thick (Ambrose and Bowie, 2020). Microbial laminations, cross-laminations (Fig. 8e), and mud cracks (Fig. 8g) are present in some carbonate beds. Siliciclastic and carbonate conglomerate/breccia layers, with clast sizes from granule to pebble, are found locally (Fig. 8h).

Windermere Supergroup

The Neoproterozoic Windermere Supergroup lies with angular unconformity over older strata of the Hematite Creek and Pinguicula groups. In the map area, the Windermere Supergroup includes the Callison Lake Formation and the Rapitan, Hay Creek and Rackla groups. Only the Callison Lake Formation and Rapitan Group are exposed in the area mapped in 2021. Ambrose and Bowie (2020) previously described the Hay Creek and Rackla group rocks that are exposed in the southwestern part of the map area.



Figure 7. *Field photographs of the Rubble Creek Formation.* ***(a-b)*** *Thinly bedded pinstriped dolostone.* ***(c)*** *Veined and brecciated dolostone.* ***(d)*** *Recessive, brown weathering, lime mudstone with fold highlighted by relatively resistant limestone beds. View to northeast.* ***(e)*** *Recessive, brown weathering, lime mudstone interval beneath cliffs of grey weathering pinstriped dolostone more typical of the unit. Lighting accentuates two east-west striking dikes in the foreground. Northeastern part of the map area, looking south.* ***(f)*** *Brecciated, pale tan-weathering dolostone near the contact with the overlying Hematite Creek Group.*

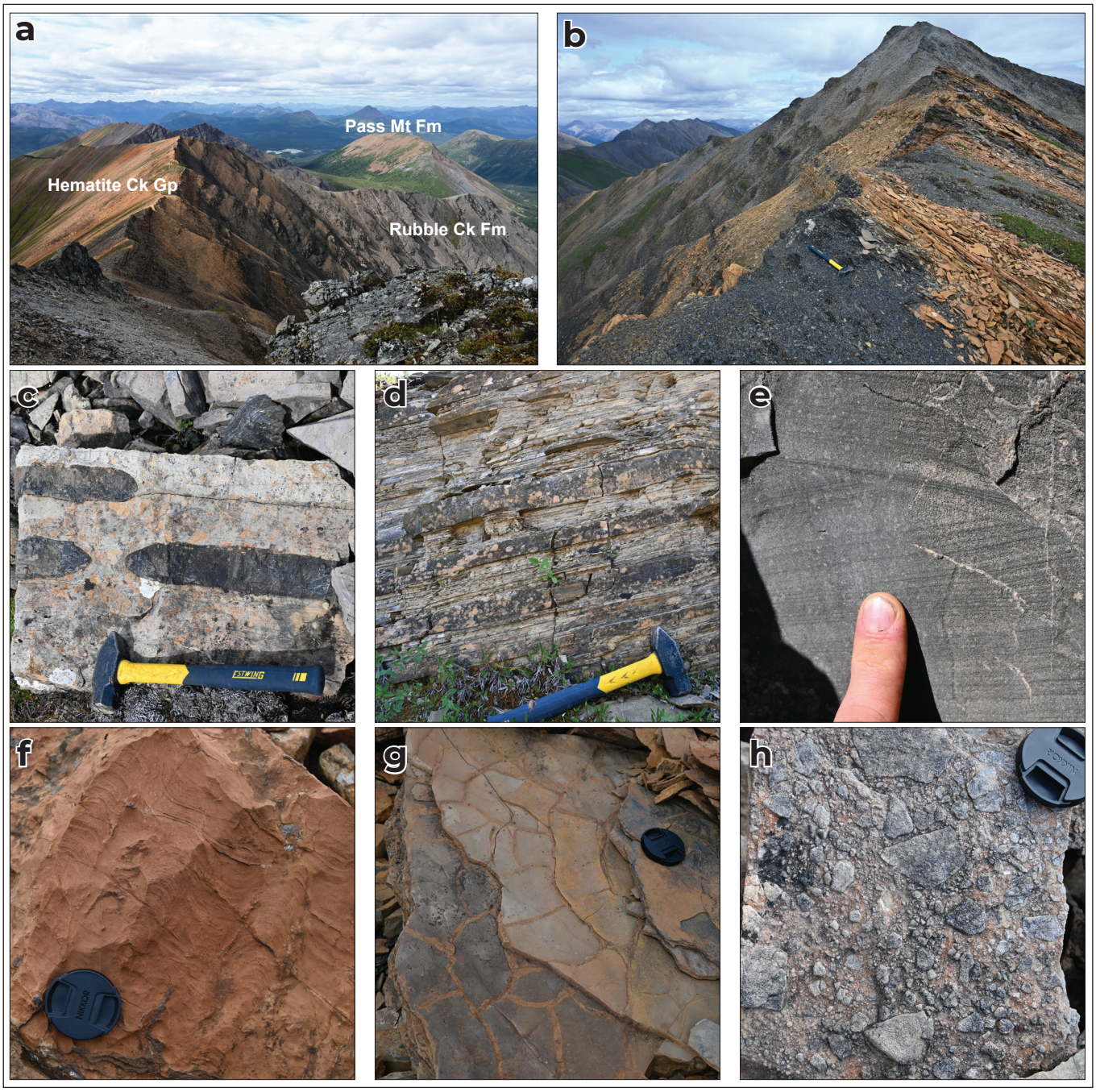


Figure 8. *Field photographs of the Hematite Creek Group.* ***(a)*** *Interbedded orange-weathering silty dolostone and black shale/siltstone of the Hematite Creek Group overlying grey-weathering dolostone of the Rubble Creek Formation. Bottom of photo is grey-weathering sandstone of the Hematite Creek Group.* ***(b)*** *Interbedded orange weathering, silty dolostone and black shale. Peak in back is grey weathering sandstone.* ***(c)*** *Black chert nodules in cream weathering laminated dolostone.* ***(d)*** *Very thin to thinly bedded lime mudstone-grainstone.* ***(e)*** *Planar cross-laminated lime grainstone.* ***(f)*** *Orange weathering stromatolitic dolostone bed.* ***(g)*** *Mud cracks in orange-brown weathering thinly bedded dolostone.* ***(h)*** *Carbonate clast conglomerate with sandy dolostone matrix.*

Callison Lake Formation

The Tonian Callison Lake Formation (Abbott, 1997; Strauss *et al.*, 2015) forms the base of the Windermere Supergroup in the area (Fig. 3). The base of the unit is angular unconformity that cuts down section from the Hematite Creek Group in the west to the Rubble Creek Formation in the east (Fig. 2). Ambrose and Bowie (2020) first described the Callison Lake Formation in the Wernecke inlier; previously, it had only been documented in the Coal Creek and Hart River inliers to the west.

The Callison Lake Formation consists of grey to cream weathering, thin to thickly bedded, commonly faintly laminated, cliff-forming dolostone with irregular discontinuous dark grey to black chert layers (Fig. 9a,e). Some dolostone beds exhibit faint, planar to wavy laminations. Silicified oolitic grainstone forms irregular pods and nodules tens of centimetres wide (Fig. 9b). Beds rarely consist of grey weathering dolowackestone–floatstone (Fig. 9c). Red weathering, hematite-cemented, carbonate-clast conglomerate/breccia is present at several localities across the map area (Fig. 9d).

Rapitan Group

The Cryogenian Rapitan Group (Yeo, 1978) overlies the Callison Lake Formation and Hematite Creek Group with angular unconformity. It consists of maroon, brown, and orange weathering, matrix to clast-supported conglomerate and diamictite, and maroon, orange, grey and green weathering shale, siltstone and fine-grained sandstone (Fig. 10). Clasts in the conglomerate/diamictite range from granule to boulder size and include carbonate, chert, jasper, siltstone, sandstone and rarely stromatolitic dolostone (Fig. 10c) and mafic volcanic rocks. Sandstone and siltstone beds are commonly laminated (Fig. 10b).

Bouvette Formation

The Cambrian to Devonian Bouvette Formation (Morrow, 1999) is the youngest unit in the map area (Fig. 3). It overlies the Windermere Supergroup and Hematite Creek Group with angular unconformity (Fig. 2). Based on observations in the southwestern part of the map area, Ambrose and Bowie (2020) and Ambrose (2020) divided the formation into three members. Only the upper member is exposed in the area mapped in 2021. The lower member consists of light grey weathering sucrosic dolostone and minor chert. The volcaniclastic member consists of up to 200 m of dark green, grey and orange weathering, thin to medium-bedded, volcaniclastic sandstone and conglomerate. It is composed of fragments of mafic volcanic rock and limestone in a carbonate matrix. Fossils are locally abundant and include graptolites, brachiopods, trilobites, sponges, crinoids, bryozoans and echinoids. An assessment of the fossil assemblage indicates a Middle Ordovician to Early Silurian age (Ambrose and Bowie, 2020).

The upper member consists of light grey weathering, thin to medium-bedded dolostone and minor limestone (Fig. 11). The base of the upper Bouvette is an angular unconformity that cuts down stratigraphic section from the volcanic member in the west to rocks as old as the Hematite Creek Group in the east (Fig. 2). In contrast to the lower member, fossils are locally abundant and include corals and gastropods. The fossil assemblage from a locality in the southwestern part of the map area indicates a Silurian age. In the absence of the volcaniclastic horizon and/or fossil assemblages, it is not always possible to distinguish the lower and upper members.

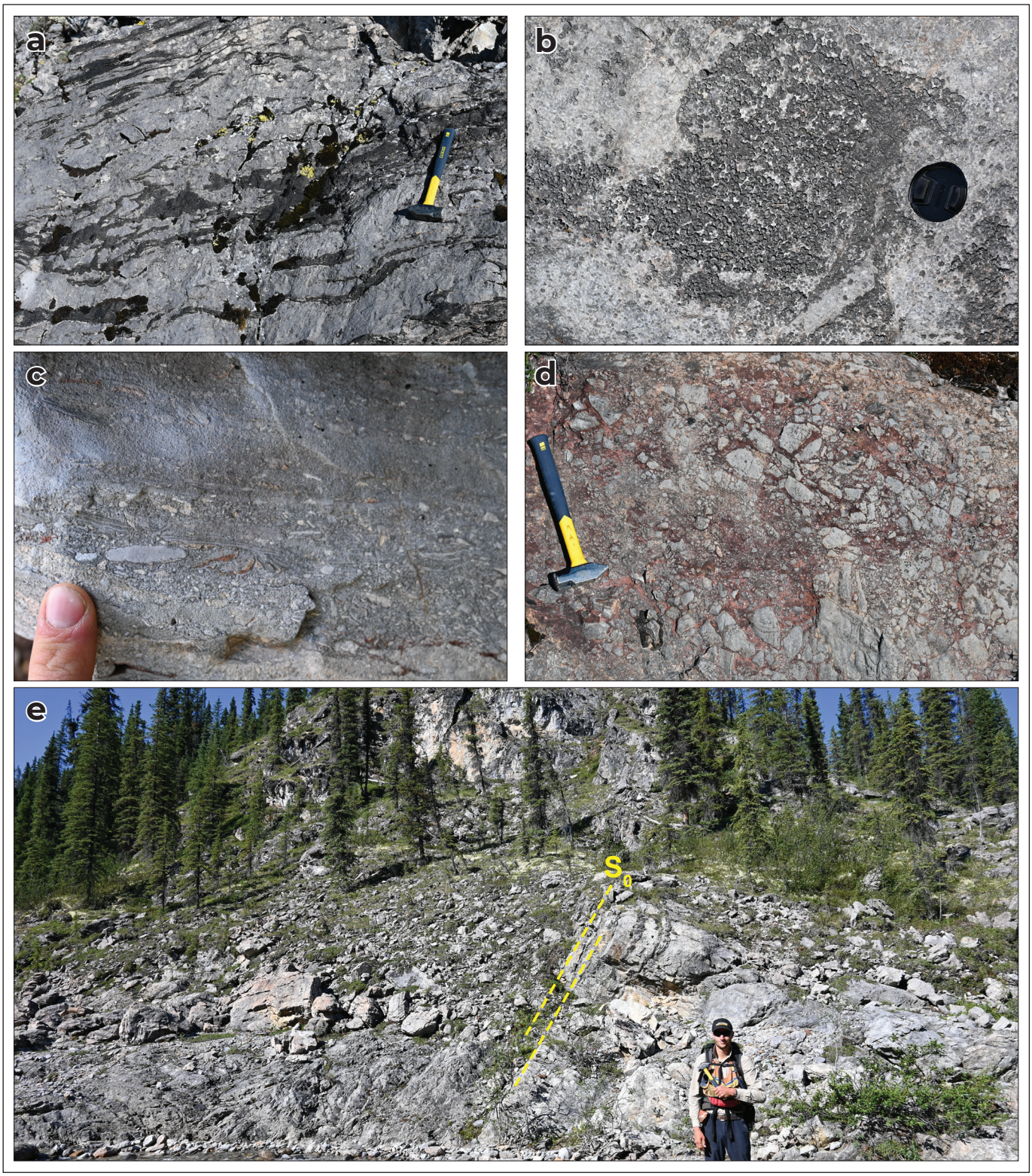


Figure 9. *Field photographs of the Callison Lake Formation.* ***(a)*** *Irregular black chert layers in light grey dolostone.* ***(b)*** *Silicified oolitic grainstone nodule.* ***(c)*** *Dolowackestone and floatstone layers.* ***(d)*** *Hematite cemented, carbonate-clast breccia.* ***(e)*** *Cliffs of Callison Lake Formation with bedding dipping steeply to the south. View to west.*

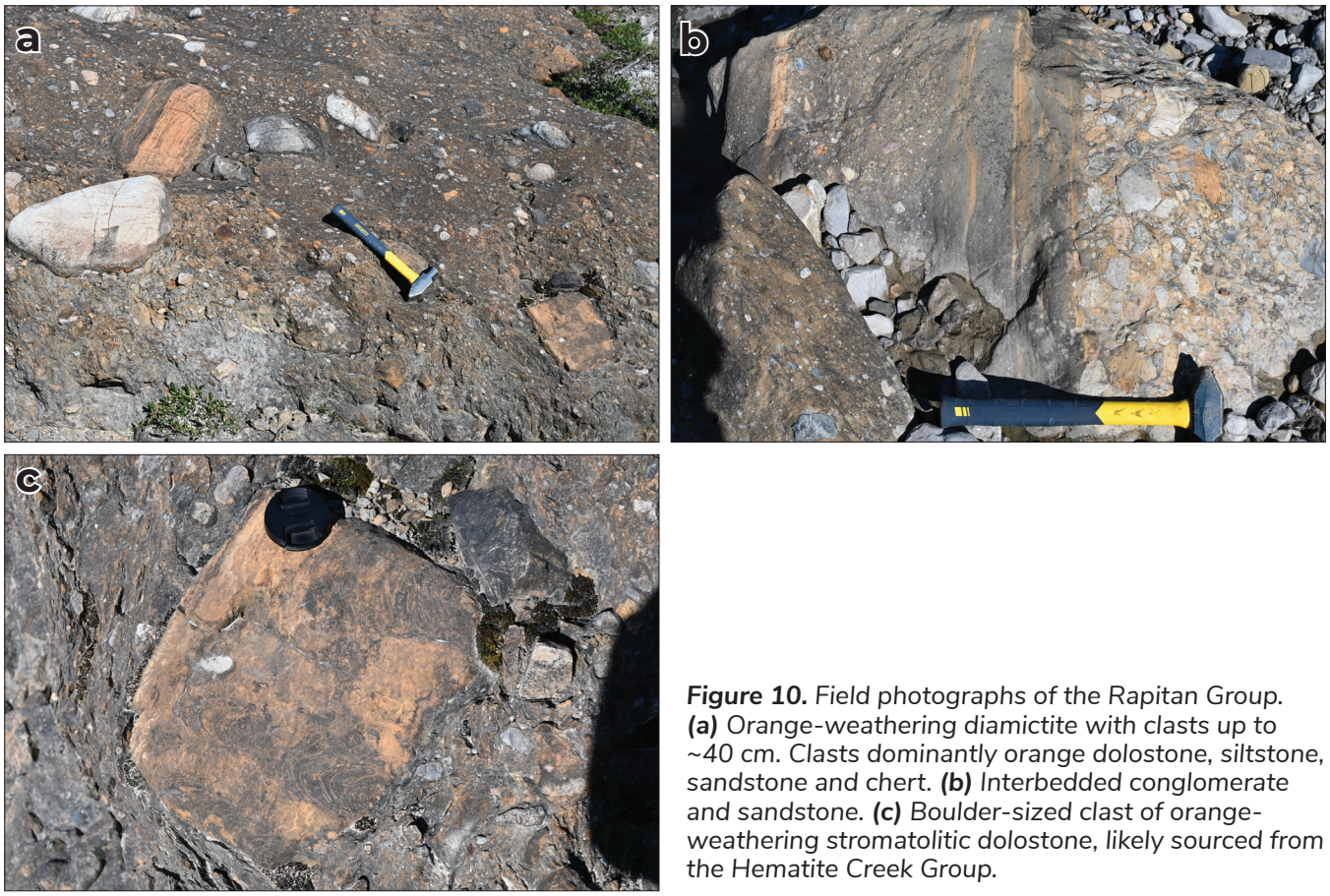


Figure 10. *Field photographs of the Rapitan Group.* ***(a)*** *Orange-weathering diamictite with clasts up to ~40 cm. Clasts dominantly orange dolostone, siltstone, sandstone and chert.* ***(b)*** *Interbedded conglomerate and sandstone.* ***(c)*** *Boulder-sized clast of orange-weathering stromatolitic dolostone, likely sourced from the Hematite Creek Group.*

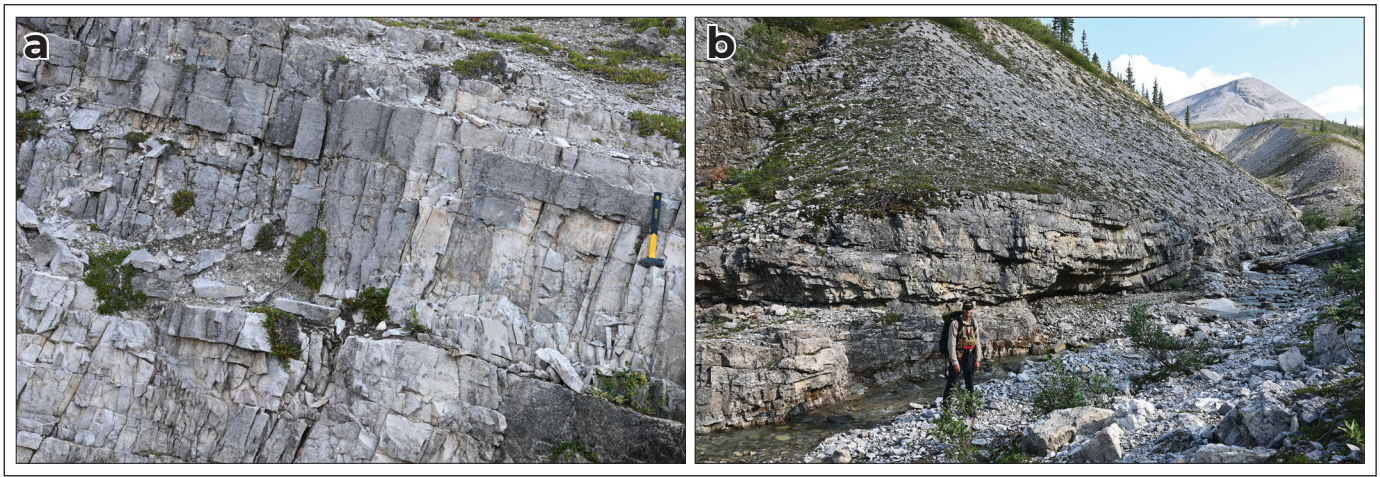


Figure 11. *Field photographs of the Bouvette Formation.* ***(a)*** *Medium-bedded, light grey dolostone.* ***(b)*** *Gently undulating, medium to thick-bedded dolostone.*

Intrusive Rocks

Hart River Sills

Gabbro and diorite of the ca. 1.38 Ga Hart River suite (Abbott, 1997; Verbaas et *al.*, 2018) intrude the Gillespie Lake Group (Figs. 2, 3 and 12). Dikes are uncommon and typically only a few metres wide. Sills are up to 250 m thick, 15 km long, and preferentially intruded the recessive, mixed siliciclastic-carbonate packages (Figs. 2 and 12a,b). Adjacent to intrusions, siliciclastic rocks are commonly orange weathering and pyritic (Fig. 12a,b), and carbonate rocks are locally bright white weathering. The primary igneous mineralogy is dominantly plagioclase and clinopyroxene with minor quartz and opaque minerals (Ambrose, 2021). Secondary minerals include chlorite, epidote group minerals, sericite and carbonate. The intrusions weather light to medium grey and commonly have a slight pinkish/orange colour (Fig. 12c). Ambrose (2021) showed that the Hart River sills in the map area have the geochemical composition of mid-ocean ridge basalts comparable to sills studied by Verbaas et *al.* (2018) to the west.

Magnetic east-west striking dikes

A swarm of approximately vertical and east-west striking dikes intrude strata at least as young as the Tonian Hematite Creek Group (Figs. 2, 3 and 13). Ambrose and Bowie (2020) noted a single, intensely altered, one metre wide mafic dike with a similar orientation cutting the Rapitan Group in the southwestern part of the map area that suggests these dikes intrude into Cryogenian strata locally. The dikes are typically 2–3 m thick and weather medium to dark grey. The colour contrast with the Pass Mountain Formation and Gillespie Lake Group makes them conspicuous. In darker weathering strata, such as the Mount Landreville Formation and siliciclastic rocks of the Gillespie Lake Group, the dikes are less apparent. Their mineralogy is dominated by variably altered plagioclase and clinopyroxene with minor olivine and opaque minerals. The magnetism, presence of olivine, lack of quartz, small size and consistent orientation distinguish these dikes from the Hart River sills. In contrast to the Hart River sills, the magnetic dikes have the geochemical composition of alkali basalt similar to ocean island basalts (Ambrose, 2021).

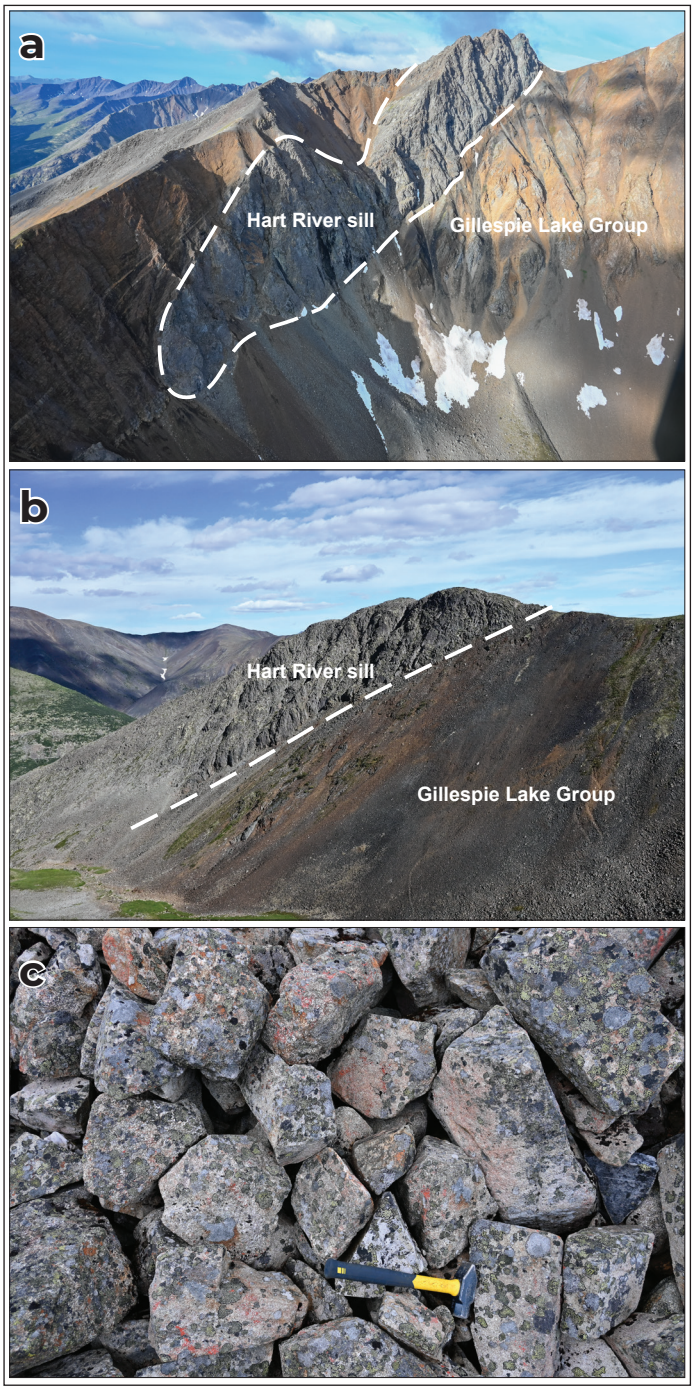


Figure 12. *Field photographs of the Hart River suite.* ***(a)*** *East-dipping mafic sill in orange weathering, recessive siliciclastic rocks of the Gillespie Lake Group. View to south. Distance from top of gabbro peak to snow at the base of the cliff is around 300 metres.* ***(b)*** *Grey weathering Hart River sill in dark and rusty weathering, fine-grained siliciclastic rocks of the Gillespie Lake Group. View to southeast. Bedding dipping to east (left of photo).* ***(c)*** *Boulders of gabbro showing the common orangey-pink colouration of weathered surfaces.*

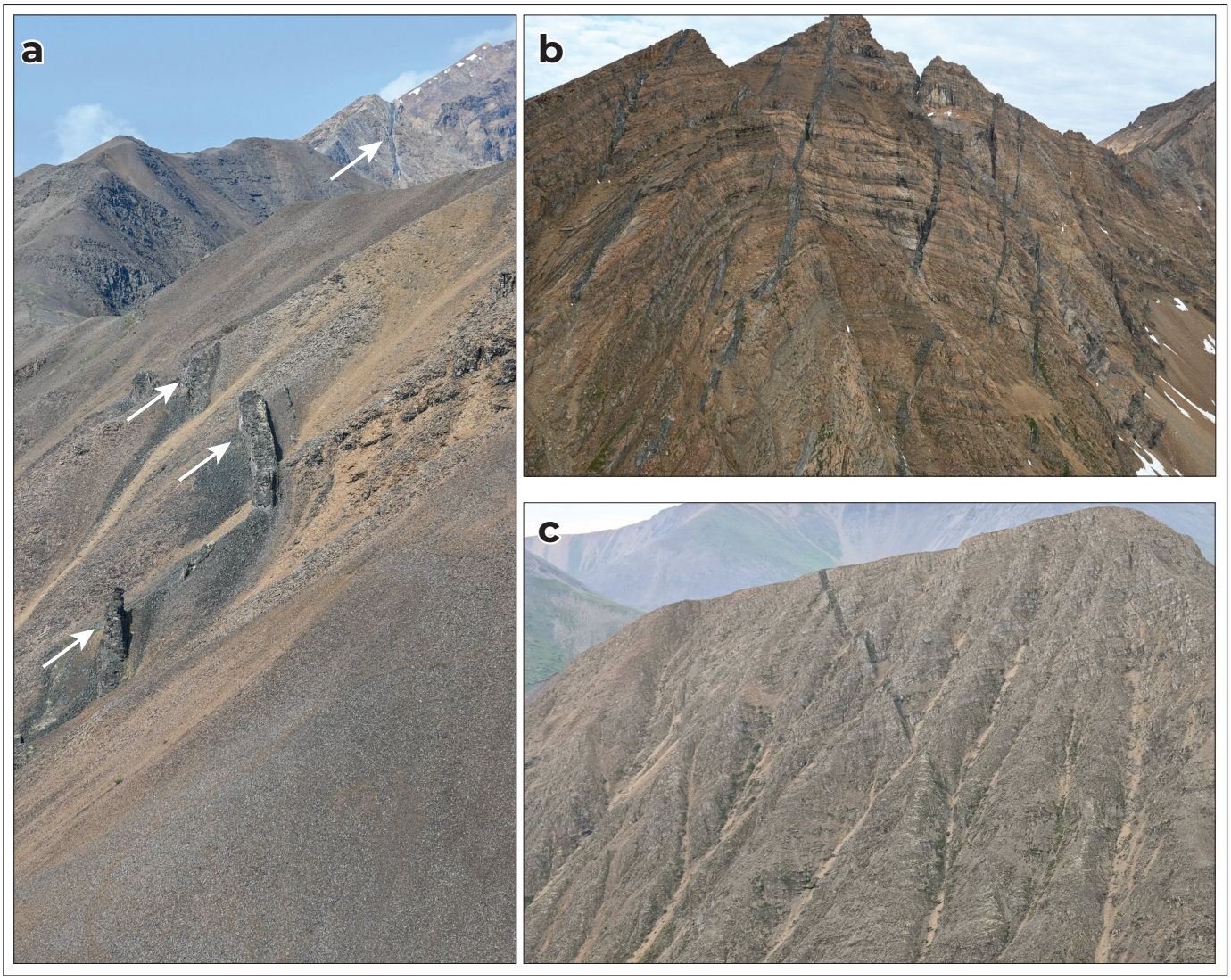


Figure 13. *Field photographs of the east-west striking dikes.* ***(a)*** *Cutting recessive mixed siliciclastic-carbonate interval of the Gillespie Lake Group. In top right of photo is cliff of red-weathering dolostone cut by dike. View to west. Bedding is folded but generally east dipping.* ***(b)*** *Dikes cutting folded Gillespie Lake Group. Note the small jogs of some dikes in the hinge zone of the fold. Cliff is ~ 400 m tall in centre of photo. View to west.*
(c) *Dike cutting carbonate of the Pass Mountain Formation, Pinguicula Group. Top of ridge is ~ 500 m long. View to southeast.*

Structure

The map area can be divided into three structural domains (northwestern, northeastern, and southern) where structures have distinct orientations (Figs. 14 and 15). The boundaries between the domains are transitional and in some places the placement is somewhat arbitrary. In each domain, structures include centimetre to kilometre-scale folds and a penetrative cleavage (Fig. 16).

Northwestern domain

The northwestern domain exposes rocks mainly of the Gillespie Lake Group and Hart River sills (Figs. 2 and 14). The eastern limit of the domain also includes exposures of the Pinguicula Group. This domain is characterized by northeast-southwest oriented structures (Figs. 14 and 15). Folds are generally open to close, upright to steeply inclined, and shallowly plunging to the northeast or southwest. Major folds are best observed in the Gillespie Lake Group

(Figs. 13b, 14 and 15), but are also present in the Pinguicula Group and Hart River sills. Minor folds are uncommon but locally well developed in the Gillespie Lake Group (Figs. 4a and 16a) and Pass Mountain Formation. Sedimentary structures in the Gillespie Lake Group and Pass Mountain Formation demonstrate that bedding is generally right way up and rarely overturned on the steep limb of folds. Folds are locally cut by the east-west striking dikes (Fig. 13b). A moderate to steeply dipping, northeast-southwest striking penetrative cleavage is common in fine-grained beds of the Gillespie Lake Group (Figs. 5c, 14 and 15) and Mount Landreville Formation.

The northwestern domain also includes steeply dipping faults that are generally parallel to the dominant cleavage and fold orientation (Fig. 2). These faults are locally identified by discrete breaks in bedding orientation and the offset of grey-weathered siliciclastic intervals (see Figure 9a in Ambrose, 2021).

Northeastern domain

The northeastern domain exposes Neoproterozoic and older strata with structures that are dominantly oriented north-south to northwest-southeast (Figs. 14 and 15). Major folds are typically gentle to close, upright, and shallowly plunging to the south-southeast or north-northwest (Figs. 14 and 15). Folding is tight in the hinge zone of some major folds (Fig. 16b). Minor folds are best developed in siliciclastic and carbonate rocks of the Pinguicula Group (Fig. 6b). A steeply dipping penetrative cleavage is common in the Mount Landreville Formation, rare in the Pass Mountain Formation (Fig. 6c), and locally well developed in siltstone and the matrix of diamictite in the Rapitan Group.

Southern domain

The southern domain exposes Paleoproterozoic to Paleozoic strata characterized by east-southeast to west-northwest oriented structures (Figs. 14 and 15). Major folds are generally gentle to open, upright and plunge shallowly to the northwest or southeast. Minor folds are uncommon and poorly developed, but found locally in rocks of the Gillespie Lake Group and Pass Mountain Formation (see bottom right of

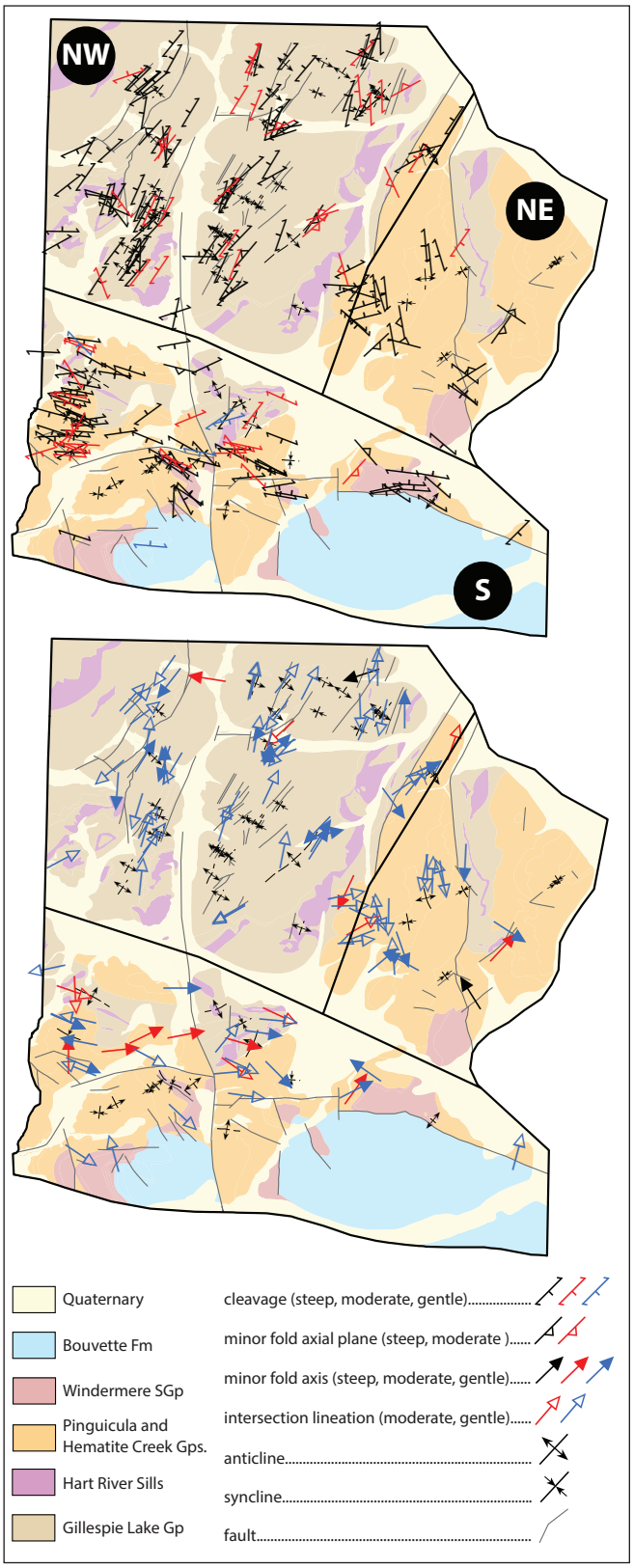


Figure 14. *Simplified geological map with three structural domains outlined in thick black line. For clarity, planar and linear structures are plotted separately.*

Figure 15 of Ambrose, 2021). A steeply dipping, southeast-northwest striking penetrative cleavage is variably developed in fine-grained siliciclastic rocks and silty carbonates of the Gillespie Lake Group, Mount Landreville Formation and Pass Mountain Formation. A well developed cleavage with the same orientation is also common within the matrix of diamictite in the Rapitan Group (see Figure 16e,f of Ambrose and Bowie, 2020). A cleavage that dips moderately to the north was observed at one locality in the volcaniclastic member of the Bouvette Formation. Northwest-southeast trending gentle folds were observed in the Bouvette Formation (Fig. 12b).

A major, east-west striking fault runs across the entire southern part of the map area. In the east, it separates Windermere Supergroup and Hematite Creek Group rocks to the north from Bouvette Formation rocks to the south. In the west, it separates Mount Landreville Formation and Pass Mountain Formation rocks to the north from younger rocks to the south. Given the similar orientation, the fault is likely related to the same event that produced folding and cleavage in the southern domain.

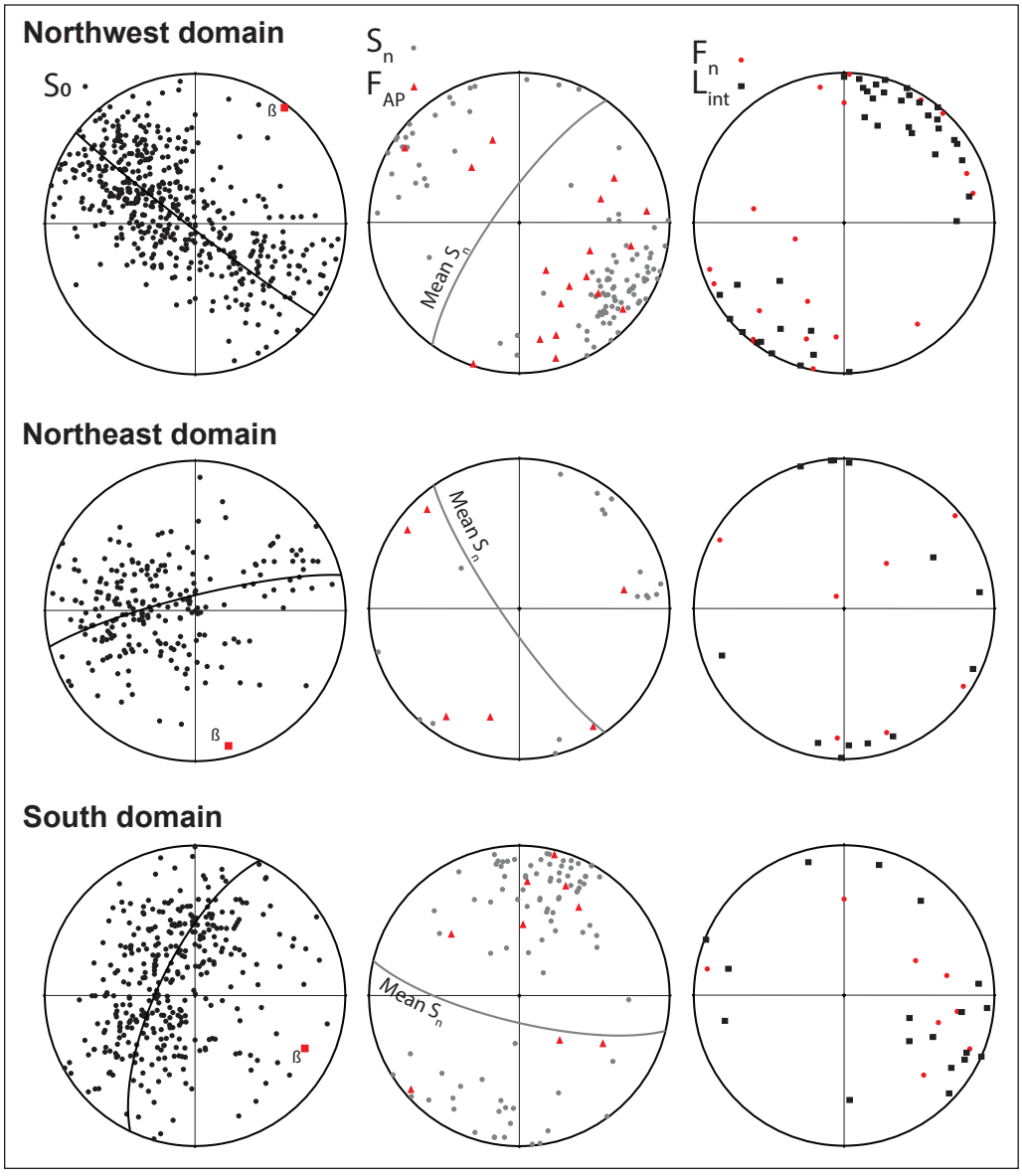


Figure 15. *Structural data from each domain plotted on lower hemisphere, equal area stereonets. S_0: bedding, S_n: cleavage, F_{AP}: fold axial plane, Fn: fold axis, L_{int}: intersection lineation.*



Figure 16. ***(a)*** *Northeast-southwest trending minor fold of Gillespie Lake Group dolostone. Northeastern structural domain. View to southwest.* ***(b)*** *Hinge zone of a north-south trending syncline with chaotic open to isoclinal folds in dolostone of the Rubble Creek Formation. Northeastern structural domain. View to north. From the peak to the base of the photo is a vertical distance ~450 m. See Figure 6a for a more extensive view of the same mountain side.*

Timing of deformation

The oldest structures in the map area are likely the northeast-southwest oriented folds and associated cleavage in the northwestern domain. The northwest-southeast directed shortening event that produced these structures postdates deposition of the late Mesoproterozoic Pinguicula Group and is therefore younger than the ca. 1.6 Ga Racklan orogeny (Gabrielse, 1967; Eisbacher, 1978; Thorkelson *et al.*, 2005; Furlanetto *et al.*, 2013). Based on the paraconformable relationship with the Pinguicula Group, deformation also postdates deposition of the Tonian Hematite Creek Group. Deformation predates intrusion of the undated east-west striking dikes (Fig. 13b). The presence of an angular unconformity beneath the Tonian Callison Lake Formation may provide a minimum age constraint for deformation. Together, these relationships bracket the timing of deformation between ~1 Ga (deposition of Hematite Creek Group; Rainbird *et al.*, 1997; Thorkelson, 2000) and ~780 Ma (deposition of Callison Lake Formation; Strauss *et al.*, 2015), which correlates with timing of the Corn Creek orogeny to the north (Eisbacher, 1981; Thorkelson, 2000). In the southern and northeastern domains, structures are parallel and likely related to younger Mesozoic-Cenozoic structures to the south (*e.g.*, Dawson and Kathleen Lakes faults) and east (Richardson fault array), respectively.

Late faulting

A major, north-south striking normal fault runs through the centre of the map area for ~25 km. In the southern part of the map area it separates Gillespie Lake and Pinguicula group rocks to the east from younger rocks to the west. In the northwestern domain, where it coincides with the North Rackla River valley, it displaces carbonate and siliciclastic rocks of the Gillespie Lake Group and gabbro of the Hart River sills. In the northeastern part of the map area, two major north-south to northeast-southwest striking normal faults separate down-dropped Mesoproterozoic and Neoproterozoic strata from older Paleoproterozoic and Mesoproterozoic rocks to the east and west. The location of these faults roughly coincides with the boundary between the northwestern and northeastern domains.

Mineralization

The map area contains several notable Pb-Zn-Ag occurrences, including the Vera (Yukon MINFILE 106C 083, 114 and 137–148), North Rackla (Yukon MINFILE 106C 088, 108 and 110–113), and "Val" (Yukon MINFILE 106C 085, 115–119, 131, 133–136, 149 and 150) occurrences.

The main mineralization at Vera occurs in a steeply dipping, north-northeast striking fault-vein system in red weathering, brecciated, stromatolitic and microbially laminated dolostone of the Gillespie Lake Group. Veins consist of quartz and carbonate with massive and disseminated sphalerite, galena, tetrahedrite, siderite, ankerite and limonite (Sivertz, 1985; Kammerer and Eaton, 2011). The host dolostone is surrounded to the north, east and south by fine-grained siliciclastic rocks of the Gillespie Lake Group. The rheological contrast between the carbonate and siliciclastic rocks may have influenced faulting and mineralization. The northern and southern dolostone-siliciclastic contacts are roughly parallel with the fault-vein system and may also be faults. Vera has a historical resource estimate of 352.7 kt at 607.0 g/t Ag, 3.18% Pb and 3.47% Zn (Casselman, 2021).

Like Vera, mineralization at North Rackla is hosted in a steeply dipping, northeast-southwest striking fault-vein system in red weathering, microbially laminated and stromatolitic, brecciated dolostone of the Gillespie Lake Group (Fig. 2). Sphalerite and galena occur as disseminations and stringers along with dolomite, siderite and other Fe-Mg-Mn carbonate minerals. In high-grade zones, sphalerite and galena form the matrix of the fault-hydrothermal breccia. The mineralized zone is within carbonate rocks but is directly adjacent to a fault contact with a package of variably dolomitic-calcareous, dark weathering, fine-grained siliciclastic rocks to the northwest. As with Vera, the juxtaposition of different rock types may have provided favourable conditions for mineralization.

A collection of Pb-Zn-Ag occurrences, commonly referred to as the Val occurrences, lie to the south of Rusty Mountain (Fig. 2). Mineralization consists primarily of massive and disseminated sphalerite, galena and tetrahedrite within breccia zones and

sparry dolomite veins in the Rubble Creek Formation (Sivertz, 1980; Kammerer and Eaton, 2011). The Val occurrences are proximal and may be related to the major east-west striking normal fault describe above. Val has a historical resource estimate of 20 kt at 1029 g/t Ag, 26.7% Pb and 7.3% Zn (Casselman, 2021).

Acknowledgements

Thanks to Sarah Bowie, Amanda O'Connor, Kory Sutton and Manas Toews for assistance in the field, and David Moynihan and Maurice Colpron for helpful discussion. A detailed review by Maurice Colpron considerably improved the manuscript. Karen MacFarlane is thanked for editorial assistance. Thanks to Horizon Helicopters and Alkan Air for transport. Cantex is thanked for providing logistical support, lodging and meals.

References

Abbott, J.G., 1997. Geology of the Upper Hart River Area, Eastern Ogilvie Mountains, Yukon Territory (116A/10, 116A/11). Exploration and Geological Services Division, Yukon Region, Indian and Northern Affairs Canada, Bulletin 9, 92 p.

Ambrose, T., 2020. Preliminary bedrock geology map of the southern Rusty Mountain area, southern Wernecke Mountains, Yukon (parts of NTS 106C/4, 5 and 106D/1, 8). Yukon Geological Survey, Open File 2020-2, scale 1:50 000.

Ambrose, T., 2021, Update on the bedrock geology of the Rusty Mountain area, southern Wernecke Mountains, Yukon (parts of: NTS106C/4,5,12 and 106D/1,8) *In:* Yukon Exploration and Geology 2020, K.E. MacFarlane (ed.), Yukon Geological Survey, p. 95–113.

Ambrose, T., 2022. Preliminary bedrock geology map of the Rusty Mountain and Bonnet Plume Pass areas, southern Wernecke Mountains, Yukon (parts of NTS 106C/3, 4, 5, 6, 11, 12 and 106D/1, 8). Yukon Geological Survey, Open File 2022-5, scale 1:50 000.

Ambrose, T. and Bowie, S., 2020. Preliminary report on the bedrock geology of the Rackla River area, southern Wernecke Mountains, Yukon (parts of NTS 106C/4, 5 and 106D/1, 8). *In:* Yukon Exploration and Geology 2019, K.E. MacFarlane (ed.), Yukon Geological Survey, p. 1–21.

Casselman, S. (compiler), 2021. Yukon Mineral Deposits Summary 2021. Yukon Geological Survey, 26 p.

Colpron, M., Israel, S., Murphy, D., Pigage, L. and Moynihan, D., 2016. Yukon bedrock geology map. Yukon Geological Survey, Open File 2016-1, scale 1:1 000 000.

Delaney, G.D., 1981. The mid-Proterozoic Wernecke Supergroup, Wernecke Mountains, Yukon Territory. In: Proterozoic Basins of Canada, F.H.A. Campbell (eds.), Geological Survey of Canada, Paper 81-10, p. 1–23.

Eisbacher, G.H., 1978. Two major Proterozoic unconformities, northern Cordillera. Geological Survey of Canada, Current Research Part A, Paper 78-1A, p. 53–58.

Eisbacher, G.H., 1981. Sedimentary tectonics and glacial record in the Windermere Supergroup, Mackenzie Mountains, northwestern Canada. Geological Survey of Canada, Paper 80–27, 40 p., doi.org/10.4095/119453.

Estève, C., Audet, P., Schaeffer, A.J., Schutt, D., Aster, R.C. and Cubley, J., 2020. The upper mantle structure of Northwestern Canada from teleseismic body wave tomography. Journal of Geophysical Research, Solid Earth, vol. 125, doi.org/10.1029/2019JB018837.

Furlanetto, F., Thorkelson, D.J., Gibson, H.D., Marshall, D.D., Rainbird, R.H., Davis, W.J., Crowley, J.L. and Vervoort, J.D., 2013. Late Paleoproterozoic terrane accretion in northwestern Canada and the case for circum-Columbian orogenesis. Precambrian Research, vol. 224, p. 512–528, doi.org/10.1016/j.precamres.2012.10.010.

Gabrielse, H., 1967. Tectonic evolution of the northern Canadian cordillera. Canadian Journal of Earth Sciences, vol. 4, p. 271–298, doi:10.1139/e67-013.

Jeletsky, J.A., 1962. Pre-Cretaceous Richardson Mountains Trough – its place in the tectonic framework of Arctic Canada and its bearing on some geosynclinals concepts. Transactions of the Royal Society of Canada, vol. 56, p. 55–84.

Kammerer, M. and Eaton, W.D., 2010. Geological mapping, prospecting and geochemical sampling at the Rusty Property. Yukon Energy, Mines and Resources Assessment Report 095720.

Medig, K.P.R., Turner, E.C., Thorkelson, D.J. and Rainbird, R.H., 2016. Rifting of Columbia to form a deep-water siliciclastic to carbonate succession: The Mesoproterozoic Pinguicula Group of northern Yukon, Canada. Precambrian Research, vol. 278, p. 179–206, doi.org/10.1016/j.precamres.2016.03.021.

Morrow, D.W., 1999. Lower Paleozoic stratigraphy of northern Yukon Territory and northwestern District of Mackenzie. Geological Survey of Canada, Bulletin 538, 202 p., doi:10.4095/210998.

Moynihan, D.P., Strauss, J.V., Nelson, L.L. and Padget, C.D., 2019. Upper Windermere Supergroup and the transition from rifting to continent-margin sedimentation, Nadaleen River area, northern Canadian Cordillera. GSA Bulletin, vol. 131, p. 1673–1701, doi:10.1130/B32039.1.

Mustard, P.S., Roots, C.F. and Donaldson, J.A., 1990. Stratigraphy of the middle Proterozoic Gillespie Lake Group in the southern Wernecke Mountains, Yukon. Geological Survey of Canada, Current Research Part E, Paper 90-1E.

Norris, D.K., 1997. The geology, mineral and hydrocarbon potential of northern Yukon Territory and northwestern District of Mackenzie. Geological Survey of Canada, Bulletin 422, 401 p., doi.org/10.4095/208886.

Rainbird, R.H., McNicoll, V.J., Thériault, R.J., Heaman, L.M., Abbott, J.G., Long, D.G.F. and Thorkelson, D.J. 1997. Pan-Continental River System Draining Grenville Orogen Recorded by U-Pb and Sm-Nd Geochronology of Neoproterozoic Quartzarenites and Mudrocks, Northwestern Canada. Journal of Geology, vol. 105, p. 1–17, doi.org/10.1086/606144.

Sivertz, G.W., 1980. Assessment Report on Geology, Geochemistry and Drilling at Val 1-318 Claims 1980. Yukon Energy, Mines and Resources Assessment Report 090511.

Sivertz, G.W., 1985. Summary Report on the Val-Vera Property, Kathleen Lakes Area, Yukon Territory. Yukon Energy, Mines and Resources Assessment Report 062208.

Strauss, J.V., MacDonald, F.A., Halverson, G.P., Tosca, N.J., Schrag, D.P. and Knoll, A.H., 2015. Stratigraphic evolution of the Neoproterozoic Callison Lake Formation: Linking the break-up of Rodinia to the Islay carbon isotope excursion. American Journal of Science, vol. 315, p. 881–944, doi:10.2475/10.2015.01.

Thorkelson, D., 2000. Geology and Mineral Occurrences of Slats Creek, Fairchild Lake and "Dolores Creek" Areas, Wernecke Mountains (106D/16, 106C/13, 106C/14), Yukon Territory. Exploration and Geological Services Division, Yukon, Indian and Northern Affairs Canada, Bulletin 10, 73 p.

Thorkelson, D.J., Abbott, J.G., Mortensen, J.K., Creaser, R.A., Villeneuve, M.E., McNicoll, V.J. and Layer, P.W., 2005. Early and Middle Proterozoic evolution of Yukon, Canada. Canadian Journal of Earth Sciences, vol. 42, p. 1045–1071, doi.org/10.1139/e04-075.

Turner, E.C., 2011. Stratigraphy of the Mackenzie Mountains Supergroup in the Wernecke Mountains, Yukon. *In:* Yukon Exploration and Geology 2010, K.E. MacFarlane, L.H. Weston and C. Relf (eds.), Yukon Geological Survey, p. 207–231.

Verbaas, J., Thorkelson, D.J., Milidragovic, D., Crowley, J.L., Foster, D., Gibson, H.D. and Marshall, D.D., 2018. Rifting of western Laurentia at 1.38 Ga: The Hart River sills of Yukon, Canada. Lithos, vol. 316-317, p. 243–260, doi.org/10.1016/j.lithos.2018.06.018.

Yeo, G.M., 1978, Iron-formation in the Rapitan Group, Mackenzie Mountains, Yukon and Northwest Territories. DIAND Mineral Industry Report, Economic Geology Series 1978-5, p. 170–175.

Yukon Geological Survey, 2021. Yukon Digital Bedrock Geology. Yukon Geological Survey, http://datatest.geology.gov.yk.ca/Compilation/3, [accessed November, 2021].

Yukon MINFILE, 2019. Yukon MINFILE – A database of mineral occurrences. Yukon Geological Survey, https://data.geology.gov.yk.ca, [accessed November, 2021].

Yukon Permafrost Database: A new baseline data resource

Panya S. Lipovsky*, Jennifer K. Humphries, Emilie T. Stewart-Jones and Derek C. Cronmiller
Yukon Geological Survey

Lipovsky, P.S., Humphries, J.K., Stewart-Jones, E.T. and Cronmiller, D.C., 2022. Yukon Permafrost Database: A new baseline data resource. *In:* Yukon Exploration and Geology 2021, K.E. MacFarlane (ed.), Yukon Geological Survey, p. 37–49.

Abstract

The Yukon Geological Survey (YGS) has compiled available geotechnical and ground temperature data and related literature from government, industry and other contributors into the Yukon Permafrost Database. This paper reviews the database development process and structure, provides a snapshot of the primary datasets that have been loaded to date and discusses some of its limitations. The database is publicly accessible from an online portal (https://yukon.ca/en/yukon-permafrost) where data may be explored interactively in web maps, tables, and time series and ground temperature envelope graphics. Database contents are also available for download in a variety of formats. The Yukon Permafrost Database provides easily accessible data on permafrost distribution and thermal regime to support the assessment of thaw-related hazard and risk, and works towards the integration of disparate permafrost data at a territorial scale. The database will be maintained and updated regularly and YGS welcomes data contributions from government, industry and academic researchers to facilitate ongoing improvements to our collective knowledge of permafrost in Yukon.

* Panya.Lipovsky@yukon.ca

Introduction

Permafrost degradation is impacting communities and public infrastructure at an increasing rate, often with costly consequences. *Our Clean Future: A Yukon Strategy for Climate Change, Energy and a Green Economy* (Government of Yukon, 2020) identifies permafrost thaw as one of the major climate change-related issues in Yukon and lists several actions that aim to address it. The most critical risks of permafrost thaw are related to ground movements (e.g., landslides and subsidence) which may increase maintenance costs for affected infrastructure such as roads and buildings, sever transportation corridors, and/or cause loss of life. Other risks associated with permafrost thaw include the release of greenhouse gases (Schuur *et al.*, 2015) and contaminants such as mercury into the ecosystem (Schaefer *et al.*, 2020).

Despite the importance of thawing permafrost, data on the distribution and character of permafrost to support risk assessments across Yukon have not been easily accessible to date. Permafrost information has largely existed as disparate datasets held by numerous researchers, government organizations, industry and consultants. These include data from instrumented boreholes owned by university researchers, unpublished geological survey data (both Yukon and Canada), and geotechnical data collected under Government of Yukon contracts in communities and along road infrastructure. Much of the latter previously resided only as paper reports held by various departments.

Since permafrost data are a critical underpinning of any thaw-related risk assessment, a first step toward improving access to these data has been to develop a centralized permafrost database for Yukon. Such a database has been recognized as a gap for many years, and the *Our Clean Future* strategy catalyzed its development.

This paper describes how the database was developed and outlines its organization and structure. It also provides a summary of the primary datasets that have been loaded to date and identifies some limitations of use.

Database development process

YGS is well-positioned to lead the development of the Yukon Permafrost Database (the Database) given its strong history of managing and serving public geoscience data. The initial phase of database development began in 2019 with a review and evaluation of existing permafrost database structures, platforms, nomenclature standards, and quality assurance and quality control (QA/QC) processes. The Mackenzie Valley Geotechnical Database published by the Geological Survey of Canada (GSC; Smith *et al.*, 2005) was selected as the initial template to modify and build upon for the geotechnical component of the Yukon Permafrost Database. Carleton University's Cryospheric Observations Longterm Database and Storage System (COLDASS; Carleton University, 2021) was used as the initial template to modify and build upon for the temperature component of the database. Drawing on these pre-existing works saved significant time and resources toward initial database design.

Database development occurred in consultation with a local working group comprising various stakeholders who collect and use permafrost data in the territory: YG Energy, Mines and Resources (Yukon Geological Survey, Assessment and Abandoned Mines, and Land Management branches); YG Highways and Public Works (Transportation Engineering and Property Management branches); YG Community Services (Land Development and Infrastructure Development branches); YG Environment (Water Resources branch and Climate Change Secretariat); and YukonU Research Centre (Yukon University).

YGS also engaged with a variety of other agencies outside Yukon who are involved in similar initiatives to manage permafrost data: Natural Sciences and Engineering Research Council (NSERC) PermafrostNet (2021); the Geological Survey of Canada (Permafrost Information Network, 2021; O'Neill *et al.*, 2018); and the Northwest Territories Geological Survey (2021). This collaboration offered great benefits to all parties by minimizing duplication, sharing standards and methodologies, and ensuring interoperability and consistency where possible.

Data modeling (*i.e.*, design of tables and their relationships) and loading of data into the database occurred concurrently with development of a web application. This approach allowed us to test and validate both the loaded data and the data model structure. The web application was refined iteratively based on ongoing feedback from the development team, working group and various users.

Database structure

Three primary types of data are handled within the Yukon Permafrost Database: geotechnical data, temperature data, and related reports or documents. Geotechnical and temperature data are stored in sets of tables within an Oracle relational database management system (RDBMS): 13 tables for the geotechnical data (Table 1), and 7 for the temperature data (Table 2). Oracle was selected as the primary database platform for its robust ability to store and serve large volumes of data, as well as to facilitate integration into the Yukon Geological Survey's Integrated Data System (YGSIDS). Reports and documents pertaining to permafrost and geotechnical investigations in Yukon are stored in the Government of Yukon's operational spatial data infrastructure (OPR), which is then linked to the Yukon Permafrost Database through a database connection.

Geotechnical data

Geotechnical data come from investigations typically performed by geotechnical engineers to obtain information on the physical properties of soil, rock and ice underlying a site for proposed structures or development. Site investigations often include subsurface sampling and laboratory testing of the soil samples retrieved. Test pits, trenching and drilling may also be used to learn about soil conditions at depth. Geotechnical data are relevant to the permafrost database as they contain logs of ground conditions and ice encountered at various depths, providing information about the distribution, and often, characteristics of ground ice. Additionally, the geotechnical properties of the materials at the site are an important control on the effects of permafrost thaw.

The geotechnical data tables were designed to reflect the workflow traditionally followed during geotechnical investigations: site selection and description; field data collection; instrumentation installation; laboratory testing; and reporting (Table 1). Data are typically initially entered into some type of relational database software (e.g., ESEBASE, gINT, or Holebase) which is used to produce geotechnical logs for inclusion in geotechnical reports. Most geotechnical logging software can export to a variety of tabular formats (e.g., .csv, .xls or .mdb files) which may be imported into the Yukon Permafrost Database.

In the Yukon Permafrost Database there are 13 relational tables (Table 1) with capacity for the range of geotechnical data commonly collected. Tables are connected by one-to-many relationships[1] extending from the primary geotechnical table (PF_LOCATIONS) through a common field (SITE_ID).

As each investigation has unique objectives, the amount and type of data collected vary by project. For a given project some fields (*i.e.*, columns) or entire tables may be left blank if they are irrelevant to the investigation. For example, while soil description data are provided for all of the approximately 15 000 boreholes currently loaded into the database, only half have some geotechnical testing data available (e.g., moisture content and/or grain size analyses). About one-fifth of the boreholes entered have permafrost description data. Boreholes lacking permafrost information were intentionally retained in the database because it is equally valuable to know where permafrost was not observed and what the associated ground conditions are.

Data summary

As of November 2021, the geotechnical component of the database has 15 349 boreholes loaded (Fig. 1). The majority of the geotechnical data were acquired from

[1] *One-to-many relationships allow for one record in a table to be associated with one or more records in another table or multiple tables. For example, each geotechnical site (SITE_ID) can have many soil stratums or permafrost cryostructure layers associated with that single site within the PF_SOIL_DESC or PF_PERMAFROST_DESC tables respectively.*

Table 1. *Summary of data tables contained within the geotechnical component of the Yukon Permafrost Database. Tables highlighted in bold text are most commonly used and therefore have the greatest number of records.*

Data Collection Workflow Phase	Table Name	General Description	Content
site selection and observation	**PF_LOCATIONS**	primary geotechnical table, with essential site location and project context information	site ID, location (UTM and/or lat/long), elevation, project name, start/end dates, consultant, client, contractor, equipment, drilling details (core diameter, flush material, borehole plunge/azimuth, hole type and depth), groundwater table
	PF_SURFACE_DESC	information on immediate surroundings of a site	vegetation, organic thickness, topography, drainage, surficial geology, terrain features, snow, slope, aspect, disturbances, ecoregion
data collected during drilling	**PF_SOIL_DESC**	soil information observed in the field for a single interval or stratum during data collection	depth to the top and bottom of the soil interval/ stratum, nature of the lower boundary, soil description, soil classification system (e.g., USCS), USCS code
	PF_PERMAFROST_DESC	frozen ground observations made during field data collection. May include frozen ground not related to permafrost (e.g. seasonal frost)	depth to the top and bottom of the frozen ground interval/stratum, temperature, thaw depth, permafrost cryostructure description, ground ice description, classification system, visual estimate of volumetric ice content
	PF_RECOVERY	information on borehole sample recovery and quality	depth to the top and bottom of the drill run, rock quality designation (*i.e.*, degree of jointing/fracture), core recovery %, fracture frequency
	PF_INSITU	information on *in situ* testing completed	depth to the top and bottom of the test interval, hydraulic conductivity, shear strength, shear wave velocity, penetration resistance, strength test type, strength, stress
	PF_SAMPLE	information on the soil and material samples collected	depth to the top and bottom of the sample, diameter of core, sample type, USC code for material type, penetration tests
instrumentation installation	PF_INSTALL_DESC	information on instrumentation installed	installation type (e.g., monitoring well, piezometer, inclinometer, ground temperature cable), depth, capped height, type of protector
	PF_BACKFILL	describes backfill used at site	depth to the top and bottom of the backfill, type of backfill (e.g., bentonite, sand, drill cuttings, slough, asphalt, cement, grout, pea gravel, topsoil)
laboratory testing	**PF_GEOTECH_TESTING**	geotechnical test results completed on soil samples	depth to the top of the sample, bulk and dry density, specific gravity, gravimetric moisture content, Atterberg limits, plasticity index, grain size analyses, organic content, soluble sulphate content, salinity
	PF_ENVIRONMENTAL	environmental test results completed on soil samples	depth to the top and bottom of the test interval, hydrocarbon vapour concentration, lower explosive limit of vapour, soil vapour concentration of volatile organic compounds, electrical conductivity, chloride content, methane content
	PF_PERMAFROST_ TESTING	permafrost test results completed on soil samples	depth to the top and bottom of the test interval, thaw weakening susceptibility, thaw strain consolidation, unfrozen water or ice content, creep properties, adfreeze strength, thermal conductivity, latent heat of fusion
reports and logs	PF_GEOTECH_PRODUCTS	metadata for documents that describe a site (e.g., drill logs, reports, journal articles)	document type, URL/web address

*Tables highlighted in bold text are most commonly used, and therefore have the greatest number of records, as of November 2021.
**Tables highlighted in blue contain no records, as of November 2021, but are available for use in future data submissions.

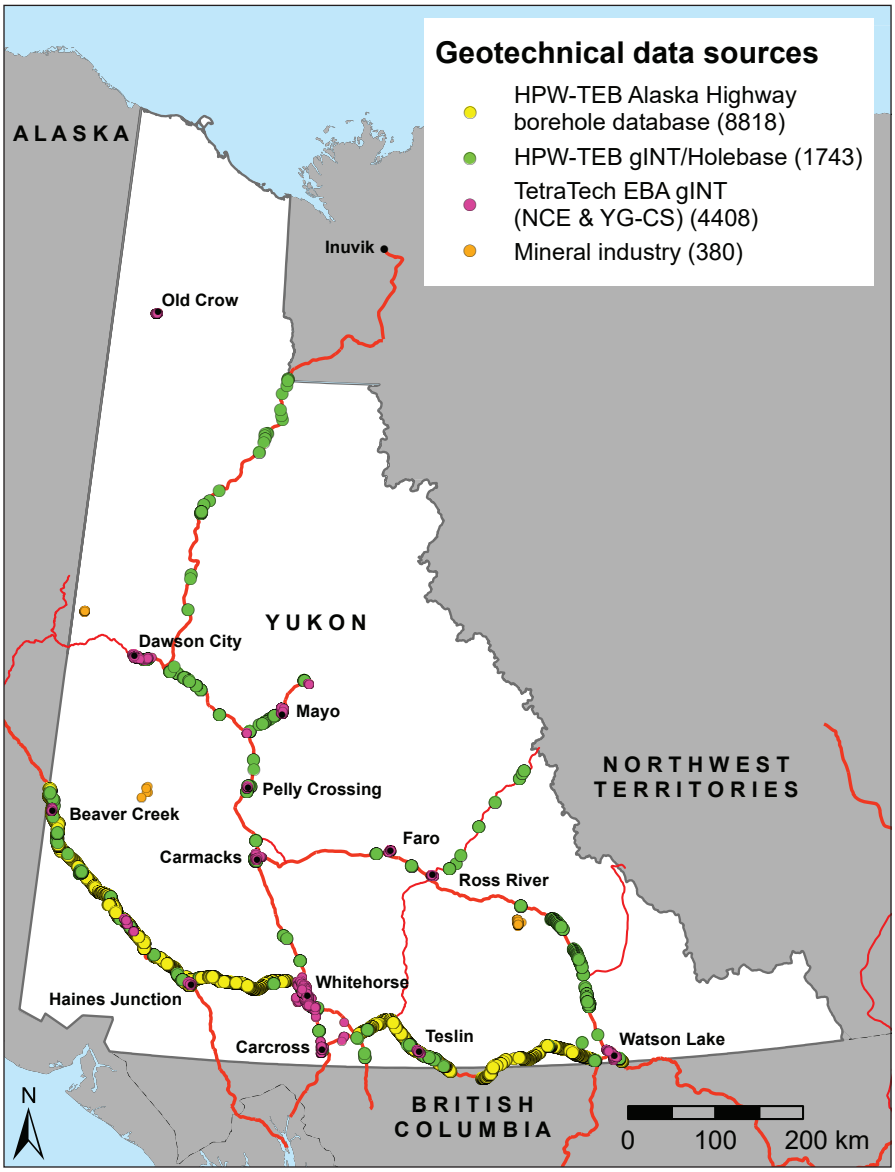


Figure 1. *Locations and primary sources of geotechnical data loaded into Yukon Permafrost Database. The number of sites from each source is indicated in brackets. Most of the sites are located within infrastructure corridors and communities, but some are located at more remote mineral properties.*

the Alaska Highway Borehole Database (AHBD), Tetra Tech EBA records acquired by Yukon College's Northern Climate ExChange (NCE; now YukonU Research Centre, Yukon University), and Yukon Government (YG) Department of Highways and Public Works (HPW) Transportation Engineering Branch (TEB). Additional data were acquired from private mining industry firms, YG Community Services (YG-CS), and YG Assessment and Abandoned Mines (YG-AAM).

The Alaska Highway Borehole Database was compiled by the YGS between 2005 and 2009 (Lipovsky, 2009). While some records were imported from their ESEBASE database, the data were largely captured from HPW-TEB's hard copy logbooks from the 1970s to 1990s. The AHBD boreholes were drilled approximately every 100 m down the Alaska Highway centerline and average 5 to 6 m deep. Of the 8818 boreholes in the AHBD dataset, about ⅓ of them encountered some form of permafrost.

HPW-TEB also contributed geotechnical data for 1743 boreholes drilled within various highway corridors between 2011 and 2019; these data were exported from their internal gINT and Holebase databases.

In 2011, Yukon College's Northern Climate ExChange acquired a compilation of Tetra Tech EBA's gINT geotechnical data that were collected for various public agencies from 1971 to mid-2010 (Tetra Tech EBA, 2011). Tetra Tech EBA also provided gINT geotechnical data collected from approximately 56 additional boreholes drilled for YG Department of Community Services (YG-CS) between 2011 and 2017.

The Geological Survey of Canada (GSC) has also compiled geotechnical data for approximately 600 boreholes within Yukon (primarily located along the Alaska Highway and the north coast), and approximately 14000 boreholes from nearby Mackenzie Valley in Northwest Territories. These data are not included in the Yukon Permafrost Database since they are managed federally. The GSC data may be explored and downloaded from the Permafrost Information Network (PIN) web application (https://pin.geosciences.ca/).

Temperature data

Temperature data, typically in time series format, come from investigations performed by government agencies, geotechnical engineers and consultants, academics and others to obtain information on the air or ground temperature conditions at a particular location. Ground temperature investigations generally include the installation of temperature sensors at a variety of depths below ground and data loggers which record the temperatures at regular time intervals (e.g., hourly or daily) for varying periods ranging from a few days to several years. Ground temperature investigations also often involve the installation or monitoring of above-ground weather stations which provide data required to understand the relationship between the ground thermal regime and local climate. For this reason, the temperature component of the Database was designed to include air temperature and other climate data (e.g., surface description, permafrost description, ground temperature, thaw depth, air humidity, air temperature, soil moisture, water level, wind speed and wind direction).

In the Database, temperature data are stored in seven tables (Table 2) within an Oracle relational database management system (RDBMS). As each investigation has unique objectives, the level and type of data collected vary by project.

Table 2. *Summary of data tables contained within the temperature component of the Yukon Permafrost Database.*

Table Name	General Description	Content
PFT_LOCATIONS	site location and basic site metadata	site name, location (latitude/longitude), location accuracy, elevation, elevation accuracy, local relief, permafrost presence, comments
PFT_OBSERVATIONS	primary table in the temperature component of the database, containing all observations	depth to the top and bottom of the observation, start and end time of observation, observation value and type (e.g., air humidity, air temperature, ground temperature, permafrost characterization, soil moisture, surface description, surface temperature, thaw depth, water level, wind direction, wind speed)
PFT_WHO	information on data ownership	contact name, and institution or affiliation
PFT_METHOD	information on instrumentation installed at a site	sensor and data logger manufacturer and model; measurement precision, accuracy and units; radiation shield description
PFT_DISTURBANCE	description of disturbances that have occurred at or near a site	disturbance type (e.g., road, trail, excavation, urban, building, fire, stream, lake, thermokarst), proximity to disturbance, estimated date of disturbance, comments
PFT_DOIS	metadata for documents that describe a site	DOI (Digital Object Identifier) of document, and associated notes (e.g., document type)
PFT_OBSERVATION_DOI	intermediate table used to link records between tables	ID fields referring to records in the PFT_OBSERVATIONS and PFT_DOIS tables

**Tables highlighted in blue contain no records, as of November 2021, but are available for use in future data submissions.

Data summary

As of November 2021, 128 sites have been loaded into the temperature component of the Yukon Permafrost Database. Temperature data were provided by the YG Department of Highways and Public Works Transportation and Engineering Branch (HPW-TEB), Yukon Geological Survey, Assessment and Abandoned Mines, and the mineral industry (Fig. 2; Table 3).

Permafrost is confirmed at 70 sites and is not present at 34 sites (Fig. 2). Permafrost presence is undetermined at 16 sites for various reasons: boreholes are too shallow (*i.e.*, <2 m depth); ground temperatures are so close to 0°C that perennially frozen ground can't be verified within the precision limitations of the instruments; the record of measurement is too short; or there are gaps in the data.

HPW-TEB has 73 temperature monitoring sites across the territory (Table 3), largely operated within their Intelligent Transportation System (ITS) network. Eight of these sites are weather stations. Many of the HPW-TEB sites are clustered near specific areas of interest. For example, there are 27 sites at Beaver Creek and the nearby Shakwak test section (km 1865 Alaska Highway); 11 sites at the Dry Creek thermosiphon installation (km 1841 Alaska Highway); 9 sites along the Dempster Highway (km 0, 65, 124 and 421); 4

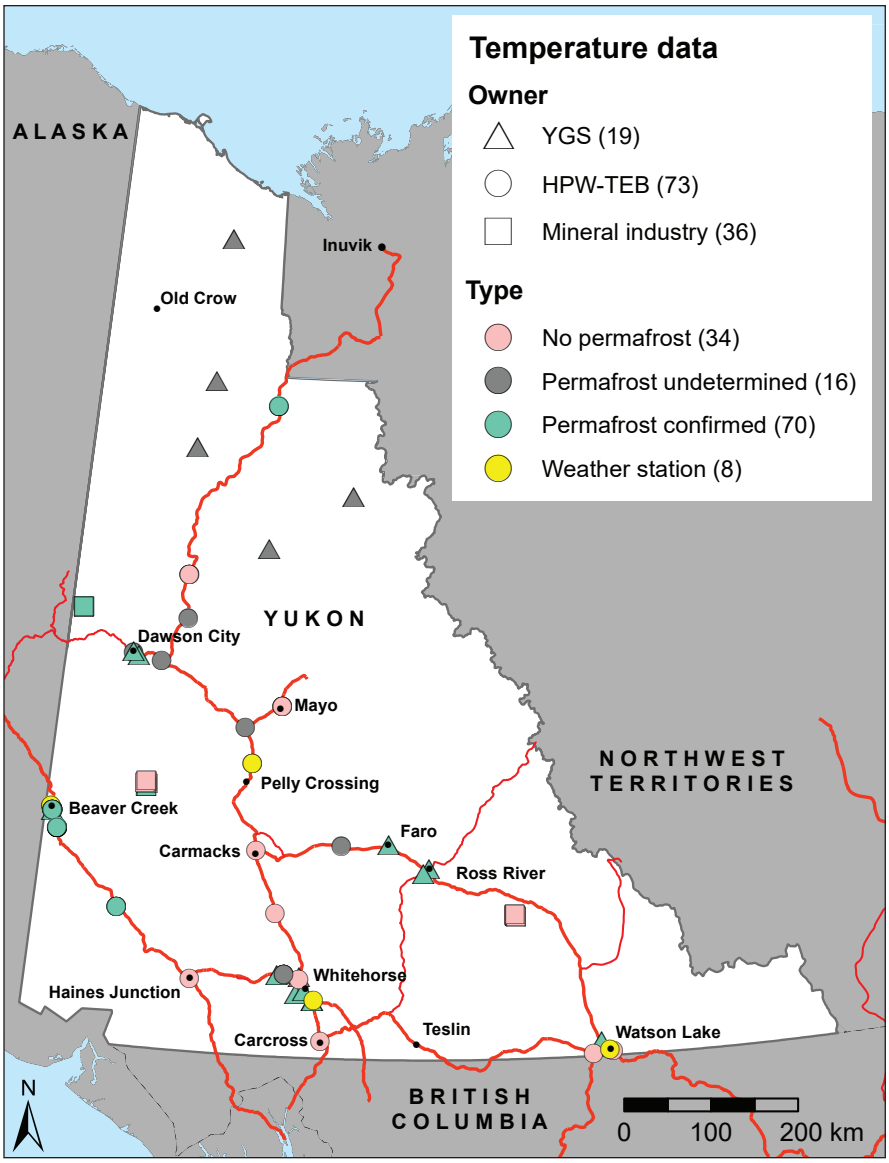


Figure 2. *Locations and primary sources of temperature data loaded into Yukon Permafrost Database. The number of sites is indicated in brackets.*

Table 3. *Key attributes of the 128 temperature monitoring sites included in the Yukon Permafrost Database, including period of data collection, borehole depth, and presence of permafrost.*

Source	Area	Location**	Number of sites	BH's in permafrost	BH Bottom Depth (m)	Data collection period
HPW-TEB	Beaver Creek and Shakwak test section	AH km 1865, 1870	27*	25	8-16	1997/2008-2019
	Dry Creek	AH km 1841	11*	10	12.5-15	2019-2020
	Dempster Highway	DH km 0, 65, 124, 421	9	1	2-20	2007-2021
	Burwash Creek	AH km 1715	4*	3	10	2015-2021
	Takhini Valley	AH km 1457	4*	1	10	2014-2021
	Mayo Airstrip		4*	?	10	2014-2021
	Watson Lake	AH km 1002, 980, 976	3*	0	2-4	2008-2020
	Haines Junction bridge	HR km 245.5	1	0	4	2008-2019
	Carcross	SK km 106 (at Tagish Rd junction)	1	0	4.2	2009-2019
	Braeburn	NK km 281	1	0	4.1	2005-2019
	Carmacks	NK km 359	1	0	2	2008-2019
	Pelly Crossing	NK km 488	2*	?	2	2017-2021
	Stewart Crossing	NK km 534	1	?	4	2007-2019
	Dawson City at Dome Rd	NK km 713	1	?	2	2008-2019
	Alaska Highway at North Klondike Highway junction	AH km 1437	1	0	4.1	2013-2020
	Alaska Highway at South Klondike Highway junction	AH km 1404	1*	0	4.0	2014-2018
	Drury Creek	RC km 468	1	?	2	2014-2020
YGS	North Yukon, US Array sites		5	?	0.5-1.5	2017-2019 & 2019-2021
	South Canol Rd (Tintina well)	SC km 216	1	1	58.43	2018 (Apr. 20 - Sept. 18)
	Beaver Creek test section	AH km 1865	1	1	5	2007-2021
	Dawson City	School and dump	2	2	2-3.4	2007-2021
	Faro		1	1	4	2007-2019
	Ross River	School	1	1	13	2007-2018
	Watson Lake	RC km 16.5	1	1	2.8	2009-2015
	Greater Whitehorse:					
	Cowley Creek		2	2	5	2007-2020
	Hamilton Blvd		1	1	2.2	2019-2021
	Fish Lake		1	1	3	2020-2021
	Hidden Valley		1	?	18.8	2019-2020
	Takhini thaw slump	AH km 1456.5	1	1	20	2020-2021
	Takhini Valley	AH km 1465	1	1	18.8	2019-2021

Table 3 continued.

Source	Area	Location**	Number of sites	BH's in permafrost	BH Bottom Depth (m)	Data collection period
AAM	Clinton Ck Mine		11	8	14-70	2018-2019
	Casino property		12	6	27-76	1994 & 2010-2019
	Kudz Ze Kayah property		13	0	29-70	2016-2017

** includes 1 weather station*
? indicates unknown
***AH = Alaska Highway, DH = Dempster Highway, HR = Haines Road, SK = South Klondike Highway, NK = North Klondike Highway, SC = South Canol Road, RC = Robert Campbell Highway*

sites at each of the Mayo airstrip, Takhini Valley (km 1457 Alaska Highway) and Burwash Creek area (km 1715 Alaska Highway); and 3 sites near Watson Lake (km 976, 980 and 1002 Alaska Highway). Haines Junction, Carcross, Braeburn, Carmacks, Pelly Crossing, Dawson City, Alaska Highway at North Klondike Highway junction, and Drury Creek each have one site nearby.

Data from 19 Yukon Geological Survey sites are included in the database (Table 3). Five shallow (0.5–1.5 m depth) holes were instrumented from 2017 to 2019 in the remote Richardson and Ogilvie Mountains of north Yukon as part of the US Array campaign (http://www.usarray.org/Alaska). Ground temperature data down to 58 m depth are available for the Tintina geothermal well (Fraser *et al.*, 2019), located at km 216 of the South Canol Road. Long-term ground temperature data dating back to 2007 are available for six community permafrost monitoring sites located in Beaver Creek, Dawson, Faro, Ross River and Watson Lake (Lipovsky and Yoshikawa, 2009 and Lipovsky, 2014). The database also includes ground temperatures from seven permafrost monitoring sites that YGS maintains in the greater Whitehorse area (Roy *et al.*, 2021).

Data from 36 sites at three mineral properties were submitted (Table 3): 25 from private industry; and 11 sites from YG Assessment and Abandoned Mines (YG-AAM) for the Clinton Creek Mine. Data from the mineral industry are particularly valuable as many were collected from very deep boreholes that extend up to 76 m. The data also provide insight into permafrost conditions at elevations higher (*i.e.*, >1100 m) than most other sites. For example, very deep permafrost is recorded in the Dip Creek valley near the Casino property, extending from approximately 4 m depth to at least 50 m depth (CAS_DH12-01). In undisturbed ground adjacent to Clinton Creek mine, two boreholes (BH18-08 and BH18-15) record permafrost down to at least 14 m depth, with active layers of 4 and 5 m, respectively.

Reports

The reports component of the Yukon Permafrost Database comprises a spatial catalogue of reports, maps, posters, journal articles and academic theses pertaining to permafrost and geotechnical investigations in Yukon. Each document was georeferenced ("footprinted") in ESRI ArcGIS to capture the spatial extent of the work as a point, line (e.g., a section of highway), or polygon feature class as appropriate. Attributes collected for each feature include the title, author, year published, document type, general location of work and download URL.

Permafrost-related documents come from many sources, only some of which are openly accessible. Within the catalogue links are provided, where available, to download publicly available documents from an FTP site, while proprietary URLs or DOI links are provided for documents that do not have open access, such as selected journal articles.

Overall, this component of the database provides a comprehensive summary of the permafrost literature available in Yukon. It offers an accessible and convenient method of determining what permafrost-related work has been done in the territory and where, and will facilitate gathering relevant literature for specific areas of interest. The collection will be updated annually to incorporate new permafrost-related literature directly pertaining to Yukon.

As of November 2021, the documents catalogued in the reports component of the Yukon Permafrost Database include 167 journal articles, 56 academic theses, 121 geotechnical reports, and 111 other documents such as internal reports, maps, and conference posters. The locations of these documents are shown in Figure 3.

Web application

The database is accessible through a web application at https://yukon.ca/en/yukon-permafrost. Locations of geotechnical investigation and ground temperature monitoring sites are presented in interactive web map platforms. Borehole logs and sample analyses for individual geotechnical sites may be viewed in tabular format, while data for individual ground temperature monitoring sites may be visualized in interactive time-series graphs, ground temperature envelopes and tables. Other modules of the web application allow users to explore Yukon permafrost-related reports and publications, and previously released permafrost products such as a permafrost probability model



Figure 3. *Locations of work described within reports loaded into the Yukon Permafrost Database. Yellow highlighting indicates road segments described in geotechnical reports.*

(Bonnanventure et *al.*, 2012) and a periglacial landform atlas (Huscroft et *al.*, 2021). All database tables are available for download in CSV format, while site locations may be downloaded in a variety of spatial data formats (ESRI feature geodatabase, ESRI shapefile and Google Earth KMZ). Standardized templates for data submissions are also available for download.

Quality control and data processing

Some data cleaning and processing were required to convert data to a format consistent with the data model and to facilitate loading into the Database. Quality assurance and quality control (QA/QC) measures adopted include the automation of data processing where possible using R scripts, manually verifying and inspecting data at regular intervals, and documentation of processing steps.

Due to the range of data sources and formats, geotechnical data were processed using a combination of manual and automated methods. This involved some restructuring of the raw data tables, and conversion of location coordinates and date/time formats. No modifications were made to original soil and permafrost descriptions, terminology or testing values.

Temperature data were cleaned to a minimal extent using automated processing, largely to optimize the web application data visualization tools. Null values and major outliers were removed, and temporal data were converted to a standardized time and date format. Raw unprocessed data and R scripts used for processing may be provided by YGS upon request.

Data limitations

The data presented in the Database are an amalgamation of multiple data sources and decades of geotechnical investigations in Yukon. While the database was designed to allow for all data that may reasonably be collected at a site, this approach also presented some challenges in assimilating the diversity of geotechnical logging styles encountered, and in some cases results in data that are difficult to compare with other sources. Geotechnical field logs and laboratory testing on discrete samples inherently impart some degree of generalization for any given site. The data were collected based on specific objectives of host organizations and the geotechnical standards at the time, which may differ from those at present, and with variable equipment, procedures, standards and personnel. The precision and accuracy of site coordinates may also vary as positioning systems have varied over time. Site conditions may have changed since the collection of historical data, such as slope stability investigations, foundation evaluations for future infrastructure, or granular resource investigations where material may have since been excavated. Site conditions at ground temperature investigation sites may also have changed since data collection, for example through thermal or mechanical erosion or landscape change.

A substantial proportion of the geotechnical and temperature data included in the Database do not include any permafrost information. These data were retained because it may be valuable to know where permafrost was not observed and the associated ground conditions. However, the absence of permafrost descriptions in geotechnical logs does not necessarily mean that permafrost is not present at that location. In some cases, it can be very difficult to tell whether permafrost is present or not at the time of drilling (e.g., in ice-poor ground, or in ground that is marginally frozen and possibly thawed during the drilling process), so it may not have been noted at the time of recording, or it may be present at greater depth.

The contents of the Database are made available “as is” and without warranty of any kind. Despite our best quality control efforts, errors, gaps or omissions may still exist. Please contact ygs-surficial@yukon.ca to report any issues encountered so they may be corrected.

The Database serves as a reference to aid in understanding areas of interest and planning further data collection programs. Professional judgement and interpretation should be used where possible to assess the value and validity of these data for a particular purpose.

Data ownership and use policy

Geotechnical and temperature data ownership resides with the original data sources summarized above (Figs. 1 and 2) and is also indicated in the metadata tabs of the web application. These data providers have agreed to make data publicly available within the Database for third party use with the provision that any publications which reference these data cite the Database as the source. Any enquiries about the data should be directed towards YGS and not the original owners.

Data submissions

The Database will be maintained and updated regularly and we strongly encourage ongoing data contributions from any source. We would particularly welcome submissions from the mineral industry to enhance our understanding of deep permafrost in the territory, outside public infrastructure corridors.

Templates have been developed to optimize the process of importing new geotechnical and temperature data (available from https://service.yukon.ca/permafrost/Downloads.html), ensuring they are provided in a consistent manner compatible with the Database. We are working to incorporate these standardized templates in all future geotechnical contracts tendered by the Government of Yukon.

Summary

The Yukon Permafrost Database is a compilation of geotechnical and ground temperature data and related literature from a variety of sources including government and industry. Data may be explored interactively and downloaded in a variety of formats from a publicly accessible web application (https://yukon.ca/en/yukon-permafrost).

The Database is a valuable resource for a variety of stakeholders, including land use planners, regulators, First Nations governments, municipal governments, Government of Yukon branches, academic researchers, geotechnical consultants and contractors. The Database may also support a variety of applications, including permafrost distribution and thermal regime evaluations, thaw-related hazard and risk assessments, climate change modeling, development of community adaptation plans, infrastructure planning and maintenance, and environmental assessments.

The Database is an evolving product that is updated regularly as new data become available. We welcome submissions from any contributors in order to maximize our collective knowledge of permafrost in Yukon.

Acknowledgements

Brett Elliot, Kisa Elmer and Moya Painter have been integral to the development and maintenance of the Yukon Permafrost Database, which would never have become a reality without their substantial efforts. We are extremely grateful for all the feedback shared by the Yukon permafrost database working group, and for helpful permafrost data management discussions and support offered by Nick Brown (NSERC PermafrostNet), Sharon Smith (Geological Survey of Canada), and Ashley Rudy (Northwest Territories Geological Survey). We are also very appreciative of Niels Weiss and Karen MacFarlane for their thorough reviewing and editing efforts. Finally, many thanks to all our data contributors, particularly Western Copper and Gold Corporation and BMC Minerals.

References

Carleton University, 2021. Cryospheric Observations Longterm Database and Storage System. https://carleton.ca/permafrost/?p=644, [accessed 26 August 2021].

Bonnaventure, P.P., Lewkowicz, A.G., Kremer, M. and Sawada, M.C., 2012. A permafrost probability model for the southern Yukon and northern British Columbia, Canada. Permafrost and Periglacial Processes, vol. 23, p. 52–68, https://doi.org/10.1002/ppp.1733.

Fraser, T., Colpron, M. and Relf, C., 2019. Evaluating geothermal potential in Yukon through temperature gradient drilling. *In:* Yukon Exploration and Geology 2018, K.E. MacFarlane (ed.), Yukon Geological Survey, p. 75–90.

Government of Yukon, 2020. Our Clean Future: A Yukon Strategy for Climate Change, Energy and a Green Economy, 72 p.

Huscroft, C.A., Elliot, B.T. and Lipovsky, P.S., 2021. Yukon Landform Atlas: permafrost and other periglacial landforms. Yukon Geological Survey storymap, https://yukon.maps.arcgis.com/apps/MapSeries/index.html?appid=8deacc9f1da84690aebce3dfd11c2958, [accessed 27 September 2021].

Lipovsky, P.L. 2009. Interim release of Alaska Highway Borehole Database. Yukon Geological Survey, interim report, March 24, 2009, http://ygsftp.gov.yk.ca/data/surficial_geology/Alaska_Highway_borehole_database_interim_release_March2009/Alaska_Highway_borehole_database_interim_release_March2009.zip, [accessed 16 September 2021].

Lipovsky, P.S., 2014. Summary of Yukon Geological Survey permafrost monitoring network results, 2008–2013. *In:* Yukon Exploration and Geology 2014, K.E. MacFarlane, M.G. Nordling and P.J. Sack (eds.), Yukon Geological Survey, p. 113–122.

Lipovsky, P.S. and Yoshikawa, K., 2009. Initial results from the first year of the Permafrost Outreach Program, Yukon, Canada. *In:* Yukon Exploration and Geology 2008, L.H. Weston, L.R. Blackburn and L.L. Lewis (eds.), Yukon Geological Survey, p. 161–172.

NSERC PermafrostNet, 2021.PermafrostNet website, https://www.permafrostnet.ca/, [accessed 12 July 2021].

Northwest Territories Geological Survey, 2021. Building a Northwest Territories Permafrost Database, https://www.nwtgeoscience.ca/services/building-northwest-territories-permafrost-database, [accessed 23 November 2021]

O'Neill, H.B., Duchesne, C., Jardine, S. and Smith, S.L. 2018. Permafrost Information Network (PIN) Geotechnical Borehole Database (beta), summary and database field descriptions. Geological Survey of Canada, 9 p.

Permafrost Information Network, 2021. The permafrost information network, https://pin.geosciences.ca/, [accessed 12 July 2021].

Roy, L.-P., Lipovsky, P.S., Calmels, F., Laurent, C., Humphries, J. and Vogt, N., 2021. Greater Whitehorse area permafrost characterization. Yukon Geological Survey, Miscellaneous Report MR-22, 185 p., including appendices.

Schaefer, K., Elshorbany, Y., Jafarov, E., Schuster, P.F., Striegl, R.G., Wickland, K.P. and Sunderland, E.M. 2020. Potential impacts of mercury released from thawing permafrost. Nature Communications, vol. 11, 6 p., https://doi.org/10.1038/s41467-020-18398-5

Schuur, E.A.G., McGuire, A.D., Schädel, C., Grosse, G., Harden, J.W., Hayes, D.J., Hugelius, G., Koven, C.D., Kuhry, P., Lawrence, D. M., Natali, S. M., Olefeldt, D., Romanovsky, V.E., Schaefer, K., Turetsky, M.R., Treat, C.C. and Vonk, J.E. 2015. Climate change and the permafrost carbon feedback. Nature, vol. 520, p. 171–179, https://doi.org/10.1038/nature14338.

Smith, S.L., Burgess, M.M., Chartrand, J. and Lawrence, D.E., 2005. Digital borehole geotechnical database for the Mackenzie Valley/Delta region. Geological Survey of Canada, Open File 4924, 25 p., https://doi.org/10.4095/220383.

Tetra Tech EBA, 2011. Geotechnical testhole database for hazards mapping – Yukon communities. EBA File W14101378, January 19, 2011.

Placer gold settings within an alpine glaciated environment, Granite Creek, Yukon (NTS 105M/14)

Jessi L. Steinke and Brent C. Ward
Earth Sciences, Simon Fraser University

Jeffrey D. Bond
Yukon Geological Survey

Steinke, J.L, Bond, J.D. and Ward, B.C., 2022. Placer gold settings within an alpine glaciated environment, Granite Creek, Yukon (NTS 105M/14). *In:* Yukon Exploration and Geology 2021, K.E. MacFarlane (ed.), Yukon Geological Survey, p. 51–82.

Abstract

Alpine glaciers from cirques of Granite and Albert creeks have deformed and reworked sediments in the Granite Creek valley and deposited locally sourced gold. Placer mining operations in the valley allowed detailed study of sedimentary deposits. The main units identified are from at least two glacial episodes which advanced farther than the previously mapped limits. Thick sequences of advance and retreat outwash blanket the till and represent high energy depositional environments. At least one proglacial lake formed due to ice-damming of lower Granite Creek by the Cordilleran Ice Sheet. We provide a stratigraphic record extending approximately 130 000 years and have correlated alpine till units to MIS 4, which has not been identified elsewhere in central Yukon. Multiple gold-bearing sedimentary units are found in the stratigraphy, representing glacial, interglacial/interstadial, and modern processes. This work highlights processes important to gold concentration that can be applied to other alpine glaciated areas with proximal gold mineralization.

* jessi_steinke@sfu.ca

Introduction

Placer deposits are concentrations of heavy minerals generally formed by fluvial action. In glaciated terrain, placer deposits may underlie or be incorporated into glacial sediments (LeBarge et *al.*, 2002). This can increase the complexity when exploring for the deposits, but also introduce opportunities for increased erosion and concentration of gold-bearing material. This study describes the depositional processes of placer gold deposits in an alpine glaciated environment in central Yukon. We utilized extensive placer mining excavations to identify sedimentary units and reconstruct the glacial history of Granite Creek valley. We identified glacial, interglacial and modern placer-forming environments, and key gold-bearing units. The result is a composite stratigraphic log representing all units found in the upper Granite Creek basin with relative gold concentrations, and glacial models which demonstrate the mode of deposition. Results of this work can be applied to other alpine environments in the Cordillera that host gold mineralization.

Location and Physiography

The study area is in Granite Creek in central Yukon, approximately 400 km north of Whitehorse (Fig. 1). The Ecoregion is the Yukon Plateau-North (Smith et *al.*, 2004) and the physiographic region is the Stewart Plateau, though the adjacent Wernecke Mountains to the north are in very close proximity (Mathews, 1986). The area is part of the Omineca morphological belt, which is dissected by the Tintina Trench. Glacial landforms on the northeastern part of the belt include rounded hills and U-shaped valleys (Smith et *al.*, 2004). The study area is within the Gustavus Range, which includes Mount Hinton and several other summits around 2000 m in elevation (Fig. 2). There are cirques throughout the range, which either drain southward into Granite or Keystone creeks, or northward into Duncan, Lightning or Faith creeks. The headwaters of Granite Creek drain the eastern side of Mount Hinton and empty into Roop Lakes.

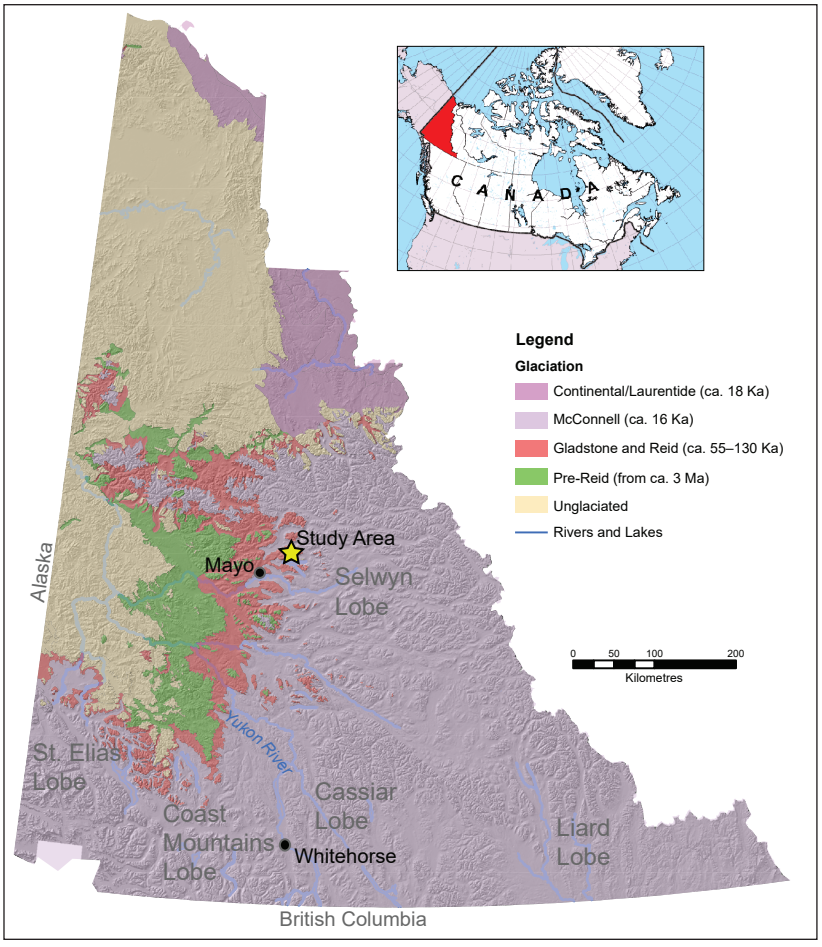


Figure 1. *Glacial limits map modified from Duk-Rodkin (1999).*

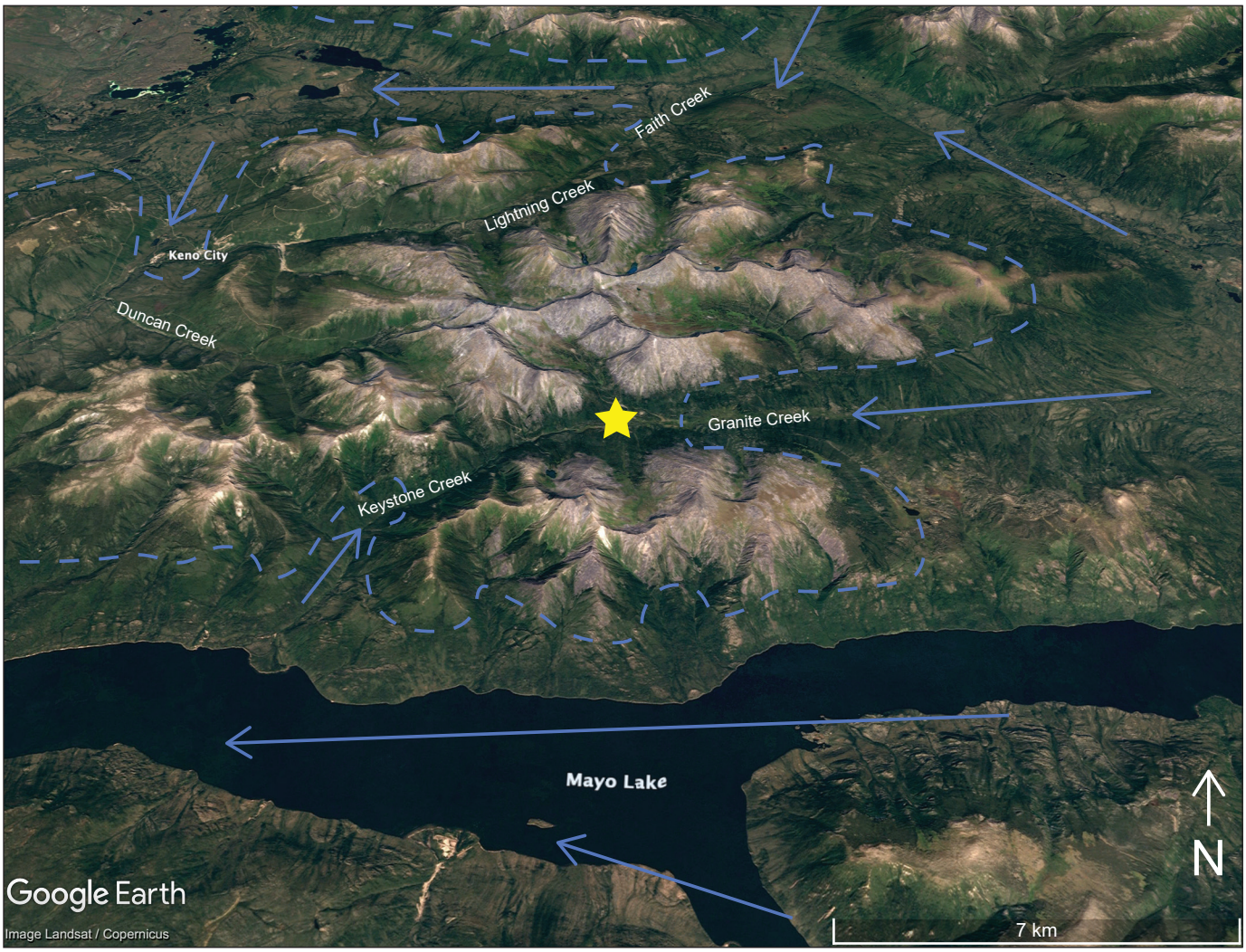


Figure 2. *Location map from Google Earth showing location of field camp. Ice flow direction is indicated with blue arrows and approximate MIS 2 glacial limit is shown with dashed blue line.*

Glacial History

The Yukon Plateau-North region in central Yukon was glaciated by the Selwyn Lobe of the Cordilleran Ice Sheet (CIS), which flowed west-northwest during Marine Isotope Stage (MIS) 2 (Table 1; Bond, 1999). As in the rest of Yukon, glaciers were largely topographically controlled, with widespread nunataks (Jackson et *al.*, 1991). Glaciers emanated out of upland areas such as the Selwyn Mountains and local cirques. Of the exposed limits in central Yukon, each subsequent glaciation was less extensive than those prior (Fig. 1; Bostock, 1966; Jackson et *al.*, 1991; Smith et *al.*, 2004). Yukon glaciations have previously been considered coherent advances, but Ward et *al.* (2008) challenged the synchrony of the penultimate glaciation across Yukon. Terrestrial cosmogenic nuclide-dated boulders at the mapped penultimate limit in southwestern Yukon were MIS 4, while Old Crow Tephra found in deglacial sediments along the Pelly River dates the penultimate surface to MIS 6. This indicates that the penultimate glacial limit is not synchronous across the territory.

Bond (1999) completed glacial limits and surficial geology mapping in the Mayo region and identified McConnell and Reid-age moraines in the Granite Creek study area. Ice flow of the CIS was dominantly west in central Yukon during the McConnell Glaciation (Bond, 1999). In Granite Creek, the Selwyn Lobe of the CIS terminated 1 km east of the divide with Keystone

Table 1. *Alternating warm and cool periods of Earth's climate derived from oxygen isotope data. These climatic periods, which control glacial and non-glacial processes of the Northern Cordilleran Ice Sheet (NCIS), are referenced throughout the paper.*

Marine Isotope Stage (MIS)	Temperature	NCIS Name	Age (years B.P.)
1	warm	Holocene	11 700 to present
2	cool	McConnell	29 000 to 11 700
3	warm	Interstadial	57 000 to 29 000
4	cool	Gladstone	57 000 to 71 000
5	warm	Interglacial	71 000 to 130 000
6	cool	Reid	130 000 to 191 000

Creek (Bond, 1998) based on moraines and ice-contact features. The age of MIS 2 deglaciation was confirmed by terrestrial cosmogenic nuclide dating (Ward and Bond, unpublished data). Alpine glaciers from upper Granite and Albert creeks terminated in the Keystone-Granite pass area, just beyond the limit of the CIS (Bond, 1999). Reid glacial deposits around Granite Creek are confined to higher elevations and pre-Reid deposits are sparse and occur as erratics on stable surfaces at elevations of 1615 and 1645 m (Bond, 1999, 1998). During the Reid glacial advance, ice followed regional drainages and flowed west, like the McConnell Glaciation. The lower Granite Creek valley was a conduit for ice advancing from the east (Bond, 1998). The MIS 4 Gladstone Glaciation had not been identified at the time of previous surficial geology and glacial limits mapping.

Regional Bedrock Geology

Central Yukon is underlain the extensive Neoproterozoic to Paleozoic Selwyn basin (Roots, 1997). Regional bedrock geology of the Mayo area is composed the following sedimentary sequences: Upper Proterozoic–Lower Cambrian Hyland Group metasandstone, conglomerate, siltstone, shale and phyllite, which underlie Selwyn basin strata; Ordovician Road River Group siltstone and chert; Devonian Earn Group coarse chert-pebble conglomerate, sandstone, siltstone, with minor dark grey to black limestone and chert; and Mississippian Keno Hill Quartzite (Roots, 1997). Read et *al.* (2021) separated the Keno Hill Quartzite into two members: the Basal Quartzite Member is composed of quartzite, graphitic shist, and sericite and chlorite schist; and the overlying Sourdough Hill Member is composed of quartzite, alternating schist, limestone, grit and chlorite. Two regional thrust sheets, the Robert Service and Tombstone, are located just south and north of the study area, respectively (Fig. 3). The Roop Lakes stock lies east of the study area and is associated with the Tombstone-Tungsten magmatic belt (Murphy, 1997; Mair et *al.*, 2006).

Deformation and Mineralization

Regional deformation began in the Middle Jurassic to the Early Cretaceous resulting in upright and overturned folds. The Robert Service thrust displaced Hyland Group rocks, and Tombstone thrusting resulted in shearing and foliation. The 93 ± 3 Ma Tombstone intrusions are composed of undeformed granite and granodiorite (Mair et *al.*, 2006; Roots, 1997). The Basal Quartzite Member identified by Read et *al.* (2021) is the host rock for most of the mineralized veins. Read et *al.* (2021) studied the geology of mineralized veins near Keno Hill, just northwest of Granite Creek and in similar rocks. They note that there are five stages of faulting, two associated with vein faulting. Vein faults are longitudinal and formed between 89 and 68 Ma, transverse vein faults formed afterwards. Rare indicators of oblique-left normal to dip-slip movement are visible in veins exposed at the surface. Their model

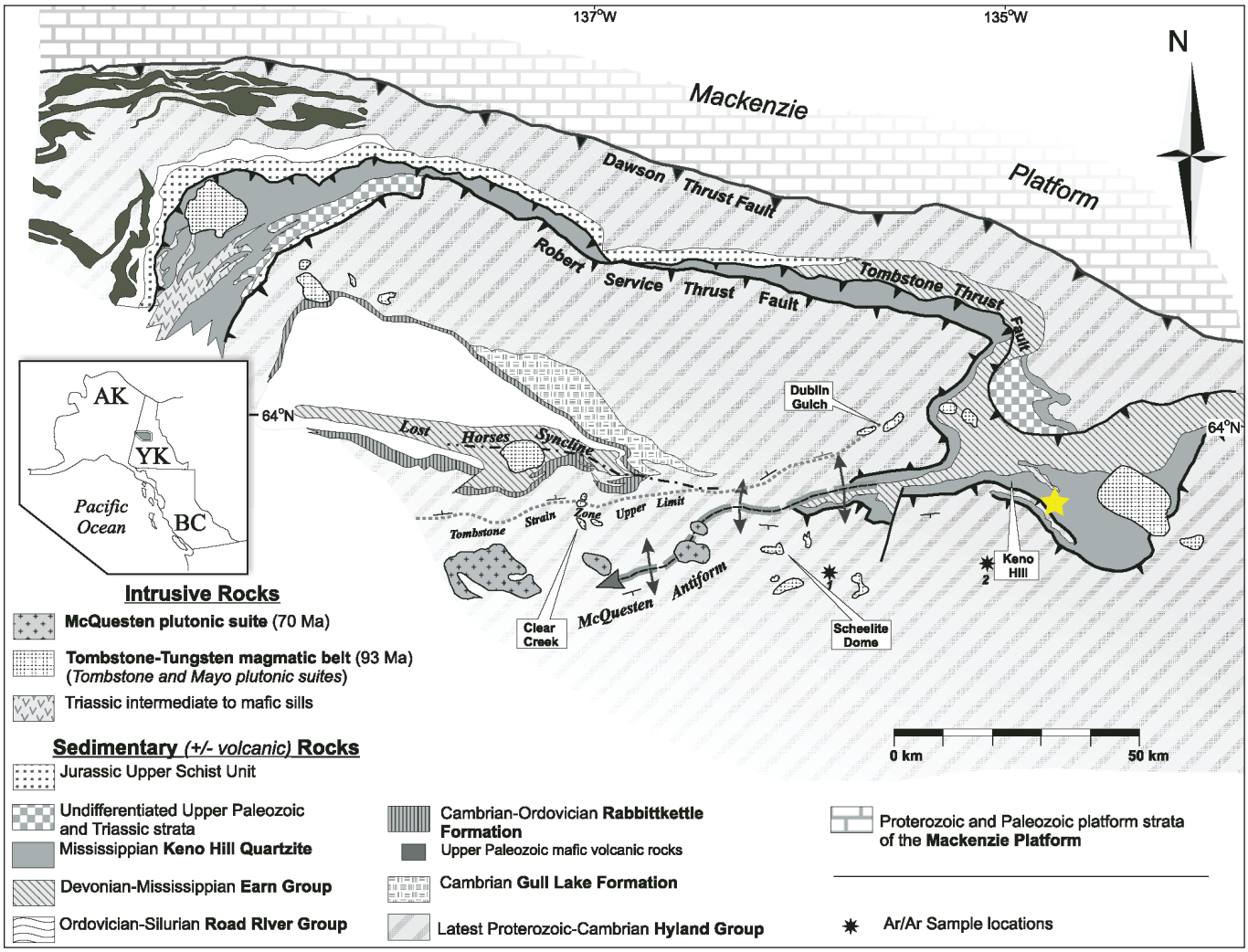


Figure 3. *Regional geology map modified from Mair et al. (2006). Study area is shown with star.*

for mineralization, built on Boyle (1965), reported faults dip steeply in competent quartzite and gently or moderately in schist in Keno Hill Quartzite. Read et *al.* (2021) note that open space for mineralization depends on direction of fault movement, and this period may have allowed formation of open space for veins. Long east-northeast striking longitudinal veins contain early phase mineralization, which is thought to be the source of gold, as well as late phase mineralization either as cemented brecciated zones or thin, secondary veins parallel to early veins (Reid, 2021). Late phase veins are short north-northeast striking transverse veins with late-stage mineralization.

Mining and Exploration

Mining in the Mayo area began with the discovery of placer gold on the Stewart River in 1883 and Duncan Creek in 1901, prompting the establishment of the Mayo townsite. Lead and silver discoveries were made in the Keno region by 1906 and were staked by 1919; development followed soon after (MacDonald et *al.*, 1990). Activity continued throughout the 20th century, increasing with rising gold prices. Between 1978 and 2021, the Mayo Mining district produced 192,815 crude ounces of placer gold. Additionally, there have been many silver-lead-zinc mines in the Keno area, with the main operator being the United Keno Hill Mines. Keno Hill was once Canada's second largest producer

of silver (LeBarge et *al*., 2002). During the summer of 2021, four placer operations were actively mining in the Granite Creek area, and one mineral exploration project was ongoing in the Granite Creek cirque targeting the hardrock gold veins. Since 2015 Granite Creek has produced 16,393 crude ounces of placer gold.

Placer Gold Development

Placer-forming environments in the Mayo region are characterized by LeBarge et *al.* (2002) and grouped into modern, interglacial, glacial and periglacial settings. Modern placers are Holocene-age deposits usually found in floodplains, alluvial terraces, fans, fan-deltas and gulches. These are the most targeted environment for placers. Buried interglacial placers are similar to modern deposits in that they are commonly found in alluvial deposits such as plains, fans and terraces, and also in reworked gulch deposits. In glaciated terrain, placer deposits commonly form during interglacial periods and are most commonly preserved at the margin of glaciers where deposition dominates erosion. Interglacial placers are commonly buried by periglacial, colluvial or glacial deposits. Glacial placers are less common, but can be found in till and outwash material, especially where glaciers reconcentrate interglacial material, or erode mineralized bedrock. Periglacial placers form outside the glacial limit where weathering and erosion dominate, where paleoplacers are reworked, or where mineralized bedrock is eroded. Deposition occurs as periglacial fans, floodplains, or colluvial deposits (LeBarge et *al*., 2002).

Methods

Desktop Mapping

Preliminary mapping consisted of using scanned 1:20 000 air photos obtained from the Energy, Mines and Resources Library in Whitehorse, and a stereoscope to map surficial geology. A series of polygons were created and included surficial material, expression, and any processes or modifiers. Polygon labels followed the method described in Howes and Kenk (1997) and modified for Yukon.

Field Mapping

Field mapping took place in the summer of 2021. Surficial geology field sites were accessed using a pickup truck on mining roads or by foot traverse. Landform sedimentology relied on soil pits, mine cuts and natural exposures to document characteristics. At each field site the following information was collected: location, measurements of the pit/exposure, landform, geomorphic processes, sorting, texture, abundance of clasts, colour, and soil horizons. Photos were taken and sketches made at each site.

Stratigraphic and Sedimentological Data

Granite Creek stratigraphic sections were logged at placer mining excavations, road cuts and stream cuts (Fig. 4). Detailed information collected includes unit thickness, grain size, texture, colour, bedding, contacts, proportion of clasts and matrix, clast lithology and rounding, fabric, and presence of structures or organics. Fabrics consisted of a minimum of 25 clasts where possible, and were plotted as contoured data on an equal area Schmidt net (Table 2). A site map is included in Figure 4 showing locations of excavations.

Results

Stratigraphy: Unit Descriptions

A composite section of units found in the study area of upper Granite Creek is shown in Figure 5. There are 16 units representing a particular depositional environment derived from a total of 12 sites. In the absence of dating control, age estimates and correlation of units are based on stratigraphic position with Unit 1 being the oldest unit.

Unit 1: Weathered bedrock

Unit 1 is weathered grey to black phyllite and quartzite bedrock of the Mississippian Keno Hill Formation. The bedrock surface is undulatory and only exposed in sections GRC-02N, GRC-03A, GRC-03H and GRC-04W (Fig. 6). The bedrock is fractured, folded and foliated, and hosts mineralized quartz veins that are the primary source of placer gold at Granite Creek.

Table 2. *Till clast fabric details. Locations and stereonet plots shown in Figure 7.*

Section Number	Lithostratigraphic Unit	Clasts Measured	Global Mean Trend (°)	Global Mean Plunge (°)	Eigenvalue	Apparent Ice Flow
GRC-01W	Unit 5	25	20	3.2	0.579	Southwest
GRC-01W	Unit 3	23	143	14.6	0.673	Southeast
GRC-01S	Unit 11	15	309	16.6	0.609	Southeast
GRC-02W	Unit 2	14	117	10.4	0.588	Southeast
GRC-02S	Unit 11	15	236	5.4	0.641	Southwest
GRC-03A	Unit 11	15	359	1.4	0.687	North
GRC-04E	Unit 5	25	139	9.2	0.682	North

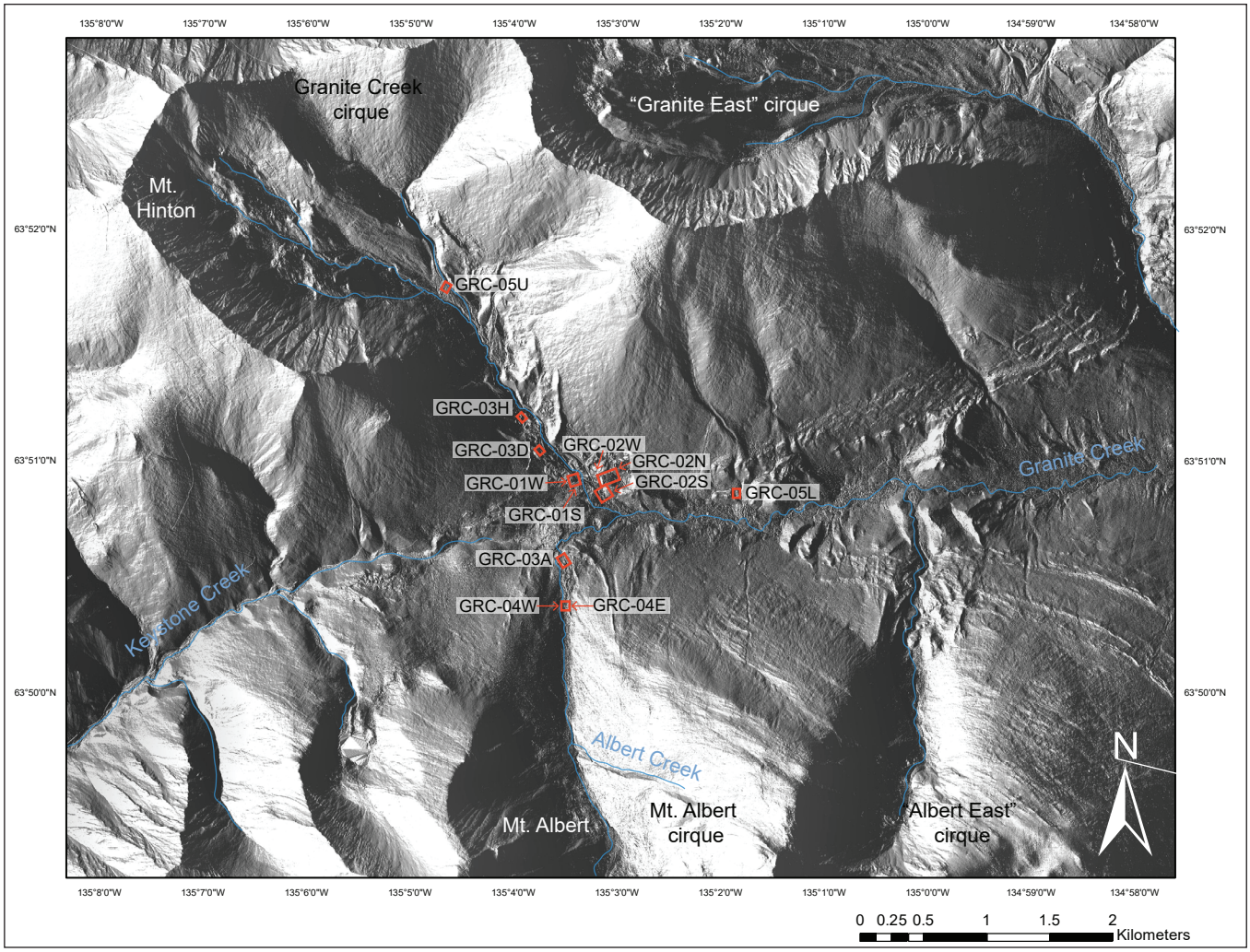


Figure 4. *Lidar imagery showing placer excavation locations, cirques, named mountains and creeks in the study area.*

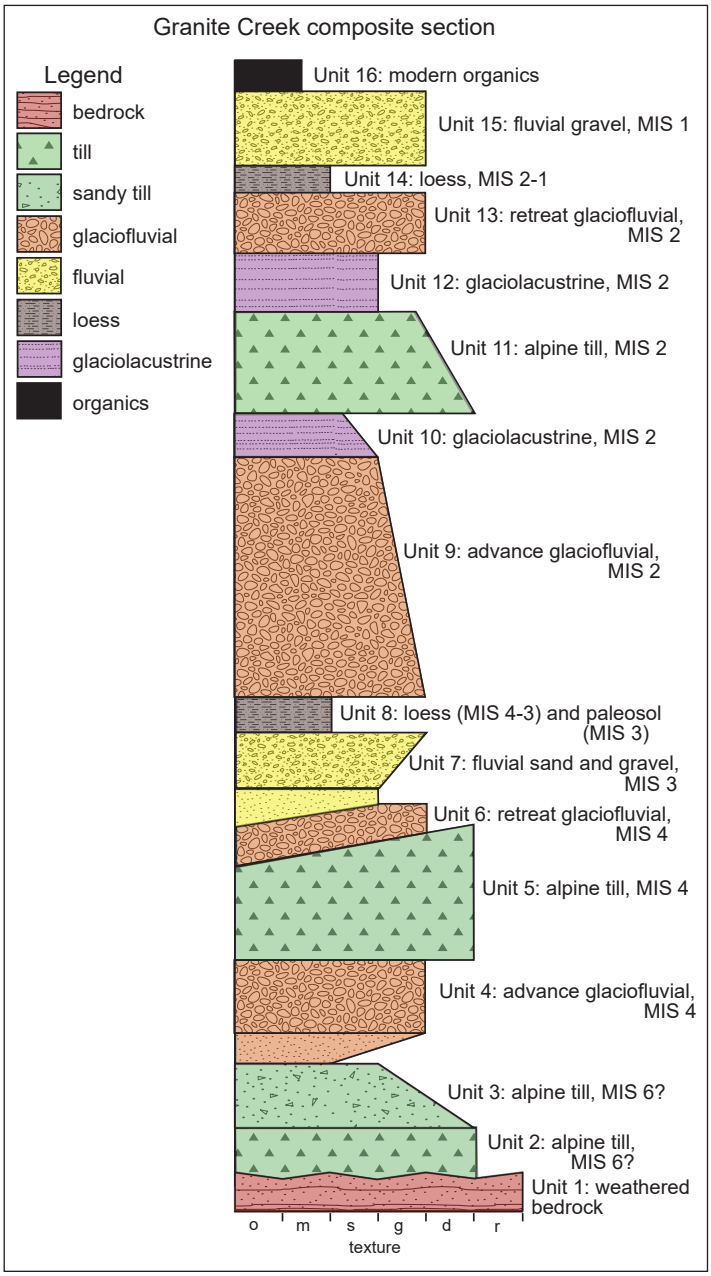


Figure 5. *Composite stratigraphic log illustrating all units found in the upper Granite Creek basin.*

Veins contain fine to coarse-grained quartz, milky white quartz, or quartz breccia. Mineralized zones are highly oxidized.

Unit 2: Alpine till, MIS 6

Unit 2 is an overconsolidated black diamict with abundant clasts of local quartzite and phyllite, and only found in section GRC-02N. This unit is discontinuous and has a variable thickness of 0.5–1.5 m, filling in undulations in bedrock at the base of GRC-02N. Clast content averages 30%, with 80% pebbles and 20% cobbles. Clasts are subangular to subround. The matrix is silty sand. The lower contact is undulatory and sharp with bedrock below. Gold values were subeconomic.

Unit 2 is interpreted as being MIS 6 alpine till due to stratigraphic position below MIS 4 till and fabric indicating flow out the Granite Creek cirque (Fig. 7).

Unit 3: Alpine till, MIS 6

Unit 3 is a discontinuous, silty, overconsolidated olive brown to beige diamict with abundant round to subround clasts. This unit, found only in GRC-01W, is discontinuous and has a thickness of 0–3 m. Clast content is highly variable and averages 35%, with 20% pebbles, 75% cobbles and 5% boulders. The matrix is medium sand with some thin silt beds found under boulders. Clasts are subround to round. The clast lithology of Unit 3 is dominantly quartzite, but 10 highly weathered granitic pebbles and cobbles were found in section GRC-01W. The lower contact was not exposed. This unit contains low amounts of gold.

This unit is interpreted as being till due the presence of erratics and clast fabric indicating flow out of the Granite Creek cirque. The presence of weathered granitic erratics suggests that this unit reworked sediments deposited by the retreat of the CIS during an older glaciation. Granite bedrock is not present in the upper Granite Creek basin and erratics originate from the Roop Lakes Pluton, approximately 20 km to the east. The age is interpreted as MIS 6 due to its stratigraphic position underlying inferred MIS 4 till at location GRC-01, however it is possible that this deposit is from an older glaciation or an earlier phase of the MIS 4 advance.

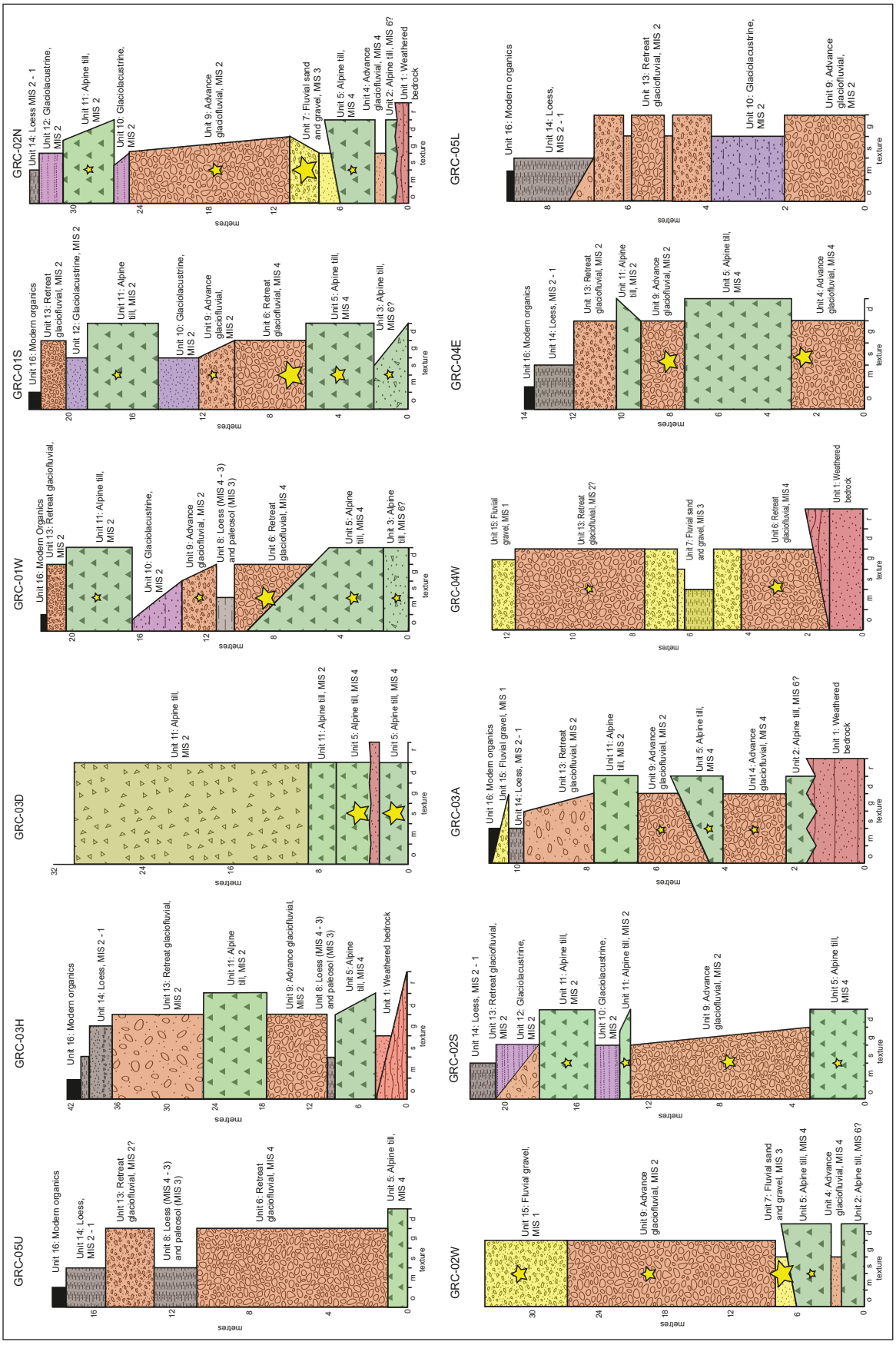


Figure 6. *Key stratigraphic sections, locations in Figure 4. Relative size of yellow star correlates to relative gold value.*

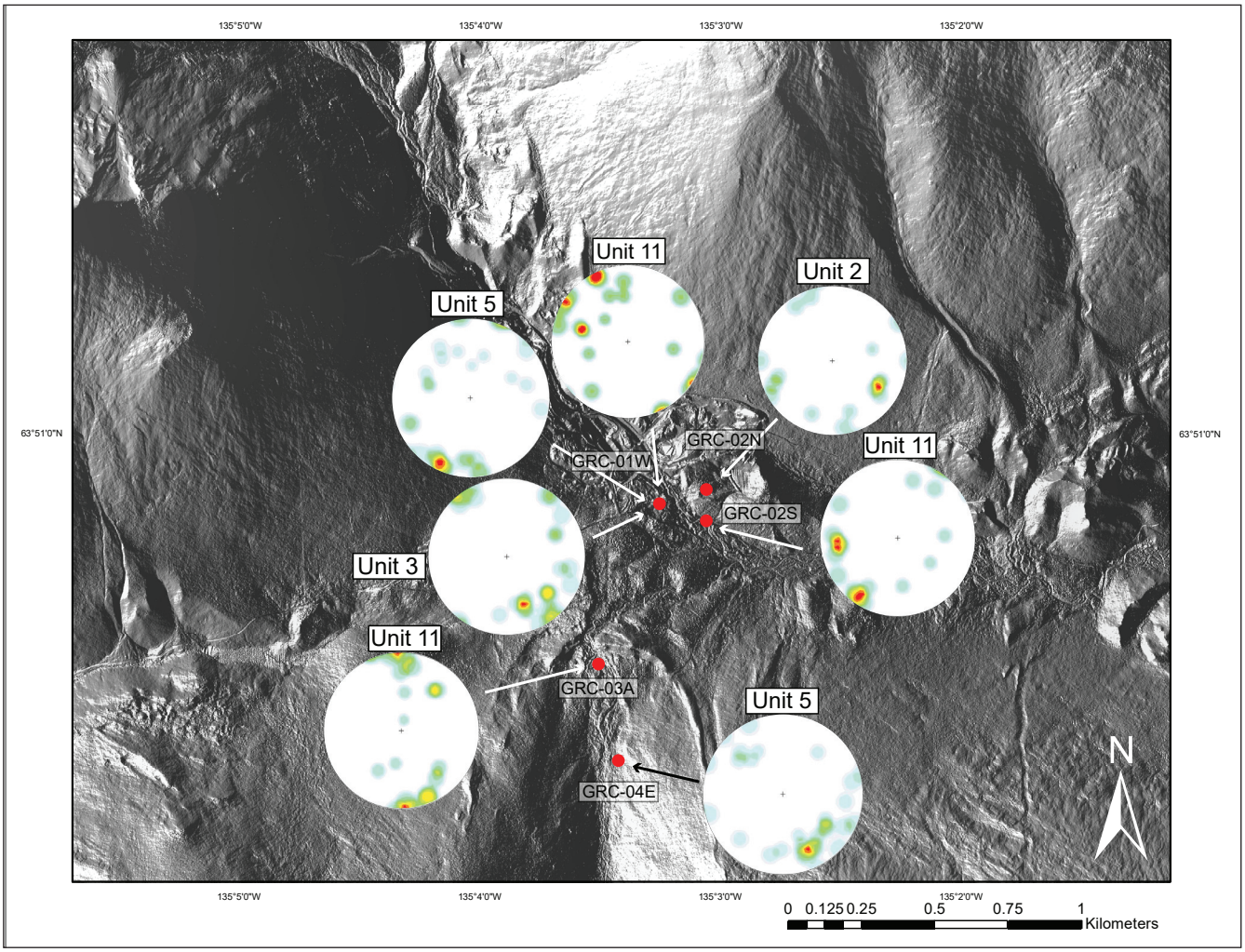


Figure 7. *Clast fabrics with unit number and section location.*

Unit 4: Advance glaciofluvial, MIS 4

Unit 4 is a horizontally bedded, fine-grained, oxidized sand that grades into coarse, moderately sorted gravel. The unit is laterally discontinuous and found at GRC-02N, GRC-04E and GRC-03A. The unit is at least 2 m thick, but only exposed in the base of the excavations. The sand is fine grained and laminated, and gradually coarsens upward into subround to round gravel having a clast content averaging 75%, with 90% pebbles and 10% cobbles. In some locations, there is a sharp contact between the sand and coarse gravel, which has a clast content averaging 80%, with 35% pebbles, 45% cobbles and 20% boulders that are subangular to subround. The matrix is medium sand with some fine sand. The lower contact is undulatory and interstratified with Unit 2. This unit is gold-bearing at location GRC-04.

The unit is interpreted as being advance outwash gravel due to the coarsening upward sequence and stratigraphic position below Unit 5, interpreted to be MIS 4 age till.

Unit 5: Alpine till, MIS 4

Unit 5 is an oxidized, overconsolidated, matrix-supported diamict. This unit is 1–3 m thick and laterally continuous, and present at locations GRC-01W, GRC-01S, GRC-02N, GRC-02S, GRC-04E, GRC-03H, GRC-03A and GRC-03D. Clast content is variable and

averages 35%, with 45% pebbles, 40% cobbles and 15% boulders. Clasts are subangular to subround. The matrix is variable, ranging from silt with some fine sand to medium sand with some fine sand. The clast lithology is dominantly quartzite, phyllite and diorite, with rare granite. Intraclasts of sand and glaciotectonized sandy silt beds were found at GRC-01W and GRC-01S. The lower contact is variable as the unit is found overlying till (GRC-01), bedrock (GRC-02N and GRC-03H) and advance gravel (GRC-04, GRC-03A).

Unit 5 is interpreted as being MIS 4 alpine till due to stratigraphic position, glaciotectonized forms, and till fabric which indicates flow out of a Granite Creek cirque. This unit may contain reworked outwash from the CIS due to presence of at least one granitic boulder. Unit 5 contains a variable amount of gold depending on what was reworked by the alpine glacier. Near the mouth of the Granite Creek cirque (GRC-05D), Unit 5 contains fluvially rounded boulders and oxidized bedrock fragments including vein quartz, suggesting nearby erosion of stream gravel and mineralized bedrock. In these settings Unit 5 contains high amounts of gold. More distal to the mouth of the cirque, Unit 5 contains lower amounts of gold suggesting limited incorporation of mineralized bedrock or enriched stream gravel.

Unit 6: Retreat glaciofluvial, MIS 4

Unit 6 is a coarse, poorly sorted gravel with sandy matrix. This unit is discontinuous and may be in direct contact with MIS 2 advance gravel in some locations suggesting an unconformity is present, or that it is beyond the limit of alpine glaciation. This unit is found in GRC-01W, GRC-01S and GRC-04W. Thickness is 0.5–2.5 m, and exposures are poor due to sloughing of excavation walls. Clast content averages 75%, with 15% pebbles, 45% cobbles and 40% boulders. The matrix is silty sand. The lower contact is sharp and undulatory.

The unit is interpreted as being deglacial gravel due to its stratigraphic position, lack of organics and sorting.

Unit 7: Fluvial sand and gravel, MIS 3

Unit 7 is a finely bedded sand grading into a coarse oxidized gravel with manganese staining. The unit is 0.5–3 m thick and laterally discontinuous, found only in GRC-02N, GRC-02S and GRC-04W. Gravel matrix is medium to fine sand and averages 15%. Clasts are subround to subangular and 30% pebbles, 40% cobbles and 30% boulders. The lower contact at GRC-02N is sharp and the unit dips steeply toward the east, consistent with flow out of the Granite Creek cirque.

The unit is interpreted as fluvial gravel likely deposited during MIS 3 due to its oxidation and stratigraphic position. This unit contains high concentrations of placer gold.

Unit 8: Loess (MIS 4-3) and paleosol (MIS 3)

Unit 8 is thin, 0.25–1.25 m thick, discontinuous, oxidized silt with some sand, has crude horizontal bedding, and is mottled. This unit is laterally discontinuous and found only in GRC-0W1 and GRC-03H. It has approximately 15% pebbles incorporated in the top 0.75 m. At location GRC-01W, the lower contact is sharp, and is draped over Unit 5, which may be a buried MIS 4 alpine moraine. Oxidation and mottling within the loess is gradational and extends into the underlying morainal sediment.

This unit is interpreted as MIS 4 and 3 loess with a paleosol formed during MIS 3. The lower 0.5 m in GRC-01 was sampled for optically stimulated luminescence dating. Results are pending.

Unit 9: Advance glaciofluvial, MIS 2

Unit 9 is a coarse gravel that fines upward into interbedded sand and gravel that interfingers with Unit 10. This unit is laterally continuous and is found in nearly all sections, and has a thickness of 5–15 m. Matrix content is highly variable but averages 15% and consists of sand and some silt. Clasts are subround to subangular and consist of 40% pebbles, 45% cobbles and 15% boulders. The clast lithology is dominantly quartzite, gabbro and phyllite. Imbrication indicates flow out of alpine cirques. The lower contact is undulatory.

This unit is interpreted as being an advance glaciofluvial gravel due to the stratigraphic position interfingering with glaciolacustrine sands above. This unit contains moderately economic amounts of gold that is distributed throughout the section.

Unit 10: Glaciolacustrine, MIS 2

Unit 10 is a horizontally bedded to deformed and glaciotectonized silty to medium sand. This unit is undulatory due to erosive till which deforms the unit and is found toward the top of most excavations located near the Granite-Keystone creek pass area. Thickness is highly variable and ranges from 0–4 m. Clasts are rarely found but some cobbles are present. The advance glaciofluvial gravel below interfingers with this glaciolacustrine sand.

This unit is interpreted as being glaciolacustrine sand deposited when the Cordilleran Ice Sheet advanced up lower Granite Creek and impounded the drainage. This interpretation was made based on the sedimentology of the unit, stratigraphic position below Unit 11 which is interpreted as being MIS 2 alpine till and surficial geology mapping of the CIS terminal moraines that block the drainage. Additionally, no organics were found in this unit and some dropstones were observed. This unit is folded and faulted by the overlying alpine till.

Unit 11: Alpine till, MIS 2

Unit 11 is an overconsolidated, very dark grey, matrix-supported diamict. This unit is 0.25–2 m thick, laterally continuous, and is found in most excavations. Clasts are subangular to subround and average 35%, with 45% pebbles, 40% cobbles and 15% boulders. The clast lithology is dominantly local quartzite and phyllite. Some vertically oriented clasts are present. Matrix is highly variable but predominantly silty sand. The lower contact is variable, undulatory and erosive. Till fabrics are consistent with flow out of respective cirques.

This unit is interpreted as being MIS 2 alpine till due to its lateral extent, fabric, local clast content and overconsolidation. This unit contains low amounts of gold, however values may increase closer to the Granite Creek cirque where the till is in contact with bedrock and more completely eroded pre-existing sediment.

Unit 12: Glaciolacustrine, MIS 2

Unit 12 is a 1–3 m thick, continuous, horizontally bedded, silty sand to medium sand. This unit is laterally continuous and found at locations GRC-02N, GRC-02S and GRC-01S. Clasts are rare, but some pebbles are present in the top of the unit as it grades into a soil in some locations. The lower contact is sharp and undulatory, draped over Unit 11.

This unit is interpreted as glaciolacustrine sand deposited after the alpine glaciers began to retreat and the CIS still blocked the drainage. This is based on stratigraphic position above Unit 11 alpine till, sedimentology of the unit, its extensive nature and lack of organics.

Unit 13: Retreat glaciofluvial, MIS 2

Unit 13 is a coarse, moderately sorted, clast-supported gravel. The unit is laterally continuous and is found at most locations. Thickness is 0.25–1.5 m. Clast content is highly variable but averages 75%; 45% pebbles, 35% cobbles and 15% boulders. Some crude imbrication is found indicating flow out of Granite Creek cirques. The matrix is variable but averages fine to medium sand. Clasts are subround to subangular. Lithology is dominantly local phyllite, quartzite and diorite. The contact is variable and ranges from gradational to sharp and undulatory when in contact with Unit 11.

This unit is interpreted as retreat glaciofluvial gravel deposited by outwash from melting alpine glaciers. The interpretation is based on its texture, lack of sorting, stratigraphic position and crude imbrication. This unit may contain Holocene gravel at the top of the unit as it is difficult to differentiate in some locations. Unit 13 contains economically low amounts of gold.

Unit 14: Loess, MIS 2-1

Unit 14 is 0.25–3 m of massive to crudely stratified, oxidized silt and fine sand. This unit is laterally continuous and is found at the top of most exposures in Granite Creek valley where preservation allows.

The lower contact varies from being sharp, to being intermixed with colluvium. At some locations, this unit is in direct contact with overlying organic material forming the A horizon. Where this occurs, B horizon oxidation is present within the unit. The lower contact is variable, ranging from gradational to sharp.

This unit is interpreted as being loess deposited following MIS 2 glaciation due to its texture and massive structure.

Unit 15: Fluvial gravel, MIS 1

Unit 15 is a poorly sorted, clast-supported gravel. The unit is restricted in extent and found at locations GRC-02W, GRC-03A, GRC-03H. Thickness is 0.5–5 m. This unit is thickest at lower elevations and generally thinner closer to the cirque. Clast content averages 80%, with 30% pebbles, 50% cobbles and 20% boulders. Clasts are subround to subangular. Lithology within the gravel is dominantly phyllite and quartzite. The lower contact is erosional.

This unit is interpreted as being Holocene fluvial gravel due to its proximity to modern Granite Creek and stratigraphic position. This unit contains moderate amounts of gold at GRC-02W and becomes more enriched toward the lower contact.

Unit 16: Modern organics

Unit 16 is modern organics that range in thickness from approximately 0.25–0.5 m. This unit is composed of modern soil horizons and vegetation. The organics are commonly stripped from excavations during preparation and set aside for reclamation.

Location Descriptions

GRC-01 (GRC-01W and GRC-01S)

GRC-01 is inside the maximum limit of the Granite Creek alpine glacier during the last glaciation (MIS 2). Two walls of this section were logged; GRC-01W (Fig. 8) and GRC-01S (Fig. 9). Modern Granite Creek flows just east of the excavation. Units are shown in Fig. 6. Many of the laterally continuous units are present in this section, but this is the only location where Unit 3 was found. It is interpreted that this unit reworked a recessional deposit from the retreat of the CIS. This excavation contains glacial and interstadial sediment extending back to the MIS 6 Reid Glaciation. The lowermost units consist of till from this time frame and are overlain by outwash and till from the ensuing MIS 4 Gladstone Glaciation. The MIS 4 glacial sediments are capped by a veneer of loess that contains a paleosol likely from the MIS 3 interstadial warm period. This unit is overlain by MIS 2 glacial sediments that include alpine till and glaciolacustrine material from the damming of Granite Creek by the CIS. These units are illustrated in a southwest to northeast cross section that intersects GRC-01, Granite Creek, and GRC-02 (Fig. 10).

GRC-02 (GRC-02N, GRC-02W and GRC-02S)

GRC-02N (Fig. 11) and GRC-02W (Fig. 12) are at the confluence of alpine glaciers and near the MIS 2 CIS limit. This location is southeast of GRC-01. Section GRC-02W differs from GRC-02N and GRC-02S (Fig. 13) because it includes the Holocene fluvial gravel and the unconformity associated with its deposition. In this location some preceding glacial units have been reworked. GRC-02S is located farther south on the toe side of a potential ice stagnation complex from the CIS. Units are shown in Figure 6. The base of the excavation intersected a steeply dipping bedrock surface only visible in the northwestern corner. The lowermost units consist of sediment from the Reid Glaciation, which infill bedrock undulations. These units are overlain by alpine till from the Gladstone Glaciation and are also gold-bearing. In the northeastern corner, the richest gold-bearing unit is an interstadial fluvial gravel from MIS 3. Overlying this gravel is a thick, gold-bearing, advance McConnell glaciofluvial gravel which fines into interbedded sand and gravel. In the northeastern corner, discontinuous retreat glaciofluvial gravel overlies the MIS 2 till. Glaciolacustrine sand, subeconomic gold-bearing till and loess cap the exposure (Fig. 10).

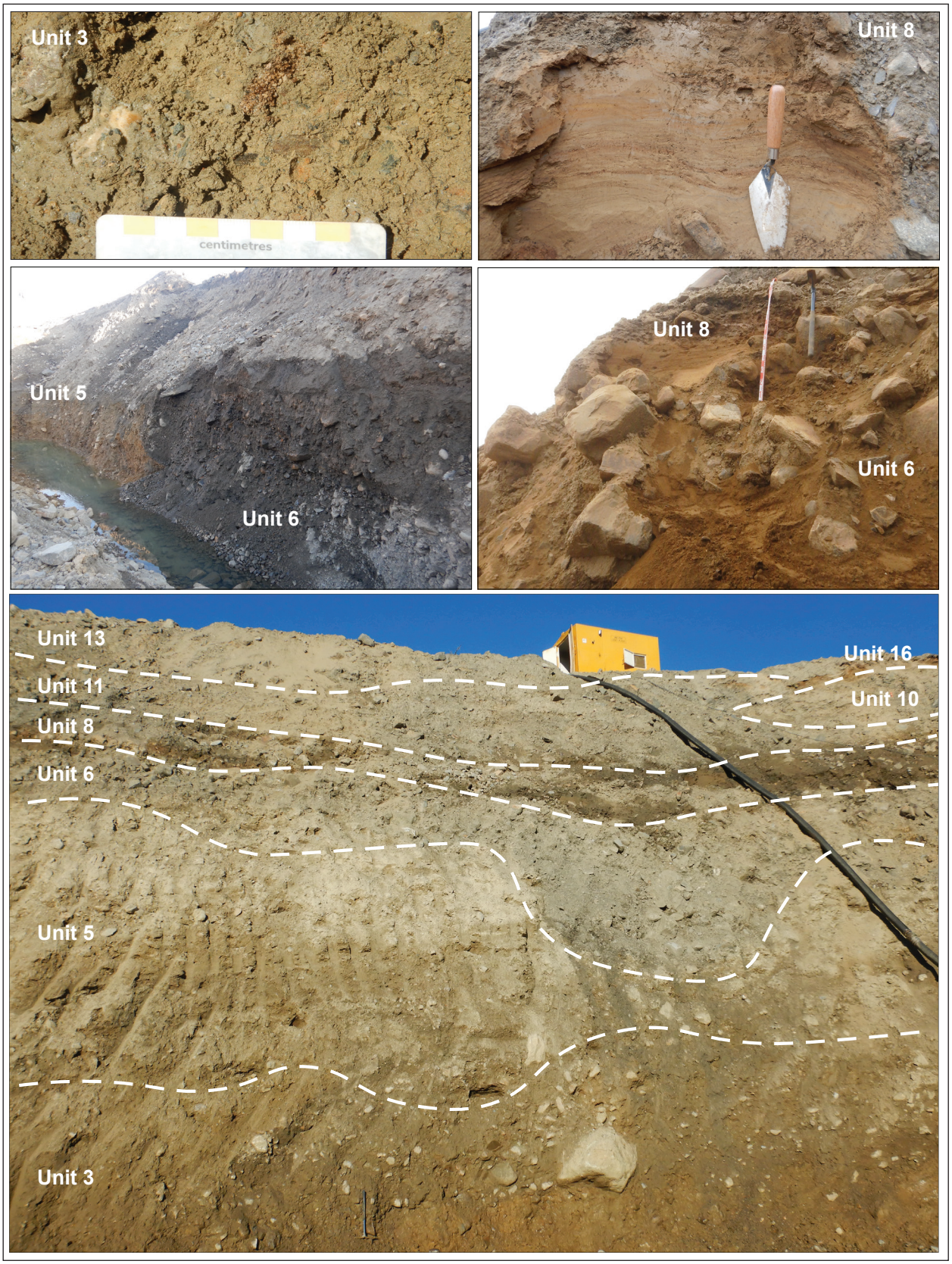


Figure 8. *Main stratigraphic units at GRC-01W.*



***Figure 9**. Main stratigraphic units at GRC-01S.*

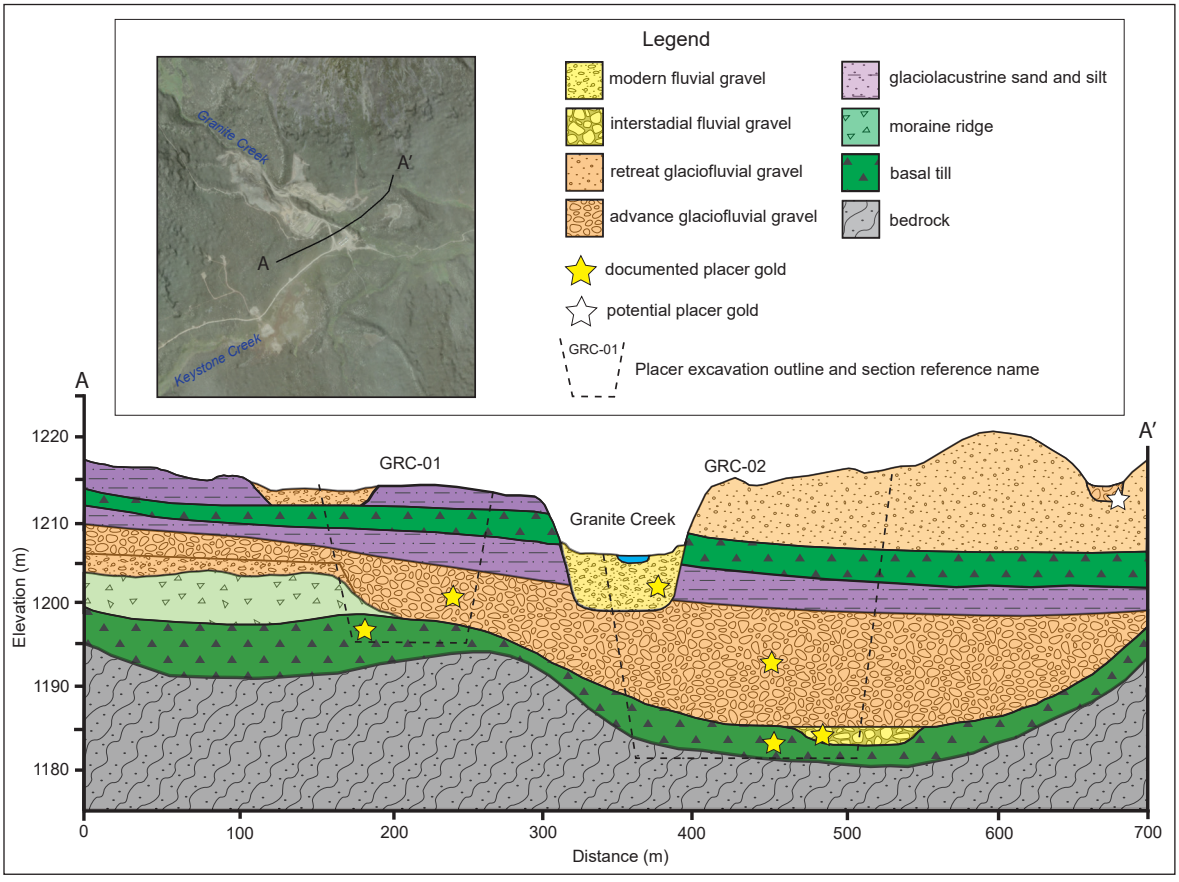


***Figure 10.** Simplified units in cross section at exposures GRC-01 and GRC-02. Transect is roughly southwest to northeast.*

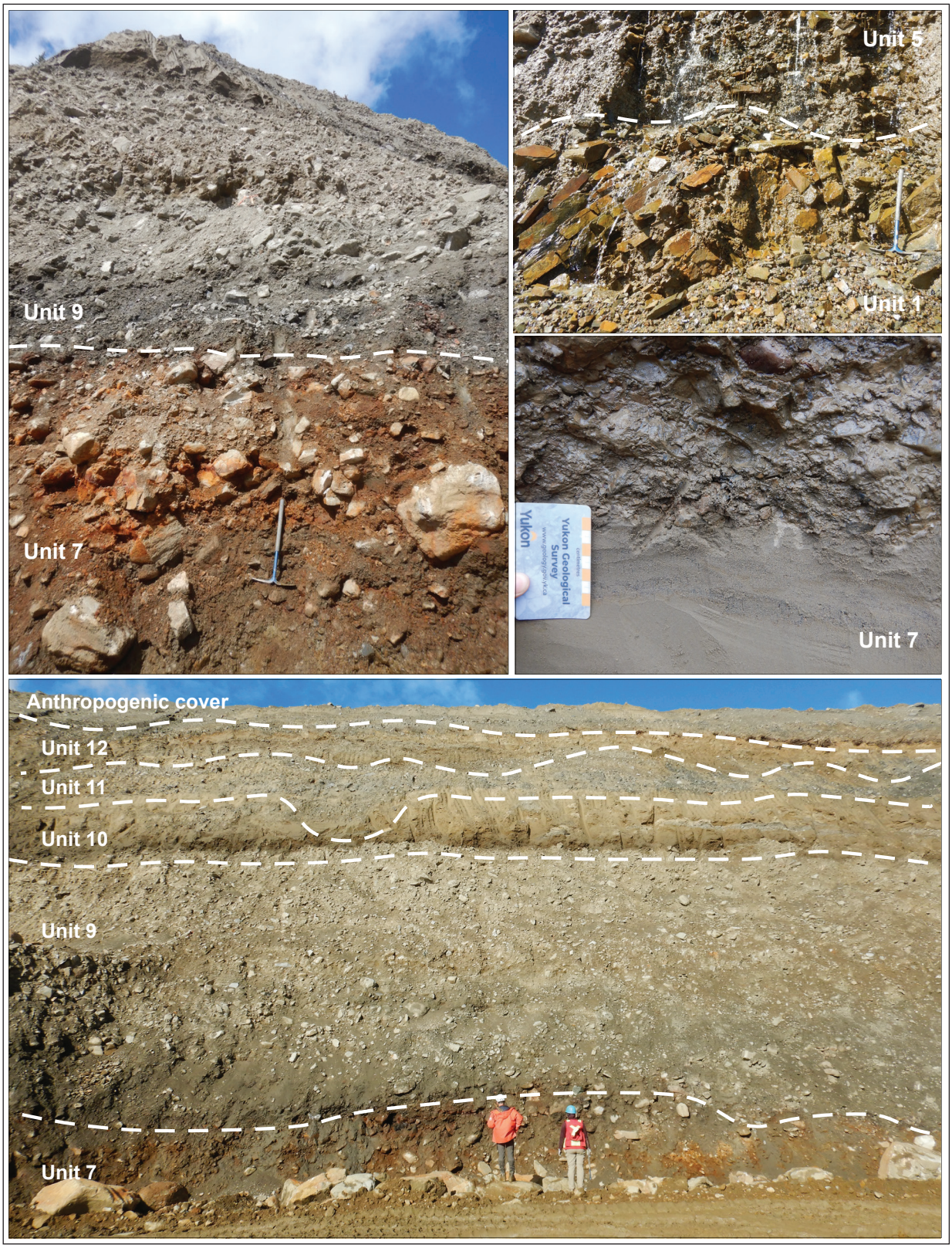


Figure 11. *Main stratigraphic units at GRC-02N.*

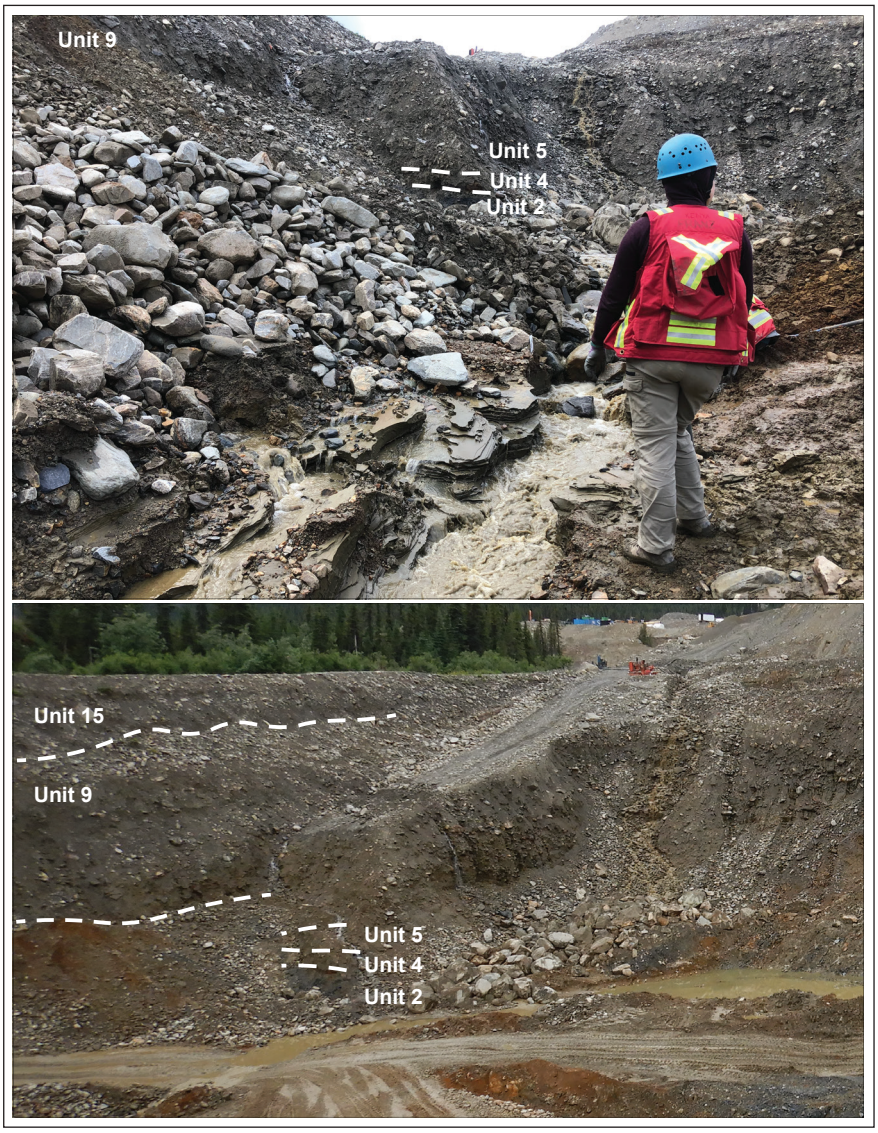


Figure 12. *Main stratigraphic units at GRC-02W. The view in the lower photograph is to the northwest.*

GRC-03D and GRC-03H

GRC-03H (Fig. 14) is just west of modern Granite Creek, up-valley of a recessional moraine formed by the Granite Creek alpine glacier. GRC-03D (Fig. 15) is just south of GRC-03H. Units are shown in Figure 6. The lowermost unit at GRC-03H is highly weathered and presumably altered bedrock overlain by MIS 4 age alpine till, which is also found in GRC-03D. At GRC-03D this unit is thicker, consisting of basal till that contains thrusted sheets of bedrock. Both contain high economic concentrations of placer gold, likely due to nearby mineralized veins in the valley bottom. GRC-03D is the original discovery pit excavated in 2017. At this site only MIS 2 basal till is present overlying the MIS 4 till. At GRC-03H, the MIS 4 till is overlain by interstadial sediments correlating to MIS 3, followed by advance gravel and till from MIS 2. Modern organics and thick loess overlie the MIS 2 deposits.

GRC-03A

GRC-03A is inside the prominent recessional moraine from the Albert Creek cirque glacier (Fig. 16), just west of modern Albert Creek. This location would have been an outwash fan during advance and retreat of alpine glaciers, and close to paleo-streams formed during interglacial periods. Units are shown in Figure 6.

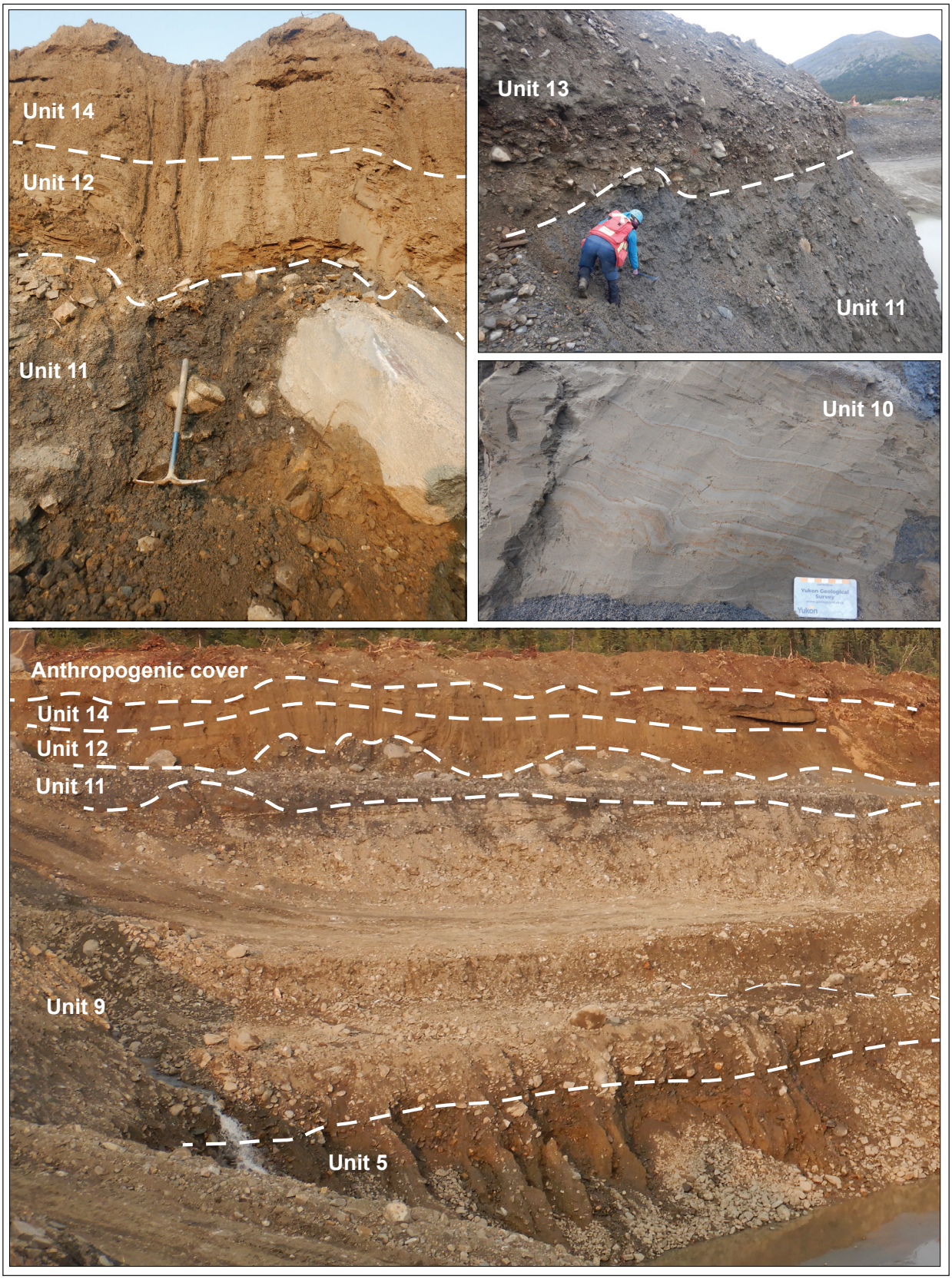


Figure 13. *Main stratigraphic units at GRC-02S.*

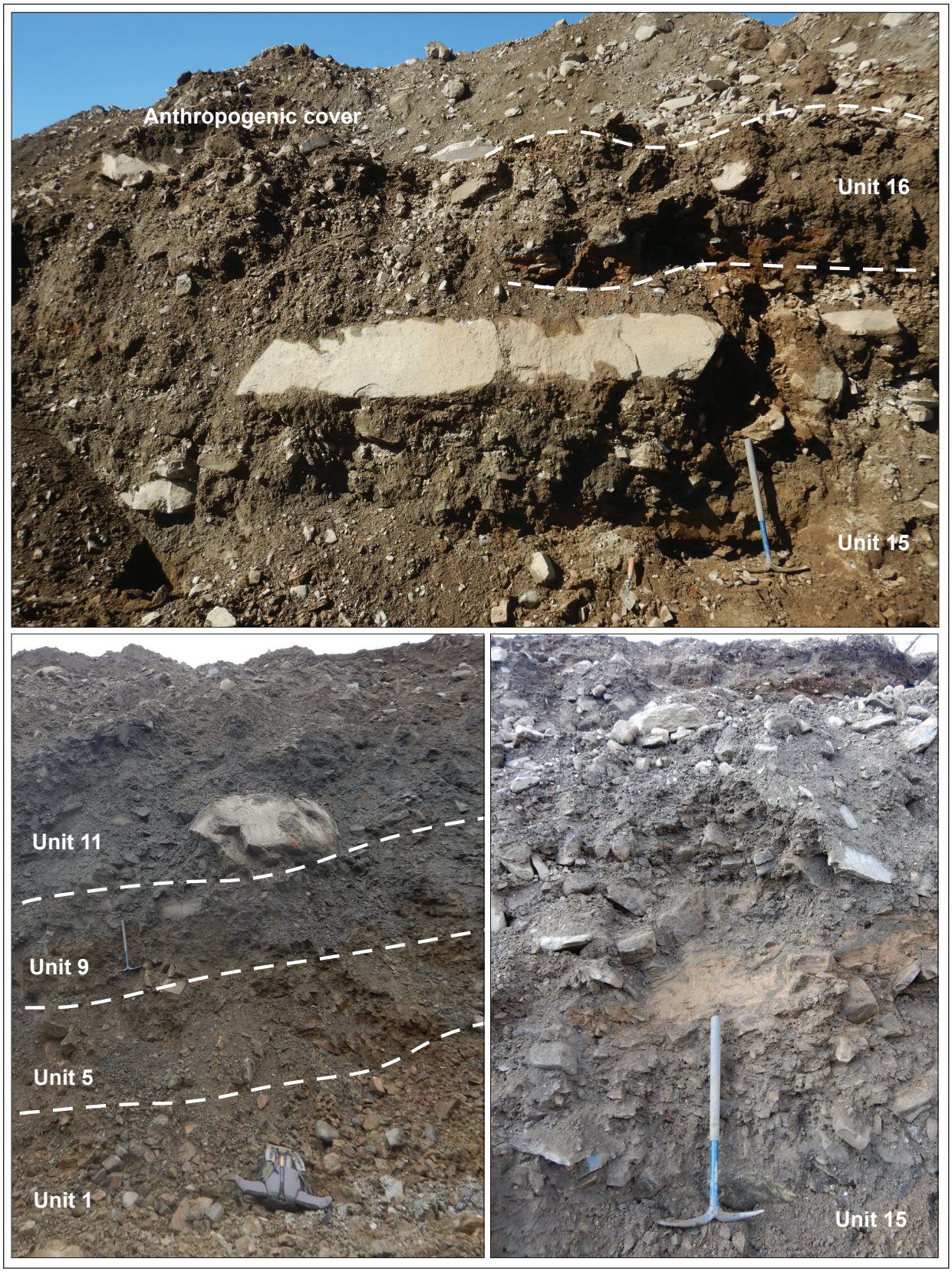


Figure 14. *Main stratigraphic units at GRC-03H.*

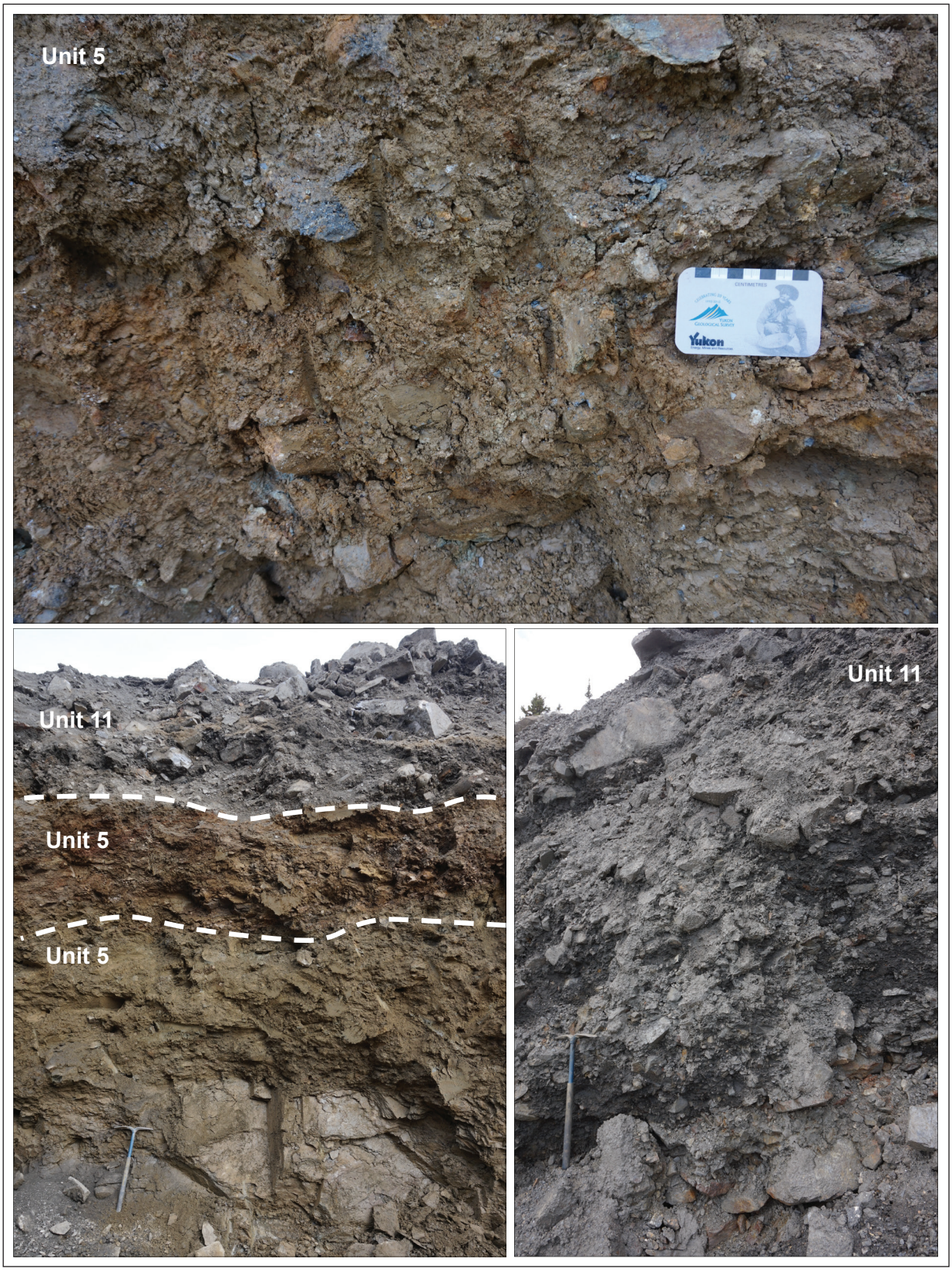


Figure 15. *Main stratigraphic units at GRC-03D.*

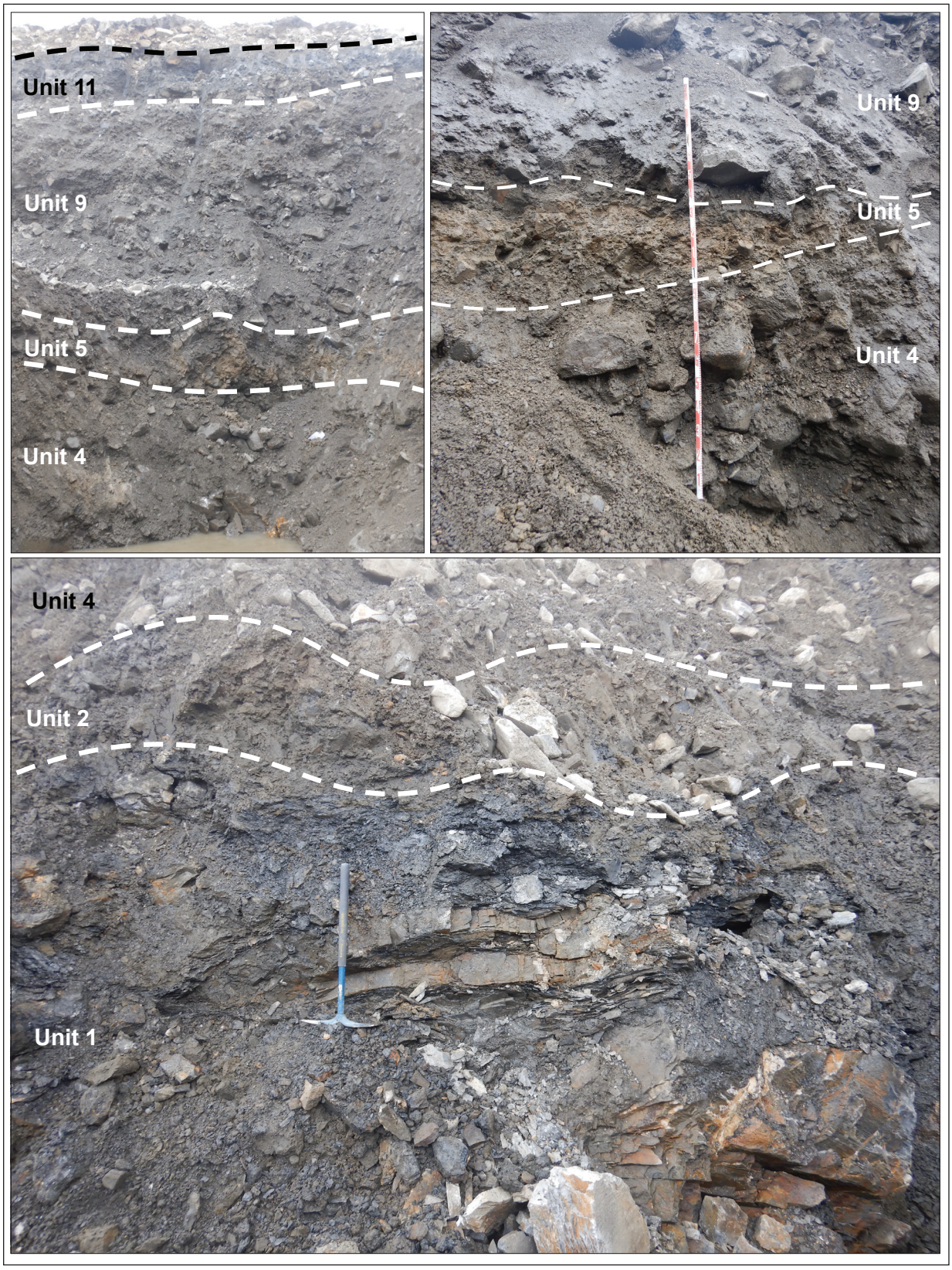


Figure 16. *Main stratigraphic units at GRC-03A.*

Bedrock outcrops on the north and west sides of the excavation and is not found in the rest of the cut. Discontinuous till inferred to be MIS 6 Reid overlies the bedrock and is unconformably overlain by a gold-bearing, yet not economic, advance gravel and till sequence from MIS 4. The next glacial units consist of an advance gravel, till and retreat gravel of MIS 2 age, which also contain low economic values of gold. Thick loess, fluvial gravel and organics overlie the glacial deposits. Gold values are generally low in this deposit, however, could be economic with greater through-put capacity in a wash plant.

GRC-04E and GRC-04W

GRC-04E and GRC-04W are up-valley of the prominent Albert Creek alpine moraine, and to the east of the modern creek. Two walls of this section were logged: GRC-04E (Fig. 17) and GRC-04W (Fig. 18). Units are shown in Figure 6. The units found on each wall of the excavation differ greatly due to the proximity of the modern creek that likely would have been inundated with outwash during glacier advance and retreat, resulting in variable erosion and deposition. Bedrock outcrops on the west wall and is not found on the east wall. Advance gravel and till of MIS 4 age are preserved on the east wall and contain some gold though the absolute values are not known. Deglacial MIS 4 gravel is found on the west wall and overlain by fluvial sand and gravel likely deposited in the MIS 3 interstadial. These units have potential for placer gold. None of the till units were preserved in the west wall, closest to the present creek. Advance gravel containing some placer gold, till and retreat gravel inferred to date to MIS 2 are found on the east and west walls. Fluvial gravel caps the sequence on the west wall and thick loess overlies the sequence on the east wall.

GRC-05L and GRC-05U

These are two separate, abandoned excavations from previous mining operations. GRC-05L (Fig. 19) is in the path of a former meltwater channel from the CIS, inferred from geomorphic position and mapping. GRC-05U (Fig. 20) is inferred as being in the path of a former outwash channel that may have drained a temporary glacial lake in the Granite Creek cirque. Units are shown in Figure 6. Operators at Granite Creek report that gold values in these excavations were not economic. From the lack of placer gold concentrations and geomorphic position, we interpret that these locations were areas of deglacial outwash erosion and deposition that did not rework sediment containing significant gold concentrations. At GRC-05L this is understandable because CIS morainal sediment, which contains very low quantities of placer gold was reworked. At GRC-05U, till that was reworked by the outwash must be sufficiently depleted in placer gold as well.

Discussion

Glacial and Interglacial History

Phase 1

Phase 1 (Fig. 21) represents modern and interglacial periods. In these environments, fluvial erosion and deposition is a common process, and is efficient at concentrating placer gold from surrounding surficial sediment and the bedrock. Within the study area this includes Unit 7 fluvial sand and gravel and Unit 15 modern fluvial gravel. Modern Granite Creek is a proxy for the size of creeks during interglacial periods. Interglacial deposits are not as voluminous as glacial outwash deposits due to the low discharge and velocity of these creeks, which transport less sediment than glacial advance or retreat meltwater environments. The source of material being eroded will impact the placer gold grades in these deposits. In addition, the length of time that the fluvial placers have to develop and concentrate heavy minerals will also impact their grades. Periglacial processes such as frost shattering and cryoturbation, associated with the subalpine and alpine environment of the study area, also liberates bedrock into the valley bottom, which can then be reworked by fluvial activity or incorporated into advancing glaciers.

Phase 2

Phase 2 represents the onset of glaciation. Alpine glaciers respond more quickly to the colder temperatures and advance prior to the arrival of the ice sheet into the area. Alpine glaciers erode bedrock, including mineralized veins in the Granite Creek cirque.

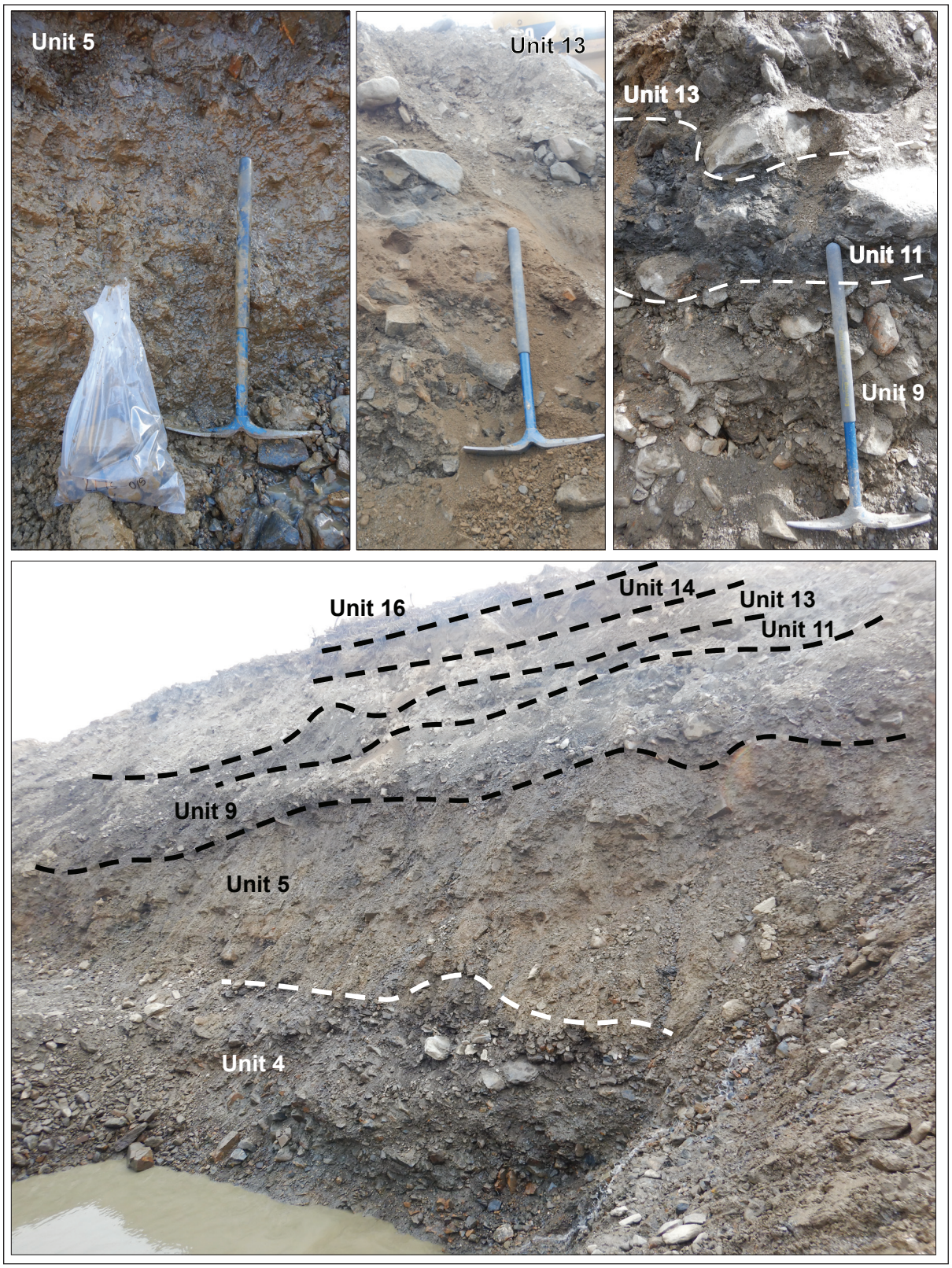


Figure 17. *Main stratigraphic units at GRC-04E.*



Figure 18. *Main stratigraphic units at GRC-04W.*

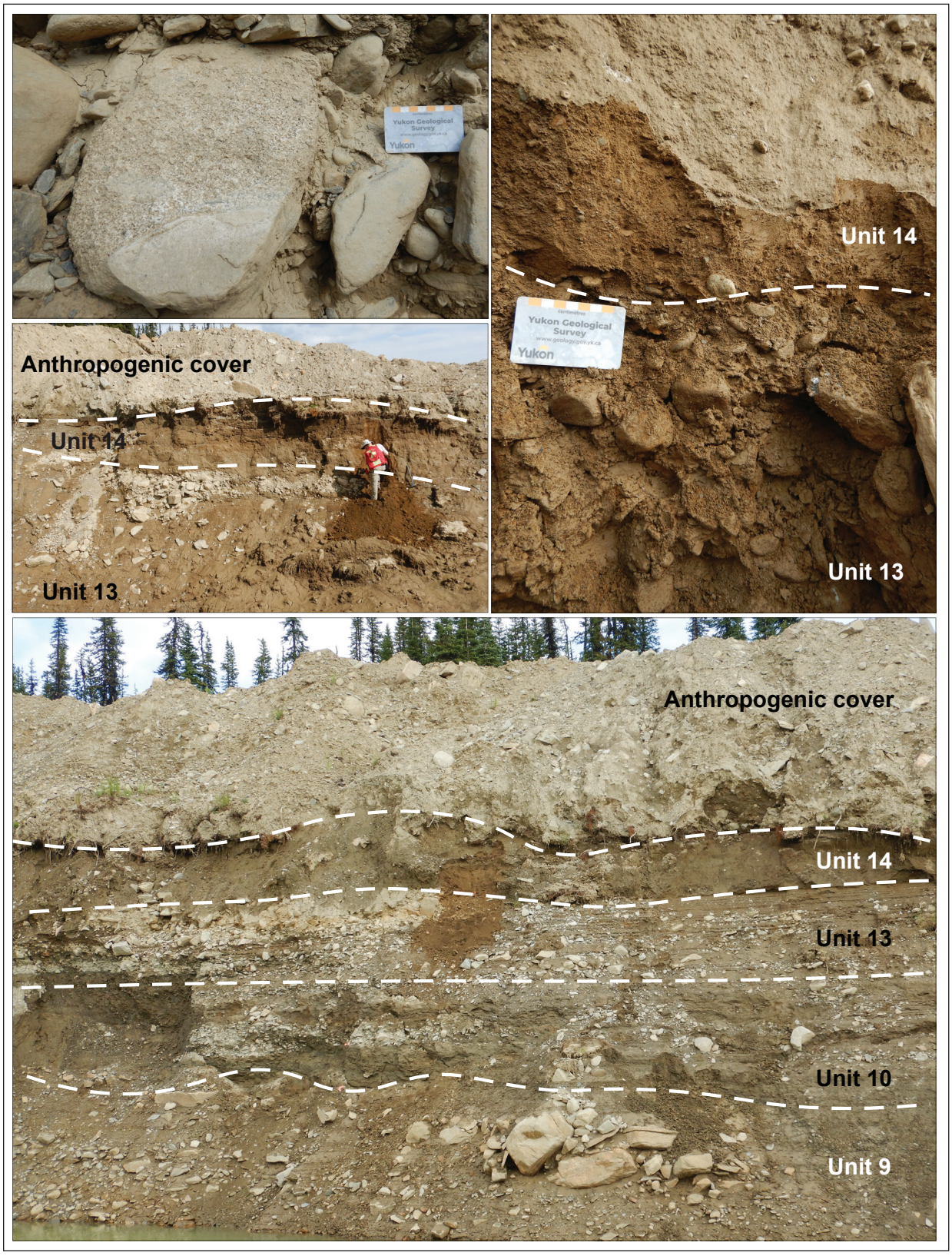


Figure 19. *Main stratigraphic units at GRC-05L including a granite boulder (top left corner) due to the proximity of the CIS MIS 2 moraine.*

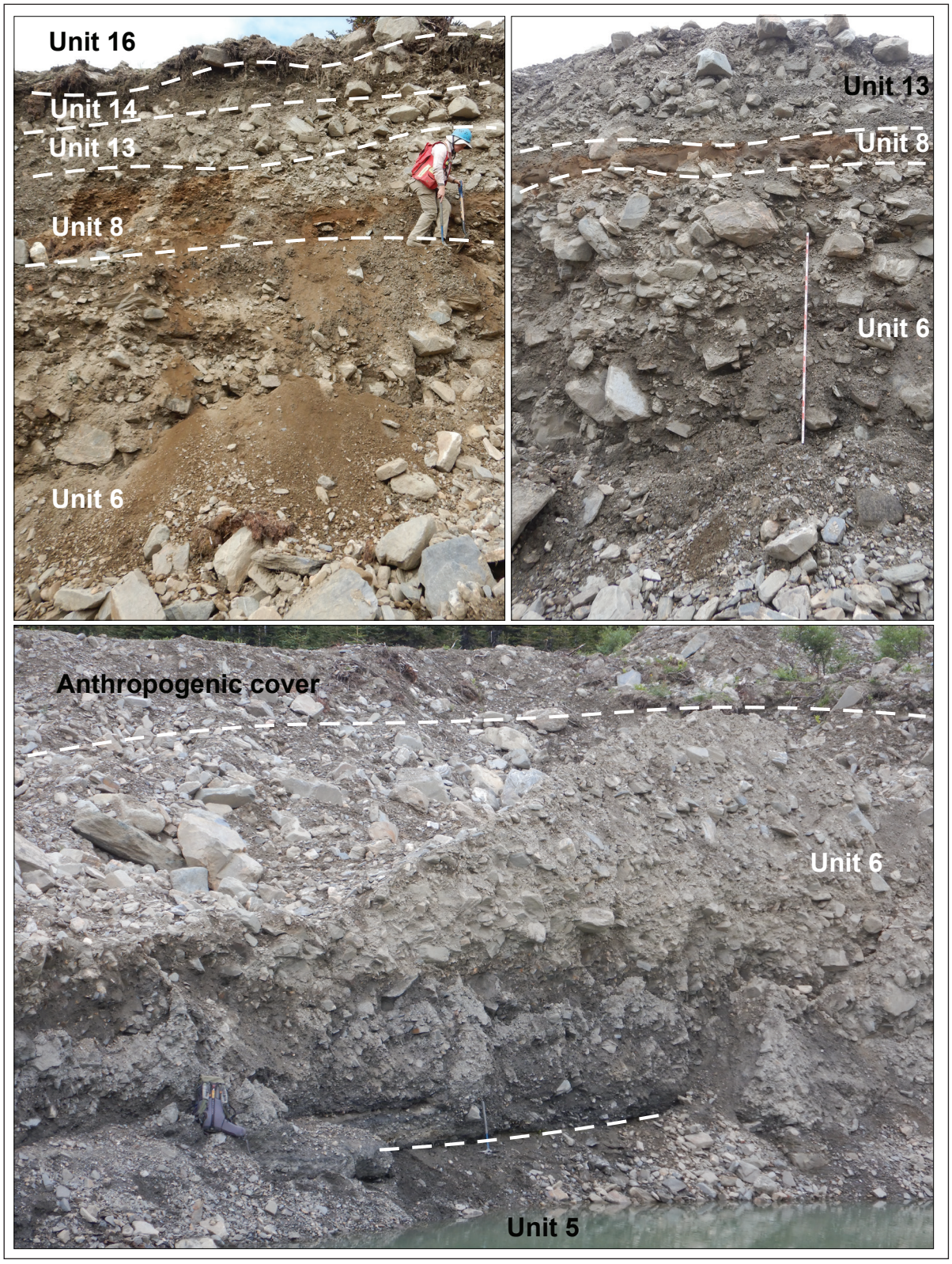


Figure 20. *Main stratigraphic units at GRC-05U.*

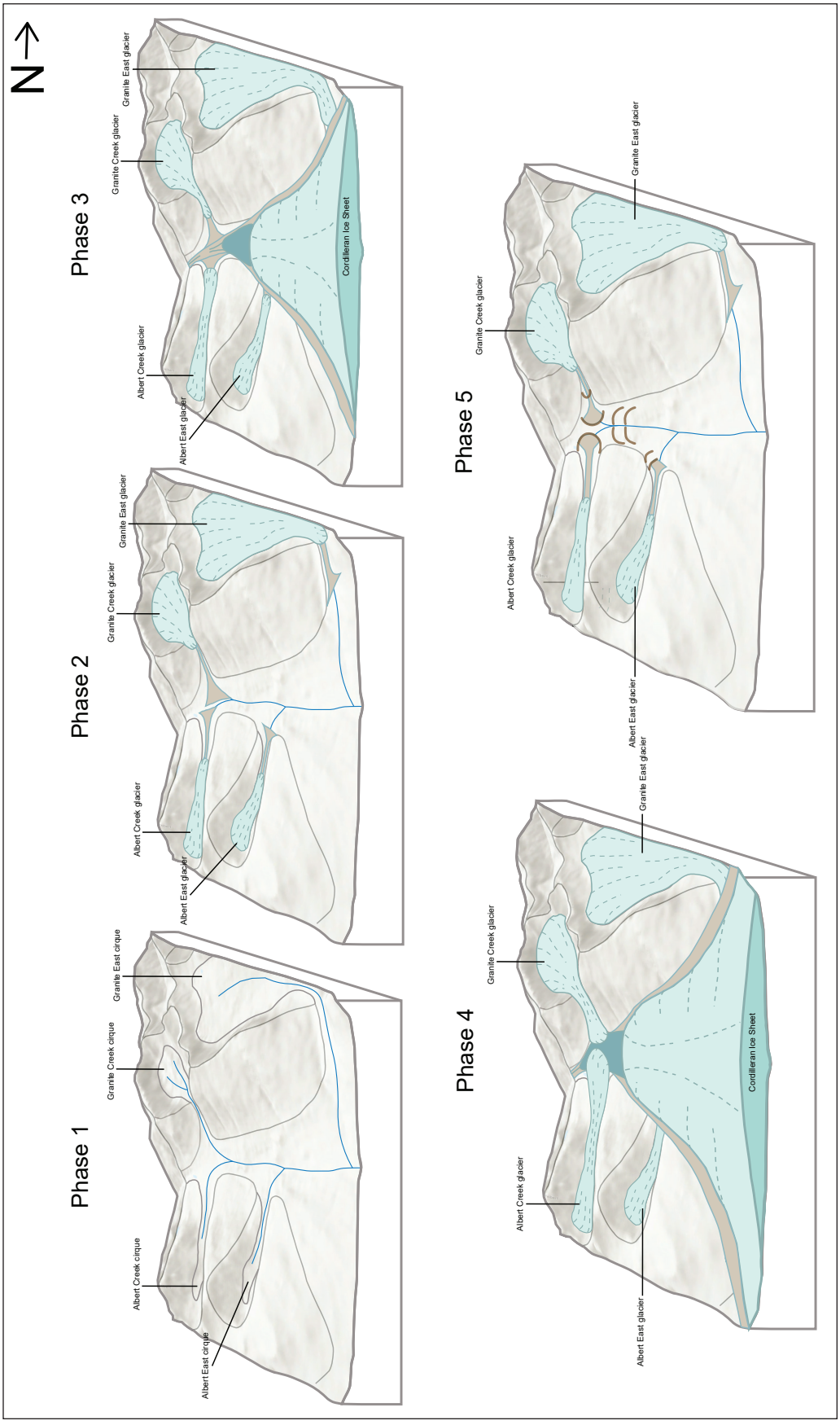


Figure 21. *Block models representing different phases of glaciation in the upper Granite Creek basin. Phase 1: Modern or previous interglacial environment. Phase 2: Onset of glaciation. Phase 3: Cordilleran Ice Sheet advancing up lower Granite Creek. Phase 4: Last glacial maximum (MIS 2). Phase 5: Deglaciation.*

Based on placer gold distribution, mineralized veins are also interpreted to extend into the Mt. Albert cirque. Erosion of these veins and incorporation of gold into till is a significant mechanism for enriching the alpine till. In addition, alpine glaciers erode and incorporate pre-existing gold bearing fluvial deposits. Coarse advance gravel is deposited in outwash fans at the terminus of the alpine glaciers. These deposits are thicker than deglacial deposits due to the aggradational environment associated with their proximity to the advancing ice front. Advance outwash deposits form the thickest placer deposits in the local area. This phase occurs during all glaciations.

Phase 3

Phase 3 represents the presence of the Cordilleran Ice Sheet as it flows up Granite Creek valley, blocking the drainage of Granite Creek and Albert Creek during MIS 2 and MIS 6. In this environment, an ice contact, proglacial lake forms. Meltwater channels form along the margins of the ice sheet. This phase is represented as a coarsening upward sequence in the stratigraphy due to changing base levels as the alpine glaciers and CIS advance. No evidence of this sequence exists for MIS 4, indicating the CIS did not reach the Granite Creek valley or Gustavus Range.

Phase 4

Phase 4 represents the increasing size of the glaciers and glacial lake as the CIS continues to advance up Granite Creek. The drainage changes direction and overtops the divide, flowing west into Keystone Creek. More fine-grained sediment is deposited in the valley. The CIS and alpine glaciers continue advancing into the lake and deform the sand. Topographic representation of the maximum alpine ice position are not preserved likely due to the glaciers terminating into the glacial lake, which would inhibit moraine formation. The prominent moraines visible in the area represent recessional margins. This phase would have occurred during MIS 2 and 6. During MIS 6, the ice sheet would have continued to thicken and eventually flowed through the valley into Keystone Creek.

Phase 5

Phase 5 represents MIS 2 deglaciation. Alpine glaciers retreat, depositing several recessional moraines which indicate that alpine deglaciation was punctuated by significant standstills and potentially readvances. Retreat gravel deposits are thinner and have a finer texture than advance gravels due to the shorter duration of the deglacial phase and reduced outwash flow. Albert and Granite creeks flow east into Roop Lakes after the CIS retreats. Loess blankets the sections, deposited during deglaciation when katabatic winds from the glaciers entrain deglacial sediment, particularly the abandoned glacial lake plain. Fluvial processes downcut into glacial deposits and colluvium from steep slopes accumulate.

Placer Setting landforms

Interglacial Placer Settings

Interglacial placer settings provide some of the most economically viable deposits in Granite Creek due to their high concentration of placer gold. These units include the Unit 7 fluvial sand and gravel deposited during the warm period (MIS 3) prior to the last glaciation, and Unit 15, the modern fluvial gravel (Fig. 10). In the Granite Creek cirque valley, Unit 7 was likely eroded by MIS 2 alpine glacial advance gravel or by the bed of the glacier and reworked into the till. Similarly, this would have occurred during MIS 4 alpine glaciation of the valley when MIS 5 interglacial sediment was reworked. The oxidized fluvial gravel is relatively thin, laterally discontinuous, and only preserved in a few of the sections at Granite Creek. However, there is potential for more deposits in this area due to the sinuous nature of fluvial deposits. Identifying the extent of this unit should be a priority for exploration near GRC-02. Modern fluvial gravel is a second interglacial deposit that contains economic amounts of gold at Granite Creek. Unit 15 modern fluvial gravel was found in sections lower in the valley as well as in upper reaches of Albert Creek. This unit tends to become more enriched toward the lower contact, as the creek reworks and concentrates glacial sediment during fluvial downcutting.

Glacial Placer Settings

Glacial placer deposits comprise the most voluminous gold-bearing deposits at Granite Creek. These units include:

- Unit 4 and 9—advance outwash gravel from the last two glaciations (MIS 2 and 4);
- Unit 5 and 11—alpine basal till (MIS 2 and 4); and
- Unit 13—Retreat gravel, MIS 2

One of the glacial placer settings first discovered in Granite Creek was in a basal lodgement till. In at least one section, lodgement till eroded and thrusted sheets of bedrock, and contained highly economic amounts of placer gold. In this case, the alpine glacier eroded a nearby mineralized bedrock source. Freezing of the glacier onto the bedrock surface, and subsequent plucking and thrusting of the bedrock sheet, can occur near the terminus of a glacier where the ice mass is thinner and not as insulative. In addition to nearby mineralized bedrock, large well-rounded boulders in the till suggest a stream gravel may have also been incorporated into the till. Differentiating between the placer gold-enriched alpine till and the barren till from the CIS can be readily completed by comparing the abundance of foreign versus local material in the till. This can be useful in drilling programs that intersect multiple till units and explain variations in the gold content. However, not all alpine tills contained economic gold concentrations due to the variable distribution of enriched material in the valley. For this reason, detailed exploration drilling is recommended prior to development.

The second glacial placer setting is in advance glaciofluvial gravel, which forms during the onset of glaciation. Advance gravel may rework interglacial deposits that contain economic placer deposits or concentrate large volumes of morainal sediment. These sediments originate as meltwater draining under and alongside the former glacier. In contact with the ice, erosion is common and placer gold is likely carried in high energy streams. Beyond the toe of the glacier, deposition dominates and an outwash fan forms. These deposits are voluminous due to the high input of sediment from the erosional glacial environment and potentially long period in which they develop. Gold concentrates at the contact of competent surfaces such as bedrock or till and is generally dispersed throughout the gravel sequence. As a result, these deposits are important low to moderate-grade bulk tonnage targets.

Placer potential

Placer operations in the upper Granite Creek basin target multiple gold-bearing units in the drainage (Fig. 10). The amount of gold in any one of these units is variable and depends on the mode of deposition, proximity to bedrock mineralization, or previously concentrated placer accumulations. Placer potential is highest in units that form during interglacial/interstadial periods. Recent interglacials spanned periods of time from 50 000 to 30 000 years, which allowed for significant concentration opportunities. Targeting former creek channels or alluvial fans, especially where the gravel is oxidized has the most potential for being economic, depending on thickness of overlying sediments and its gold content. These deposits have the highest preservation potential on the lee side of bedrock highs or in narrow troughs that escaped glacial erosion (Levson and Blyth, 1993). Exploring for these deposits relies on geophysics and drilling to understand their local extent.

Processes that erode mineralized bedrock and deposit it close to the source, such as the formation of alpine till deposits, are found to be enriched in placer gold that is coarse and still retains vein quartz material. Commonly these gold grains are very angular and pristine (Fig. 22). Where bedrock sheets have been thrust into the till, this can be a good indication that erosional processes are occurring nearby and can entrain mineralized bedrock if present. Understanding the structural orientations of mineralized veins in the upper Granite Creek valley bottom will aid in finding new gold-bearing till deposits. The alpine glaciers are also effective at eroding pre-existing stream gravel that contained high concentrations of gold. The presence of well-rounded and water-sculpted boulders in the till provides good evidence of this process.



Figure 22. *Angular gold grains recovered from Granite Creek exposure.*

Glacial meltwater deposits are another potential target. Advance outwash gravel from the alpine glaciers that erodes preglacial gravel or gold-enriched till have high potential, especially when the outwash overlies a competent surface such as bedrock or till. Targeting locations where outwash has eroded into till, which acts as a "false bedrock surface", have proven to be economic at Granite Creek. These deposits can form very thick units of pay.

In summary, interglacial placer settings are economically viable although discontinuous and low volume, but the potential for more of these deposits exists. Modern fluvial gravel that has reworked and reconcentrated glacial deposits may be preserved in proximity to modern creeks, although they have been largely exploited in recent years in Granite Creek. Glacial placer settings are voluminous and occur as advance outwash, till and retreat gravel. These deposits are the most economic where alpine glaciers erode mineralized bedrock or interglacial placer deposits, resulting in high concentrations of placer gold in till. Advance gravel can contain gold dispersed throughout voluminous deposits and can concentrate on competent surfaces such as till.

There are multiple gold-bearing units at Granite Creek. Exploration programs can benefit from studying the composition of till (local versus erratic material) and employ techniques such as geophysics and drilling to evaluate and map buried economic units. Placer gold concentrations are variable and reflect the complex climatic cycles that have impacted the study area over the past 130 000 years. Future exploration and development in the upper Granite Creek basin will benefit from stratigraphic and sedimentological modeling to understand the mode of deposition of various units. These can be correlated with the 16 units compiled from this study, which will aid in predicting unit continuity across local exploration areas.

Alpine glaciated environments have likely been overlooked in the past, based on the assumption that placer preservation potential is low in areas that have been glaciated multiple times. This study, and the efforts of the Granite Creek mining community, counteracts this assumption. Targeting areas where known high-grade gold veins are present in an alpine glacier-dominated environment would form the basis for exploration.

Conclusion

The glacial history of the upper Granite Creek basin is recorded in a series of interglacial and glacial deposits. The stratigraphy and sedimentology accessed due to extensive placer mining has allowed reconstruction of the geologic history of the last 130 000 years. This sequence is complex and includes interglacial deposits such as fluvial sand and gravel, and a large proportion of glacial deposits such as outwash, glaciolacustrine and till. Glacial material that correlates to an alpine advance during MIS 4 was identified, which has not been found elsewhere in central Yukon. However, no MIS 4 Cordilleran Ice Sheet deposits affected the upper Granite Creek basin, suggesting the advance did not reach the Gustavus Range. The advance of the CIS into the Granite Creek valley during MIS 2 and MIS 6 caused base level changes in the form of ponding and redirection of local drainage to the west.

Placer gold is dispersed throughout the stratigraphy in several units at varying depths and concentrations. Modern, interglacial and glacial placer deposits were identified in several units across the Granite Creek

valley. One of the main controls on placer gold content is the material that is incorporated into deposits. The presence of local mineralized gold veins can result in till that is enriched in coarse, nuggety placer gold. Glacial processes that entrain interglacial placer deposits can also be economic and result in concentrations of placer gold at false bedrock contacts. Detailed exploration into these units allow for more targeted exploration into these deep environments. These findings can be extended to other formerly alpine glaciated areas in the Cordillera such as northern BC, or in Alaska.

Acknowledgements

This project took place in the Traditional Territory of the Na-Cho Nyäk Dun First Nation. The authors would like to thank Granite Creek Resources, Dulac Mining, Earth and Iron Mines Ltd., Gem Steel Edmonton Ltd., and Archer, Cathro & Associates (1981) Limited for access to mining exposures, hospitality and knowledge. We thank Kenya Franz for providing field assistance. This study was supported by the Yukon Geological Survey, the Natural Sciences and Engineering Research Council of Canada and Polar Canada's Northern Scientific Training Program. Special thanks to Derek Cronmiller and Sydney van Loon for their technical review of this paper. Thank you to Karen MacFarlane of the YGS for a great job with editing and layout.

References

Bond, J.D., 1998. Surficial geology of Keno Hill, Central Yukon (105 M/14). Exploration and Geological Sciences Division, Yukon Region, Indian and Northern Affairs, Canada, Geoscience Map 1998-4.

Bond, J.D., 1999. Glacial limits and ice-flow map, Mayo area, central Yukon (1:250 000 scale). Exploration and Geological Sciences Division, Yukon Region, Indian and Northern Affairs Canada, Open File 1999-13.

Bostock, H.S., 1966. Notes on glaciation in central Yukon Territory. Geological Survey of Canada, Paper 65-36, 25 p, https://doi.org/10.4095/100937.

Boyle, R.W., 1965. Geology, Geochemistry, and Origin of the Lead-Zinc-Silver Deposits of the Keno Hill-Galena Hill Area, Yukon Territory. Geological Survey of Canada, Bulletin 111, 302 p.

Duk-Rodkin, A., 1999. Glacial limits map of Yukon. Geological Survey of Canada, Open File 3694; Exploration and Geological Sciences Division, Yukon Region, Indian and Northern Affairs Canada, Geoscience Map 1999-2, scale 1:1 000 000..

Howes, D.E. and Kenk, E., 1997. Terrain classification system for British Columbia. Version 2. British Columbia Ministry of Environment, Land and Parks, Victoria, B.C.

Jackson, L.E., Ward, B., Duk-Rodkin, A. and Hughes, O.L., 1991. The Last Cordilleran Ice Sheet in Southern Yukon Territory. Géographie Physique et Quaternaire, vol. 45, p. 341–354, https://doi.org/10.7202/032880ar.

LeBarge, W.P., Bond, J.D. and Hein, F.J., 2002. Placer gold deposits of the Mayo area, central Yukon. Exploration and Geological Services Division, Yukon Region, Indian and Northern Affairs Canada, Bulletin 13, 209 p.

Levson, V.M. and Blyth, H., 1993. Applications of Quaternary geology to placer deposit investigations in glaciated areas; a case study, Atlin, British Columbia. Quaternary International, vol. 20, p. 93–105, https://doi.org/10.1016/1040-6182(93)90039-I.

MacDonald, L.E.T. and Bleiler, L.R., 1990. Gold & galena: A history of the Mayo District. The Mayo Historical Society.

Mair, J.L., Hart, C.J.R. and Stephens, J.R., 2006. Deformation history of the northwestern Selwyn Basin, Yukon, Canada: Implications for orogen evolution and mid-Cretaceous magmatism. Geological Society of America Bulletin, vol. 118, p. 304–323, https://doi.org/10.1130/B25763.1.

Mathews, W.H., 1986. Physiographic map of the Canadian Cordillera. Geological Survey of Canada, "A" series map 1701A, https://doi.org/10.4095/122821.

Murphy, D.C., 1997. Geology of the McQuesten River Region, Northern McQuesten and Mayo Map Areas, Yukon Territory (115P/14, 15, 16; 105M/13, 14). Exploration and Geological Services Division, Yukon, Indian and Northern Affairs Canada, Bulletin 6, 122 p.

Read, P.B., McOnie, A. and Iles, S., 2021. Keno Hill Mining Camp. Yukon Geological Survey, Miscellaneous Report MR-21, 35 p.

Roots, C., 1997. Geology of the Mayo Map Area, Yukon Territory (NTS 105M). Exploration and Geological Services Division, Yukon, Indian and Northern Affairs Canada, Bulletin 7, 82 p.

Smith, C.A.S., Meikle, J.C. and Roots, C.F., 2004. Ecoregions of the Yukon Territory: Biophysical properties of Yukon landscapes. Agriculture and Agri-Food Canada, PARC Technical Bulletin No. 04-01, Summerland, British Columbia, 313 p.

Ward, B.C., Bond, J.D., Froese, D. and Jensen, B., 2008. Old Crow tephra (140 ± 10ka) constrains penultimate Reid glaciation in central Yukon Territory. Quaternary Science Reviews, vol. 27, p. 1909–1915. https://doi.org/10.1016/j.quascirev.2008.07.012.

Preliminary results and structural interpretations from drone lidar surveys over the Eastern Denali fault, Yukon

Theron Finley*, Guy Salomon and Edwin Nissen
School of Earth and Ocean Sciences, University of Victoria

Roger Stephen
Department of Geography, University of Victoria

John Cassidy
Pacific Geoscience Centre, Geological Survey of Canada, Natural Resources Canada

Brian Menounos
Department of Geography, Earth, and Environmental Sciences, University of Northern British Columbia

Finley, T., Salomon, G., Stephen, R., Nissen, E., Cassidy, J. and Menounos, B., 2022. Preliminary results and structural interpretations from drone lidar surveys over the Eastern Denali fault, Yukon. *In:* Yukon Exploration and Geology 2021, K.E. MacFarlane (ed.), Yukon Geological Survey, p. 83–105.

Abstract

The Yukon Geological Survey and Kluane First Nation intend to drill a temperature gradient well near Burwash Landing, YT, to evaluate the geothermal energy potential of the area. The preferred drill site is located immediately southwest of the Eastern Denali fault (EDF), which has ruptured multiple times in the Holocene. The kinematics and recent activity of the fault are important factors to consider when developing a geothermal resource, for two purposes: 1. identifying zones of enhanced permeability due to local fault geometry and 2. assessing the seismic hazard of drilling and developing a geothermal system along an active fault. Here, we present new lidar data collected from a drone platform, which enabled the production of 30 cm spatial resolution bare-earth Digital Terrain Models (DTMs) over several segments of the EDF. These products offer a considerable increase in both spatial resolution and canopy penetration compared to existing spaceborne and airborne photogrammetric Digital Surface Models (DSMs) and DTMs of the area. We use hillshades to map segments of the EDF surface trace in detail, and we make preliminary interpretations about the structure and kinematics of the fault. Offset stream channels and hill slopes that cross the fault at high angles indicate dextral offsets ranging between 5 and 75 m. Vertical separation ranges between 0 and 20 m, varying between northeast and southwest-side up. We confirm previous interpretations that the geothermal drill site is located at a minor releasing bend in the fault. Previous fault maps based on ArcticDEM data showed multiple fault splays parallel to the EDF at the geothermal drill site, whereas the lidar data indicate strain is concentrated to a singular fault plane in this area. The EDF is characterized by a series of sediment mounds that we interpret to be positive flower structures. The higher spatial resolution achieved by the drone reveals possible compressional structures (fault tips or folds) consistent with dextral transpression on the surface of these mounds. We recommend additional drone lidar acquisition, field studies, geophysical analysis, and kinematic modeling to be carried out over the coming year.

* tfinley@uvic.ca

Introduction & Motivation

Geothermal Resource Exploration

As part of an effort to assess the potential for geothermal resource extraction in Yukon, the Yukon Geological Survey (YGS) is working with the Kluane First Nation (KFN) to drill a temperature gradient well near the community of Burwash Landing, YT. Burwash Landing is a small community of <100 people and is one of several remote communities in the territory that still relies on diesel fuel for electricity generation. Geothermal energy could, at the very least, provide direct heating for buildings, offsetting demand for electricity. There is particular interest in using geothermal energy for greenhouses, thereby contributing to food security in the community. If the geothermal resource is hot enough, it could also be used for electricity generation. Geothermal energy is one of only a few renewable energy sources that provides base-load (non-intermittent) power, and it does so while emitting very little carbon and requiring minimal physical infrastructure (Kristmannsdóttir and Ármannsson, 2003; IPCC, 2014). Discovering a geothermal resource would be highly beneficial for this community, and Yukon as a whole.

Geothermal conditions in Yukon are generally favourable for development; terrestrial heat flow is in the range of 80–100 mW m^{-2} over a broad area of the territory, which is comparable to values in geothermal fields in the southwestern United States (Blackwell and Richards, 2004; Majorowicz and Grasby, 2010). Despite the high heat flow, there are limited expressions of geothermal activity at the surface (e.g., thermal springs). If significant geothermal resources do exist, they are mostly "blind", suppressed from reaching the surface by permeable surficial deposits, or shallow, cold groundwater plumes (Dobson, 2016). To de-risk drilling, predictive mapping using a variety of geological and geophysical techniques must be employed to prioritize the most favourable zones. Geothermal resources in Yukon are likely amagmatic, fault-controlled, convective hydrothermal systems (Moeck, 2014). In this resource type—best exemplified by the geothermal systems in the Basin and Range province of Nevada—major fault zones act both as reservoirs and conduits for fluid, facilitating deep circulation into the crust (Faulds and Hinz, 2015; Jolie *et al.*, 2015; Craig, 2018). As has been demonstrated in the Basin and Range, detailed mapping of structural features and neotectonic setting can facilitate prediction of where plumes of thermal water might reach economic drilling depths (Faulds *et al.*, 2016; Craig, 2018).

The fault zone that is of interest for geothermal exploration near Burwash Landing is the Eastern Denali fault (EDF), a major Holocene-active structure with significant strike-slip, and possibly dip-slip offset. It has been speculated that the EDF might provide the necessary permeability to allow thermal fluid to ascend to the near surface where it might be economically accessible via drilling (Witter, 2020). A critical part of the geothermal exploration process in fault-controlled domains is locating specific segments of the fault that are likely to be most permeable, and host to the greatest volume of thermal fluid. There are several related factors that contribute to fault permeability, the most important of which are: fault age, strain rate, stress orientation and kinematics. Young, seismically active faults are generally more permeable due to episodic refracturing of mineral precipitate that would otherwise seal the fault (Curewitz and Karson, 1997). Faults with higher strain rate are also generally more permeable, because the re-fracturing occurs more frequently (Faulds *et al.*, 2012). Faults that are oriented favourably in the stress field for slip or dilation tend to remain more permeable, whereas those oriented perpendicular to the stress-field are clamped shut (Meixner *et al.*, 2016). Finally, fault kinematics play a role in the directionality of fluid flow; it has been shown that fluid tends to flow preferentially parallel to σ_2, which implies that strike-slip faults are more conducive to vertical convection of fluid (Sibson, 1996). In the well-studied structurally-controlled geothermal fields of Nevada and elsewhere, detailed structural mapping combined with geophysical data has allowed for the identification of the most favourable structural settings (Curewitz and Karson, 1997; Faulds and Hinz, 2015). These settings include fault tips, stepovers and relays, and intersections where increased fracture density favours hydrothermal upwelling.

There are several methods that are useful for constraining the parameters most relevant to geothermal fluid flow: field-based structural geology, remote sensing, geodesy, and seismology. In a pilot study of geothermal resource potential along the Tintina Fault near Ross River, field-based structural mapping was used to constrain crustal strain, and thus target specific fault strands identified in geophysical models and bedrock mapping (Mira Geoscience, 2015). However, mapping of strain preserved in geologic structures does not reliably provide information about current stress and strain, only strain that occurred sometime in the past. Remote sensing (e.g., LiDAR), geodesy and seismology are therefore helpful tools to evaluate the current tectonic setting of fault-controlled geothermal resources. In a comprehensive early assessment of the geothermal system at Burwash Landing, Witter (2020) used existing photogrammetric DSMs and DTMs (Bender and Haeussler, 2017; Porter *et al.*, 2018) to map out the surface trace of the Denali fault. However, these existing data sets are not quite adequate for the purposes of Holocene fault mapping as they are not true bare-earth DTMs with vegetation stripped away. A key recommendation put forth by Witter (2020) was the acquisition of lidar over the project area to accurately map Holocene faults, and distinguish faults from glacial lineations that run parallel to the EDF. This recommendation was echoed by Blais-Stevens *et al.* (2020) as a means to better understand the kinematics and seismic history of the fault. This report details our efforts to begin to address this data gap.

Previous paleoseismic and remote sensing studies of the EDF

In Alaska, the Central Denali fault has hosted large earthquakes in recorded history, including a M7.9 event in 2002 (Eberhart-Phillips *et al.*, 2003), but the seismic history and hazard on the EDF in Yukon are less well constrained despite nearly 70 years of study. Some of the earliest maps of the EDF were produced by Bostock (1952) using air photos and extensive field investigations. It was possible to recognize the surface trace of the EDF at a broad level without sophisticated remote sensing techniques due to the preferential growth of Black Spruce on a series of sediment mounds that occur along the fault. Bostock recognized that the fault must be young due to the lack of glacial overprint on the fault scarp but did not specify an age range for past ruptures. Clague (1979) built on Bostock's work with further investigation of air photos and glacial geology. He was able to determine that the EDF had likely ruptured in the early and mid-Holocene, but not more recently than 500 years ago, based on undisturbed paleo-shorelines of Kluane Lake. Three paleoseismic trenches were excavated on the EDF near the Duke River by USGS, YGS and Simon Fraser University researchers (Seitz *et al.*, 2008; Lipovsky *et al.*, 2009) but the results were not formally published beyond conference abstracts. Blais-Stevens *et al.* (2020) re-excavated these trenches and integrated other data from lake sediment cores and exposures of Holocene sediment, ultimately concluding that up to four >M_w 6 events have occurred in the last 6000 years. Various geophysical studies have also examined the EDF: Leonard *et al.* (2008) used the earthquake catalog to estimate a slip rate of ~2 mm/yr across this segment of the fault and Marechal *et al.* (2015) obtained a similar slip rate from GNSS velocities. However, it has also been speculated that most of the strain accommodated on the Central Denali fault in Alaska is subsequently partitioned onto either a hypothetical "Connector Fault" through the St. Elias Mountains (Spotila and Berger, 2010; Marechal *et al.*, 2015) or in a diffuse zone to the southwest of the Eastern Denali fault (Choi *et al.*, 2021), in both cases bypassing the EDF itself.

Due to financial constraints, the EDF has not, until now, been widely covered by lidar data. Transport Canada has apparently previously flown lidar over the Denali fault, but these data have not been made available to researchers (Bender and Haeussler, 2017). Small sections of the Denali fault are also captured in lidar data acquired by Yukon Highways and Public Works (https://yukon.ca/en/statistics-and-data/mapping/view-yukon-elevation-data), but these are not sufficient for detailed mapping along strike. In an effort to complement lidar imagery acquired over the Alaskan segment of the Denali fault, Bender and Haeussler (2017) used Agisoft Photoscan (now Metashape) structure-from-motion software to create a 4 m-resolution DSM from legacy aerial photos. This DSM was then used to digitally

map the Denali fault. Marechal et *al.* (2018) also used aerial photogrammetry to measure geometry of distinct tectonic scarps along the fault, and the newly released ArcticDEM data set offers a 2 m-resolution DSM derived from satellite stereo-photographs. However, none of these data sets derived from optical imagery allow for the removal of vegetation from the landscape, adding uncertainty to locations and exact measurements of the fault scarp. In this report, we detail the acquisition of new high-resolution (30 cm pixel) bare earth lidar DTM from a drone platform.

Unanswered questions about the EDF

Despite the number of studies on the EDF, there remain several unanswered questions that lidar data may be able to help answer:

- Efforts to measure the vertical and lateral offset of the EDF have been challenged by large uncertainties in photogrammetric DSMs. For example, Haeussler et *al.* (2017) arrived at a rough estimate of 20–30 m dextral slip based on two offset groves of Black Spruce on sediment mounds. The total offset can be divided to estimate the magnitude of multiple individual events identified in previous studies (e.g., Blais-Stevens et *al.*, 2020). Additionally, lidar data may allow for the discernment of multiple rupture events from variations in marker offsets along strike (e.g., Zielke et *al.*, 2010).
- Limited structural mapping in the vicinity of the proposed geothermal drill site (Witter, 2020) has suggested that the EDF is a broad fault zone with multiple subparallel strands. Existing photogrammetric DSMs do not have the resolution to determine whether multiple strands have ruptured the surface sediments. Lidar data will help confirm whether these subtle parallel lineaments are fault-related or simply glacial features.
- The EDF is characterized by a series of sediment mounds that are interpreted to be positive flower structures (Haeussler et *al.*, 2017; Blais-Stevens et *al.*, 2020). The exact morphology of these mounds is imperfectly represented by the preferential growth of Black Spruce trees on them. Lidar data will allow for the removal of the trees to obtain more accurate measurement of their structure.
- Existing fault maps based on photogrammetric DSMs do not capture fine-scale (10–100 m) variations in fault strike. Lidar data will help identify and measure subtle releasing and restraining bends, which are of particular interest for identifying local zones of extension that may be more permeable to hydrothermal fluid flow.

Data and Methods

Drone Lidar

Over a 10-day period in September of 2021, high resolution lidar data were acquired using a Riegl miniVUX 1UAV lidar scanner mounted on a DJI M600 Pro drone platform (Fig. 1a); sensor position and orientation were concurrently logged with an Applanix APX-20 UAV GNSS-Inertial system. Flight mission and survey planning was done in Map Pilot Pro for iPadOS, utilizing a resampled 30 m resolution DSM derived from ArcticDEM as a baseline for terrain following. Individual flight lines were planned to provide a field of view of ± 30°, with 50% sidelap of adjacent flight lines. For each project area a set of orthogonal flight lines were acquired for boresight calibration. We used standardized flight parameters of 81 m above ground level at a speed of 6 m/s. One flight (Survey 3a) was conducted at half-speed (3 m/s) to acquire points at higher density over a subtle scarp feature. These chosen parameters reflect a trade off between areal coverage and point density that we have arrived at through experimentation. Lower and slower flights allow for data acquisition at much higher point densities, but the areal coverage possible in a single battery set is reduced. At the standard parameters, we achieved a point density of 35–40 pts/m^2 per flight line, and 70–80 pts/m^2 over the majority of each survey area where flight lines overlapped. Flight segments for an individual project area were limited in duration to approximately 20 minutes, necessitating multiple platform launches for most sites and continual recharging of battery sets throughout the day with an on-site generator. At typical survey acquisition parameters, we were able to cover an average of 0.25 km^2 for each set of batteries, although this coverage varied depending on the launch location, transit time to and from the survey, and weather conditions.

Transport Canada strictly regulates the operation of drones in Canada. All three field crew members possessed Advanced Small RPAS Pilot licenses. In every survey, the drone remained within visual line of sight (VLOS) of the pilot-in-command or a remote visual observer in contact via radio. The low height (10–20 m) and low density of the Black Spruce forests made the study area conducive to VLOS flight up to ~1.5 km from an observer. In addition to battery life, a major practical restriction on the length of each survey was connectivity with the controller, which degraded at ~1.5 km in some cases where there was obstructing terrain. In its current configuration, the entire drone system including GNSS survey equipment cannot be easily transported on foot, meaning that the drone must be launched from a site accessible by vehicle. This limitation prevented us from accessing remote segments of the EDF; in the future we hope to develop a more portable system.

A Trimble R12 Real-Time Kinematic Global Navigation Satellite System (RTK-GNSS) consisting of a static base station and a rover was deployed at each project area. The base station (Fig. 1a) was deployed in a location with a clear view of the sky for the length of the airborne survey, typically a few hours, logging GNSS observables. The logged base station data in RINEX format were uploaded to NRCan's Precise Point Positioning tool to determine an absolute base station coordinate referenced to NAD83 CSRS 2002.0. A rover unit (Fig. 1b) was used to survey locations of ground control points deployed in the field. Reflective 1 by 1 m

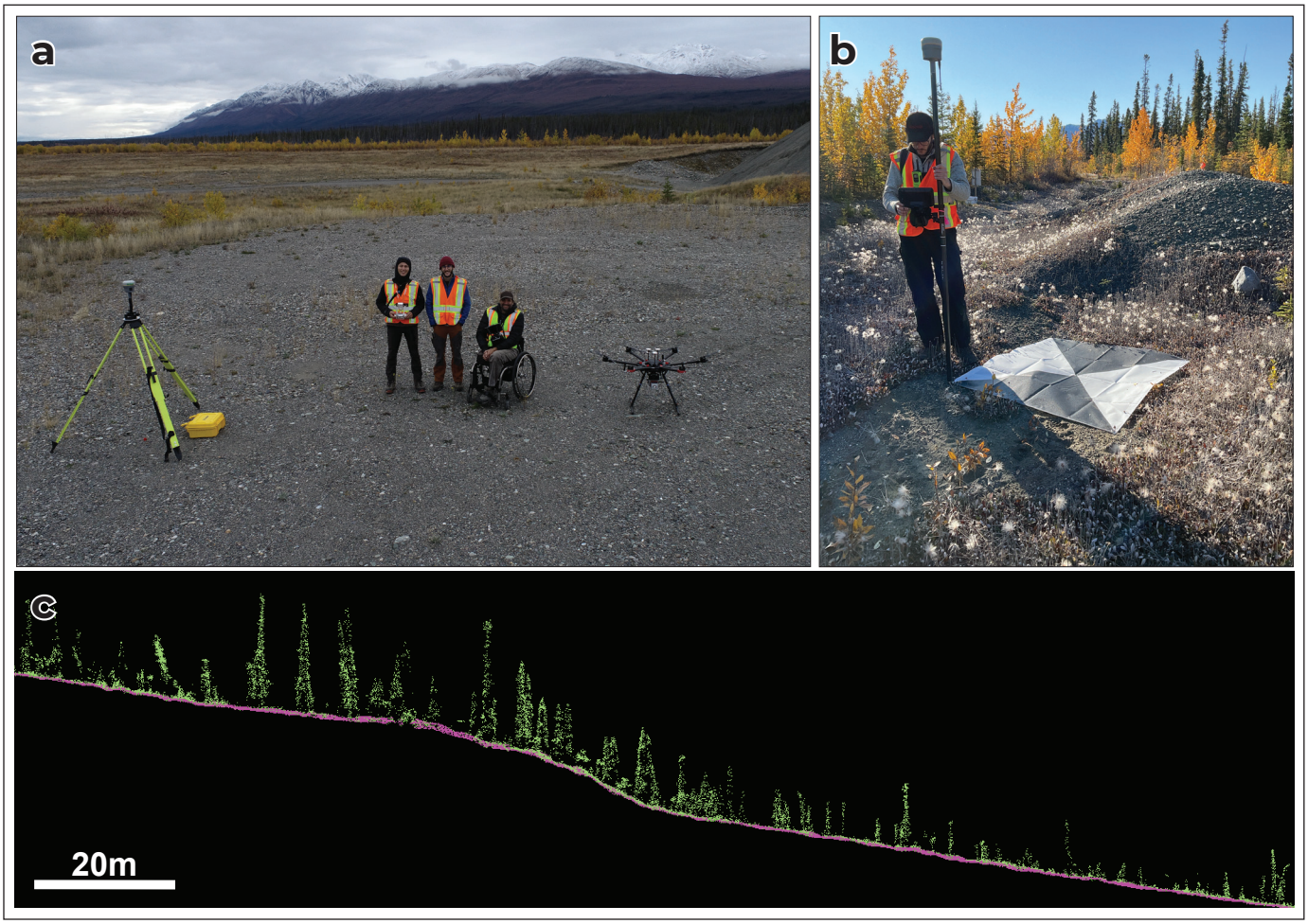


Figure 1. (a) *The field crew at launch site in gravel pit southeast of Duke River, with the DJI Matrice M600 drone, and RTK GNSS base station.* ***(b)*** *Collecting ground control point coordinates with the RTK rover unit and portable 1 m² fabric targets.* ***(c)*** *Lidar point cloud swath profile (5 m wide) across EDF scarp at Quill Creek. Points are coloured according to classification: ground (pink) and vegetation (green). Note that some points on the ground are coloured green, indicating the classification scheme could be improved.*

fabric squares with black and white quadrants were used as ground control targets (Fig. 1b). Following the field acquisition, rover acquired GNSS positions were calibrated and referenced to the base station absolute coordinates.

Trajectories acquired with the APX-20 GNSS-Inertial system were refined and post processed in single base mode with the Trimble GNSS base station using POSPac UAV. Laser data were processed using Riegl's RiProcess package. A rudimentary point classification was applied in RiProcess. As shown in Figure 1c the classification does not perfectly separate ground (pink) and vegetation (green) returns, and future efforts will focus on improving this classification. The resulting .las file was converted to a bare-earth DTM using a Triangular Irregular Network (TIN) algorithm in the LAStools software suite. Experimentation showed that a 30 cm pixel size was appropriate for the point density; attempts at finer resolution suffered from excess noise. The DTMs presented in this report are not final. Future efforts will focus on calibrating between individual flight lines, which do not currently align perfectly. Finally, the current data sets have not yet been adjusted with ground control points, so while they are relatively internally consistent, their spatial accuracy can be improved.

Survey Locations

Drone survey locations were selected and prioritized based on their scientific merit as well as the practical constraints of drone surveying, as discussed in the preceding section. The highest priority sites were located along the east and west sides of the Duke River, where geothermal drilling is to take place in the coming year. Secondary sites of interest were selected based on interesting features (e.g., potential offset markers) observed in existing satellite imagery that warranted closer examination. The regional map in Figure 2 shows the locations of the drone surveys in relation to one another along the EDF. In total, 4 km^2 of lidar data were acquired. A summary of each survey site follows.

Duke River Central (Surveys 1-3)

Three areas (Surveys 1–3) centred on the Duke River, collectively totaling 1.55 km^2, were surveyed over a period of 3 days (Fig. 3). An additional 0.19 km^2 survey (Survey 3a) was flown at half speed (3 m/s) to acquire higher resolution data over a subtle scarp feature on the abandoned river terrace. This topographic surface is likely younger than other locations where the fault is observed, and thus could constitute a tighter bound on the age of the most recent fault activity. The drone was launched from several open spots on the dirt road

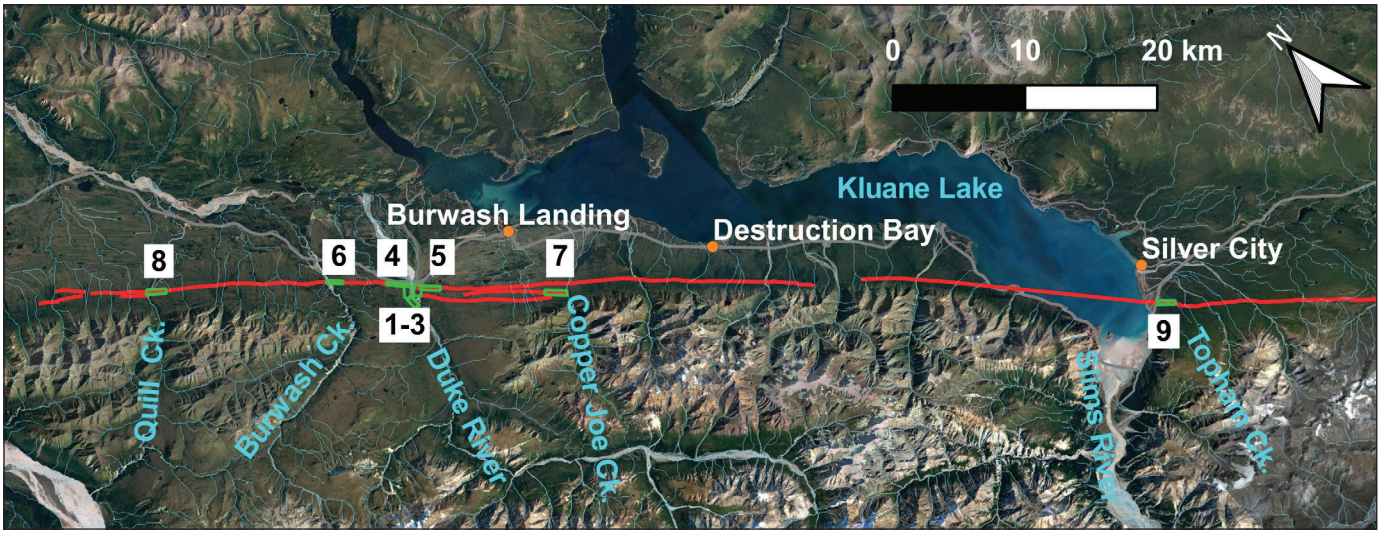


Figure 2. *Regional map of study area on southwest side of Kluane Lake. EDF surface trace (red line) is from Bender and Haeussler (2017). Numbered green polygons indicate the locations of high-resolution drone lidar acquisitions: 1–3. Duke River Central; 4. Duke River Northwest; 5. Duke River Southeast; 6. Burwash Creek; 7. Copper Joe Creek; 8. Quill Creek; 9. Topham Creek. See Figure 3 for detailed map of surveys 1–5, and Figure 4 for detailed maps of surveys 6–9.*

leading to the Donjek Route trailhead on the northwest side of the Duke River, and from two open meadows on the abandoned river terrace on the southeastern side of the Duke River. Visual observers were stationed in open meadows at the edges of the survey areas farthest from the launch sites to maintain constant VLOS. These survey areas were selected to cover the highest priority geothermal drill sites proposed by Witter (2020). The final selection for the geothermal test well is contained within Survey 1, and two other recommended sites are contained in Survey 3. Survey 2 was conducted to provide continuous lidar coverage from the known EDF fault trace (Survey 4) to the selected drill site (Survey 1). Based on ArcticDEM data, Witter (2020) suggested a possible secondary parallel strand of the EDF only 200 m northeast of the final drill site selection (Fig. 3). A critical goal of Survey 2 was to determine whether this fault strand disturbs the Holocene land surface, or whether the observed features are just glacial lineaments. The results of Surveys 1–3 are shown in Figure 5.

Duke River Northwest (Survey 4)

A linear swath totaling 0.42 km^2 was surveyed on the northwest side of the Duke River along the known trace of the EDF, requiring a half-day deployment (Fig. 3). The drone was launched from the broad ditch on the northeast side of the Alaska Highway and a visual observer was stationed on the southwest side of the EDF. This survey is immediately northwest along strike

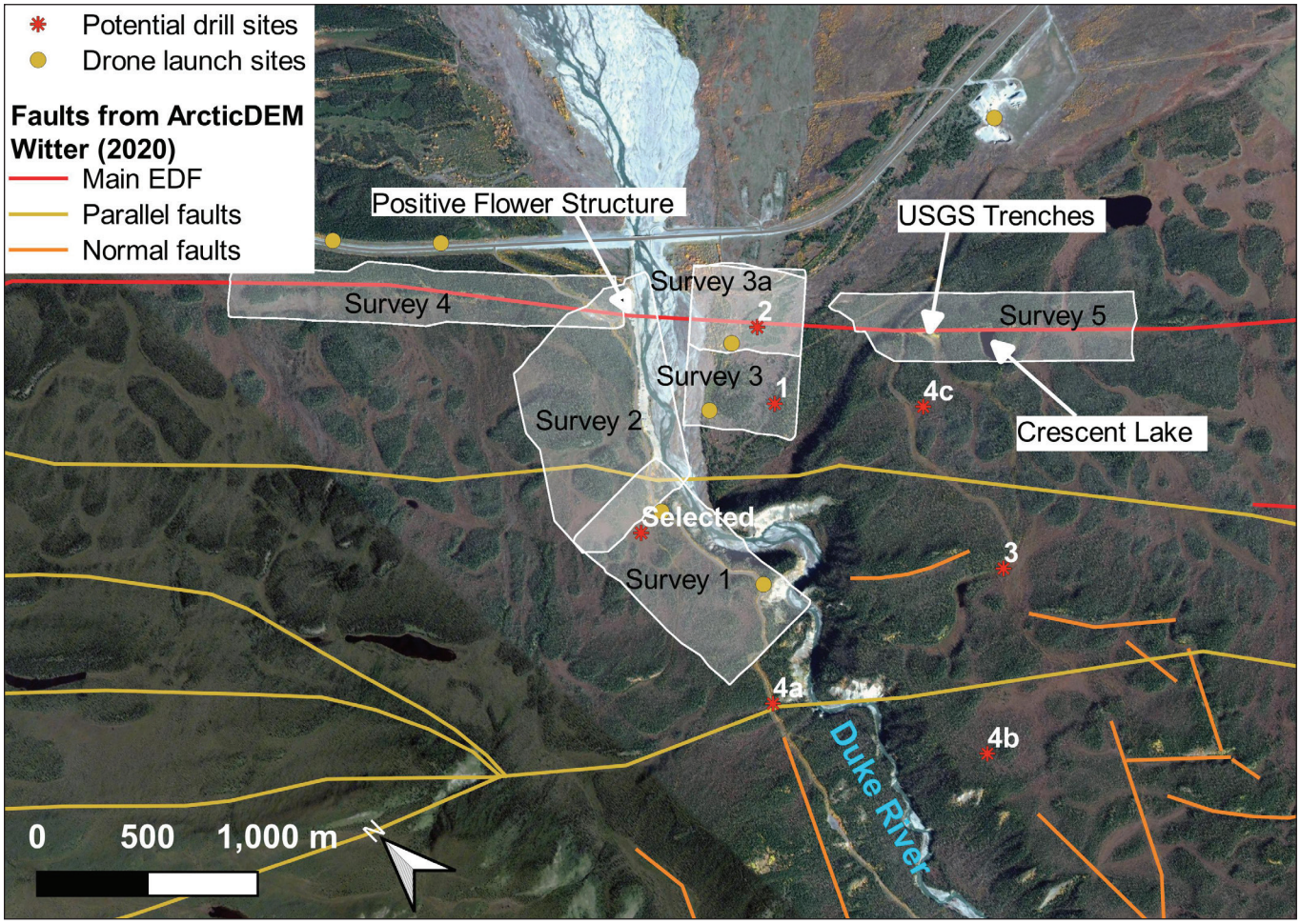


Figure 3. *Map of Surveys 1–5 (transparent polygons) in the vicinity of the Duke River. Faults interpreted by Witter (2020) are based on lineaments in ArcticDEM data. Preferred geothermal drill sites from Witter (2020) are also indicated with red dots. Locations of paleoseismic study sites discussed in Blais-Stevens et al. (2020) are labelled.*

from a positive flower structure that is bisected by the Duke River, as discussed by Blais-Stevens et *al.* (2020). The main goal of this survey was to cover sediment mounds along strike that are inferred to be similar structures. The results of Survey 4 are shown in Figure 6.

Duke River Southeast (Survey 5)

A linear swath totaling 0.39 km^2 was surveyed on the southeast side of the Duke River along the known trace of the EDF, requiring a half-day deployment (Fig. 3). The drone was launched from a Department of Highways and Public Works gravel pit on the southwest side of the Alaska Highway. Good sight lines from the launch site meant that no remote visual observer was necessary for this survey. This survey was designed to cover the highly studied segment of the EDF, where paleoseismic trenches and sediment cores from Crescent Lake have been used to infer up to 4 major earthquakes in the past 6000 years (Lipovsky et *al.*, 2009; Haeussler et *al.*, 2017; Blais-Stevens et *al.*, 2020). The results of Survey 5 are shown in Figure 7.

Burwash Creek (Survey 6)

An area of 0.37 km^2 was surveyed on the southeast side of Burwash Creek, 6 km northwest of the Duke River, requiring a half-day deployment (Fig. 4a). The drone was launched from a flat gravel area adjacent to a dirt road used by placer miners and a visual observer was stationed in the central part of the survey area to ensure VLOS. The intention of this survey was to capture the Denali fault at the nearest accessible location along strike from the central Duke River study area. Additionally, it appeared as though the fault crosses at least one abandoned terrace of Burwash Creek (Fig. 4a), which may provide some constraint on multi-event earthquake chronology. The results of Survey 6 are shown in Figure 8.

Copper Joe Creek (Survey 7)

An area of 0.43 km^2 was surveyed on the northwest side of Copper Joe Creek, 12 km southeast of the Duke River, requiring a half-day deployment (Fig. 4b). The drone was launched from a small gravel parking area at the trailhead for the Donjek Route. VLOS for the pilot

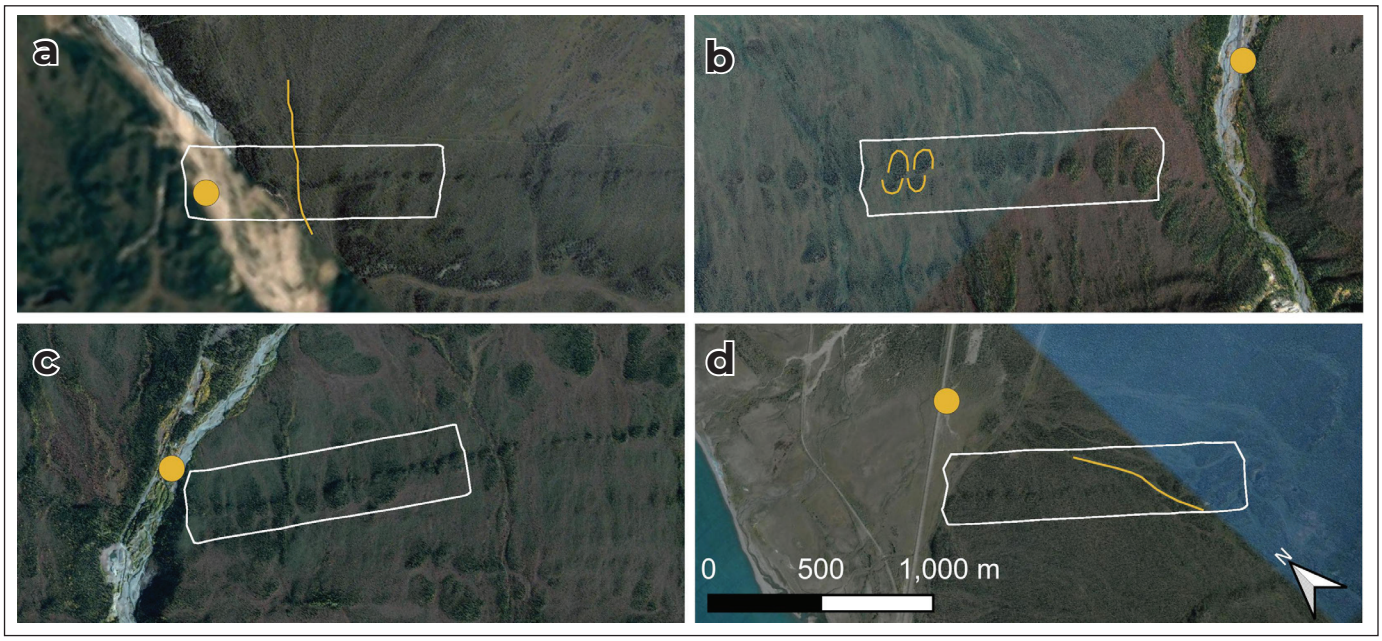


Figure 4. *Satellite imagery showing local context of Surveys 6–9. All maps are at the same scale and orientation. Yellow dots indicate drone launch sites.* ***(a)*** *Survey 6 on the southeast side of Burwash Creek. Yellow line shows possible edge of abandoned river terrace;* ***(b)*** *Survey 7 on the northwest side of Copper Joe Creek. Yellow lines show two offset mounds discussed by Haeussler et al. (2017) and Blais-Stevens et al. (2020);* ***(c)*** *Survey 8 on the southeast side of Quill Creek;* ***(d)*** *Survey 9 at the southeast end of Kluane Lake at Topham Creek. Yellow line shows trace of Topham Creek as it crosses the fault scarp.*

in command was challenging at this site due to a hill near the launch site blocking the view to the northwest, so a visual observer hiked approximately 1 km along the survey footprint to maintain visual contact with the drone. The primary goal of this survey was to capture lidar imagery of sediment mounds along the fault that have been interpreted in previous studies (Bender and Haeussler, 2017; Blais-Stevens *et al.*, 2020) as evidence of 20–30 m of dextral offset (Fig. 4b). The results of Survey 7 are shown in Figure 9.

Quill Creek (Survey 8)

An area of 0.39 km^2 was surveyed on the southeast side of Quill Creek, 20 km northwest of the central Duke River study area, requiring a half-day deployment (Fig. 4c). The drone was launched from a gravel pull out adjacent to a prospector's cabin on the northwest side of the river. A large hill halfway along the survey swath obscured the view of the farthest extent of the survey, so a visual observer hiked to this location to maintain VLOS. This site was chosen to extend our survey coverage as far to the northwest as was practically possible within this field season. Additionally, this fault segment strikes ~10° more westerly than the other segments and appears to have a distinct right-stepping bend highlighted by a large grove of Black Spruce (Fig. 4c). The results of Survey 8 are shown in Figure 10.

Topham Creek (Survey 9)

An area of 0.41 km^2 was surveyed at the southeast end of Kluane Lake adjacent to Topham Creek, 56 km southeast of the Duke River study area, requiring a half-day deployment (Fig. 4d). The drone was launched from a flat gravel area on the south side of the Alaska Highway. This is the farthest southeast location where the EDF trace is both accessible and clearly observable in satellite imagery; obtaining measurements here is important for understanding the size and length of past surface ruptures. Additionally, this is one of few locations where the fault climbs significantly in elevation along-strike, which may help with measuring 3D fault offset. Finally, Topham Creek crosses the fault at an oblique angle here and we speculated it might be used as a displacement maker (Fig. 4d). The results of Survey 9 are shown in Figure 11.

Results and preliminary interpretations

Duke River Central Area (Surveys 1–3)

Likely owing to ease of access, the central Duke River area is one of the most thoroughly studied sections of the EDF, and is featured in papers and reports by Clague (1979), Seitz *et al.* (2008), Lipovsky *et al.* (2009), Witter (2020) and Blais-Stevens *et al.* (2020). Nevertheless, lidar data do provide some new insight for this area. Most notably, the fault makes a distinct 7° right-stepping bend as it crosses the low-lying abandoned river terrace on the southeastern side of the Duke River (Fig. 5). This right-stepping bend likely represents a releasing bend in a dextral system, and although it was identified by Witter (2020) in ArcticDEM data, the lidar data allow for a more accurate determination of the true geometry. The red dots in Figure 5 indicate discrete inflection points where the fault changes strike. Also noteworthy here is the fact that the fault scarp on the abandoned river terrace is sharper and narrower than the fault trace to the east and west (Fig. 5 inset). Vertical separation is less than 2 m, down to the northeast. The sediment mounds that characterize the majority of the EDF elsewhere along strike are non-existent on this short segment. This segment is one of very few places along the fault where a scarp is observed deforming a young fluvial surface, as opposed to an older glacially-affected surface. Furthermore, there appears to be a stream channel offset by 5–10 m across this scarp (Fig. 5 inset), which is smaller than dextral offsets measured elsewhere along strike. It may be that the fault scarp here records only the youngest rupture event, whereas the larger more complex fault traces elsewhere represent multiple ruptures. The lack of sediment mounds and the slight change in strike is consistent with this segment undergoing oblique dip-slip faulting to accommodate localized extension in this dextral releasing bend.

The lidar data also allow for definitive classification of other lineaments as non-tectonic. Witter (2020) used ArcticDEM data to trace out potential parallel strands of the EDF. One of these lineaments is indicated with the white arrows in Figure 5. This feature does appear to be a southwest-side-up terrace of some sort, but there is not a distinct fault scarp observed in the lidar here.

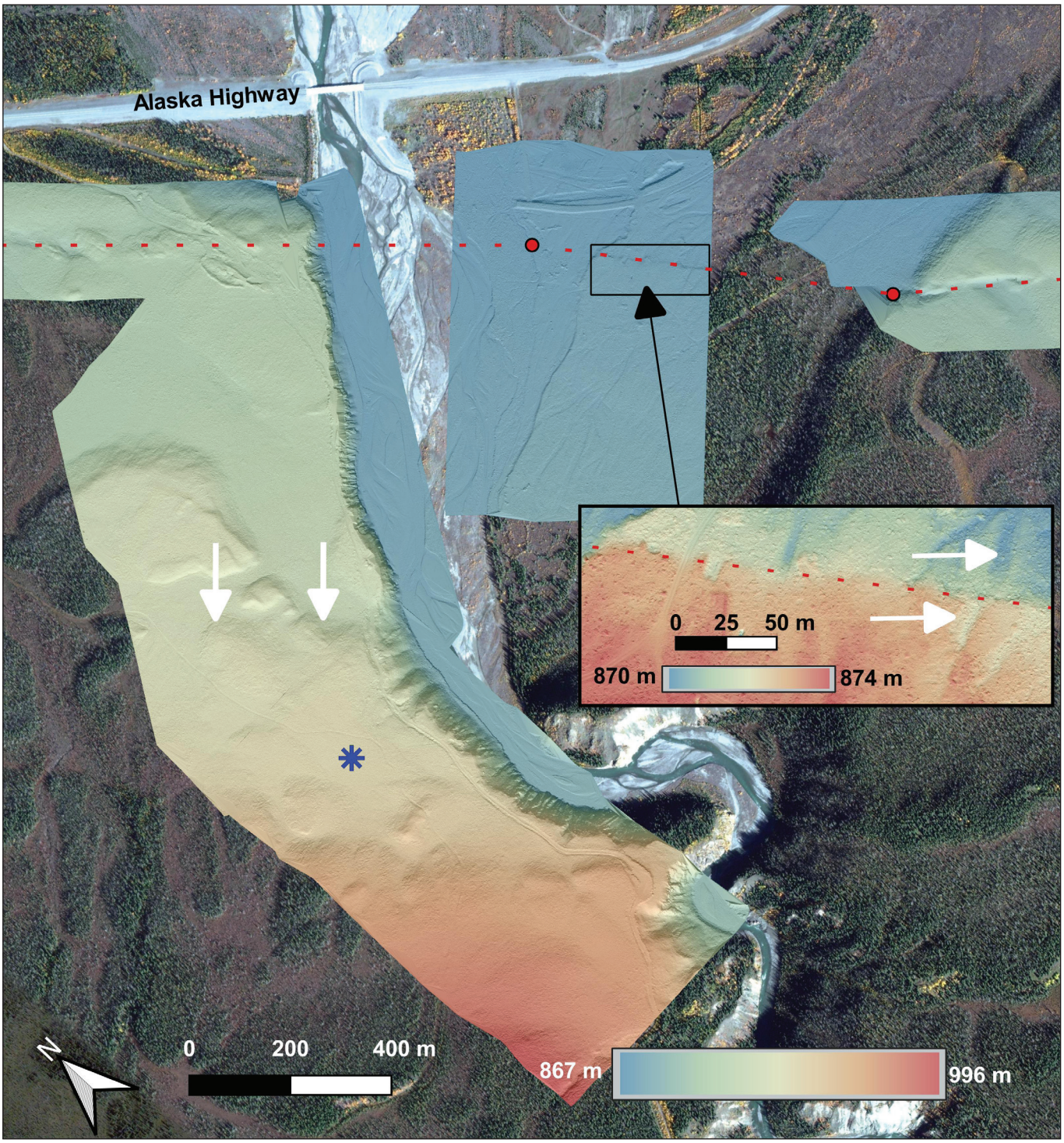


Figure 5. *Lidar hillshade (30 cm resolution) of the central Duke River study area (Surveys 1–3 and parts of 4 and 5). Dashed line shows the surface trace of the main strand of the EDF. Red dots indicate inflection points where the fault makes a discrete 7° right-stepping bend to form a possible releasing bend. White arrows indicate a feature interpreted by Witter (2020) as a Holocene fault scarp. The blue star shows the chosen drill site, 1 km southwest of the main EDF. Inset hillshade shows detail of fault scarp at 10 cm resolution (Survey 3a) where it crosses abandoned river terrace; white arrows indicate possible 5–10 m dextral offset in old stream channel at southeast end of inset.*

If this lineament is a fault scarp it is much older than the main trace of the EDF, having had time to become eroded and more diffuse.

The selected geothermal drill site is shown with the blue star in Figure 5. It is approximately 1 km southwest of the main strand of the Denali fault. The lidar data indicate there are no Holocene fault scarps in the immediate vicinity of the drill site. However, while in the field, we examined the cliffs on the northwest side of the Duke River immediately below a topographic bench interpreted as a fault by Witter (2020). In the cliff, there does appear to be a significant bedrock fault that coincides with this topographic feature, but it is unclear whether it breaks through into unconsolidated Late Quaternary sediments. These observations (which will be reported in more detail in subsequent reports), and mapping of numerous bedrock faults in the canyon walls of Burwash Creek by Witter (2020) together indicate that the EDF is a broad fault zone, with only one strand currently active and visible in lidar. The older strands that do not have apparent Holocene surface ruptures, may still be permeable to hydrothermal fluid.

Duke River Northwest (Survey 4)

The fault scarp is subdued and relatively narrow at the Duke River Northwest site (Fig. 6). There does not appear to be any consistent sense of vertical separation across the fault in this survey area. A series of small sediment mounds occur along the fault trace here. These mounds are roughly 40 by 40 m (smaller than many other mounds observed along strike). We interpret these mounds to represent en echelon push-ups (Fig. 6 inset), or "mole tracks" which are often associated with large strike-slip displacements (Little *et al.*, 2021).

Duke River Southeast (Survey 5)

The fault scarp is very distinct at the Duke River Southeast site (Fig. 7). This survey covers the locations of three paleoseismic trenches excavated by Seitz *et al.* (2008) and revisited by Blais-Stevens *et al.* (2020). Crescent Lake, from which sediment cores were retrieved and studied by Blais-Stevens *et al.* (2020), is also covered. This segment of the fault is northeast-side-up, with a vertical separation in the range of 3–8 m. Although not fully covered by the drone survey, the old riverbank at the northwestern end of the survey appears to be dextrally offset by 30–40 m. On the northeast side of the fault, a regular pattern of east-west trending lineations repeated on an ~5 m wavelength appear on the outer edge of broad mounds (Fig. 7 inset). These features are not simply artifacts of the hillshade effect and appear regardless of light source azimuth. These may record north-south compression in the surficial sediments, though it is also possible they are related to frost slumping. They

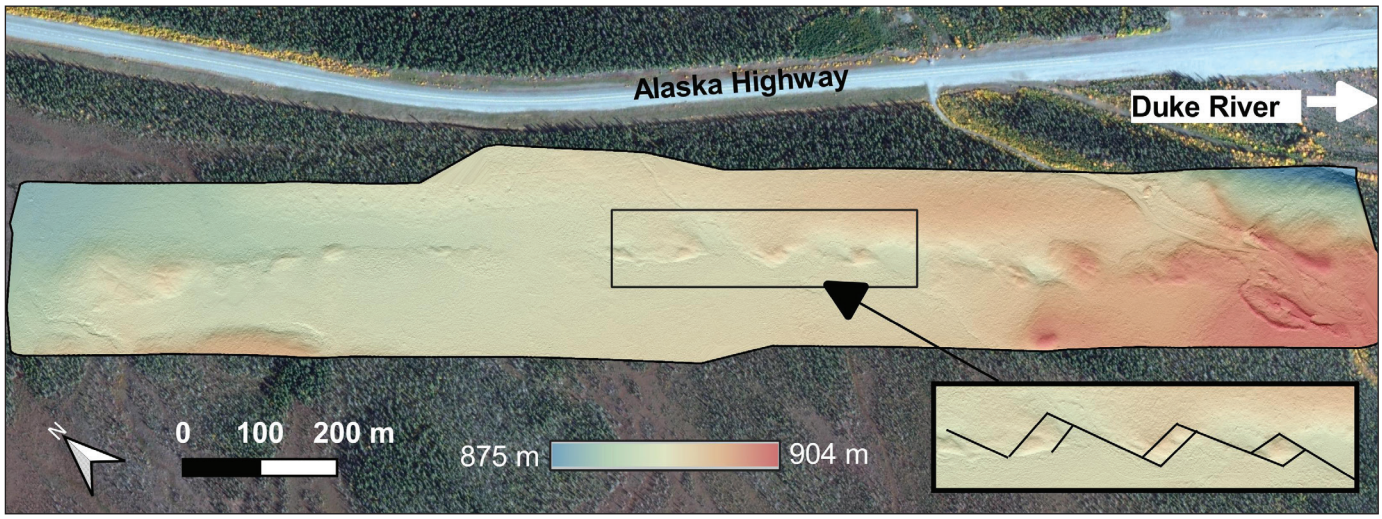


Figure 6. *Survey 4 lidar hillshade (30 cm resolution) of the EDF on the northwestern side of the Duke River. Inset shows possible interpretation of sedimentary mounds as en echelon positive flower structures.*

will be more thoroughly investigated as possible strain recorders in future work. It is worth noting that these features would not be easily discerned in typical 1 m resolution airborne lidar.

Burwash Creek (Survey 6)

The fault scarp at Burwash Creek (Fig. 8) is moderately distinct in the landscape, although the surface expression in the northwestern part of the survey area is obscured by the braided river channel and recent placer mining excavations on the riverbanks. At this site, the fault scarp does not have distinct vertical separation, although the fault trace itself is characterized by several sediment mounds. The curvature of the hill in the southwestern corner of the survey appears to be dextrally offset, but this is an imprecise marker. Similar to Survey 5, linear east-west structures are observed on the northern slopes of the sediment mounds (Fig. 8 inset). It is possible these are related to freeze-thaw cycles on north-facing slopes, but if so, it is difficult to understand why they occur at oblique angles (45°) to the slope dip direction in most cases.

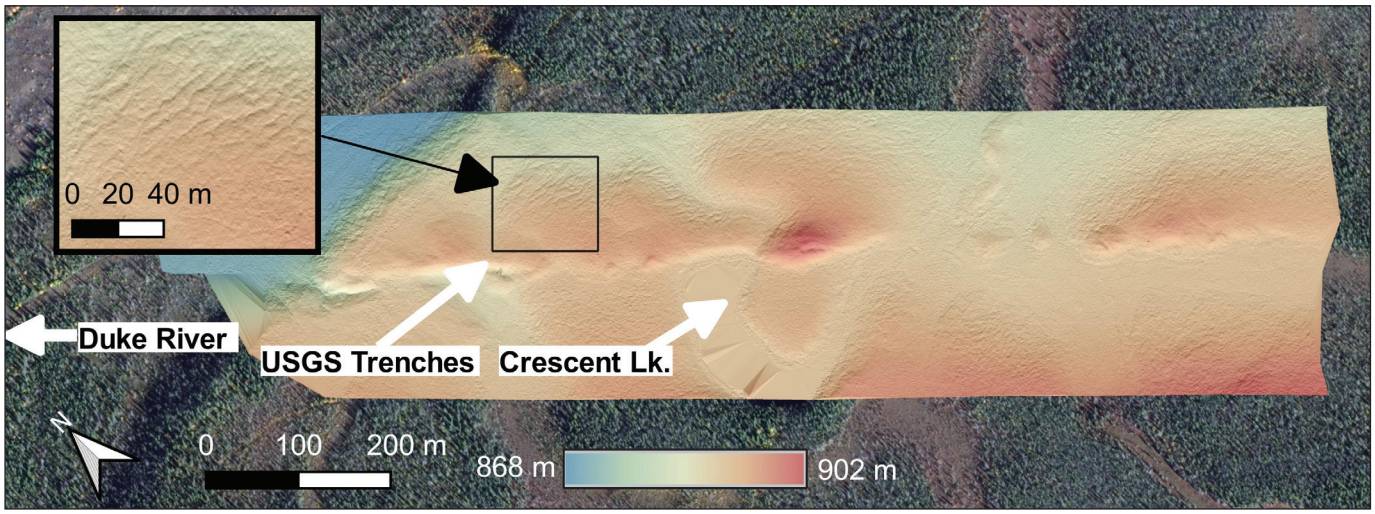


Figure 7. *Survey 5 lidar hillshade (30 cm resolution) of the EDF on the southeastern side of the Duke River. Locations of the USGS trenches and Crescent Lake (discussed by Blais-Stevens et al. (2020)) are indicated. Inset shows east-west trending fold-like structures.*

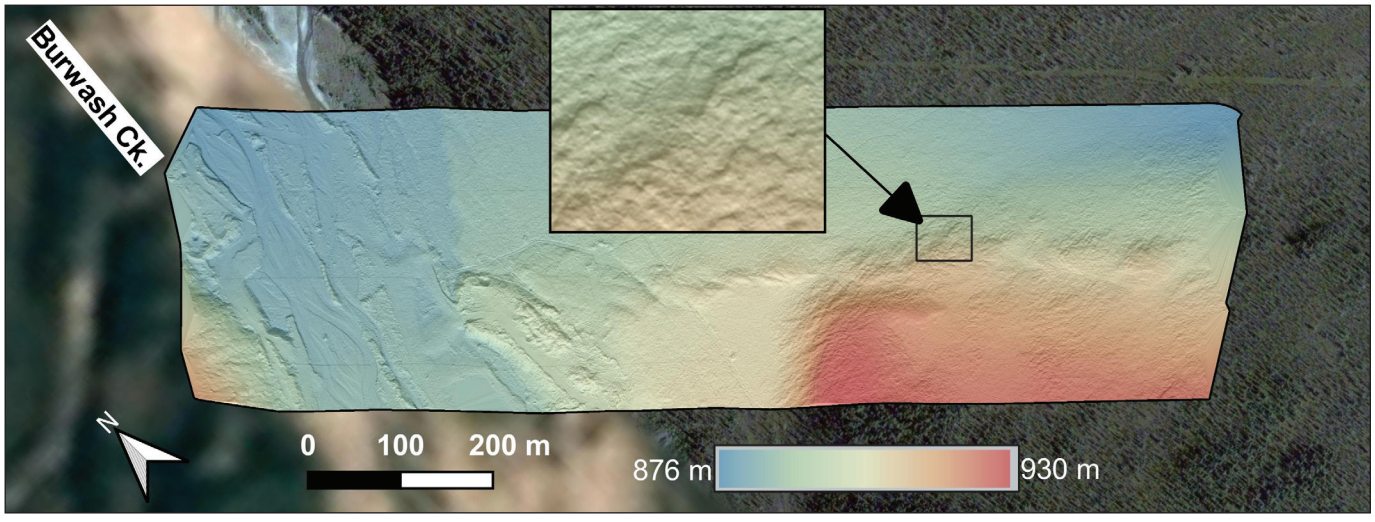


Figure 8. *Survey 6 lidar hillshade (30 cm resolution) of the EDF on the southeastern side of Burwash Creek, 13 km northwest of Burwash Landing. Inset shows east-west trending lineations.*

Copper Joe Creek (Survey 7)

Despite being quite distinct in satellite imagery, the fault scarp at Copper Joe Creek is not very distinct in the lidar hillshade (Fig. 9). The strike of the fault appears variable, and it is not clear if there is any vertical separation. The pair of mounds at the northwestern end of the survey are the same pair of mounds from which Haeussler et *al.* (2017) estimated a dextral offset of 22.5 +7.5/–2.5 m. It may be possible to derive a more accurate estimate of offset from the lidar data, however, with the vegetation stripped away, the boundaries of these markers actually become less distinct than the Black Spruce groves visible in satellite imagery (Fig. 4b). Notably, no other mounds in this survey area appear to be offset by the fault trace. It may be that the apparent offset of the Black Spruce groves is deceptive and there is not actually any discrete offset between the mounds; rather, the mounds may just be coincidentally shaped in a way that gives the illusion of offset. If the mounds are offset, they must record multiple earthquake ruptures: at least one to have formed them in the first place, and probably at least two more to achieve such large lateral separation. In the southeastern end of the survey area, the fault appears to make a 100 m right-stepping bend, which may represent a releasing bend. Similar to Surveys 5 and 6, a series of ~5 m wavelength east-west trending lineations appear on the north slopes of the sediment mounds (Fig. 9 inset).

Quill Creek (Survey 8)

The fault scarp at Quill Creek is very distinct in the lidar hillshade (Fig. 10). It is consistently southwest-side up, with a vertical separation of 8–16 m. The southeastern part of the surveyed fault segment is characterized by a series of 10 distinct en echelon mounds with their long axes oriented east-west, and short axes oriented north-south. The northwestern part of the survey area has mounds, but they are less distinct. The largest mound, in the centre of Figure 10, is ~100 × 120 m and rises 20 m above the down-dropped (northeastern) side of the fault. This mound corresponds to a distinct left-stepping bend in the fault and is therefore likely a restraining bend/positive flower structure (Fig. 10 inset). The northern slope of this mound exhibits east-west trending lineations similar to those observed in previous surveys.

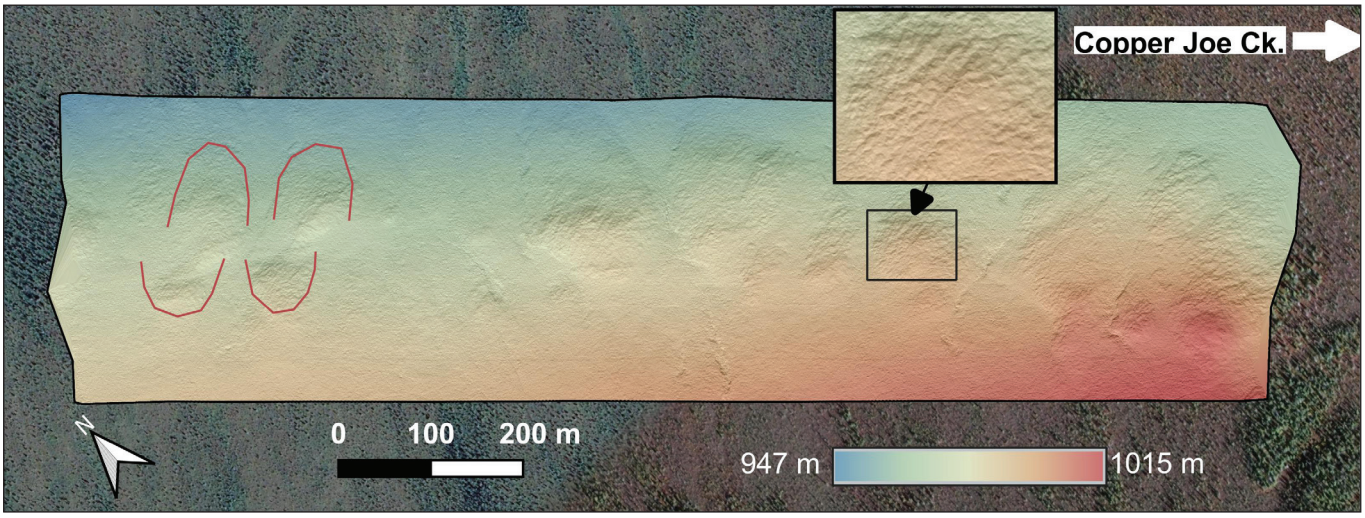


Figure 9. *Survey 7 lidar hillshade (30 cm resolution) of the EDF on the northwestern side of Copper Joe Creek, 5 km south of Burwash Landing. Pink lines show outlines of possible offset mounds discussed in Haeussler et al., (2017) and Blais-Stevens et al. (2020). Linework is based on the boundaries of Black Spruce groves, as the boundaries of the mounds are less distinct. Inset shows detail of east-west lineations visible on north sides of all sedimentary mounds, similar to Survey 5 and 6.*

Topham Creek (Survey 9)

The fault scarp at Topham Creek is very distinct in the lidar hillshade (Fig. 11). It is consistently southwest-side up, with a vertical separation of approximately 8–12 m. Where Topham Creek crosses the fault scarp, it deviates course by ~20°. This channel offset is suggestive of dextral displacement up to a maximum of 75 m. However, due to the oblique angle at which the stream intersects the fault, obtaining an good estimate of offset is challenging; software tools such as LaDiCaoz (Zielke and Arrowsmith, 2012) or 3D Fault Offsets (Stewart et *al.*, 2018) may be appropriate for obtaining more accurate measurements of displacement.

Discussion

Fault kinematics and displacement

Compared to previously available DEMs of the EDF, the drone lidar data allow for much higher-confidence estimations of kinematics and fault displacement from geomorphological features (Fig. 12). Lateral offsets observed in multiple surveys and the geometry of the "mole tracks" all consistently indicate dextral slip. The amount of apparent dextral slip varies from a minimum of 5 m at the Duke River abandoned river terrace to 75 m at the Topham Creek site.

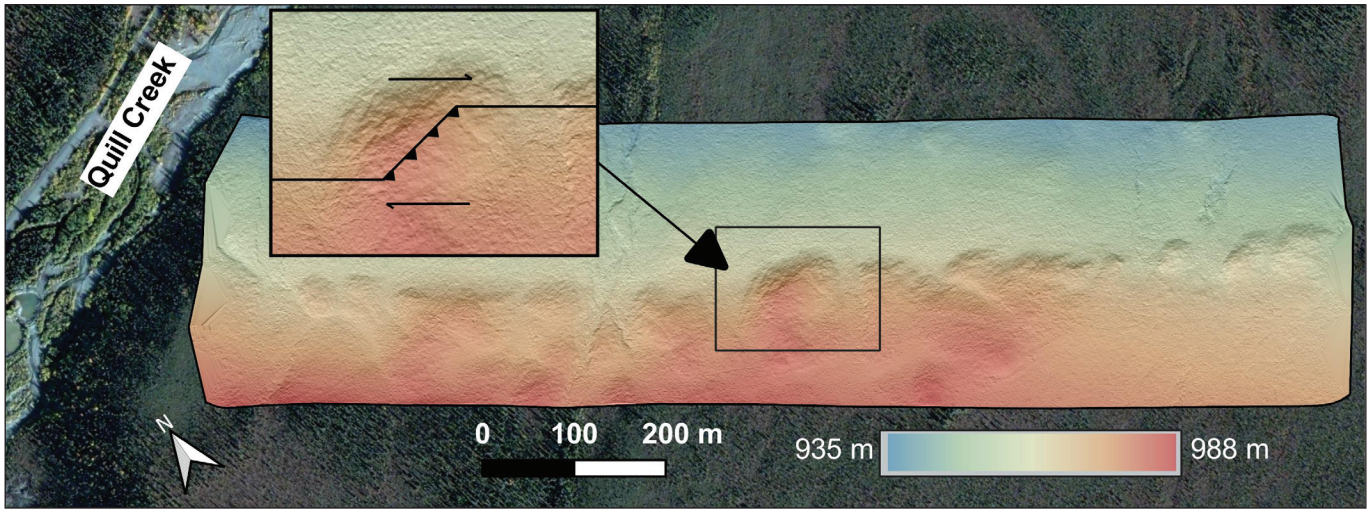


Figure 10. *Survey 8 lidar hillshade (30 cm resolution) of the EDF on the southeastern side of Quill Creek, 27 km northwest of Burwash Landing. Inset shows interpretation of large sediment mound as a restraining bend.*

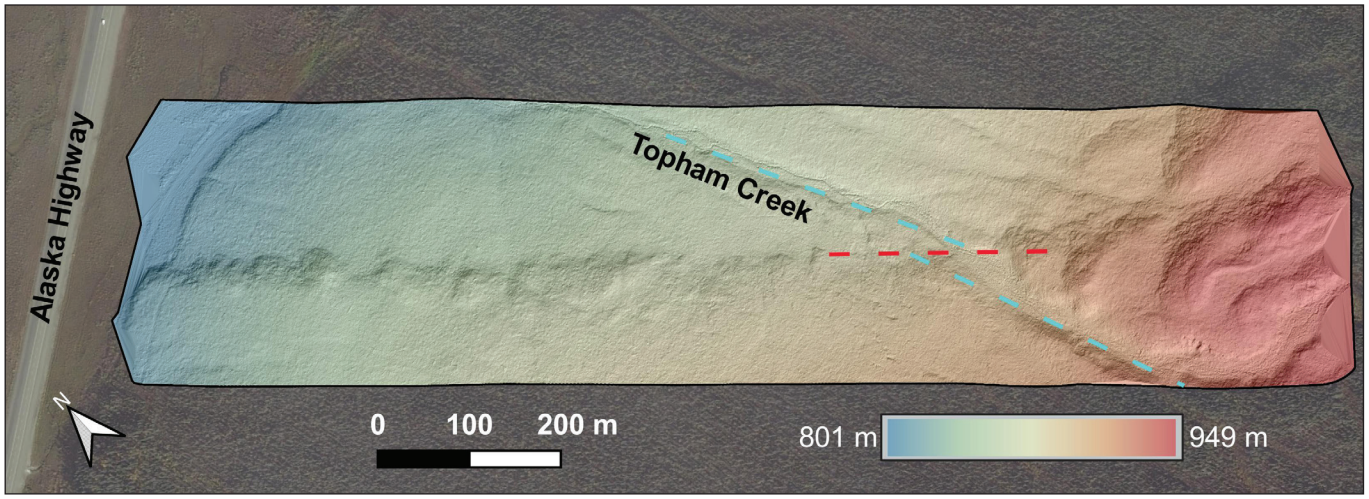


Figure 11. *Survey 9 lidar hillshade (30 cm resolution) of the EDF at Topham Creek near the southeastern end of Kluane Lake. Red dashed line is the approximate trace of the fault; cyan dashed lines are the offset projections of Topham Creek channel on either side of the fault, indicating a possible dextral offset of ~75 m.*

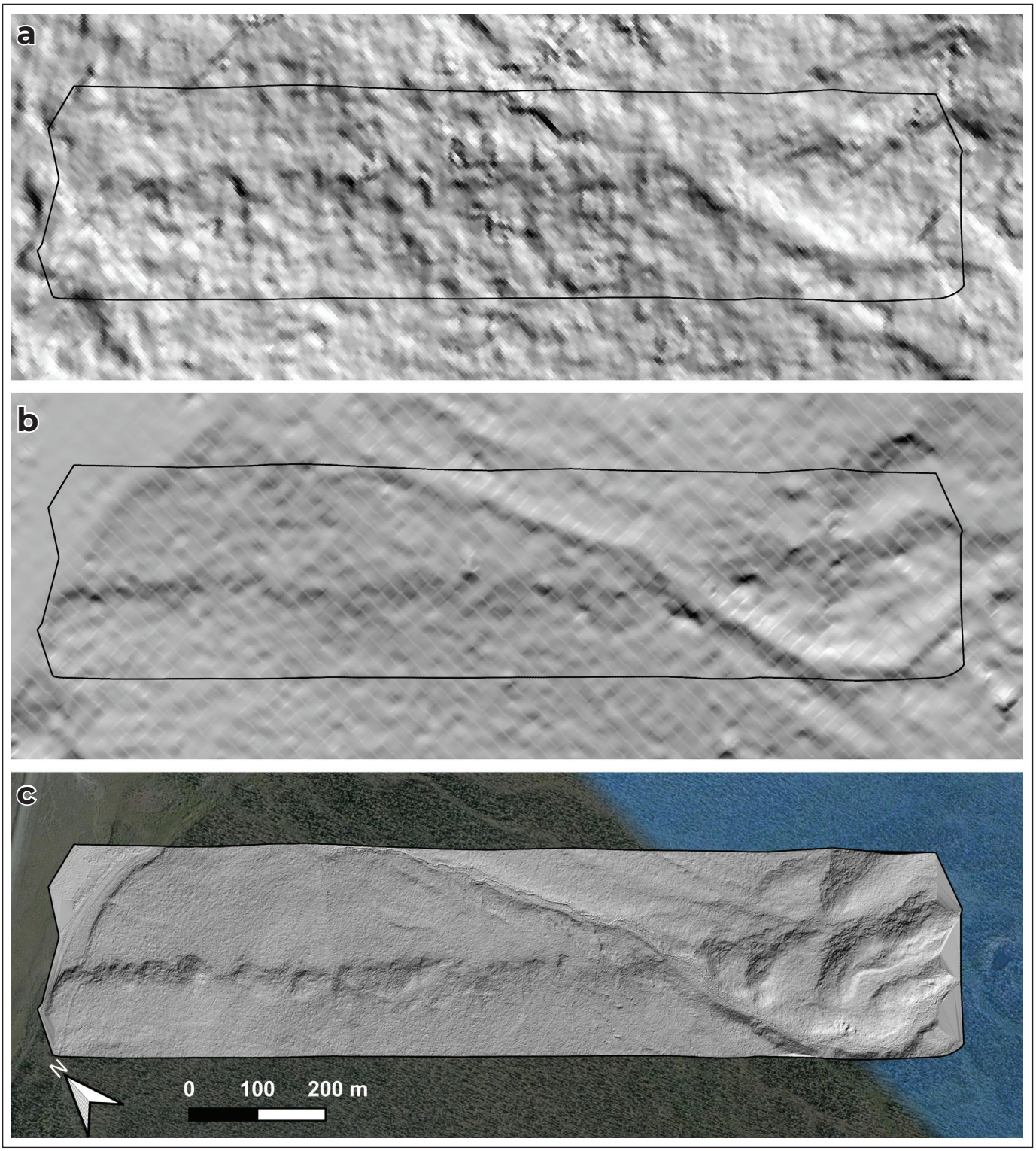


Figure 12. *Comparison between the drone lidar DTM from this study and DSMs from which previous maps and interpretations of the EDF have been made. All panels are the same scale and orientation at the Topham Creek site (Survey 9).* ***(a)*** *The 4 m photogrammetric DSM hillshade produced from air photos by Bender and Haeussler (2017).* ***(b)*** *The 2 m ArcticDEM hillshade produced from optical satellite imagery by Porter et al. (2018).* ***(c)*** *30 cm DTM produced by our lidar drone platform.*

If these offsets are valid, the larger ones likely record multiple earthquake ruptures, while the smaller ones on younger fluvial surfaces may only record a single rupture. Vertical separation is more variable, ranging among no separation, <2 m to 20 m of southwest-side-up separation at Duke River, Quill Creek and Topham Creek, and 3–8 m of northeast-side-up separation at Duke River Southeast. The variability of vertical separation along strike supports the notion that rupture on the EDF is predominantly strike-slip. Several features, in particular the offset channel of Topham Creek (Fig. 11), the offset sediment mounds at Copper Joe Creek (Fig. 9), and the offset river channel on the abandoned Duke River (Fig. 5 inset), may allow for accurate estimates of three-dimensional fault displacement using software tools such as LaDiCaoz (Zielke and Arrowsmith, 2012) or 3D-Fault-Offsets (Stewart *et al*., 2018).

The high spatial resolution of the drone lidar is also useful in allowing an improved understanding of the structure of the somewhat enigmatic sediment mounds which occur along the fault trace. It is apparent that in many places these mounds have a preferred east-west orientation to their long axes (*e.g.*, Quill Creek segment, Fig. 10). In many cases, there are east-west-trending lineations on the northern slopes of these sediment mounds; we tentatively interpret these as folds or fault tips resulting from north-south compression across these mounds. However, more work, including ground-truthing in the field will be required to confirm a tectonic cause. They instead could be caused by slumping due to freeze-thaw cycles on north-facing slopes, but if so, it is unclear why they are often oriented oblique (~45°) to the slope fall line (*e.g.*, Fig. 8). They are not an artifact of the hillshade effect and are visible at a variety of light source azimuths. It is worth noting that these features would not be easily discerned in traditional 1 m resolution lidar data, so if they are records of strain, the utility of high-resolution drone lidar is clear. However, more work is required to prove their origin definitively.

Width and complexity of the EDF

At the central Duke River study site, the combined areas of Surveys 1–4 cover ground up to 2 km from the main EDF trace. In this area, the lidar data do not reveal any parallel splays of the main EDF as originally interpreted by Witter (2020), indicating that strain on this segment is concentrated to one fault plane. Given that complex faults with wide damage zones and high fracture density are generally more permeable to fluid flow (Caine *et al*., 1996), this finding suggests hydrothermal circulation may be limited. However, preliminary mapping by ourselves and by Witter (2020) found evidence for multiple significant bedrock faults in the Burwash Creek and Duke River canyons; although these faults do not appear to rupture to the surface, or at least not to the degree required to generate clear topographic expressions, they still may be relatively young: for example McDermott *et al.* (2021) obtained Pliocene ages from EDF fault surfaces using hematite thermochronometry.

The amount of off-fault deformation at the surface varies along strike. The width of the zone of clearly deformed sediments varies from ~2 m (Duke River; Fig. 5 inset) to >100 m (Copper Joe Creek; Fig. 9 inset). This may reflect changes in bedrock fault zone dimensions along strike, or it may simply reflect the depth and type of Late Quaternary sediment through which the fault has ruptured. For example, a wider zone of deformation may be indicative of a deeper layer of sediment, in which deformation becomes more diffuse towards the surface. Alternatively, the width of the deformed zone of sediment may be a proxy for the amount of Late Quaternary slip that has been accommodated along that particular segment (*i.e.*, the gravel on the abandoned river terrace at Duke River has potentially only experienced one rupture event).

Fault geometry and geothermal favourability

Projecting the traces of the EDF scarps from either side of the Duke River shows that the fault makes a 7° right-stepping bend, and the fault trace shifts ~100 m laterally. Considering the ample evidence for dextral kinematics, this right-stepping bend is interpreted as a releasing bend with a component of localized extension. In the structurally controlled geothermal systems of Nevada, zones with localized extension tend to be more permeable to hydrothermal fluid flow. The selected drill site is approximately 1 km to the west of the fault bend, and it is unclear whether extensional strain would have an effect at that distance.

Stepovers can also be identified at other survey sites. The Quill Creek segment has a distinct 100 m left-stepping bend, which is interpreted to be a restraining bend giving rise to an exceptionally large sediment mound. The Copper Joe Creek segment appears to have a right-stepping bend, which may represent another local zone of extension. The proximity of the Copper Joe site to Burwash Landing makes this another potential candidate for geothermal energy extraction.

Future Work

These data and interpretations are preliminary, and further data collection and analysis will occur over the coming months and years. The following sections describe planned and suggested future work.

Improvement to the drone system

The use of a lidar-equipped drone for fault mapping is novel, and this deployment pushed the system to its limits in terms of flight time and distance from launch point. The data from the system are already useful, but the utility of the system would be even greater if the drone could fly for longer distances. There are several ways the flight distance could be improved, including:

- Mounting a small camera to the airframe to provide a real-time video feed to the pilot in command. This addition would allow for improved situational awareness when the drone is far from the launch point and the flight direction is difficult to discern.
- Upgrading the batteries. DJI does manufacture higher capacity batteries, but these would not be allowed in standard air cargo, limiting the deployment of the drone to locations within driving distance of the University of Victoria.
- Using a larger generator for recharging. In 2021 we used a 1000-watt generator, which was only capable of charging one set of batteries at a time. For future fieldwork we could reduce inefficiency by using a generator with higher wattage.
- Packaging the drone system appropriately to allow for transport via an ATV to more remote launch sites. In 2021 we were limited to launch sites accessible with a truck.
- Applying for Special Flight Operations Certificate (SFOC) from Transport Canada to allow for controller hand-off between multiple pilots stationed along a flight line. This allowance would enable a much longer survey, without requiring beyond-visual line-of-sight flight. Currently, such a system requires a bespoke control system not commercially available.
- Applying for an SFOC from Transport Canada to allow for beyond-visual-line-of-sight flight. This allowance has thus far only been granted to a handful of commercial operators. Furthermore, operating beyond visual line of sight would require a high degree of trust in the flight programming software, which currently experiences enough glitches to render it untrustworthy. Considering the cost of the drone system, and high consequences of a crash, considerable testing would be required before implementing such a high-risk flight.

Additional drone lidar acquisition

The preliminary results presented in this report show that the 3 to 10-fold increase in resolution achieved with the drone lidar as compared to traditional fixed-wing lidar, is useful for mapping fault structure in this particular region. Permanent strain recorders such as laterally-offset stream channels, and possible compressional structures in sediment mounds, would be barely-discernible, or at least less convincing, in traditional lidar, but are easily mapped with drone lidar. We propose collecting more drone lidar data at exposures of the EDF we were unable to cover in 2021. This includes filling in gaps in the data coverage at existing study sites and expanding coverage to the northwest and southeast. In addition to fault-parallel surveys, we suggest collecting several swaths perpendicular to the main fault to ascertain whether or not other lineaments in the hillside represent Holocene fault scarps.

Figure 13 shows proposed sites for additional coverage and the access considerations and scientific justifications are presented in Table 1. The highest priority sites (5–10 in Fig. 13) are proximal to the proposed geothermal site. More distant sites will be

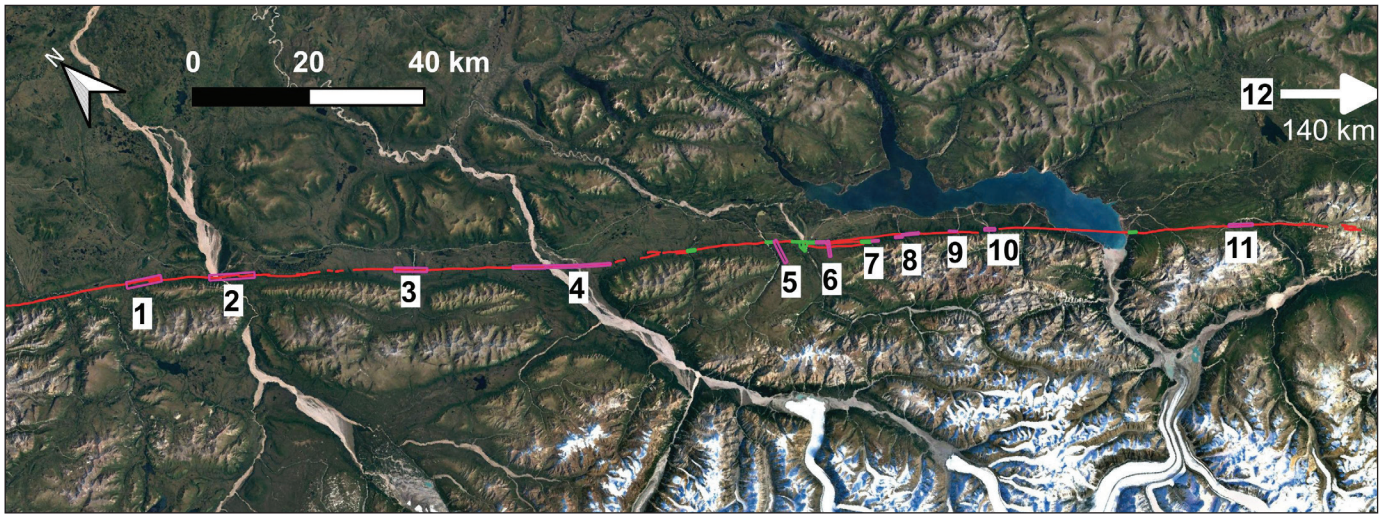


Figure 13. *Proposed locations (pink rectangles) for future drone lidar acquisition along the EDF. Green rectangles show areas captured in the present study. Numbers correspond to entries in Table 1.*

Table 1. *Proposed future study sites, access routes, and scientific justification.*

No.	Location	Access Route	Reason
1	Sanpete Creek	Road and ATV track	Farthest NW, close to US border; Several creeks with possible lateral offset.
2	White River	Adjacent to highway	Possible knickpoint in river; Unusual undulatory fault geometry.
3	Koidern River	Road on NW side of river	Possible disturbance of abandoned river terrace.
4	Donjek River	ATV tracks on river bars	Fault at high angle to local glacial lineations (possible offset markers); Possible disturbance of abandoned river terrace.
5	Burwash Creek Cross Profile	Road on NW side of creek	Distinguish any parallel fault splays (4 were identified by Witter (2020)).
6	Duke River Cross Profile	Dept. of Highway's Gravel Pit	Distinguish any parallel fault splays (3 were identified by Bender and Haeussler (2017)).
7	Copper Joe Southeast	Road on SE side of creek	Possible continuation of fault not identified by Bender and Haeussler (2017).
8	Lewis Creek	ATV up gravel creek bed?	Suspected deviation from EDF fault map created by Bender and Haeussler (2017).
9	Bocks Creek	Road and ATV track	Suspected deviation from EDF fault map created by Bender and Haeussler (2017).
10	Nines Creek	ATV track up creek bed	Possible disturbance of abandoned river terrace.
11	Telluride Creek	ATV/hiking route up Mt. Cairnes	Farthest accessible exposure of EDF mapped by Bender and Haeussler to SE.
12	Chilkat Pass	Adjacent to Haines Highway	Site of 2017 earthquake doublet (Choi *et al.*, 2021). Possible scarp/lineament observed in satellite imagery.

of more use for understanding the regional tectonics of the EDF. Many of the proposed future sites will be challenging to access via road, and may require the use of an ATV to transport the drone system to a suitable launch site.

Field studies and ground truthing

Witter (2020) documented multiple bedrock faults in the cliffs along Burwash Creek and Duke River. Future effort should be undertaken to map these faults in detail, including their widths, kinematic indicators, and whether they disturb unconsolidated Quaternary sediments that drape over top of them. Although there is no clear evidence in lidar data that these faults disturb the surface, this does not rule out a Quaternary age; it may be possible to observe disturbed Quaternary sediments in cross section, even if the surface trace is muted. Furthermore, mapping out the fault zone architecture (*i.e.*, damage zone and fault core) will help constrain fault zone permeability.

The east-west lineations observed on the north slopes of the sediment mounds also need to be investigated in the field. Given their subtle nature, they were not obvious on the ground during 2021 fieldwork. It may be possible to excavate a shallow trench across them to view a cross section of their internal structure. Additionally, it would be worth searching for similar features on slopes not adjacent to the EDF. If they are ubiquitous on north facing slopes in the area, they likely all have a non-tectonic origin.

Slip and dilation tendency modeling of the 2D fault map

In addition to drone surveys and fieldwork, we plan to conduct kinematic modeling based on the detailed lidar-derived fault map. Earthquake focal mechanisms will be used to estimate stress directions and magnitudes using a Bayesian stress inversion (e.g., Balfour et *al.*, 2011). Ristau et *al.* (2007) conducted this sort of analysis for earthquakes in western Canada with M_w>4, but an additional 14 years of seismicity could be added to the catalog to further refine our understanding of the regional stress field. The recent addition of data from the Earthscope Transportable Array in Alaska and across the Mackenzie Mountains (Baker et *al.*, 2019; Busby and Aderhold, 2020) will greatly improve focal mechanism determinations in the region. Choi et *al.*, (2021) relocated earthquakes and determined stress directions using focal mechanism inversions along the southern section of the EDF, but a similar reanalysis has not yet been conducted in the vicinity of the geothermal drill site. The detailed fault maps obtained with the lidar drone (or future airplane) will be integrated with seismological stress axes and other data sources to model kinematics on the EDF. Specifically, slip and dilation tendency will be calculated for fault segments identified in lidar imagery. Slip tendency (T_S) is the likelihood of a fault to slip in a certain stress field, and is quantified as the ratio between shear stress (τ) and normal stress (σ_n) relative to the friction coefficient of the rocks (μ_s):

$$T_S = \frac{\tau}{\sigma_n} \geq \mu_s$$

Dilation tendency (T_D) is controlled by the relative orientation of the maximum and minimum compressive stresses (σ_1 and σ_3) and normal stress (σ_n) acting on a fault plane; when the normal stress is parallel to the principal stress, the dilation tendency will be 0, and when the normal stress is parallel to the minimum stress, dilation tendency will be 1:

$$T_D = \frac{\sigma_1 - \sigma_n}{\sigma_1 - \sigma_3}$$

The tendency of a fault to slip or dilate is a proxy for permeability, and this technique has been used to aid in drill-targeting at numerous fault-controlled geothermal systems around the world (e.g., Moeck et *al.*, 2009; Jolie et *al.*, 2015; Meixner et *al.*, 2016, 2018).

Currently, the subsurface geometry of the EDF is only roughly constrained. Lidar imagery will refine surface maps of the fault trace, and while this is useful, other geophysical techniques will be necessary to properly model subsurface structure and kinematics. Seismicity patterns (from relocation algorithms), and geophysical data (e.g., EM, seismic tomography, gravity, magnetics) obtained as part of the YGS's geothermal project, could provide a more detailed view of subsurface fault

geometry, and thus inform kinematic modeling. Existing regional geophysical surveys of the Yukon may also help with this task. However, even with poorly constrained subsurface geometry, the slip and dilation tendency can be modeled for a range of dip angles given high resolution fault segment mapping on the surface (*e.g.*, Meixner et *al.*, 2018).

Conclusion

The preliminary results presented in this report demonstrate the utility of high-resolution drone lidar for active fault mapping. We were able to: 1. map fine scale fault geometry that could be conducive to hydrothermal fluid flow, and 2. improve constraints on the kinematics and rupture magnitude of prehistoric earthquakes on the EDF, both of which are important factors for developing fault-hosted geothermal systems. The bare-earth DEMs and hillshades derived from the lidar point clouds are three times the resolution of traditional fixed-wing lidar and allow for much higher resolution mapping of the EDF surface trace than was possible with existing photogrammetric DEM products (*e.g.*, Bender and Haeussler, 2017). The overall cost of deploying the lidar drone is a fraction of traditional airborne lidar systems, although airborne systems are more efficient at covering a much larger area. The true utility of the drone system is its ability to target known fault segments with very high spatial resolution. We observe subtle strain markers such as offset channels and deformed surface sediments that can be used to estimate kinematics and slip magnitudes of past ruptures. We can resolve small restraining and releasing bends, some of which were not previously mapped; the releasing bends are considered conducive for hydrothermal fluid circulation. In the future, we will use these data to perform slip and dilation tendency modeling of the EDF but recommend that more drone lidar data be acquired in subsequent field seasons. Additionally, structural mapping of bedrock faults in drainages crossing the EDF will help to elucidate the relationship between the recent ruptures, and older faulting.

Acknowledgements

Excellent food, lodging and research infrastructure was provided by the Kluane Lake Research Station/ Arctic Institute of North America. Special thanks to Harry Penn for accommodating our myriad of requests. Funding and logistical support was provided by the Yukon Geological Survey. Sincere thanks are due to Maurice Colpron, Carolyn Relf and Sarah Sternbergh for facilitating our visit. Lucinda Leonard provided a constructive critical review of this manuscript. This is NRCan contribution number 20210433.

References

Baker, M.G., Heath, D.C., Schutt, D.L., Aster, R.C., Cubley, J.F. and Freymueller, J.T., 2019. The Mackenzie Mountains EarthScope Project: Studying Active Deformation in the Northern North American Cordillera from Margin to Craton. Seismological Research Letters, vol. 91, p. 521–532, doi:10.1785/0220190139.

Balfour, N.J., Cassidy, J.F., Dosso, S.E. and Mazzotti, S., 2011. Mapping crustal stress and strain in southwest British Columbia. Journal of Geophysical Research, vol. 116, p. 1–11, doi:10.1029/2010JB008003.

Bender, A. and Haeussler, P., 2017. Eastern Denali Fault Surface Trace Map, Eastern Alaska and Yukon, Canada. U.S. Geological Survey, Open-File Report 2017–1049, 10 p., https://doi.org/10.3133/of20171049.

Blackwell, D.D. and Richards, M., 2004. Geothermal Map of North America. American Association of Petroleum Geologists Map, https://www.smu.edu/Dedman/Academics/Departments/EarthSciences/Research/GeothermalLab/DataMaps/GeothermalMapofNorthAmerica, [accessed July 2019].

Blais-Stevens, A., Clague, J.J., Brahney, J., Lipovsky, P., Haeussler, P.J. and Menounos, B., 2020. Evidence for Large Holocene Earthquakes along the Denali Fault in Southwest Yukon, Canada. Environmental and Engineering Geoscience, vol. 26, p. 149–166, doi:10.2113/EEG-2263.

Bostock, H.S., 1952. Geology of the northwest Shakwak Valley, Yukon Territory. Geological Survey of Canada, Memoir 267, 50 p.

Busby, R.W. and Aderhold, K., 2020. The Alaska Transportable Array: As Built. Seismological Research Letters, v0l. 91, p. 3017–3027, doi:10.1785/0220200154.

Caine, J.S., Evans, J.P. and Forster, C.B., 1996. Fault zone architecture and permeability structure. Geology, vol. 24, p. 1025–1028, doi:10.1130/0091-7613(1996)024<1025.

Choi, M., Eaton, D.W. and Enkelmann, E., 2021. Is the Eastern Denali fault still active? Geology, vol. 49, doi:10.1130/G48461.1.

Clague, J.J., 1979. The Denali Fault System in southwest Yukon Territory -a geologic hazard? Geological Survey of Canada, Paper No. 79-1A, p. 169–178, doi:10.4095/104844.

Craig, J.W., 2018. Discovery and Analysis of a Blind Geothermal System in Southeastern Gabbs Valley, Western Nevada. Unpublished MSc thesis, University of Nevada, Reno, 121 p.

Curewitz, D. and Karson, J.A., 1997. Structural settings of hydrothermal outflow: Fracture permeability maintained by fault propagation and interaction. Journal of Volcanology and Geothermal Research, vol. 79, p. 149–168, doi:10.1016/S0377-0273(97)00027-9.

Dobson, P.F., 2016. A Review of Exploration Methods for Discovering Hidden Geothermal Systems. GRC Transactions, vol. 40, p. 695–706.

Eberhart-Phillips, D. *et al.*, 2003. The 2002 Denali Fault Earthquake, Alaska: A Large Magnitude, Slip-Partitioned Event. Science, vol. 300, p. 1113–1118, doi:10.1126/science.1082703.

Faulds, J. and Hinz, N., 2015. Favorable Tectonic and Structural Settings of Geothermal Systems in the Great Basin Region, Western USA: Proxies for Discovering Blind Geothermal Systems. Proceedings World Geothermal Congress 2015, Melbourne, Australia, p. 19–25.

Faulds, J.E., Hinz, N., Kreemer, C. and Coolbaugh, M., 2012. Regional Patterns of Geothermal Activity in the Great Basin Region, Western USA: Correlation With Strain Rates. GRC Transactions, vol. 36, p. 6.

Haeussler, P.J., Matmon, A., Schwartz, D.P. and Seitz, G.G., 2017. Neotectonics of interior Alaska and the late Quaternary slip rate along the Denali fault system. Geosphere, vol. 13, p. 1445–1463, doi:10.1130/GES01447.1.

IPCC, 2014. AR5 Climate Change 2014: Mitigation of Climate Change. Contribution of Working Group III to the Fifth Assessment Report of the Intergovernmental Panel on Climate Change, Cambridge University Press, 1967 p.

Jolie, E., Moeck, I. and Faulds, J.E., 2015. Quantitative structural-geological exploration of fault-controlled geothermal systems-A case study from the Basin-and-Range Province, Nevada (USA). Geothermics, vol. 54, p. 54–67, doi:10.1016/j.geothermics.2014.10.003.

Kristmannsdóttir, H. and Ármannsson, H., 2003. Environmental aspects of geothermal energy utilization. Geothermics, vol. 32, p. 451–461, doi:10.1016/S0375-6505(03)00052-X.

Leonard, L.J., Mazzotti, S. and Hyndman, R.D., 2008. Deformation rates estimated from earthquakes in the northern Cordillera of Canada and eastern Alaska. Journal of Geophysical Research: Solid Earth, vol. 113, p. 1–18, doi:10.1029/2007JB005456.

Lipovsky, P.S., Seitz, G., Haeussler, P.J., Crone, A.J., Schwartz, D.P., Clague, J.J., Mazotti, S. and Cobbett, R., 2009. Neotectonic investigations in southwest Yukon. In: Canadian Quaternary Association Meeting, Vancouver, BC, Canada.

Little, T.A., Morris, P., Hill, M.P., Kearse, J., Van Dissen, R.J., Manousakis, J., Zekkos, D. and Howell, A., 2021. Coseismic deformation of the ground during large-slip strike-slip ruptures: Finite evolution of “mole tracks”. Geosphere, vol. 17, p. 1170–1192, doi:10.1130/GES02336.1.

Majorowicz, J. and Grasby, S.E., 2010. Heat flow, depth–temperature variations and stored thermal energy for enhanced geothermal systems in Canada. Journal of Geophysics and Engineering, vol. 7, p. 232–241, doi:10.1088/1742-2132/7/3/002.

Marechal, A., Mazzotti, S., Elliott, J.L., Freymueller, J.T. and Schmidt, M., 2015. Indentor-corner tectonics in the Yakutat-St. Elias collision constrained by GPS. Journal of Geophysical Research: Solid Earth, vol. 120, p. 3897–3908, doi:10.1002/2014JB011842.

Marechal, A., Ritz, J.-F., Ferry, M., Mazzotti, S., Blard, P.-H., Braucher, R. and Saint-Carlier, D., 2018. Active tectonics around the Yakutat indentor: New geomorphological constraints on the eastern Denali, Totschunda and Duke River Faults. Earth and Planetary Science Letters, vol. 482, p. 71–80, doi:10.1016/j.epsl.2017.10.051.

McDermott, R.G., Ault, A.K. and Caine, J.S., 2021. Dating fault damage along the eastern Denali fault zone with hematite (U-Th)/He thermochronometry. Earth and Planetary Science Letters, vol. 563, doi:10.1016/j.epsl.2021.116872.

Meixner, J., Grimmer, J.C., Becker, A., Schill, E. and Kohl, T., 2018. Comparison of different digital elevation models and satellite imagery for lineament analysis: Implications for identification and spatial arrangement of fault zones in crystalline basement rocks of the southern Black Forest (Germany). Journal of Structural Geology, vol. 108, p. 256–268, doi:10.1016/j.jsg.2017.11.006.

Meixner, J., Schill, E., Grimmer, J.C., Gaucher, E., Kohl, T. and Klingler, P., 2016. Structural control of geothermal reservoirs in extensional tectonic settings: An example from the Upper Rhine Graben. Journal of Structural Geology, vol. 82, p. 1–15, doi:10.1016/j.jsg.2015.11.003.

Mira Geoscience, 2015. Ross River geothermal exploration project: Review of the 2014 work program. Yukon Geological Survey, Miscellaneous Report MR-18, 141 p.

Moeck, I.S., 2014. Catalog of geothermal play types based on geologic controls. Renewable and Sustainable Energy Reviews, vol. 37, p. 867–882, doi:10.1016/j.rser.2014.05.032.

Moeck, I., Kwiatek, G. and Zimmermann, G., 2009. Slip tendency analysis, fault reactivation potential and induced seismicity in a deep geothermal reservoir. Journal of Structural Geology, vol. 31, p. 1174–1182, doi:10.1016/j.jsg.2009.06.012.

Porter, C. *et al.*, 2018. ArcticDEM:, doi:10.7910/DVN/OHHUKH.

Ristau, J., Rogers, G.C. and Cassidy, J.F., 2007. Stress in western Canada from regional moment tensor analysis. Canadian Journal of Earth Sciences, vol. 44, p. 127–148, doi:10.1139/e06-057.

Seitz, G., Haeussler, P.J., Crone, A.J., Lipovsky, P.S. and Schwartz, D.P., 2008. Eastern Denali fault slip rate and paleoseismic history, Kluane Lake area, Yukon Territory, Canada. In: American Geophysical Union Fall Meeting, Abstract T53B-1947. AGU meeting, December 15–19, 2008, San Francisco, CA, USA.

Sibson, H., 1996. Structural permeability of fluid-driven fault-fracture meshes. Journal of Structural Geology, vol. 18, p. 1–12, doi:10.1016/0191-8141(96)00032-6.

Spotila, J.A. and Berger, A.L., 2010. Exhumation at orogenic indentor corners under long-term glacial conditions: Example of the St. Elias orogen, Southern Alaska. Tectonophysics, vol. 490, p. 241–256, doi:10.1016/j.tecto.2010.05.015.

Stewart, N., Gaudemer, Y., Manighetti, I., Serreau, L., Vincendeau, A., Dominguez, S., Mattéo, L. and Malavieille, J., 2018. "3D_Fault_Offsets," a Matlab Code to Automatically Measure Lateral and Vertical Fault Offsets in Topographic Data: Application to San Andreas, Owens Valley, and Hope Faults. Journal of Geophysical Research: Solid Earth, vol. 123, p. 815–835, https://doi.org/10.1002/2017JB014863.

Witter, J.B., 2020. Early-stage exploration for geothermal energy resources along the Denali fault near Duke River, Yukon. Yukon Geological Survey, Open File 2020-3, 70 p.

Zielke, O. and Arrowsmith, J.R., 2012. LaDiCaoz and LiDARimager—MATLAB GUIs for LiDAR data handling and lateral displacement measurement. Geosphere, vol. 8, p. 206–221, doi:10.1130/GES00686.1.

Zielke, O., Arrowsmith, J.R., Ludwig, L.G. and Akçiz, S.O., 2010. Slip in the 1857 and Earlier Large Earthquakes Along the Carrizo Plain, San Andreas Fault. Science, vol. 327, p. 1119–1122, doi:10.1126/science.1182781.

Surficial geochemical setting of the southern Carmacks-Minto copper belt

Kristen Kennedy*, Patrick J. Sack and Heather Clarke
Yukon Geological Survey

Kennedy, K., Sack, P.J. and Clarke, H., 2022. Surficial geochemical setting of the southern Carmacks-Minto copper belt. *In:* Yukon Exploration and Geology 2021, K.E. MacFarlane (ed.), Yukon Geological Survey, p. 107–124.

Abstract

Preliminary surficial geological investigations of the southern Carmacks-Minto copper belt (NTS 115I/7) include material thicknesses, distribution and observations of thermal conditions. The Quaternary setting is discussed in relationship to material genesis and geomorphological processes operating on the landscape. Surficial material distribution is controlled by ice flow direction, prevailing wind direction and aspect-related differences in gravity and thermal-driven surficial processes.

Valley bottoms and north-facing slopes have moderate to thick surficial cover that include far-travelled sediments such as till, loess and glaciolacustrine sand. Drainage can be poor in these landscapes and permafrost is present in many areas. Valley bottoms contain thick Quaternary fill and are unsuitable for traditional soil surveys. North-facing slopes may provide good geochemical results if sampled carefully for first-order bedrock derivatives. Upland and south-facing slopes have thin to moderate surficial cover and can provide good conditions for traditional C-horizon soil sampling surveys. Windblown sand, silt and volcanic ash are deposited thickly, but unevenly, across the landscape. These sediments dilute surficial geochemical samples and are often incorporated into other materials through cryoturbation, and fluvial and gravitational reworking. Geochemical dilution by eolian materials is more significant near the Yukon River floodplain and in the central Carmacks-Minto copper belt.

Future surficial geochemical surveys should use a variety of methods suited to landscape characteristics and well-described surficial material characterizations. Applying surficial landscape models to existing soils data may also improve their utility for exploration. High quality surficial mapping is a critical part of surficial geochemical surveys and new products in this area will benefit from the use of airborne lidar.

* Kristen.Kennedy@yukon.ca

Introduction

Copper deposits extending from Carmacks Copper (Cu-Au-Ag; Yukon MINFILE 115I 008) to Minto (Cu-Au; Yukon MINFILE 115I 021 and 115I 022), and including the Stu prospect (Cu-Ag; Yukon MINFILE 115I 011), together form a northwest trending corridor known as the Minto or Carmacks copper belt (Fig. 1). Much of the existing mineralization in this region has been identified in landscape positions where surficial cover is absent or thin, typically on or near ridge tops. Exploration of landscapes characterized by thick surficial cover will require a better understanding of surficial materials distribution and genesis.

Challenges associated with surficial geochemical sampling in the region are well-known (Casselman, 2015; James, 2019; Paulter, 2015, 2016). Traditional soil sampling methods have had limited success at identifying known targets in areas of variable cover (Casselman, 2015) while applications of selective leach mobile metal ion and biological samples have had somewhat more success when used over thick cover (Paulter, 2016). Both methods require robust interpretations of surficial material distributions and careful sampling in the field. Existing surficial material and glacial limit maps (Jackson, 2000; Duk-Rodkin, 1999) lack the spatial resolution for property scale mineral exploration applications. This project aims to facilitate high-quality sediment surveys by describing the distribution and genesis of surficial materials in the southern part of the copper belt including the Carmacks Copper and Stu properties (also known as Carmacks and Carmacks North, respectively).

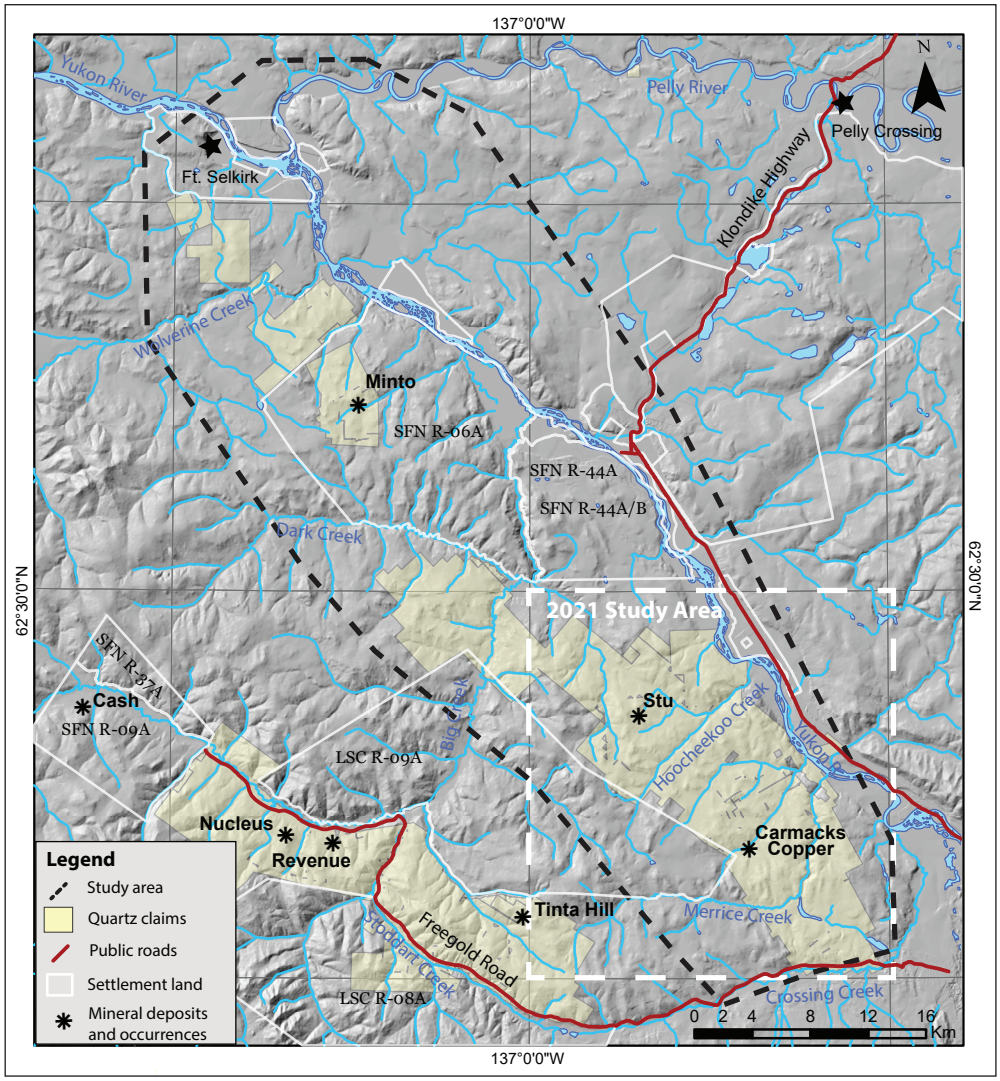


Figure 1. *Land tenure, access and major features of the study area in central Yukon. Quartz claims are shown in yellow shaded polygons and settlement land is labeled by reserve block number and First Nation (LSC: Little Salmon Carmacks First Nation; SFN: Selkirk First Nation). Mineral deposits and significant occurrences are marked with an asterisks symbol.*

Regional setting

Land tenure and development

The study area includes the Traditional Territories of the Selkirk and Little Salmon Carmacks First Nations. Land management is overseen by both First Nation governments as well as the Government of Yukon. Quartz claims cover much of the study area and, along with Selkirk First Nation settlement land, form a nearly continuous belt of tenured land from Crossing Creek to Fort Selkirk (Fig. 1). Road access to the southern part of the study area is via the seasonal publically maintained Freegold Road, as well as various privately maintained mining and exploration roads. The northern part of the study area has limited accessibility with the exception of the Minto mine which is serviced via barge and private roads from the Klondike Highway.

Pre-Quaternary geology

Located within the Yukon Plateau, the Carmacks-Minto copper belt lies east of the Dawson Range in an area of subdued relief west of the Teslin fault (Fig. 2). Bedrock geology in the region is primarily a series of Late Triassic to Early Jurassic Minto suite plutons that likely form a continuous batholith ~120 km long by ~15–20 km wide (Sack et *al.*, 2020). The batholith likely

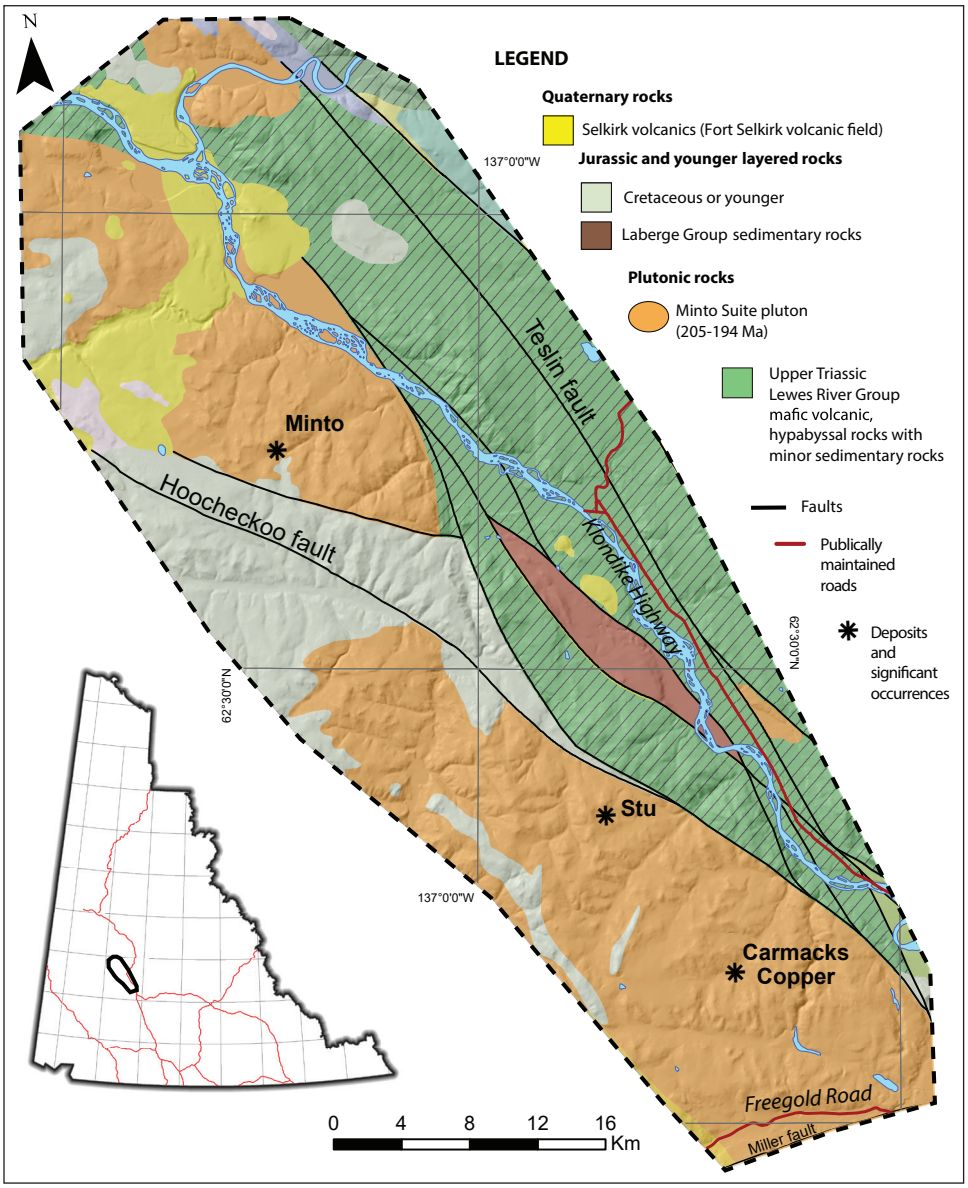


Figure 2. *Simplified bedrock geology of the Minto-Carmacks copper belt. Geology from Yukon Geological Survey (2020a). Minto-Carmacks copper belt boundary from Sack and Colpron (2020). Occurrences from Yukon Geological Survey (2020b).*

intruded metamorphic basement rocks of the Yukon-Tanana terrane and Late Triassic mafic volcanic rocks of the Povoas Formation. Copper (± gold and silver) deposits and occurrences within the copper belt are associated with Late Triassic to Early Jurassic rocks, the most economically significant of these are found as rafts within the plutons (Kovacs et *al.*, 2020; Sack et *al.*, 2020).

Mid-Cretaceous and older rocks are unconformably overlain by Late Cretaceous basalt and immature sedimentary rocks which were deposited on a deeply weathered erosional surface of considerable relief (Grond et *al.*, 1984). Some volcanic rocks are highly prone to failure and complex kilometre-scale landslides are present in the southeastern part of the study area (Jackson, 2000). Although the Late Cretaceous landscape has remained largely intact through the Cenozoic, its overall physiography and surface expression has been modified by Quaternary volcanism and glaciation.

Quaternary geologic setting

The Carmacks copper belt has a complex Quaternary history that includes at least six periods of glaciation from two distinct sectors of the Cordilleran Ice Sheet. Glaciations occurred contemporaneously with volcanism in the Fort Selkirk volcanic field (Jackson et *al.*, 1996, 2012) and both processes contributed to significant changes in fluvial drainage patterns in the region (Fig. 3; Huscroft et *al.*, 2004).

Glaciation in central Yukon occurred via a complex of semi-independent topographically-controlled ice lobes that periodically coalesced to form the northern Cordilleran Ice Sheet (Duk-Rodkin et *al.*, 2010; Jackson et *al.*, 1991). The Selwyn Lobe advanced over the northern part of study area from the east while the Cassiar Lobe advanced from the southeast (Fig. 4; Bostock, 1936, 1966; Hughes et *al.*, 1969; Jackson, 2000). The ice lobes became increasingly precipitation limited during the Quaternary (Ward et *al.*, 2007) although they remained generally synchronous and in-step with global periods of ice advance and retreat.

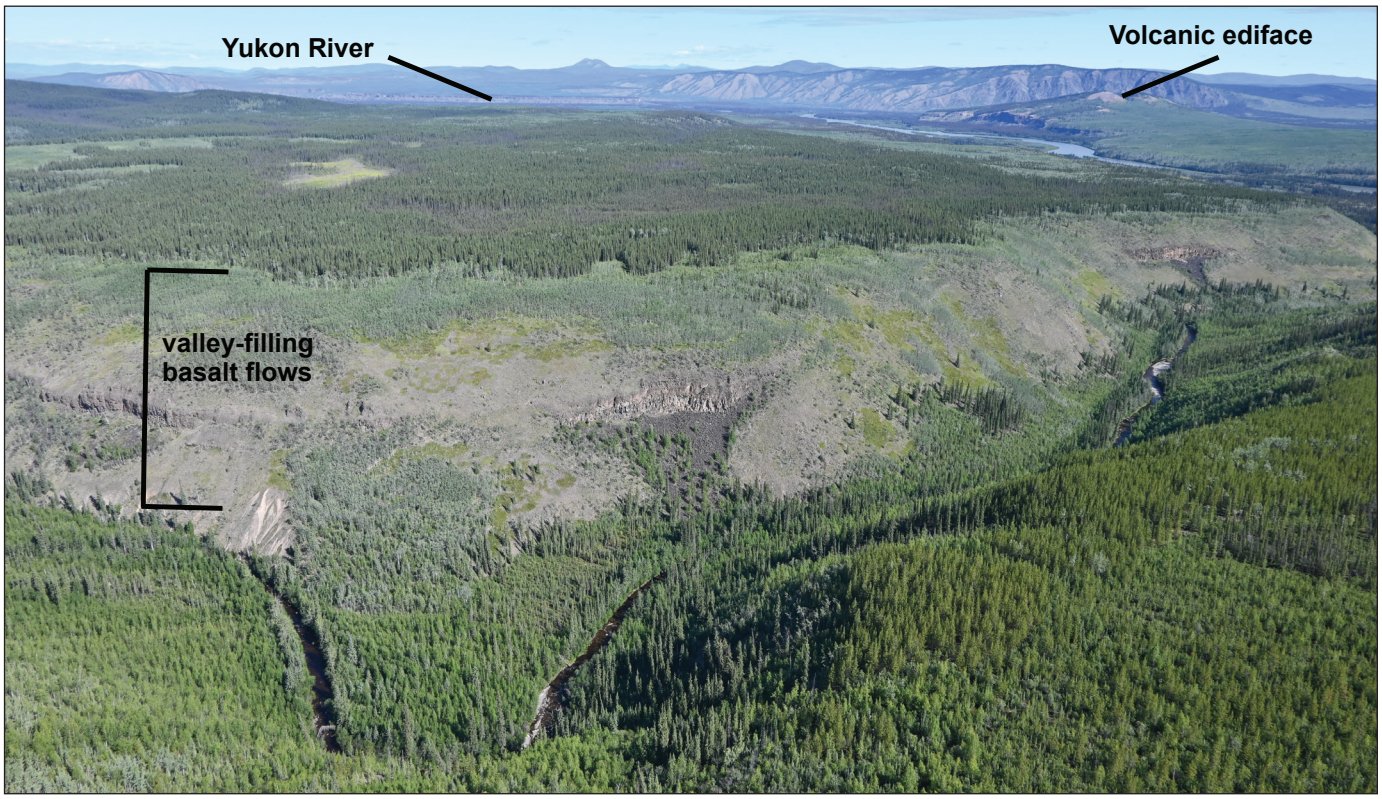


Figure 3. *View north across Wolverine Creek toward the Yukon River. Cenozoic volcanism filled valleys in the northern part of the study area and significantly altered earlier drainage systems.*

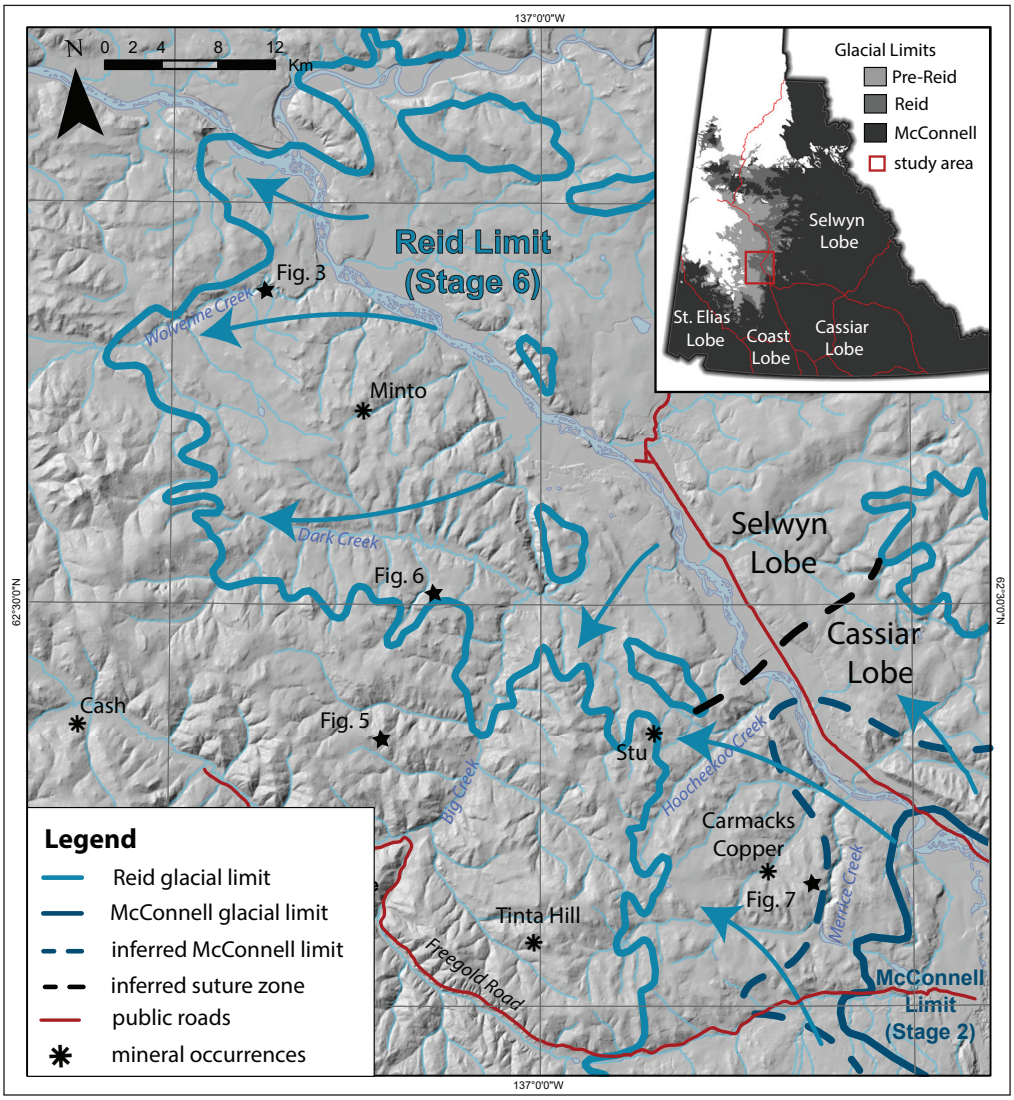


Figure 4. *Limits of the Selwyn and Cassiar lobes of the Cordilleran Ice Sheet during the Reid and McConnell glaciations (from Duk-Rodkin, 1999). A hypothetical suture zone between Selwyn and Cassiar lobe ice is represented by the black dashed line. A more extensive limit for the McConnell Glaciation indicated from new observations and mapping by Jackson (2000) is shown in dashed blue line along Merrice Creek.*

The chronology of Cordilleran glaciation in central Yukon is built from Selwyn Lobe records that include at least three "pre-Reid" advances between 2.1 Ma and 0.78 Ma (Jackson et *al.*, 1996, 2012; Nelson et *al.*, 2009; Westgate et *al.*, 2001). These glaciations were more extensive than later advances and extended beyond the study area (Duk-Rodkin et *al.*, 1999). Pre-Reid surfaces are difficult to distinguish from unglaciated terrain and are characterized by their absence of glaciogenic landforms and geomorphology reflective of dominantly fluvial regimes (Bond and Lipovsky, 2010). Uplands in pre-Reid terrain in the study area may have escaped glaciation altogether and are indistinguishable from unglaciated uplands of the eastern Dawson Range (Fig. 5).

The penultimate Reid Glaciation occurred ~140 000 years ago (Ward et *al.*, 2008; Preece et *al.*, 2011; Demuro et *al.*, 2012) and reached its maximum extent within the study area (Fig. 4). Landforms and limits associated with the Reid Glaciation are subdued and weathered, but still visible on the landscape (Fig. 6). Impoundment of east-flowing Yukon River tributaries including Merrice, Williams, Hoocheekoo, Big and Wolverine creeks likely occurred at the close of the Reid Glaciation and resulted in the creation of glacial lakes in these valleys.

The McConnell Glaciation was the least extensive advance of ice over the study area and reached its maximum extent near Merrice Creek (Fig. 4).

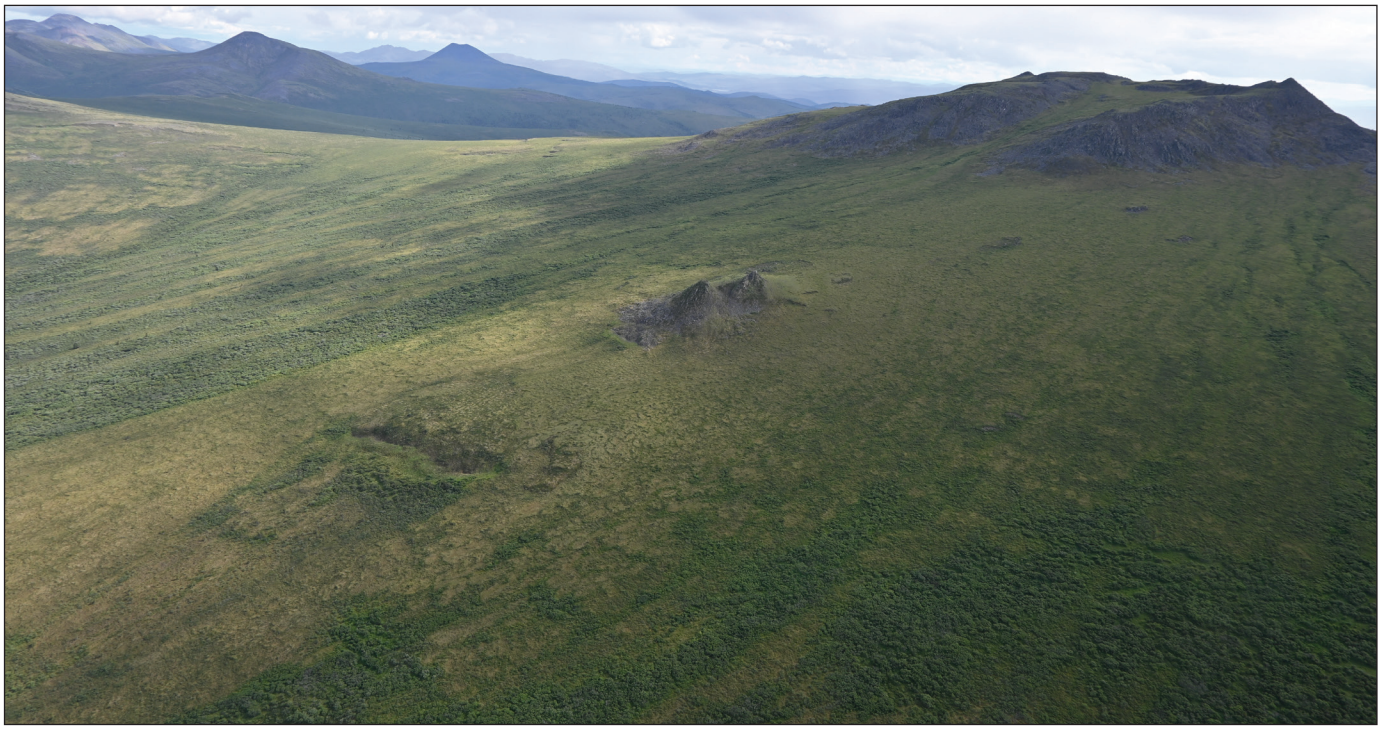


Figure 5. *Subdued terrain and thick blankets of weathered bedrock are characteristic of pre-Reid and unglaciated terrain in the study area. Upland surfaces that were glaciated during the pre-Reid glaciations are largely indistinguishable from unglaciated terrain*



Figure 6. *Erosional and depositional features associated with the Reid Glaciation are subdued, but still visible on the landscape. A Reid-aged moraine ridge is marked here with a dashed line.*

The McConnell Glaciation is thought to have advanced over central Yukon ~30 000 years ago (Matthews et *al.*, 1990; Jackson and Harington, 1991) and recession was likely underway ~15 000 years ago (Menounos et *al.*, 2017). High relief and sharply defined erosional (Fig. 7) and depositional landforms associated with the McConnell Glaciation are limited to areas southeast of Merrice Creek.

To the southwest of the study area, the St. Elias and Coast Mountain lobes of the Cordilleran Ice Sheet also had extensive advances during the Gladstone Glaciation (~60 000 years ago; Turner et *al.*, 2013; Ward et *al.*, 2007), however, this glaciation hasn't yet been recognized in areas glaciated by the Cassiar or Selwyn lobes. Additionally, mountainous areas of the eastern Dawson Range generated alpine glaciers during early Quaternary glaciations (LeBarge, 1995; Englehart et *al.*, 2016) that may have extended into some parts of the western study area.

Post-glacial landscape adjustment in the latest Pleistocene and Holocene is associated with eolian sedimentation and re-establishment of fluvial drainage systems. East-flowing drainages such as Merrice and Williams creeks may have been impounded by McConnell ice in the Yukon River valley, but would have rapidly incised through fine-grained sediments as deglaciation progressed. Eolian processes were active as glaciers receded and largely stabilized by vegetation ~9000 years ago (Wolfe et *al.*, 2011).

In the latest Holocene, White River Ash (volcanic tephra) was deposited ~1147 years ago over a broad swath of central Yukon (Clague et *al.*, 1995; Lerbekmo, 2008). It is distributed in a cone-shaped plume across the study area and mapped thicknesses range from more than 30 cm over Carmacks Copper to less than 5 cm at Wolverine Creek (Fig. 8; Lerbeckmo and Campbell, 1969). Field observations in the study area suggest the thickest accumulations are centered on the Stu property where primary ash-fall deposits of more than 30 cm are well-preserved on stable, flat, or shallow sloping surfaces. Other authors in the region have noted accumulations of up to a metre in depth (Casselman, 2015; Paulter, 2015) although these thicknesses may be related to resedimentation of these highly mobile materials.



Figure 7. *McConnell-aged erosional landforms such as this meltwater channel display greater relief than similar features in Reid-aged terrain.*

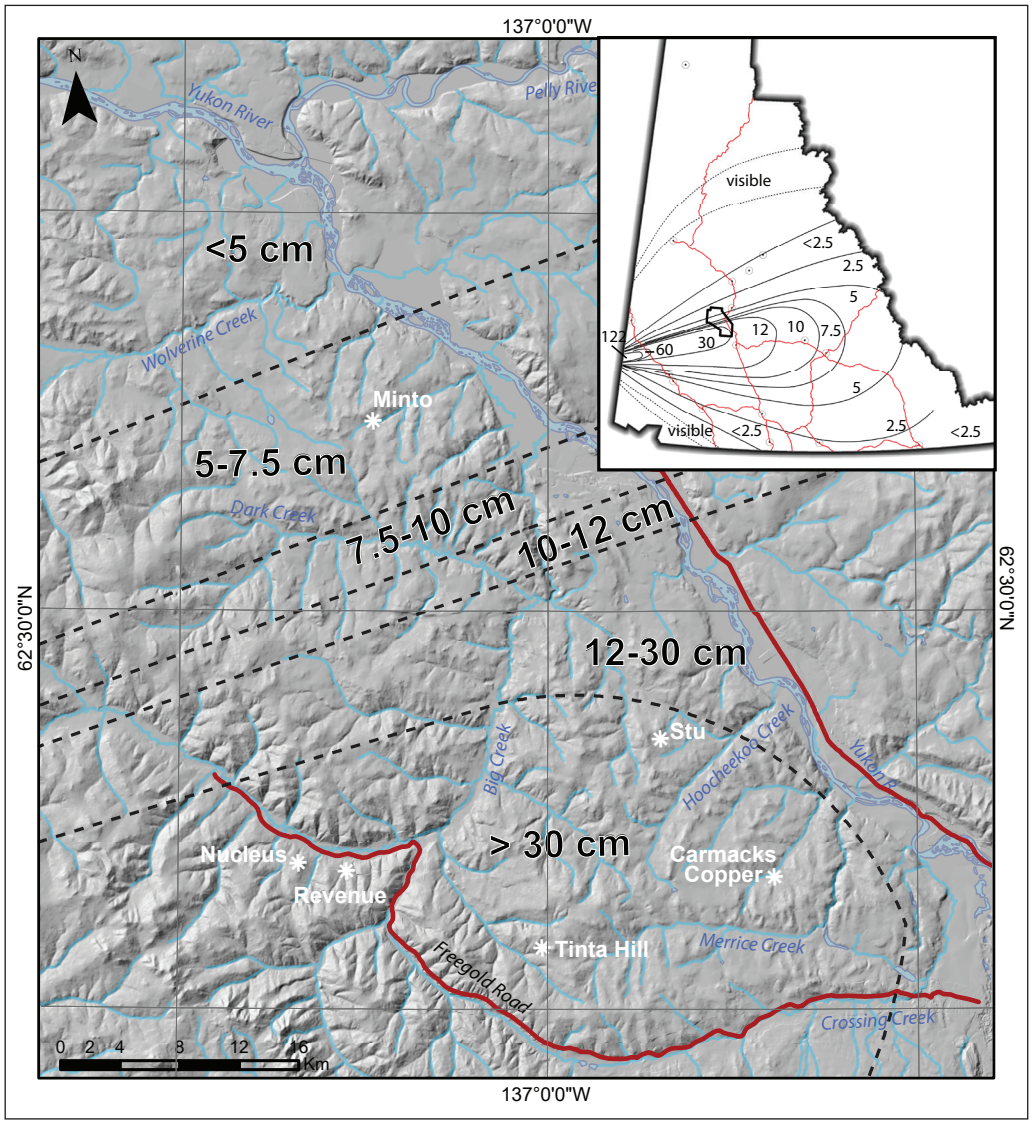


Figure 8. *Isopachs (cm) map of the east lobe of the White River Ash over the study area (from Mulliken et al., 2018). The study area coincides with an area of tightly spaced isopachs that mark a sharp decrease in thickness of ash north of the Stu claims. The southern part of the study area coincides with some of the thickest ash deposits in central Yukon.*

Surficial geochemical setting

In early stages of mineral exploration, surficial geochemical samples are commonly collected from soil parent materials (B or C-horizons) and stream sediments (silt-sized fraction). Less commonly, surveys of coarse-fraction stream sediments, A-horizon soils, and biological samples are undertaken (*i.e.*, Heberlein and Samson, 2010; Heberlein *et al.*, 2013). First-derivative surficial materials transported by gravity, water, or ice can be useful analogues for bedrock but are subject to varying degrees of dilution from other materials. The ideal medium has simple transport vectors and is evenly distributed across the landscape.

Regional geochemical survey (RGS) stream sediment data have been effective at identifying mineral occurrences in the study area, however, overall sample quality in the region is negatively affected by subdued relief, large catchment sizes, thick surficial cover, and organic scavenging (Mackie *et al.*, 2016, 2017). Infill sampling of large basins could produce targeted anomalies in areas of thick cover, particularly in the eastern part of the study area.

Stream silts are subject to dilution from abundant eolian materials on the landscape. One method that may be more resilient in these conditions is the examination of coarse-fraction heavy minerals in stream sediment samples. This technique has been successful at characterizing known minerals from the nearby Casino deposit and ongoing work on water chemistry may further support enhanced regional and targeted stream geochemical surveys (McClenaghan *et al.*, 2020).

Soil geochemistry quality depends on a wide number of site-specific factors including total soil depth, permafrost depth, surface organic thickness, loess thickness, transport distance, and type of geochemical anomaly (McKillop *et al.*, 2013). Existing soil sampling programs in the study area have had variable success (Casselman, 2015; James, 2019), but are generally under-used because of the complexity of the surficial setting. Understanding soil parent material genesis and distribution is a critical part of planning good surveys and reducing uncertainty in geochemical results.

Surficial materials distribution

Pre-Reid landscapes

Pre-Reid landscapes in the eastern part of the study area are dominated by weathered bedrock and colluvium. Glacial sediments deposited during pre-Reid glaciations have largely been moved downslope by gravity and have accumulated in valley bottoms and on stable topographic settings that have escaped erosion. Pre-Reid glacial sediments have been observed in borrow pit materials near Tinta Hill, and in deep excavations and drill core from tributaries to Big Creek. Pre-Reid landscapes and materials in the nearby McQuesten map sheet (NTS 115P) are discussed in detail in Bond and Lipovsky (2010).

Reid landscapes

Reid-aged landscapes comprise the surficial setting for existing mineral deposits and significant occurrences in the Carmacks-Minto copper belt, and as such, are addressed in detail here. The rounded uplands, shallow hillslopes, and broad, flat valley bottoms of the upper Merrice (Fig. 9) and Williams creek valleys make useful analogues for a number of similar drainages in the region. In order to illustrate the distribution of surficial sediments in the southern part of the copper belt, idealized valley profiles were constructed for characteristic landscape positions (Figs. 10c, 12a, 13a and 14d). Idealized distributions are based on observations from soil pits, road cuts, trenches and drill core in Williams, Nancy Lee and Hoocheekoo valleys.



Figure 9. *View down (east) upper Merrice Creek from Tinta Hill. The gentle topography and flat valley floor is typical of many east-flowing tributaries to the Yukon River in the study area.*

Valley bottoms

Broad, flat valley bottoms are common in many east-flowing tributaries to the Yukon River, and reflect Quaternary infilling of formerly v-shaped fluvial drainages (Fig. 10a,b). Impoundment of Yukon River tributaries during the Reid Glaciation (and possibly the McConnell as well) resulted in glaciolacustrine deposits in many valley bottoms. These materials range from fine silt to coarse sand and are often associated with deltas and other shoreline deposits preserved ~2 to 20 m above the modern valley floor (Fig. 11). Glaciolacustrine and deltaic landforms are better exposed along the base of south-facing hillslopes and may be partially buried by eolian sediments at the base of north-facing hillslopes (Fig. 10c). Fine-grained glaciolacustrine and glaciofluvial or deltaic materials can be challenging to distinguish from eolian sand deposits and may, in part, be sources for these materials.

Valley bottom sediments are generally not exposed in the study area, but drilling at Carmacks Copper suggests up to 80 m of unconsolidated sediments beneath the modern valley floor (Fig. 10c). Valley filling sediments commonly comprise glacial, glaciofluvial, lacustrine and fluvial sediments, but may also include pre-Quaternary sedimentary and volcanic materials. Permafrost is common in valley bottoms where poor drainage contributes to saturated conditions and thick organic cover.

It is not recommended that traditional parent-material soil samples be collected in valley bottom settings in the southern Carmacks-Minto copper belt. Bedrock may be close to (or at) surface in some areas, but valley bottom landscapes lack the even distribution and simple transport vectors required to generate high quality geochemical results. Existing samples collected

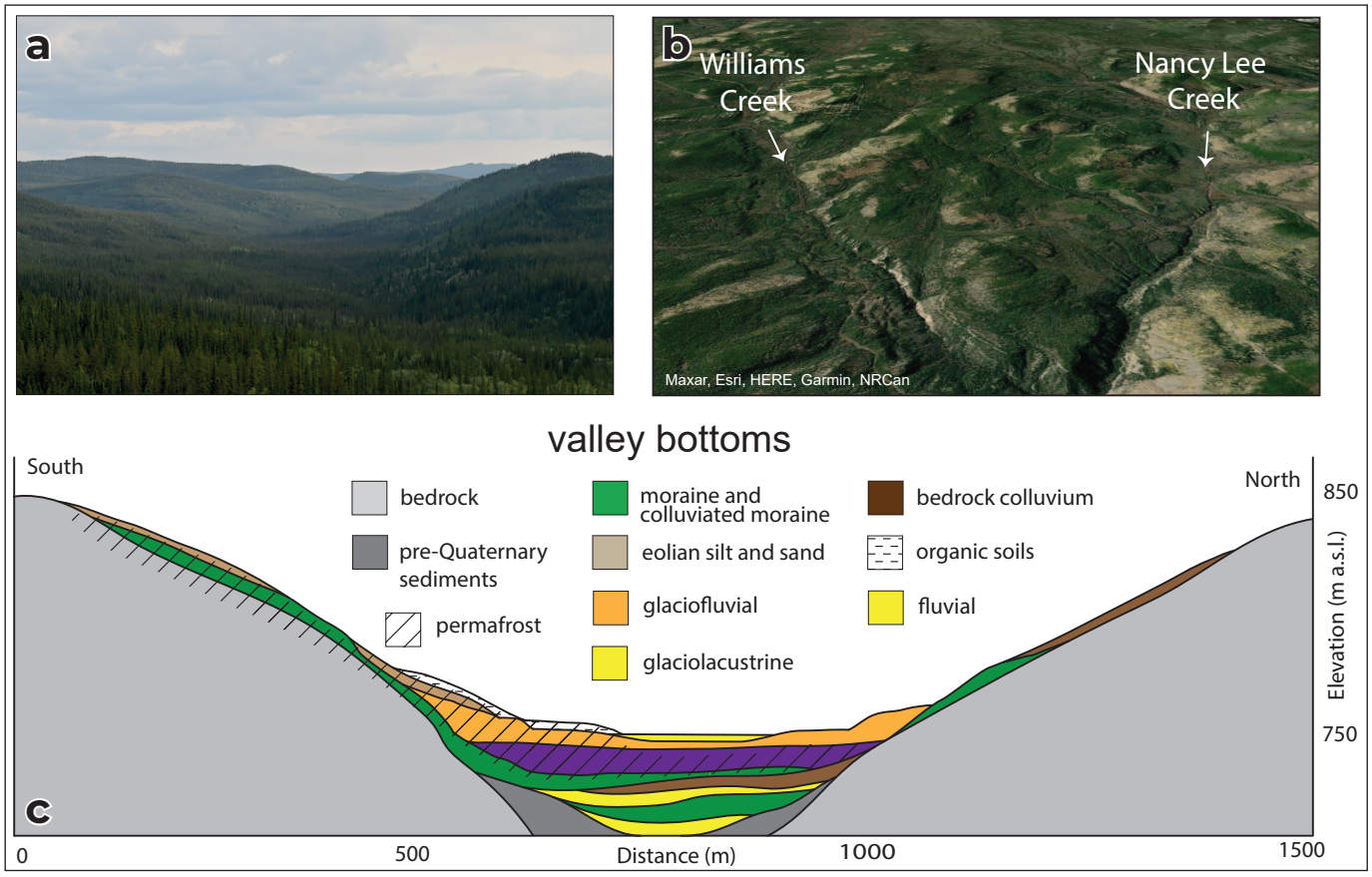


Figure 10. (a) *View west up Williams Creek from near its confluence with the Yukon River.* ***(b)*** *View west over Williams and Nancy Lee creeks (image from ArcGIS Earth).* ***(c)*** *Idealized cross valley profile of Williams Creek from observations of east-flowing drainages between the Carmacks Copper and Stu properties. Hypothetical valley fill comprises a range of glacial and non-glacial materials. Eolian deposits (including ash) are present on most surfaces.*

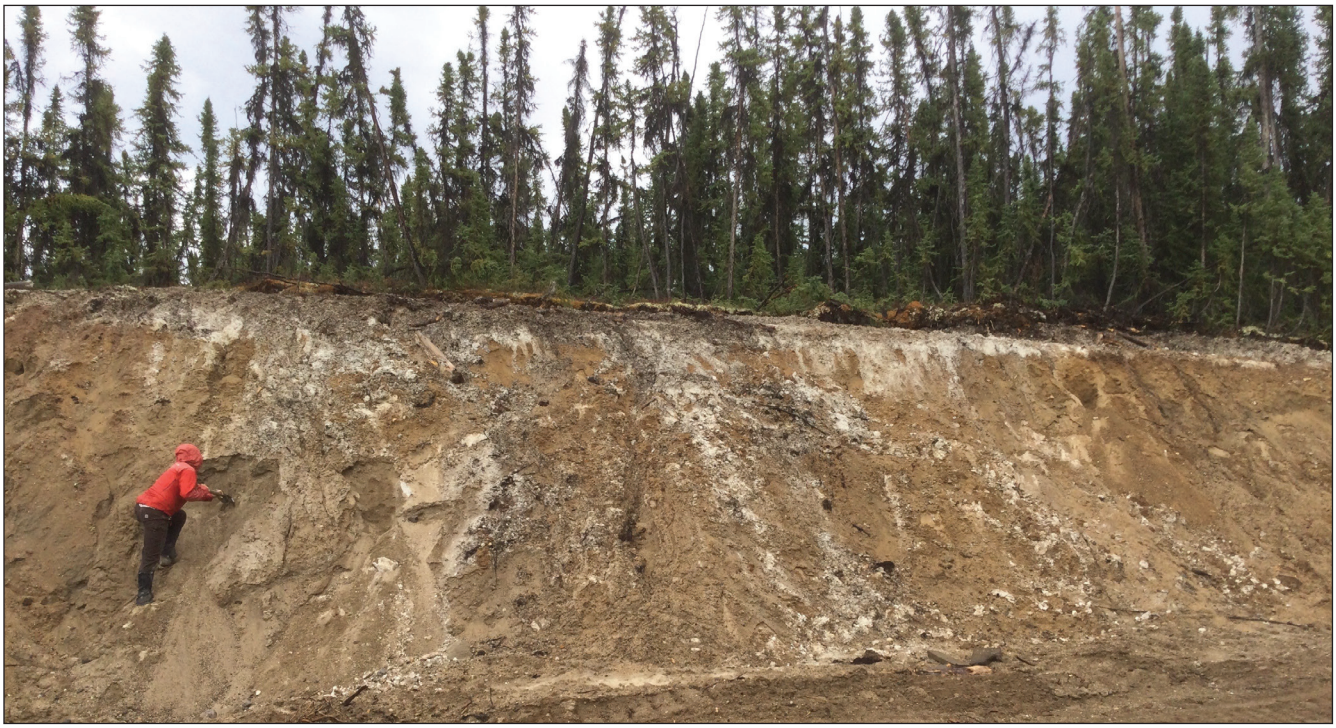


Figure 11. *Sandy glaciolacustrine or deltaic sediments form a flat terrace on this north-facing slope ~10 m above the modern valley floor.*

using traditional soil sampling methods are unlikely to accurately reflect underlying bedrock in valley bottom settings.

North-facing hillslopes

North-facing slopes are characterized by cold thermal conditions and relatively intact surficial materials (Fig. 12a). Moraine (till) is found in both blankets (>1 m thick) and veneers on higher positions on valley sides and commonly comprises a sandy cobble diamict with a silt-rich matrix. Till preservation is discontinuous on hillslopes and can fill topographic depressions where it reaches observed thicknesses of at least 2.5 m.

Moraine exposed in a north-facing trench above Williams Creek (Fig. 12b) can be subdivided based on texture, lithology and degree of compaction into three diamict units: a lower mixed facies containing local bedrock (unit 3 on Fig. 12c); a silty compact facies of non-local materials (unit 4); and a modified, loose upper facies of predominantly non-local materials (unit 5). Copper values from each unit are generally representative of transport distance. High copper in mixed bedrock and till at the lower contact of unit 2 (3220 ppm Cu) and bedrock-enriched till in unit 3 (700 ppm Cu) contrast with low copper values in overlying silty, compact, and far-travelled materials of units 4 and 5 (38.3 and 38.8 ppm Cu). Slightly elevated copper values in unit 6 (108.5 ppm Cu) are likely related to the incorporation of upslope bedrock materials into this unit.

Eolian sand deposits are most common near glacial limits where prolonged katabatic winds developed sand sheets, dunes and blankets. These landforms and materials are best preserved on leeward (north-northwest facing) slopes and in hollows and depressions (Fig. 12e). Eolian deposits are thickest near the Yukon River valley and around other floodplain sources of sand and silt. Windblown sand and silt deposits are derived from both proximal and distal sources, are well-homogenized, and record cooler, windier, glacial and periglacial conditions (Muhs, 2017). Ice-rich organic materials are common at the bottom of north-facing hillslopes (Fig. 12d).

North-facing hillslopes can be challenging settings for surficial geochemical sampling. Highly-transported glacial and eolian materials are poor proxies for bedrock and may accumulate in thicknesses that make traditional sampling impractical. Existing samples from these areas should be used with caution unless parent materials are clearly documented. Shallow auger drills would be useful for new surveys where glacial or eolian materials are preserved in thicknesses that limit hand sampling. It isn't clear how permafrost may affect partial-leach mobile metal applications, but its widespread presence should be taken into account in these sampling programs.

South-facing hillslopes

South-facing hillslopes are warmer and drier than north-facing slopes in the study area. Gravity-driven processes dominate south-facing slopes and much of the surficial cover has been moved into lower slope and valley bottom positions on the landscape (Fig. 13). Silt-enriched weathered bedrock and weathered bedrock colluvium are common on middle and upper slope positions (Fig. 13b).

South-facing hillslopes provide many good settings for surficial geochemical sampling. Care should be taken to avoid thick surficial cover, confirm bedrock parent materials, and recognize silt-enrichment at the top of the soil profile. On some south-facing slopes, ongoing

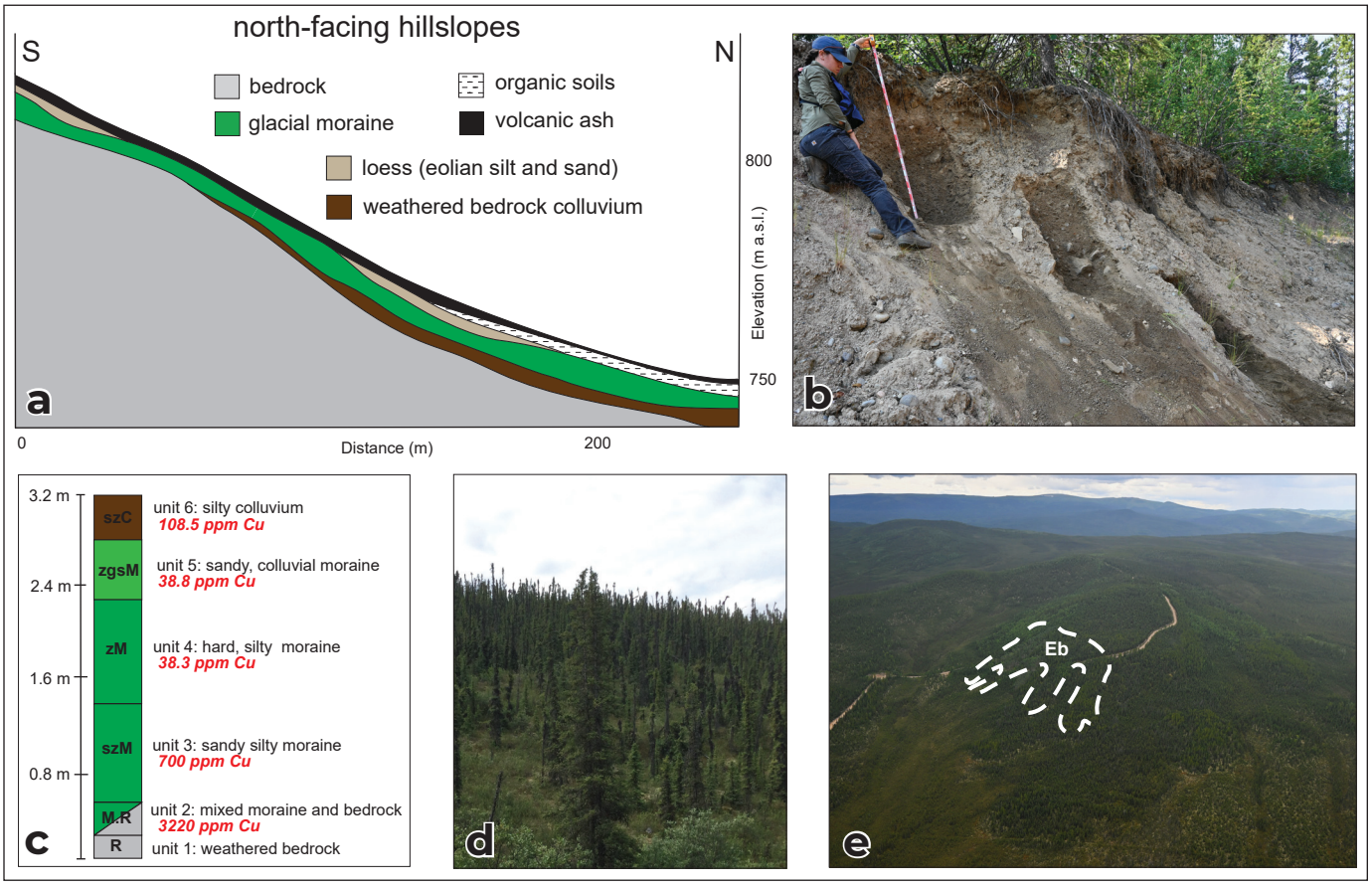


Figure 12. (a) *Idealized valley profile of a north-facing hillslope in the study area. Blankets and veneers of till are preserved above bedrock, weathered bedrock, and colluvium on most surfaces. Eolian silt, sand, and ash is well-preserved and may be overlain by, or interbedded with, ice-rich organic materials. Permafrost is not shown, but is present on most north-facing slopes.* ***(b)*** *Moraine exposed in a ~3 m deep trench above Williams Creek.* ***(c)*** *Stratigraphic profile of the units exposed in* ***(b)*** *with results from silt-fraction geochemistry.* ***(d)*** *Permafrost is common on north-facing slopes and can be associated with thick organic soils and stunted forest.* ***(e)*** *This sandy eolian blanket was deposited on a northwest-facing slope above Williams Creek. Cold soils and thick vegetation likely helped preserve these sediments.*

weathering of exposed bedrock has generated thin veneers of weathered bedrock colluvium that can obscure underlying extra-basinal sediments (Fig. 13c). These materials may be good representations of upslope bedrock if sampled correctly, but could confound the results of programs focusing on A-horizon or biological samples.

Upland surfaces

Flat to gently sloping upland surfaces are commonly characterized by bedrock or weathered bedrock variably overlain by windblown silt (loess) and ash (Fig. 14). With background or lower than background metal values (Preece *et al.*, 2014), windblown ash can mask underlying mineralized soils when incorporated into geochemical samples. This dilution of soil samples is well-known and primary ash fall is easily recognizable in the field. Similarly, numerous publications have discussed the poor suitability of loess for geochemical sampling in the Dawson Range, and their findings apply to this study area as well (McKillop, 2013; Bond and Lipovsky, 2011).

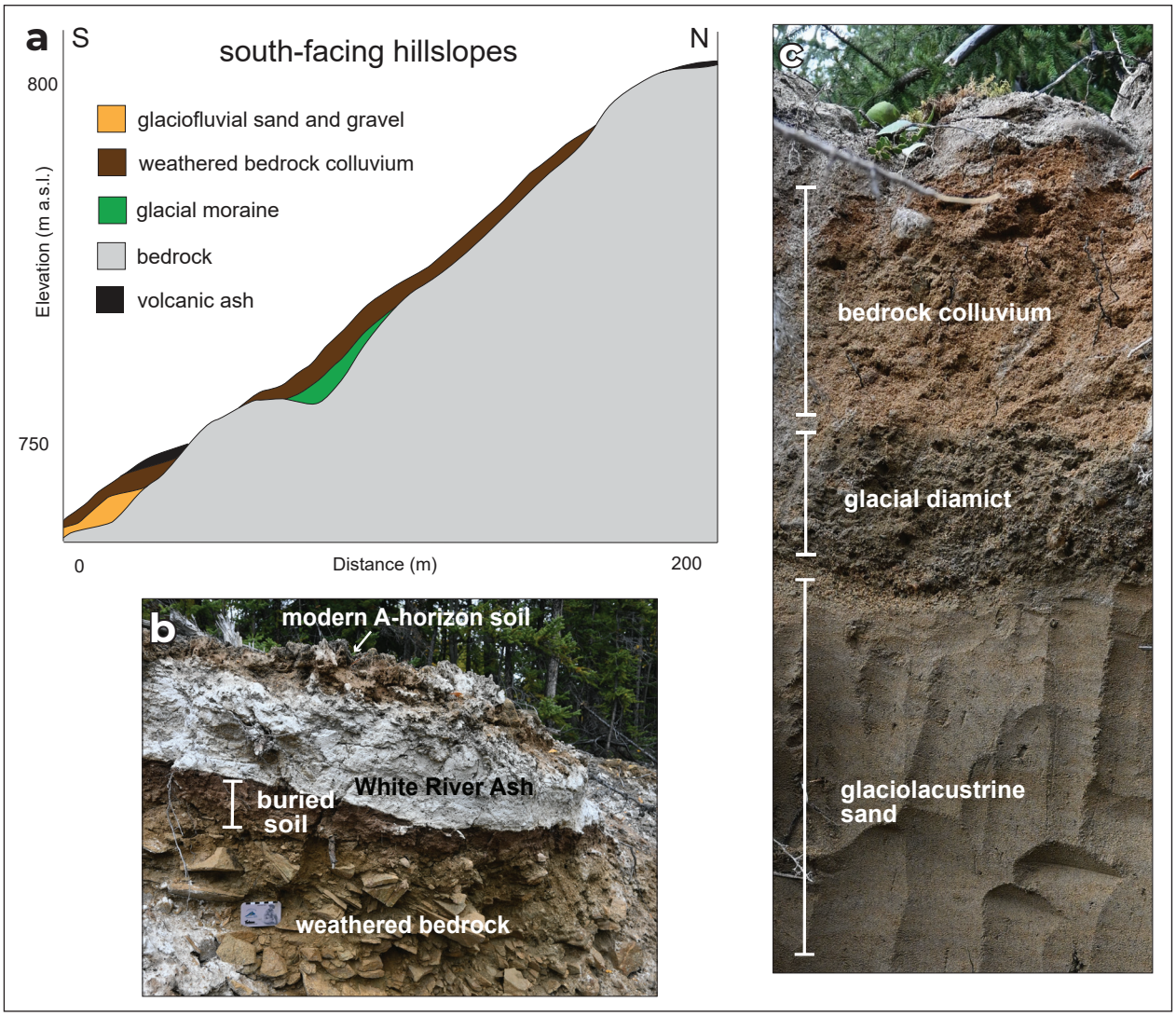


Figure 13. ***(a)*** *Idealized valley profile of a south-facing hillslope in the study area. Upper slopes are characterized by thin surficial cover and abundant bedrock, weathered bedrock, and weathered bedrock colluvium.* ***(b)*** *White River Ash is preserved above a well-developed soil in local weathered bedrock materials.* ***(c)*** *A veneer of weathered granite bedrock overlies till and glaciolacustrine sediments on this south-facing section near the bottom of a hillslope on Nancy Lee Creek.*

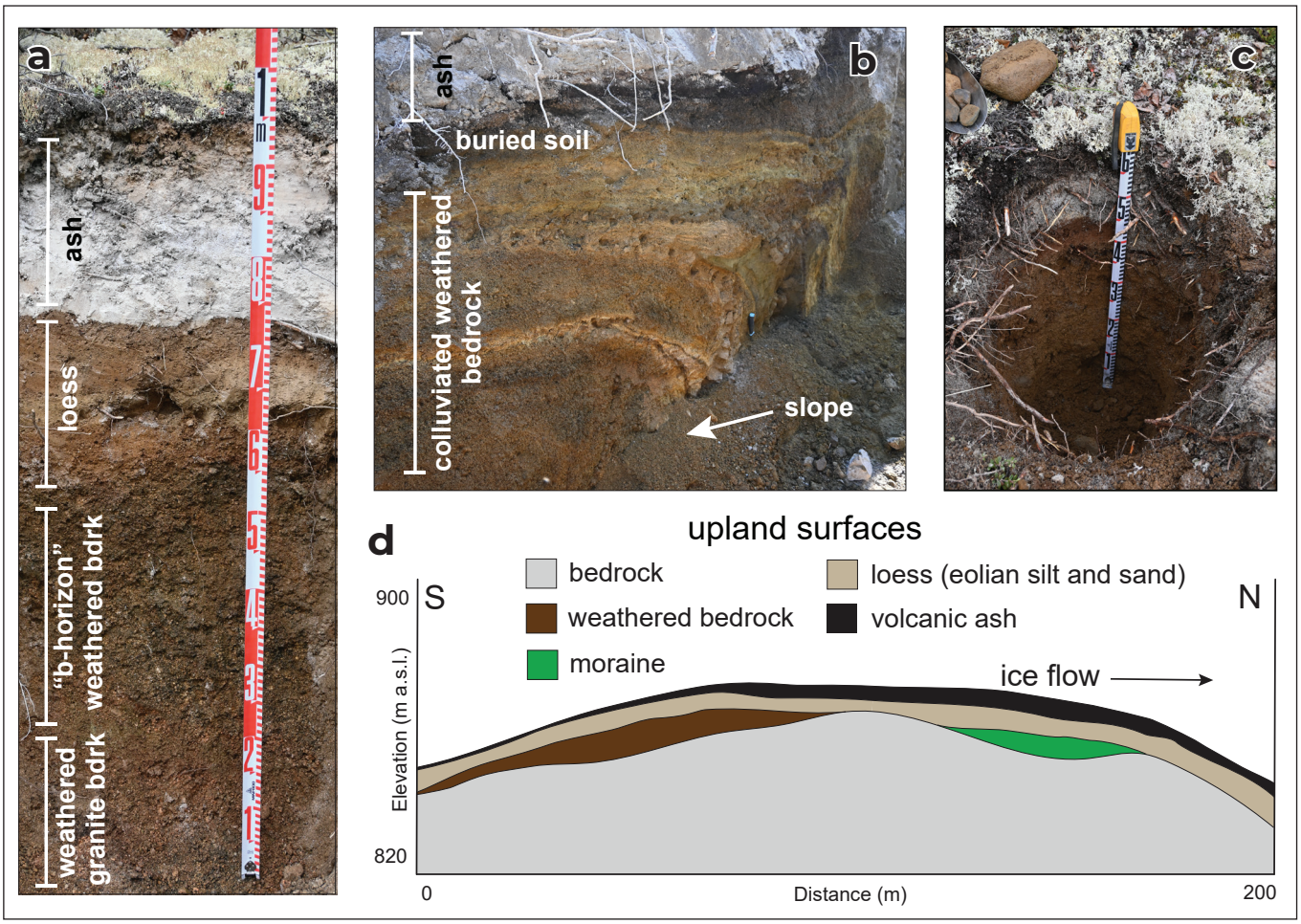


Figure 14. (a) *The stratigraphy seen in this road cut is common on upland surfaces that have seen limited erosion. Granite bedrock and weathered granite bedrock are overlain by windblown silt (loess) and ash.* ***(b)*** *Weathered bedrock in this trench on the Stu property is creeping downslope (toward the left). Deeply weathered and fractured bedrock is overlain by a well-developed paleosol and thick accumulations of White River Ash.* ***(c)*** *A typical soil pit on a Reid-aged upland surface is characterized by ash (~10–15 cm) and loess (~20 cm) overlying silty, oxidized, pebble-cobble glacial diamict.* ***(d)*** *Upland surfaces preserve relatively thin (<1 m) in situ accumulations of weathered bedrock and eolian sediments.*

Intact weathered bedrock and moderately transported weathered bedrock are ideal surficial geochemical materials and analytical results for these medium are straight-forward to interpret. While windblown materials are generally thin on upland surfaces, they may accumulate in topographic swales or other protected areas. Loess can also be incorporated into parent materials through cryoturbation and have a significant impact on geochemical results (Bond and Sanborn, 2006). Regardless, both loess and volcanic ash are easy to identify and avoid in flat to gently sloping upland environments.

McConnell landscapes

McConnell-aged landscapes have a limited extent in the study area and are primarily restricted to the Yukon River valley and areas south of Merrice Creek (Fig. 4). Materials associated with McConnell glaciation are generally thicker and more continuous than glacial deposits associated with earlier glaciations. Detailed descriptions of McConnell-aged materials are available in Cronmiller (2020) for the nearby Carmacks area.

Indicator mineral analysis

Fieldwork in 2021 included sampling for indicator minerals from both bedrock and stream sediment sources. Drill core samples containing a range of mineralized and unmineralized rocks from the Minto and Carmacks deposits have been submitted to Overburden Drilling Management for indicator mineral characterization. The results of these samples will be compared to five stream sediment samples collected from upstream and downstream of the Carmacks deposit on Williams Creek and tributaries. Preliminary results will be reported at a later date, and follow-up sampling and analysis may be undertaken.

Conclusions

Assessment reports for the Carmacks-Minto copper belt routinely report that <10% of the landscape is suitable for traditional prospecting. The remaining 90% of the landscape requires dealing with surficial geology. Understanding the genesis and distribution of these materials will inevitably improve exploration results.

When used with an understanding of surficial materials, traditional soil sampling has been shown to work well in this region (James, 2019). Identifying areas of thick cover is essential to leveling results and obtaining reliable samples with the least amount of time and effort. Windblown silt and ash are variably deposited across the study area and have the potential to significantly dilute surficial geochemical samples. Traditional soils will need to be supported by alternative sampling programs (*i.e.*, shallow drilling or selective leach geochemistry) over areas of thick surficial cover. The landscape model presented here can also be used to evaluate existing soil geochemistry data and highlight areas that may require targeted sampling through alternative methods. Ultimately, it may be useful to level data according to topographic position in order to minimize the diluting effects of thick surficial cover.

Although general genetic processes and distributions are discussed here, property-scale surficial mapping is a critical base layer for designing and interpreting surficial geochemical surveys. Given the subdued geomorphology, pervasive eolian cover and dense vegetation, any future mapping should be based on stereo-photography coupled with high-resolution airborne lidar. Ongoing work in the region will focus on updating glacial limits, expanding our knowledge of the surficial geology, and testing the utility of stream sediment indicator minerals for ongoing exploration.

Acknowledgements

Little Salmon Carmacks and Selkirk First Nations are thanked for sharing access to their Traditional Territories in order for this work to be completed. Granite Creek Copper provided camp and logistical support for fieldwork on their Carmacks and Carmacks North properties. Debbie James and Owen Peer were gracious hosts and provided invaluable property-scale geological knowledge. Conversations with Jeff Bond, Scott Casselman, Maurice Colpron, Nicolette Kovacs, Povilas Grigutis and Jacob Longridge contributed significantly to our understanding of regional and property-scale geology. Emily Halle and Jesse Halle are also thanked for supporting logistical aspects of this work, providing local expertise, and sharing deep “overburden” core from the Freegold Mountain project. A review of this manuscript by Jeff Bond added breadth and depth to the paper, and Jeff is thanked for his contribution. Karen MacFarlane’s careful and thoughtful editing is very much appreciated.

References

Bond, J.D. and Sanborn, P.T., 2006. Morphology and geochemistry of soils formed on colluviated weathered bedrock: Case studies from unglaciated upland slopes in west-central Yukon. Yukon Geological Survey, Open File 2006-19, 70 p.

Bond, J.D. and Lipovsky, P.S., 2010. Pre-Reid surficial geology investigations in southwest McQuesten map area (115P). *In:* Yukon Exploration and Geology 2009, K.E. MacFarlane, L.H. Weston and L.R. Blackburn (eds.), Yukon Geological Survey, p. 103–117.

Bond, J.D. and Lipovsky, P.S., 2011. Surficial geology, soils and permafrost of the northern Dawson Range. *In:* Yukon Exploration and Geology 2010, K.E. MacFarlane, L.H. Weston and C. Relf (eds.), Yukon Geological Survey, 19–32.

Bostock, H.S., 1936. Carmacks district, Yukon. Geological Survey of Canada, Memoir 189, 58 p.

Bostock, H.S., 1966. Notes on glaciation in central Yukon Territory. Geological Survey of Canada, Paper 65-56, 18 p.

Casselman, S., 2015. Assessment report for the Carmacks Copper Project. Yukon Energy, Mines and Resources Assessment Report 96688, 220 p. including appendices.

Clague, J.J., Evans, S.G., Rampton, V.N. and Woodsworth, G.J., 1995. Improved age estimates for the White River and Bridge River tephras, western Canada. Canadian Journal of Earth Sciences, vol. 32, no. 8, p.1172–1179.

Cronmiller, D.C., 2020. Surficial geology, Carmacks area, Yukon (parts of NTS 115I/1). Yukon Geological Survey, Open File 2020-43, scale 1:15000.

Duk-Rodkin, A., 1999. Glacial limits map of Yukon Territory. Geological Survey of Canada Open File 3694; Exploration and Geological Services Division, Yukon Region, Indian and Northern Affairs Canada, Geoscience Map 1999-2, scale 1:1 000 000.

Duk-Rodkin, A., Barendregt, R.W. and White, J.M., 2010. An extensive late Cenozoic terrestrial record of multiple glaciations preserved in the Tintina Trench, west-central Yukon: stratigraphy, paleomagnetism, paleosols, and pollen. Canadian Journal of Earth Science, vol. 47, p. 1003–1028.

Demuro, M., Froese, D.G., Arnold, L.J. and Roberts, R.G., 2012. Single-grain OSL dating of glaciofluvial quartz constrains Reid glaciation in NW Canada to MIS 6. Quaternary Research, vol. 77, p. 305–316.

Englehardt, P.O., Ward, B.C., Bond J.D. and Coleman, M.J., 2016. Early Pleistocene glaciation and implications for placer gold deposits in Back Creek, Mount Nansen area, Yukon. *In:* Yukon Exploration and Geology 2015, K.E. MacFarlane and M.G. Nordling (eds.), Yukon Geological Survey, p. 111–129.

Grond, H.C., Churchill, S.J., Armstrong, R.L., Harakal, J.E. and Nixon, G.T., 1984. Late Cretaceous age of the Hutshi, Mount Nansen, and Carmacks groups, southwestern Yukon Territory and northwestern British Columbia. Canadian Journal of Earth Sciences, vol. 21, p. 554–558.

Heberlein, D.R., Dunn, C.E. and Macfarlane, W., 2013. Use of organic media in the geochemical detection of blind porphyry copper-gold mineralization in the Woodjam property area, south-central British Columbia (NTS 093A/03, /06). *In:* Geoscience BC Summary of Activities 2012, Geoscience BC, Report 2013-1, p. 47–62.

Heberlein D.R. and Samson H., 2010. An assessment of soil geochemical methods for detecting copper-gold porphyry mineralization through Quaternary glaciofluvial sediments at the Kwanika central zone, north-central British Columbia. Geoscience BC Report 2010-03, 97 p.

Hughes, O.L., Campbell, R.B., Muller, J.E. and Wheeler, J.O., 1969. Glacial limits and flow patterns, Yukon Territory, south of 65 degrees north latitude. Geological Survey of Canada, Paper 68–34, 9 p.

Huscroft, C.A., Ward, B.C., Barendregt, R.W., Jackson, L.E., Jr. and Opdyke, N.D., 2004. Pleistocene volcanic damming of Yukon River and the maximum age of the Reid Glaciation, west-central Yukon. Canadian Journal of Earth Sciences, vol. 41, p. 151–164.

Jackson, Jr., L.E., and Harington, C.R., 1991. Middle Wisconsinan mammals, stratigraphy, and sedimentology at the Ketza River site, Yukon Territory. Geographie physique et Quaternaire, vol. 45, p. 69–77.

Jackson, Jr., L.E., Ward, B.C., Duk-Rodkin, A. and Hughes, O.L., 1991. The latest Cordilleran ice sheet in Yukon Territory. Geographie Physique et Quaternaire, vol. 45-3, p. 341–354.

Jackson, Jr., L.E., Nelson, F.E., Huscroft, C.A., Villeneuve, M., Barendregt, R.W., Storer, J.E. and Ward, B.C., 2012. Pliocene and Pleistocene volcanic interaction with Cordilleran ice sheets, damming Yukon River and vertebrate palaeontology, Fort Selkirk Volcanic Group, west-central Yukon, Canada. Quaternary International, vol. 260, p. 3–20.

Jackson, Jr., L.E., Barendregt, R.W., Baker, J. and Irving, E., 1996. Early Pleistocene volcanism and glaciation in central Yukon: a new chronology from field studies and paleomagnetism. Canadian Journal of Earth Science, vol. 33, p. 904–916.

Jackson, Jr., L.E., 2000. Quaternary Geology of the Carmacks map area, Yukon Territory. Geological Survey of Canada, Bulletin 539, 74 p., plus maps and appendices.

James, D., 2019. Geological and Geochemical Exploration Program on the Stu Copper Property. Yukon Energy, Mines and Resources Assessment Report 97373, 68 p.

Kovacs, N., Allan, M.M., Crowley, J.L., Colpron, M., Hart, C.J.R., Zagorevski, A. and Creaser, R.A., 2020. Carmacks Copper Cu-Au-Ag deposit: mineralization and post-ore migmatization of a Stikine arc porphyry copper system in Yukon, Canada. Economic Geology, vol. 115, p. 1413–1442.

LeBarge, W.P., 1995. Sedimentology of placer gravels near Mt. Nansen, central Yukon Territory. Exploration and Geological Services Division, Indian and Northern Affairs Canada, Yukon Region, Bulletin 4, 155 p.

Lerbekmo, J.F., 2008. The White River Ash: largest Holocene Plinian tephra. Canadian Journal of Earth Sciences, vol. 45, p. 693–700.

Lerbekmo, J.F. and Campbell, F.A., 1969. Distribution, composition, and source of the White River ash, Yukon Territory. Canadian Journal of Earth Sciences, vol. 6, p. 109–116.

Mackie, R., Arne, D. and Pennimpede, C., 2016. Enhanced interpretation of stream sediment geochemical data for NTS 115I. Yukon Geological Survey, Open File 2016-14, 15 maps.

Mackie, R.A., Arne, D.C. and Pennimpede, C., 2017. Assessment of Yukon regional stream sediment catchment basin and geochemical data quality. Yukon Geological Survey, Open File 2017-4, 29 p. and digital files.

Matthews, J.V., Schweger, C.E. and Janssens, J.A., 1990. The last (Koy-Yukon) interglaciation in the northern Yukon: evidence from Unit 4 at Ch'ijee's Bluff, Bluefish Basin. Geographie Physique et Quaternaire, vol. 44, p. 341–362.

McClenaghan, M.B., McCurdy, M.W., Beckett-Brown, C.E. and Casselman, S.C., 2020. Indicator-mineral signatures of the Casino porphyry Cu-Au-Mo deposit, Yukon. Geological Survey of Canada, Open File 8711, 42 p. and 11 maps.

McKillop, R., Turner, D., Johnston, K. and Bond, J., 2013. Property-scale classification of surficial geology for soil geochemical sampling in the unglaciated Klondike Plateau, west-central Yukon. Yukon Geological Survey, Open File 2013-15, 85 p. including appendices.

Menounos, B., Goehring, B.M., Osborn, G., Margold, M., Ward, B., Bond, J., Clarke, G.K.C., Clague, J.J., Lakeman, T., Koch, J., Caffee, M.W., Gosse, J., Stroeven, A.P., Seguinot, J. and Heyman, J., 2017. Cordilleran Ice Sheet mass loss preceded climate reversals near the Pleistocene Termination. Science, vol. 358, p. 781–784.

Muhs, D.R. 2017. The geochemistry of loess: Asian and North American deposits compared. Journal of Asian Earth Sciences, vol. 155, p. 81–115.

Mulliken, K.M., Schaefer, J.R. and Cameron, C.E., 2018. Geospatial distribution of tephra fall in Alaska: a geodatabase compilation of published tephra fall occurrences from the Pleistocene to the present. Alaska Division of Geological and Geophysical Surveys, Miscellaneous Publication 164, 46 p., https://doi.org/10.14509/29847.

Nelson, F.E., Barendregt, R.W. and Villeneuve, M., 2009. Stratigraphy of the Fort Selkirk volcanogenic complex in central Yukon and its paleoclimatic significance: Ar/Ar and paleomagnetic data. Canadian Journal of Earth Science, vol. 46, p. 381–401.

Paulter, J., 2015. Geological, geochemical, trenching and archaeological report on the Stu Project in the Carmacks Copper-Gold Belt, Yukon. Yukon Energy, Mines and Resources Assessment Report 96761, 74 p. including appendices.

Paulter, J. 2016. Compilation report on the Williams South Project in the Carmacks Copper-Gold Belt, Yukon Territory. Yukon Energy, Mines and Resources Assessment Report 96798, 534 p. including appendices.

Preece, S.J., Pearce, N.J.G., Westgate, J.A., Froese, D.G., Jensen, B.J.L. and Perkins, W.T., 2011. Old Crow tephra across eastern Beringia: a single cataclysmic eruption at the close of Marine Isotope Stage 6. Quaternary Science Reviews, vol. 30, p. 2069–2090.

Preece, S.J., McGimsey, R.G., Westgate, J.A., Pearce, N.J.G., Hart, W.K. and Perkins, W.T., 2014. Chemical complexity and source of the White River Ash, Alaska and Yukon. Geosphere, vol. 10, p. 1020–1042.

Sack, P.J., Colpron, M., Crowley, J.L., Ryan, J.J., Allan, M.M., Beranek, L.P. and Joyce, N.L., 2020. Atlas of Late Triassic to Jurassic plutons in the Intermontane terranes of Yukon. Yukon Geological Survey, Open File 2020-1, 365 p.

Sack and Colpron (2021). Magmatic-hydrothermal deposits in central Yukon: Variations on a theme. Unpublished fieldtrip guide, Yukon Geological Survey.

Turner, D.G., Ward, B.C., Bond, J.D., Jensen, B.J.L., Froese, D.G., Telka, A.M., Zazula, G.D. and Bigelow, N.H., 2013. Middle to Late Pleistocene ice extents, tephrochronology and paleoenvironments of the White River area, southwest Yukon. Quaternary Science Reviews, vol. 75, p. 59–77.

Ward, B.C., Bond, J.D. and Gosse, J.C., 2007. Evidence for a 55–50 ka (early Wisconsin) glaciation of the Cordilleran ice sheet, Yukon Territory, Canada. Quaternary Research, vol. 68, p. 141–150.

Ward, B.C., Bond, J.D., Froese, D. and Jensen, B., 2008. Old Crow tephra (140 ± 10 ka) constrains penultimate Reid glaciations in central Yukon Territory. Quaternary Science Reviews, vol. 27, p. 1909–1915.

Westgate, J.A., Preece, S.J., Froese, D.G., Walter, R.C. and Sandhu, A.S., 2001. Dating Early and Middle (Reid) Pleistocene glaciations in central Yukon by tephrachronology. Quaternary Research, vol. 56, p. 335–348.

Wolfe, S., Bond, J. and Lamothe, M., 2011. Dune stabilization in central and southern Yukon in relation to early Holocene environmental change, northwestern North America. Quaternary Science Reviews, vol. 30, p. 324–334.

Yukon Geological Survey, 2020a. Yukon digital bedrock geology. Yukon Geological Survey, https://data.geology.gov.yk.ca/Compilation/3, [accessed December 3, 2021].

Yukon Geological Survey, 2020b. Yukon MINFILE – A database of mineral occurrences. Yukon Geological Survey, https://data.geology.gov.yk.ca, [accessed December 3, 2021].

Geology of the Carpenter Creek and McKay Hill areas (NTS 106D/6, 11), central Yukon

Rosie Cobbett*
Yukon Geological Survey

Cobbett, R., 2022. Geology of the Carpenter Creek and McKay Hill areas (NTS 106D/6, 11), central Yukon. *In:* Yukon Exploration and Geology 2021, K.E. MacFarlane (ed.), Yukon Geological Survey, p. 125–142.

Abstract

The Carpenter Creek area straddles the Paleozoic basin-platform transition which is coincident with the Dawson thrust in north-central Yukon. North of the thrust, the strata can be broadly divided into two groups: (1) Proterozoic sedimentary and intrusive rocks, and (2) Paleozoic platformal strata with volcanic rock horizons. The two groups of rocks are separated by an angular unconformity. Below the unconformity, Hart River gabbro sills and dikes (ca. 1.38 Ga) intrude the Gillespie Lake Group. Younger Proterozoic rocks that are not intruded by the gabbro occur on the other side of a fault that traces through the Carpenter Creek valley. These rocks are interpreted to be younger than Gillespie Lake Group and are tentatively assigned to Pinguicula Group. Above the unconformity, Paleozoic volcanic and volcaniclastic rocks are interstratified with carbonate rocks. The volcanic rocks occur near the base and top of the Bouvette Formation.

South of the Dawson thrust, in its direct hangingwall, volcanic and volcaniclastic rocks are interlayered with shale, chert and sandstone and intruded by discontinuous gabbro bodies of unknown age. Rare limestone lenses within the volcanic rocks contain coral fossils that constrain the age of these rocks to Middle Ordovician or younger. Hyland Group rocks are thrust over the volcanic unit and comprise shale, quartz grit and limestone. Shale exhibits a well-developed foliation, oriented parallel to the northwest-trending structural grain. Tight folds with NW-SE-striking axial planes repeats stratigraphy south of the Dawson thrust.

Within the mapped area, Ag-Pb-Zn ± Au mineralization near Grey Copper Hill occurs right along the unconformity between Upper (?) Proterozoic rocks and the Bouvette Formation (Figs. 1 and 2). Au-Ag-Cu-Pb-mineralization is spatially associated with a strike-slip fault that offsets shale, volcanic rocks and small gabbro bodies near McKay Hill (Figs. 1 and 2).

* Rosie.Cobbett@yukon.ca

Introduction

Detailed mapping (1:25 000-scale) centred on Carpenter Creek was carried out over the summers of 2019 to 2021 to provide geologic context to the igneous rocks exposed in the area and to several mineral showings in the region. The Carpenter Creek area includes parts of NTS map sheets 106D/6, 11, and part of the area is described in detail in an earlier report (Cobbett, 2020). The area is located approximately 60 km north of Keno Hill, Yukon (Fig. 1a), where previous work includes reconnaissance-scale mapping by Green (1972) and detailed, property-scale mapping by local exploration companies since the 1920s (Fig. 1; e.g., Blackburn 2010). Of note is McKay Hill (Fig. 1b), a mineral occurrence that is located south of the Dawson fault, where exploration efforts have discovered Au-Ag-Cu mineralization (e.g., Blackburn, 2010; Blackburn and Haid, 2018). Several other mineral occurrences occur north of the Dawson thrust including Grey Copper Hill, a polymetallic Ag-Pb-Zn vein prospect (Fig. 1b), where mineral exploration was conducted between 1920 and 1974, and more recently explored by Metallic Minerals in 2019 (e.g., Haid and Blackburn, 2019).

Paleozoic volcanic rocks are documented along the length of the Canadian Cordilleran in autochthonous western Laurentian stratigraphy (e.g., Abbott, 1997; Colpron *et al.*, 2002; Pigage, 2004; Pigage *et al.*, 2015; Eyster *et al.*, 2018). The volcanic rocks are linked to rifting along the western Laurentian margin during the early Paleozoic, but there is a paucity of information about their age and significance (e.g., Campbell *et al.*, 2019). This report describes the results of detailed geologic mapping undertaken to provide context to, and better characterize, volcanic rocks that occur in the Carpenter Creek area. The area includes igneous rocks that range in age from Mesoproterozoic to Late Ordovician and possibly younger. The map, cross sections, and detailed stratigraphic sections presented and described in this report provide geologic framework for future studies that will examine the geochemistry and geochronology of the volcanic rocks (Fig. 2).

Geologic Framework

The mapped area straddles the Paleozoic basin-platform transition, which coincides in this region with the Dawson thrust (Figs. 1b and 2). South of the fault, basinal facies of the Selwyn basin crop out, including Hyland Group shale, sandstone and limestone, and Ordovician shale and volcanic rocks (Skipton, 2022; Fig. 2). North of the fault, carbonate rocks of the McKenzie Platform, including the Bouvette Formation, are exposed along two east-west trending belts in the north and central parts of the map (e.g., Cecile *et al.*, 1997). Proterozoic sedimentary rocks are exposed in an east-west trending belt that occupies the centre of the mapped area between two belts of Bouvette Formation strata.

Stratigraphy in the Carpenter Creek area includes rocks as old as lower Proterozoic (Gillespie Lake Group) and as young as Devonian (upper parts of the Bouvette Formation). The older rocks are part of the Mesoproterozoic Wernecke Supergroup, which comprise clastic and carbonate rocks that were deposited in response to subsidence and subsequent basin infilling (Thorkelson, 2000). These rocks were intruded by the Hart River gabbro sills and dikes, which have been dated at *ca.* 1.38 Ga (Abbott 1997; Verbaas 2017). Upper (?) Proterozoic sedimentary rocks that are not intruded by gabbro sills and dikes are interpreted to be younger than 1.38 Ga, forming part of the Pinguicula Group that unconformably overlies the Gillespie Lake Group (Abbott 1997; Thorkelson, 2000; Medig *et al.*, 2009). Deposition of the Bouvette Formation occurs above an angular unconformity on top of these older units.

South of the Dawson thrust, the Hyland Group is thrust over Ordovician volcanic and sedimentary rocks that have been tentatively assigned to the Road River Group.

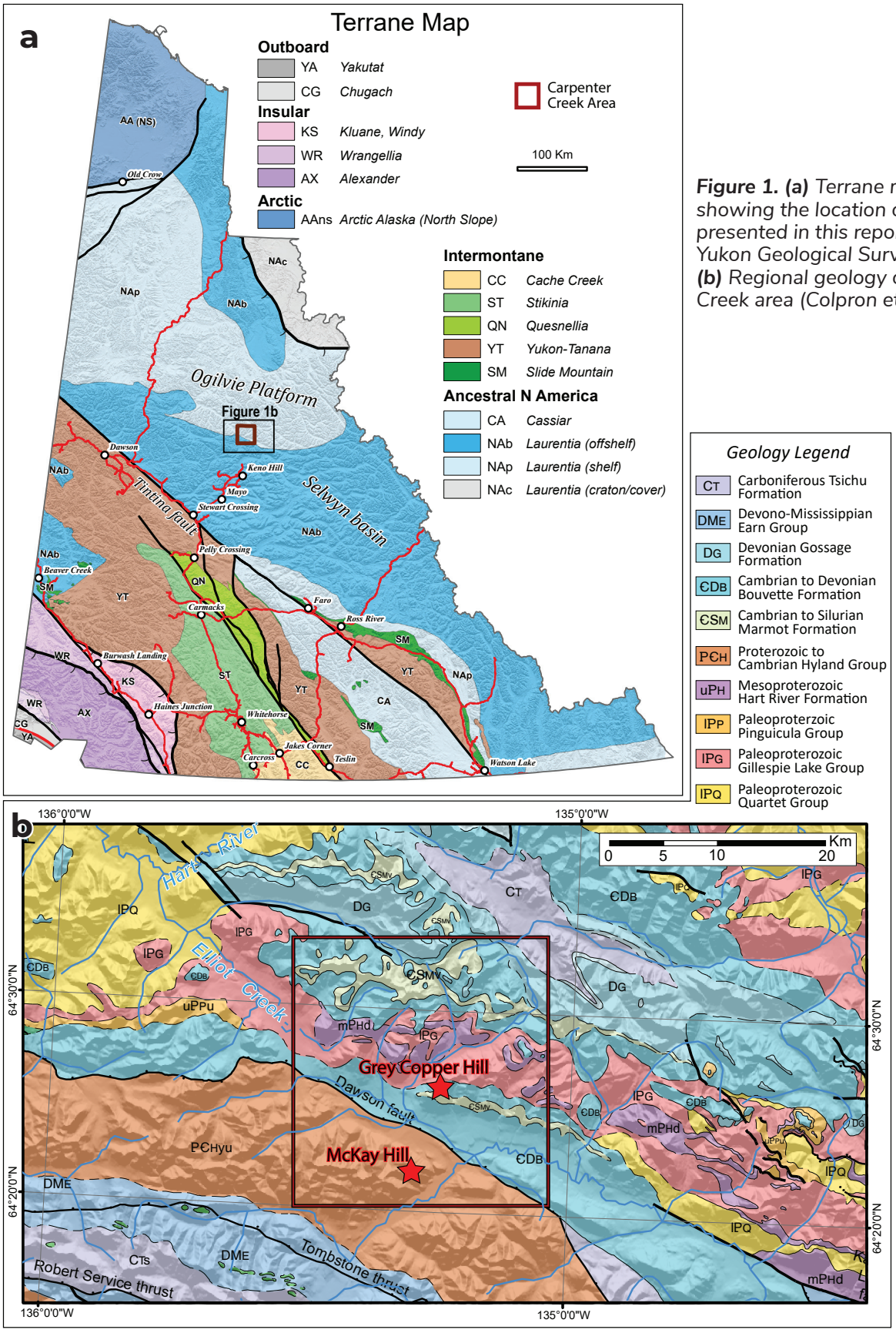


Figure 1. (a) *Terrane map of Yukon showing the location of map area presented in this report. Modified from Yukon Geological Survey, 2021.* ***(b)*** *Regional geology of the Carpenter Creek area (Colpron et al., 2016).*

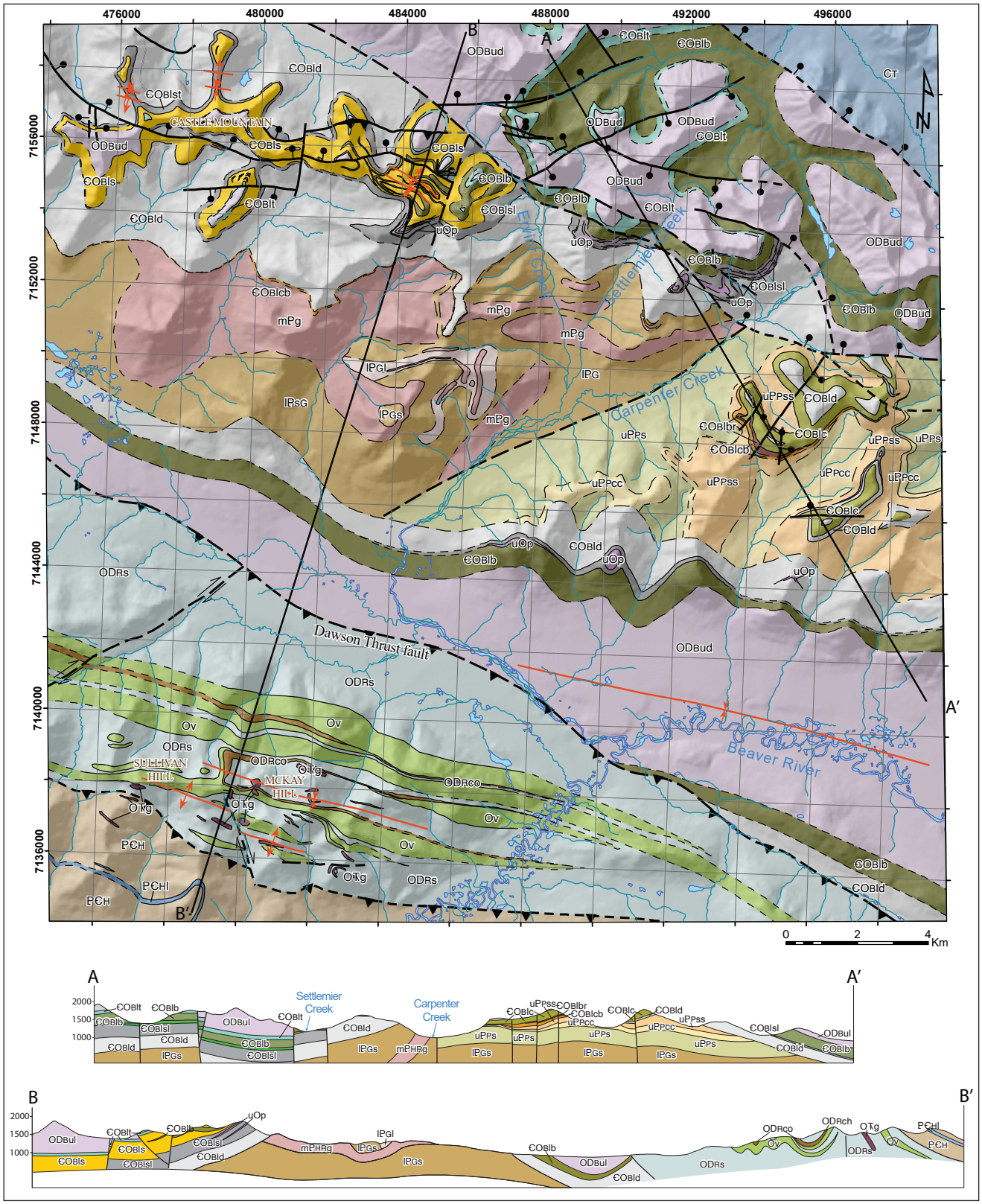


Figure 2. *Geologic map, cross sections and legend (see next page) of Carpenter Creek-McKay Hill area.*

North of Dawson Thrust Intrusive Rocks

uOp — Porphyritic augite-bearing gabbro

mPHRg — Hart River: dark green coarse-grained gabbro

Layered Rocks

Carboniferous

Tsichu Formation

CT — Tsichu: limestone, shale, chert

Cambrian to Devonian

Upper Bouvette Formation

ODBud — limestone: grey and beige-weathering, thick to thin-bedded, fossiliferous dolostone and limestone.

LowerBouvette Formation

€OBlt — tuff: biotite-phyric, crystal-lithic tuff, sandstone, chert pebble conglomerate, volcanic conglomerate, fossiliferous limestone.

€OBlb — volcanic rocks: pyroxene-phyric basalt, variably amygdaloidal, rarely pillowed; hyaloclastite breccia; mafic tuff breccia; agglomerate; minor limestone

€OBls — sandstone: brown weathering, green-grey and green fresh, variably calcareous, thin-bedded siltstone and sandstone; volcaniclastic sandstone; organge-brown weathering silty limestone with fossils

€OBlsl — silty limestone: recessive, dark grey weathering, thin to medium-bedded, graptolitic silty limestone with minor black chert beds.

€OBld — dolostone: light grey and buff weathering, massive to thick-bedded dolostone; rare silicified stromatolites.

€OBlc — conglomerate: dark green-grey weathering, conglomerate with dominantly rounded volcanic clast, minor volcaniclastic sandstone and basalt.

€OBlbr — breccia: maroon weathering, sandy breccia.

€OBlcb — carbonate breccia: bright orange weathering, beige fresh, matrix-supported breccia comprising angular clasts of dolostone, sandstone, and siltstone in a sandy matrix.

Upper Proterozoic

Pinguicula Group

uPPch — chert: dark grey to black weathering and fresh siltstone and chert.

uPPss — sandstone: brown, beige and reddish weathering, mildly calcareous, fine-grained arkosic to lithic sandstone with rare basal sections of flat lying shale chips and upper sections that are cross-bedded. Rare, orange weathering conglomerate and iron carbonate beds.

uPPcc — iron carbonate: orange-weathering iron carbonate interbedded with brown-weathering sandstone

uPPs — siltstone: thin-bedded, siltstone with minor fine-grained, orange-weathering, sandstone interbeds.

Lower Proterozoic

Gillespie Lake Group

lPGl — limestone: light-grey weathering, medium-bedded, silty limestone, calcareous siltstone and grainstone.

lPGs — siltstone: thin and medium-bedded, iron carbonate, calcareous siltstone, silty limestone and limestone all interbedded.

South of Dawson Thrust Intrusive Rocks

OTg — gabbro; minor pyroxenite

Layered Rocks

Ordovician to Devonian

Road River Group

ODRs — shale: light grey and brown shale, minor siltstone and calcareous sandstone

ODRco — conglomerate: brown weathering conglomerate with a sandy lithic matrix; clasts are dominated by sandstone, siltstone, and quartzite; dark weathering, thin to medium-bedded chert.

Cambrian to Ordovician

Ov — volcanic rocks: green fresh and weathering, mafic tuff breccia comprising angular basalt clasts in a crystal-rich, sandy matrix; pillow basalt; agglomerate.

Proterozoic to Cambrian

Hyland Group

P€H — shale: green, maroon and brown shale with minor thick beds of brown, coarse-grained, quartz-rich sandstone.

P€Hl — limestone: grey-weathering, medium-bedded, fetid limestone

Symbols

geological contacts:
defined, approximate, inferred

normal fault:
defined, approximate, inferred

strike slip:
dextral, approximate

thrust:
defined, approximate, inferred

unknown fault:
defined, approximate, inferred

fold axis; anticline, syncline

Figure 2 *continued.*

Stratigraphy north of the Dawson thrust

The stratigraphy north of the Dawson thrust can be divided into three groups based on two unconformities. The first unconformity, that separates Proterozoic sedimentary rocks and Hart River gabbro from the Paleozoic Bouvette Formation, is angular (Fig. 3). The second is a disconformity that occurs at the break between volcanic and coarse-grained clastic rocks of the lower Bouvette Formation and reefal limestone and dolostone of the upper Bouvette Formation (Fig. 3). Below are detailed descriptions of each unit and their relationships with adjacent strata.

Lower Proterozoic Gillespie Lake Group (lPGs, lPGl)

The oldest rocks in the mapped area are broadly divided into limestone and bedded carbonates, which form steep ridges that trend north-northeast between Carpenter Creek and Castle Mountain (Fig. 2). The relationship between the two units is obscured by abundant Hart River gabbro sills and dikes that intrude into the bedded rocks. The limestone unit (lPGl) comprises medium-bedded, light grey weathering limestone to silty limestone interbedded with orange and brown weathering iron carbonate and calcareous siltstone beds (Fig. 4a). The silty limestone beds rarely show cross-stratification and are hornfelsed near gabbro. The remaining volume of sedimentary rocks that make up this succession comprise thin-bedded, orange weathering, dark grey fresh, dolo-siltstone interbedded with bright orange dolo-sandstone and iron carbonate (Fig. 4b). Minor, green and dark grey, laminated to thin-bedded siltstone crop out locally but are not sufficiently extensive to map as a separate unit at 1:25 000-scale.

As the gabbro intrusions complicate structural mapping and impede lithological correlations between outcrops, it is difficult to estimate the thickness of the Gillespie Lake Group in this area. Consistently steeply-dipping bedded rocks occur continuously along one ridge (Fig. 4c). Unless the rocks are isoclinally folded across this section (no field relationships were observed to suggest this), the minimum thickness of the Gillespie Lake Group is inferred to be 1 km. The base of the Gillespie Lake Group was not observed in the mapped area. The upper contact with the Bouvette Formation is marked by an angular unconformity characterized by steeply dipping Gillespie Lake siltstone overlain by subhorizontal beds of dolostone of the Bouvette Formation (Fig. 5).

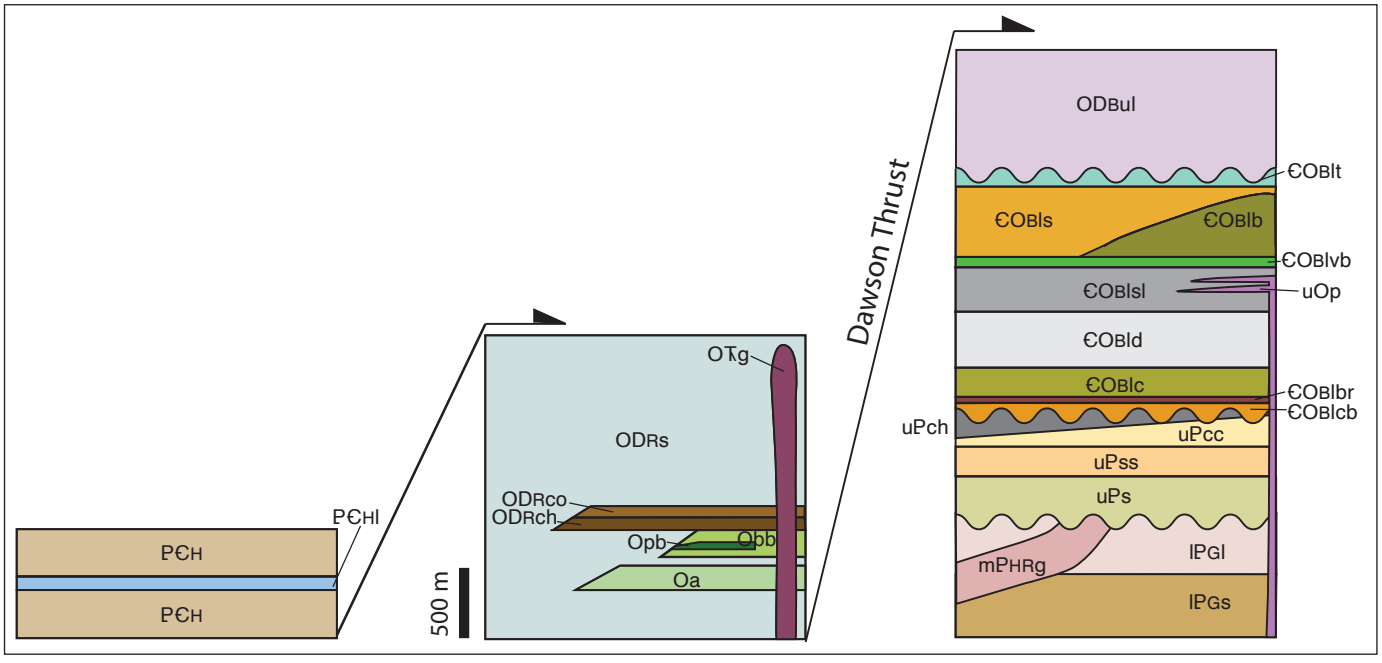


Figure 3. *Schematic stratigraphy of the Carpenter Creek area.*

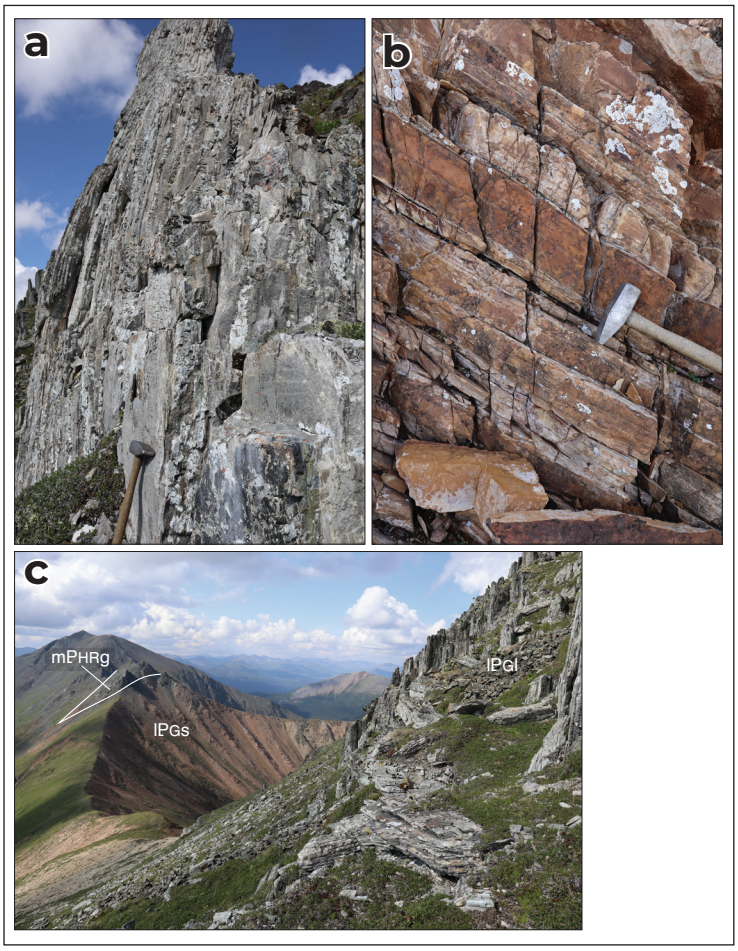


Figure 4. *Gillespie Lake Group rocks and Hart River gabbro.* ***(a)*** *Thin bedded, variably hornfelsed limestone of the Gillespie Lake Group. Beds dip near vertical in this photo (485197E, 7150267N).* ***(b)*** *Medium-bedded, dolostone, siltstone and dolo-sandstone of Gillespie Lake Group (485197E, 7150267N).* ***(c)*** *Photograph looking south at Gillespie Lake limestone in the foreground and the orange weathering dolomitic rocks in the middle ground. The dark coloring rocks at the far end of the ridge is gabbro (485197E, 7150267N). All coordinates are UTM Zone 8 NAD83.*

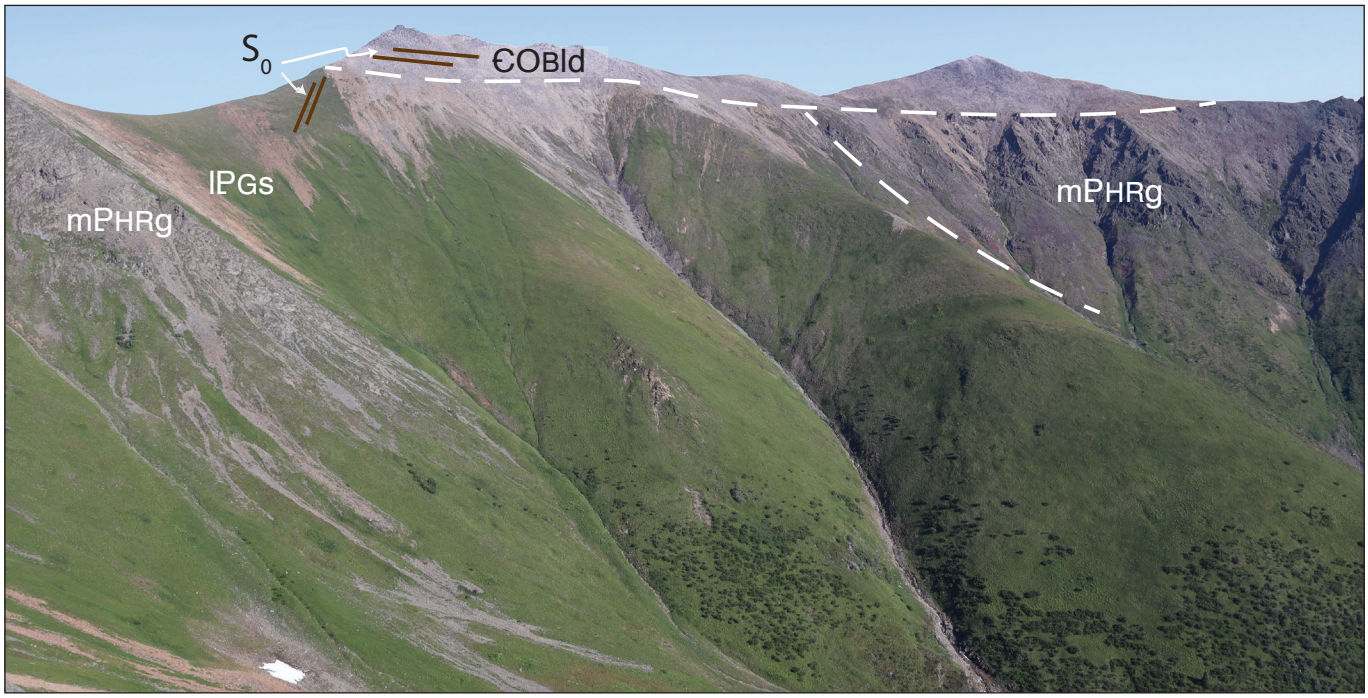


Figure 5. *The lower Bouvette Formation overlies the Gillespie Lake Group and Hart River gabbro along an angular unconformity (horizontal white dashed line).*

Upper (?) Proterozoic Pinguicula Group
(uPPs, uPPcc, uPPss, uPPch)

Southeast of Carpenter Creek a succession of siliciclastic and lesser carbonate rocks are exposed in the east-central part of the map area. The succession can be subdivided into three units which are described below from stratigraphically deepest to shallowest.

The deepest part of the stratigraphy was only observed along the eastern boundary of the mapped area, where several creek exposures comprise dark brown weathering, grey fresh, thin-bedded siltstone with minor orange-brown weathering, fine-grained sandstone (uPPs). Stratigraphically above the siltstone unit, orange-brown weathering, thin-bedded, sandstone is interlayered with bright reddish-orange iron carbonate beds and rare medium-sized beds of floatstone (uPPcc). Near the eastern boundary of the map area, this unit comprises thick-bedded, orange weathering dolostone, matrix-supported conglomerate and pebbly dolo-sandstone (Fig. 6a). The conglomerate has pebble to boulder sized clasts of carbonate, sandstone and quartz-rich sandstone supported by a sandy, carbonate-dominated matrix. Stratigraphically above the orange weathering dolostone unit, exposed along the north-south striking ridge in the east-central part of the map area, lies thick-bedded sandstone that weathers in shades of orange, brown and red (uPPss; Fig. 6b). The sandstone ranges from arkosic to lithic in composition and grades upwards from pebbly sandstone to siltstone. The base of the beds commonly contains shale chips that are oriented parallel to bedding. Farther east, the sandstone unit (uPPSS) includes brown weathering and fresh, thin to medium-bedded fine-grained sandstone with rare cross-beds (Fig. 6c). Locally, dark grey to black, thin to medium bedded chert lies on top of the iron carbonate rocks at the same stratigraphic level as the sandstone (uPPch; Fig. 3).

Assuming an overall flat-lying configuration for this succession, the minimum thickness for the upper Proterozoic strata is 800 m. The stratigraphic relationship between these rocks and the Gillespie Lake Group was not observed because the contact is faulted (Fig. 2). The base of the succession was not observed

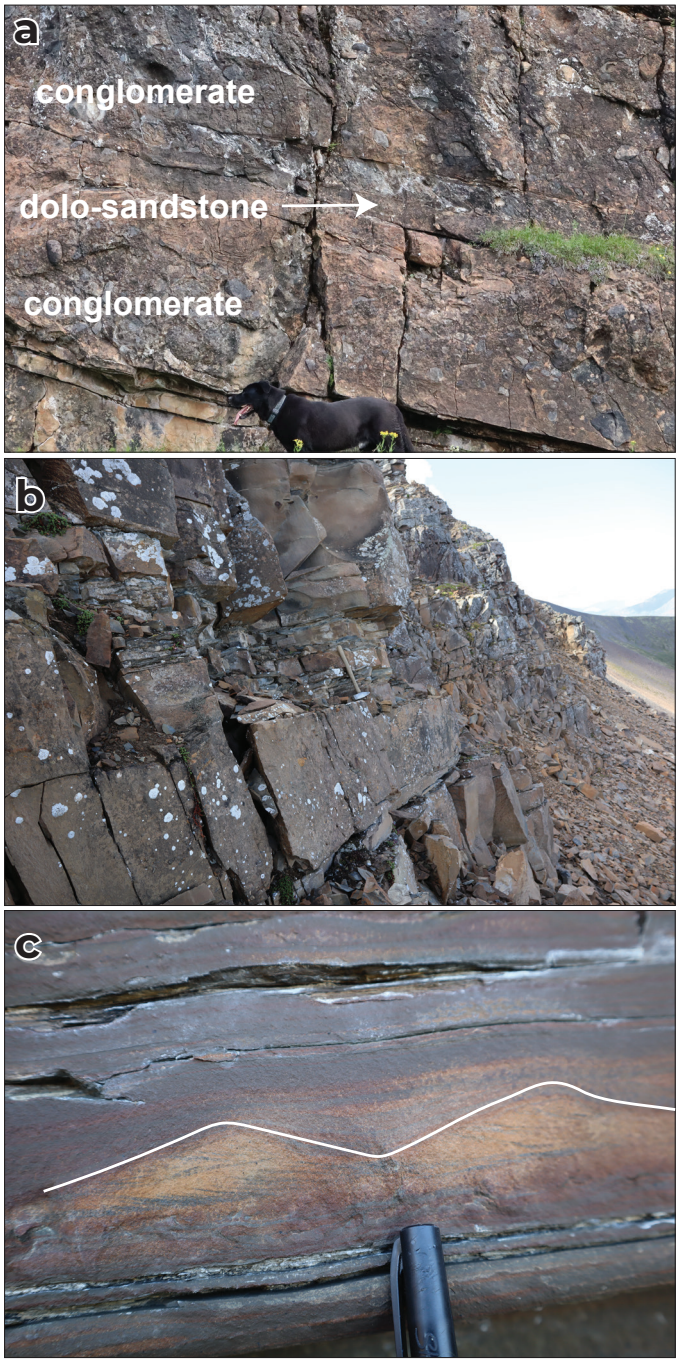


Figure 6. *Upper Proterozoic rocks exposed southeast of Carpenter Creek.* ***(a)*** *Orange weathering thick-bedded, matrix supported conglomerate is interbedded with medium beds of pebbly, dolo-sandstone (496074E, 7147037N). Dog for scale is 1 m long.* ***(b)*** *Brown weathering, medium to thick-bedded lithic sandstone that grades up into siltstone and has pebble trains near the bases of the beds (493598N, 7147627E).* ***(c)*** *Dark brown weathering, well-bedded sandstone with asymmetric ripples with internal cross-stratification (497486E, 7148274N). All coordinates are UTM Zone 8 NAD83.*

but is assumed to unconformably overlie the Gillespie Lake Group. (e.g., Medig et al., 2009). The upper contact with the Bouvette Formation is an angular unconformity best observed where chert beds are cut off by overlying dolostone of the Bouvette Formation (Fig. 2).

Cambrian (?) to Ordovician Lower Bouvette Formation (ЄOBlt, ЄOlBv, ЄOlBs, ЄOBlsl, ЄOBld)

Rocks of the lower Bouvette Formation are exposed throughout the northern two-thirds of the mapped area. The stratigraphy across the northern part of the area and the band across in the middle is comparable, and therefore, described together. Lower Bouvette rocks that are exposed southeast of Carpenter Creek are described separately because, (1) they are in fault contact with other Bouvette Formation outcrops, (2) the stratigraphy is different than the Bouvette Formation elsewhere in the mapped area, and (3) the correlation with the lower Bouvette Formation is inferred as there were no geochronological data to confidently ascertain the age of this strata (Fig. 2).

Castle Mountain stratigraphy is described in detail in Cobbett (2020). A summary is provided below, followed by more detailed descriptions for the rocks exposed in the northeastern corner of the map. Along the east-west trending ridge system where Castle Mountain is centred, the stratigraphically lowest exposed rocks consist of distinctly orange weathering, beige fresh, sandy breccia comprising clasts of dolostone, sandstone and siltstone in a calcareous, sandy matrix. This unit ranges in thickness from 0 to 10 m. Conformably above the breccia, light grey and beige weathering, massive dolostone (ЄOBld) with rare horizons of silicified stromatolites comprise a large part of the lower slopes of Castle Mountain. Up section, recessive, dark grey weathering, thin and medium-bedded, graptolitic, silty limestone with black chert horizons (ЄOBlsl) form a band around Castle Mountain. In the eastern part of the map area, this unit is intruded by two, porphyritic, gabbro sills (uOp). Conformably overlying the silty limestone, a succession of calcareous, variably volcaniclastic siltstone and sandstone is well-bedded and commonly fossiliferous (ЄOBls). Fossils in this part of the stratigraphy include trilobites, ammonites, brachiopods, cephalopods, sponges and corals. Farther east from the summit of Castle Mountain this unit includes basalt and tuff (ЄOBlv), and on the easternmost end of the Castle Mountain ridge system, light grey limestone is interbedded with basalt. A lithologically diverse succession of distinctly dark and sometimes red weathering, volcanic, carbonate and clastic rocks comprise the overlying unit (ЄOBlt) and the highest part of the stratigraphy that is included in the lower Bouvette subdivision. For example, this unit includes crystal-lithic tuff, conglomerate, sandstone, siltstone and fossiliferous limestone in varying abundances and thicknesses across the northern part of the area. Common fossils in this unit include bivalves, gastropods and corals.

Between Carpenter Creek and Ervin Creek, the lower Bouvette Formation includes primarily volcanic rocks and overlying sedimentary rocks. Above the silty limestone unit in this area, up to 300 m of combined volcaniclastic rocks and basalt are locally interbedded with lenses of limestone. Some areas include a basal basalt breccia, volcaniclastic siltstone and sandstone, or volcanic-derived conglomerate comprising rounded clasts of basalt in a volcanic-derived, sandy matrix (Fig. 7a,b). Light grey weathering limestone forms discontinuous bands surrounded by basalt. Some bands have strongly undulating basal contacts and flat upper contacts (Fig. 7c). The basalt includes pyroxene-phyric and aphanitic flows and locally has amygdaloidal tops. Stratigraphically above the basalt, red weathering siltstone and arkosic sandstone (red beds) becomes interbedded with micrite up-section (Fig. 7d). Gastropods and bivalves commonly occur in this part of the stratigraphy. Above the red beds, brown and grey weathering, pebbly, lithic sandstone grades upwards into a calcareous, locally fossiliferous, muddy, siltstone.

North of the Beaver River, the mafic volcanic rocks include fine-grained basalt with amoeboid-shaped, variably fossiliferous limestone clasts (Fig. 7e), crudely bedded volcanic-derived, variably cross-bedded sandstone, and basalt with brecciated tops.

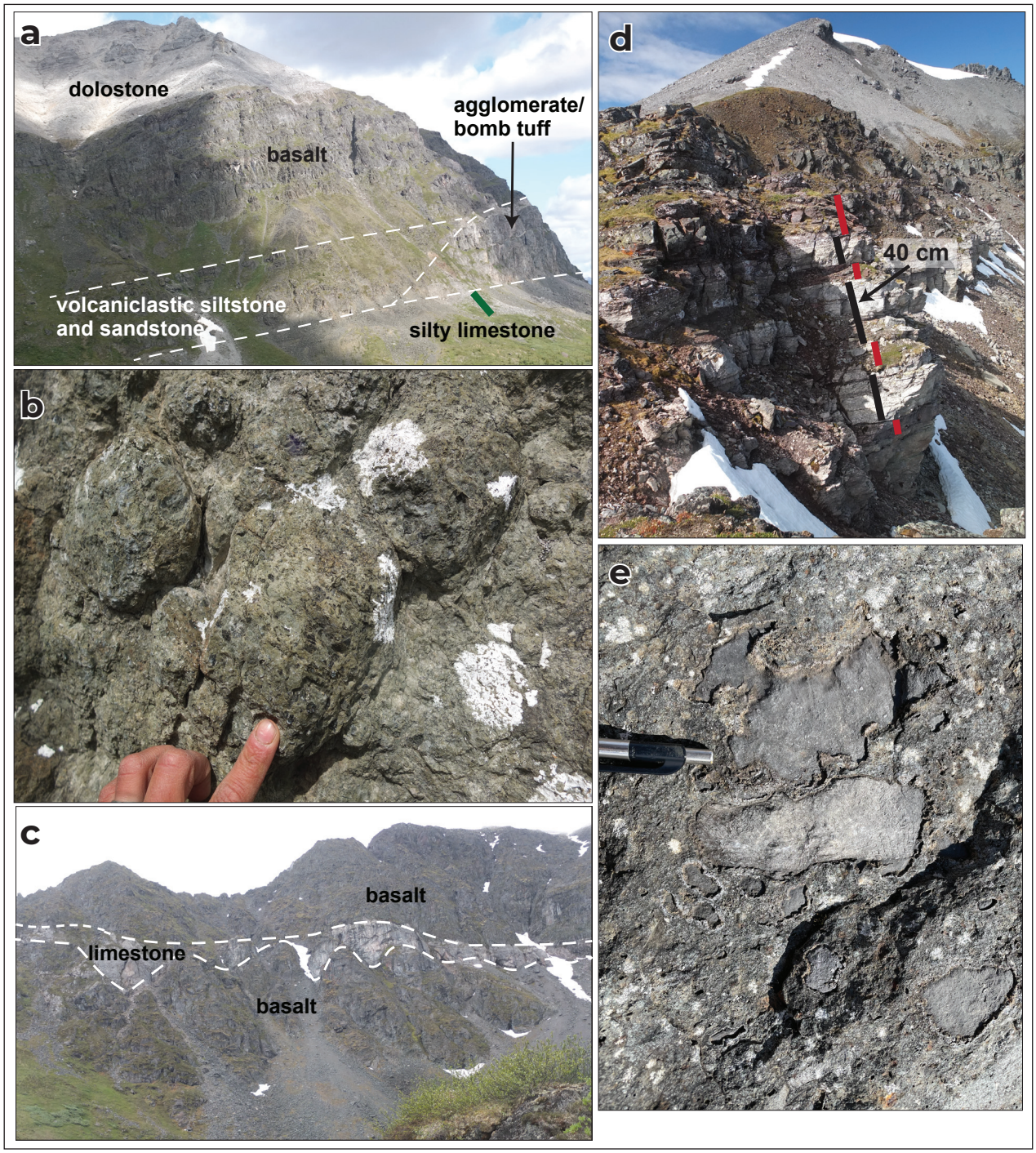


Figure 7. *Lower Bouvette Formation rocks exposed between Ervin and Carpenter Creeks, and north of Beaver River.* ***(a)*** *Volcanic rocks typical of the stratigraphy east of Ervin Creek. The base of the volcanic section includes a lens-shaped pile of agglomerate or block and bomb tuff comprising rounded cobbles of pyroxene-phyric basalt with interstitial volcanic-derived sandstone. A mafic dike (green line) cuts through the silty limestone below the volcanic rocks. For scale, the basalt and volcaniclastic rocks together are approximately 300 m thick (493855E, 7153011N).* ***(b)*** *Rounded clasts of pyroxene-phyric basalt with interstitial basaltic material. Similar rocks comprise the lens of volcanic material highlighted in (a; 485894E, 7154567N).* ***(c)*** *A limestone bed that conforms to the irregular flow top shape of the underlying basalt flow and has a generally flat top, which dictates the basal form of the overlying flow (489802E, 7157926N).* ***(d)*** *Interbedded red weathering sandstone (red lines) and light weathering micrite (black lines; 487365E, 7156937N). For scale, the micrite bed that the black arrow points to is approximately 40 cm thick.* ***(e)*** *Amoeboid-shaped limestone clasts in basalt (492295E, 7144590N).*

The thickness of the volcanic-dominated lower Bouvette Formation in the northern part of the area ranges from 700 to 1200 m. It is thickest near Ervin Creek where basalt reaches its maximum thickness of nearly 300 m. West of Castle Mountain the absence of basalt, basalt breccia and volcanic-derived conglomerate reduces the total thickness. The lower Bouvette sits unconformably on the Gillespie Lake Group (Fig. 2). The upper contact with the upper Bouvette is a disconformity marked in places by a boulder conglomerate (Cobbett, 2020).

South of Carpenter Creek in the east-central part of the map area, rocks that have been included in the lower Bouvette Formation are dominantly clastic with some volcanic intervals and dolostone (Fig. 8a). The lowest part of the stratigraphy comprises an orange weathering, beige fresh, carbonate breccia comprising pebble to boulder sized clasts of carbonate and siliciclastic rocks in a calcareous sandy matrix (Fig. 8b). Above this lies a maroon weathering and fresh, sandy, matrix-supported volcanic breccia comprising subangular clasts of carbonate and quartz surrounded by a matrix of subangular quartz grains and euhedral feldspar (altered to sericite) crystals that commonly have concentric zoning (Fig. 8c). This unit grades into a green weathering and fresh, volcanic-derived conglomerate comprising rounded clasts of basalt in a volcanic-derived sandstone matrix (Fig. 8d).

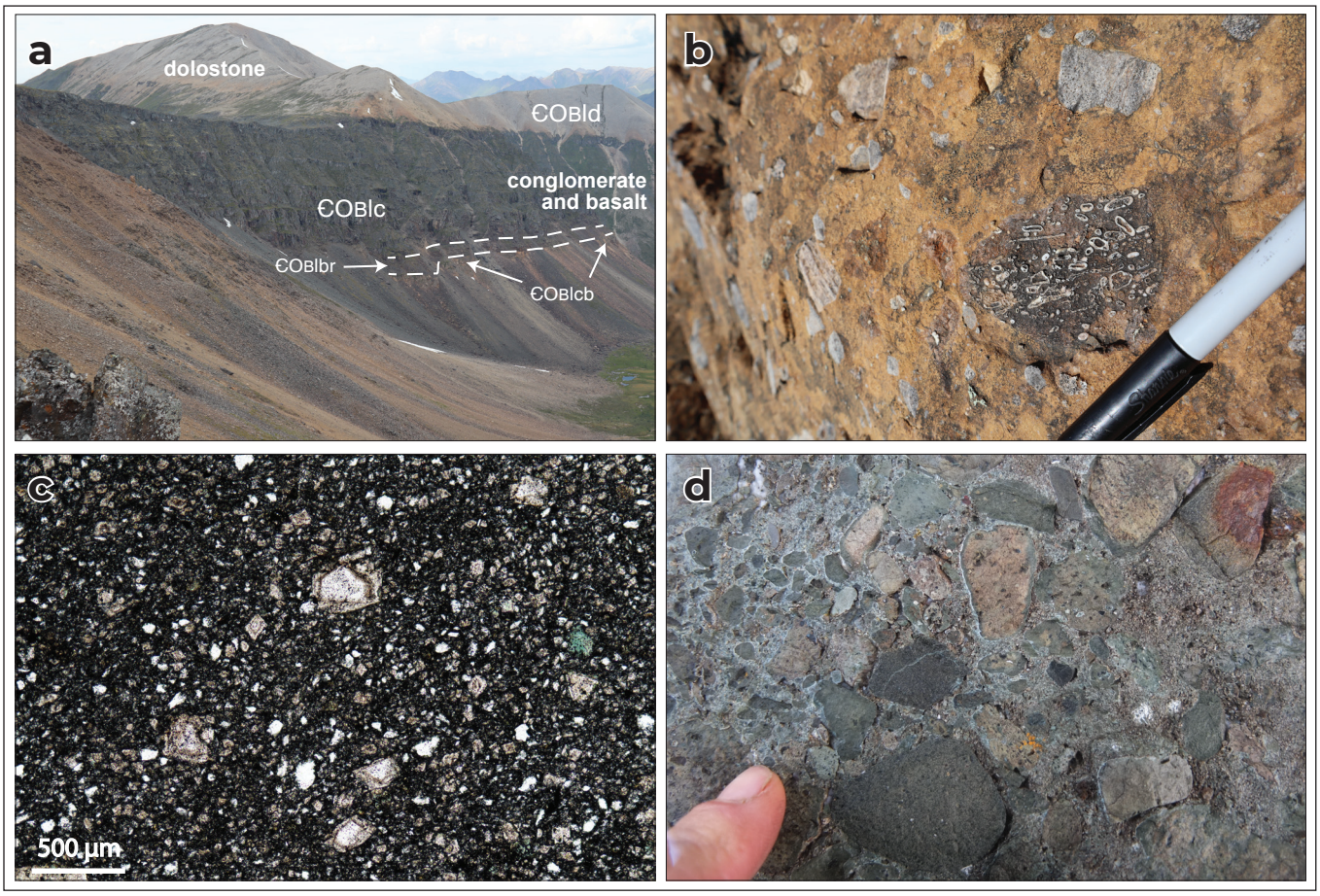


Figure 8. *Lower Bouvette stratigraphy exposed southeast of Carpenter Creek.* ***(a)*** *A sequence of volcanic conglomerate and sandstone with minor basalt flows (exposed in the dark grey cliff in the middle of the photograph) overlain by grey massive dolostone and underlain by orange-brown weathering sandy breccia and carbonate breccia (497778E, 7150096N).* ***(b)*** *Orange weathering carbonate conglomerate comprising clasts of carbonate floating in a sandy dolomitic matrix (494175E, 7148144N).* ***(c)*** *Photo micrograph of maroon weathering, sandy breccia. Photo shows zoned feldspar crystals in a matrix of smaller lithic and volcanic grains (493756E, 7148866N).* ***(d)*** *Volcanic conglomerate comprising volcanic clasts in a sandy matrix (495445E, 7148298N).* *Figure continued on next page.*

Green weathering and fresh, medium-bedded, coarse-grained, volcanic-derived sandstone comprise the top of very thick beds of conglomerate and is commonly cross-bedded. Locally interbedded with the volcanic conglomerate are basalt flows. The lowermost flow has feldspar phenocrysts and two flows higher up in the succession are aphanitic (Fig. 8e). Rarely, basalt flows are directly overlain by basalt breccia comprising angular clasts of basalt in a glassy to basaltic matrix or volcanic breccia comprising irregular shaped, vesicular clasts ranging in size from 0.5–5 cm with interstitial calcite (Fig. 8f).

Above the volcanic and volcaniclastic rock units is a single thick bed of beige weathering, quartz-rich, fine-grained sandstone that is overlain by beige weathering, grey fresh, thick-bedded to massive dolostone (Fig. 8a).

Locally the two breccia units are absent, and the volcanic-derived conglomerate sits instead on, (1) orange to pink weathering, thick-bedded dolostone, or (2) orange weathering, medium-bedded dolo-sandstone interbedded with beige-brown weathering, lithic, pebble conglomerate comprising well-rounded clasts of quartz arenite, chert and siltstone (Fig. 8g). Maroon weathering sandy siltstone rarely occurs within this part of the stratigraphy.

South of Carpenter Creek, the thickness of the volcanic strata, including volcanic-derived conglomerate and basalt, ranges from 150 to 200 m. The orange carbonate conglomerate ranges in thickness from 0 to 20 m and is exaggerated on the cross section on Figure 2. The maroon sandy breccia that occurs locally between the orange carbonate conglomerate and the volcanic rocks ranges in thickness from 0 to 10 m. The contact with the underlying dark weathering sedimentary rocks is not conformable but this is difficult to confirm in outcrop because all strata is relatively flat lying where the volcanic rocks are exposed.

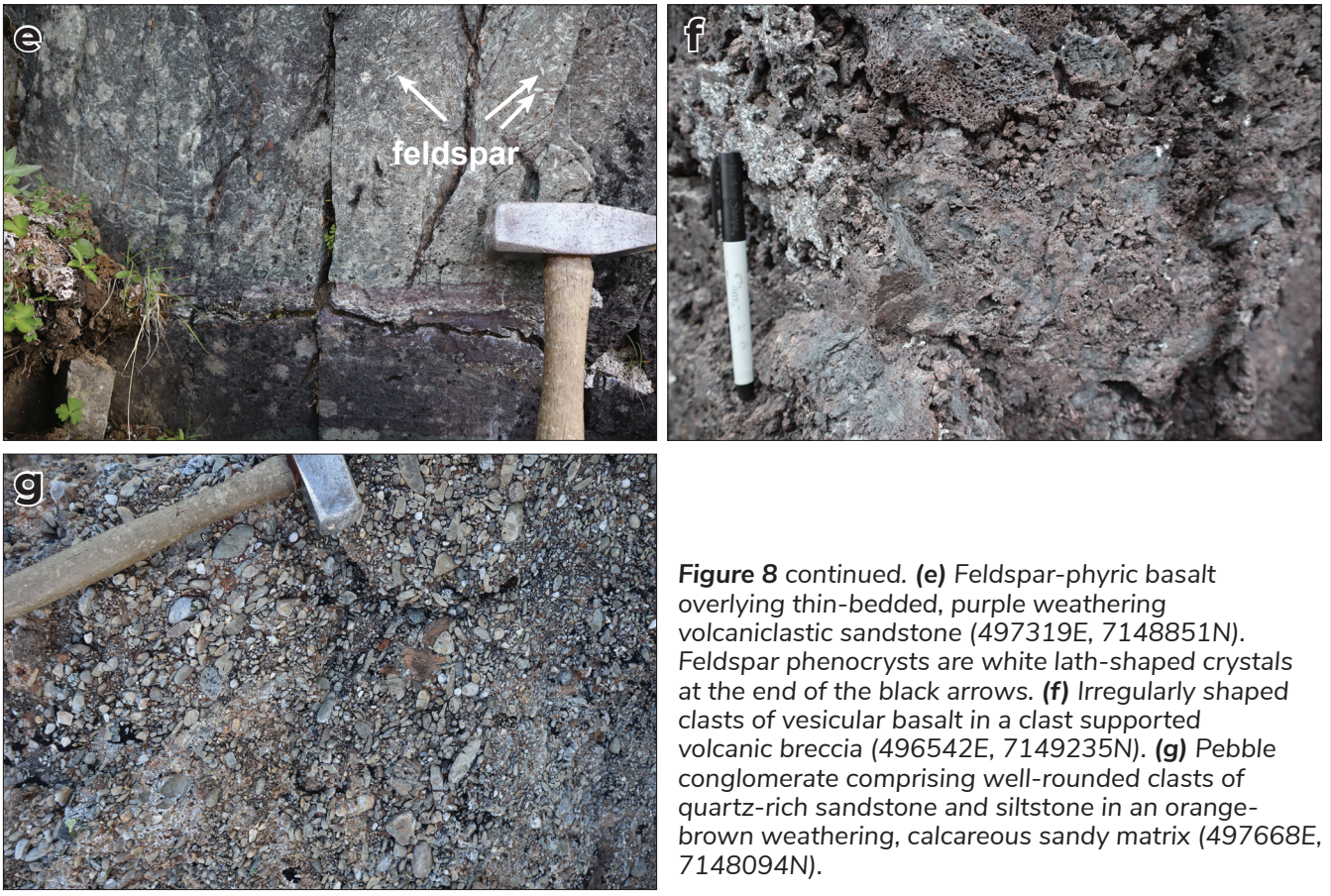


Figure 8 *continued.* ***(e)*** *Feldspar-phyric basalt overlying thin-bedded, purple weathering volcaniclastic sandstone (497319E, 7148851N). Feldspar phenocrysts are white lath-shaped crystals at the end of the black arrows.* ***(f)*** *Irregularly shaped clasts of vesicular basalt in a clast supported volcanic breccia (496542E, 7149235N).* ***(g)*** *Pebble conglomerate comprising well-rounded clasts of quartz-rich sandstone and siltstone in an orange-brown weathering, calcareous sandy matrix (497668E, 7148094N).*

Ordovician to Devonian upper Bouvette Formation (ODBud)

Across the entire northern part of the map area, the youngest rocks belong to the upper Bouvette Formation (ODBud). Upwards of 500 m of limestone and dolostone crop out above the lower Bouvette tuff unit (ЄOBlt). Light to dark grey weathering and fresh, thin to thick-bedded, variably fossiliferous limestone and dolostone make up many ridge tops, including those of Castle Mountain (Fig. 9a). Common fossils include corals, crinoids and bivalves (Fig. 9b).

The lower and upper Bouvette stratigraphy is repeated in a band parallel to the Dawson thrust, directly north of the Beaver River valley, where it unconformably overlies Proterozoic rocks (Fig. 2).

The upper Bouvette Formation is separated by a disconformity from the lower Bouvette and is marked by the first occurrence of fossiliferous carbonate above the volcanic and clastic rocks. The top of the Bouvette Formation is not exposed in the map area.

Stratigraphy south of the Dawson Thrust fault

Two groups of rocks were mapped south of the Dawson thrust. Near Sullivan and McKay hills, volcanic and volcaniclastic rocks are interbedded with fine-grained siliciclastic rocks. On the southern ends of the north-south trending ridges, south of the volcanic rocks, are exposures of Hyland Group shale, quartz grit and limestone.

The Hyland Group within the mapped area comprises maroon, green, grey, and brown shale (PЄH). Brown weathering, coarse-grained, quartz-rich sandstone occurs as metre-scale interbeds that occur locally within the shale. Stratigraphically above the shale and sandstone is light grey weathering, medium-bedded limestone (PЄHl). In one location, the limestone is overlain by dark weathering, dark grey fresh, thin-bedded siltstone interbedded thickly with dark grey quartz arenite, but these rocks are grouped with the shale unit (PЄH) in Figure 2.

In fault contact with the Hyland Group rocks, volcanic and sedimentary rocks crop out along north-south trending ridges that comprise Sullivan and McKay hills. A stratigraphic column is difficult to construct with confidence due to folding and lack of regular upright bedding indicators. Two volcanic horizons are separated by brown shale and siltstone. The lower volcanic horizon is dominated by green weathering and fresh variably calcareous volcanic-derived conglomerate comprising well-rounded clasts of basalt and volcaniclastic sandstone in a sandy or crystal-rich matrix (Fig. 10a). Locally, basalt breccia forms lenses up to 200 m thick (Fig. 10b). The upper volcanic horizon includes pillow basalt, basalt breccia and pillow-basalt breccia.

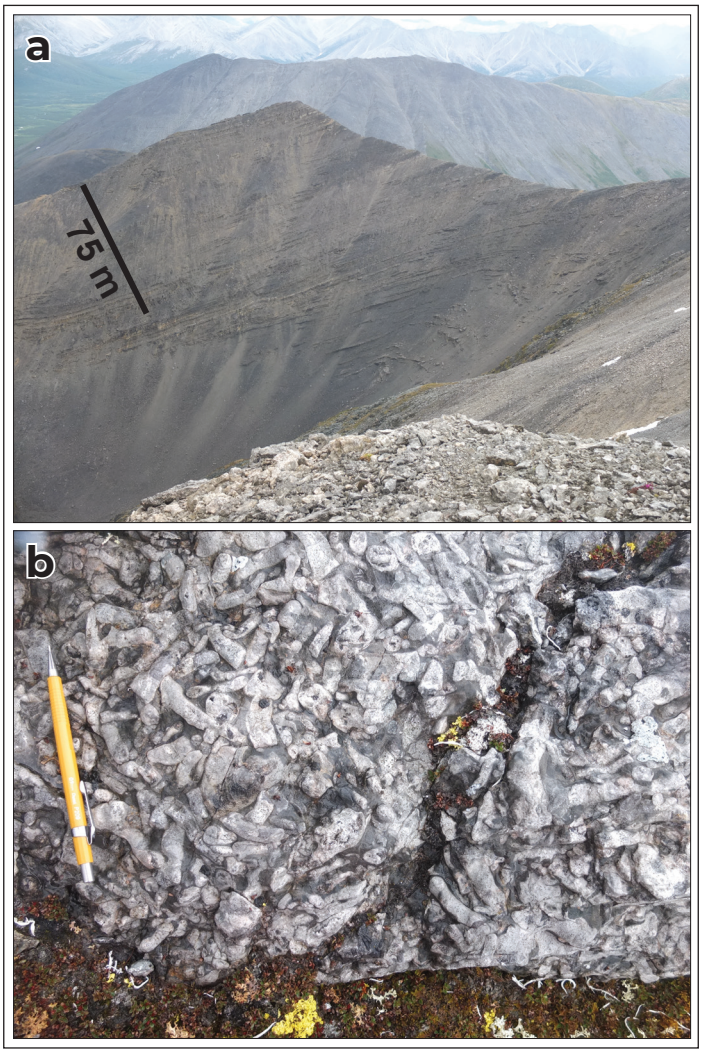


Figure 9. *Upper Bouvette dolostone and limestone.* ***(a)*** *Ridge tops comprising upper Bouvette interbedded limestone and dolostone.* ***(b)*** *Coral fossils typical of parts of the upper Bouvette stratigraphy (493306E, 7153555N).*

Pillow basalt forms beds that are several metres to tens of metres thick and contains rare limestone lenses with coral fossils (Fig. 10c,d). Spatially associated with the pillow basalt and basalt breccia is a highly calcareous volcanic rock characterized by hexagon shaped vesicles(?) that are filled with calcite and are surrounded by glassy material, (Fig. 10e) which crops out on the main ridge between Sullivan Hill and McKay Hill. Included in the upper volcanic horizon is interbedded green-grey weathering, thin-bedded mudstone, calcareous volcanic-derived sandstone and volcanic-derived conglomerate. The conglomerate is composed of lapilli-sized clasts in a fine-grained matrix. The volcanic rocks are overlain by, and possibly partially interbedded with, brown weathering, lithic conglomerate with varying amounts of volcanic detritus, shale, and dark grey weathering, banded chert. Milky-white quartz veins are exposed along a ridge southwest of McKay Hill where gabbro and shale exhibit orange weathering near the veins.

The lower volcanic horizon is approximately 200 m thick and the upper volcanic horizon is up to 150 m thick; however, because the volcanic horizons are lenticular, they vary in thickness over a few kilometers (Fig. 10f). The presence of coral-bearing limestone (Fig. 10d) within the basalt constrains the age of the volcanic rocks to Middle Ordovician to Permian based on the range of ages of fossil in the Cordillera (Nelson, 1975).

Intrusive Rocks

Hart River intrusions (mPHRg)

The Gillespie Lake Formation is extensively intruded by gabbro sills and dikes. The gabbro is grey-brown weathering, green-grey fresh, medium to coarse-grained and is commonly chlorite-altered. The gabbro comprises sills up to 2 km long, and dikes that can be up to 200 m thick. Two samples of the gabbro from Carpenter Ridge were dated at 1385.8 ± 1.9 Ma and 1383.0 +5.9/-5.2 Ma (Abbott, 1997).

Upper Ordovician Porphyritic gabbro (uOp)

Between Castle Mountain and Carpenter Creek, in the northern quarter of the map area, the silty limestone unit (ЄOBlsl) is intruded by two porphyritic sills. Similar sills are also hosted by the silty limestone unit just north of Beaver River. The sills only occur where basalt is part of the lower Bouvette stratigraphy (Fig. 2). The sills comprise fine-grained, pyroxene-phyric gabbro in most areas but near the cores of larger sills, they consist of medium-grained pyroxene-bearing gabbro. A metre thick, aphanitic dike cuts through the silty limestone near Ervin Creek and is traced to the base of the volcanic rocks (Fig. 7a).

Gabbro of unknown age (OTg)

Several gabbro bodies intrude into the Hyland Group rocks. These are grey-green weathering, coarse-grained, pyroxene gabbro that form 10 to 20 m thick bodies, which are oriented parallel to the main structural fabric. Similar bodies intrude into the Road River Group shales near Sullivan and McKay hills, where they are locally associated with pyroxenite. The ultramafic bodies are orange weathering, medium to coarse-grained, and primarily comprise clinopyroxene.

Feldspar porphyritic sills and dikes

Southeast of Carpenter Creek, several occurrences of feldspar-phyric diorite are observed both cutting the stratigraphy and intruding along bedding. However, these bodies are too small (1–5 m thick) to be included as separate units on the map. The diorite is a brown weathering, variably altered, fine-grained, feldspar ± pyroxene-phyric diorite.

Structure

North of the Dawson fault

Proterozoic rocks exposed across the central part of the map area were deformed prior to the deposition of overlying Paleozoic strata. A very clear angular unconformity exists between the two successions. For example, in Figure 5, near vertical beds that belong to Gillespie Lake siltstone are overlain by flat-lying lower Bouvette Formation. Folding and faulting was not directly observed in the Proterozoic strata, so the structures responsible for the steep bedding orientations remains uncertain.

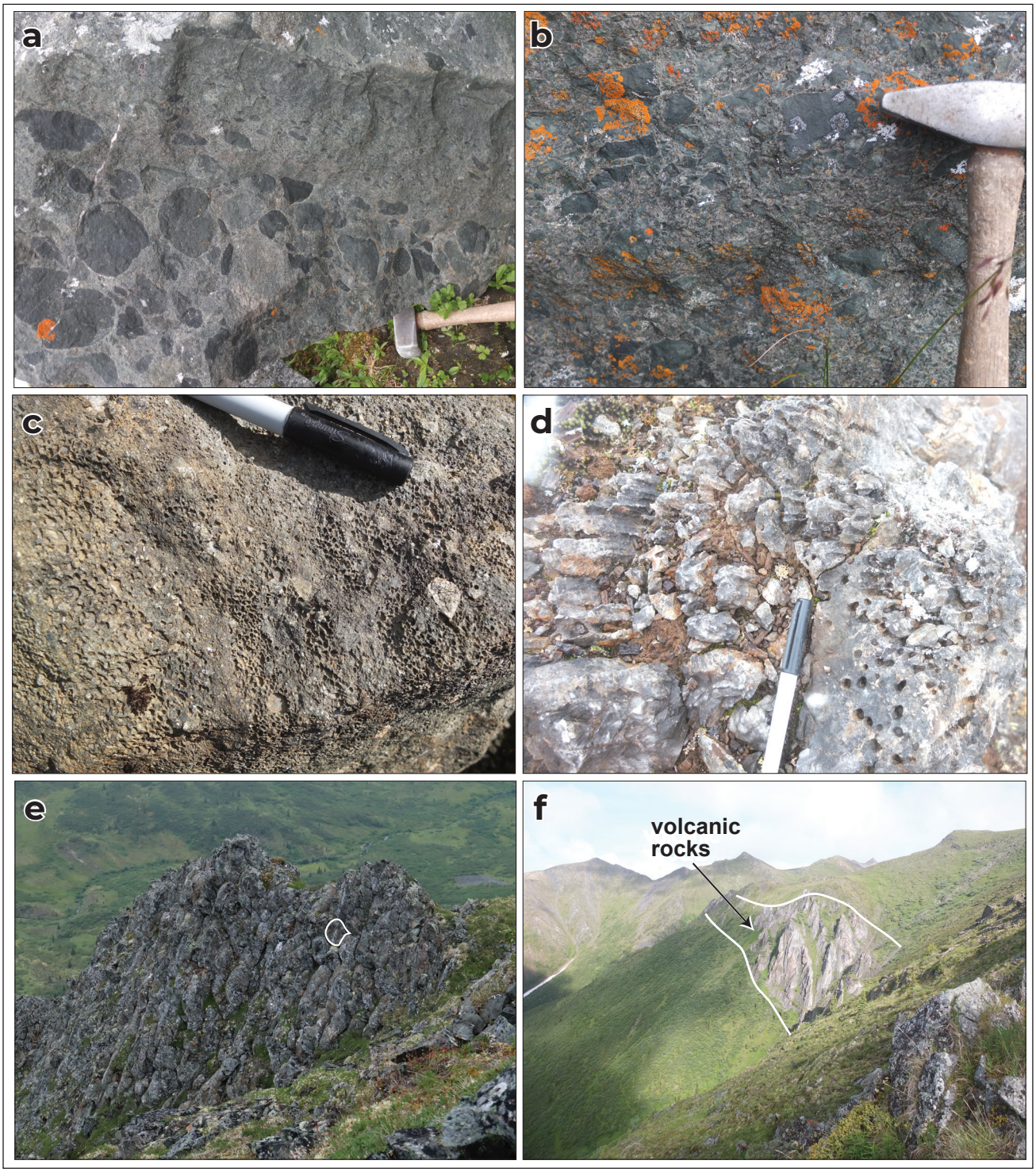


Figure 10. *Volcanic rocks at McKay Hill, south of the Dawson Thrust fault.* ***(a)*** *Agglomerate comprising rounded volcanic rocks in a calcareous, sandy matrix (481587E, 7139702N).* ***(b)*** *Mafic tuff breccia comprising angular clasts of basalt in a devitrified glass matrix (484347E, 7138301N).* ***(c)*** *Very calcareous volcanic rock comprising hexagonal shaped vesicles filled with calcite with minor white weathering, angular clasts (478807E, 7138037N).* ***(d)*** *Limestone with fasciculate coral fossils that have been replaced by rusty weathering sulphides (479453E, 7137976N).* ***(e)*** *Ridge comprised of pillow basalt that is approximately 10 m high. Pillows clearly show bottoms and tops, as highlighted by the white outline indicating this sequence of rocks young to the southwest (476325E, 7138362N).* ***(f)*** *Looking northwest at McKay Hill, where light grey weathering cliff-forming rocks comprise a tapering lens of pillow basalt.*

A buried fault follows the trace of Carpenter Creek and accommodates the placement of upper Proterozoic rocks at a similar level as the Gillespie Lake Group rocks (Fig. 2). However, because the age of the strata southeast of Carpenter Creek is unknown, the nature of movement along that fault is uncertain.

North of the Dawson thrust, Paleozoic rocks are openly folded with fold axial traces plunging gently west-northwest. East-west striking normal faults cut through Castle Mountain stratigraphy offsetting rocks by as much as 300 m. One of the more significant faults in the northern part of the map area has dropped the stratigraphy in the northeast corner down, so that much of lower Bouvette Formation remains buried.

South of the Dawson fault

A strong structural trend exists south of the Dawson thrust where most foliation and bedding strikes west-northwest/east-southeast. Foliation dips between 80 and 89° and is well-developed in the shale but is not commonly observed in the volcanic rocks and gabbro. Several tight regional folds follow the structural trends and locally repeat the stratigraphy. A right-lateral strike-slip fault has offset these strata by several hundred metres near McKay Hill.

The Hyland Group is in fault contact with the volcanic strata along a moderately south-southwest dipping thrust fault. The fault was drawn at the first occurrence of maroon and green shale.

Discussion

Stratigraphic relationships

The map area is unique because of the igneous rocks exposed here. Based on stratigraphic position and crosscutting relationships, there are at least three distinct episodes of magmatism, possibly as many as five. These are represented by (1) the Mesoproterozoic Hart River gabbro bodies, (2) the volcanic and volcaniclastic rocks in the lowest part of the lower Bouvette Formation, and (3) the Ordovician volcanic rocks exposed on both sides of the Dawson thrust fault (*i.e.*, the upper parts of the lower Bouvette near Castle Mountain and Ervin Creek and the volcanic rocks exposed at McKay Hill). The feldspar-porphyritic rocks that occur as dikes and sills southeast of Carpenter Creek intrude and are therefore younger than the older lower Bouvette Formation volcanic rocks with no upper age constraint. Based on the current age constraints for these rocks, they could represent a fourth magmatic episode. The gabbro that intrudes the Dawson fault hangingwall rocks intrudes into the Road River Group rocks constraining its age to younger than Middle Ordovician, suggesting that these rocks could also represent a temporally distinct magmatic episode. The wide valley that the Beaver River partially occupies may represent a long-lived basement structure that facilitated the migration of magma to and near the surface.

The lack of gabbro in the upper Proterozoic rocks, south of Carpenter Creek, is interpreted to indicate that the younger succession unconformably overlies Gillespie Lake rocks, as shown on the cross sections in Figure 2. However, because the Carpenter Creek fault separated the two successions, this could not be verified.

Significance of volcanic facies

The basaltic rocks and sills in the northeastern part of the map area (near Ervin Creek, Fig. 2) represent the thickest accumulation of volcanic rocks in this part of the stratigraphy. The lens shaped mound of volcanic-derived conglomerate that sits below the basalt (Fig. 7a,b) is interpreted to be a block and bomb tuff based on the shape and size of the clasts and the lack of a lithic component (*i.e.*, the entire lens comprises volcanic-derived material). The only dike that was confidently identified in the northern part of the map area is right below the block and bomb tuff, where a metre-wide, steeply dipping, aphanitic, mafic dike was observed cutting through the silty limestone unit trending into (but not cutting) the overlying tuff and basalt flows (Fig. 7a). Block and bomb tuffs are vent-proximal facies because the large size of the bombs requires them to be deposited quickly after they are ejected (Head and Wilson, 2003). Feeder dikes are typically preserved near vents, and basalt flows are considered vent-proximal facies; however, during effusive eruptions that are typical of basaltic compositions, flows can spread out laterally many kilometres from a vent (e.g., Cas and Wright, 2012).

North of Beaver River, the amoeboid-shaped limestone clasts that occur locally in basalt are interpreted to be formed from basalt flowing into unconsolidated limey sediments. This indicates that the fossils found in some of the limestone clasts directly date the age of the eruptions. Cross-bedded, volcanic derived sandstone is interpreted to form from pyroclastic surges that sort ash to lapilli-sized volcanic fragments during transport (e.g., Cas and Wright, 2012).

The bedded volcanic-derived siltstone and sandstone that occur adjacent to the block and bomb tuff are interpreted to be syn-eruptive facies. Ash and lapilli ejected during explosive eruptions were sorted during transport through air or water shortly after the block and bomb tuff was deposited resulting in well-bedded deposits. These pyroclastic rocks that occur as the basal volcanic unit near Ervin Creek suggest early eruptions may have been explosive, followed by more effusive eruptions represented by the basalt flows above the tuffaceous rocks. Also, in the northeastern part of the map area, discontinuous limestone in basalt represents a break in volcanism (Fig. 7c). The limestone conformed to the irregular shape of the top of the underlying flow.

The volcanic-derived conglomerate that occurs near the base of the Bouvette Formation is interpreted to be reworked deposits from collapse of a steep volcanic edifice. The well-rounded nature of clasts suggest they have been transported. Further, the general fining upwards of the beds into cross-bedded volcanic-derived sandstone indicated sorting during transport (e.g., Cas and Wright, 2012). Rare volcanic breccia that occurs near the top of basalt is interpreted to be a flow-top breccia (Fig. 8f) that formed from fragmenting of a vesicular basalt rind (Cas and Wright, 2012).

Mineralization

Mineralization at McKay Hill is associated with milky-white quartz veins and orange weathering surface alteration of gabbro. Veins and mineralization are interpreted to be linked to late strike-slip faulting (Blackburn, *pers. comm.*). Competency contrasts between rigid gabbro bodies and shale are important controls for vein growth at McKay Hill because they undergo brittle deformation during faulting, allowing space for fluids (Blackburn, 2010). Volcanic rocks are spatially associated with the mineralization at McKay Hill but it is unclear whether they are an important control for mineralization.

Little is known about the mineralization at Grey Copper Hill but historical trenches were dug parallel to the contact between the Bouvette Formation and the underlying Pinguicula Group suggesting the unconformity between these two formations is a control for mineralization.

Acknowledgements

Heather Clarke and Jake Charlton provided outstanding assistance during the three field seasons it took to map this area. Julia Lake, Adam Coultier and Lauren Blackburn were very generous with their support for this project by accommodating us in their camps and offering helicopter availability whenever it was needed. Lauren Blackburn provided detailed field maps that were incorporated into the compilation. Diane Skipton and Lauren Blackburn provided valuable feedback on the manuscript.

References

Abbott, G., 1997. Geology of the Upper Hart River area, Eastern Ogilvie Mountains, Yukon Territory (116A/10, 116A/11). *In:* Exploration and Geological Services Division, Yukon, Indian and Northern Affairs Canada, Bulletin 9, 92 p.

Blackburn, L.R., 2010. High-sulphidation epithermal Au-Ag-Cu mineralization at the McKay Hill property — a revised deposit model. *In:* Yukon Exploration and Geology 2009, K.E. MacFarlane, L.H. Weston and L.R. Blackburn (eds.), Yukon Geological Survey, p. 85–101.

Blackburn, L.R. and Haid, T., 2018. Rock Geochemistry, Soil Geochemistry, Bedrock Mapping Geology, Backhoe Trenching, Hand Trenching at the McKay Hill Propoerty. Yukon Energy, Mines, and Resources Assessment Report 09781.

Campbell, R.W., Beranek, L.P., Piercey, S.J. and Friedman, R., 2019. Early Paleozoic post-breakup magmatism along the Cordilleran margin of western North America: New zircon U-Pb age and whole-rock Nd-and Hf-isotope and lithogeochemical results from the Kechika group, Yukon, Canada. Geosphere, vol. 15, 29 p., https://doi.org/10.1130/GES02044.1.

Cas, R.A.F. and Wright, J.V. ,2012. Volcanic successions modern and ancient: A geological approach to processes, products and successions. Springer Science & Business Media.

Cecile, M., Morrow, D. and Williams, G., 1997. Early Paleozoic (Cambrian to Early Devonian) tectonic framework, Canadian Cordillera. Bulletin of Canadian Petroleum Geology, vol. 45, p. 54–74.

Cobbett, R., 2020. Preliminary report on the bedrock geology of Castle Mountain area, Yukon (parts of NTS 105D/6). *In:* Yukon Exploration and Geology 2019, K.E. MacFarlane(ed.), Yukon Geological Survey, p. 43–55.

Colpron, M., Logan, J.M. and Mortensen, J.K., 2002. U-Pb zircon age constraint for late Neoproterozoic rifting and initiation of the lower Paleozoic passive margin of western Laurentia. Canadian Journal of Earth Sciences, vol. 39, p. 133–143.

Eyster, A., Ferri, F., Schmitz, M.D. and Macdonald, F.A., 2018. One diamictite and two rifts: Stratigraphy and geochronology of the Gataga Mountain of northern British Columbia. American Journal of Science, vol. 318, p. 167–207.

Green, L.H., 1972. Geology of Nash Creek, Larsen Creek, and Dawson Map-Areas, Yukon Territory. Geological Survey of Canada, Memoir 364, 157 p.

Haid, T. and Blackburn, L.R., 2019. 2019 Assessment Report on the McKay Hill Project, Yukon. Yukon Energy, Mines, and Resources Assessment Report 097343.

Head III, J.W. and Wilson, L. 2003. Deep submarine pyroclastic eruptions: theory and predicted landforms and deposits. Journal of Volcanology and Geothermal Research, vol. 121, p. 155–193.

Medig, K., Thorkelson, D. and Dunlop, R., 2010. The Proterozoic Pinguicula Group: stratigraphy, contact relationships and possible correlations. Yukon Exploration and Geology 2009, K.E. MacFarlane, L.H. Weston and L.R. Blackburn (eds.), Yukon Geological Survey, p. 265–278.

Nelson, S.J., 1975. Paleontological Field Guides Northern Canada and Alaska. Bulletin of Canadian Petroleum Geology, vol. 23, p. 428–683.

Pigage, L., Roots, C. and Abbott, J., 2015. Regional bedrock geology for Coal River map area (NTS 95D), southeast Yukon. Yukon Geological Survey, Bulletin 17, 155 p.

Pigage, L.C., 2004. Bedrock geology compilation of the Anvil District (parts of 105K/2, 3, 5, 6, 7 and 11), central Yukon. Yukon Geological Survey, Bulletin 15, 103 p.

Thorkelson, D., 2000. Geology and mineral occurrences of the Slats Creek, Fairchild Lake and 'Dolores Creek' areas, Wernecke Mountains, Yukon Territory. Exploration and Geological Services Division, Yukon Region, Indian and Northern Affairs Canada, Bulletin 10, p. 73.

Verbaas, J., 2017. Paleoproterozoic to Mesopropterozoic evolution of Yukon Territory, Canada. Unpublished PhD thesis, Department of Earth Sciences, Simon Fraser University.

Yukon Geological Survey, 2021. A digital atlas of terranes for the northern Cordillera. Yukon Geological Survey, https://data.geology.gov.yk.ca/Compilation/2, [accessed December, 2021].

The Yukon Digital Bedrock Geology compilation

Maurice Colpron
Yukon Geological Survey

Colpron, M., 2022. The Yukon Digital Bedrock Geology compilation. *In:* Yukon Exploration and Geology 2021, K.E. MacFarlane (ed.), Yukon Geological Survey, p. 143–159.

Abstract

The Yukon Digital Bedrock Geology dataset was first released in 1999. It was rebuilt and expanded in 2016 and has since received regular updates. This paper summarizes the enhancements made to the bedrock geology dataset since 2016, the other ancillary geoscience datasets available, and the various ways to access and use the dataset.

Introduction

Gordey and Makepeace (1999) produced the first comprehensive GIS (geographic information system) compilation of the Yukon bedrock geology (Fig. 1). This digital compilation was inspired in large parts by the tectonic assemblage map of Wheeler and McFeely (1991) for which a GIS version was produced by Journeay and Williams (1995). The tectonic assemblage map of the Canadian Cordillera was a "classic" compilation map in that the compilers made decisions to simplify the source information to produce the published 1:2 000 000-scale map. The GIS capture of this map by Journeay and Williams (1995) was faithful to the 1:2 000 000 map and therefore lacked the details from the source maps. In contrast, Gordey and Makepeace (1999) captured the geological information at the scale of publication, without compromise. For most of Yukon, Gordey and Makepeace (1999) digitized the geology from the 1:250 000-scale regional maps published by the Geological Survey of Canada (GSC), but they also included locally more detailed maps published at 1:50 000-scale. This approach allowed for more detailed capture of the 1:250 000 or larger scale maps, more precise contact locations, incorporation of more rock units and more detailed description of those units than on the Cordillera-wide compilation of Wheeler and McFeely (1991).

* Maurice.Colpron@yukon.ca

Following the digital release (on CD at the time), a "wall map" and graphical legend were produced at the 1:1 000 000-scale (Gordey and Makepeace, 2001). At the same time, the Gordey and Makepeace (1999) GIS compilation was used to develop the first online map by the Yukon Geological Survey (YGS' Map Gallery, ca. 2001). It was the base for further development of online map applications for nearly 15 years and the Gordey and Makepeace (1999) compilation became the primary source of geological information for Yukon.

One issue with the Gordey and Makepeace (1999) compilation was that it was not easy to update and

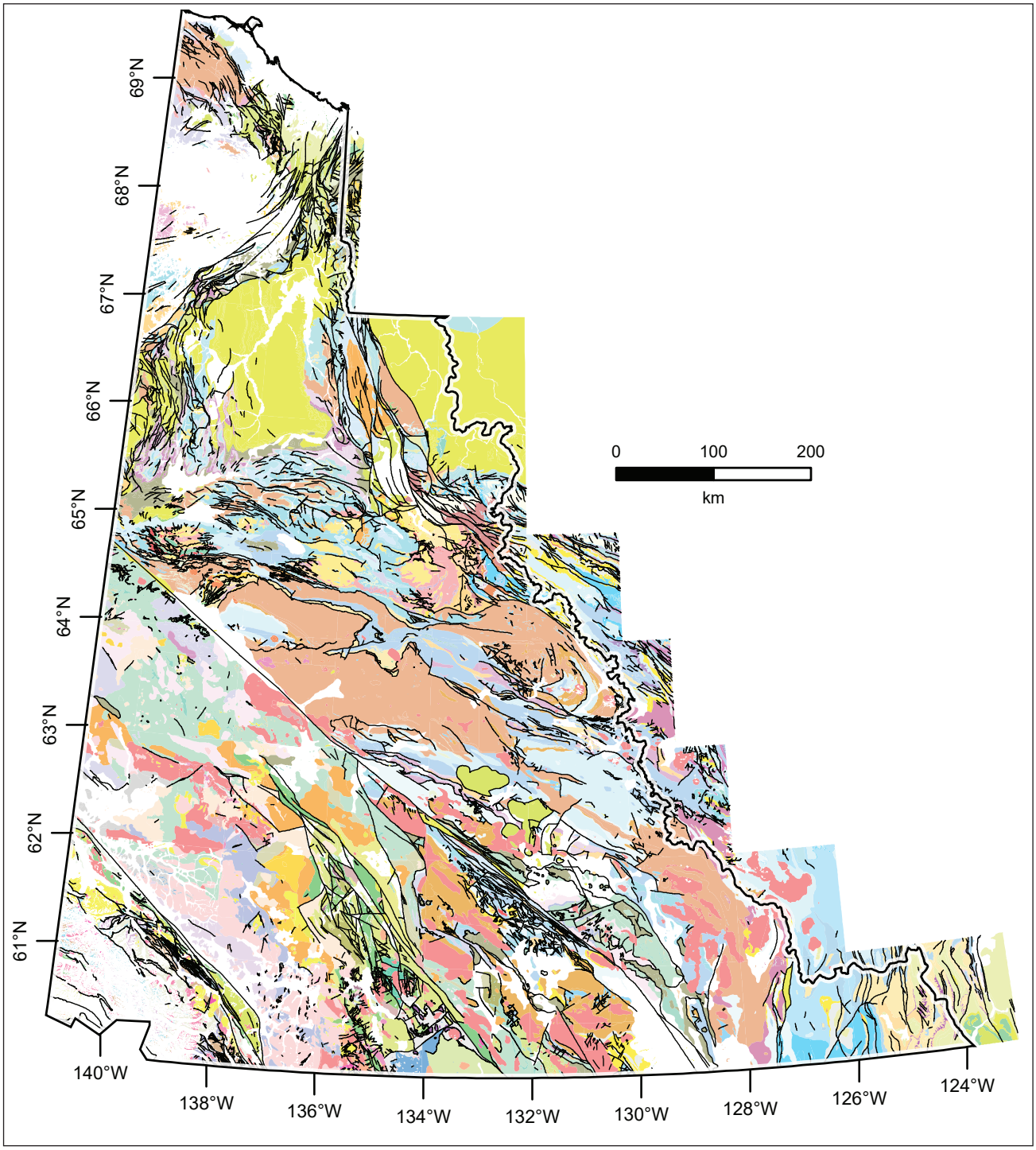


Figure 1. *Bedrock geology compilation of Gordey and Makepeace (1999).*

incorporate new detailed mapping into it. The digital geology compilation rapidly became out-of-date as new detailed bedrock maps were published, generally at a scale of 1:50 000, by the Yukon Geological Survey (and its precursor, the Yukon Geology Program) and the GSC. Because the digital bedrock geology had become the primary source of geological information, the difficulty in updating this dataset resulted in users not always getting the most current data available.

A partial update of the digital bedrock geology that included some newer detailed maps was released by Gordey and Makepeace (2003) but the new maps were only included as overlays to the original compilation and not integrated in the main GIS dataset. As a result, the 1999 compilation remained the *de facto* source of geological information for Yukon, a source that did not accurately reflect the evolving knowledge over time.

As of writing of this paper, new maps published since 1999 covered approximately 40% of Yukon (33% when excluding 1:250 000-scale maps published after 1999 but compiled in the original GIS dataset; Fig. 2a). Approximately 32% of the territory has been mapped in greater detail (1:150 000-scale or larger) since 1999, with 15% of Yukon mapped at 1:50 000-scale (Fig. 2b). These figures are constantly growing as the Yukon Geological Survey publishes new detailed bedrock geology maps annually.

The Ancient Pacific Margin NATMAP project (1999–2003) was a major impetus for updating the Yukon bedrock geology compilation. This collaborative mapping project involved geologists from the Geological Survey of Canada, British Columbia Geological Survey, Yukon Geological Survey and the United States Geological Survey and resulted in extensive detailed mapping and redefinition of the pericratonic Yukon-Tanana and Slide Mountain terranes in the northern Cordillera (Colpron and Nelson, 2006). Colpron (2006) produced a 1:1 000 000-scale compilation map to illustrate this new knowledge of Yukon-Tanana and related terranes, and this raised the need for an update to the Yukon digital bedrock geology.

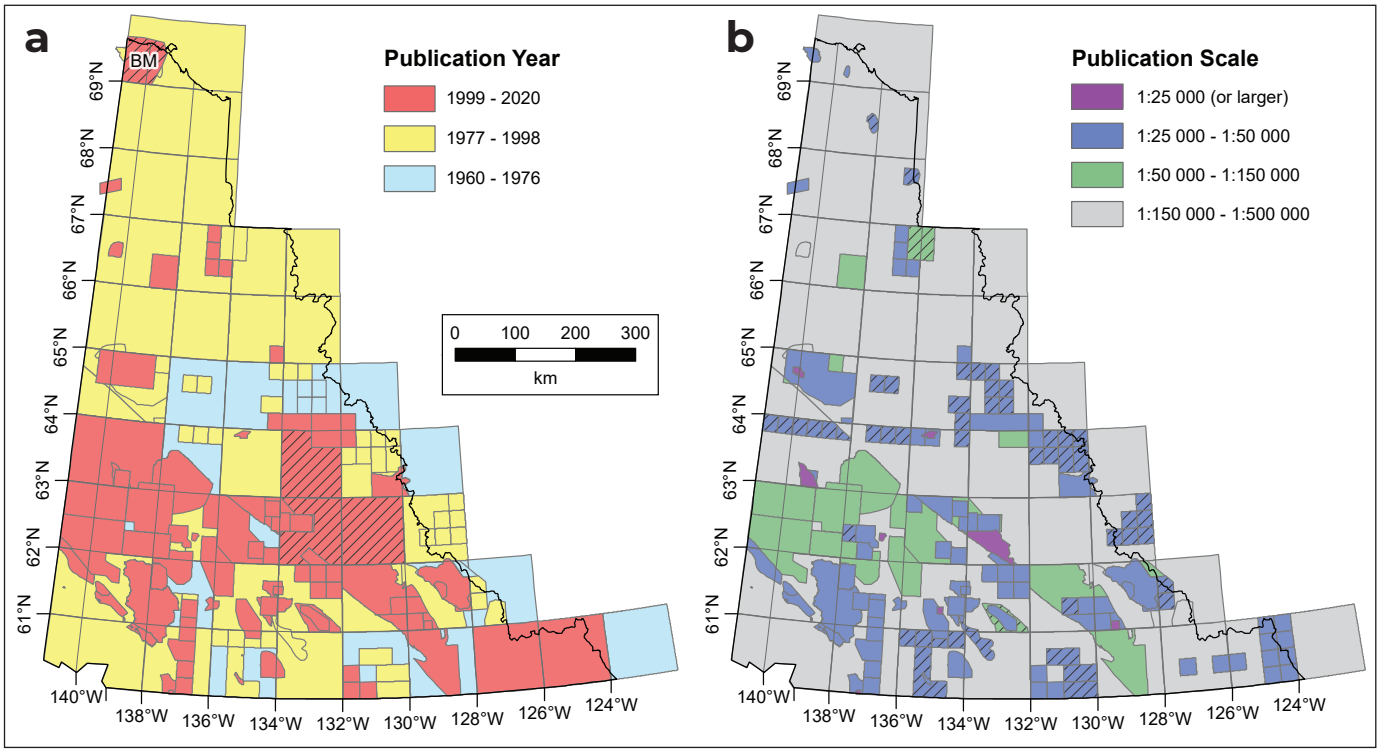


Figure 2. *Status of bedrock mapping in Yukon. The source geology maps used in the digital bedrock geology compilation are symbolized according to year* ***(a)*** *and scale* ***(b)*** *of publication. Hatched areas in* ***(a)*** *are 1:250 000-scale maps published after 1999 but compiled in the original GIS dataset (Gordey and Makepeace, 1999). Note that the geology map of the British Mountains (BM) in North Yukon was only published as part of the Gordey and Makepeace (1999) compilation. Hatched areas in B are detailed maps that were included in the original GIS compilation (1:50 000 in blue; 1:125 000 in green).*

A key objective in developing an update of the digital bedrock geology was to ensure that future updates of the dataset could be done efficiently and more frequently, such that the more detailed geological information could be disseminated through the various online portals in a timely manner. This was achieved in 2016 and the Yukon bedrock geology GIS compilation has been "live" and seen periodic updates since. This paper summarizes the concepts that guided the overhaul of the Yukon digital bedrock geology dataset, and the enhancements in data organization and presentation the user will find in the modern GIS compilation. The various ways in which the dataset can be accessed and used are described, as well as the ongoing development of ancillary geoscience datasets that complement the bedrock geology map.

Rebuilding the Yukon Bedrock Geology Compilation

The original compilation of Gordey and Makepeace (1999) was constructed in ArcInfo as a set of lines and polygons that were attributed using codes that referenced external database tables. The polygon structure made it difficult to integrate new maps into the dataset. Most users accessed the data as shapefiles on other GIS software and therefore couldn't benefit from ArcInfo interconnectivity between tables and the code-base attribution of the GIS features made it cumbersome to build queries and symbolize the data. The attribute structure of GIS tables in the Gordey and Makepeace (1999) compilation were designed to be lean and minimize file sizes (Fig. 3). A few attributes contained plain language entries that were readily understood but many included concatenated text difficult to query. Polygon attributes did not include stratigraphic information and the user needed to be acquainted with the unit codes (e.g., REG_UNIT) to readily extract this information. The polygons were keyed to an HTML legend (PICKINFO field; Fig. 3b) but this assumed proper link to the HTML files, an assumption that did not necessarily apply for most users.

The update of the digital bedrock geology dataset aimed at producing a more flexible and user-friendly map. To facilitate more regular updates of the map, the polygons from the Gordey and Makepeace (1999) compilation were first converted to centroids. A centroid is a point feature that carries all the attribute information for a given map unit bound by geological contacts. Using lines and centroids, topologically correct polygons can be generated quickly using a series of ArcGIS tools. The workflow begins with merging the linework (faults, contacts, extent polygon) using the Merge (Data Management) tool, then cleaning to remove topology errors with the Trim Line (Editing) tool, and then creating polygons from the enclosed spaces that the lines create using the Feature to Polygon (Data Management) tool. Finally, the geological attributes are spatially joined from the centroid to the newly created polygon feature class using the Spatial Join (Analysis) tool. This workflow is saved as a model builder tool in ArcGIS so it can be run consistently with the same parameters (Fig. 4). Although the data are still delivered to the end-user as lines and polygons, the centroid-based master files at the YGS allow for regular updates as new maps are published, and easy corrections to the data as errors are being detected.

The following step in rebuilding the bedrock geology dataset was to develop an extended attribute structure for both line and centroid/polygon features (Fig. 3). Several fields were added to the new data tables and were assigned names that are readily recognized by most users (Appendix 1). The coding from the original Gordey and Makepeace (1999) dataset was converted to text and previously concatenated attributes (e.g., AGE) were distributed over multiple fields to facilitate queries. New fields were introduced to provide the full stratigraphic information for each map unit (e.g., Group, Formation, etc...), and a short unit description (10 words or less) was added for rapid investigation of the GIS dataset and easy production of abbreviated legends. Line features are now provided in separate feature classes (or shapefiles) for faults and contacts (Fig. 3a). Both line feature classes have identical attribute structures (Appendix 1), but they are provided individually for easy symbolization. The "map boundary" lines that were part of the Gordey and Makepeace (1999) dataset were removed to produce comprehensive unit polygons (Fig. 5). In the updated dataset, the source information is provided as a separate polygon feature class (Bedrock Map Index)

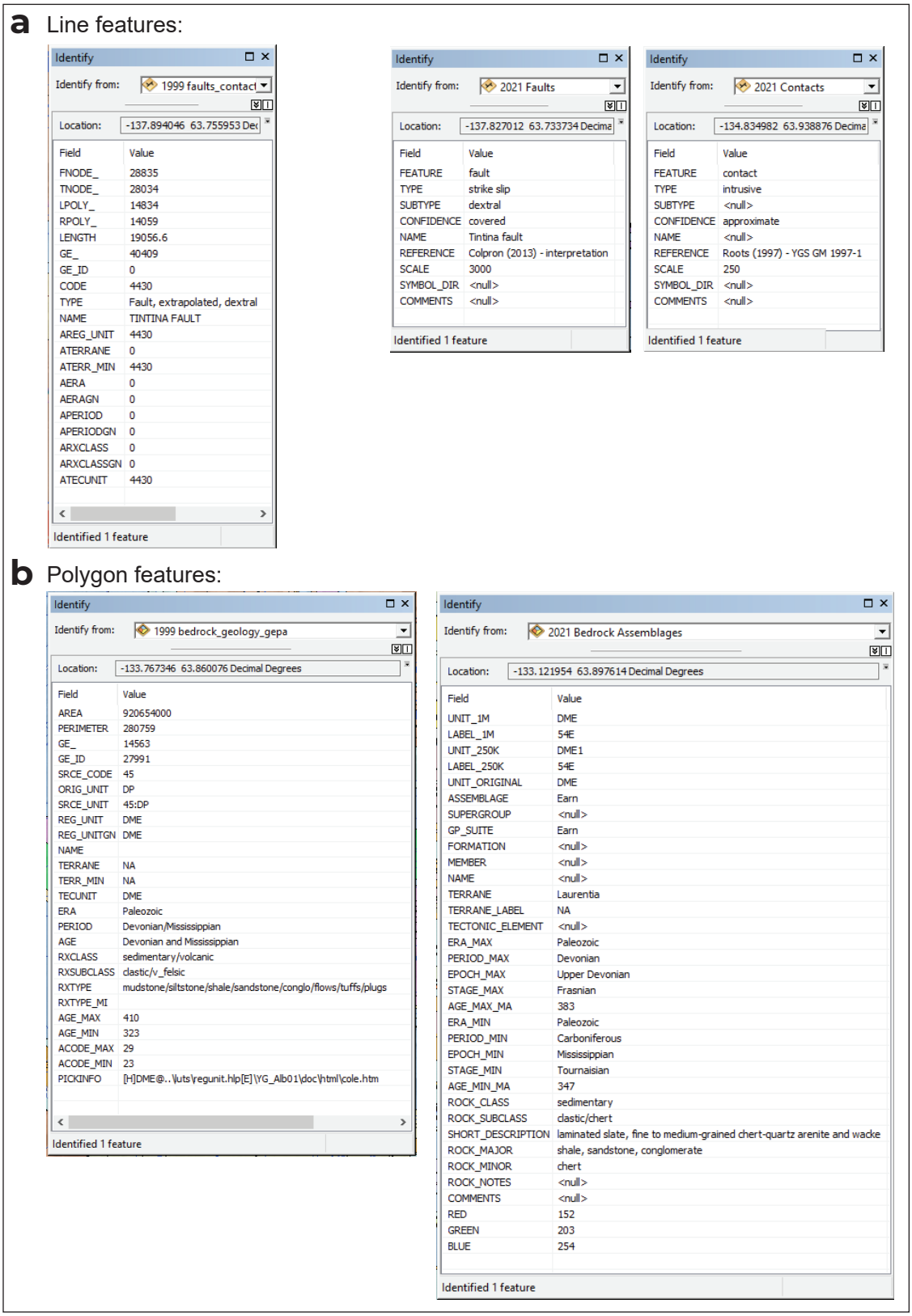


Figure 3. *Comparison of attribute structures for line* ***(a)*** *and polygon* ***(b)*** *features between the original digital compilation of Gordey and Makepeace (1999; left) and the current version of the bedrock geology dataset (Yukon Geological Survey, 2022; right).*

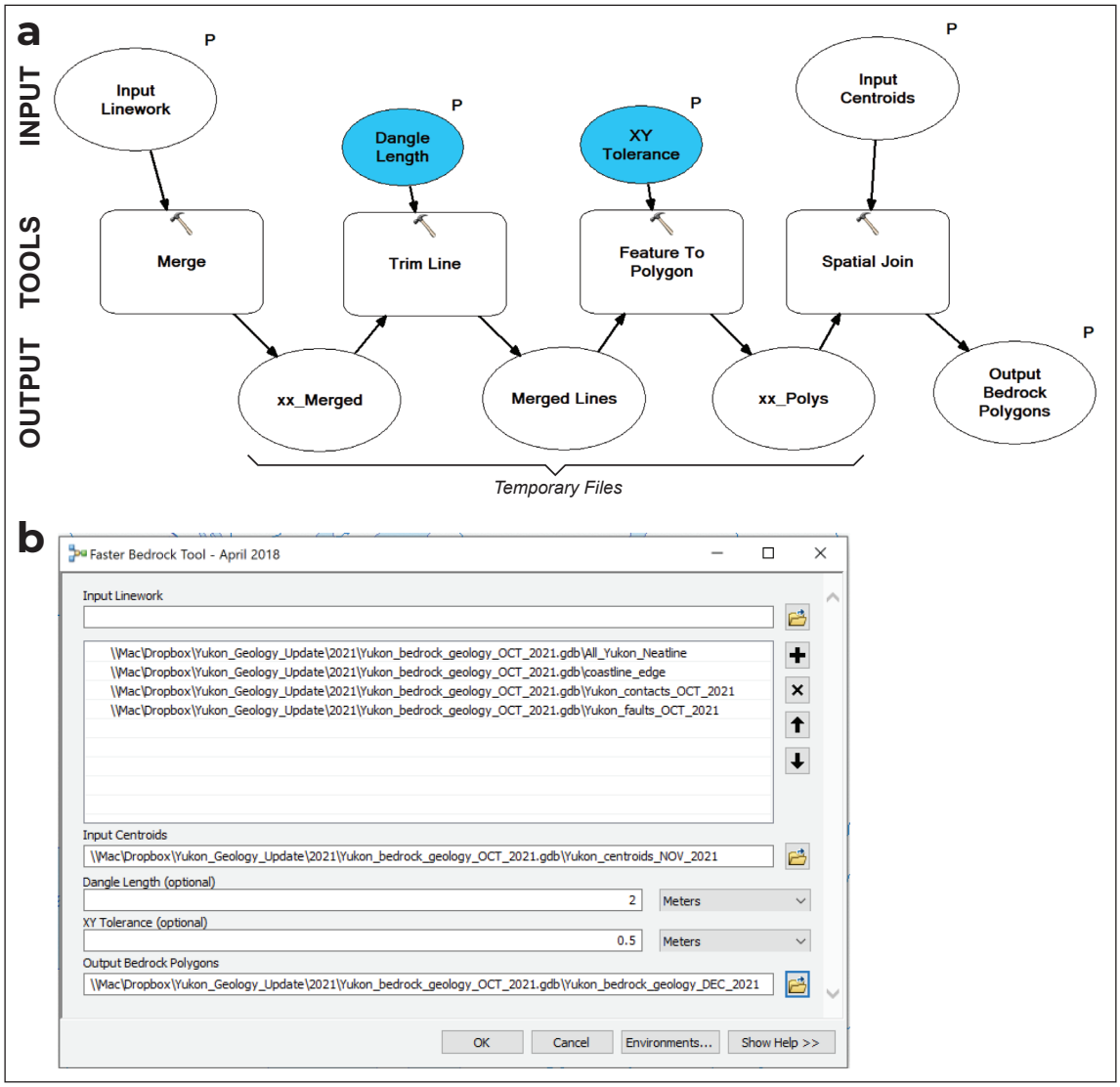


Figure 4. (a) *ArcGIS workflow employed for polygon creation at the Yukon Geological Survey. Input data and parameters are shown at the top, ArcGIS tools (indicated by hammer symbol) in the middle, and output files at the bottom. Parameters shown in blue at the top can be adjusted in the user interface shown in* ***(b)****. For polygon creation in the Yukon bedrock geology dataset, Dangle Length is set at 2 m and XY Tolerance at 0.5 m.*

and source attribution is now included in the line feature classes, rather than within unit polygon attributes. References to source maps are also given as shorthand text attributes that are readily recognizable (Figs. 3a and 5c).

Another objective in updating the GIS dataset was to extrapolate the interpretation of the bedrock geology through many of the areas shown as Quaternary cover (Q) in the Gordey and Makepeace (1999) compilation (compare Fig. 5a and 5b). Interpretations were guided using remote sensing images such as aeromagnetic maps and satellite images, resulting in a more coherent bedrock geology map with only limited regions of extensive Quaternary cover left (e.g., Old Crow Flats; Fig. 6). Users can still access information about surficial geology by using the YGS surficial geology dataset (https://data.geology.gov.yk.ca/Compilation/33) in concert with the bedrock geology dataset. Surficial geology mapping does not yet cover all of Yukon.

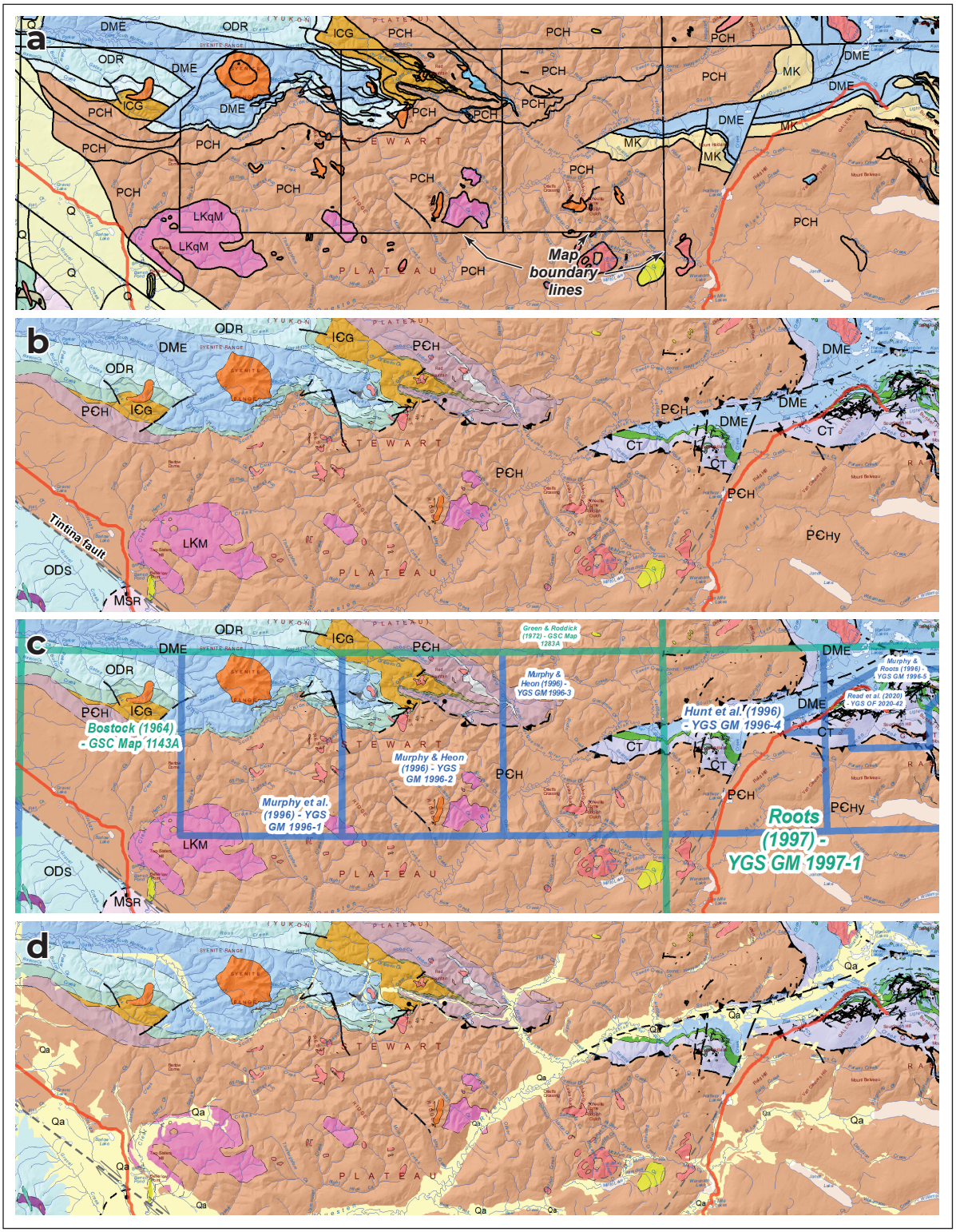


Figure 5. *Comparison between the original compilation of Gordey and Makepeace (1999)* **(a)** *and the current version of the bedrock geology map* **(b–d)**. **(b)** *In the current GIS compilation, the bedrock geology is extrapolated through region of extensive Quaternary cover (Q in* **(a)***) and unit polygons are seamless across map boundaries.* **(c)** *Information about the source maps compiled into the bedrock geology map is now provided in a separate feature class.* **(d)** *Areas of extensive Quaternary colluvium and alluvium deposits (Qa) are now provided as a distinct feature class extracted from the surficial geology dataset.*

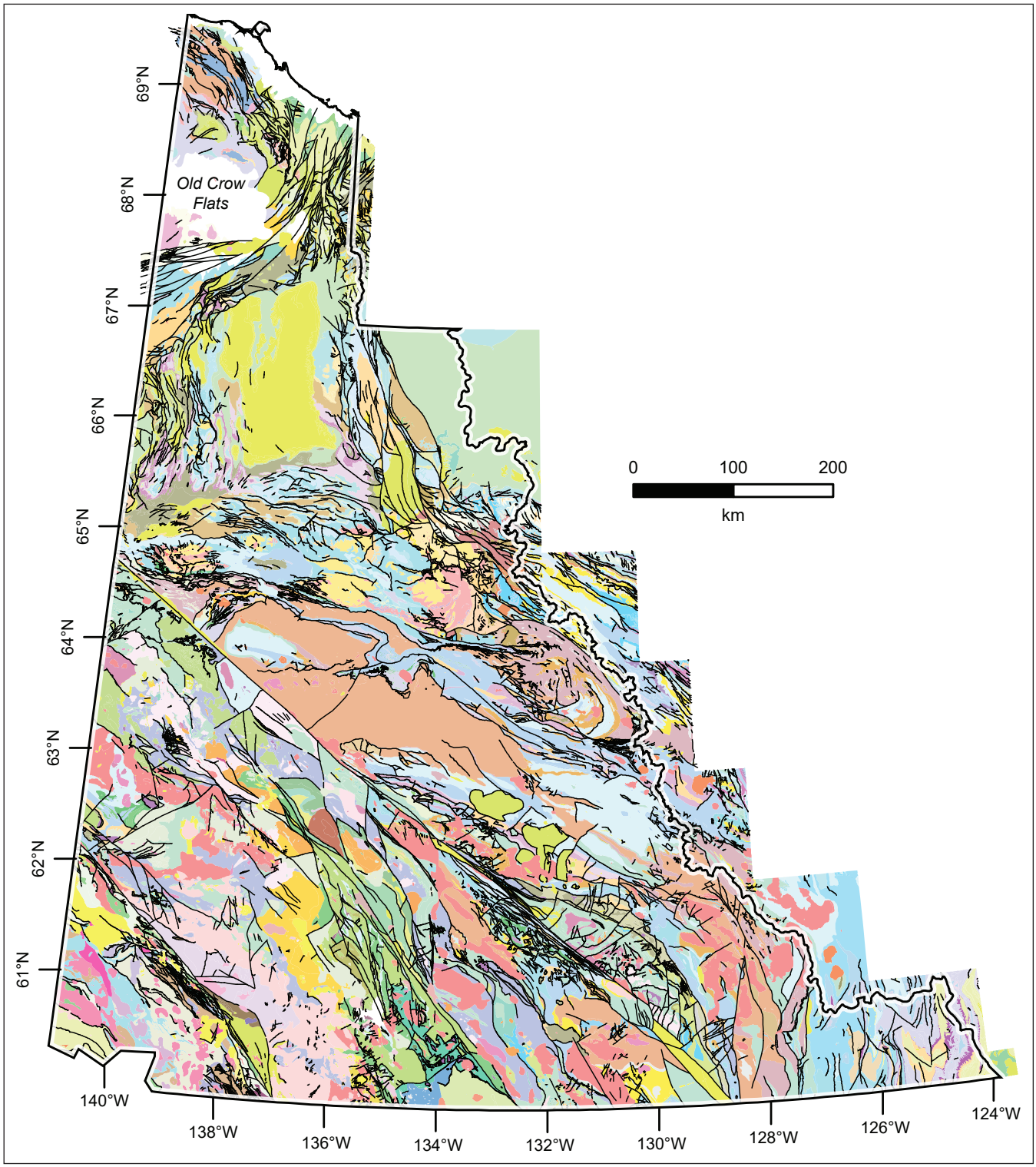


Figure 6. *The current version of the GIS compilation provides an interpretation of the bedrock geology beneath Quaternary cover over much of the territory, except in few locations such as Old Crow Flats in North Yukon (Yukon Geological Survey, 2022). Compare with the Gordey and Makepeace (1999) map in Figure 1.*

To facilitate overlay with the bedrock geology map, regions where extensive alluvial and colluvial deposits hinder bedrock exposures were extracted as a "Quaternary Alluvium" feature class from existing regional surficial maps (Qa; Fig. 5d). Following Gordey and Makepeace (1999), the bedrock geology compilation and accompanying spatial datasets are provided in Yukon Albers projection (Appendix 2).

The first comprehensive update to the Yukon bedrock geology GIS dataset was available for download in early 2016, and the dataset has seen periodic updates since. Online map services were also updated in 2016 to show the latest version of the bedrock geology dataset and are updated at the same frequency as the GIS dataset. With each update, new detailed maps are added to the dataset, errors in previous data captures are corrected, and feature attributions are improved. Since 2016, the Yukon bedrock geology map has become "live" online such that the end-user can now access the best information available in a timely manner.

Map and Legend Organization

Gordey and Makepeace (1999) used the Wheeler and McFeely (1991) tectonic assemblage map as the basis for organization of their map, choice of colours and regional unit names, but aimed to provide more of a stratigraphic map (*vs.* tectonic assemblages) by preserving details from the source maps. Gordey and Makepeace (2001) produced a 1:1 000 000-scale "wall map" accompanied by a graphic legend with more detailed unit descriptions. The 2016 update of the Yukon bedrock geology dataset was also accompanied by release of a revised 1:1 000 000 "wall map" and legend which followed the same general organization as previous maps but integrated more recent interpretations of regional stratigraphic units (Colpron *et al.*, 2016). With ongoing mapping in various parts of Yukon, there has been sufficient additional improvements to the regional stratigraphy in the last 5 years to warrant a new revision to the Yukon bedrock geology 1:1 000 000-scale "wall map" and legend (Colpron, 2022).

The new bedrock geology map (Colpron, 2022) is symbolized and labeled for display at the 1:1 000 000 scale but was generated from the full GIS dataset (Yukon Geological Survey, 2022). The map includes 1:5 000 000-scale inset maps of terranes (Yukon Geological Survey, 2020), glacial limits (Duk-Rodkin, 1999), total field aeromagnetic (Oneschuk *et al.*, 2019) and bouguer gravity (compilation by N. Hayward, December 2021; data available from: http://gdr.agg.nrcan.gc.ca/).

The graphic legend that accompanies the 1:1 000 000-scale geology map (Colpron, 2022) provides more detailed descriptions of regional map units compared to short descriptions built into the GIS compilation. The legend is organized in a series of columns that correspond to geographic areas of Yukon characterized by distinct geology (Fig. 7). Columns in the legend are generally arranged from southwest to east and north.

- Column A, in southwestern Yukon, includes units of the Insular and Outboard terranes and their Mesozoic and younger overlap assemblages.
- Units in Column B, in western Yukon, are the extension of parautochthonous Ancestral North American (Laurentian) rocks of the Yukon-Tanana Uplands of east-central Alaska (Dusel-Bacon *et al.*, 2006; Murphy, 2007), and their Mesozoic overlap assemblages. Many units in Column B are considered equivalents to units in Selwyn basin described in Column E.
- Column C contains description of units in the Intermontane terranes, including the Yukon-Tanana, Slide Mountain, Stikinia, Quesnellia and Cache Creek terranes, overlapping Mesozoic sedimentary (e.g., Whitehorse trough) and volcanic units (e.g., Carmacks Group), and the numerous Mesozoic–Cenozoic plutons that intrude the region.
- In Column D, units of the Cassiar terrane and its contained Cretaceous and Eocene plutons are described.

- Column E covers the "Selwyn basin region" of central and eastern Yukon (Fig. 6). Selwyn basin *sensu stricto* comprises lower Paleozoic, mainly siliciclastic, off shelf strata (Gordey and Anderson, 1993; Gordey, 2013) but the term Selwyn basin (*sensu lato*) is commonly used to refer to the region underlain by the Selwyn Mountains (west of Mackenzie Mountains and south of Ogilvie-Wernecke Mountains) and encompasses Neoproterozoic to lower Mesozoic strata and the numerous Cretaceous plutons that intrude them.
- Columns F and G describe the mainly continental shelf, carbonate and siliciclastic lower Paleozoic strata of the Mackenzie/MacDonald platform to the east (F) and the Ogilvie platform to the north (G). Both regions are overlapped by Mesozoic foreland basin strata and include older Neoproterozoic 'rift' facies. Column G covers the region known as the Yukon block (Fritz, 1996) and includes the oldest rocks in the northern Cordillera (Wernecke Supergroup).
- Finally, Column H describes displaced continental margin strata of Neoproterozoic to Devonian age exposed north of the Porcupine shear zone and west of the Yukon fault in North Yukon. These rocks are overlapped by upper Paleozoic and younger strata described in column G.

Within these columns, brackets to the left group units according to terrane affinities, overlap successions or post-accretionary intrusions. Stratified units are symbolized with rectangles, while intrusive units are shown with oval swatches (Fig. 8).

Ancillary Datasets

The bedrock geology compilation is complemented by a series of ancillary datasets, including compilations of radiometric ages (Geochronology – https://data.geology.gov.yk.ca/Compilation/22), whole rock geochemistry (Lithogeochemistry – https://data.geology.gov.yk.ca/Compilation/35), and mineral occurrences (MINFILE – https://data.geology.gov.yk.ca/Compilation/24).

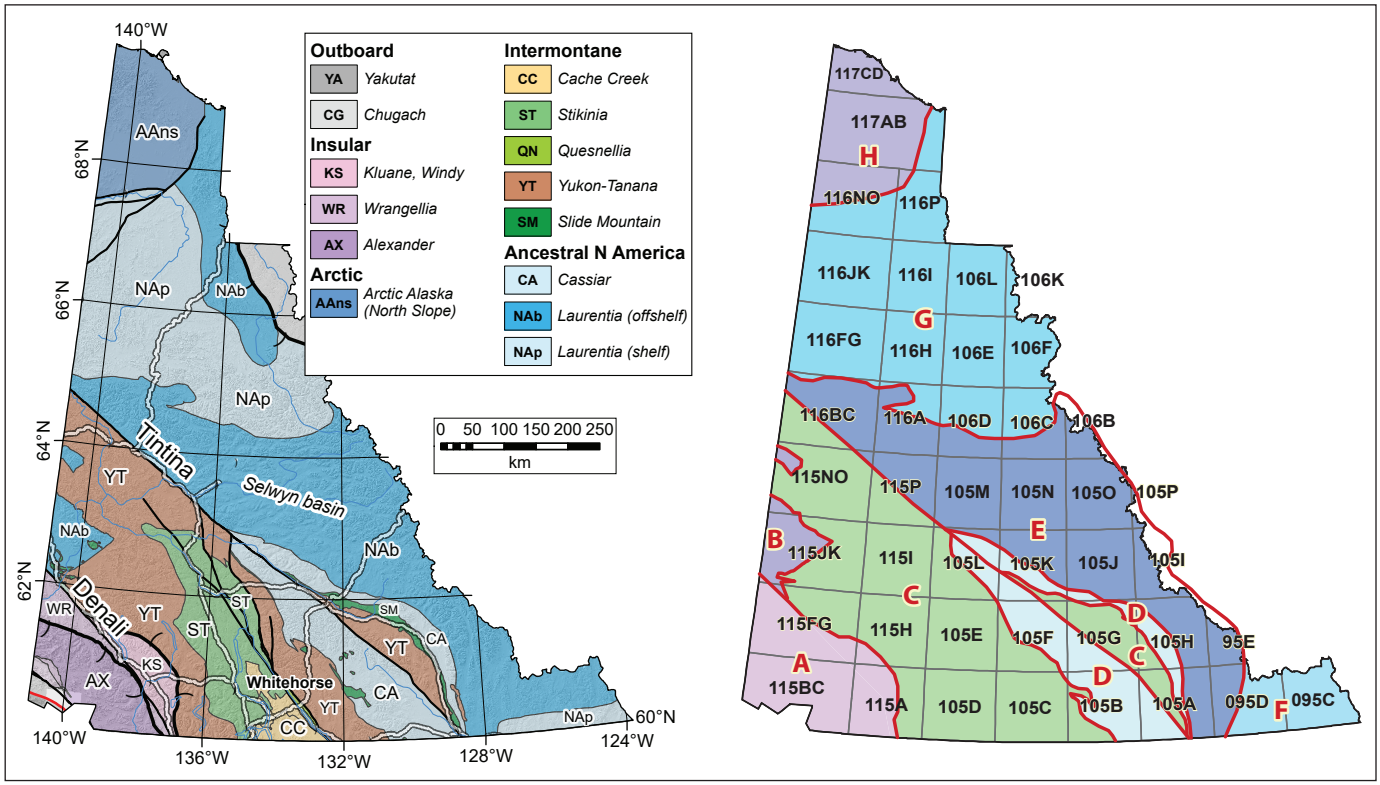


Figure 7. (a) *Terrane map of Yukon (Yukon Geological Survey, 2020).* ***(b)*** *Organization of map legend where areas A–H correspond to columns in the legend of Colpron (2022).*

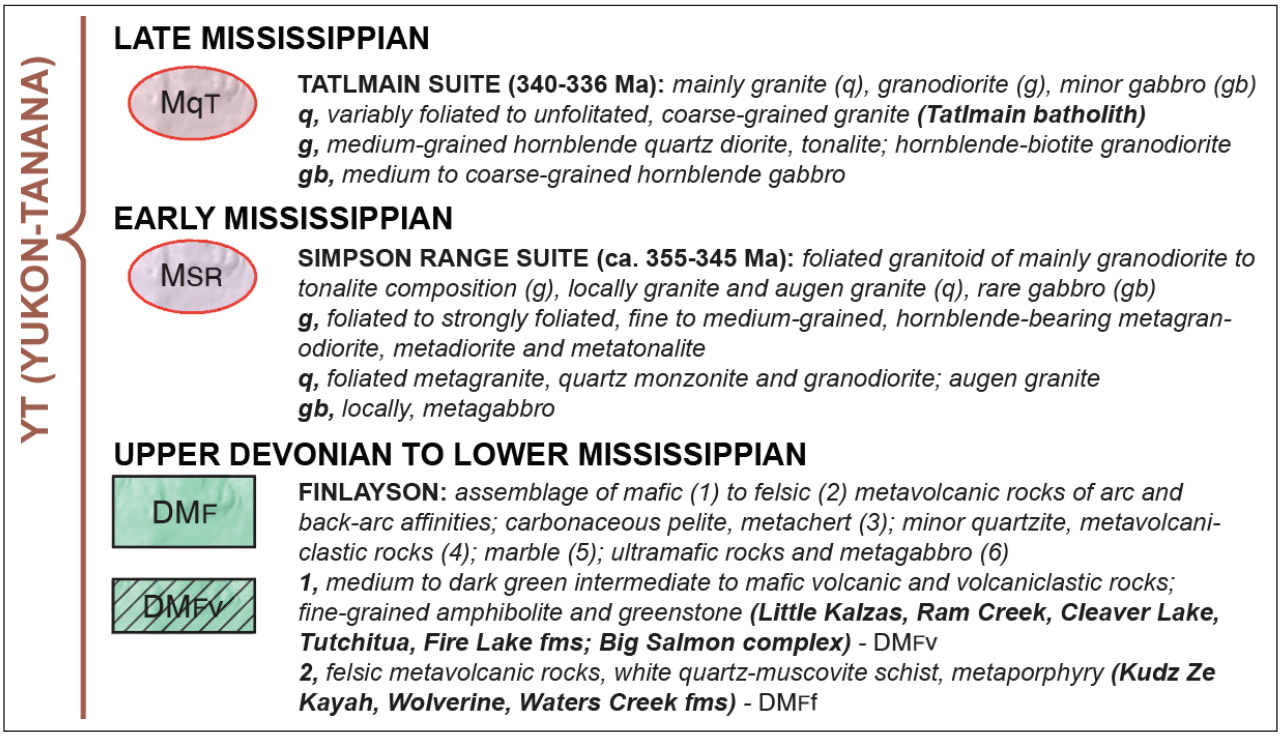


Figure 8. *Portion of the legend that accompanies the "wall map" (Colpron, 2022) showing some key symbolization features. Stratified units are represented with rectangular swatches (e.g., DMF) while plutonic units are shown with ovals with red outline (e.g., MSR). The assemblage or suite names are shown in capitalized bold letters at the start of the descriptions, while regional stratigraphic or intrusive units are listed in bold-italic after some rock descriptions where appropriate. Map labels of regional units (UNIT_1M and LABEL_1M fields in the geodatabase, Fig. 3b) are typically shown in the unit swatch (e.g., DMF and MSR) while compositional grouping shown by bold-italic letters or numbers at the start of unit descriptions correspond to attributes in the UNIT_250K field. Compositions of plutonic rocks are indicated by letters that are inserted between age and unit descriptors in labels (e.g., MgSR, where M is for Mississippian, g granodiorite, and SR Simpson Range). Stratified units are listed in numerical order (e.g., DMF1, DMF2, etc...). The corresponding map label (LABEL_250K) is listed last after rock descriptions for some units (e.g., DMFv, DMFf). Map labels require the gscGeology true-type font for proper display. For some subunits, pattern overlays are used to distinguish facies. In the example shown here, the diagonal hatch pattern for subunit DMFv (or DMF1) indicates a mafic volcanic facies.*

The Geochronology dataset was developed based on the YukonAge database of Breitsprecher and Mortensen (2004). YukonAge was a relational database that provided a querying interface in Microsoft Access, but that wasn't easily integrated with GIS platforms (for spatial queries) and required database skills for maintenance. The YukonAge database was converted to a 'flatfile' format (comma-separated values [CSV] and shapefile) that is more readily used on any software platform and easily updated. The Geochronology feature class is easily integrated with the bedrock geology GIS dataset allowing for spatial interrogation of the data. The Geochronology dataset contains a compilation of all known radiometric ages from igneous and metamorphic rocks in Yukon, including U/Pb, K/Ar, $^{40}Ar/^{39}Ar$, and other dating methods, as well as mineralization ages determined by the Re/Os method. For some geochronology samples, images of the age plot are included to provide a means of evaluating the confidence of the age determinations. Future development should include links to published isotopic data tables. Detrital zircon U/Pb ages are excluded from the Geochronology dataset, except for samples that have a precisely determined maximum depositional age that is interpreted to closely reflect the age of strata.

A separate compilation of detrital zircon data is under development. The Geochronology dataset was first made available on the YGS website in 2018 and has been updated annually with the addition of new age determinations from YGS projects, other publications and identified gaps.

The Lithogeochemistry dataset was first posted online in 2019. The whole rock geochemistry compilation was first developed to facilitate calculation of radiogenic heat production from Yukon granitoids as part of YGS' geothermal energy research program (Friend and Colpron, 2017; Colpron, 2019); and data for volcanic, sedimentary and metamorphic rocks were subsequently added. The dataset is a compilation of all known published and archival YGS data (many unpublished). The Lithogeochemistry dataset benefited substantially from large datasets released by the GSC (Milidragovic et *al*., 2016; Ryan et *al*., 2018; Zagorevski, 2020). Annual updates fill identified gaps in the dataset and add new data from the literature and from ongoing YGS projects.

The MINFILE database is maintained by the Minerals Geology unit of YGS and is interfaced with assessment report files and the YGS drill core collection. Other datasets being developed at the time of writing this report include compilations of structural and rock property data collected during bedrock mapping programs by the YGS. Finally, a terrane map is also available for more generalized representations of the geology of the northern Cordillera at scale of 1:5 000 000 and smaller (Fig. 6a; https://data.geology.gov.yk.ca/Compilation/2).

Accessing and Using the Bedrock Geology Datasets

The Yukon Bedrock Geology dataset can be accessed in a wide range of formats. The authoritative resource for accessing the latest version of the Yukon Bedrock Geology dataset is through YGS's publication database (https://data.geology.gov.yk.ca/Compilation/3). The dataset can be viewed as layers within many of the web mapping applications created by YGS (https://data.geology.gov.yk.ca/WebMaps/) and Yukon government, including GeoYukon (https://mapservices.gov.yk.ca/GeoYukon/). Advanced users can download the data for use with their own desktop GIS software from the YGS website (https://data.geology.gov.yk.ca/Compilation/3) or Geomatics Yukon (ftp://ftp.geomaticsyukon.ca/GeoYukon). The Yukon geology map can also be downloaded in PDF format from the YGS website (https://data.geology.gov.yk.ca/Compilation/3) either as a Yukon-wide 1:1 000 000-scale compilation (or "wall map" with legend; Colpron, 2022) or as a series of 1:250 000-scale tiles for each NTS sheet in Yukon (total of 43 maps; https://data.geology.gov.yk.ca/Compilation/23). These PDF tiles are georeferenced maps that can be viewed interactively on mobile devices using the Avenza Maps™ app (www.avenzamaps.com). When downloaded (for free) directly from the Avenza Maps Store (https://www.avenzamaps.com/vendor/3337/yukon-geological-survey) the user can view the Yukon geology maps on the free Avenza Maps™ app. The georeferenced PDF maps allow for real-time tracking and navigation on the geology base using any GPS-enabled mobile devices (e.g., smartphones and tablets). Each 1:250 000-scale map contains a legend specific to the NTS sheet to the right of the geology map and displays subsets of the geochronology (U/Pb, K/Ar and $^{40}Ar/^{39}Ar$ dates) and mineral occurrences datasets on the map (Fig. 9).

From Outcrop to Digital Map

New, detailed bedrock geology maps produced by the Yukon Geological Survey are built within the same GIS framework as the Yukon-wide compilation, therefore facilitating easy integration within the regional geodatabase. In the field, geologists capture site information (e.g., stations, lithology, structural data, rock magnetic susceptibility, etc.) on mobile devices and these point data are transferred to ArcGIS in the office. Maps are digitized in ArcGIS using the same attribute structures as the regional compilation. At completion of a mapping project, the new geology map is then easily substituted into the regional compilation and integrated following some edge-matching by YGS geologists. Once incorporated into the bedrock geology geodatabase, the updated data can easily be substituted on the various web services, thus making the Yukon bedrock geology map a "live" map.

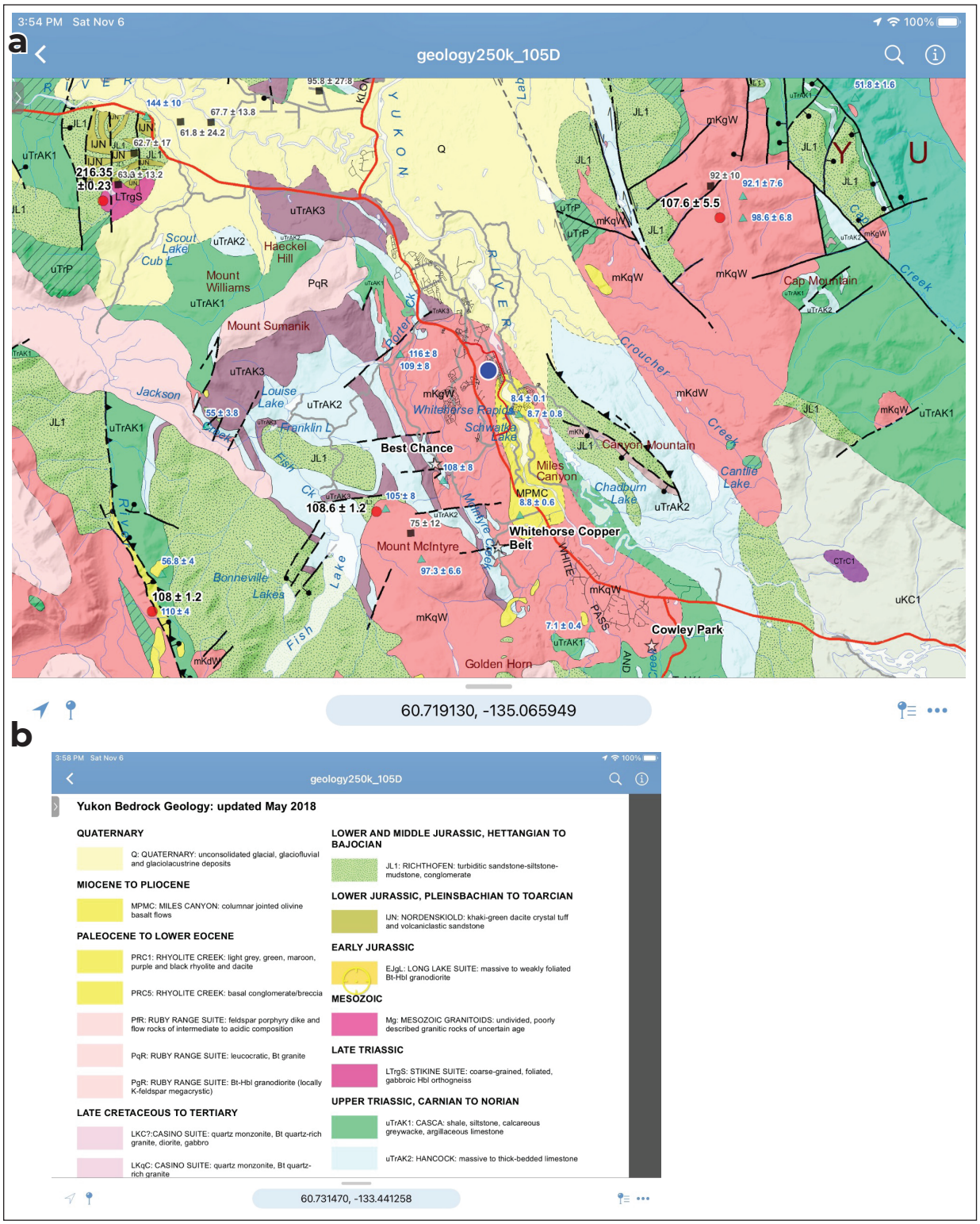


Figure 9. (a) *Geology of the Whitehorse area as viewed on the Avenza Maps™ app on a tablet. The blue dot at the centre of the map indicates the "current" GPS position on the map, with coordinates shown at the bottom of the screen (latitude and longitude; WGS84 projection).* ***(b)*** *When scrolling to the right edge of the PDF map, the user can view a geological legend filtered for units present on the NTS sheet.*

Some Key Points to Remember

- The Yukon Bedrock Geology dataset is in constant evolution with continued corrections, new data and maps added as they become available. As such, the user is encouraged to visit the YGS website regularly to ensure they are working with the latest version of the dataset.
- The bedrock geology GIS compilation was captured at the scale of publication. Therefore, the Yukon digital geology map does not have a unique scale. There is a common misconception that the Yukon bedrock geology map and data are at a scale of 1:1 000 000, because this is the scale of publication for the open file "wall map" (Gordey and Makepeace, 2001; Colpron *et al.*, 2016; Colpron, 2022). For the most part, the bedrock geology data were captured at a scale of 1:250 000 or better. This last point is important to note, as a growing proportion of the Yukon map comprises data captured at 1:50 000 or larger scale (Fig. 2b).
- Although the Yukon bedrock geology GIS dataset offers a convenient way to access the latest information, with increasing better accuracy over time, the source maps remain the ultimate resource for any part of Yukon. The users should always consult the more detailed published maps when working in specific areas. Any discrepancies noted by the user should be reported to the Yukon Geological Survey (YGS-Bedrock@yukon.ca).
- User comments have made important contributions to improving the quality and accuracy of the bedrock geology dataset over the years. The Yukon Geological Survey aims to provide users with the best available geoscience data for Yukon. Any revisions or additional geological information known to the user would be welcomed by the Yukon Geological Survey.

Acknowledgements

The original Digital Bedrock Geology compilation of Gordey and Makepeace (1999) provided the solid foundation from which the YGS' modern geodatabase could evolve. The pioneering work of Steve Gordey and Andrew Makepeace helped propel the Yukon geology into the digital age. The update of the bedrock geology dataset was a lengthy and laborious process that involved many geologists and geological assistants at YGS over nearly a decade: Lee Pigage, Don Murphy, Steve Israel, David Moynihan, Grant Abbott, Esther Bordet, Olwyn Bruce, Panya Lipovsky, Kristy Kennedy, Samantha Darling, Liz Westberg, Brett Elliot and many others. I thank Kristy Kennedy for providing the Quaternary Alluvium (Qa) extract from the Surficial geology maps for use as an overlay to the bedrock geology map. Brett Elliot provided comments on an early version of this paper.

References

Breitsprecher, K. and Mortensen, J.K. (compilers), 2004. Yukonage 2004: A database of isotopic age determinations for rock units from Yukon Territory, Canada. Yukon Geological Survey, CD-ROM.

Colpron, M., 2006. Tectonic assemblage map of Yukon-Tanana and related terranes in Yukon and northern British Columbia. Yukon Geological Survey, Open File 2006-1, scale 1:1 000 000.

Colpron, M., 2019. Potential radiogenic heat production from granitoid plutons in Yukon. Yukon Geological Survey, Open File 2019-16.

Colpron, M., 2022. Yukon bedrock geology map. Yukon Geological Survey, Open File 2022-1, scale 1:1 000 000.

Colpron, M. and Nelson, J.L., 2006. Paleozoic evolution and metallogeny of pericratonic terranes at the ancient Pacific margin of North America, Canadian and Alaskan Cordillera. Geological Association of Canada, Special Paper 45, 523 p.

Colpron, M., Israel, S., Murphy, D.C., Pigage, L.C. and Moynihan, D., 2016. Yukon Bedrock Geology Map. Yukon Geological Survey, Open File 2016-1, scale 1:1 000 000.

Duk-Rodkin, A., 1999. Glacial Limits Map of Yukon. Yukon Geological Survey, Geoscience Map 1999-2, scale 1:1 000 000.

Dusel-Bacon, C., Hopkins, M.J., Mortensen, J.K., Dashevsky, S.S., Bressler, J.R. and Day, W.C., 2006. Paleozoic tectonic and metallogenic evolution of the pericratonic rocks of east-central Alaska and adjacent Yukon. *In:* Paleozoic Evolution and Metallogeny of Pericratonic Terranes at the Ancient Pacific Margin of North America, Canadian and Alaskan Cordillera, M. Colpron and J.L. Nelson (eds.), Geological Association of Canada, Special Paper 45, p. 25–74.

Friend, M. and Colpron, M., 2017. Potential radiogenic heat production from Cretaceous and younger granitoid plutons in southern Yukon. Yukon Geological Survey, Open File 2017-60, scale 1:1 000 000.

Fritz, W.H., 1996. Cambrian. *In:* The Geology, Mineral and Hydrocarbon Potential of Northern Yukon Territory and Northwestern District of Mackenzie, D.K. Norris (ed.), Geological Survey of Canada, Bulletin 422, p. 85–117.

Gordey, S.P., 2013. Evolution of the Selwyn Basin region, Sheldon Lake (105J) and Tay River (105K) map areas, central Yukon Territory. Geological Survey of Canada, Bulletin 599, 190 p.

Gordey, S.P. and Anderson, R.G., 1993. Evolution of the northern Cordilleran miogeocline, Nahanni map area (105I), Yukon and Northwest Territories. Geological Survey of Canada, Memoir 428, 214 p.

Gordey, S.P. and Makepeace, A.J., 1999. Yukon digital geology. Geological Survey of Canada, Open File D3826.

Gordey, S.P. and Makepeace, A.J., 2001. Bedrock geology, Yukon Territory. Geological Survey of Canada, Open File 3754, scale 1:1 000 000.

Gordey, S.P. and Makepeace, A.J., 2003. Yukon digital geology (version 2). Geological Survey of Canada, Open File 1749.

Journeay, J.M. and Williams, S.P., 1995. GIS Map Library; A Window on Cordilleran Geology. Geological Survey of Canada, Open File 2948.

Milidragovic, D., Ryan, J.J., Zagorevski, A. and Piercey, S.J., 2016. Geochemistry of Permian rocks of the Yukon-Tanana terrane, western Yukon: GEM 2 Cordillera project. Geological Survey of Canada, Open File 8170, 21 p.

Murphy, D.C., 2007. The three 'Windy Mckinley' terranes of Stevenson Ridge (115JK), western Yukon. *In*: Yukon Exploration and Geology 2006, D.S. Emond, L.L. Lewis and L.H. Weston (eds.), Yukon Geological Survey, p. 223–236.

Oneschuk, D., Miles, W.F., Saltus, R.W. and Hayward, N., 2019. Alaska and Yukon magnetic compilation, residual total field. Geological Survey of Canada, Open File 7862, scale 1:1 125 000.

Ryan, J.J., Zagorevski, A. and Piercey, S.J., 2018. Geochemical data of Yukon-Tanana and Slide Mountain terranes and their successor rocks in Yukon and northern British Columbia. Geological Survey of Canada, Open File 8500, 11 p.

Wheeler, J.O. and McFeely, P., 1991. Tectonic assemblage map of the Canadian Cordillera and adjacent parts of the United States of America. Geological Survey of Canada, Map 1712A, scale 1:2 000 000.

Yukon Geological Survey, 2020. A digital Atlas of terranes for the northern Cordillera. Yukon Geological Survey, https://data.geology.gov.yk.ca/Compilation/2, [accessed January 25, 2022].

Yukon Geological Survey, 2022. Yukon digital bedrock geology. Yukon Geological Survey, https://data.geology.gov.yk.ca/Compilation/3#InfoTab, [accessed November 20, 2021].

Zagorevski, A., 2020. Whole-rock geochemical data compilation supporting Geo-mapping for Energy and Minerals Cordillera syntheses, British Columbia and Yukon. Geological Survey of Canada, Open File 8674, 7 p. and spreadsheet.

Appendix 1

Yukon bedrock geology – centroid/polygon attribute

FIELD NAME	ALIAS	DESCRIPTION	TYPE	LENGTH
UNIT_1M	UNIT_1M	1 million-scale map unit	TEXT	25
LABEL_1M	Map_label_1M	Code for 1M label using gscGeology font	TEXT	12
UNIT_250K	UNIT_250K	1:250 000-scale map unit	TEXT	25
LABEL_250k	Map_label_250k	Code for 250k label using gscGeology font	TEXT	12
UNIT_ORIG	UNIT_ORIGINAL	Original map unit – at scale of capture (from published map)	TEXT	25
ASSEMBLAGE	ASSEMBLAGE	Tectonic assemblage (may include various stratigraphic units)	TEXT	50
SUPERGROUP	SUPERGROUP	Supergroup	TEXT	50
GP_SUITE	GP_SUITE	Group (stratigraphic); Suite (plutonic, metamorphic); Complex; Assemblage	TEXT	50
FORMATION	FORMATION	Formation (stratigraphic) and equivalents	TEXT	50
MEMBER	MEMBER	Member (stratigraphic) and equivalents	TEXT	50
NAME	NAME	Name of geological features such as plutons and batholiths	TEXT	50
TERRANE	TERRANE	Terrane	TEXT	50
TERR_LABEL	TERRANE_LABEL	Short label for terrane (*e.g.* YT, AX, SM…)	TEXT	10
TECT_ELEM	TECTONIC_ELEMENT	Tectonic element (*e.g.* Selwyn basin, Whitehorse trough)	TEXT	50
ERA_MAX	ERA_MAX	Maximum age – Era (timescale)	TEXT	50
PERIOD_MAX	PERIOD_MAX	Maximum age – Period/System (timescale)	TEXT	50
EPOCH_MAX	EPOCH_MAX	Maximum age – Epoch/Series (timescale)	TEXT	50
STAGE_MAX	STAGE_MAX	Maximum age – Stage/Age (timescale)	TEXT	50
AGE_MAX_MA	AGE_MAX_MA	Maximum age – numerical (in m.y.); derived from IUGS timescale for stratigraphic units OR from geochronological constraints for igneous rocks (date + error)	NUMBER	FLOAT
ERA_MIN	ERA_MIN	Minimum age – Era (timescale)	TEXT	50
PERIOD_ MIN	PERIOD_ MIN	Minimum age – Period/System (timescale)	TEXT	50
EPOCH_ MIN	EPOCH_ MIN	Minimum age – Epoch/Series (timescale)	TEXT	50
STAGE_ MIN	STAGE_ MIN	Minimum age – Stage/Age (timescale)	TEXT	50
AGE_ MIN_MA	AGE_ MIN_MA	Minimum age – numerical (in m.y.); derived from IUGS timescale for stratigraphic units OR from geochronological constraints for igneous rocks (date - error)	NUMBER	FLOAT
ROCK_CLASS	ROCK_CLASS	Rock classification – sedimentary, metamorphic, plutonic, volcanic	TEXT	50
ROCK_SUBCL	ROCK_SUBCLASS	Rock subclassification – clastic, carbonate, chert…; Prefix – 'm' = metamorphic, v = volcanic, p = plutonic; Suffix – for igneous rocks: 'mafic', 'inter' = intermediate, 'felsic', 'ultram' = ultramafic	TEXT	50
SHORT_DESC	SHORT_DESCRIPTION	Short unit description	TEXT	254
ROCK_MAJOR	ROCK_MAJOR	Major lithology(ies) within map unit	TEXT	100
ROCK_MINOR	ROCK_MINOR	Minor lithology(ies) within map unit	TEXT	100
ROCK_NOTES	ROCK_NOTES	Comment(s) for rock type	TEXT	254
COMMENTS	COMMENTS	Other comments	TEXT	250
RED	RED	Red value for unit RGB colour	NUMBER	Short Integer
GREEN	GREEN	Green value for unit RGB colour	NUMBER	Short Integer
BLUE	BLUE	Blue value for unit RGB colour	NUMBER	Short Integer

Appendix 1 continued.

Yukon bedrock geology – fault and contact attributes

FIELD NAME	ALIAS	DESCRIPTION	TYPE	LENGTH
FEATURE	FEATURE	Fault, contact (*needed for query from merge line set)*	TEXT	25
TYPE	TYPE	Type of fault – thrust, normal, strike slip, unknown; or contact – stratigraphic, intrusive	TEXT	30
SUBTYPE	SUBTYPE	Fault – Dextral, sinistral, upright, overturned, unknown Contact – Unconformity, facies change, gradational… BLANK = Conformable	TEXT	30
CONFIDENCE	CONFIDENCE	Reliability – defined, approximate, inferred, covered	TEXT	15
NAME	NAME	Name of fault *(ignore for contacts)*	TEXT	50
REFERENCE	REFERENCE	Source (publication)	TEXT	254
SCALE	SCALE	Minimum scale for display (x 1000) – 1000, 250, 50…	NUMBER	INTEGER
SYM_DIR	SYM_DIR	Direction of symbols for faults (*e.g.* NE, SW, *etc*…)	TEXT	10
COMMENTS	COMMENTS	Comments	TEXT	250

Appendix 2

Projection information for YGS datasets:

Projection ALBERS
Datum NAD83
Zunits NO
Units METRES
Spheroid GRS1980
Xshift 0.0000000000
Yshift 0.0000000000

Parameters

61° 40’ 0.000” – 1st standard parallel
68° 00’ 0.000” – 2nd standard parallel
-132° 30’ 0.000” – central meridian
59° 00’ 0.000” – latitude of projection’s origin
500000.00000 – false easting (metres)
500000.00000 – false northing (metres)

Updated bedrock geology of the southern Nash Creek area in central Yukon (parts of NTS 106D/2, 3, 6 and 7)

Diane Skipton
Yukon Geological Survey

Skipton, D., 2022. Updated bedrock geology of the southern Nash Creek area in central Yukon (parts of NTS 106D/2, 3, 6 and 7). *In:* Yukon Exploration and Geology 2021, K.E. MacFarlane (ed.), Yukon Geological Survey, p. 161–183.

Abstract

The southern Nash Creek area is located along the northern boundary of the Selwyn basin, and is underlain mainly by the Ediacaran–Cambrian Hyland Group, the Devonian–Mississippian Earn Group and the Mississippian Tsichu Group. Several Au and polymetallic mineral deposits are hosted by the Hyland Group and Paleozoic platformal carbonate rocks in the surrounding region. The southern Nash Creek area is bordered by regional-scale, southeast-striking thrust faults, which include the Dawson thrust to the northeast and the Robert Service thrust to the southwest. Based on stratigraphic relationships identified during 1:50 000-scale bedrock mapping, Hyland Group rocks in the area are considered to belong to the Cryogenian–Ediacaran Yusezyu Formation, the Ediacaran Algae Formation and the Ediacaran–Terreneuvian Narchilla Formation. Earn Group rocks include mainly shale and lesser amounts of interbedded dolostone, sandstone and shale. Tsichu Group rocks mostly comprise quartzite. The Yusezyu and Narchilla formations host (Paleozoic?) gabbro sills, and the Earn and Tsichu groups host gabbro sills that are considered to belong to the Triassic Galena suite. Rocks in the southern Nash Creek area exhibit a northeast-to-southwest-dipping foliation that is axial planar to southeast-trending folds.

* Diane.Skipton@yukon.ca

Introduction

This article presents the results of 1:50 000-scale bedrock mapping conducted in 2019 and 2021 in the southern Nash Creek area of central Yukon, which includes parts of NTS sheets 106D/2, 3, 6 and 7. The southern Nash Creek area is located along the northern boundary of the Selwyn basin (Gordey and Anderson, 1993), where the Neoproterozoic–Cambrian Hyland Group is juxtaposed against Paleozoic slope and shelf rocks of the Ogilvie Platform along the Dawson thrust zone (Figs. 1 and 2; Green, 1972a,b; Colpron et *al.*, 2013). The surrounding region hosts several mineral deposits (Fig. 2), including carbonate-hosted intrusion-related Au-Ag (Tiger), epithermal Au-Ag-Cu (McKay Hill), manto Ag-Pb-Zn (Clark), plutonic-related Au (Dublin Gulch), vein polymetallic Ag (Keno) and volcanogenic massive sulphide Cu-Pb-Zn (Marg).

The region was initially mapped at 1:250 000-scale by the Geological Survey of Canada as part of a regional mapping project that included the Nash Creek, Larsen Creek and Dawson areas (Green, 1972a,b). Several 1:50 000 and 1:75 000-scale mapping projects have improved our understanding of regional stratigraphic and structural relationships across the Dawson

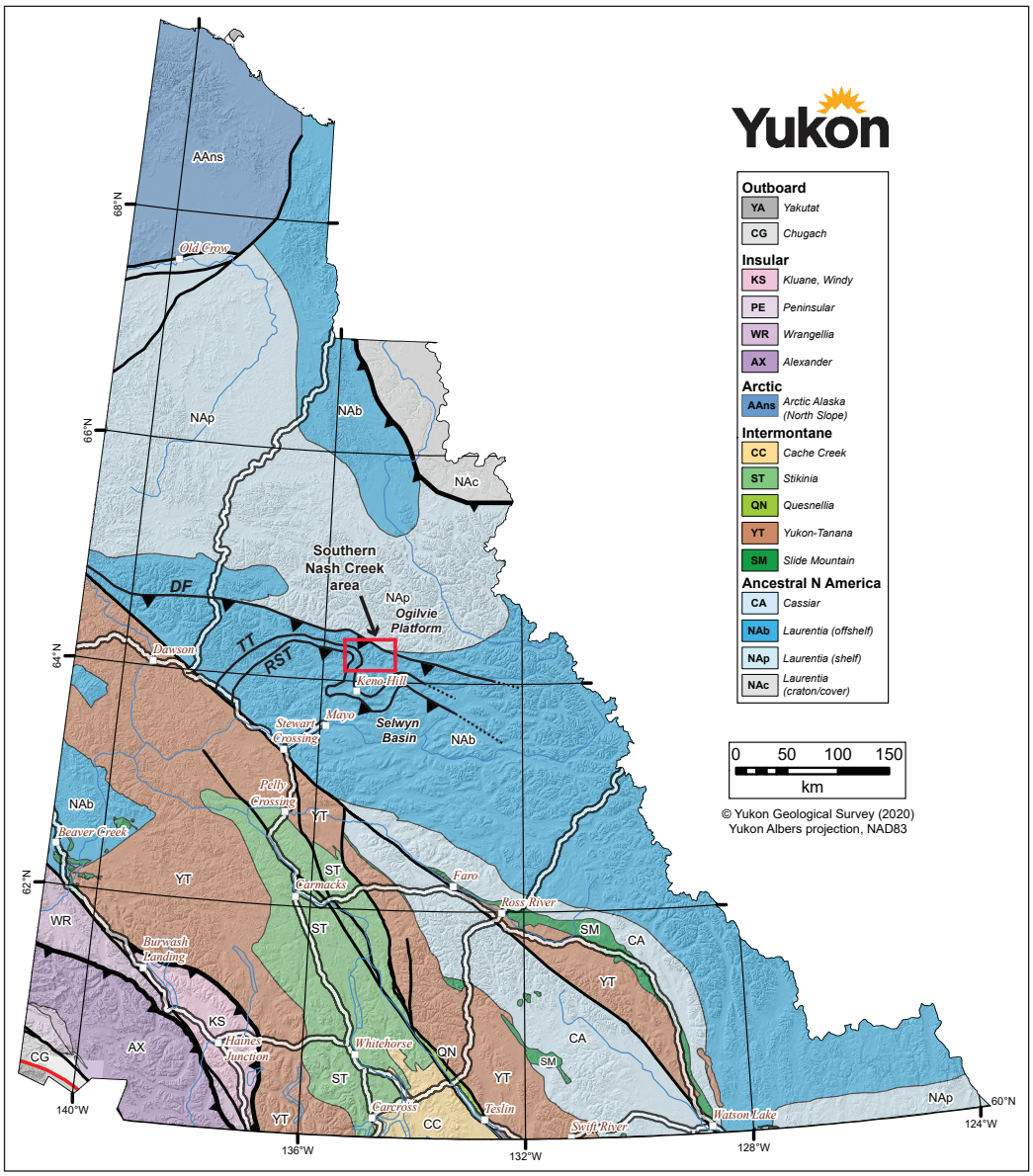


Figure 1. *Map of the geological terranes that comprise the northern Cordillera (modified after Yukon Geological Survey, 2021b). The study area (southern Nash Creek) is located in central Yukon, and outlined in red. DF = Dawson fault; TT = Tombstone thrust; RST = Robert Service thrust.*

thrust zone in the Ogilvie and Wernecke mountains (Abbott, 1990a,b, 1997a,b,c; Colpron *et al.*, 2013; Moynihan, 2014, 2016a) and across the Tombstone and Robert Service thrust zones in the McQuesten River and Mayo areas (Murphy, 1997; Roots, 1997). However, the southern Nash Creek area has not seen upgraded bedrock mapping until this study, which involved detailed (1:50 000-scale) mapping to address outstanding questions regarding stratigraphy, structural history and mineral potential. The preliminary bedrock map (Fig. 3; Skipton, 2022) and stratigraphic–structural framework presented herein supersede those presented by Skipton and Maw (2021).

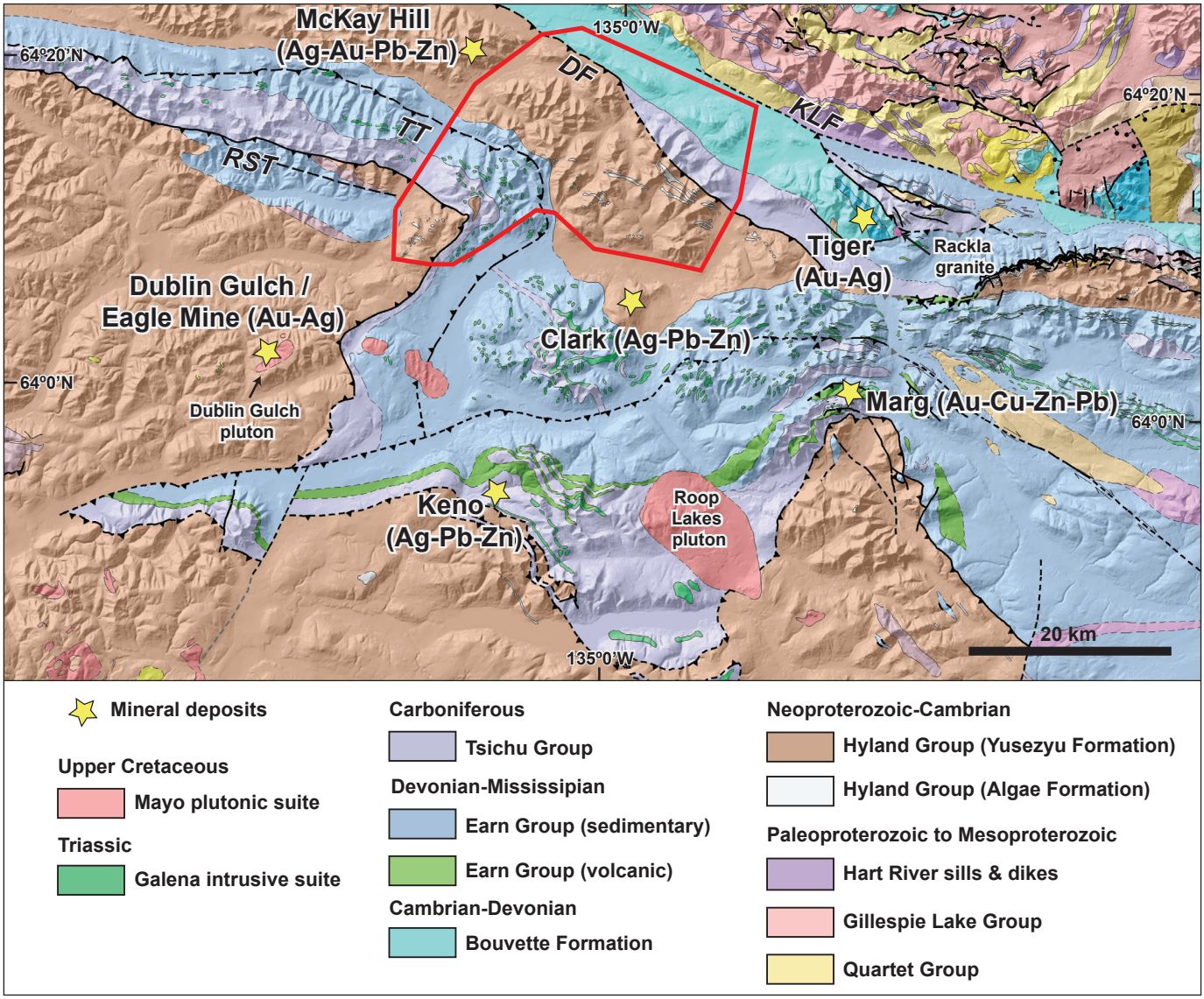


Figure 2. *Geological map of Paleoproterozoic to Carboniferous sedimentary rocks and younger plutons along the northern margin of the Selwyn basin in the region of the Keno, Tiger and McKay Hill mineral deposits (from the digital compilation map of Yukon; Yukon Geological Survey, 2021a). The area mapped in detail in 2019–2021 (this study) is outlined in red. DF = Dawson fault; TT = Tombstone thrust; RST = Robert Service thrust; KLF = Kathleen Lakes fault.*

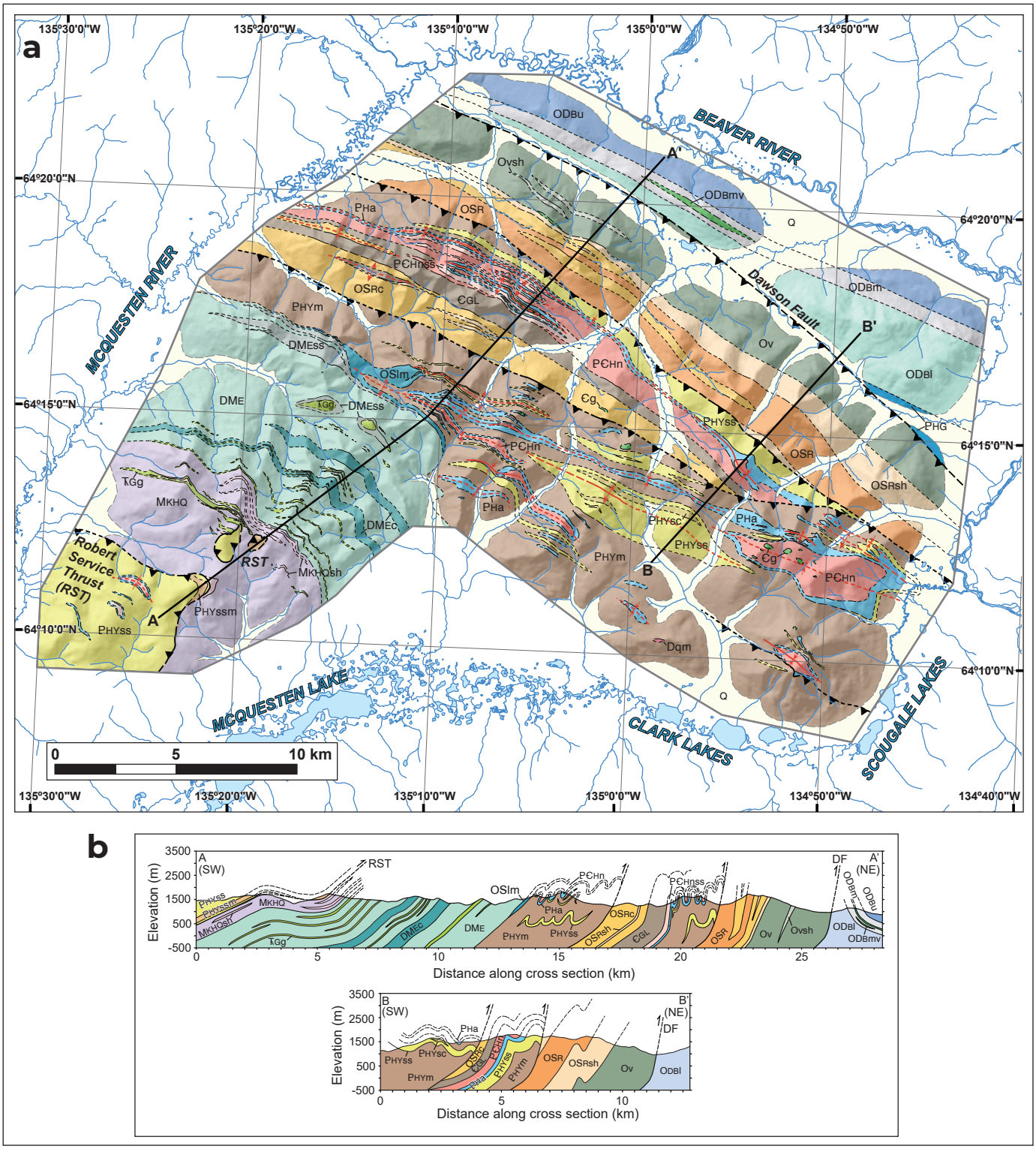


Figure 3. (a) *Preliminary geological map of the southern Nash Creek area (parts of NTS 106D/2, 3, 6, 7) based on 1:50 000-scale bedrock mapping conducted in 2019 and 2021 (simplified after Skipton (2022)). Map legend is provided in Figure 3c.* ***(b)*** *Cross sections corresponding to the preliminary geological map of the southern Nash Creek area shown in Figure 3a. Figure continued on next page.*

QUATERNARY

Q — **QUATERNARY:** unconsolidated alluvial, colluvial, fluvial and glacial deposits.

TRIASSIC

TGg — **GALENA SUITE, GABBRO:** Dark grey to dark green-weathered, dark green gabbro sills; medium-grained; locally fine-grained with plagioclase phenocrysts.

MISSISSIPPIAN

MKHQ — **TSICHU GROUP, KENO HILL QUARTZITE:** Medium to thick bedded grey quartz arenite; medium-grained, crystalline texture; local interbeds of buff to orange-weathered, medium-grained quartz-rich sandstone with dolomite cement; rare interbeds of dark grey shale.

MKHQsh — **TSICHU GROUP, KENO HILL QUARTZITE, shale member:** Dark grey shale; thinly interbedded to laminated; locally light to dark green weathered; locally rich in chlorite ± white mica (schistose); interstratified with Keno Hill Quartzite.

DEVONIAN TO MISSISSIPPIAN

DME — **EARN GROUP, undivided:** Dark grey shale; thinly bedded to laminated; local thin interbeds of grey-brown siltstone ranging to very fine grained sandstone.

DMEc — **EARN GROUP, carbonate member:** Rhythmically interbedded orange-weathered dolostone, white-weathered fine-grained sandstone and dark grey to dark green shale, with local chert interbeds; thinly bedded, locally medium bedded.

DMEss — **EARN GROUP, sandstone member:** Brown-weathered, fine-to-medium-grained, grey-brown quartz arenite; medium-bedded; shiny, sugary-textured fresh surface.

DEVONIAN(?)

Dqm — Medium-grained quartz monzonite with carbonate-quartz alteration.

ORDOVICIAN TO DEVONIAN (?)

ODBu — **BOUVETTE FORMATION, UPPER:** Pale grey to white-weathered, thick-bedded to massive dolostone; fine-to-medium-grained dolomitic sandstone and mudstone; lesser pebble conglomerate with dolostone, mudstone and rare limestone clasts; two-hole and star crinoids are common.

ODBmv — **BOUVETTE FORMATION, MIDDLE, volcanic member:** Dark green to brown weathered vesicular basalt; carbonate-cemented hyaloclastite breccia; volcanic sandstone, grit and pebble to cobble conglomerate.

ODBm — **BOUVETTE FORMATION, MIDDLE, undivided:** Thin to medium-bedded, grey and buff weathered silty limestone; massive, white limestone; grey to light grey bioclastic limestone; local interbedded pale yellow and grey limestone and dolostone.

ODBl — **BOUVETTE FORMATION, LOWER:** Light grey-weathered, massive to medium-bedded, variably dolomitized pale grey limestone, dolostone, oncolitic dolostone; light grey quartzite and sandy dolostone.

ORDOVICIAN TO SILURIAN (?)

OSlm — Fine-grained, medium-bedded, light grey-weathered, fetid grey limestone; commonly contains silica nodules; hosts non-abundant fossils; local pebble conglomerate with a grey limestone matrix.

ORDOVICIAN TO SILURIAN

OSR — **ROAD RIVER GROUP, undivided:** Thinly, rhythmically interbedded, grey-weathered, dark grey to black mudstone, grey siliceous siltstone and chert.

OSRsh — **ROAD RIVER GROUP, shale member:** Grey-green shale to phyllite; dark grey and black shale; minor maroon shale; local interbeds of black mudstone, siliceous siltstone ± chert.

OSRc — **ROAD RIVER GROUP, chert member:** Thin to medium-bedded, dark grey-weathered chert with rhythmic dark grey and light grey interbeds; locally white-weathered; locally massive.

ORDOVIAN (?)

Ov — Dark grey, dark brown and dark green mafic volcaniclastic rocks; lesser dark green amygdaloidal basalt and mafic tuff; minor reddish-brown-weathered intermediate volcaniclastic rocks.

Ovsh — Blue-grey to silver-weathered, dark grey to black shale; interstratified with volcaniclastic rocks (COv).

CAMBRIAN

ЄGL — **GULL LAKE FORMATION:** Thinly, rhythmically interbedded grey-brown to chocolate-brown-weathered siltstone and shale (~50/50%) with grey fresh surfaces; locally siltstone-rich (~70%) and medium-bedded.

CAMBRIAN(?)

Єg — Medium to coarse-grained, brownish-green, clinopyroxene gabbro sills and plugs; local melanocratic hornblende diorite.

NEOPROTEROZOIC (EDIACARAN) TO LOWER CAMBRIAN

PЄHn — **HYLAND GROUP, NARCHILLA FORMATION, undivided:** Dark grey, green and maroon shale; grey and green siltstone to phyllite; minor fine-grained, white, thinly bedded sandstone; rare medium-bedded, brown to grey quartz grit to quartz arenite.

PЄHnss — **HYLAND GROUP, NARCHILLA FORMATION, sandstone member:** Medium-bedded, brown to grey quartz quartz grit sandstone and lesser quartz arenite; local interbeds of dark grey, green and maroon shale and grey-green siltstone to phyllite.

NEOPROTEROZOIC (EDIACARAN)

PHa — **ALGAE FORMATION:** Grey, fine-grained, massive to medium-bedded limestone with local laminations; minor orange-weathered, medium-bedded dolostone.

PHYm — **HYLAND GROUP, YUSEZYU FORMATION, "MIXED" UNIT:** Green and grey siltstone to phyllite; dark grey, green and maroon shale; minor medium-bedded, brown to grey quartz arenite and quartz grit with local quartz-pebble conglomerate.

PHYss — **HYLAND GROUP, YUSEZYU FORMATION, SANDSTONE-DOMINATED UNIT, undivided:** Medium to thickly bedded, brown to grey quartz arenite and quartz grit sandstone with local quartz-pebble conglomerate; rare dark grey and green shale and siltstone to phyllite.

PHYsc — **HYLAND GROUP, YUSEZYU FORMATION, SANDSTONE-DOMINATED UNIT, calcareous member:** Medium to thick-bedded, orange-weathered quartz-rich sandstone with dolomitic cement; local interbeds of grey limestone, orange-weathered dolostone and green-grey shale.

PHYssm — **HYLAND GROUP, YUSEZYU FORMATION, SANDSTONE-DOMINATED UNIT, "mixed" member:** Thinly interbedded siliciclastic and calcareous rocks, including: grey-to-tan quartz grit sandstone; dark grey-green shale to phyllite; orange-weathered quartz grit sandstone with dolomite cement; grey limestone; orange-weathered dolostone.

PHG — **GAMETRAIL FORMATION:** Orange, yellow and grey-weathered dolostone, dolomitic siltstone/sandstone and limestone, commonly planar and or cross-laminated; carbonate-clast breccia and conglomerate; minor maroon shale.

SYMBOLS

Geological contact (defined, approximate, inferred)

Thrust fault (defined, approximate, inferred)

Anticline axial trace (defined, approximate, inferred)

Syncline axial trace (defined, approximate, inferred)

Limit of mapping (this study)

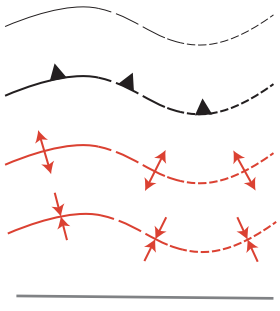


Figure 3 continued. ***(c)*** *Legend corresponding to the preliminary geological map and cross sections of the southern Nash Creek area presented in Figure 3a and 3b.*

Geological setting

The southern Nash Creek area mostly comprises sedimentary rocks that were deposited along the western Laurentian continental margin. These include clastic and carbonate rocks of the Neoproterozoic–Cambrian Hyland Group, which are unconformably overlain by the Devono-Mississippian Earn Group and the Carboniferous to Permian Tsichu Group (Fig. 2; Green, 1972a,b).

The study area forms part of the Selwyn fold belt, which trends NW–SE across central Yukon, and formed in response to Jura-Cretaceous shortening during the Cordilleran orogeny (Gordey and Anderson, 1993). Hyland Group strata have been juxtaposed over Ordovician–Devonian(?) platformal carbonate rocks (Bouvette Formation) across the Dawson thrust, which extends northwest-southeast across central Yukon (Figs. 1 and 2; Yukon Geological Survey, 2021a). Detailed mapping in the Rackla belt (Colpron *et al.*, 2013) has shown that the Dawson fault forms the frontal thrust in a series of imbricates that comprise the Dawson fault zone, which has a width of at least ~500 m and up to 2–4 km locally. Movement along the fault zone may have initiated in the Neoproterozoic, with reactivation in the Paleozoic and during Mesozoic (mid-Cretaceous?) shortening associated with Cordilleran orogenesis (*e.g.*, Abbott, 1997a; Colpron *et al.*, 2013).

The southern Nash Creek area includes several additional northwest–southeast-striking thrusts. Southwest of the Dawson fault, previous maps show that the Hyland Group has been juxtaposed over the Devonian–Mississippian Earn and Tsichu groups by the Robert Service thrust, and the Earn Group has been repeated by the Tombstone thrust (Figs. 1 and 2; Green and Roddick, 1962; Tempelman-Kluit, 1970; Thompson *et al.*, 1990; Anderson, 1987; Roots, 1988; Murphy, 1997). The Robert Service thrust is plugged by the Roop Lakes pluton (Fig. 2; 92.8 ± 0.5 Ma; Roots, 1997). In the Keno and Mayo areas, the hanging wall of the Tombstone thrust is affected by a several-km thick interval of intensely deformed, lower-to-middle-greenschist-facies metasedimentary rocks (Devonian Earn Group, Mississippian Keno Hill Quartzite), termed the Tombstone high-strain zone (Murphy, 1997). Muscovite from the hanging wall of the Robert Service thrust, which is considered to have been overprinted by the Tombstone high-strain zone, yielded $^{40}Ar/^{39}Ar$ dates of *ca.* 104–100 Ma, interpreted as the age of latest Tombstone thrust deformation (Mair *et al.*, 2006). The *ca.* 63–59 Ma crystallization age of the post-kinematic Rackla granite (Kingston *et al.*, 2010) at the Tiger Au deposit (Fig. 2) may represent a minimum age limit on regional deformation.

Stratigraphy

The southern Nash Creek area mainly consists of siliciclastic and carbonate rocks that occupy several southwest-dipping thrust panels (Figs. 3 and 4). Based on lithofacies mapping and comparisons with stratigraphic relationships in the broader Selwyn basin (*e.g.*, the eastern Wernecke Mountains, the Hyland River area, the Ogilvie Mountains, the McQuesten River and Mayo areas; Abbott, 1997a,b,c; Murphy, 1997; Roots, 1997; Colpron *et al.*, 2013; Moynihan, 2014, 2016b), most of the rocks are considered equivalent to the Cryogenian–Terreneuvian Hyland Group, the Cambrian Gull Lake Formation, the Ordovician–Silurian Road River Group, the Devonian–Mississippian Earn Group, and the Mississippian Tsichu Group. These stratigraphic correlations are preliminary, and may be refined following additional bedrock mapping and geochronology.

Ediacaran Hyland Group: Yusezyu, Algae, Narchilla and Gametrail formations (PHYm, PHYss, PHYsc, PHYssm, PHa, PЄHn, PЄHnss, PHG)

Ediacaran to Lower Cambrian strata of the Hyland Group are extensive in the study area, and predominantly include Cryogenian–Ediacaran sandstone and fine-grained siliciclastic rocks of the Yusezyu Formation. Based on lithofacies associations, the Yusezyu Formation has been divided into four units. The heterogeneous "mixed" unit (PHYm) consists of approximately equal proportions of green-grey siltstone and grey, green or maroon shale, with lesser amounts of medium-bedded brown-grey quartz grit sandstone (Fig. 5a), quartz arenite and rare quartz-pebble conglomerate. The sandstone-dominated unit

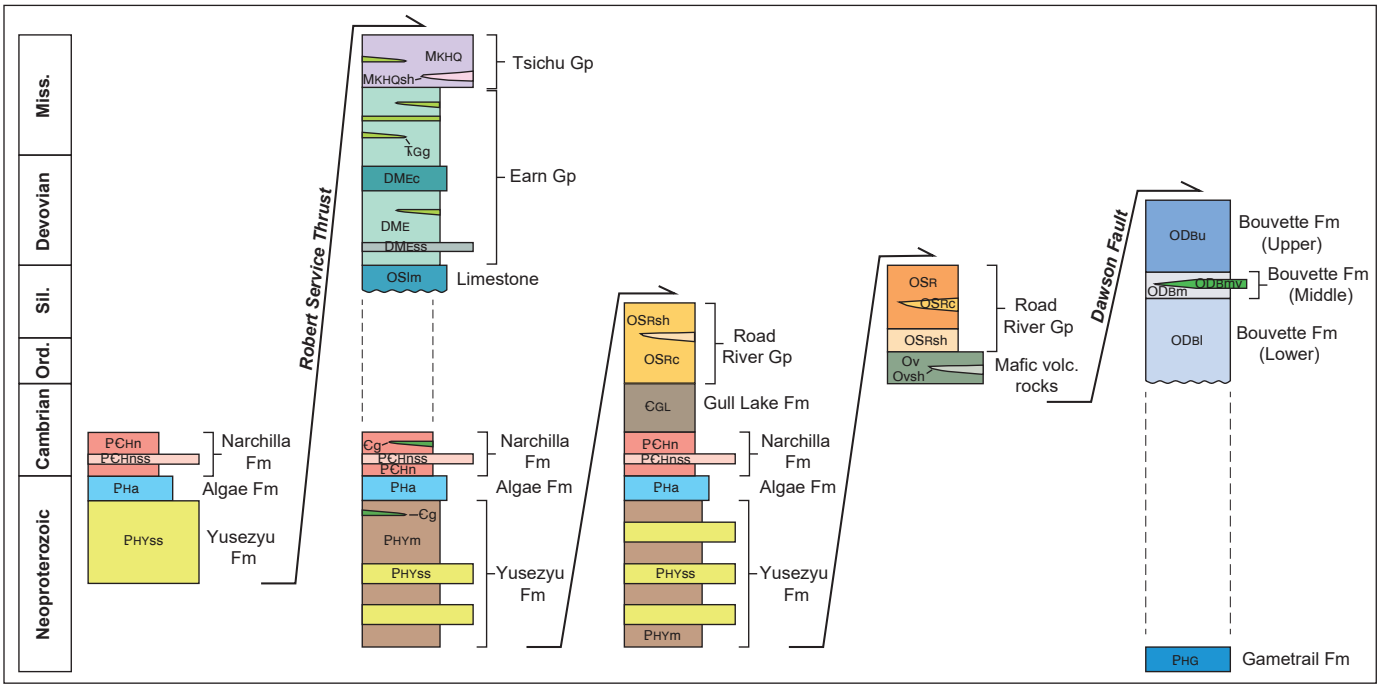


Figure 4. *Schematic diagram illustrating the preliminary stratigraphic framework and thrust relationships in the southern Nash Creek area.*

(PHYss) in the Yusezyu Formation includes medium to thick-bedded, brown-grey quartz arenite and quartz grit sandstone with local quartz-pebble conglomerate and rare interbeds of grey-green shale and siltstone. Field relationships suggest that the sandstone-dominated unit forms laterally discontinuous layers at different stratigraphic levels within the "mixed" unit, and may represent channel-fill deposits. In places, the sandstone-dominated unit contains calcareous rocks (calcareous member; PHYsc), including medium to thick-bedded, orange-weathered quartz-rich sandstone with dolomite cement and lesser interbeds of grey limestone, orange-weathered dolostone and green-grey shale. In the hanging wall of the Robert Service thrust, the sandstone-dominated unit of the Yusezyu Formation contains ~20–40 m-thick intervals of thinly interbedded siliciclastic and calcareous rocks ("mixed" member; PHYssm). These interbedded rocks include grey-to-tan-coloured quartz grit sandstone, dark green-grey siltstone to phyllite, orange-weathered quartz grit sandstone with dolomite cement, grey limestone and orange-weathered dolostone.

The Yusezyu Formation is overlain by fine-grained grey limestone of the Algae Formation (PHa) along a sharp contact. The limestone exhibits a light grey weathering colour that is distinctive from the overlying Narchilla and underlying Yusezyu formations, which have dark grey-brown weathering colours overall (Fig. 5c,e,f). The Algae Formation limestone is massive to medium bedded (Fig. 5c), laminated in places, and locally contains minor proportions of orange-weathered dolostone interbeds. The Algae Formation in the study area has an estimated observed thickness of ~30 to 50 m, although the thickness is poorly constrained in several places due to complex folding.

The Narchilla Formation (undivided; PCHn) overlies the Algae Formation along a sharp contact, and comprises fine-grained siliciclastic rocks, including dark grey, green and maroon shale and grey-green siltstone to phyllite (Fig. 5d). It contains lesser amounts of fine-grained white, thinly bedded sandstone, interbedded green-grey to white fine-grained sandstone and siltstone, and rare interbeds of brown-grey quartz grit to quartz arenite. The Narchilla Formation locally contains relatively thick sandstone-rich horizons (sandstone member; PCHnss), which dominantly comprise medium-bedded brown-grey quartz grit sandstone (Fig. 5b) and lesser quartz arenite.

Southwest of the Tiger Au deposit (Fig. 2), preliminary mapping by the author and others (S. Israel, R. Cobbett, pers. comm. 2021) has shown that the Bouvette Formation (discussed below) unconformably overlies the Gametrail Formation (PHG). The Bouvette and Gametrail formations are inferred to extend northwest along-strike in the Beaver River valley (Fig. 3). The Gametrail Formation is composed of mostly orange, yellow and grey-weathered dolostone that is typically planar or cross-laminated, as well as carbonate-clast breccia and conglomerate. Based on stratigraphic relationships defined in the eastern Rackla belt (Moynihan, 2014), the Gametrail Formation is considered to underlie the Yusezyu Formation.

Cambrian Gull Lake Formation (ЄGL)

The Gull Lake Formation (ЄGL) overlies the Narchilla Formation (PЄHn, PЄHnss) along a sharp contact (Fig. 6a). It consists of thinly, rhythmically interbedded light to dark grey weathering siltstone and dark grey to brown weathering shale (Fig. 6b). The fresh surfaces of shale beds are dark grey, and those of siltstone are

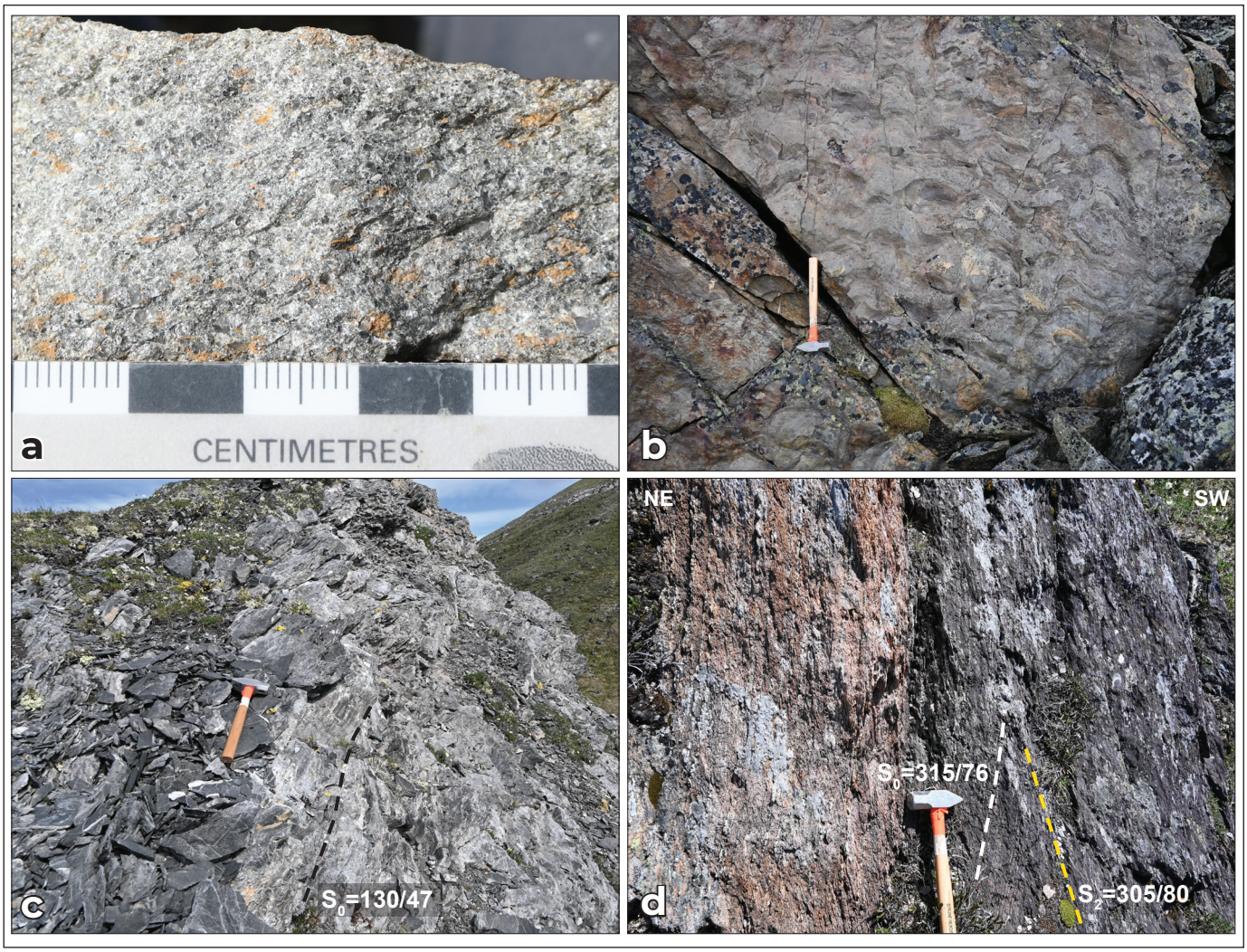


Figure 5. *Field photographs of the Ediacaran to Lower Cambrian Hyland Group. Planar structural orientations are indicated in right-hand-rule format here and throughout the manuscript.* **(a)** *Fresh surface of quartz grit sandstone (Yusezyu Formation, "mixed" unit,* PHYm). **(b)** *Ripple marks on the bedding plane of quartz grit sandstone (Narchilla Formation, sandstone member,* PЄHnss). **(c)** *Light to dark-grey weathered, thin to medium-bedded limestone with calcite veining (Algae Formation,* PHa). **(d)** *Thinly bedded beige siltstone (left) and dark grey to maroon shale (right), with a well-developed foliation (S_2) oriented at an angle to bedding (Narchilla Formation,* PЄHn). *Figure continued on next page.*

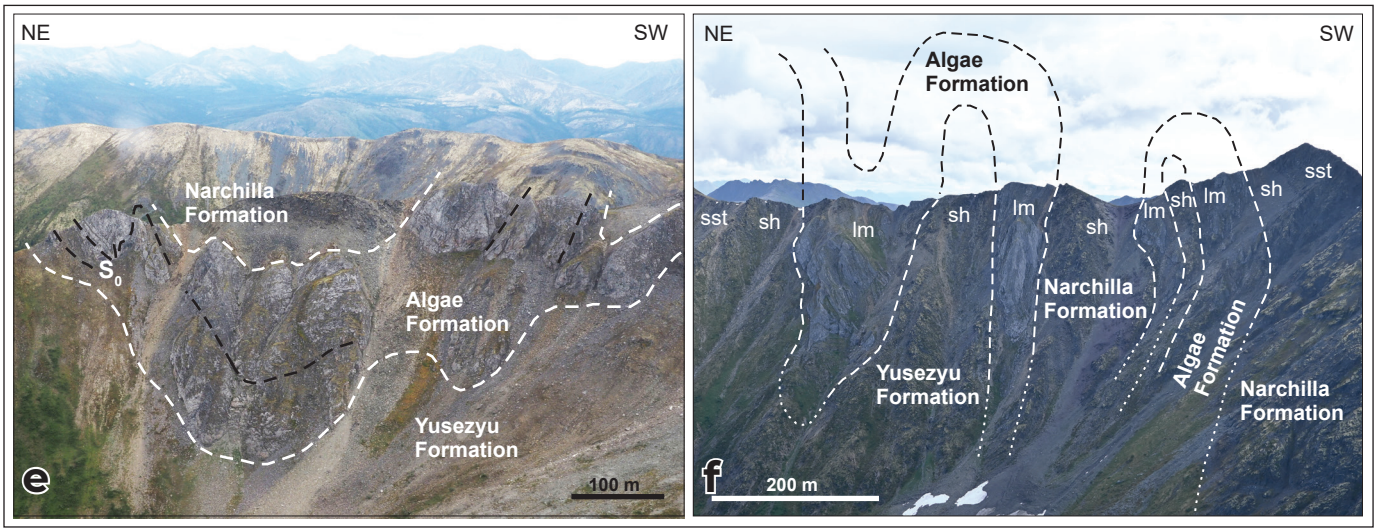


***Figure 5** continued.* ***(e)** F2-folded strata of the Yusezyu, Algae and Narchilla formations with a broadly synclinal geometry. Smaller folds occur within the limbs of the syncline, including a synclinal chevron fold in the northeastern limb (left side of photo). White dashed lines indicate geological contacts and black dashed lines delineate bedding.* ***(f)** Steeply dipping, isoclinally folded strata of the Yusezyu, Algae and Narchilla formations. Bedding orientations measured along the ridgetop range from ~80° NE to 80° SW. The rock types mapped along the ridgetop are indicated as follows: sh = grey, green and/or maroon shale and lesser grey siltstone; sst = grey to brown quartz arenite and/or quartz grit; lm = grey limestone. White lines represent geological contacts as mapped along the ridgetop (dashed pattern) or as inferred from remote observations (dotted pattern). Black dashed lines represent interpreted pre-erosional geological contacts.*

typically light grey. Shale beds weather recessively relative to the siltstone beds, giving the unit a ridged appearance in outcrops. The unit forms both ridgetops and saddles, but in both cases generally forms scree slopes, which exhibit a distinctive chocolate-brown colour from a distance (Fig. 6a). Siltstone and shale are typically in equal proportions, but the unit is locally siltstone-rich (up to ~70%).

Ordovician (?) volcanic rocks (Ov)

Volcanic rocks (Ov) crop out in the northeastern part of the map (Fig. 3). They consist of dark green and dark grey-brown-weathered volcaniclastic rocks and lesser amounts of mafic volcanic rocks, and are locally interstratified with silver-weathered shale with a black fresh surface (Ovsh). The volcaniclastic rocks comprise a fine-to-medium-grained mafic matrix that surrounds subrounded to angular pebble-to-cobble-sized clasts of mostly mafic-to-intermediate volcanic rocks (Fig. 6c). The matrix of some volcaniclastic rocks has an intermediate composition and weathers reddish-brown with a grey fresh surface (Fig. 6d). The volcanic sequence also includes fine-grained basalt and mafic volcanic breccia, some of which contain medium-to-coarse-grained phenocrysts of pyroxene, hornblende or plagioclase. Some volcanic rocks contain calcite-filled amygdules, and the volcanic sequence has been pervasively altered by calcite and chlorite.

The sequence of volcanic rocks (Ov) is overlain by the Road River Group (discussed below) along a sharp contact, and the lower limit of the volcanic sequence is inferred to be the Dawson fault (discussed below).

The volcanic rocks mapped here (Ov) are lithologically similar to and located along-strike from those exposed on McKay Hill to the northwest (Fig. 2), suggesting that they are part of the same volcanic sequence. The age of the volcanic rocks (Ov) is yet to be determined, but they are estimated to be younger than Middle Ordovician, based on preliminary identification of fossils from limestone interbedded with volcanic rocks in the McKay Hill area (R. Cobbett, pers. comm. 2021).

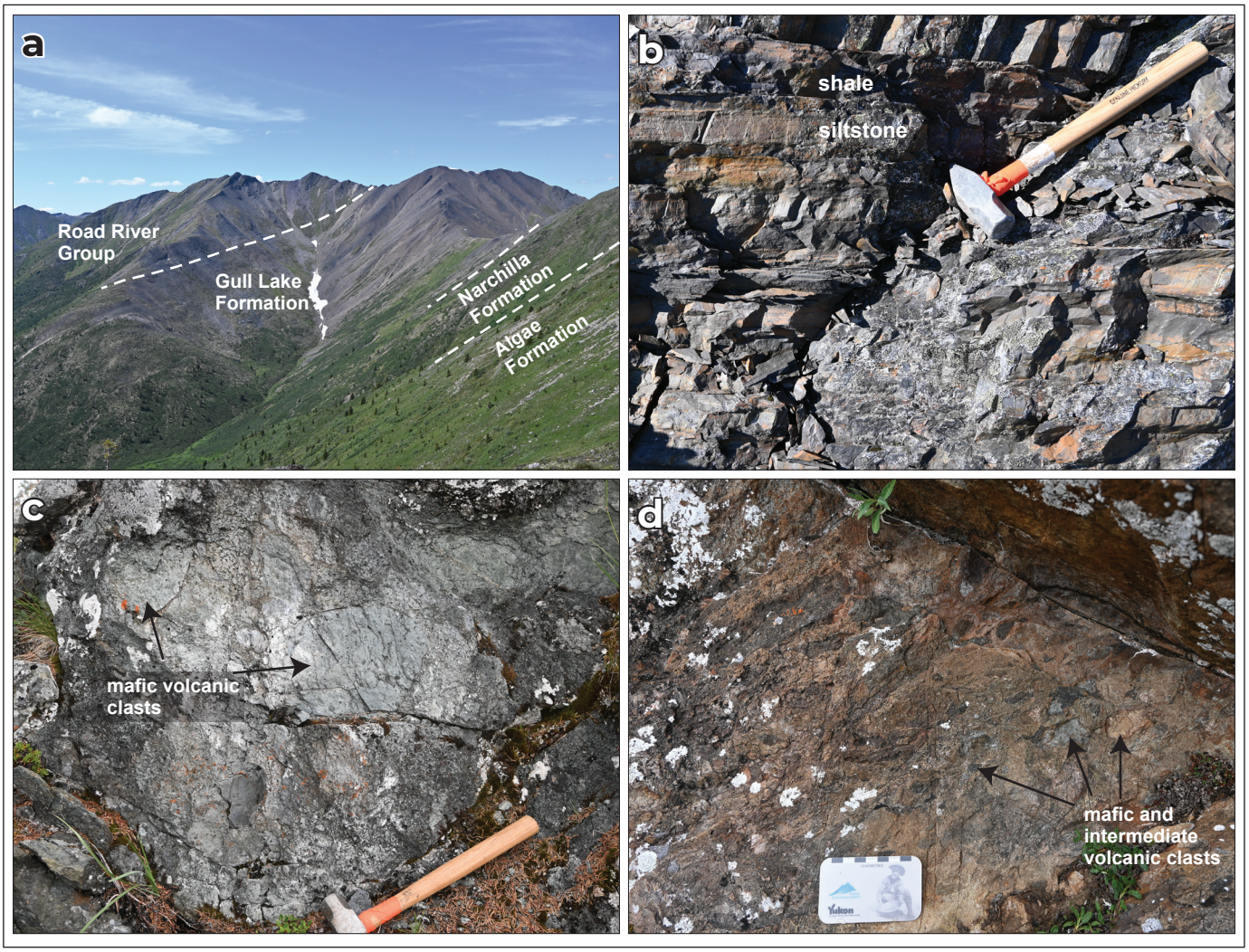


Figure 6. *Field photographs of the Cambrian Gull Lake Formation and Ordovician(?) volcaniclastic rocks.* ***(a)*** *Chocolate-brown-weathered scree slopes formed by the Gull Lake Formation (ЄGL), overlain by chert and shale of the Road River Group (OSRc, OSRsh) and underlain by siliciclastic and carbonate rocks of the Hyland Group. Horizontal field of view is ~2 km.* ***(b)*** *Thin, rhythmic interbeds of dark grey to brown-weathered siltstone and dark grey shale in the Gull Lake Formation.* ***(c)*** *Volcaniclastic rock comprising green-weathered clasts of hornblende-porphyritic mafic volcanic clasts in a green-grey-weathered sandy mafic matrix (Ov).* ***(d)*** *Volcaniclastic rock comprising black, light brown and light grey-weathered mafic and intermediate clasts in a reddish-brown-weathered intermediate matrix (Ov).*

Ordovician to Silurian Road River Group (OSR, OSRc, OSRsh)

The Road River Group is exposed in two southeast-striking bands across the northern third of the map area (Fig. 3). The undivided unit of the Road River Group (OSR) comprises thinly, rhythmically interbedded, grey-weathered mudstone with dark grey to black fresh surfaces, grey siliceous siltstone and chert (Fig. 7a,b). These rocks locally contain ~250–400 m-thick horizons of chert (chert member; OSRc), which is the dominant lithology in southwestern exposures of the Road River Group in the study area. The chert member of the Road River Group consists of thin-to-medium-bedded chert with rhythmic dark grey and light grey ~1–3 cm-thick interbeds (Fig. 7c,d). It generally exhibits a dark grey weathering colour (Fig. 7c), but is locally light grey to white-weathered. In places, the chert member is medium-to-thick-bedded and the beds are internally massive. The Road River Group (OSR, OSRc) locally contains ~100 m to ~1.5 km-thick interstratifications of shale (shale member; OSRsh), which includes grey-green shale to phyllite, dark grey to black shale, and local maroon shale.

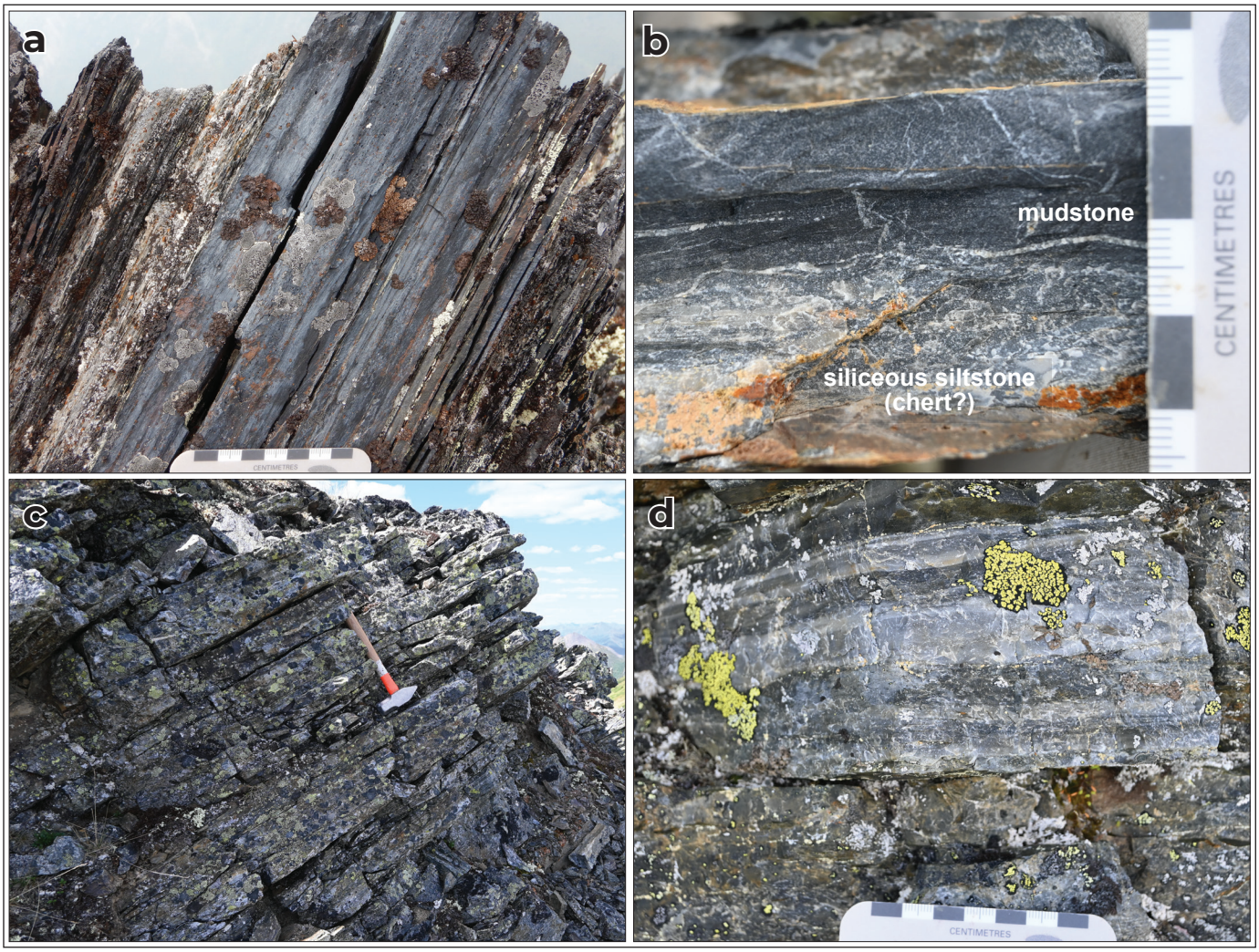


Figure 7. *Field photographs of the Ordovician to Silurian Road River Group.* ***(a)*** *Thinly bedded to laminated dark grey to light grey mudstone with minor light grey siltstone interbeds (OSR).* ***(b)*** *Thinly interbedded black mudstone and light grey siliceous siltstone (chert?; OSR).* ***(c)*** *Thin-to-medium-bedded, dark grey-weathered chert (OSRc).* ***(d)*** *Thin-to-medium-bedded chert with thin, rhythmic, dark and light grey interbeds (OSRc).*

Ordovician to Silurian (?) limestone (OSlm)

This unit (OSlm) is exposed in the west-central part of the map area. It consists of fine-grained, medium-bedded grey limestone, and is distinguished from the Algae Formation primarily on the presence of fossils (Fig. 8a,b). Fossils are not abundant and are generally poorly preserved, but preliminary fossil identifications of gastropods and brachiopods suggest a possible Late Ordovician to Silurian age for the limestone (R. Blodgett, pers. comm., 2021). Part of this limestone was initially mapped in the 1960s and interpreted as Permian based on fossil identifications, although it was noted that the fossils "are poorly preserved and the identifications are uncertain" (Green, 1972b). Unlike the Algae Formation, the fossiliferous limestone has a strong fetid odour and contains black silica nodules (Fig. 8a), white-weathered bedding-parallel bands of diagenetic silica (Fig. 8c) and local chert beds. In places, it also contains pebble-conglomerate beds up to ~0.5 m thick, which comprise a fine-grained grey limestone matrix surrounding quartz pebbles and dark grey chert clasts (Fig. 8d).

Where mapped, the limestone overlies sandstone, siltstone and shale ("mixed" unit; PHYm) of the Yusezyu Formation (Hyland Group). The contacts of the limestone are covered, and bedding orientations are concordant with those in underlying and overlying strata (the Hyland and Earn groups, respectively). The limestone appears to pinch out to the southeast and northwest, along the contact between the Hyland and Earn groups.

Ordovician to Devonian (?) Bouvette Formation (ODBl, ODBm, ODBmv, ODBu)

The Bouvette Formation consists of carbonate platformal rocks and forms limited exposures in the Beaver River valley in the northeastern part of the map area (Fig. 3). These exposures consist of light grey weathered limestone with a fine-to-medium-grained crystalline fresh surface. The limestone contains abundant quartz and(or) carbonate veins, and has a weak reaction to 10% hydrochloric acid, consistent with pervasive dolomitization. Based on lithological similarities and stratigraphic relationships in the Bouvette Formation along-strike to the east (e.g., Tiger deposit area; Fig. 2; Abbott, 1990a; Colpron *et al.*, 2013; Yukon Geological Survey, 2021a) and northwest (Castle Mountain area; Cobbett, 2020, 2022), the limestone encountered in this study in the Beaver River valley is inferred to be the lower Bouvette Formation of Cobbett (2022; ODBl).

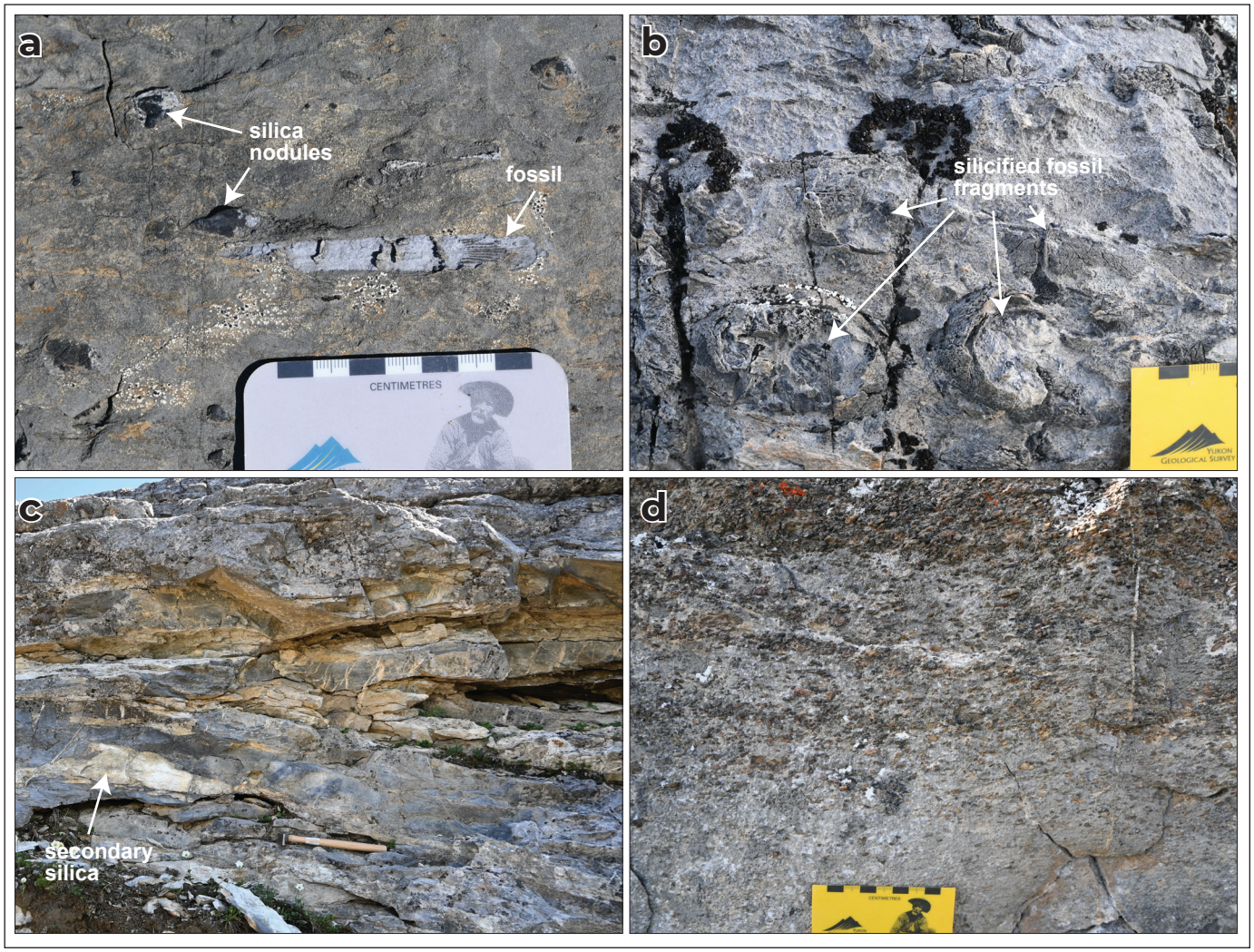


Figure 8. *Field photographs of fossiliferous limestone of estimated Ordovician-Silurian age (OSlm).* ***(a)*** *Grey limestone containing black chert nodules and a partial coral fossil.* ***(b)*** *Light grey limestone containing silicified fossil fragments.* ***(c)*** *Medium-bedded, fine-grained grey limestone with white-weathered, discontinuous, bedding-parallel bands of silica alteration.* ***(d)*** *Pebble-conglomerate interbed, comprising mostly quartz pebbles and chert clasts in a fine-grained, light grey limestone matrix.*

Mafic volcanic rocks (ODBmv) occur in isolated hilltop outcrops in the Beaver River valley (Fig. 3) and comprise fine-grained mafic volcanic breccia with hornblende phenocrysts. Although their contacts are unconstrained, the location of these rocks suggests that they represent a volcanic interval within the Bouvette Formation, perhaps equivalent to similar mafic volcanic rocks in the middle Bouvette Formation near the Tiger deposit (Abbott, 1990a; Colpron *et al.*, 2013; Yukon Geological Survey, 2021a), at Castle Mountain (Cobbett, 2020, 2022), and in the southern Wernecke Mountains (Ambrose and Bowie, 2020).

The middle (ODBm) and upper (ODBu) parts of the Bouvette Formation (*e.g.*, Cobbett, 2022) were not encountered during mapping, but are inferred to lie in the Beaver River valley (Fig. 3), based on along-strike stratigraphic relationships in the Tiger and Castle Mountain areas (Cobbett, 2022). In those areas, the upper Bouvette Formation mainly consists of grey to buff-weathered limestone and dolostone, and contains abundant two-hole and star-shaped crinoids, coral and bivalve fossils (*e.g.*, Colpron *et al.*, 2013; Cobbett, 2020, 2022).

Devonian to Mississippian Earn Group (DME, DMEss, DMEc)

The Devonian to Mississippian Earn Group occurs in the southwestern part of the map area, overlying the fossiliferous limestone (OSlm) along an inferred stratigraphic contact (pending fossil identification and age interpretation of the limestone; discussed above). The unconformity between the Earn and Hyland groups was not encountered during mapping in the study area, but has been documented on previous regional maps (*e.g.*, Green, 1972a).

The Earn Group (undivided; DME) mostly consists of homogeneous, dark grey, thinly interbedded to laminated shale (Fig. 9a). It locally contains minor amounts (<10%) of thin-to-medium-sized grey-brown siltstone interbeds, which range in grain size to very fine grained sandstone. A ~1–2 m-thick bed of medium-grained, white-weathered, beige quartz arenite was observed at one locality. Neither chert nor chert-pebble conglomerate were observed, in contrast to the Earn Group in the surrounding region (*e.g.*, Tiger area and Rackla belt; Abbott, 1990a; Colpron *et al.*, 2013).

Thick (~200–500 m) intervals of fine-to-medium-grained quartz arenite (sandstone member; DMEss) occur within the lower part of the Earn Group shale (DME). The sandstone is medium-bedded, grey-brown weathered and exhibits a grey-brown fresh surface with a shiny, sugary texture. Based on its apparent stratigraphic level and the occurrence of interbeds of similar sandstone within Earn Group shale (DME), the sandstone member may represent discrete sandstone deposits in the Earn Group.

Farther south, near the middle of the Earn Group sequence exposed in the map area, there are two ~350 m-thick intervals of rhythmically interbedded dolostone, sandstone, dark grey-green shale and minor chert (carbonate member; DMEc). This unit is thin-to-medium-bedded and has a distinctive, orange-and-white striped appearance (Fig. 9a,b). Dolostone beds are orange-weathered and have a grey fresh surface with a medium-grained crystalline texture. Sandstone beds are very fine grained, and white-weathered with a grey fresh surface. This unit has gradational stratigraphic contacts with underlying and overlying Earn Group shale.

Mississippian Tsichu Group: Keno Hill Quartzite (MKQH, MKHQsh)

The Mississippian Keno Hill Quartzite (MKHQ) occurs in the southwestern part of the map area, above the Earn Group (Fig. 3). It comprises homogeneous, medium-to-thick-bedded, medium-grained quartz arenite with a light to dark grey weathered surface (Fig. 9c). Beds are internally massive and exhibit a light grey fresh surface with an equigranular crystalline texture (Fig. 9d). Locally, the sandstone contains minor (<5%) clasts of dark grey fine-grained shale or chert (Fig. 9d). In many places, it includes minor (<2%) interbeds of orange-weathered, medium-grained quartz-rich sandstone with dolomite cement. The Keno Hill Quartzite tends to form prominent ridges and talus piles, which exhibit a distinctive, steel-grey weathering colour from a distance (Fig. 10c). Dark grey shale (MKHQsh) forms ~30–70 m-thick intervals that are interstratified with the quartzite. The shale is locally green-weathered and rich in chlorite ± white mica (phyllitic).

Intrusive rocks

Cambrian (?) gabbro (Ꞓg)

Gabbro intrusions (Ꞓg) were emplaced into siltstone and shale of the Narchilla and upper Yusezyu formations, forming discontinuous sills and plugs with maximum dimensions estimated to be ~150 m at the bedrock surface. Gabbro is medium-grained, locally foliated, and has been extensively replaced by greenschist-facies minerals (chlorite, actinolite, epidote) and carbonate alteration (see Fig. 7 in Skipton and Maw (2021)). Igneous textures have been preserved locally, and relics of igneous clinopyroxene crystals are visible in thin section. In places, igneous hornblende occurs instead of clinopyroxene, indicating that the intrusions have a compositional range from gabbro to melanocratic hornblende diorite. As the intrusions are hosted by the Narchilla Formation, they are inferred to be Terreneuvian or younger. Whole-rock geochemical compositions suggest that the gabbro and hornblende

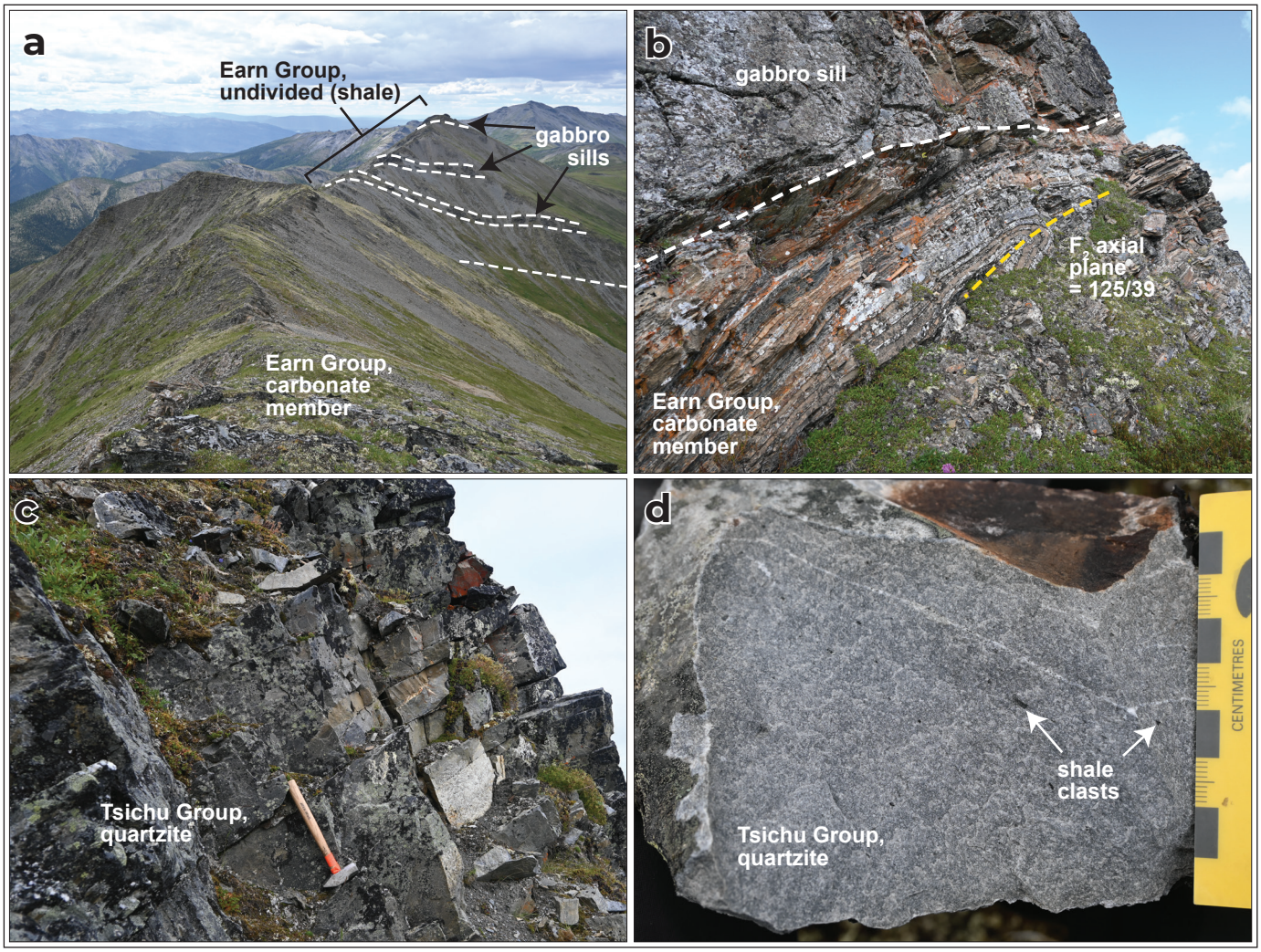


Figure 9. *Field photographs of the Devonian-Mississippian Earn Group, the Mississippian Tsichu Group and Triassic gabbro sills (Galena suite). White dashed lines indicate geological contacts.* ***(a)*** *Rhythmically interbedded carbonate, sandstone and dark grey shale in the Earn Group (carbonate member,* DMEc*) in the foreground of the photo, overlain by dark grey shale of the Earn Group (*DME*), which hosts several gabbro sills (Galena suite,* ŦGg*). Horizontal field of view is ~1 km.* ***(b)*** *Isoclinally folded (F2), rhythmically interbedded orange-weathered carbonate, white-weathered sandstone (± chert) and dark grey shale of the Earn Group (carbonate member,* DMEc*), hosting a gabbro sill (Galena suite). Photo was taken looking towards the northwest.* ***(c)*** *Medium-bedded, dark grey-weathered quartzite in the Tsichu Group (Keno Hill Quartzite,* MKHQ*).* ***(d)*** *Light grey fresh surface of quartzite in the Tsichu Group (*MKHQ*). Figure continued on next page.*

diorite intrusions have alkali basaltic compositions that are transitional between those of typical oceanic island basalt and enriched mid-ocean ridge basalt (Skipton and Maw, 2021). Preliminary geochemical comparisons with Cambrian and younger mafic to intermediate rocks in the region suggest that the gabbro and diorite intrusions are distinct from the Triassic Galena suite sills (Skipton and Maw, 2021). Instead, they may share affinity with Paleozoic sills, dikes and volcanic rocks (Dempster volcanics), such as those in the Upper Hart River area (Abbott, 1997c).

Devonian(?) quartz monzonite (Dqm)

Foliated quartz monzonite (Dqm) occurs in the southern part of the map area, hosted in siltstone of the Yusezyu Formation mixed unit. The quartz monzonite has a pitted, orange-brown weathered surface and a green-grey fresh surface. It consists of medium to coarse-grained K-feldspar, plagioclase feldspar and minor quartz. It has undergone pervasive carbonate, quartz and sericite alteration and hosts abundant carbonate (± quartz) veins (see Fig. 7 in Skipton and Maw (2021)). The intrusion's extent is poorly defined, mainly owing to poor outcrop exposure. The age of the intrusion is unknown, but it may share affinity with felsic rocks in the surrounding region (Fig. 2), such as the Rackla granite (*ca.* 63–59 Ma; Kingston *et al.*, 2010), Dublin Gulch pluton (*ca.* 93.5–92.8 Ma; Murphy, 1997), or *ca.* 380–378 Ma felsic volcanic rocks in the Earn Group (Murphy, 1997).

Triassic Galena suite: gabbro sills (ŦGg)

Gabbro sills of the Triassic Galena suite (ŦGg) are emplaced in the Devonian–Mississippian Earn Group (Fig. 9a,b) and the Mississippian Tsichu Group in the southwestern part of the map area (Fig. 3). The sills form prominent 'ribs' of outcrop that stand out from recessively-weathered Earn Group host rocks, including shale (DME; Fig. 9a) and the carbonate member (DMEc; Fig. 9b). Where hosted in the Tsichu Group, the sills have a similar weathering habit and colour to the Keno Hill Quartzite (MKHQ), and anastomose within and between shale horizons (MKHQsh).

The gabbro sills mostly range from ~2 to 15 m in thickness, but are locally up to ~60 m thick. Gabbro sills are dark grey-weathered with a dark green fresh surface, and are generally medium-grained and equigranular (Fig. 9e). In places, particularly near intrusion margins, they are fine-grained and locally contain euhedral to subhedral, ~2–5 mm-sized plagioclase phenocrysts (Fig. 9f).

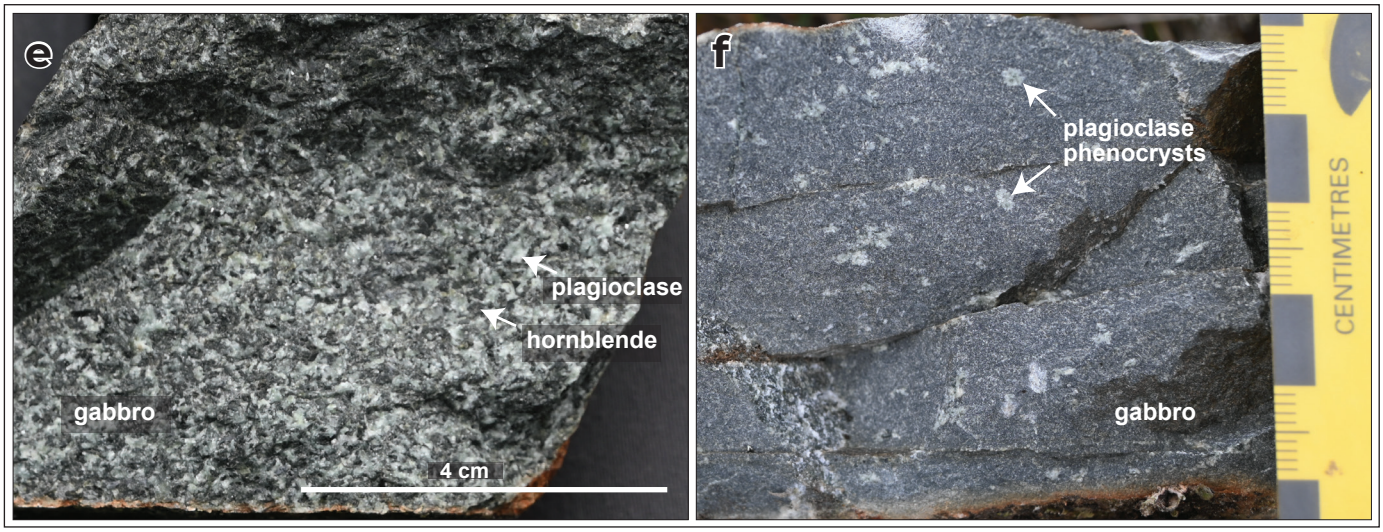


***Figure 9** continued.* ***(e)** Medium-grained gabbro (ŦGg) containing subhedral plagioclase and hornblende.* ***(f)** Fine-grained gabbro (ŦGg) with clusters of subhedral to euhedral plagioclase phenocrysts.*

Deformation

The mapped area records a complex compressional deformation history that produced a predominantly NW–SE-striking, SW-dipping structural architecture. The area includes at least five southeast-striking thrust sheets, from the hanging wall of the Robert Service thrust in the southwest to the footwall of the Dawson fault in the northeast (Figs. 3 and 4). Compression resulted in significant folding, crenulation lineations, and a regional lower-greenschist-facies foliation. For ease of discussion in this report, these folds and fabrics are grouped together within the same generation of deformation (D_2) throughout the mapped area.

Foliations (S_1 and S_2)

Two regional foliations were identified during mapping (S_1 and S_2). An early foliation (S_1) is defined by very fine grained white mica and chlorite aligned parallel to bedding in sedimentary rocks. Bedding and S_1 typically dip towards the southwest, but are northeast-dipping in places due to reorientation by subsequent folding (F_2, discussed below). The early, bedding-parallel foliation (S_1) may record burial during initial crustal thickening.

In fine-grained siliciclastic rocks, the S_2 foliation is defined by aligned fine-grained white mica (± chlorite), which commonly forms a crenulation cleavage. In carbonate rocks and sandstone, S_2 is less pervasive and typically presents as a spaced cleavage. In general, S_2 dips towards the southwest or northeast, and is oblique to bedding (and S_1) at angles up to 90° (Fig. 5d). S_2 is interpreted to have formed as an axial planar cleavage to F_2 folds (Fig. 10d), and the variable dip directions of S_2 are interpreted as the result of cleavage fanning and refraction in rocks of contrasting competencies. The S_2 foliation is parallel to S_1 in some F_2 fold limbs (described in detail in Skipton and Maw (2021)).

Folds (F_2)

F2 folds occur from the micro-scale to map-scale, have northwest–southeast-striking axial planes, and fold axes that plunge shallowly to moderately towards the northwest or southeast. F_2 crenulations have wavelengths as small as 0.25 mm, and form northwest or southeast-plunging crenulation lineations (L_2; see Fig. 10d in Skipton and Maw (2021)). At the outcrop-scale, F_2 folds generally have wavelengths of ~10–60 cm (Fig. 10b,d,f). Larger folds are common, with wavelengths ranging from tens of metres to ~3 km (Figs. 3b and 5e,f). F_2 folds form several different types: open (Figs. 5e and 10a) to isoclinal (Figs. 5f, 9b and 10d), symmetric and asymmetric (Fig. 10b,f), cylindrical and non-cylindrical, harmonic and disharmonic (Fig. 10f), upright (Fig. 5e,f) to inclined

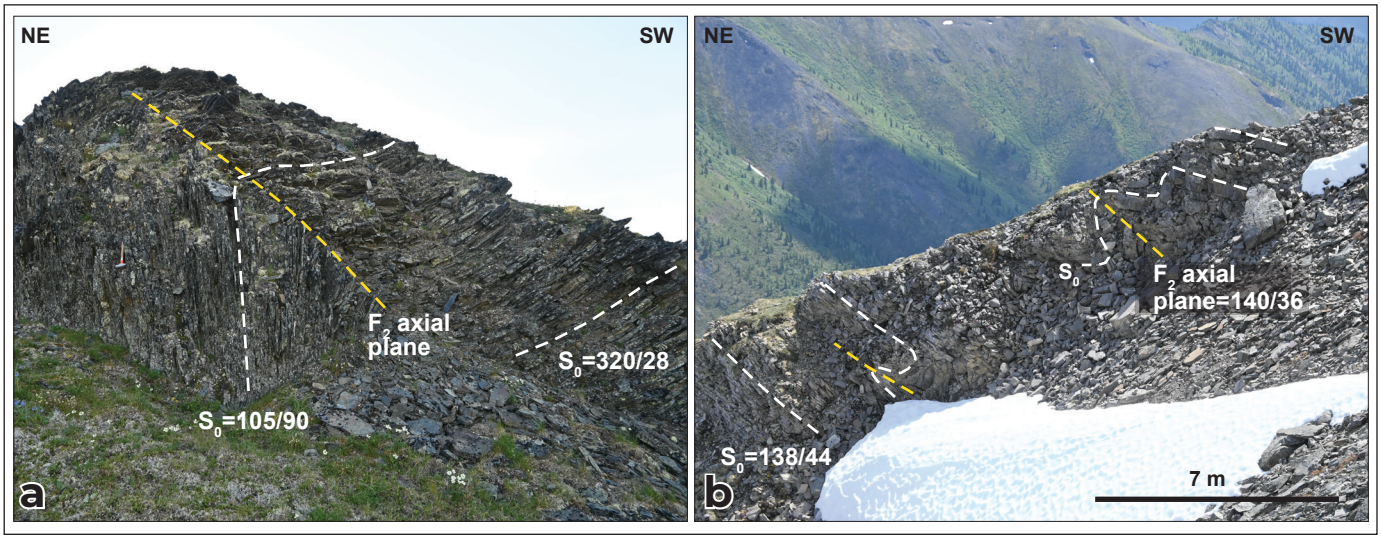


Figure 10. *Field photographs of deformation structures. Deformation fabrics are indicated by yellow dashed lines. Linear fabric orientations are indicated in plunge-trend notation here and throughout the manuscript.* ***(a)*** *Thinly interbedded black mudstone and chert (Road River Group, OSR) folded by an open southwest-dipping anticline;* ***(b)*** *Asymmetric, tight, southwest-dipping folds of limestone beds (Algae Formation, PHa), suggesting vergence towards the northeast.* *Figure continued on next page.*

(Fig. 10a,b,d,f), and chevron (Fig. 5e). The northeastern limbs of asymmetric F_2 folds are short and steeply-dipping (Fig. 10b,f), suggesting northeast vergence, consistent with the southwestern dip of F_2 axial planes.

In folded sequences of the Hyland Group, map-scale folds have preserved upper stratigraphic levels in synclinal keels (e.g., the Algae and Narchilla formations; Figs. 3 and 5e,f) and revealed lower stratigraphic levels in antiformal cores (e.g., Yusezyu Formation; Figs. 3 and 5f). In areas where fold closures are covered or have been eroded away, large-scale folds are interpreted from the repetition of stratigraphy, together with the presence of parasitic folds on the micro-to-outcrop-scale and the associated axial planar cleavage (S_2). Several units are discontinuous along-strike (Fig. 3a) as a result of non-cylindrical map-scale folds with northwest or southeast-plunging axes, in combination with lateral facies changes and topographic relief.

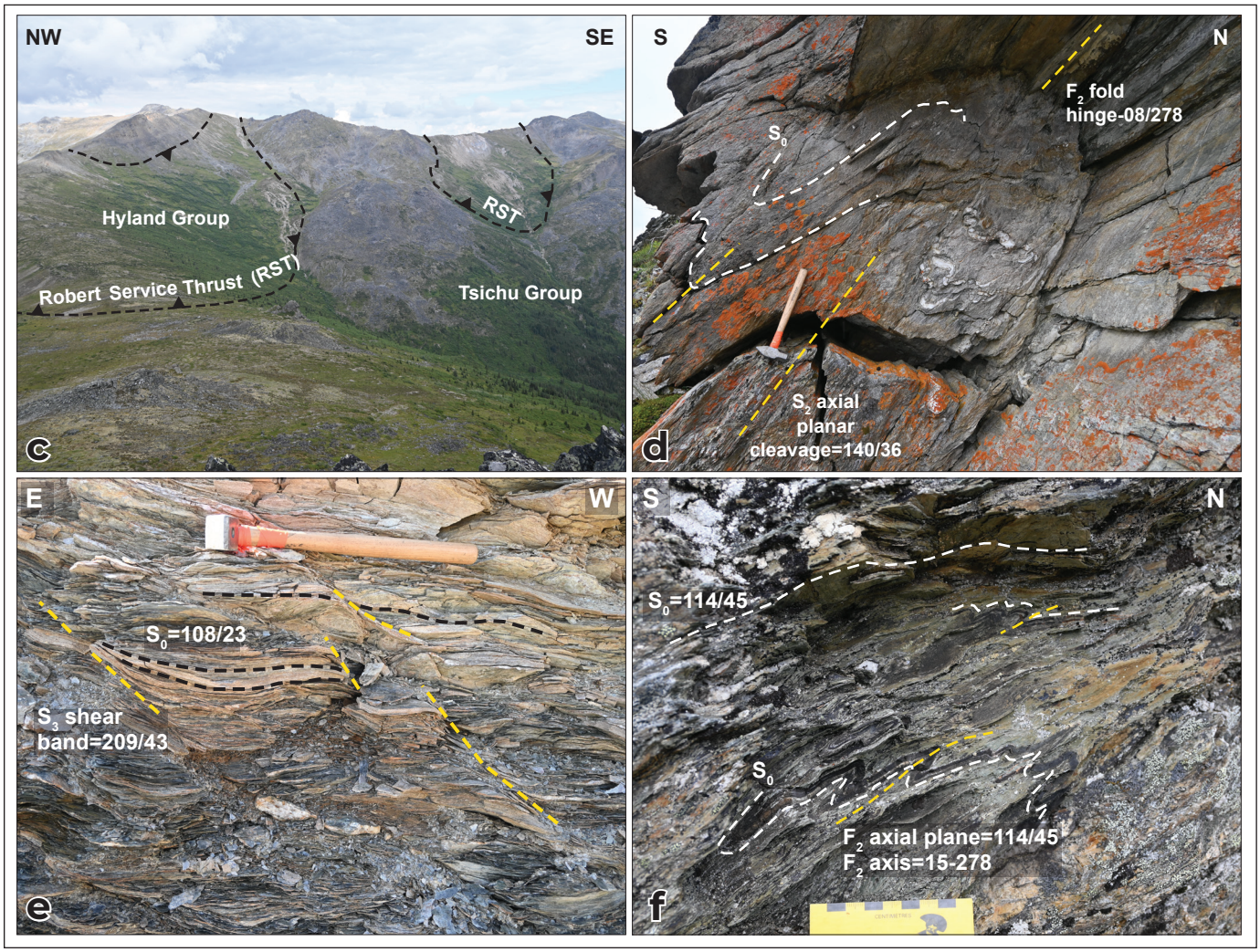


***Figure 10** continued.* ***(c)** Tan-weathered quartz grit sandstone and phyllite (Hyland Group, Yusezyu Formation,* PHYss, PHYssm*) in the hanging wall of Robert Service thrust klippen, juxtaposed over grey-weathered quartzite (Tsichu Group, Keno Hill Quartzite,* MKHQ*) in the footwall (horizontal field of view is ~1.7 km).* ***(d)** South-dipping isoclinal anticline in quartz grit sandstone (Hyland Group, Yusezyu Formation,* PHYss*) in the hanging wall of the Robert Service thrust, with numerous parasitic folds and well-developed axial planar cleavage.* ***(e)** Thinly interbedded dark green phyllite and orange-weathered dolostone and quartz grit with carbonate cement (Hyland Group, Yusezyu Formation,* PHYssm*) with west-dipping shear bands in the hanging wall of the Robert Service thrust zone.* ***(f)** Tight, disharmonic, asymmetric folds of bedding (and S_1) in interbedded dark grey mudstone and grey-green phyllite (Earn Group,* DME*) in the footwall of the Robert Service thrust. South-dipping axial planes and steep, short northern limbs indicate vergence towards the north.*

Thrusts

Robert Service thrust

Initially mapped by Green (1972a), the locations of the Robert Service thrust and klippen have been refined based on the detailed mapping conducted in this study (Figs. 3a and 10c). The Robert Service thrust juxtaposes Ediacaran–Lower Cambrian Hyland Group rocks over the Mississippian Keno Hill Quartzite (MKHQ). Bedding orientations and the presence of klippen indicate that the thrust surface dips shallowly to moderately toward the south-southwest overall, and has been folded by an open anticline-syncline pair with west-to-northwest-striking axial planes (Fig. 3b).

Rocks in the Robert Service thrust hanging wall are intensely deformed, especially within a few hundred metres above the thrust. They exhibit a strong S_2 foliation that is defined mainly by aligned muscovite (± chlorite), and is axial planar to moderately south–southwest-dipping F_2 folds (Fig. 10d). Bedding orientations are variable, but generally dip shallowly to moderately towards the south–southwest. In places, hanging wall rocks have been affected by post-S_2 west-dipping shear bands (S_3) that imply top-to-the-west movement (Fig. 10e).

In the footwall of the Robert Service thrust, the Earn Group (DME, DMEc) and the margins of gabbro sills (ŦGg) are strongly foliated, and the Earn Group locally contains isoclinal folds with well-developed S_2 axial planar cleavage (Fig. 9b). Earn Group shale within ~100 m below the thrust exhibits tight, disharmonic, asymmetric, north-vergent F_2 folds of bedding and the early bedding-parallel (S_1) foliation (Fig. 10f).

Tombstone thrust

In the mapped area, the Tombstone thrust was previously inferred to occur in the Earn Group near its northeastern (basal) contact (Fig. 2). However, detailed mapping across well-exposed rocks in the area where the fault trace was previously inferred (and several kilometres on either side of it) yielded no apparent structural evidence for the thrust or its associated high-strain zone. Structural fabrics include a southwest-dipping foliation and southeast-plunging crenulation lineations and fold axes, which are typical of those elsewhere in the study area (discussed above; see also Skipton and Maw (2021)). In particular, the previously inferred location of the Tombstone thrust lacks northwest-vergent structures, which are considered diagnostic of the thrust and its associated high-strain zone in the Keno and Mayo areas (e.g., Murphy, 1997). Minor occurrences of west-dipping shear bands (Fig. 10e) in the Robert Service thrust zone may signify an overprint of strain related to the Tombstone thrust, but additional investigation is required to test this hypothesis.

Thrusts located between the Robert Service and Dawson thrusts

In the thrust panel that forms the footwall to the Robert Service thrust, Hyland Group strata have been juxtaposed above the younger Road River Group (OSRc, OSRsh), along an interpreted steeply-dipping thrust fault (Figs. 3 and 4). Farther northeast, an additional steeply-dipping thrust fault is interpreted to have juxtaposed the Hyland Group over the Road River Group (OSR, OSRc, OSRsh; Figs. 3 and 4).

Map-scale variations in fold patterns (e.g., open *vs.* isoclinal) and stratigraphic dips (e.g., shallow southwest vs. subvertical) within and between different thrust sheets suggest that protracted thrusting and variably overlapping strain footprints may have produced distinct structural domains. For example, in the northwestern part of the thrust panel that forms the footwall to the Robert Service thrust, Earn and Hyland Group strata dip moderately towards the southwest, and the Hyland Group forms several tight-to-isoclinal map-scale F_2 folds (Fig. 3). To the southeast, Hyland Group rocks in the same thrust panel form upright, open map-scale F_2 folds (Figs. 3 and 5e) and have variable southwest–northeast-dipping bedding orientations.

In contrast, the Road River Group, Gull Lake Formation (ЄGL) and Hyland Group that occupy the thrust sheet in the middle of the map dip subvertically. Bedding orientations range from ~80° NE to ~80° SW, varying about tight-to-isoclinal F_2 folds with subvertical axial planes (Figs. 3 and 5f). In the thrust sheet to the northeast (which forms the hanging wall to the Dawson fault, discussed below), bedding in the Road River Group and volcanic rocks (Ov, Ovsh) mostly dips

steeply towards the southwest, but orientations are variable due to tight F_2 folds.

Dawson thrust

The frontal Dawson thrust is inferred to lie along the southeastern edge of the Beaver River valley (Fig. 3a), coinciding with a distinct linear signature on aeromagnetic maps of Kiss (2020; see also Fig. 9 in Skipton and Maw (2021)). In the region surrounding the study area, the Dawson Fault separates the Ediacaran–Lower Cambrian Hyland Group in the hanging wall from the Ordovician–Devonian(?) Bouvette Formation in the footwall (Fig. 2; Green and Roddick, 1972; Colpron *et al.*, 2013). Previous maps of the study area document the same relationship (Green and Roddick, 1972), or include the Mississippian Tsichu Group locally in the immediate footwall (Fig. 2; digital compilation map of Yukon; Yukon Geological Survey, 2021a). Based on the detailed mapping presented herein, rocks formerly assigned to the Tsichu Group in the footwall of the Dawson fault here are considered to belong to the Ordovician–Silurian Road River Group. The latter rocks are underlain, at least in part, by volcanic rocks of possible Ordovician age (Ov), which may have been thrust over the Bouvette Formation along the frontal Dawson fault (Figs. 3 and 4). The Dawson fault cuts at similarly young stratigraphic levels west of the study area in the Ogilvie Mountains, where it has juxtaposed the Gull Lake Formation over the Road River Group (Abbott, 1997b). These relationships demonstrate the complexity of the Dawson fault zone, whereby rocks of different stratigraphic levels and ages appear to have been transported in the hanging wall.

It is important to note that the Bouvette Formation is known to unconformably overlie older rocks in the region surrounding the study area (e.g., in the southern Wernecke Mountains and eastern Rackla belt; Colpron *et al.*, 2013; Moynihan *et al.*, 2019; Ambrose and Bowie, 2020). Therefore, it is possible that the contact between the Bouvette Formation and the volcanic rocks (Ov) is an unconformity, rather than the frontal Dawson fault. It also remains uncertain what role the Kathleen Lakes strike-slip fault (Fig. 2; Roots, 1990; Abbott, 1990a) may have played in the juxtaposition of different-aged rock units in the Beaver River valley. In an alternative scenario, the frontal Dawson fault may lie farther southwest in the study area, where the Hyland Group overlies the Road River Group (OSR; Fig. 3).

Metamorphism

The southern Nash Creek area has been regionally metamorphosed at lower-greenschist-facies conditions (chlorite zone; e.g., Spear, 1993). Metamorphic assemblages in siliciclastic rocks are characterized by very fine grained white mica and chlorite (± epidote ± calcite). Phyllite and siltstone in the southeastern part of the mapped area locally contain chloritoid porphyroblasts up to 1.5 mm long. Metamorphic minerals in carbonate rocks include recrystallized calcite and/or dolomite, minor fine-grained white mica and, rarely, fine-grained tremolite. Metamorphic mineral assemblages in gabbro and diorite include chlorite, epidote, actinolite, calcite and white mica (± titanite ± apatite). Throughout the map area, the S_1 and S_2 foliations are defined by lower-greenschist-facies minerals, suggesting that they formed during regional lower-greenschist-facies metamorphism.

In siliciclastic rocks within few hundred metres of the Robert Service thrust, metamorphic white mica (± chlorite) is generally more abundant than elsewhere. The metamorphic mineral assemblages suggest lower-greenschist-facies conditions, similar to the rest of the mapped area.

Some mafic-to-intermediate intrusions (Cg, TKgg) are surrounded by narrow (≤1–2 m) contact metamorphic aureoles. The aureoles are subtly different from the host rocks, and are characterized by a lighter green or grey colour and higher contents of white mica and chlorite. Rarely, the aureoles contain ~1–2 mm-wide, grey, oval-shaped aggregates of chlorite and quartz, which may represent former porphyroblasts (e.g., cordierite).

Mineralization

Located between several Au and polymetallic mineral deposits (Fig. 2), the study area has been classified as “prospective” to “highly prospective” in mineral

potential models (Bullen, 2020). Stratigraphic units mapped here are known to host mineral deposits in the surrounding region. For example, the Hyland Group hosts the past-producing polymetallic manto-style Clark deposit (Fig. 2). The McKay Hill polymetallic vein deposit (Fig. 2) is hosted by a sequence of volcanic and sedimentary rocks (Cobbett, 2022) that may be equivalent to those mapped in the study area (Ov).

Quartz veins are relatively common in the mapped area, and typically contain calcite, white mica and/or chlorite. Sulphides are rare and generally comprise pyrite, although several veins contain a reddish-brown material, which may be a product of weathering or alteration of sulphides (Fig. 11a). Some wall rocks exhibit gossanous weathering. Quartz veins are predominantly hosted by the Narchilla and Yusezyu formations in the Hyland Group (Fig. 11a), by chert in the Road River Group (OSRc) and by the Keno Hill Quartzite (MKHQ; Fig. 11b). Less commonly, they are hosted by gabbro (Ꞓg) and by the Algae Formation (PHa) where it has been intruded by gabbro (Skipton and Maw, 2021). The quartz veins dominantly strike northwest–southeast, parallel to the regional structural grain, but they have variable orientations and locally form networks. As some vein surfaces are lineated (L_2; Fig. 11b), regional D_2 deformation outlasted vein emplacement in some cases.

Assay results from grab-samples of several quartz veins and altered (e.g., silicified or gossanous) rocks are presented in Table 1. A southeast-dipping quartz vein hosted in quartz arenite (Narchilla Formation, PꞒHnss) contains blue and green minerals (azurite and malachite?; Fig. 11a) and yielded anomalously high contents of Au, Ag, Cu, Zn and other elements (sample 21DS-050-1-1; Table 1).

Acknowledgements

Amaya Cherian-Hall and Liam Maw are thanked for their outstanding assistance in the field. Helicopter support was provided by Horizon Helicopters (2019) and Fireweed Helicopters (2021). Julia Lane, Adam Coulter and ATAC Resources Ltd. provided generous logistical support for this project in 2019. Maurice Colpron, Rosie Cobbett, David Moynihan, Steve Israel and Don Murphy are acknowledged for numerous helpful discussions. Rosie Cobbett is thanked for providing a critical review that improved the quality of the manuscript, and Karen MacFarlane is thanked for her editorial handling of the paper. Fieldwork was conducted in the traditional territory of the First Nation of Na-Cho Nyäk Dun.

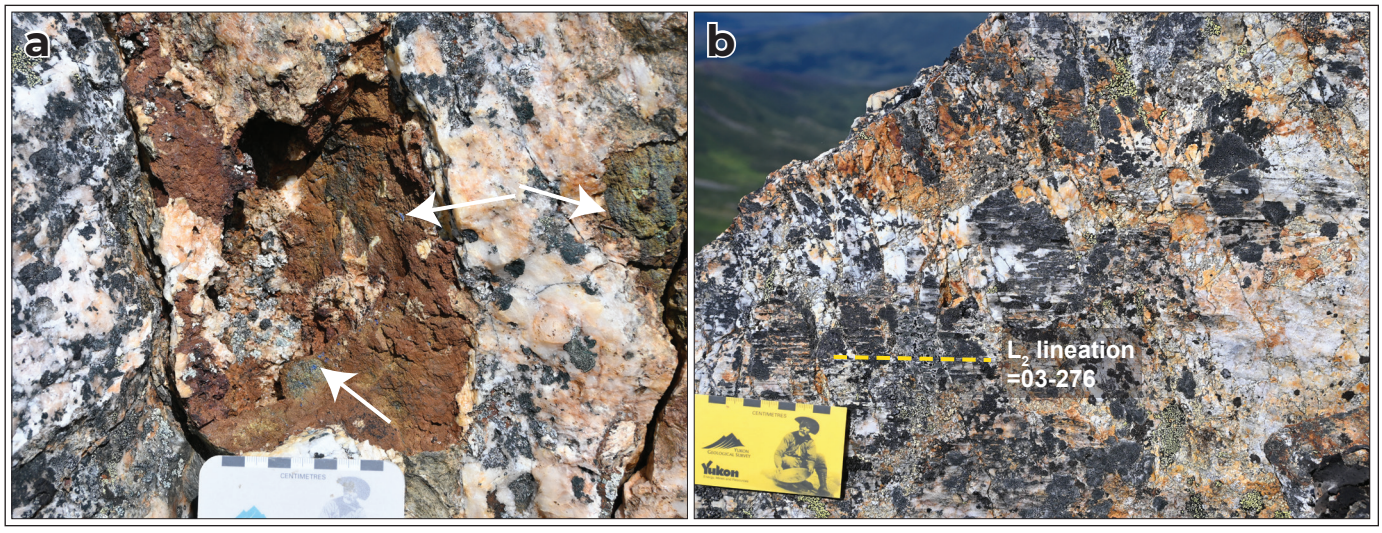


Figure 11. *Field photographs of quartz veins.* ***(a)*** *Quartz vein containing a reddish-brown alteration material and blue and green minerals (azurite and malachite?; indicated by white arrows). The quartz vein orientation is 055/62 and the vein is hosted in quartz arenite (Narchilla Formation, sandstone member,* PꞒHnss*).* ***(b)*** *Quartz vein surface exhibiting well-developed* L_2 *lineations. The quartz vein is hosted in quartzite (Tsichu Group, Keno Hill Quartzite,* MKHQ*).*

Table 1. *Assay results from rock samples collected during geological mapping in the southern Nash Creek area.*

Sample	Rock type	Latitude	Longitude	Au	Ag	As	Bi	Cd	Cu	Pb	Sb	Zn
				(ppm)	(ppm)	(ppm)	(ppm)	(ppm)	(ppm)	(ppm)	(ppm)	(ppm)
21DS-050-1-1	Quartz vein	64.299684	-135.084658	5.58	71.1	4310	32.1	73.2	22300	3980	>10000	10250
21DS-056-1-2	Altered siltstone	64.293649	-135.140764	0.02	0.87	25.5	0.286	0.325	142	21.7	52.8	153
21DS-094-1-1	Altered mafic volcaniclastic rock	64.340803	-135.104251	<0.01	0.151	6.41	0.066	0.416	85.6	7.75	51.5	71.8
21DS-098-1-3	Altered chert	64.298977	-135.200566	0.01	0.076	14.45	0.118	0.475	93.3	9.62	10.6	28.6
21DS-176-1-2	Altered quartzite with quartz veins	64.214353	-135.354614	<0.01	0.1	17.6	0.043	0.157	67.4	3.7	22.7	243
19DS-012-2-1	Quartz vein	64.210713	-134.886781	<0.01	0.003	4.75	0.035	0.023	0.84	2.44	0.32	59.3
19DS-040-1-2	Gabbro with quartz vein	64.201451	-134.830385	<0.01	0.03	12.7	0.079	0.126	43.7	52.5	0.47	314
19DS-042-1-2	Altered siltstone	64.203576	-134.819603	0.01	0.024	0.68	0.484	<0.005	11.9	2.36	0.18	35
19DS-058-1-2	Quartz vein	64.1671	-134.842987	<0.01	0.009	1.43	0.105	0.013	2.1	3.08	0.54	82
19DS-058-1-3	Quartz vein	64.1671	-134.842987	<0.01	0.01	1.28	0.105	0.068	9.58	4.49	0.72	72.1
19DS-136-1-1	Limestone with quartz veins	64.255204	-135.101553	0.01	0.018	7.51	0.021	0.038	59.4	0.6	0.05	94.1

Notes: Geochemical analyses were performed by ALS Geochemistry (Whitehorse, Yukon) using the following methods: Au, fire assay and atomic absorption spectroscopy (AAS); Ag, As, Cu, Pb, Sb, Zn, four acid digestion with inductively-coupled plasma mass spectrometry (ICP-MS).

References

Abbott, G., 1990a. Geological map of Mt. Westman map area (106D/1). Exploration and Geological Services Division, Yukon Region, Indian and Northern Affairs Canada, Open File 1990-1, scale 1:50 000.

Abbott, G., 1990b. Preliminary results of the stratigraphy and structure of the Mt. Westman area, central Yukon. Current Research, Part E: Cordillera and Pacific Margin. Geological Survey of Canada, Paper 90-1E, p. 15–22.

Abbott, G., 1997a. Geology of the Upper Hart River Area, Eastern Ogilvie Mountains, Yukon Territory (116A/10, 116A/11). Exploration and Geological Services Division, Yukon Region, Indian and Northern Affairs Canada, Bulletin 9, 92 p.

Abbott, G., 1997b. Geology of NTS map area 116A/10, eastern Ogilvie Mountains, Yukon. Exploration and Geological Services Division, Yukon Region, Indian and Northern Affairs Canada, Geoscience Map 1997-2, scale 1:50 000.

Abbott, G., 1997c. Geology of Two Beaver Lake map area, eastern Ogilvie Mountains, Yukon (NTS 116A/11). Exploration and Geological Services Division, Yukon Region, Indian and Northern Affairs Canada, Geoscience Map 1997-3, scale 1:50 000.

Ambrose, T. and Bowie, S., 2020. Preliminary report on the bedrock geology of the Rackla River area, southern Wernecke Mountains, Yukon (parts of NTS 106C/4, 5 and 106D/1, 8). *In:* Yukon Exploration and Geology 2019, K.E. MacFarlane (ed.), Yukon Geological Survey, p. 1–21.

Anderson, R.G., 1987. Plutonic rocks in the Dawson map area, Yukon Territory. *In:* Current Research, Part A, Geological Survey of Canada, Paper 87-1A, p. 689–697.

Bullen, W., 2020. New mineral potential mapping methodology for Yukon: Case studies from the Beaver River and Dawson regional land use planning areas. *In*: Yukon Exploration and Geology 2019, K.E. MacFarlane (ed.), Yukon Geological Survey, p. 23–42.

Cobbett, R., 2020. Preliminary report on the bedrock geology of Castle Mountain area, Yukon (parts of NTS 105D/6). *In:* Yukon Exploration and Geology 2019, K.E. MacFarlane (ed.), Yukon Geological Survey, p. 43–55.

Cobbett, R., 2022. Geology of the Carpenter Creek and McKay Hill areas (NTS 106D/6, 11), central Yukon. *In:* Yukon Exploration and Geology 2021, K.E. MacFarlane (ed.), Yukon Geological Survey.

Colpron, M., Moynihan, D., Israel, S. and Abbott, G., 2013. Geological map of the Rackla belt, east-central Yukon (NTS 106C/1–4, 106D/1). Yukon Geological Survey, Open File 2013-13, 1:50 000 scale, 5 maps and legend.

Gordey, S. and Anderson, R.G., 1993. Evolution of the northern Cordilleran miogeocline, Nahanni map area (105I), Yukon and Northwest Territories. Geological Survey of Canada, Memoir 428, 214 p.

Green, L.H. and Roddick, J.A., 1962. Dawson, Larsen Creek, and Nash Creek map-areas, Yukon Territory (116B, C, E1/2, 116A, and 106D). Geological Survey of Canada, Paper 62-7, 20 p., plus maps.

Green, L.H., 1972a. Geology, Nash Creek, Yukon Territory. Geological Survey of Canada, Department of Energy, Mines and Resources, Map 1282A, scale 1:250 000.

Green, L.H., 1972b. Geology of Nash Creek, Larsen Creek, and Dawson map-areas, Yukon Territory (106D, 116A, 116B, and 116C (E1/2)). Geological Survey of Canada, Memoir 364, 157 p.

Kingston, S., Mortensen, J.K., Dumala, M. and Gabites, J., 2010. Ar-Ar geochronology and Pb isotopic constraints on the origin of the Rau gold-rich carbonate replacement deposit, central Yukon. *In*: Yukon Exploration and Geology 2009, K.E. MacFarlane, L.H. Weston, and L.R. Blackburn (eds.), Yukon Geological Survey, p. 213–222.

Kiss, F., 2020. Aeromagnetic Survey of the Nash Creek Area, Yukon, Parts of NTS 105-M, N, 106-C, D, 115-P and 116-A. Geological Survey of Canada, Open File 8728; Yukon Geological Survey, Open File 2020-7, scale 1:100 000, https://doi.org/10.4095/326147.

Mair, J.L., Hart, C.J.R. and Stephens, J.R., 2006. Deformation history of the northwestern Selwyn Basin, Yukon, Canada: Implications for orogen evolution and mid-Cretaceous magmatism. GSA Bulletin, vol. 118, p. 304–323.

Moynihan, D., 2014. Bedrock Geology of NTS 106B/04, Eastern Rackla belt. *In*: Yukon Exploration and Geology 2013, K.E. MacFarlane, M.G. Nordling and P.J. Sack (eds.), Yukon Geological Survey, p.147–167.

Moynihan, D., 2016a. Bedrock geology compilation of the eastern Rackla belt, NTS 105N/15, 105N/16, 105O/13, 106B/4, 106C/1, 106C/2, east-central Yukon. Yukon Geological Survey, Open File 2016-2, scale 1:75 000, 2 sheets.

Moynihan, D., 2016b. Stratigraphy and structural geology of the upper Hyland River area (parts of 105H/8, 105H/9), southeast Yukon. *In*: Yukon Exploration and Geology 2015, K.E., MacFarlane and M.G. Nordling (eds.), Yukon Geological Survey, p. 187–206.

Moynihan, D., Strauss, J., Nelson, L.L. and Padget, C.D., 2019. Upper Windermere Supergroup and the transition from rifting to continent-margin sedimentation, Nadaleen River area, northern Canadian Cordillera. GSA Bulletin, vol. 131(9-10), p. 1673–1701.

Mair, J.L., Hart, C.J.R., and Stephens, J.R., 2006. Deformation history of the northwestern Selwyn Basin, Yukon, Canada: Implications for orogen evolution and mid-Cretaceous magmatism. GSA Bulletin, vol. 118(3-4), p. 304–323.

Murphy, D.C., 1997. Geology of the McQuesten River Region, Northern McQuesten and Mayo Map Area, Yukon Territory (115P/14, 15, 16; 105M/13, 14). Exploration and Geological Services Division, Yukon Region, Indian and Northern Affairs Canada, Bulletin 6, 122 p.

Read, P.B., Woodsworth, G.J., Greenwood, H.J., Ghent, E.D. and Evenchick, C.A., 1991. Metamorphic Map of the Canadian Cordillera. Geological Survey of Canada, Map 1714A, scale 1:2 000 000.

Roots, C.F., 1988. Cambro-Ordovician volcanic rocks in eastern Dawson map area, Ogilvie Mountains, Yukon. *In:* Yukon Geology, volume 2, G. Abbott (ed.), Exploration and Geological Services Division, Yukon, Indian and Northern Affairs Canada, p. 81–87.

Roots, C.F., 1990. Geology of 106D/8 and 106D/7 (East half) Map Areas. Exploration and Geological Services Division, Yukon Region, Indian and Northern Affairs Canada, Open File 1990-3, 1 sheet.

Roots, C.F., 1997. Geology of the Mayo Map Area, Yukon Territory (105M). Exploration and Geological Services Division, Yukon Region, Indian and Northern Affairs Canada, Bulletin 7, 82 p.

Skipton, D.R., 2022. Preliminary geological map of the southern Nash Creek area, central Yukon (parts of NTS 106D/2, 3, 6, 7). Yukon Geological Survey, Open File 2022-6, 1 sheet, 1:50 000-scale.

Skipton, D.R. and Maw, L., 2021. Updated geology of the Clark Lakes area in central Yukon (parts of 106D/2, 3, 6 and 7). *In:* Yukon Exploration and Geology 2020, K.E. MacFarlane (ed.), Yukon Geological Survey, p. 73–94.

Spear, F.S., 1993. Metamorphic Phase Equilibria and Pressure-Temperature-Time Paths. Mineralogical Society of America, Monograph 1, 799 p.

Tempelman-Kluit, D.J., 1970. Stratigraphy and structure of the Keno Hill quartzite in Tombstone River-Upper Klondike River map areas, Yukon Territory (116B/7, B/8). Geological Survey of Canada, Bulletin 180, 102 p. and maps.

Thompson, R.I., Roots, C.F. and Mustard, P.S., 1990. Repeated Proterozoic passive margin extension influences Late Cretaceous folding and thrusting in southern Ogilvie Mountains, Yukon. Geological Association of Canada, Program with Abstracts, vol. 15, p. 131.

Yukon Geological Survey, 2021a. Yukon Digital Bedrock Geology. Yukon Geological Survey, http://data.geology.gov.yk.ca/Compilation/3#InfoTab, [accessed November 6, 2021].

Yukon Geological Survey, 2021b. A digital atlas of terranes for the northern Cordillera. Yukon Geological Survey, https://data.geology.gov.yk.ca/Compilation/2, [accessed December, 2021].

Geology and U-Pb zircon geochronology and Pb isotope geochemistry of mid-Cretaceous plutonic rocks in the Mount Nansen map area (NTS 115I/3 and part of 115I/2)

Patrick J. Sack
Yukon Geological Survey

James L. Crowley
Boise State University

Venessa Bennett
Geomantia Consulting

Janet Gabites
University of British Columbia

Sack, P.J., Crowley, J.L., Bennett, V. and Gabites, J., 2022. Geology and U-Pb zircon geochronology and Pb isotope geochemistry of mid-Cretaceous plutonic rocks in the Mount Nansen map area (NTS 115I/3 and part of 115I/2). *In:* Yukon Exploration and Geology 2021, K.E. MacFarlane (ed.), Yukon Geological Survey, p. 185–215.

Abstract

The geology in the Mount Nansen area, of the Dawson Range, comprises a metamorphic basement overlain and intruded by mid and Late Cretaceous magmatic rocks. Mid-Cretaceous epithermal deposits are recognized in the Brown-McDade cluster in the south, and Late Cretaceous porphyry and epithermal occurrences in the centrally located Klaza cluster. Here we report eight new U-Pb zircon crystallization ages, two CA-TIMS and six LA-ICPMS, and Pb isotopic data for igneous feldspar from six samples. A 199.06 ± 0.96 Ma crystallization age demonstrates the host rock to the Brown-McDade deposit is the Late Triassic to Early Jurassic Minto suite. We report crystallization ages of 111 ± 1.8 Ma for the Dickson Hill porphyry, 107.96 ± 0.03 and 107.86 ± 0.03 Ma for the central and border phases of the Bow Creek granite, respectively, and 107.0 ± 0.72, 107.0 ± 0.78 and 107.5 ± 0.67 Ma for equigranular and porphyritic phases of the Dawson Range granodiorite. These ages confirm a mid-Cretaceous Whitehorse suite affinity for these rocks with porphyritic textures suggesting high-level emplacement. Feldspar Pb isotopic data of igneous rocks in the Mount Nansen area become more radiogenic with time and are distinct for Late Triassic to Early Jurassic plutonic rocks versus Cretaceous rocks. Cretaceous feldspar isotopic data broadly overlaps Pb isotopic values of galena from deposits throughout the Dawson Range suggesting coeval magmatic rocks are a significant source of metals.

* Patrick.Sack@yukon.ca

Regional geology

The Dawson Range area is broadly defined by the Yukon River to the east and north, the White River to the north and west and the Nisling River to the west and south (Fig. 1). The geology of the Dawson Range is predominantly composed of metamorphic Yukon-Tanana Paleozoic country rocks (Snowcap and Finlayson assemblages and the Simpson Range and Sulphur Creek metaplutonic suites) intruded by Late Triassic to Early Jurassic plutonic rocks (Pyroxene Mountain, Minto and Long Lake suites). These basement rocks were covered and intruded by Cretaceous volcanic and plutonic rocks (mid-Cretaceous Mount Nansen group and Whitehorse suite, and Late Cretaceous Carmacks group and Casino and Prospector Mountain suites; Ryan *et al.*, 2013, 2016, 2018; Sack *et al.*, 2021). The area is dissected by northwest and northeast trending faults with movement along the fault plane being Late Cretaceous and younger (e.g., Big Creek fault; Mottram *et al.*, 2020).

In the Dawson Range, Yukon-Tanana rocks were metamorphosed to greenschist and amphibolite facies as Late Triassic to Early Jurassic plutons were emplaced at >20 km depths during regional exhumation (Staples *et al.*, 2014; Clark, 2017; Gaidies *et al.*, 2020; Sack *et al.*, 2020). In contrast, mid-Cretaceous and younger rocks were emplaced at shallow crustal levels, and both plutonic and volcanic rocks of the mid-Cretaceous,

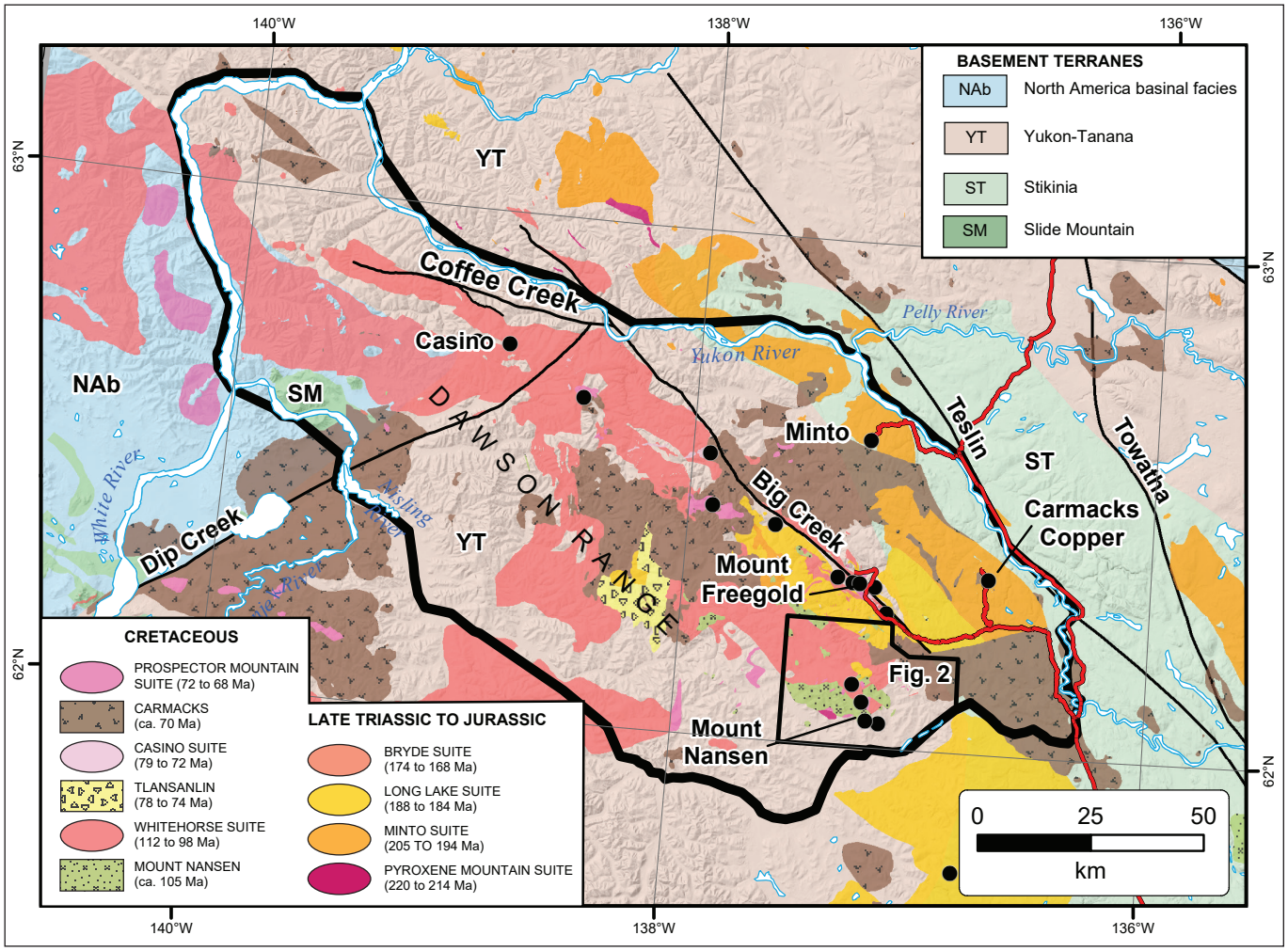


Figure 1. *Simplified regional geology map of the central Dawson Range (outlined in heavy black line). For this figure and Fig. 2, legend shape for layered units is a rectangle and for plutonic units is an oval. Significant mineral occurrences are shown with black circles. Regionally significant faults and mineral districts are labelled. Geology from YGS (2020).*

Late Cretaceous and Paleogene are preserved. From the perspective of mineral deposits, this means that the appropriate crustal level for development of porphyry systems (porphyry, epithermal and skarn deposits) is likely preserved throughout the Dawson Range for Cretaceous, but not Late Triassic to Early Jurassic, systems. The Mount Nansen area discussed in this paper is an example in the Dawson Range with both mid and Late Cretaceous porphyry system potential (e.g., Sawyer and Dickinson, 1976; Mortensen *et al.*, 2016; Mortensen and Friend, 2020; Lee, 2021).

Local geology

Basement

Basement rocks in the Mount Nansen area are primarily in the south and east (Fig. 2) where they are broadly folded along northeast trending fold axes (Sack *et al.*, 2021). With the local exception of the Snowcap amphibolite and the Minto suite, the basement has relatively low magnetic susceptibility (Table 1; Sack *et al.*, 2021) and shows up as magnetic lows on regional aeromagnetic maps (Aurora Geosciences and Bruce, 2020).

Yukon-Tanana terrane

Snowcap assemblage (PDS1 and PDS3)

The Snowcap assemblage is a Proterozoic to Devonian metasedimentary unit of quartzite and schist, and minor amphibolite of volcanic origin (Piercey and Colpron, 2009). In the Mount Nansen area, both the quartzite and schist are grey to white on weathered and fresh surfaces (Fig. 3a). The schist tends to be darker as the biotite content increases. The quartzite and schist have quartz, feldspar, muscovite, biotite and locally garnet. These rocks are strongly foliated and layered, and locally form a quartzofeldspathic schist difficult to distinguish from Simpson Range metagranitoid (MgSR). The magnetic susceptibility of the Snowcap quartzite and schist ranges from 18.10 to 0.01×10^3 SI units with a median value of 0.32 (Table 1). Snowcap amphibolite is layered dark green and white on weathered and fresh surfaces (Fig. 3b) and is fine to medium grained, equigranular and well foliated. The magnetic susceptibility of the Snowcap amphibolite ranges from 24.0 to 0.11×10^3 SI units with a median value of 4.09 (Table 1).

Finlayson assemblage (DMF1 and DMF2)

The Finlayson assemblage consists of mafic (DMF1) and felsic (DMF2) map units. The mafic unit is difficult to differentiate from the Snowcap amphibolite at the outcrop scale as the Finlayson amphibolite is also dark green, strongly foliated and locally compositionally layered. It is generally schistose, locally gneissic and more chloritic than the Snowcap amphibolite (PDS3). The magnetic susceptibility of the Finlayson amphibolite ranges from 2.93 to 0.04×10^3 SI units with a median value of 0.21 (Table 1) suggesting it may be a less magnetic unit than the Snowcap amphibolite. The felsic Finlayson unit is only found in 50 000 map scale units in the southwestern corner of the Mount Nansen map area (Fig. 2) where Ryan *et al.* (2016) describe it as a schistose, fine-grained felsic metavolcanic rock commonly with a fragmental texture. The felsic unit was deposited ca. 351 to 344 Ma (Joyce *et al.*, 2020).

Simpson Range metaplutonic suite (MgSR)

The Simpson Range metaplutonic suite is a biotite ± hornblende metagranodiorite. It is light grey to orange weathered and light grey fresh with local feldspar augen. It is well foliated and is locally compositionally banded with more mafic (biotite-hornblende-rich) and more felsic (quartz-feldspar-rich) layers making it difficult to distinguish from the quartzofeldspathic schist of the Snowcap assemblage. The Simpson Range metaplutonic suite (365 to 350 Ma) intruded Snowcap rocks and is slightly older to coeval with the Finlayson assemblage (Joyce *et al.*, 2020). The magnetic susceptibility of the Simpson Range metaplutonic suite ranges from 10.9 to 0.0005×10^3 SI units with a median value of 0.31 (Table 1).

Sulphur Creek metaplutonic suite (PgS)

One body of Sulphur Creek orthogneiss is mapped to the east of Victoria Creek (Fig. 2; Ryan et *al.*, 2016; Sack et *al.*, 2021) where it is a fine-grained, grey to pink alkali feldspar porphyritic monzonite that is moderately foliated (Fig. 3c). The magnetic susceptibility of this body ranges from 0.53 to 0.01 × 10³ SI units with a median value of 0.03 (Table 1).

Late Triassic to Early Jurassic plutons

Pyroxene Mountain suite (LTrPx)

The Pyroxene Mountain suite is medium-grained, foliated hornblende diorite to quartz diorite that intruded the Finlayson assemblage and locally the Snowcap assemblage (Ryan et *al.*, 2016). The magnetic susceptibility of the Pyroxene Mountain suite ranges from 0.41 to 0.12 × 10³ SI units with a median value of 0.26 (Table 1). The Pyroxene Mountain body on the south flank of Mount Nansen was intruded ca. 216 Ma (Colpron et *al.*, *in press*).

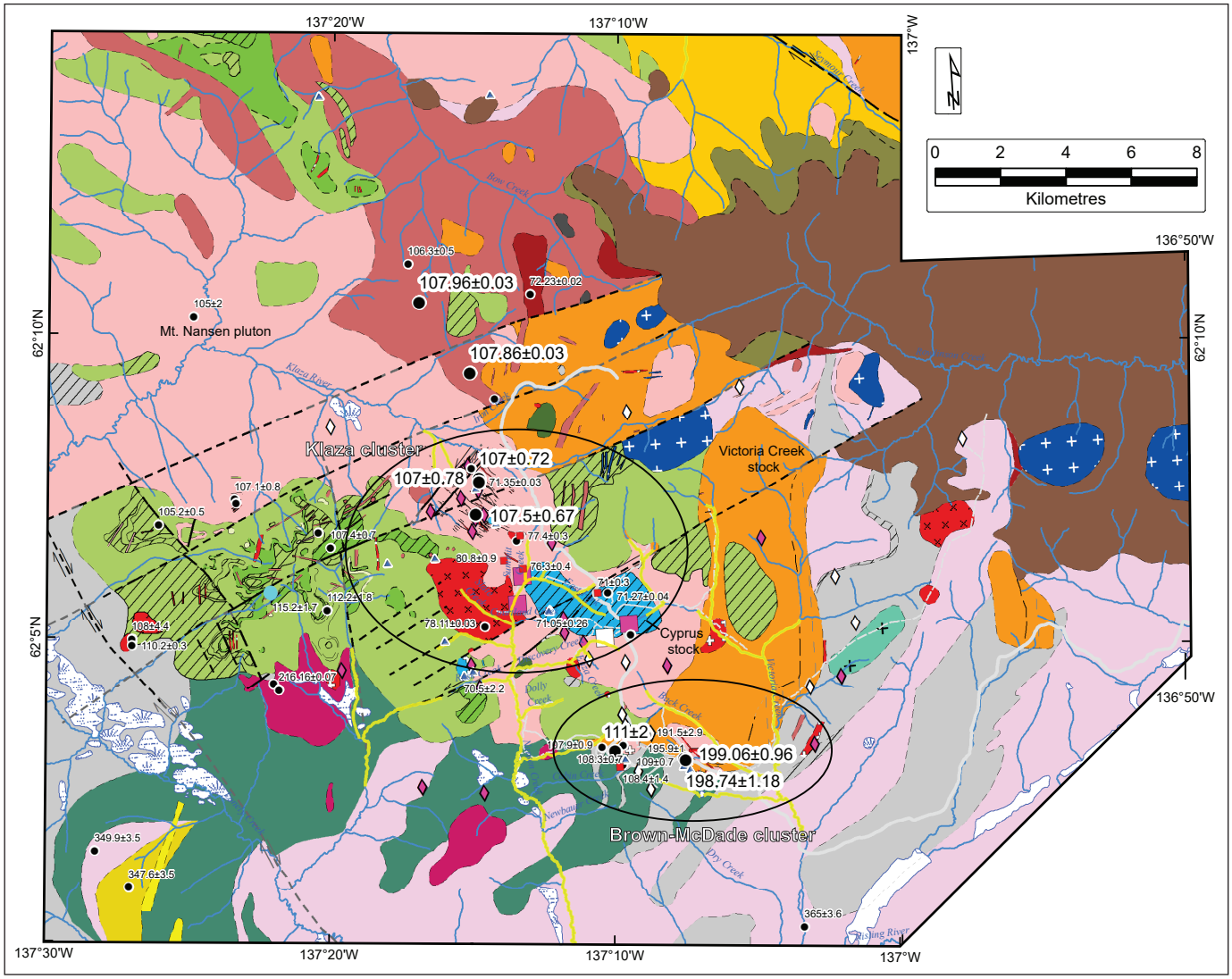


Figure 2. *Simplified geology of the Mount Nansen map area (NTS 115I/3 and part of 115I/2). Legend on following page. For Prospector Mountain suite and Mount Nansen group, units on map with angled hatching are breccia of dominantly same lithology as unhatched unit of same colour. U-Pb zircon ages presented in this paper are those shown with larger symbols and labelled with a larger font. Modified from Sack et al. (2021).*

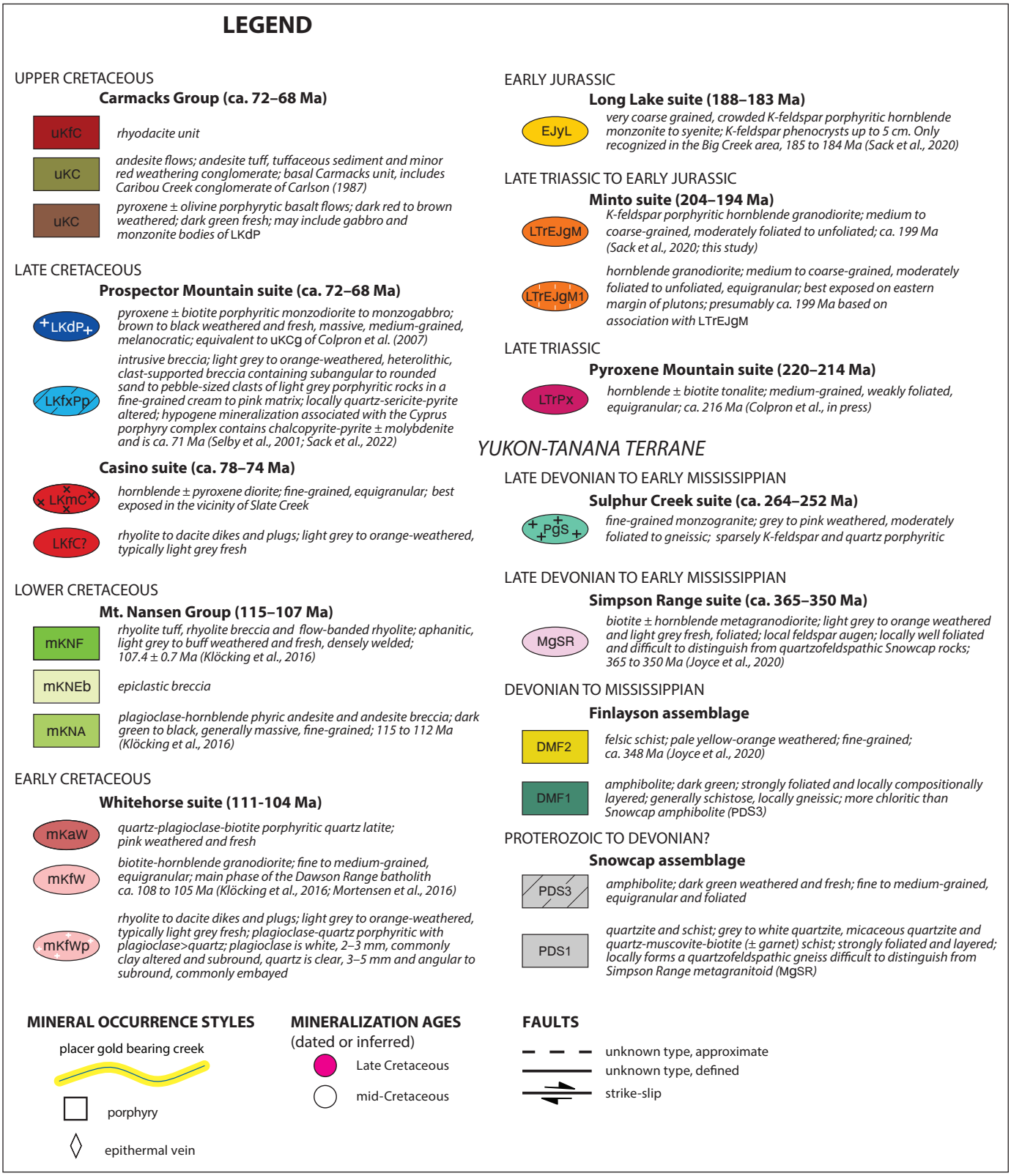


***Figure 2** continued.*

Table 1. *Magnetic susceptibility measurements from the Mount Nansen area mostly summarized by map unit. N = number of stations with a magnetic susceptibility measurement; each magnetic susceptibility measurement is the mean of five point measurements over a 1 to 2 m² area, within the same lithology. Data are in Appendix 1.*

	Map units	Mean	Median	Minimum	Maximum	Std dev	N	
Propsector Mountain (mafic)	LKdP	8.47	6.49	0.20	20.70	9.77	4	Late Cretaceous
Propsector Mountain (felsic)	LKfxPp	5.97	0.14	0.03	19.40	9.39	11	
Carmacks basalt	uKC1	10.71	10.70	8.01	15.10	2.41	8	
Carmacks felsic volcanic	uKC3	0.33	0.14	0.08	0.97	0.42	4	
Casino microdiorite	LKmC	20.87	18.95	8.19	50.70	10.13	16	
Casino felsic	LKfCp	0.12	0.05	0.04	0.32	0.14	4	
Whitehorse Pl porphyry	mKaW	19.56	23.80	4.58	30.30	13.37	3	mid-Cretaceous
Whitehorse granodiorite	mKgWT	13.22	11.10	0.13	32.80	10.18	24	
Whitehorse Qz porphyry	mKfWp	1.04	0.45	0.02	3.81	1.25	15	
Mount Nansen (felsic)	mKNFt, mKNFf	0.04	0.05	0.00	0.08	0.03	5	
Mount Nansen (intermediate)	mKNAm, mKNAb	17.10	14.60	0.09	55.80	14.09	52	
Minto	LTrEJgM, LTrEJgM1	8.25	6.18	0.09	26.00	6.91	56	metamorphic basement
Pyroxene Mountain	LTrPx	0.26	0.26	0.12	0.41	0.20	2	
Sulphur Creek	PgS	0.19	0.03	0.01	0.53	0.30	3	
Simpson Range	MgSR	1.51	0.31	0.00	10.90	2.95	13	
Finlayson amphibolite	DMF1	0.67	0.21	0.04	2.93	0.87	11	
Snowcap amphibolite	PDS3	9.27	4.09	0.11	24.00	11.12	6	
Snowcap schist	PDS1	1.69	0.32	0.01	18.10	3.88	33	

Minto suite (LTrEJgM)

Plutons of the Minto suite are relatively widespread in the central part of the Mount Nansen area (Fig. 2). Two textural varieties are recognized, a K-feldspar porphyritic hornblende granodiorite and an equigranular hornblende granodiorite (Sack *et al.*, 2021). Both phases are medium to coarse grained and moderately foliated to unfoliated; foliation intensity tends to increase on the eastern side of plutons (Sack *et al.*, 2021). We report an emplacement age for the Victoria Creek pluton of *ca.* 199 Ma, similar to other Minto suite plutons to the north and northeast that range from 205 to 194 Ma (Sack *et al.*, 2020). The magnetic susceptibility of the Minto plutonic suite ranges from 26.0 to 0.09 × 10³ SI units with a median value of 6.18 (Table 1).

Long Lake suite (EJyL)

In the Mount Nansen area, Long Lake suite rocks are only recognized near Seymour Creek at the north edge of the map (Allan and Friend, 2018). Here the Long Lake suite comprises a composite batholith, the phase that is mapped locally is very coarse grained, crowded K-feldspar porphyritic hornblende monzonite to syenite; K-feldspar phenocrysts are up to 5 cm (Carlson, 1987). This alkalic phase of the batholith was emplace *ca.* 185 Ma (Sack *et al.*, 2020).

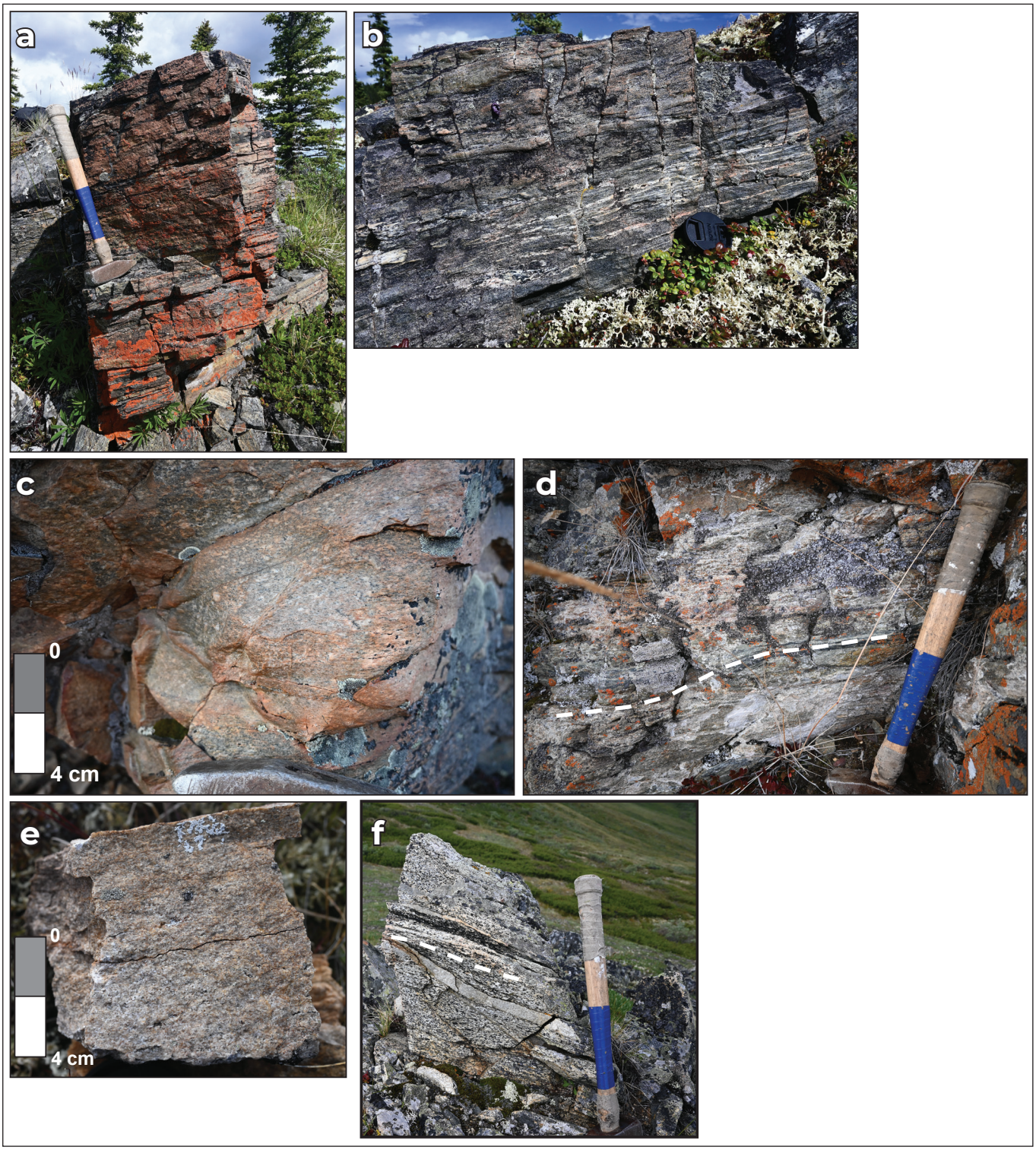


Figure 3. *Representative photos of metamorphic basement rocks in the Mount Nansen area.* **(a)** *20PS017, weathered outcrop of quartz-mica schist, the main lithology of the Snowcap assemblage in the Mount Nansen area. Hammer is 45 cm long.* **(b)** *20PS021, foliated amphibolite within the Snowcap assemblage.* **(c)** *20PS217, plagioclase augen gneiss of the Simpson Range suite.* **(d)** *20PS214, foliated amphibolite of the Finlayson assemblage. Dashed white line shows main foliation trace. Hammer is 45 cm long.* **(e)** *20PS102, fine to medium-grained, sugary metaplutonic rock of the Sulphur Creek suite.* **(f)** *20PS050, foliated, medium-grained granodiorite of the Minto suite crosscut by thin, unfoliated aplite dikes. Dashed white line shows main foliation trace. Hammer is 45 cm long.*

Mid-Cretaceous igneous rocks

Mid-Cretaceous volcanic and plutonic rocks are primarily found in the central and western parts of the Mount Nansen area (Fig. 2) and comprise a volcano-plutonic complex formed ca. 115 to 105 Ma (Klöcking et al., 2016; Ryan et al., 2016; Sack et al., 2021). The magnetic susceptibility of these rocks varies over three orders of magnitude (Table 1) but in general, these rocks have relatively high magnetic susceptibility and are mostly magnetic highs on regional aeromagnetic maps (Aurora Geosciences and Bruce, 2020).

Mount Nansen group

Volcanic rocks of the Mount Nansen group are primarily found in the central part of the area on Mount Nansen and Victoria Mountain (Fig. 2). Intermediate and felsic rocks of the Mount Nansen group are broadly coeval with crystallization ages ca. 115 to 107 Ma (Klöcking et al., 2016).

Intermediate volcanic rocks (mKNA)

The bulk of the Mount Nansen group is andesitic in composition with textural varieties that include massive, plagioclase-phyric flows, monomictic autobreccias and lesser rounded, polymictic breccias (Fig. 4). The magnetic susceptibility of the intermediate Mount Nansen rocks ranges from 55.8 to 0.09 × 10³ SI units with a median value of 14.6 (Table 1). All andesitic varieties are dark green to brown weathered and dark green to black fresh. In massive andesite, 2–5 mm white plagioclase phenocrysts give a speckled appearance (Fig. 4a).



Figure 4. *Representative photos of mid-Cretaceous volcanic rocks in the Mount Nansen area.* ***(a)*** *20PS143, weathered outcrop of massive, plagioclase phyric andesite, the most widespread lithology of the Mount Nansen group in the map area.* ***(b)*** *20PS105, volcanic, matrix supported conglomerate of primarily andesitic cobbles within an andesitic matrix. Hammer head is 13 cm.* ***(c)*** *20PS142, flow banded rhyolite of the Mount Nansen group. Scribe for scale.*

Felsic volcanic rocks (mKNF)

Felsic volcanic rocks within the Mount Nansen group are relatively rare, occurring as local flows and domes, mostly in the upper part of the stratigraphy preserved near the top of Mount Nansen (Klöcking *et al.*, 2016). These rocks are rhyolitic in composition and range from aphanitic densely welded tuff to autoclastic rhyolite breccia and flow-banded rhyolite (Fig. 4c). They are light grey to buff, weathered and fresh. The magnetic susceptibility of the felsic Mount Nansen rocks ranges from 0.08 to 0.0043 × 10³ SI units with a median value of 0.05 (Table 1).

Whitehorse suite

Porphyry plugs and dikes (mKfWp)

Small plugs and dikes associated with the main Dawson Range granodiorite phase of the Mount Nansen pluton are found throughout the Mount Nansen area (Fig. 2). The dikes are typically small, up to metres across, and porphyritic with two phenocryst assemblages: plagioclase only and quartz-plagioclase. The plagioclase only porphyries are relatively rare. They are dull grey-brown on weathered and fresh surfaces and friable. The plagioclase phenocrysts commonly have a radiating texture giving the rock a 'flower' porphyry appearance. The magnetic susceptibility of Whitehorse suite plagioclase porphyritic dikes ranges from 30.3 to 4.58 × 10³ SI units with a median value of 23.8 (Table 1).

The quartz-plagioclase porphyries are more volumetrically and economically significant and the largest of these bodies is the plug on Dickson Hill immediately north of the Flex deposit (115I 137). These dikes and plugs have rhyolitic to dacitic compositions and are light grey to orange-weathered and light grey fresh. The phenocryst assemblage has plagioclase > quartz with white subround 2–3 mm plagioclase crystals and clear 3–5 mm, angular to subround quartz crystals that are commonly embayed (Fig. 5a). The magnetic susceptibility of Whitehorse suite quartz-feldspar porphyritic dikes ranges from 3.81 to 0.02 × 10³ SI units with a median value of 0.45 (Table 1). These rocks were previously interpreted as Late Cretaceous (Sack *et al.*, 2021) however, they are now known to be mid-Cretaceous as the crystallization age of the Dickson Hill plug is 111 ± 1.8 Ma (this study).

Granodiorite (mKfW)

The main phase of the Whitehorse suite, also known as the Dawson Range granodiorite (Ryan *et al.*, 2016), in the Mount Nansen area is a fine to medium-grained, equigranular biotite-hornblende granodiorite of the Mount Nansen pluton (Fig. 6a; Sack *et al.*, 2021). The Mount Nansen pluton and associated dikes are *ca.* 107 to 105 Ma (Klöcking *et al.*, 2016; Mortensen *et al.*, 2016; this study). The magnetic susceptibility of Whitehorse suite granodiorite and granite ranges from 32.8 to 0.13 × 10³ SI units with a median value of 11.1 (Table 1).

Granite (mKaW)

The other volumetrically significant phase of the Mount Nansen pluton is the Bow Creek granite (Carlson, 1987). This phase is predominantly recognized in the headwaters of Bow Creek near the north edge of the Mount Nansen area (Fig. 2), though small dikes are recognized on the flanks of Mount Nansen as well (Klöcking *et al.*, 2016). The Bow Creek granite is a zoned pluton with a core of fine-grained equigranular, biotite ± hornblende granite and a border phase of quartz-plagioclase-biotite porphyritic granite. Both phases are pink on weathered and fresh surfaces (Fig. 6b,c). The crystallization age of both phases is *ca.* 108 Ma with the core slightly older than the border phase (this study).

Late Cretaceous igneous rocks

Casino plugs and dikes (LKC)

There are felsic and mafic Casino age (*ca.* 78 to 74 Ma) dikes and plugs in the Mount Nansen area. The felsic variety are found as dikes and are best understood in the vicinity of the Klaza deposit (15I 067). These dikes are feldspar > quartz porphyritic granodiorite with very fine grained biotite in the groundmass (Lee *et al.*, 2020). The dikes are commonly co-spatial with, and cut by, composite epithermal veins of the Klaza deposit (Lee *et al.*, 2020). The phenocryst assemblage and composition of these dikes is very similar to the mid-Cretaceous plugs and dikes, and differentiating them in the field is difficult. The age of these dikes in the vicinity of the Klaza deposit is 78 to 76 Ma (Lee, 2021).

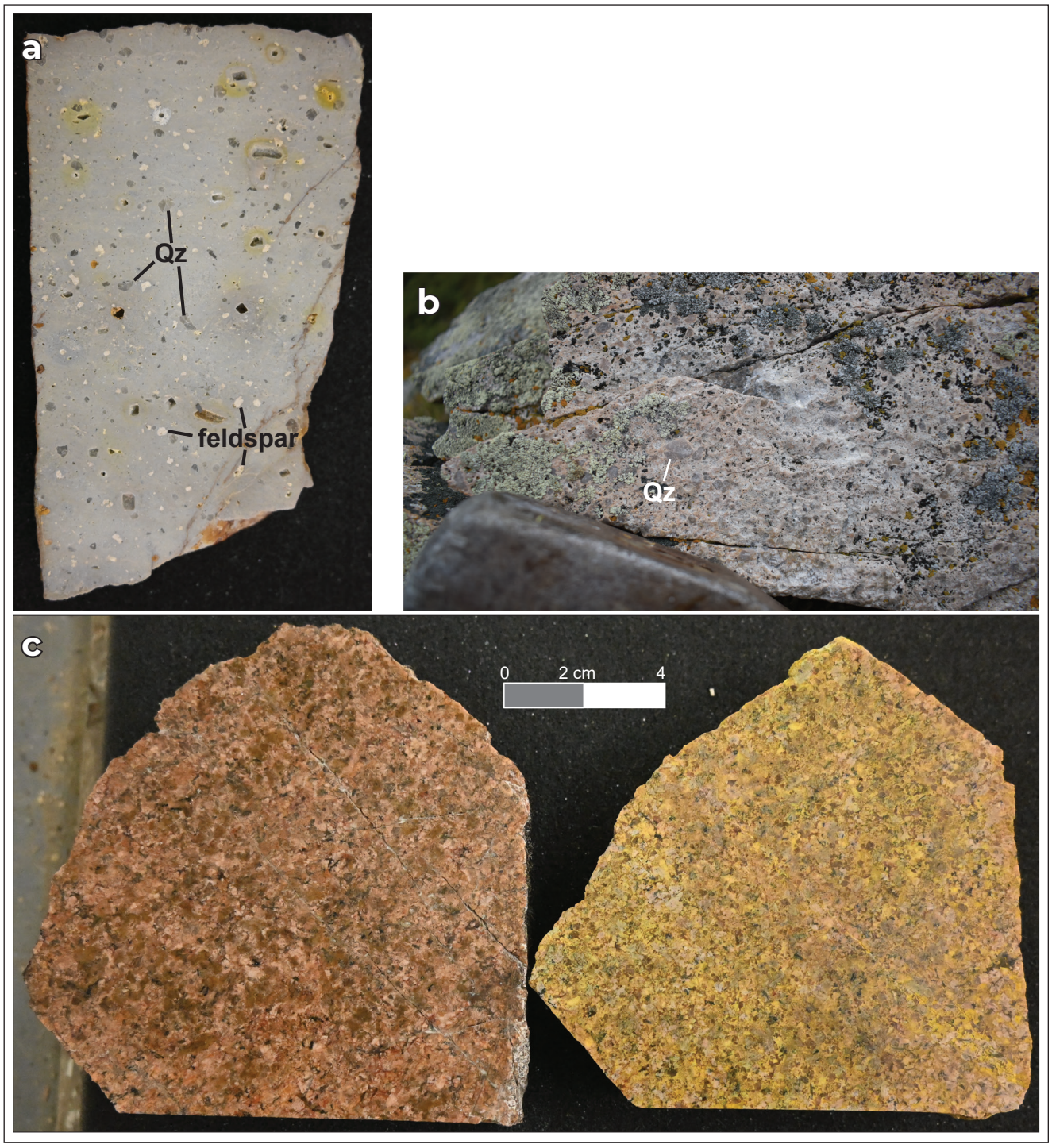


Figure 5. *Representative photos of mid-Cretaceous plutonic rocks in the Mount Nansen area analyzed for U-Pb zircon dating at Boise State University.* ***(a)*** *20PS218-1, cobaltinitrite stained slab of silica and clay altered quartz-plagioclase porphyritic rock from Dickson hill; 111 Ma. Slight yellow stain of feldspars indicate they are plagioclase.* ***(b)*** *20PS190-1, outcrop of quartz-feldspar porphyritic granite from the central phase of the Bow Creek pluton; 107.86 Ma.* ***(c)*** *20PS194-1, polished (L) and sodium cobaltinitrite stained (R) slabs of the border phase of the Bow Creek pluton, same phase as 20PS195-1 which has been dated in this study at 107.96 Ma. All photos are the same scale.*



Figure 6. *Representative photos of plutonic rocks in the Mount Nansen area analyzed for U-Pb zircon dating at Memorial University.* **(a)** *2010vb0046, medium-grained hornblende-biotite granodiorite of the Dawson Range batholith, country rock to the Klaza deposit; 107.0 Ma.* **(b)** *2010vb0047, mineralized feldspar porphyritic dike crosscutting the Dawson Range batholith at the Klaza deposit.* **(c)** *2010vb0055, deformed K-feldspar porphyritic hornblende granodiorite of the Minto suite, country rock to the Brown-McDade deposit.* **(d)** *2010vb0056, brecciated feldspar porphyritic dike crosscutting Minto suite granodiorite at the Brown-McDade pit. Centimetre graduations on scale card in each photo.*

More voluminous throughout the Mount Nansen area are a series of small, equigranular, hornblende ± pyroxene microdiorite plugs (Fig. 7a). The best exposure of this unit is in the vicinity of Slate Creek immediately south of the Klaza deposit (Fig. 2). The unit was originally recognized in early mapping (Sawyer and Dickinson, 1976) but was thought to be related to mid-Cretaceous magmatism (Sack *et al.*, 2021). Sack *et al.*, 2022 report a *ca.* 78 Ma age for the Kelly plug confirming it is coeval with the Casino suite and is likely related to the Kelly porphyry system (115I 156, 157) as Sack *et al.*, 2022 report Re-Os molybdenite ages between 81 and 76 Ma. The magnetic susceptibility of Casino suite dikes ranges from 0.32 to 0.04 × 10³ SI units with a median value of 0.05, the microdiorite plugs range from 50.7 to 18.9 × 10³ SI units with a median value of 18.95 (Table 1).

Carmacks group

The Carmacks group volcanic rocks are the youngest widespread rocks in the Mount Nansen area and are primarily preserved in the northeastern part of the area (Fig. 2). A crude stratigraphy is recognized in the Mount Nansen area with a basal felsic unit overlain by a lower andesite and capped by upper basalt flows, the most regionally extensive unit (Carlson, 1987). In the Mount Nansen area, this stratigraphy can be seen on the south side of Rowlinson Creek and the headwaters of Bow Creek (Fig. 2). Based on K-Ar and Ar-Ar dates outside the Mount Nansen area, Carmacks group rocks were deposited between 73 and 68 Ma (Grond *et al.*, 1984; Joyce *et al.*, 2015).

Felsic volcanic rocks (LKfC)

The basal felsic unit is an alkalic rhyolite crystal tuff with 5–10% quartz and feldspar shards, and 1–2% tabular biotite. The unit is flaggy, weathers pale pink and is light grey on fresh surfaces. The groundmass is very fine grained and potassic (Fig. 7b,c). The magnetic susceptibility of Carmacks group felsic rocks ranges from 0.97 to 0.08 × 10³ SI units with a median value of 0.14 (Table 1).

Intermediate volcanic rocks (uKC)

The lower andesitic rocks outcrop on the margins of the basalt unit and are primarily tuff and volcanic breccia with a phenocryst assemblage of plagioclase, hornblende and rarely pyroxene (Carlson, 1987). These rocks typically weather pink to red to reddish-brown and are grey to green on fresh surfaces (Carlson, 1987).

Mafic volcanic rocks (uKC)

These are the most regionally extensive rocks in the Carmacks group (Ryan *et al.*, 2013, 2016) and are pyroxene ± olivine porphyritic basalt flows that weather dark red to brown and are dark green on fresh surfaces (Fig. 7d). The magnetic susceptibility of Carmacks group basalt ranges from 15.1 to 8.01 × 10³ SI units with a median value of 10.7 (Table 1).

Prospector Mountain suite

Felsic plutonic rocks (LKfxPp)

Felsic rocks of Prospector Mountain suite age (72 to 68 Ma) are primarily found near the Cyprus porphyry body near the East Fork of Nansen Creek (Fig. 2). The Cyprus porphyry is an intrusive breccia complex with light grey to orange-weathered, heterolithic, clast-supported breccia containing subangular to rounded sand to pebble-sized clasts of light grey porphyritic rock in a fine-grained cream to pink matrix. It is locally quartz-sericite-pyrite altered (Sawyer and Dickinson, 1976). Porphyry mineralization is associated with the Cyprus porphyry and includes chalcopyrite-pyrite ± molybdenite stockwork veining at *ca.* 71 Ma (Selby *and Creaser,* 2001; Lee, 2021). The magnetic susceptibility of felsic Prospector Mountain rocks ranges from 19.4 to 0.03 × 10³ SI units with a median value of 0.14 (Table 1).

Mafic plutonic rocks (LKdP)

Mafic plutonic rocks of the Prospector Mountain suite are pyroxene ± biotite porphyritic monzodiorite to monzogabbro. They are brown to black on weathered and fresh surfaces and are massive, medium grained and melanocratic with an alkali groundmass (Fig. 7e,f). These plugs are best recognized south of Rowlinson Creek where they intrude Carmacks group basalt (Fig. 2).

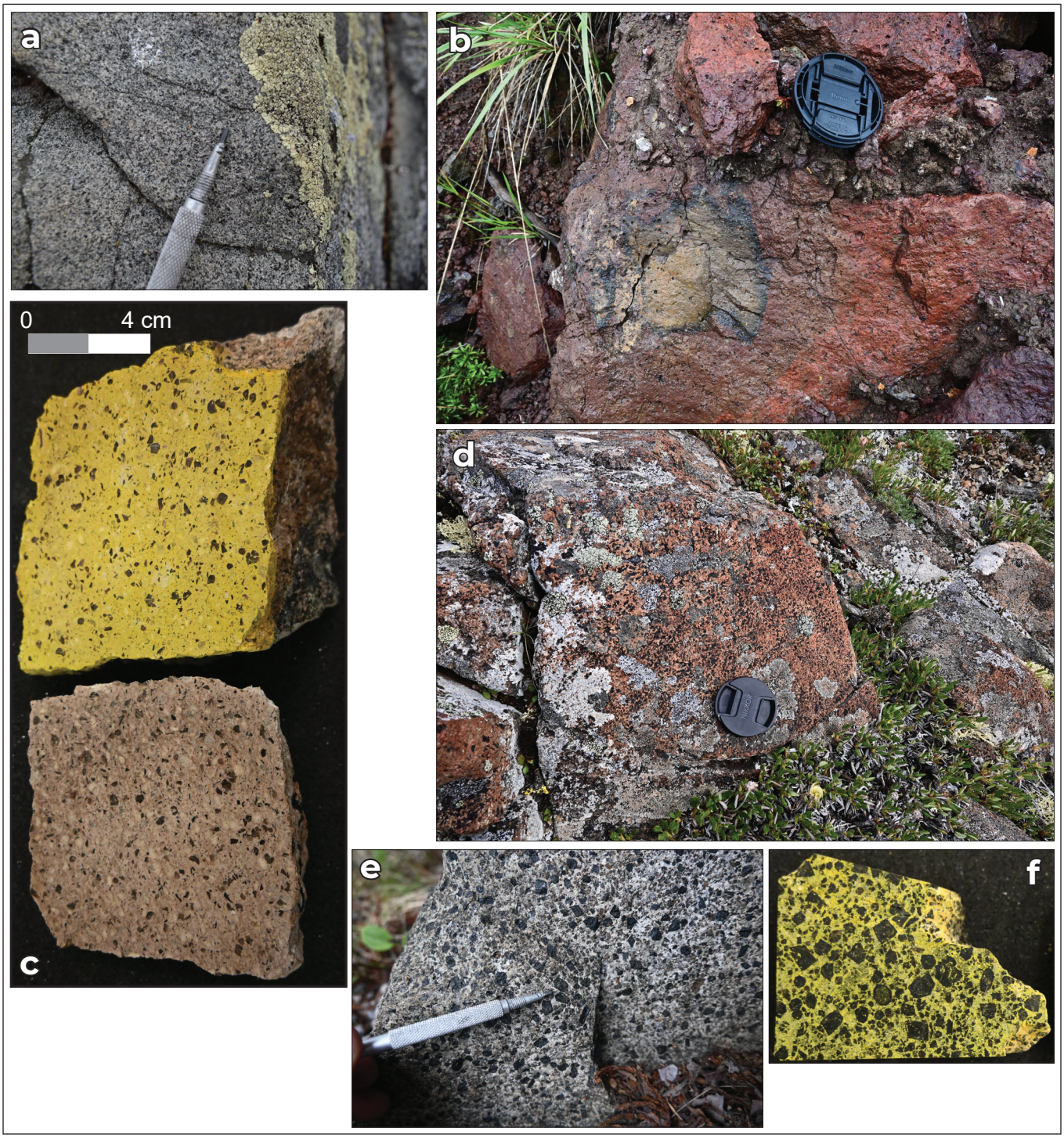


Figure 7. *Representative photos of Late Cretaceous rocks in the Mount Nansen area.* ***(a)*** *19PS046, weathered surface of microdiorite from the Kelly plug; this body has a crystallization age of 78.11 ± 0.03 Ma (Sack et al., 2022). Scribe for scale.* ***(b)*** *20PS004, weathered outcrop of intermediate to felsic volcanic breccia near the base of the Carmacks Group. Lens cap is 5 cm in diameter.* ***(c)*** *20PS161-1, sodium cobaltinitrite stained (upper) and polished (lower) slabs of alkalic crystal tuff from the lower Carmacks Group.* ***(d)*** *20PS024, red-brown weathered outcrop of olivine-pyroxene basalt from the upper (main) Carmacks Group. Lens cap is 5 cm in diameter.* ***(e)*** *20PS002, coarse-grained pyroxene-phyric gabbro that intrudes basalt of the Carmacks Group. Scribe for scale.* ***(f)*** *20PS002-1, sodium cobaltinitrite stained slab of coarse-grained pyroxene-phyric gabbro showing the alkalic nature (yellow) of the groundmass. Same scale as* ***(c)***.

The magnetic susceptibility of mafic Prospector Mountain rocks ranges from 20.7 to 0.2 × 10³ SI units with a median value of 6.49 (Table 1). These rocks are equivalent to unit uKCg of Colpron et *al.* (2007) 60 km to the east where they have a biotite K-Ar cooling age of *ca.* 68 Ma (Grond et *al.*, 1984), an age which is consistent with these plugs locally intruding Carmacks group basalt.

Paleogene igneous rocks

Rhyolite Creek dikes (PRc)

Rhyolite Creek rocks are more commonly recognized to the west of the Mount Nansen area, but porphyritic, tan to cream, locally flow banded, rhyolite dikes and sills with smoky quartz ± feldspar phenocrysts are mapped along the western part of the area (Ryan et *al.*, 2016). These rocks are *ca.* 58 Ma (Ryan et *al.*, 2016).

Methods

U-Pb zircon geochronology

Boise State University

Three mid-Cretaceous plutonic samples underwent U-Pb zircon geochronological analysis at Boise State University using a method similar to that described in Sack et *al.* (2020). This method includes reconnaissance laser ablation-inductively coupled plasma mass spectrometer (LA-ICPMS) analyses of a relatively large number of crystals per sample (up to 51 in this study) to characterize zircon populations followed by chemical abrasion-thermal ionization mass spectrometry (CA-TIMS) analysis of 5 or 6 crystals from the youngest coherent population. Appendix 2 includes a detailed description of the analytical method, cathodoluminescence (CL) images of zircon with located laser spots, as well as results of LA-ICPMS

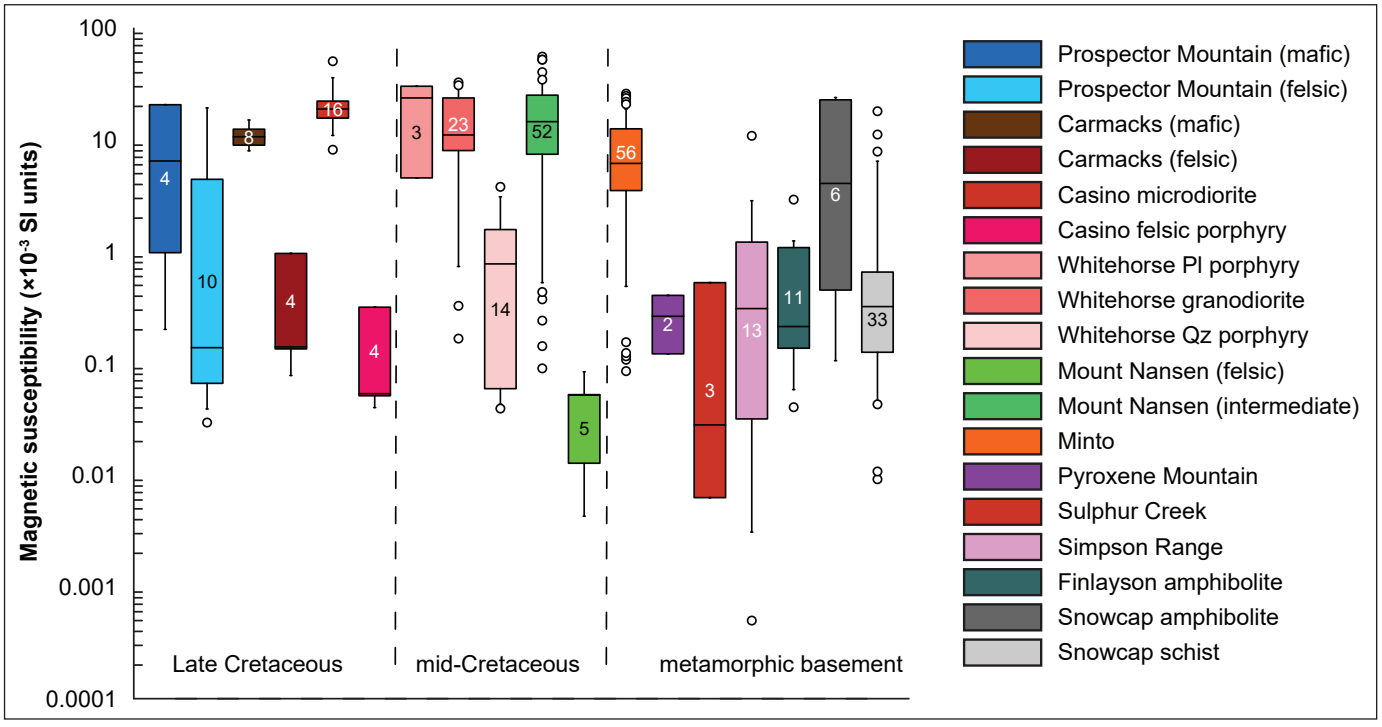


Figure 8. *Box-whisker plot of magnetic susceptibility data for rocks in the Mount Nansen area. Data in Appendix 1 and summarized in Table 1. Whiskers are 10th and 90th percentile, box edges are 25th and 75th percentile and centre line within box is median of data; small white circles represent outlier data. Number within each box is the number of stations with data. Magnetic susceptibility at each station is the average of five measurements over a 1 to 2 m² area within the same lithology.*

and CA-TIMS analyses. For two samples, we use the more precise weighted mean date of CA-TIMS analyses to determine the crystallization age of samples. For sample 19PS004-1, only nine crystals were recovered during separation and only LA-ICPMS analyses were conducted; for this sample the weighted mean date of LA-ICPMS data is used to determine the crystallization age. All errors are reported at 2σ.

Memorial University

Five plutonic samples underwent U-Pb zircon geochronological analysis at Memorial University following the method described by Bennett and Tubrett (2010). This is a LA-ICPMS method that utilizes line ablation with a 10 µm or 20 µm spot size and ablation of either a 40 µm by 40 µm raster or a line. Backscatter electron (BSE) images of zircon crystals were used to locate homogeneous zones for ablation. Results of LA-ICPMS analysis are included in Appendix 2; representative BSE images of zircon are shown in Figures 12 to 16. All errors are reported at 2σ.

Pb isotope geochemistry

The lead isotopic composition of feldspar from igneous rocks was determined at the Pacific Centre for Isotopic and Geochemical Research at the University of British Columbia. Feldspar separates were washed and dissolved in dilute hydrochloric acid, then prepared and analyzed using the TIMS method described by Mortensen and Gabites (2002). Errors are reported at 2σ. Data are in Table 4.

Results

Geochronology

Table 2 summarizes the new geochronological results for the Mount Nansen area.

Sample 20PS190-1 is a quartz-feldspar porphyritic granite collected from Bow Creek pluton (unit 8c of Carlson, 1987; Fig. 2). It yielded euhedral, concentrically zoned zircons with 2:1 aspect ratios (Fig. 9a).

Table 2. *Summary table of geochronology results.*

Sample	Latitude	Longitude	Pluton/ Location	Lithology	Method	Weighted mean $^{206}Pb/^{238}U$ date (Ma)	± 2δ (Ma)	total n	n in weighted mean	MSWD	pof	Inheritance
20PS190-1	62.156839	-137.252990	Bow Creek	quartz-feldspar porphyritic granite	CA-TIMS	107.86	0.03	5	5	0.80	0.53	none
20PS195-1	62.176095	-137.282900	Bow Creek	biotite granite	CA-TIMS	107.96	0.03	6	6	1.20	0.29	none
19PS004-1	62.053260	-136.167480	Flex knob	quartz-feldspar porphyry	LA-ICPMS	111.00	1.8	7	6	1.02	0.40	1 @ 344 Ma
2010vb0045	62.127500	-137.247167	Klaza trench 09	mineralized feldspar porphyry dike	LA-ICPMS	107.00	0.72	20	20	0.59	0.92	none
2010vb0046	62.127361	-137.247305	Klaza trench 09	hornblende-biotite granodiorite	LA-ICPMS	107.00	0.78	20	20	0.55	0.94	none
2010vb0047	62.117528	-137.248972	Klaza trench 02?	mineralized feldspar porphyry dike	LA-ICPMS	107.50	0.67	25	25	0.39	1.00	none
2010vb0055	62.051444	-137.126167	Brown-McDade pit	deformed hornblende-biotite granodiorite	LA-ICPMS	199.06	0.96	24	23	3.55	0.00	1 @ 340 Ma
2010vb0056	62.051444	-137.126167	Brown-McDade pit	brecciated feldspar porphyry dike	LA-ICPMS	198.74*	1.18	24	21	3.82	0.00	1 @ 76, 1 @ 106 Ma

* calculations for population of Early Jurassic dates from crystals interpreted as inherited

Fifty-one LA-ICPMS spot analyses yielded $^{206}Pb/^{238}U$ dates between 109 and 101 Ma. The weighted mean of all 51 LA-ICPMS dates is 105.53 ± 0.51 Ma (n = 51 of 51; Fig. 9b). Five zircons from 20PS190-1 were analyzed by CA-TIMS and yielded equivalent $^{206}Pb/^{238}U$ dates ranging from 107.90 ± 0.08 to 107.81 ± 0.08 Ma (Table 2), with a weighted mean age of 107.86 ± 0.03 Ma (MSWD = 0.8, n = 5; Fig. 9c; Table 2). This is the best estimate of the crystallization age for this phase of the Bow Creek pluton.

Sample 20PS195-1 is a quartz-feldspar porphyritic biotite granite collected from Bow Creek pluton (unit 8b of Carlson, 1987; Fig. 2). It yielded euhedral, concentrically zoned zircons with 2:1 aspect ratios (Fig. 10a). Thirty-three LA-ICPMS spot analyses yielded $^{206}Pb/^{238}U$ dates between 113 and 100 Ma. The weighted mean of all 33 LA-ICPMS dates is 104.74 ± 0.60 Ma (n = 33 of 33; Fig. 10b). Six zircons from 20PS195-1 were analyzed by CA-TIMS and yielded equivalent $^{206}Pb/^{238}U$ dates ranging from 108.02 ± 0.07 to 107.91 ± 0.07 (Table 3), with a weighted mean age of 107.96 ± 0.03 Ma (MSWD = 1.2, n = 6; Fig. 10c; Table 2). This is the best estimate of the crystallization age for this phase of the Bow Creek pluton.

Sample 19PS004-1 is a clay altered quartz-feldspar porphyry collected from north end of the Flex deposit and is interpreted to be part of the Dickson plug (Fig. 2). This sample yielded nine subhedral to euhedral, sector

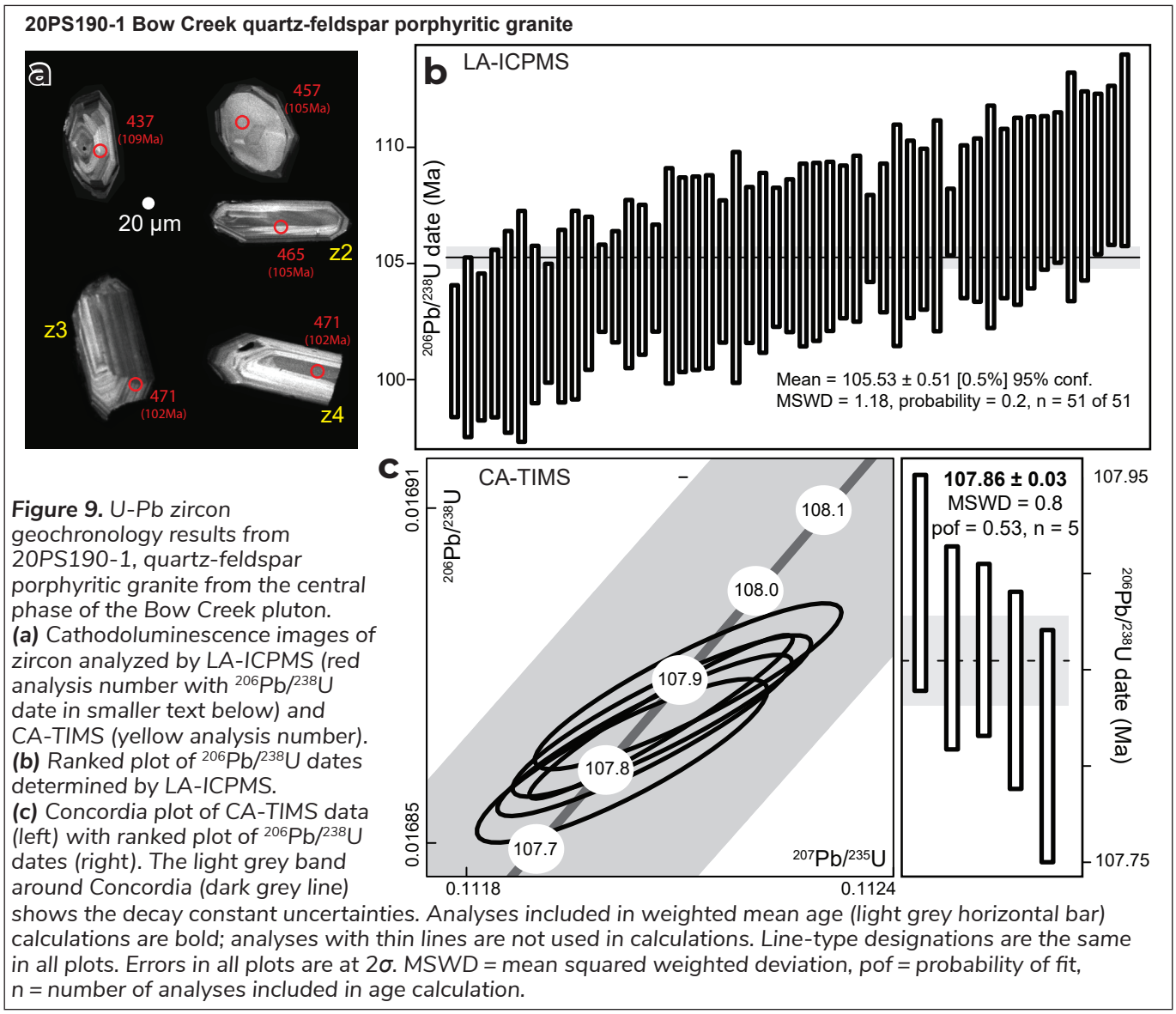


Figure 9. *U-Pb zircon geochronology results from 20PS190-1, quartz-feldspar porphyritic granite from the central phase of the Bow Creek pluton.* ***(a)*** *Cathodoluminescence images of zircon analyzed by LA-ICPMS (red analysis number with $^{206}Pb/^{238}U$ date in smaller text below) and CA-TIMS (yellow analysis number).* ***(b)*** *Ranked plot of $^{206}Pb/^{238}U$ dates determined by LA-ICPMS.* ***(c)*** *Concordia plot of CA-TIMS data (left) with ranked plot of $^{206}Pb/^{238}U$ dates (right). The light grey band around Concordia (dark grey line) shows the decay constant uncertainties. Analyses included in weighted mean age (light grey horizontal bar) calculations are bold; analyses with thin lines are not used in calculations. Line-type designations are the same in all plots. Errors in all plots are at 2σ. MSWD = mean squared weighted deviation, pof = probability of fit, n = number of analyses included in age calculation.*

zoned and weakly concentrically zoned zircons with 1:1 to 2:1 aspect ratios (Fig. 11a). Seven LA-ICPMS spot analyses yielded six $^{206}Pb/^{238}U$ dates between 114 and 108 Ma and one inherited grain at 344 Ma. The weighted mean of the six LA-ICPMS dates is 111.00 ± 1.8 Ma (n = 6 of 7; Fig. 11b; Table 2). Due to the low number of zircon crystals recovered, further CA-TIMS analyses were not done. The weighted mean of the LA-ICPMS dates is the best estimate of the crystallization age of the Dickson plug.

Sample 2010vb0045 is a mineralized feldspar porphyry dike collected from trench 9 at the Klaza deposit (Fig. 2). This sample yielded euhedral, sector zoned and concentrically zoned zircons with 1:1 to 2:1 aspect ratios and bright rims (Fig. 12a). Twenty LA-ICPMS spot analyses yielded $^{206}Pb/^{238}U$ dates between 110 and 103 Ma. The weighted mean of all 20 LA-ICPMS dates is 107.06 ± 0.73 Ma (n = 20 of 20; Fig. 12b; Table 2). The weighted mean of the LA-ICPMS dates is the best estimate of the crystallization age of this dike.

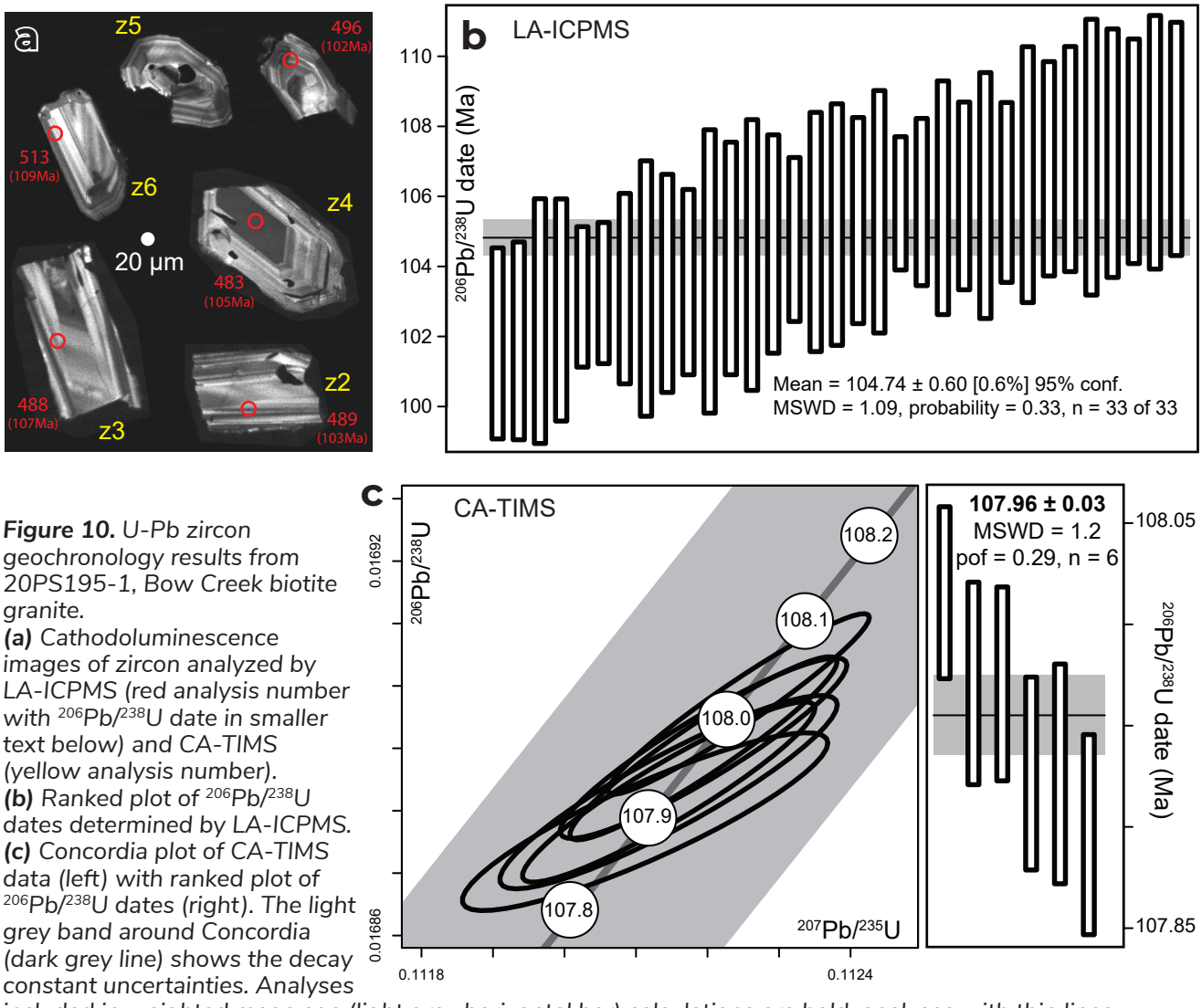


Figure 10. *U-Pb zircon geochronology results from 20PS195-1, Bow Creek biotite granite.*
(a) *Cathodoluminescence images of zircon analyzed by LA-ICPMS (red analysis number with $^{206}Pb/^{238}U$ date in smaller text below) and CA-TIMS (yellow analysis number).*
(b) *Ranked plot of $^{206}Pb/^{238}U$ dates determined by LA-ICPMS.*
(c) *Concordia plot of CA-TIMS data (left) with ranked plot of $^{206}Pb/^{238}U$ dates (right). The light grey band around Concordia (dark grey line) shows the decay constant uncertainties. Analyses included in weighted mean age (light grey horizontal bar) calculations are bold; analyses with thin lines are not used in calculations. Line-type designations are the same in all plots. Errors in all plots are at 2σ. MSWD = mean squared weighted deviation, pof = probability of fit, n = number of analyses included in age calculation.*

Table 3. *CA-TIMS U-Pb zircon data table. The data and calculations for this table are available in Appendix 2.*

										Radiogenic Isotope Ratios								Isotopic Dates						
Sample (a)	Tracer solution	LA-ICPMS spot label	Th/U (b)	$^{206}Pb^*$ x10^{-13} mol (c)	mol % $^{206}Pb^*$ (c)	Pb* (pg) (c)	Pb_c (pg) (c)	Pb*/Pb_c (c)	$^{206}Pb/^{204}Pb$ (d)	$^{208}Pb/^{206}Pb$ (e)	$^{207}Pb/^{206}Pb$ (e)	% err (f)	$^{207}Pb/^{235}U$ (e)	% err (f)	$^{206}Pb/^{238}U$ (e)	% err (f)	corr. coef.	$^{207}Pb/^{206}Pb$ (g)	± (f)	$^{207}Pb/^{235}U$ (g)	± (f)	$^{206}Pb/^{238}U$ (g)	± (f)	include in weighted mean?
20PS190-1																								
z2	BSU1B	465	0.655	0.9527	99.78%	24.72	0.18	140	8123	0.209	0.048290	0.099	0.112337	0.157	0.016880	0.072	0.890	112.43	2.35	108.10	0.16	107.90	0.08	x
z5	BSU1B	473	0.553	1.6862	99.75%	42.62	0.35	122	7237	0.177	0.048257	0.095	0.112225	0.153	0.016874	0.070	0.900	110.82	2.24	108.00	0.16	107.87	0.08	x
z1	BSU1B	461	0.527	2.0283	99.91%	50.91	0.15	330	19726	0.168	0.048264	0.071	0.112239	0.135	0.016874	0.071	0.953	111.19	1.67	108.01	0.14	107.87	0.08	x
z4	BSU1B	471	0.528	1.3363	99.79%	33.55	0.23	143	8544	0.169	0.048231	0.092	0.112137	0.151	0.016870	0.070	0.910	109.56	2.18	107.92	0.15	107.84	0.07	x
z3	BSU1B	470	0.618	1.8798	99.87%	48.32	0.20	244	14255	0.198	0.048209	0.095	0.112054	0.149	0.016865	0.071	0.863	108.49	2.25	107.84	0.15	107.81	0.08	x
20PS195																								
z4	BSU1B	483	0.913	2.8877	99.92%	79.89	0.18	435	23577	0.292	0.048243	0.069	0.112352	0.133	0.016898	0.070	0.959	110.15	1.64	108.11	0.14	108.02	0.07	x
z2	BSU1B	489	0.892	1.3841	99.85%	38.10	0.18	217	11798	0.285	0.048246	0.086	0.112313	0.146	0.016891	0.070	0.923	110.28	2.03	108.08	0.15	107.98	0.08	x
z1	BSU1B	490	0.905	2.1012	99.91%	58.03	0.15	379	20555	0.289	0.048247	0.073	0.112312	0.136	0.016891	0.071	0.945	110.33	1.73	108.08	0.14	107.98	0.08	x
z3	BSU1B	488	0.871	1.1879	99.83%	32.54	0.17	195	10698	0.279	0.048246	0.088	0.112265	0.149	0.016884	0.070	0.927	110.27	2.08	108.03	0.15	107.93	0.08	x
z6	BSU1B	513	1.095	0.7197	99.78%	20.78	0.13	160	8315	0.350	0.048199	0.109	0.112149	0.172	0.016883	0.075	0.910	108.00	2.57	107.93	0.18	107.93	0.08	x
z5	BSU1B	497	0.905	0.6000	99.72%	16.57	0.14	120	6516	0.289	0.048330	0.129	0.112438	0.186	0.016881	0.069	0.888	114.38	3.04	108.19	0.19	107.91	0.07	x

(a) z1, z2, etc. are labels for analyses composed of single zircon grains that were annealed and chemically abraded (Mattinson, 2005).
(b) Model Th/U ratio calculated from radiogenic $^{208}Pb/^{206}Pb$ ratio and $^{207}Pb/^{235}U$ date.
(c) Pb* and Pbc are radiogenic and common Pb, respectively. mol % $^{206}Pb^*$ is with respect to radiogenic and blank Pb.
(d) Measured ratio corrected for spike and fractionation only. Fractionation correction for analyses done with tracer solution BSU1B is 0.16 ± 0.03 (1 sigma) %/amu (atomic mass unit) for single-collector Daly analyses, based on analysis of EARTHTIME ^{202}Pb-^{205}Pb ET2535 tracer solution. Fractionation correction for analyses done with tracer solution ET2535 is based on measurement of $^{202}Pb/^{205}Pb$ in the tracer solution.
(e) Corrected for fractionation and spike. Common Pb in zircon analyses is assigned to procedural blank with composition of $^{206}Pb/^{204}Pb$ = 18.04 ± 0.61%; $^{207}Pb/^{204}Pb$ = 15.54 ± 0.52%; $^{208}Pb/204Pb$ = 37.69 ± 0.63% (1 sigma). $^{206}Pb/^{238}U$ and $^{207}Pb/^{206}Pb$ ratios corrected for initial disequilibrium in $^{230}Th/^{238}U$ using a D(Th/U) of 0.20 ± 0.05 (1 sigma).
(f) Errors are 2 sigma, propagated using algorithms of Schmitz and Schoene (2007) and Crowley et al. (2007).
(g) Calculations based on the decay constants of Jaffey et al. (1971). $^{206}Pb/^{238}U$ and $^{207}Pb/^{206}Pb$ dates corrected for initial disequilibrium in $^{230}Th/^{238}U$ using a D(Th/U) of 0.20 ± 0.05 (1 sigma).

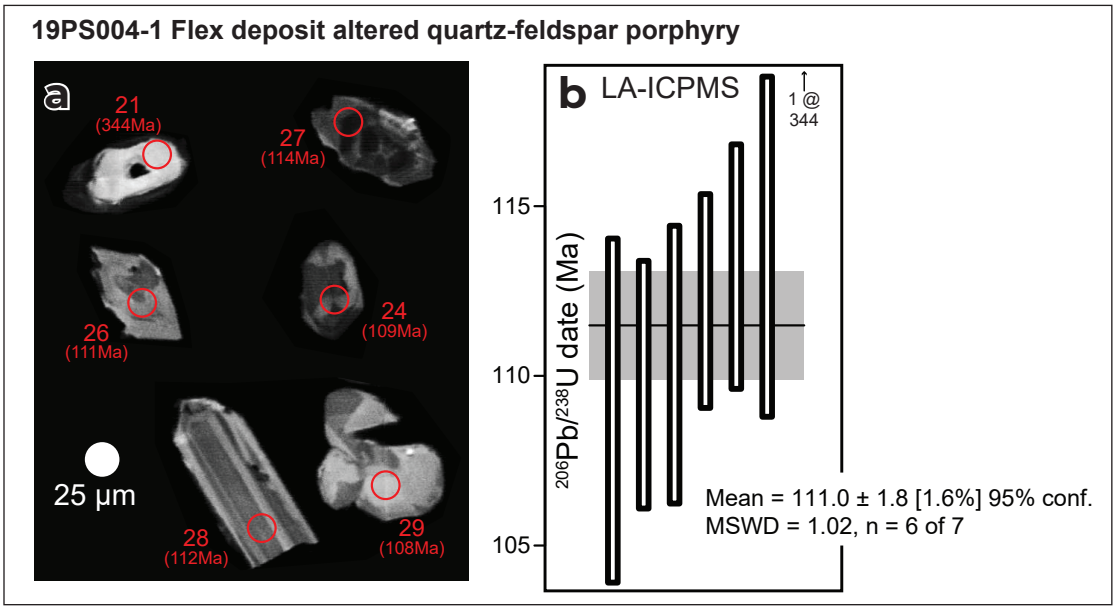


Figure 11. *U-Pb zircon geochronology results from 19PS004-1, Flex plug.* ***(a)*** *Cathodoluminescence images of zircon analyzed by LA-ICPMS (red analysis number with* $^{206}Pb/^{238}U$ *date in smaller text below; open red circle shows approximate location of spot).* ***(b)*** *Ranked plot of* $^{206}Pb/^{238}U$ *dates determined by LA-ICPMS. The light grey band around Concordia (dark grey line) shows the decay constant uncertainties. Analyses included in weighted mean age (light grey horizontal bar) calculations are bold; analyses with thin lines are not used in calculations. Errors are at 2σ. MSWD = mean squared weighted deviation, n = number of analyses included in age calculation.*

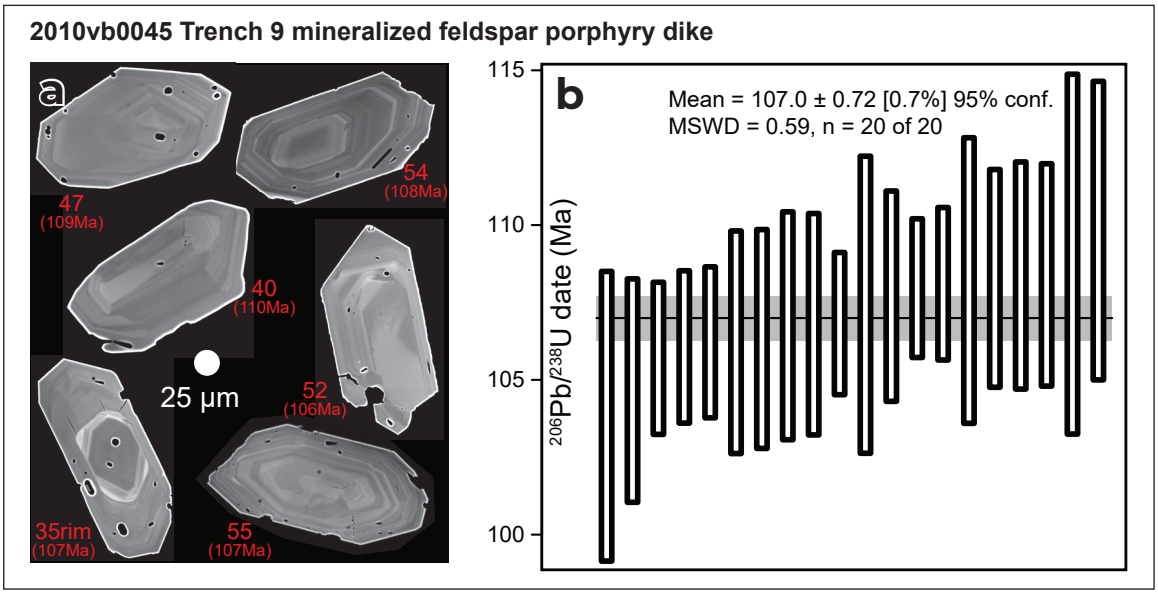


Figure 12. *U-Pb zircon geochronology results from 2010v0045, mineralized feldspar porphyry dike.* ***(a)*** *Backscatter electron (BSE) images of zircon analyzed by LA-ICPMS (red analysis number with 206Pb/238U date in smaller text below).* ***(b)*** *Ranked plot of 206Pb/238U dates determined by LA-ICPMS. The light grey band around Concordia (dark grey line) shows the decay constant uncertainties. Analyses included in weighted mean age (light grey horizontal bar) calculations are bold; analyses with thin lines are not used in calculations. Errors are at 2σ. MSWD = mean squared weighted deviation, n = number of analyses included in age calculation.*

Sample 2010vb0046 is hornblende-biotite granodiorite collected from trench 9 at the Klaza deposit (Fig. 2). It is the country rock to the mineralized feldspar porphyry dike sampled at 2010vb0045 and is part of the Dawson Range batholith. Sample 2010vb0046 yielded euhedral, sector zoned and concentrically zoned zircons with 1:1 to 2:1 aspect ratios and bright rims (Fig. 13a). Twenty LA-ICPMS spot analyses yielded $^{206}Pb/^{238}U$ dates between 109 and 105 Ma. The weighted mean of all 20 LA-ICPMS dates is 107.00 ± 0.78 Ma (n = 20 of 20; Fig. 13b; Table 2). The weighted mean of the LA-ICPMS dates is the best estimate of the crystallization age of this part of the Dawson Range batholith.

Sample 2010vb0047 is a mineralized feldspar porphyry dike collected from trench 2 at the Klaza deposit (Fig. 2). This sample yielded euhedral, sector zoned and concentrically zoned zircons with 1:1 to 2:1 aspect ratios and bright rims (Fig. 14a). Twenty-five LA-ICPMS spot analyses yielded $^{206}Pb/^{238}U$ dates between 110 and 105 Ma. The weighted mean of all 20 LA-ICPMS dates is 107.60 ± 0.71 Ma (n = 25 of 25; Fig. 14b; Table 2). The weighted mean of the LA-ICPMS dates is the best estimate of the crystallization age of this dike.

Sample 2010vb0055 is a foliated hornblende-biotite granodiorite collected from the Brown-McDade pit (Fig. 2). It is the country rock to the mineralized feldspar porphyry dike sampled at 2010vb0056 and is part of the Victoria Creek stock. Sample 2010vb0055 yielded euhedral, sector zoned and concentrically zoned zircons with 1:1 to 4:1 aspect ratios and bright rims (Fig. 15a). Twenty-four LA-ICPMS spot analyses yielded 23 $^{206}Pb/^{238}U$ dates between 215 and 182 Ma and one at 340 Ma. The weighted mean of 19 LA-ICPMS dates is 199.06 ± 0.96 Ma (n = 19 of 24; Fig. 15b; Table 2). The weighted mean of the LA-ICPMS dates is the best estimate of the crystallization age of the Victoria Creek stock.

Sample 2010vb0056 is a mineralized and brecciated feldspar porphyry dike collected from the Brown-McDade pit (Fig. 2). This sample yielded euhedral, sector zoned and concentrically zoned zircons with 1:1 to 2:1 aspect ratios and bright rims (Fig. 16a). Twenty-four LA-ICPMS spot analyses yielded $^{206}Pb/^{238}U$ dates between 213 and 74 Ma. The oldest grain is interpreted as a xenocryst and excluded from age calculations.

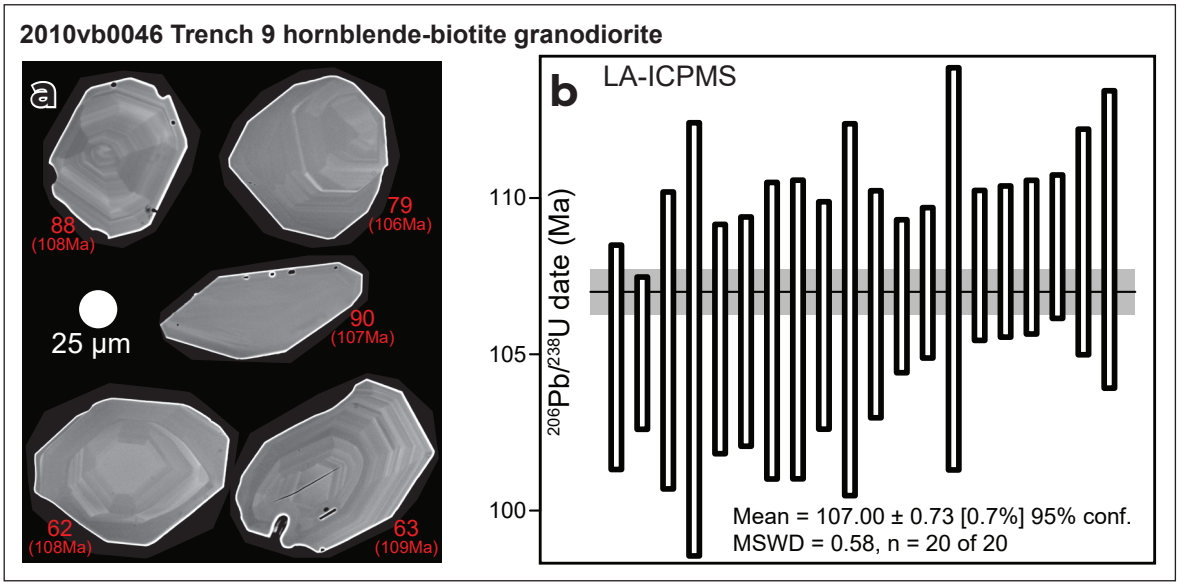


Figure 13. *U-Pb zircon geochronology results from 2010v0046, hornblende-biotite granodiorite.* ***(a)*** *BSE images of zircon analyzed by LA-ICPMS (red analysis number with $^{206}Pb/^{238}U$ date in smaller text below).* ***(b)*** *Ranked plot of $^{206}Pb/^{238}U$ dates determined by LA-ICPMS. The light grey band around Concordia (dark grey line) shows the decay constant uncertainties. Analyses included in weighted mean age (light grey horizontal bar) calculations are bold; analyses with thin lines are not used in calculations. Errors are at 2σ. MSWD = mean squared weighted deviation, n = number of analyses included in age calculation.*

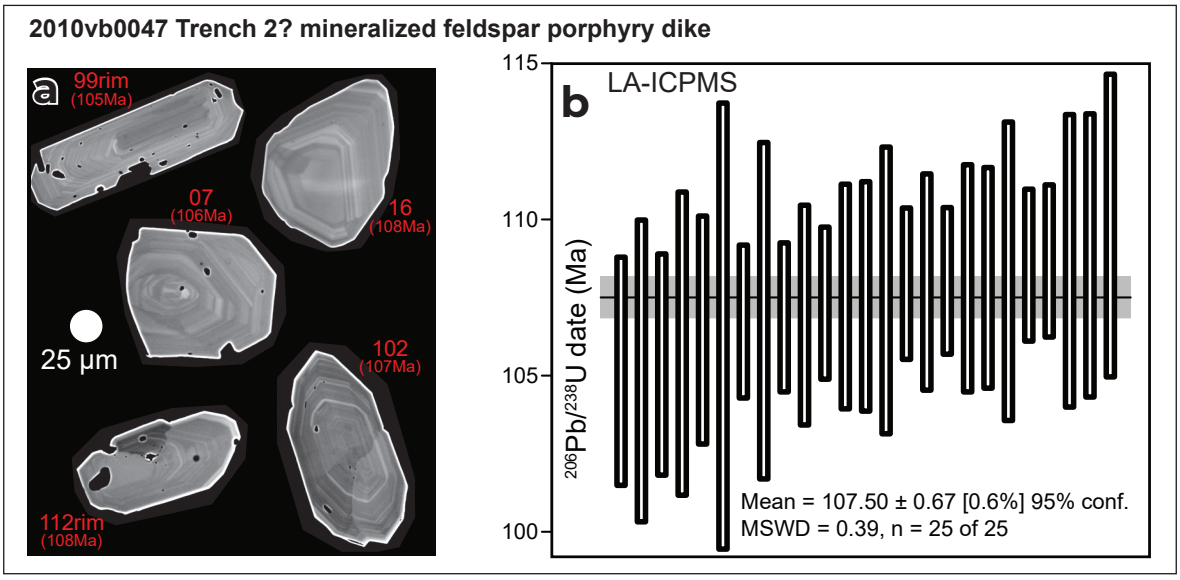


Figure 14. *U-Pb zircon geochronology results from 2010v0047, mineralized feldspar porphyry dike.* **(a)** *BSE images of zircon analyzed by LA-ICPMS (red analysis number with $^{206}Pb/^{238}U$ date in smaller text below).* **(b)** *Ranked plot of $^{206}Pb/^{238}U$ dates determined by LA-ICPMS. The light grey band around Concordia (dark grey line) shows the decay constant uncertainties. Analyses included in weighted mean age (light grey horizontal bar) calculations are bold; analyses with thin lines are not used in calculations. Errors are at 2σ. MSWD = mean squared weighted deviation, n = number of analyses included in age calculation.*

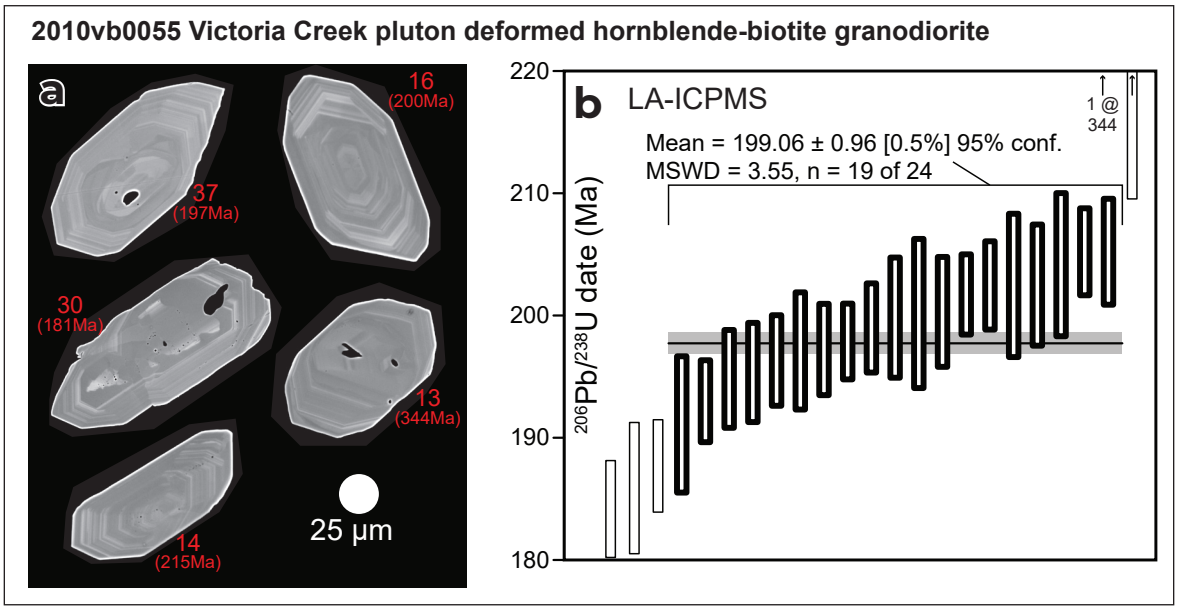


Figure 15. *U-Pb zircon geochronology results from 2010v0055, foliated hornblende-biotite granodiorite from the Brown-McDade pit.* **(a)** *BSE images of zircon analyzed by LA-ICPMS (red analysis number with $^{206}Pb/^{238}U$ date in smaller text below).* **(b)** *Ranked plot of $^{206}Pb/^{238}U$ dates determined by LA-ICPMS. The light grey band around Concordia (dark grey line) shows the decay constant uncertainties. Analyses included in weighted mean age (light grey horizontal bar) calculations are bold; analyses with thin lines are not used in calculations. Errors are at 2σ. MSWD = mean squared weighted deviation, n = number of analyses included in age calculation.*

The significance of two young grains at 106 and 74 Ma is unclear but leaves open the possibility that the dike is as young as Late Cretaceous (ca. 74 Ma). The weighted mean of 21 LA-ICPMS dates is 198.74 ± 1.18 Ma (n = 21 of 24; Fig. 16b; Table 2).The weighted mean of the LA-ICPMS dates is the best estimate of the population of inherited grains that make up the majority of grains recovered from this dike.

Pb isotopes

Radiogenic Pb isotopes ^{206}Pb, ^{207}Pb and ^{208}Pb were analyzed from feldspar from six igneous samples and are reported in Table 4; five samples are plutonic and one is volcanic. Two plutonic samples are Late Triassic to Early Jurassic and the rest of the samples are mid-Cretaceous. The two Late Triassic to Early Jurassic samples have $^{206}Pb/^{204}Pb$ values ranging from 18.960 to 18.846, $^{207}Pb/^{204}Pb$ values ranging from 15.681 to 15.600, and $^{208}Pb/^{204}Pb$ values ranging from 38.859 to 38.548. Sample 20PS218-1 was analyzed three times and is from the mid-Cretaceous Dickson Hill plug (Fig. 2) immediately north of the Flex deposit and has consistently high results with $^{206}Pb/^{204}Pb$ values ranging from 26.800 to 25.825, $^{207}Pb/^{204}Pb$ values ranging from 16.050 to 15.921, and $^{208}Pb/^{204}Pb$ values ranging from 44.474 to 42.139. The remaining three mid-Cretaceous samples, including one duplicate, have $^{206}Pb/^{204}Pb$ values ranging from 19.351 to 19.225, $^{207}Pb/^{204}Pb$ values ranging from 15.728 to 15.634, and $^{208}Pb/^{204}Pb$ values ranging from 39.462 to 38.923.

Discussion

The geology of the Mount Nansen area is presented here using geochronologic evidence to establish the age of events and Pb isotopic evidence to discuss metal sources of mineralizing fluids. For magmatic events, U-Pb zircon are considered the most robust chronometer (closure temperature >700˚C and resistant to subsequent alteration; Hodges, 2014) with CA-TIMS ages the most precise; in a few cases LA-ICPMS ages are the best data available and we use those. For mineralization, Re-Os TIMS ages of molybdenite are considered the best estimate as the closure temperature is relatively high (500 to 300˚C; Suzuki *et al.*, 1996) and the Re-Os system within

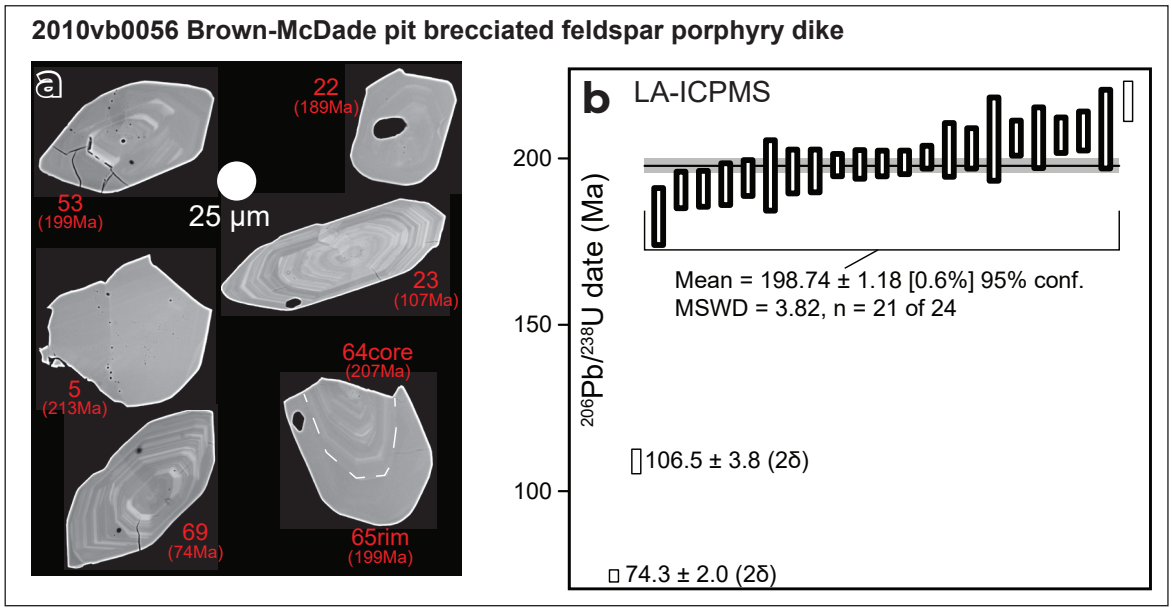


Figure 16. *U-Pb zircon geochronology results from 2010v0056, brecciated feldspar porphyry dike from the Brown-McDade pit.* ***(a)*** *BSE images of zircon analyzed by LA-ICPMS (red analysis number with $^{206}Pb/^{238}U$ date in smaller text below).* ***(b)*** *Ranked plot of $^{206}Pb/^{238}U$ dates determined by LA-ICPMS. The light grey band around Concordia (dark grey line) shows the decay constant uncertainties. Analyses included in weighted mean age (light grey horizontal bar) calculations are bold; analyses with thin lines are not used in calculations. Errors are at 2σ. MSWD = mean squared weighted deviation, n = number of analyses included in age calculation.*

Table 4. *Lead isotope data table.*

Sample	Pluton/ Location	Suite	Lithology	Age (Ma)	Age control	Latitude	Longitude	Mineral
20PS218-1	Dickson plug	Whitehorse	quartz ± feldspar porphyry	111	estimated	62.05655	-137.15871	feldspar-sericite
20PS218-1	Dickson plug	Whitehorse	quartz ± feldspar porphyry	111	estimated	62.05655	-137.15871	feldspar-sericite
20PS218-1	Dickson plug	Whitehorse	quartz ± feldspar porphyry	111	estimated	62.05655	-137.15871	feldspar-quartz
20PS195-1	Bow Creek granite	Whitehorse	quartz-feldspar porphyritic biotite granite	108	dated	62.17610	-137.28290	feldspar
19PS005-1	Klaza	Minto	hornblende ± biotite granodiorite	197	estimated	62.13802	-137.21842	feldspar
19PS024-1	Klaza	Minto	hornblende ± biotite granodiorite	198	estimated	62.13970	-137.20445	feldspar
19PS070-1	Mount Victoria	Mount Nansen	plagioclase-pyroxene porphyrytic andesite	115	estimated	62.11907	-137.17357	feldspar
KL15-291-208m	Klaza hill	Whitehorse	biotite-hornblende granodiorite	107	estimated	62.12315	-137.27227	feldspar
KL15-291-208m	Klaza hill	Whitehorse	biotite-hornblende granodiorite	108	estimated	62.12315	-137.27227	feldspar

Table 4 *continued.*

Sample	$^{206}Pb/^{204}Pb$	Error absolute	Error (%; 2δ)	$^{207}Pb/^{204}Pb$	Error absolute	Error (%; 2δ)	$^{208}Pb/^{204}Pb$	Error absolute	Error (%; 2δ)	$^{207}Pb/^{206}Pb$	Error absolute	Error (%; 2δ)	$^{208}Pb/^{206}Pb$	Error absolute	Error (%; 2δ)
20PS218-1	26.800	0.0110	0.04	16.050	0.0049	0.03	42.267	0.0178	0.04	0.5989	0.0002	0.027	1.5772	0.0002	0.010
20PS218-1	25.824	0.2421	0.94	15.921	0.0877	0.55	44.474	0.5053	1.14	0.6165	0.0047	0.759	1.7222	0.0111	0.642
20PS218-1	26.691	0.0926	0.35	15.969	0.0536	0.34	42.139	0.1876	0.45	0.5983	0.0006	0.093	1.5788	0.0044	0.279
20PS195-1	19.351	0.0053	0.03	15.728	0.0037	0.02	39.280	0.0122	0.03	0.8128	0.0001	0.014	2.0298	0.0003	0.015
19PS005-1	18.960	0.0034	0.02	15.681	0.0027	0.02	38.859	0.0082	0.02	0.8271	0.0000	0.006	2.0496	0.0002	0.011
19PS024-1	18.846	0.0014	0.01	15.600	0.0010	0.01	38.548	0.0030	0.01	0.8277	0.0000	0.004	2.0454	0.0001	0.003
19PS070-1	19.265	0.0027	0.01	15.659	0.0017	0.01	39.151	0.0061	0.02	0.8128	0.0001	0.008	2.0323	0.0001	0.007
KL15-291-208m	19.305	0.0118	0.06	15.692	0.0089	0.06	39.462	0.0248	0.06	0.8128	0.0002	0.023	2.0441	0.0003	0.016
KL15-291-208m	19.225	0.0044	0.02	15.634	0.0032	0.02	38.923	0.0111	0.03	0.8132	0.0001	0.010	2.0246	0.0003	0.017

molybdenite is relatively resistant to subsequent alteration (Stein *et al.*, 2001). We use hydrothermal minerals with lower closure temperatures (Ar-Ar in mica and feldspar and U-Pb in calcite) as chronometers of waning hydrothermal activity, typically these are several m.y. younger than Re-Os molybdenite ages from the same system (*e.g.*, Selby *et al.*, 2002). We refer to interpreted ages subsequently using magmatic, mineralization and hydrothermal designations. The Pb isotopic composition of igneous feldspar is generally thought to be similar to that of sulphides genetically related to their causative intrusion, assuming closed system behavior, which can be useful for interpreting metal sources and fluid interaction in porphyry systems (Tosdal *et al.*, 1999).

Magmatism

The U-Pb zircon data presented here help refine the magmatic ages of Late Triassic to Early Jurassic and mid-Cretaceous igneous rocks in the Mount Nansen area (Table 2; Fig. 17). The Mount Nansen area records four main magmatic episodes, from oldest youngest these are:

1. Paleozoic: Simpson Range metaplutonic suite (365 to 350 Ma) and Finlayson assemblage (351 to 344 Ma) and Sulphur Creek (264 to 252 Ma) metaplutonic suite;
2. Late Triassic to Early Jurassic: Pyroxene Mountain (220 to 214 Ma), Minto (205 to 194 Ma) and Long Lake (188 to 184 Ma) suites;
3. Mid-Cretaceous: Mount Nansen group (115 to 107 Ma) and Whitehorse suite (111 to 105 Ma); and
4. Late Cretaceous: Casino suite (78 to 74 Ma), Carmacks group (73 to 68 Ma) and Prospector Mountain suite (72 to 68 Ma).

The sample of deformed hornblende-biotite granodiorite collected from the Brown-McDade pit is 199.06 ± 0.96 Ma, within the range of the Minto suite regionally (205–194 Ma; Sack *et al.*, 2020). The second sample from the Brown-McDade pit is a quartz-feldspar porphyry, similar to both the mid and Late Cretaceous dikes seen near the Flex and Klaza deposits. The vast majority of the zircons in the sample are inherited, and based on the 198.74 ± 1.18 Ma weighted mean age using 21 of 24 grains, are sourced primarily from Minto suite country rock. A single grain at 106 Ma and another at 74 Ma can't be interpreted with confidence, but likely indicate the dike is Cretaceous; refining further to the mid or Late Cretaceous is not possible with our data.

Our new LA-ICPMS U-Pb zircon 111 ± 1.8 Ma age for the Dickson Hill plug and the similar quartz-feldspar porphyritic texture between the plug and mineralized dikes within core from the Flex deposit confirm a mid-Cretaceous age for these rocks as suggested by Mortensen *et al.* (2016). Our two CA-TIMS ages of 107.86 ± 0.03 Ma and 107.96 ± 0.03 Ma for the core and border phases, respectively, of the Bow Creek granite refine the mid-Cretaceous crystallization age of that body. At the Klaza deposit, the medium-grained biotite granodiorite of the Mount Nansen pluton and associated feldspar porphyry dikes, are all coeval with crystallization ages between 107.17 and 106.22 Ma (including errors; Table 2). Mid-Cretaceous magmatic rocks represent a volcanic complex with Mount Nansen andesite at the base, intruded by high-level plugs and dikes such as those seen on Dickson Hill and the border phase of the Bow Creek granite. Subsequently, the more voluminous Dawson Range granodiorite phase intruded the volcanic pile, again at high crustal levels as suggested by the associated porphyritic dikes at the Klaza deposit.

We don't report any new Late Cretaceous ages here for the Mount Nansen area, but recent work by Mortensen *et al.* (2016) and Lee (2021); Sack *et al.*, 2022 demonstrate that in the Klaza cluster there are both Casino (78–74 Ma) and Prospector Mountain (72–68 Ma) age magmatic rocks. The Kelly porphyry, best exposed near Slate Creek, has a crystallization age of a *ca.* 78 Ma, whereas the Cyprus porphyry immediately east of the Kelly porphyry and best exposed near the headwaters of the East Fork of Nansen Creek, has a U-Pb zircon crystallization age of *ca.* 71 Ma.

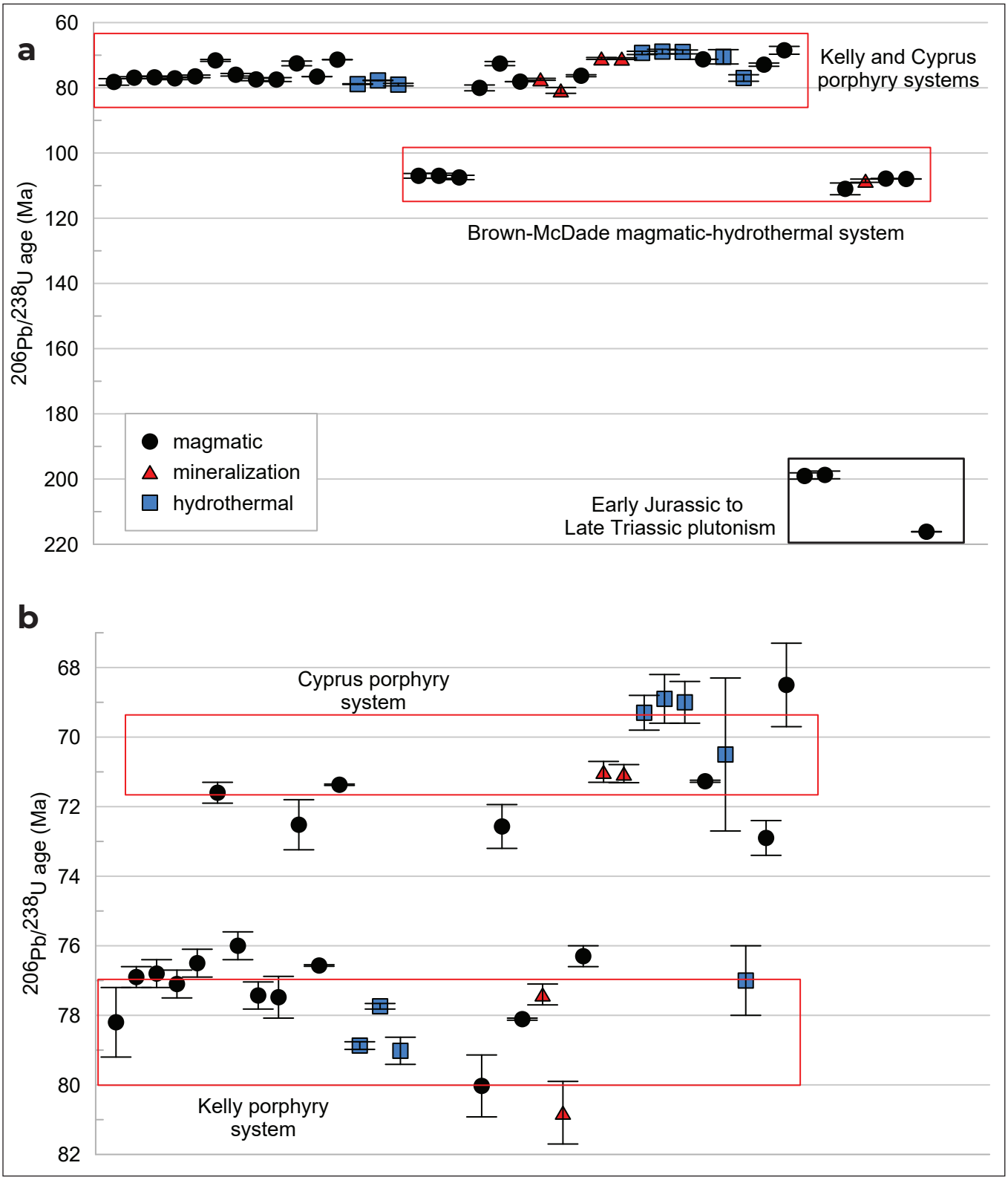


Figure 17. *Geochronology summary for the Mount Nansen area, not shown are Paleozoic ages for the ca. 365 to 350 Ma Simpson Range and ca. 264 to 252 Ma Sulphur Creek metaplutonic suites. Data plotted are from Mortensen et al. (2016), Joyce et al. (2015, 2020), Lee (2021) and this study. Ages symbolized by interpreted process; magmatic primarily U-Pb zircon analyses, mineralization Re-Os molybdenite analyses, hydrothermal U-Pb calcite and Ar-Ar muscovite. Error bars are 2δ. (a) Late Triassic to Late Cretaceous data. (b) Late Cretaceous data.*

Mineralization

A single MINFILE occurrence, Lucky Joe (115O 051), is associated with Paleozoic metaplutonic rocks of the Simpson Range 160 km northwest of the Mount Nansen area (Mortensen and Friend, 2020). Mineralization at Lucky Joe was ca. 352 to 333 Ma and mineralized rocks are clearly deformed (Mortensen and Friend, 2020). The Simpson Range metaplutonic suite is broadly coeval and cospatial with layered rocks of the Finlayson assemblage suggesting that these rocks were emplaced and deposited at an upper crustal level where porphyry system formation was possible. Furthermore, Simpson Range and Finlayson rocks are interpreted as having formed in an arc environment above a subduction zone (Piercey *et al.*, 2003) a setting permissive of porphyry system formation. Paleozoic mineral occurrences are not currently recognized in the Mount Nansen area. Rafts of rock mineralized in the Late Triassic are hosted by Minto suite intrusions 35 km to the northeast of the Mount Nansen area in the Carmacks Copper Belt (Kovacs *et al.*, 2020; Sack *et al.*, 2020). Though Minto suite intrusions are common in the Mount Nansen area, there are not any known Late Triassic mineral occurrences (Sack *et al.*, 2021).

Based on U-Pb zircon ages from mineralized dikes, previous workers have suggested the Mount Nansen area has both mid and Late Cretaceous deposits (Fig. 17; Mortensen *et al.*, 2016). The first direct mid-Cretaceous age for mineralization comes from vein-hosted molybdenite in the Flex deposit (ca. 108.5 Ma; Sack *et al.*, 2022). Brown-McDade, the other deposit in the Brown-McDade cluster, has not been directly dated and has low quality (K-Ar whole-rock) hydrothermal Late Cretaceous ages (Joyce *et al.*, 2015). In light of our equivocal U-Pb zircon data from a dike in the Brown-McDade pit, we can't refine a mid or Late Cretaceous age for mineralization at that deposit. However, based on the similar quartz-feldspar porphyry texture and the abundance of mid-Cretaceous dikes throughout the area (Mortensen *et al.*, 2016), we prefer the interpretation that mineralization in the Brown-McDade cluster was predominantly mid-Cretaceous, likely ca. 108.5 Ma.

Late Cretaceous mineralization appears to have been located primarily near the headwaters of Nansen Creek in the Klaza cluster (Fig. 2). Immediately east of Nansen Creek, chalcopyrite-molybdenite stock work veining associated with the Kelly porphyry has Re-Os ages between 81.7 and 75.9 Ma (Fig. 17; including errors; Lee, 2021). Immediately west of Nansen Creek, chalcopyrite-molybdenite stock work veining within the Cyprus porphyry has Re-Os molybdenite ages ranging from 71.3 to 70.7 Ma (Fig. 17; including errors; Selby and Creaser, 2001). Vein mineralization at the Klaza deposit is younger than the dikes in the area with U-Pb zircon, calcite and Ar-Ar muscovite ages between 77.8 and 70.1 Ma indicating a Late Cretaceous age, likely related to Prospector Mountain suite magmatism (Fig. 17).

Figure 18a,b shows the Pb isotopic ratios of the nine igneous feldspars analyses in the present study. Figure 18c, shows Pb isotopic ratios for igneous feldspar from other plutonic suites. Figure 18d and e show Pb isotopic ratios of galena from throughout the Dawson Range. The feldspar Pb isotopic analyses are divided by plutonic suite, primarily based on the U-Pb zircon magmatic ages, but because the age of all intrusions are not well constrained, suite assignment for some samples is interpreted. The shaded fields on each figure represent the majority of the data in each plutonic suite. The galena Pb isotopic analyses are symbolized first by mineralization age (shape) and deposit (colour). Again, because the age of mineralization is not well constrained for many deposits, age assignments are interpreted. For broader context, the shale curve of Godwin and Sinclair (1982) which closely approximates the Pb isotopic evolution of upper crustal rocks in the northern Cordillera (including the Yukon-Tanana terrane; Mortensen *et al.*, 2006) is shown in Figure 18a–e. The feldspar in sample 20PS218-1 are clay altered and these analyses are not considered to reflect magmatic conditions and are excluded from discussion.

Feldspar from rocks of Minto and Whitehorse suites in our study and other studies have $^{206}Pb/^{204}Pb$ ratios that range from 19.351 to 19.846 and define fields that broadly become more radiogenic with time. On $^{206}Pb/^{204}Pb$ versus $^{207}Pb/^{204}Pb$ diagrams (Fig. 18a,c,d),

most plutonic suites found in the Mount Nansen are plot below the shale curve of Godwin and Sinclair (1982), the exception is the mid-Cretaceous Whitehorse suite which plots above and below the curve. Similar grouping of feldspar isotopic compositions by plutonic suite is evident in the $^{206}Pb/^{204}Pb$ versus $^{208}Pb/^{204}Pb$ plot (Fig. 18b); $^{208}Pb/^{204}Pb$ ratios are positively correlated with increasing $^{206}Pb/^{204}Pb$, indicating an increasing radiogenic component with decreasing age. Mid-Cretaceous Whitehorse suite feldspars yielded the most radiogenic ratios. All three Cretaceous suites in the Mount Nansen area, Whitehorse, Casino and Prospector Mountain have similar feldspar Pb isotopic compositions, the Prospector Mountain suite may be slightly more radiogenic than the Whitehorse and Casino suites (Fig. 18c). The Pb isotopic compositions of galena from Cretaceous deposits (Fig. 18d,e) plot below the shale curve of Godwin and Sinclair (1982) and broadly overlap the field of feldspar Pb compositions from Cretaceous intrusions. As pointed out by Mortensen *et al.* (2016) these deposits are hosted by a variety of rocks and the age of mineralization is commonly poorly constrained, thus linking metal sources directly between plutonic suites and deposits in the Dawson Range is challenging. However, coeval feldspar and galena broadly have similar Pb isotopic ratios suggesting the magmatic rocks were a significant source of metals. We note that the existing Pb isotopic data for plutonic rocks in the Dawson Range includes more whole-rock data (*e.g.*, Selby *et al.*, 1999; Smuk, 1999) than feldspar data which has complicated previous interpretations (*e.g.*, Mortensen *et al.*, 2016). Additional Pb isotopic data from well constrained magmatic feldspar are required to refine interpretations further.

Conclusions

The U-Pb zircon and Pb isotopic data presented here refine understanding of magmatism and mineralization in the Mount Nansen area with the following conclusions:

1. The Brown-McDade deposit is hosted by Minto suite granodiorite with a crystallization age of 199.06 Ma and is intruded by dikes which likely have a Cretaceous emplacement age;
2. Magmatism and mineralization on Dickson Hill and at the adjacent Flex deposit (and likely other Brown-McDade cluster deposits) were mid-Cretaceous, *ca.* 108.5 Ma;
3. The Mount Nansen pluton is a composite Whitehorse suite body which includes a relatively small Bow Creek granite phase and a widespread Dawson Range granodiorite phase.
    a. Bow Creek granite phase is zoned with the border phase crystallizing at 107.86 Ma, slightly after the central phase which crystallized at 107.96 Ma; and
    b. Dawson Range granodiorite phase crystallized 107 to 105 Ma;
4. Mid-Cretaceous magmatism likely began with eruption of dominantly andesitic volcanic rocks, followed by intrusion of felsic, high-level porphyritic dikes and plugs such as those seen at Dickson Hill and possibly the margins of the Bow Creek body. The mid-Cretaceous magmatic cycle ended with emplacement of widespread intermediate plutonic rocks that are dominantly equigranular and fine to medium-grained. The increase in size of plutonic bodies and lack of porphyritic textures may suggest a slightly deeper emplacement level for the main Dawson Range granodiorite phase in the Mount Nansen area. The smaller, slightly older and porphyritic phases may represent a high emplacement level and thus be more prospective for porphyry and related vein deposits;
5. Feldspar Pb isotopic data throughout the Dawson range becomes more radiogenic with time and are distinct for Late Triassic to Early Jurassic plutonic rocks versus Cretaceous plutonic rocks; and
6. Cretaceous feldspar isotopic data broadly overlaps Pb isotopic values of galena from deposits throughout the Dawson Range suggesting coeval magmatic rocks are a significant source of metals.

Acknowledgements

The authors thank Matt van Loon for geology discussion and Rockhaven Resources for data sharing and hospitality.

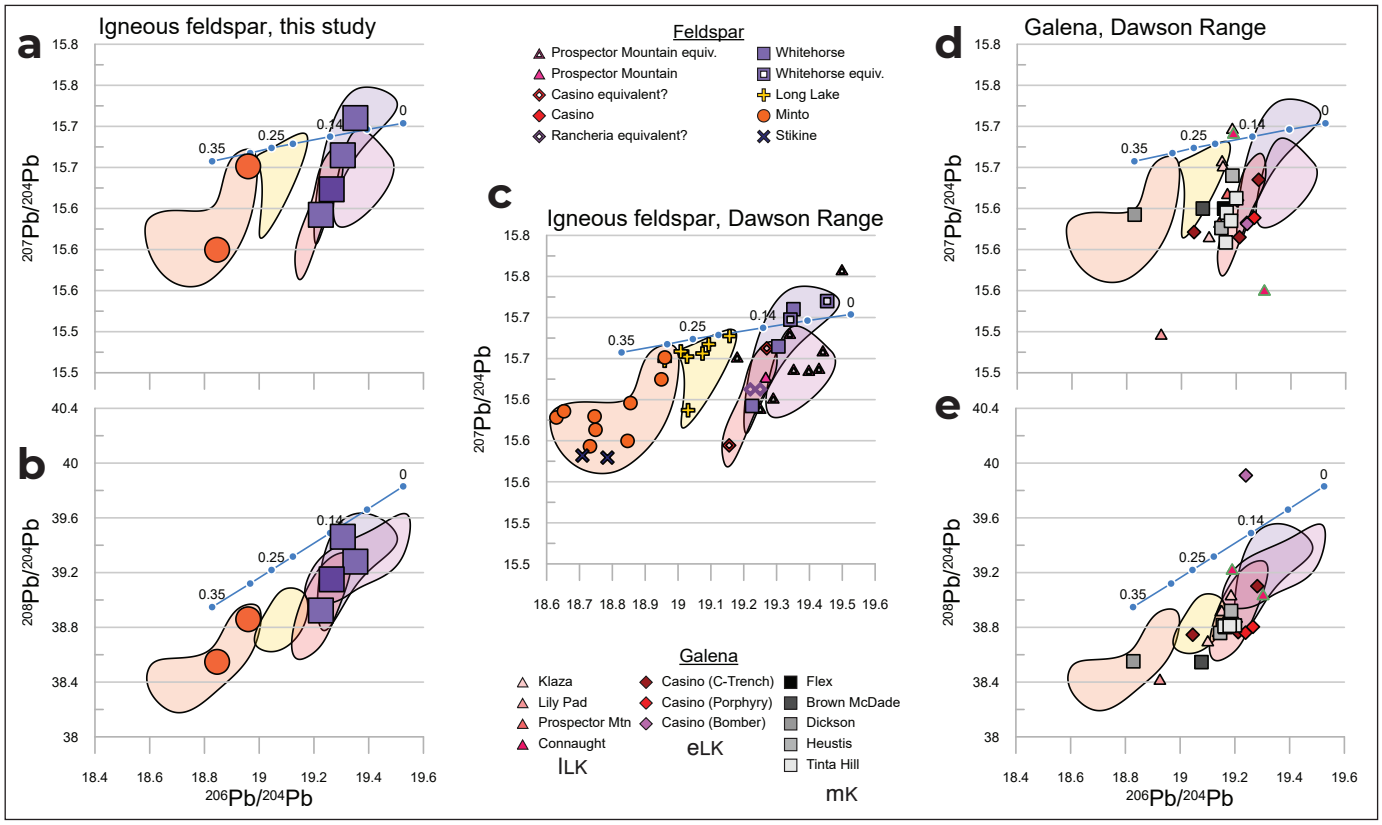


Figure 18. *$^{206}Pb/^{204}Pb$ versus $^{207}Pb/^{204}Pb$ and $^{206}Pb/^{204}Pb$ versus $^{208}Pb/^{204}Pb$ plots.* ***(a** and **b)** From this study; data for feldspar Pb are given in Table 4.* ***(c)** From plutonic rocks throughout the Dawson range and east-central Alaska; data from feldspar Pb are from Rasmussen (2013), Mortensen et al. (2016), Dusel-Bacon et al. (2015) and Sack et al. (2020).* ***(d** and **e)** From galena in vein deposits in the Mount Nansen area; data are from Smuk (1999) and Mortensen et al. (2016).*

References

Allan, M.A. and Friend, M., 2018. Bedrock geological map of the Mount Freegold district, Dawson Range (NTS 115I/6 and parts of 115I/2,3,5,7,10,11,12). Yukon Geological Survey, Open File 2018-2, scale 1:50 000.

Aurora Geosciences and Bruce, J.O., 2020. Residual total magnetic field, shaded colour contour map (NTS 115I). *In:* Reprocessing of Yukon magnetic data for NTS 115I. Yukon Geological Survey, Open File 2020-33, sheet 2 of 4.

Bennett, V. and Tubrett, M., 2010. U-Pb isotopic age dating by LAM ICP-MS, INCO Innovation Centre, Memorial University: Sample preparation methodology and analytical techniques *In*: Yukon Exploration and Geology 2009, K.E. MacFarlane, L.H. Weston and L.R. Blackburn (eds.), Yukon Geological Survey, p. 47–55.

Carlson, G.G., 1987. Geology of Mount Nansen (115-I/3) and Stoddart Creek (115-I/6) map areas Dawson Range, central Yukon. Exploration and Geological Services Division, Yukon Region, Indian and Northern Affairs Canada, Open File 1987-2, 194 p.

Clark, A.D., 2017. Tectonometamorphic history of mid-crustal rocks at Aishihik Lake, southwest Yukon. MSc thesis, Simon Fraser University, 153 p.

Colpron, M., Gordey, S., Lowey, G., White, D. and Piercey, S., 2007. Geology of the northern Whitehorse trough, Yukon (105E/12, 13 and parts of 11 and 14; 105L/4 and parts of 3 and 5; parts of 115H/9 and 16; 115I/1 and part of 8). Yukon Geological Survey, Open File 2007-6, scale 1:150 000.

Colpron, M., Sack, P.J., Crowley, J., Allan, M. and Beranek, L.P., in press. Late Triassic to Jurassic magmatic and tectonic evolution of the Intermontane terranes in Yukon, northern Canadian Cordillera: Transition from arc to syn-collisional magmatism and post-collisional lithospheric delamination. Tectonics.

Crowley, J.L., Schoene, B. and Bowring, S.A., 2007. U-Pb dating of zircon in the Bishop Tuff at the millennial scale. Geology, vol. 35, p. 1123–1126.

Dusel-Bacon, C., Aleinikoff, J.N., Day, W.C. and Mortensen, J.K., 2015. Mesozoic magmatism and timing of epigenetic Pb-Zn-Ag mineralization in the western Fortymile mining district, east-central Alaska: Zircon U-Pb geochronology, whole-rock geochemistry, and Pb isotopes. Geosphere, vol. 11, p. 786–822.

Gaidies, F., Morneau, Y.E., Petts, D.C., Jackson, S.E., Zagorevski, A. and Ryan, J.J., 2020. Major and trace element mapping of garnet: Unravelling the conditions, timing and rates of metamorphism of the Snowcap assemblage, west-central Yukon. Journal of Metamorphic Geology, vol. 39, p. 133–164.

Godwin, C.I. and Sinclair, A.J., 1982. Average lead isotope growth curves for shale-hosted zinc-lead deposits, Canadian Cordillera. Economic Geology, vol. 77, p. 675–690.

Grond, H.C., Churchill, S.J., Armstrong, R.L., Harakal, J.E. and Nixon, G.T., 1984. Late Cretaceous age of the Hutshi, Mount Nansen, and Carmacks groups, southwestern Yukon Territory and northwestern British Columbia. Canadian Journal of Earth Sciences, vol. 21, p. 554–558.

Hodges, K.V., 2014. Geochronology and Thermochronology in Orogenic Systems. *In*: Treatise on geochemistry: The crust, H.D. Holland and K.K. Turekian (eds.), Elsevier Pergamon, p. 263–292.

Jaffey, A.H., Flynn, K.F., Glendenin, L.E., Bentley, W.C. and Essling, A.M., 1971. Precision measurements of half-lives and specific activities of ^{235}U and ^{238}U. Physical Review C, vol. 4, p. 1889–1906.

Joyce, N.L., Iraheta Muniz, P., Rayner, N.M. and Ryan, J.J., 2020. Geochronology of the Mount Nansen-Nisling River area, Yukon. Geological Survey of Canada, Open File 8614, 28 p.

Joyce, N.L., Ryan, J.J., Colpron, M., Hart, C.J.R. and Murphy, D.C., 2015. A compilation of $^{40}Ar/^{39}Ar$ age determinations for igneous and metamorphic rocks, and mineral occurrences from central and southeast Yukon. Geological Survey of Canada, Open File 7924.

Klöcking, M., Mills, L., Mortensen, J. and Roots, C., 2016. Geology of mid-Cretaceous volcanic rocks at Mount Nansen, central Yukon, and their relationship to the Dawson Range batholith. Yukon Geological Survey, Open File 2016-25, 37 p.

Kovacs, N., Allan, M.M., Crowley, J.L., Colpron, M., Hart, C.J.R., Zagorevski, A. and Creaser, R.A., 2020. Carmacks Copper Cu-Au-Ag deposit: mineralization and post-ore migmatization of a Stikine arc porphyry copper system in Yukon, Canada. Economic Geology, vol. 115, p. 1413–1422.

Lee, W.-S., 2021. Metallogeny and characterization of Late Cretaceous superimposed porphyry Cu-Au-Mo and epithermal Au-Ag systems in the Dawson Range, Yukon, Canada: Case study on the Klaza deposit. PhD thesis, Laurentian University, Sudbury, Ontario, Canada.

Lee, W.-S., Kontak, D.J., Richards, J.P. and Sack, P., 2020. Updated geology and porphyry copper potential of the Klaza deposit, Mount Nansen district (Yukon MINFILE 115I 067). *In*: Yukon Exploration and Geology 2019, K.E. MacFarlane (ed.), Yukon Geological Survey, p. 75–97.

Mattinson, J.M., 2005. Zircon U-Pb chemical abrasion ("CA-TIMS") method: combined annealing and multi-step partial dissolution analysis for improved precision and accuracy of zircon ages. Chemical Geology, vol. 220, p. 47–66.

Mortensen, J.K., Dusel-Bacon, C., Hunt, J.A. and Gabites, J., 2006. Lead isotopic constraints on the metallogeny of middle and late Paleozoic syngenetic base-metal occurrences in the Yukon-Tanana and Slide Mountain/Seventymile terranes and adjacent portions of the North American miogeocline. *In*: Paleozoic Evolution and Metallogeny of Pericratonic Terranes at the Ancient Pacific Margin of North America, Canadian and Alaskan Cordillera, M. Colpron and J.L. Nelson (eds.), Geological Association of Canada, p. 261–279.

Mortensen, J. and Friend, M., 2020. An overview of porphyry style deposits in Yukon. *In*: Porphyry deposits of the northwestern Cordillera of North America: a 25-year update, E.R. Sharman, J.R. Lang and J.B. Chapman (eds.), Canadian Institute of Mining, Metallurgy and Petroleum, p. 176–193.

Mortensen, J.K. and Gabites, J.E., 2002. Lead isotopic constraints on the metallogeny of southern Wolf Lake, southeastern Teslin and northern Jennings River map areas, Yukon and British Columbia: Preliminary results. *In*: Yukon Exploration and Geology 2001, D.S. Emond, L.H. Weston and L.L. Lewis (eds.), Exploration and Geological Services Division, Yukon Region, Indian and Northern Affairs Canada, p. 179–188.

Mortensen, J.K., Hart, C.J.R., Tarswell, J. and Allan, M.M., 2016. U-Pb zircon age and Pb isotopic constraints on the age and origin of porphyry and epithermal vein mineralization in the eastern Dawson Range, Yukon. *In*: Yukon Exploration Geology 2015, K.E. MacFarlane and M.G. Nordling (eds.), Yukon Geological Survey, p. 165–185, including appendices.

Mottram, C.M., Kellett, D.A., Barresi, T., Zwingmann, H., Friend, M., Todd, A. and Percival, J.B., 2020. Syncing fault rock clocks: Direct comparison of U-Pb carbonate and K-Ar illite fault dating methods. Geology, vol. 48, p. 1179–1183.

Piercey, S.J. and Colpron, M., 2009. Composition and provenance of the Snowcap assemblage, basement to the Yukon-Tanana terrane, northern Cordillera: Implications for Cordilleran crustal growth. Geosphere, vol. 5, p. 439–464.

Piercey, S.J., Mortensen, J.K. and Creaser, R.A., 2003. Neodymium isotope geochemistry of felsic volcanic and intrusive rocks from the Yukon–Tanana Terrane in the Finlayson Lake Region, Yukon, Canada. Canadian Journal of Earth Sciences, vol. 40, p. 77–97.

Rasmussen, K.L., 2013. The timing, composition and petrogenesis of syn- to post-accretionary magmatism in the northern Cordilleran miogeocline, eastern Yukon and southwest Northwest Territories. PhD thesis, University of British Columbia, 810 p.

Ryan, J.J., Israel, S., Williams, S.P., Parsons, A.J. and Hayward, N., 2018. Bedrock geology, Klaza River area, Yukon. Geological Survey of Canada, Canadian Geoscience Map 376, scale 1:100 000.

Ryan, J.J., Westberg, E.E., Williams, S.P. and Chapman, J.B., 2016. Geology, Mount Nansen - Nisling River area, Yukon. Geological Survey of Canada, Canadian Geoscience Map 292 (ed. prelim.), 1 sheet, scale 1:100 000.

Ryan, J., Zagorevski, A., Williams, S.P., Root, C.F., Ciolkiewicz, W. and Chapman, J.B., 2013. Geology, Stevenson Ridge (northeast part), Yukon. Geological Survey of Canada, Geoscience map 116 (2nd edition, preliminary), scale 1:100 000.

Sack, P.J., Colpron, M., Crowley, J.L., Ryan, J.J., Allan, M.M., Beranek, L.P. and Joyce, N.L., 2020. Atlas of Late Triassic to Jurassic plutons in the Intermontane terranes of Yukon. Yukon Geological Survey, Open File 2020-1, 378 p.

Sack, P.J., Eriks, N. and van Loon, S., 2021. Revised geological map of the Mount Nansen area (NTS 115I/3 and part of 115I/2). Yukon Geological Survey, Open File 2021-2, 2 sheets; scales 1:50 000 and 1:20 000.

Sack, P.J., Eriks, N. and van Loon, S., 2022. Updated geological map of the Mount Nansen area (NTS 115I/3 and part of 115I/2). Yukon Geological Survey, Open File 2022-4, 2 sheets; scales 1:50 000 and 1:20 000.

Sawyer, J.P.B. and Dickinson, R.A., 1976. Mount Nansen. *In*: Porphyry deposits of the Canadian Cordillera, S.A. Brown (ed.), The Canadian Institute of Mining and Metallurgy, Special Volume 15, p. 336–343.

Schmitz, M.D. and Schoene, B., 2007. Derivation of isotope ratios, errors and error correlations for U-Pb geochronology using 205Pb-235U-(233U)-spiked isotope dilution thermal ionization mass spectrometric data. Geochemistry, Geophysics, Geosystems (G^3), vol. 8, Q08006, doi:10.1029/2006GC001492.

Selby, D. and Creaser, R.A., 2001. Late and mid-Cretaceous mineralization in the northern Canadian Cordillera: Constraints from Re-Os molybdenite dates. Economic Geology, vol. 96, p. 1461–1467.

Selby, D., Creaser, R.A., Hart, C.J.R., Rombach, C.S., Thompson, J.F.H., Smith, M.T., Bakke, A.A. and Goldfarb, R.J., 2002. Absolute timing of sulfide and gold mineralization: A comparison of Re-Os molybdenite and Ar-Ar mica methods from the Tintina Gold Belt, Alaska. Geology, vol. 30, p. 791–794.

Selby, D., Creaser, R.A. and Nesbitt, B.E., 1999. Major and trace element compositions and Sr–Nd–Pb systematics of crystalline rocks from the Dawson Range, Yukon, Canada. Canadian Journal of Earth Sciences, vol. 36, p. 1463–1481.

Smuk, K.A., 1999. Metallogeny of epithermal gold and base metal veins of the southern Dawson Range, Yukon. MSc thesis, McGill University, 188 p.

Staples, R.D., Murphy, D.C., Gibson, H.D., Colpron, M., Berman, R.G. and Ryan, J.J., 2014. Middle Jurassic to earliest Cretaceous mid-crustal tectono-metamorphism in the northern Canadian Cordillera: Recording foreland-directed migration of an orogenic front. Geological Society of America Bulletin, vol. 126, p. 1511–1530.

Stein, H.J., Markey, R.J., Morgan, J.W., Hannah, J.L. and Scherstén, A., 2001. The remarkable Re–Os chronometer in molybdenite: how and why it works. Terra Nova, vol. 13, p. 479–486.

Suzuki, K., Shimizu, H. and Masuda, A., 1996. ReOs dating of molybdenites from ore deposits in Japan: Implication for the closure temperature of the ReOs system for molybdenite and the cooling history of molybdenum ore deposits. Geochimica et Cosmochimica Acta, vol. 60, p. 3151–3159.

Tosdal, R.M., Wooden, J.L. and Bouse, R.M., 1999. Pb isotopes, ore deposits, and metallogenic terranes. *In*: Application of Radiogenic Isotopes to Ore Deposit Research and Exploration, Reviews in Economic Geology, Volume 12, D.D. Lambert and J. Ruiz (eds.), Society of Economic Geology, p. 1–28.

YGS, 2020. Yukon Digital Bedrock Geology. Yukon Geological Survey, https://data.geology.gov.yk.ca/Compilation/3#InfoTab, [accessed March 31, 2020].

Appendices

The appendices are only available as digital files. They are included in a .zip file that accompanies this document, and are available from https://data.geology.gov.yk.ca.

Appendix 1 – magnetic susceptibility

Appendix 2 – U-Pb zircon geochronology

Preliminary observations on the geology of the southern Big Salmon Range, south-central Yukon (parts of NTS 105C/13, 14, 105F/4 and 105E/1)

D. Moynihan*
Yukon Geological Survey

J.L. Crowley
Boise State University

Moynihan, D. and Crowley, J.L., 2022. Preliminary observations on the geology of the southern Big Salmon Range, south-central Yukon (parts of NTS 105C/13, 14, 105F/4 and 105E/1). *In:* Yukon Exploration and Geology 2021, K.E. MacFarlane (ed.), Yukon Geological Survey, p. 217–265.

Abstract

Penetratively deformed rocks of the Yukon-Tanana terrane and Semenof block, and unfoliated Jurassic-Cretaceous intrusions are exposed in the southern Big Salmon Range of south-central Yukon. A newly mapped area, centred on the Boswell River, is divided into three structural panels by two regional-scale discontinuities, the Little Bear fault and the Sidney Creek fault.

The panel on the northeastern side of the Little Bear fault includes units dominated by metasedimentary rocks (Slate Mountain succession), mafic volcanic and volcaniclastic rocks (Wiley succession), and a varied metasedimentary/metavolcaniclastic unit (Livingstone Creek succession). Each of these is crosscut by intermediate-mafic intrusions of the Simpson Range suite and is therefore Early Mississippian or older. Fossiliferous limestone is interpreted to unconformably overlie phyllite of the Slate Mountain succession. Other units that crop out in this region are Permian augen schist and Cretaceous plutons, including Late Cretaceous quartz monzonite that hosts the Red Mountain Mo porphyry deposit.

The central part of the area, between the Little Bear and Sidney Creek faults, is dominated by mafic volcanic and plutonic rocks of the Sawtooth succession. These are along strike from, and provisionally correlated with the Moose formation of the Boswell assemblage. The Sawtooth succession is overlain by a carbonate and chert-bearing metasedimentary unit (Rosy succession), which hosts a small foliated metagranodiorite intrusion. A younger, as yet undated, mafic metavolcanic unit (Gunsight succession) is locally preserved above the Rosy succession. The metagranodiorite in the Rosy succession formed *ca.* 336 Ma and underwent metamorphic zircon growth in the Early Jurassic (~195 Ma). This zircon growth is interpreted to have accompanied regional, epidote-amphibolite to amphibolite-facies metamorphism and deformation.

Mississippian rocks of the Simpson Range suite dominate much of the southwestern domain. These intrusions crosscut quartzose schist, graphitic phyllite and metabasaltic rocks of the Flat Creek succession, which also hosts Middle Triassic metagabbro.

* David.Moynihan@yukon.ca

All pre-Jurassic rocks in the area are deformed, while post-tectonic intrusions include members of the Early Jurassic Lokken suite, the mid-Cretaceous Quiet Lake batholith and Iron Creek stock, and the aforementioned Red Mountain suite. Most Early Jurassic intrusions are undeformed, but deformation/hydration of some minor phases suggests they were intruded during the waning stages of deformation.

The Sidney Creek fault is cut by the Early Jurassic Sawtooth stock while the Cretaceous Iron Creek stock intruded across the trace of the Little Bear fault. The Little Bear and Sidney Creek faults are interpreted to define tectonic boundaries between Yukon-Tanana terrane and rocks of the Semenof block and may form part of a regional detachment between these units.

Introduction

This report presents preliminary observations on the geology of the southern Big Salmon Range in south-central Yukon, based on approximately nine weeks of fieldwork conducted over the summers of 2020 and 2021 (Fig. 1; see also Moynihan, 2022). A simplified map and cross sections are presented (Fig. 2), along with brief descriptions and illustrations of the major units, supplemented by some new U-Pb geochronological data. The interpretations included in the report are preliminary and subject to refinement following further analytical work.

The mapped area (approximately 785 km^2) is located east of the Teslin River in the southern Big Salmon Range (Fig. 1; Moynihan, 2022). It encompasses an

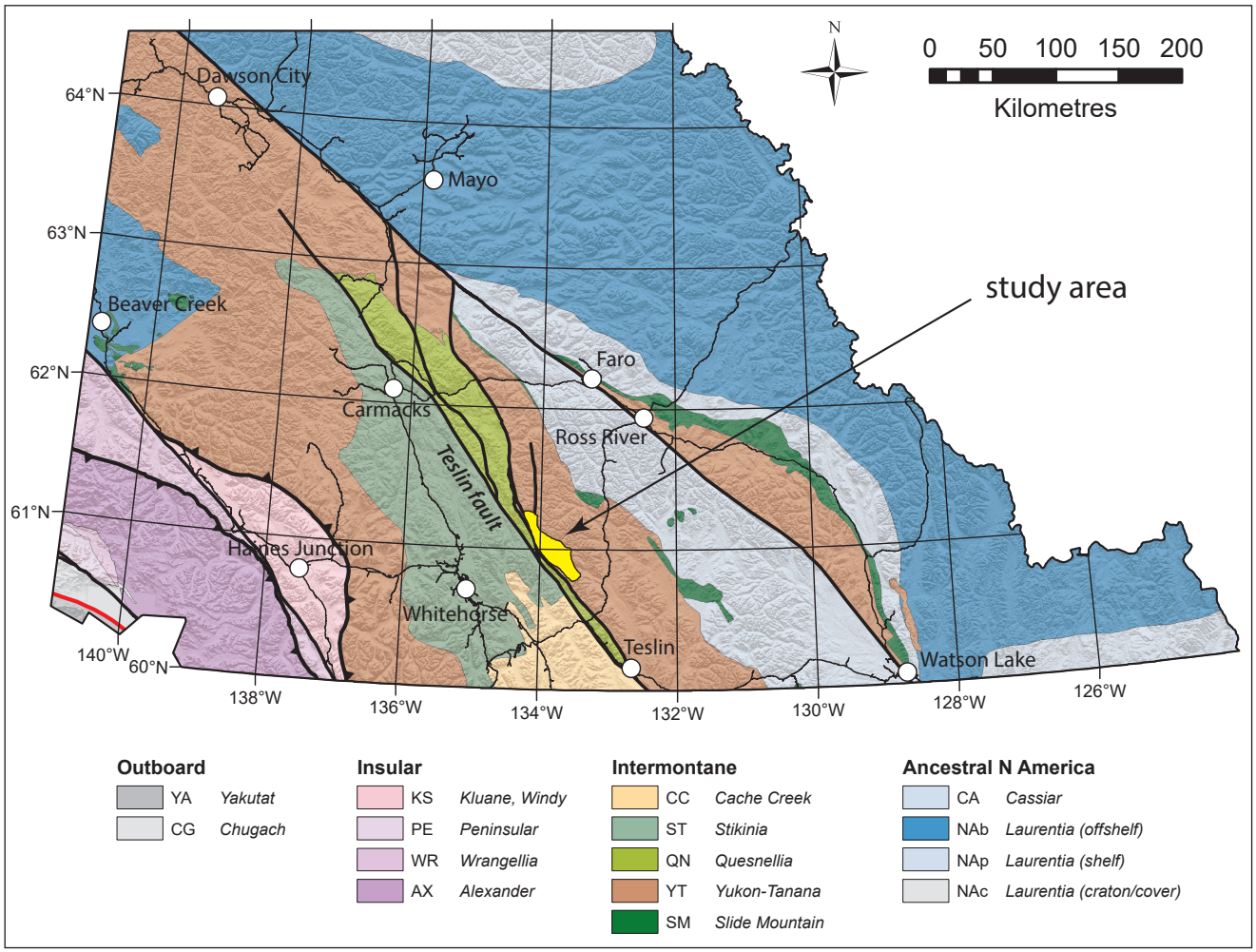


Figure 1. *Terrane map of Southern Yukon (after Colpron and Nelson, 2011). The study area is located approximately 75 km northeast of Whitehorse, east of the Teslin fault. It is mostly underlain by rocks of Yukon-Tanana terrane and the Semenof block.*

elongate NW-SE-trending strip that extends from the South Big Salmon River to upper parts of the Sidney Creek drainage (Fig. 2). The area is centred on the Sawtooth Range and the upper parts of the Boswell River; it includes parts of the Teslin (105C), Quiet Lake (105F) and Laberge (105E) map sheets.

Geological background and previous work

Early accounts of the geology of the area, based on reconnaissance mapping (1:253,440), were provided by Cockfield *et al.* (1936), Lees (1936) and Mulligan (1963); Tempelman-Kluit (1984) subsequently extended 1:250 000-scale mapping in the Lake Laberge and Carmacks areas. The first detailed (1:50 000 scale) mapping of the study area was carried out by Stevens (1994; see also Gordey and Stevens, 1994). The geology of the Semenof Hills was mapped at 1:50 000 by Simard (2003) and is described in Simard and Devine (2003). Colpron (2005a,b, 2006) and Colpron *et al.* (2017) documented the geology of the Livingstone Creek area, directly north of the study area.

The present work builds on Stevens (1994); it aims to provide more detail on the character, age and affinity of lithological units, to provide a clearer understanding of its relationships with other parts of Yukon-Tanana terrane, and to consider implications for metallogenic potential of the southern Big Salmon Range.

The study area is underlain by rocks of the Yukon-Tanana terrane and the Semenof block (Colpron *et al.*, 2003, 2006a). Yukon-Tanana includes: 1) Proterozoic-Devonian metasedimentary rocks that are interpreted to have been rifted from the Laurentian margin, and 2) metavolcanic, metasedimentary and metaplutonic rocks that formed in arc and back-arc environments that developed on and around the rifted basement during the middle to late Paleozoic. The pre-Late Devonian basement is referred to as Snowcap assemblage, while three younger, widely developed unconformity-bounded assemblages have been recognized throughout Yukon-Tanana: 1) the Late Devonian-Early Mississippian Finlayson assemblage, 2) Middle Mississippian-Early Permian Klinkit assemblage and 3) the Middle to Late Permian Klondike assemblage (Colpron *et al.*, 2006a). The Finlayson assemblage is coeval with two voluminous metaplutonic suites – the Late Devonian-Early Mississippian Grass Lakes suite (*ca.* 365–357 Ma) and Early Mississippian Simpson Range suite (*ca.* 355–345 Ma).

The 'Semenof block' (Colpron *et al.*, 2003, 2006a) includes the Semenof hills, which are along strike to the northwest of the study area. Rocks of the Boswell assemblage (Tempelman-Kluit, 1984, 2009; Simard and Devine, 2003) underlie this area. The Boswell assemblage is coeval with parts of Yukon-Tanana but its relationship with it is uncertain (Colpron *et al.* 2006a). Contacts between Yukon-Tanana and the Semenof block are tectonic, and while there are some stratigraphic similarities, particularly between their respective Mississippian-Pennsylvanian successions, definitive correlations have not been established (Colpron *et al.* 2006a).

The oldest part of the Boswell assemblage is Early Mississippian mafic and minor felsic volcanic rocks of the Moose formation. This is overlain by the Boswell formation, which includes sandstone, conglomerate, minor mafic volcanic rocks and one or more prominent Late Mississippian-Early Permian limestone units. The Moose formation is intruded by Late Mississippian-Pennsylvanian hornblende tonalite of the Kelly suite (*ca.* 335–310 Ma), which is similar in age to the Tatlmain suite of Yukon-Tanana (*ca.* 340–336 Ma). Late Triassic rocks of the Semenof Formation, which have been assigned to Stikine (Colpron *et al.*, 2002, 2003) or Quesnel terranes (Gordey and Makepeace, 2001; Colpron *et al.*, 2016) unconformably overlie the Boswell assemblage (Simard, 2003).

The boundary between Yukon-Tanana and the Semenof block is marked by the Big Salmon fault and Needlerock thrust to the north of the study area. Colpron *et al.*, (2003) interpreted the Needlerock thrust to be an early (Triassic-Jurassic) structure that is cut by the Big Salmon fault. The Big Salmon fault truncates the Late Cretaceous Carmacks Group near Little Salmon Lake, which demonstrates some Late Cretaceous or younger movement along at least part of its trace. The Teslin fault marks the western boundary of the Semenof block and Yukon-Tanana terrane at the latitude of the study area (Fig. 1).

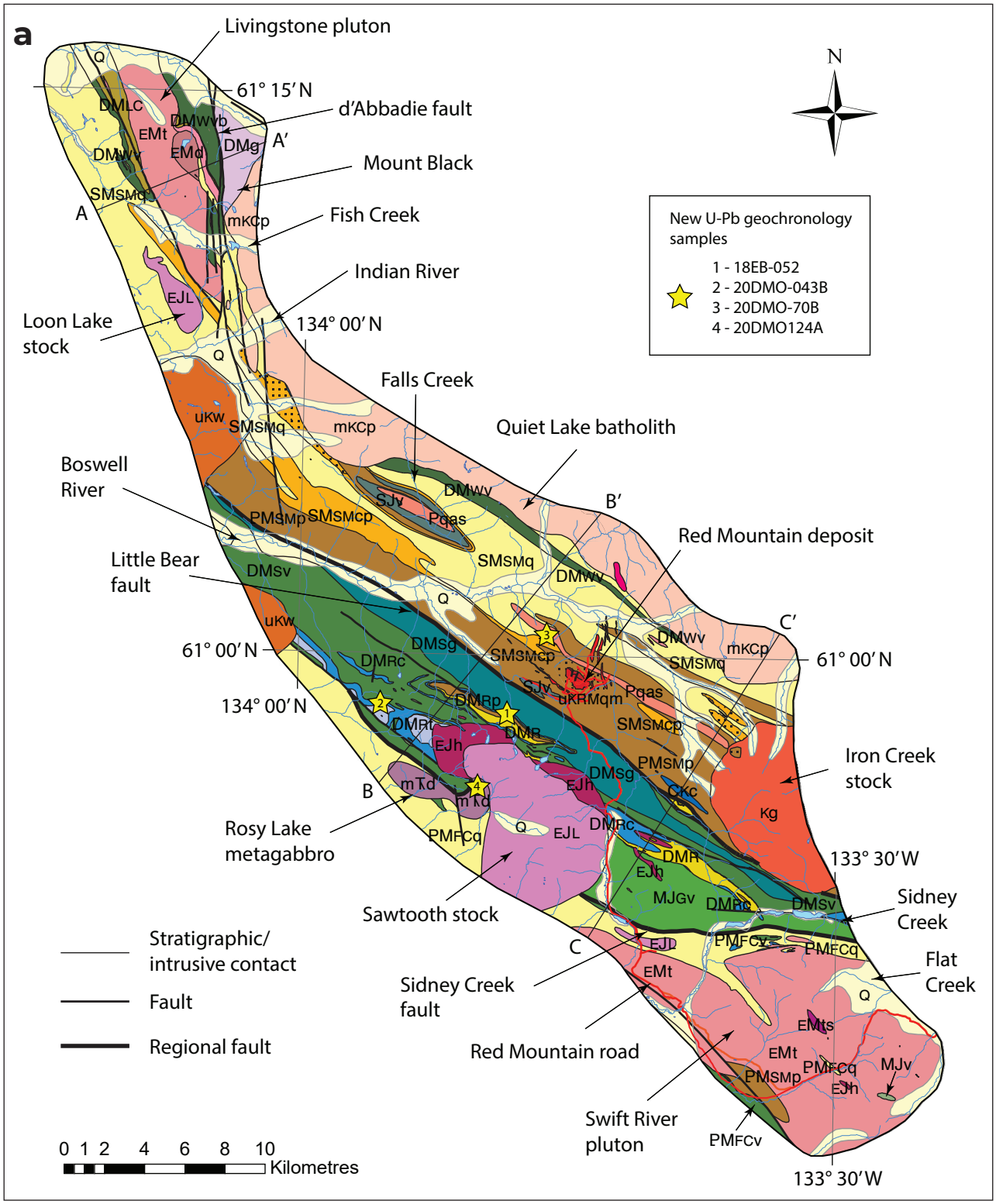


Figure 2. *Simplified geological map* **(a)**, *legend* **(b)** *and cross sections* **(c)** *of the study area (after Moynihan, 2022). Features and places named in the text are shown on the map. Legend and cross sections on following pages.*

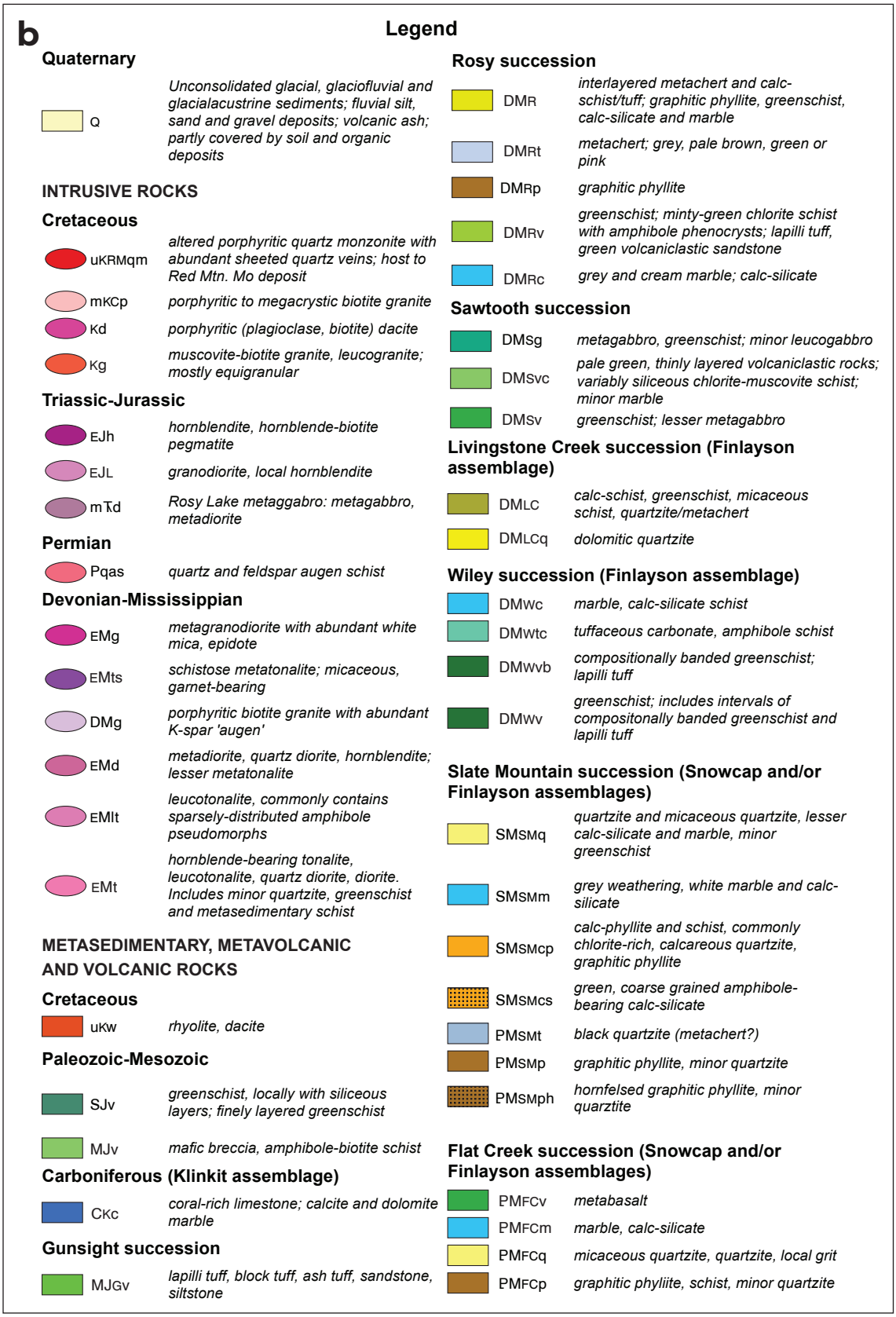


Figure 2 continued. ***(b)*** Legend.

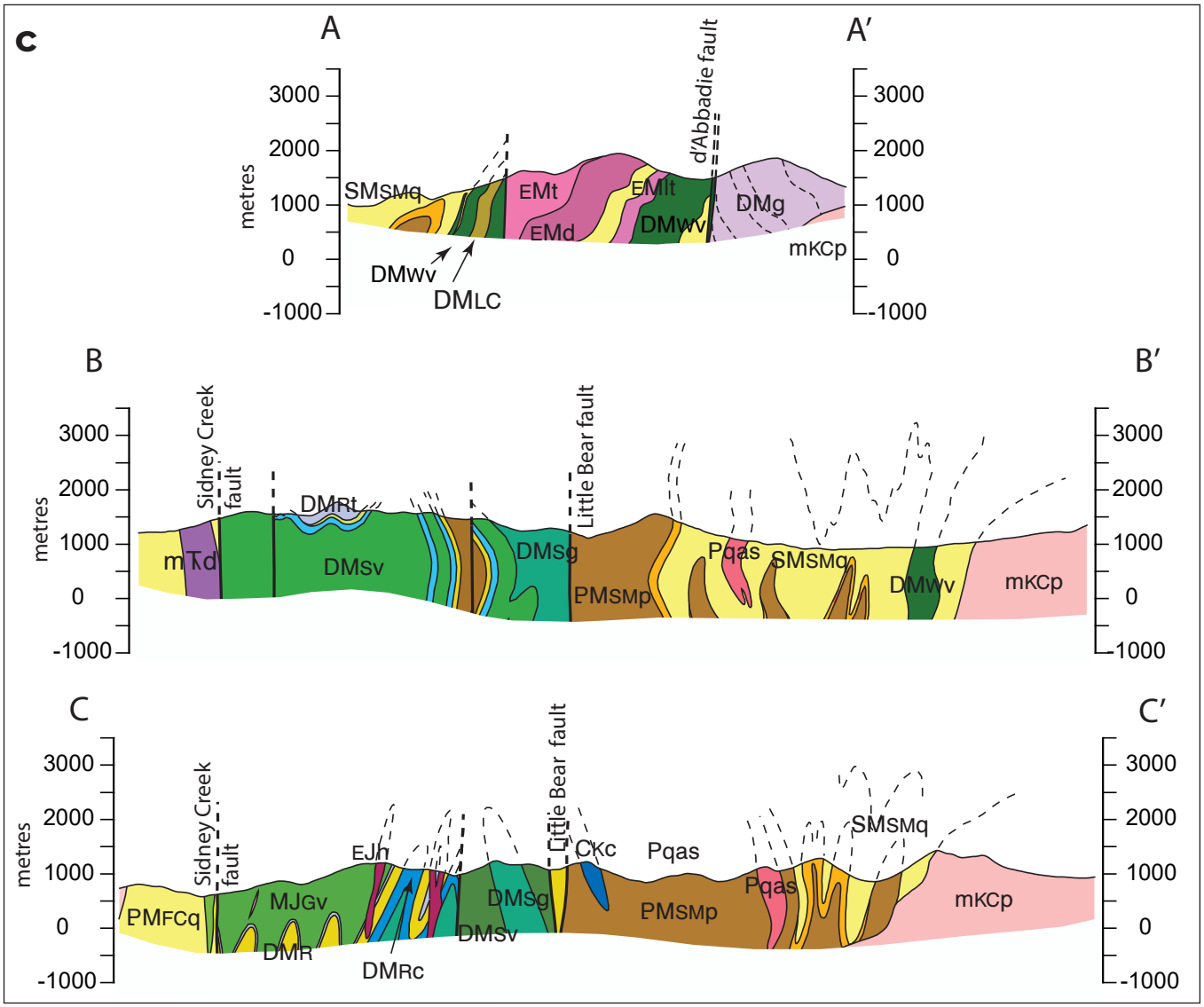


***Figure 2** continued. **(c)** Cross sections.*

Tripartite division of the study area

The mapped area is divided into three belts by the Little Bear and Sidney Creek faults (Figs. 2 and 3). The Little Bear fault separates Mississippian metaplutonic and older metasedimentary/metavolcanic rocks in the northeast from a central belt that is dominated by greenschist and metagabbro. The central region also includes some metasedimentary rocks but almost entirely lacks deformed intermediate-felsic intrusions. The Sidney Creek fault marks the southwestern boundary of the central belt and juxtaposes this region against an area dominated by intermediate Mississippian metaplutonic and older metasedimentary rocks. All three belts host largely undeformed Cretaceous intrusions (Fig. 3). The central belt is interpreted to form part of the Semenof block, while the outer regions are parts of Yukon-Tanana terrane.

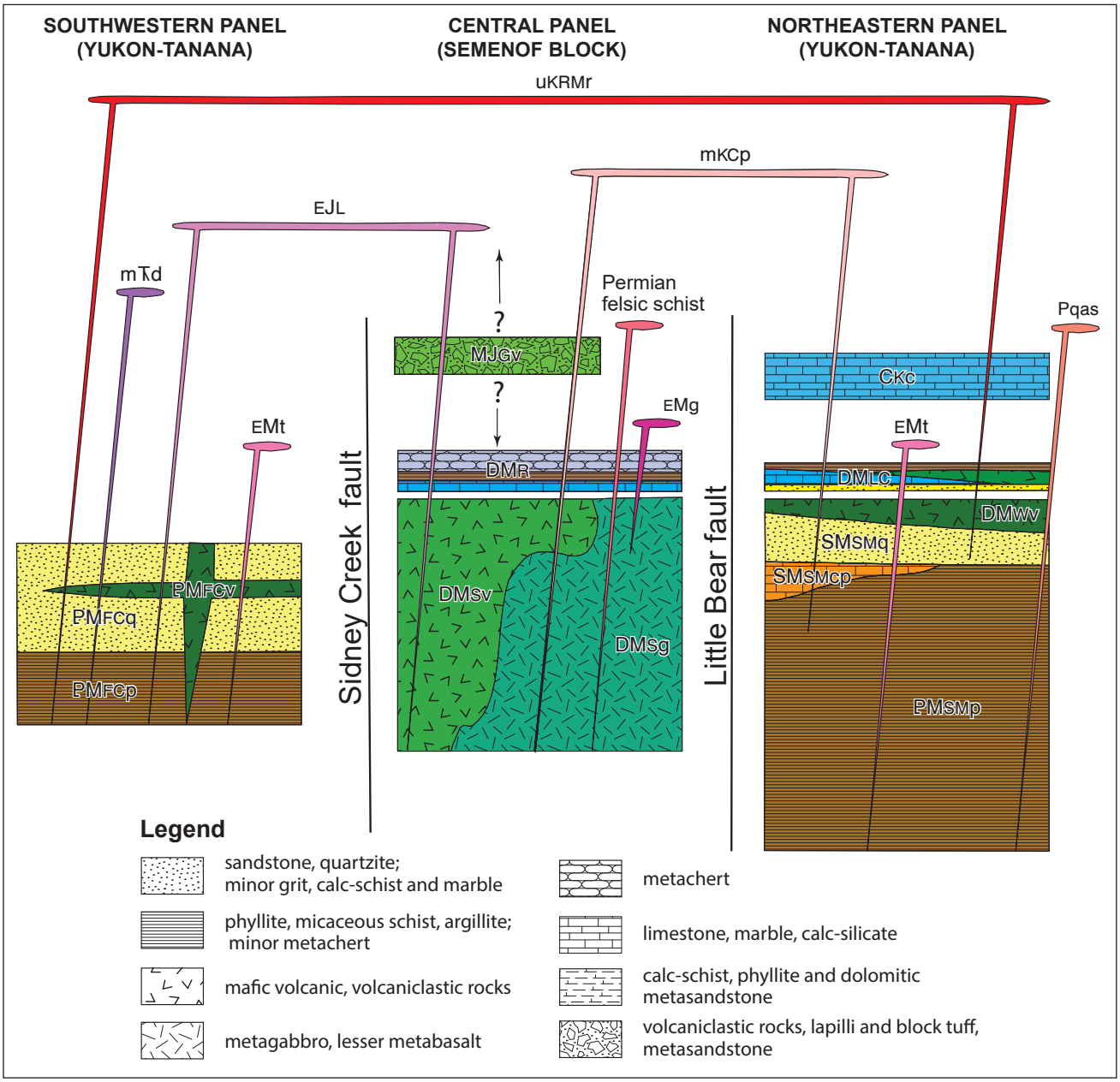


Figure 3. *Provisional interpretation of relationships between major stratigraphic and intrusive units, with relative time on the Y-axis. The Little Bear and Sidney Creek faults divide the area into three structural domains. The southwestern and northeastern domains are dominated by metasedimentary successions that are intruded by plutons assigned to the Simpson Range suite, while the central region is dominated by mafic metavolcanic/plutonic rocks and lacks Simpson range suite intrusions. Jurassic intrusions are interpreted to crosscut the Sidney Creek fault.*

Metasedimentary and metavolcanic rocks northeast of the Little Bear fault (Yukon-Tanana terrane)

Slate Mountain succession

The Slate Mountain succession is a belt of folded metasedimentary rocks that crops out between the Little Bear fault and the Quiet Lake batholith (Fig. 2), and extends the length of the mapped area. It includes three main map units: 1) a dark phyllite unit, 2) a calc-schist/calc-silicate unit, and 3) a unit dominated by metasandstone. There are gradational lithological changes between these units in many parts of the area.

Dark phyllite (PMSMp)

Much of the region immediately northeast of the Little Bear fault is underlain by dark, carbonaceous phyllite and argillite (Fig. 4a). The phyllite is typically medium grey, dark grey or black and weathers rusty brown. A particularly dark, graphite-rich interval is exposed near the top of Slate Mountain, southeast of the Boswell River. This unit also includes numerous thin (5–15 cm thick) layers of quartzite that contain dark graphitic folia, and locally metre-scale intervals of homogeneous, finely banded grey to black quartzite that may represent metamorphosed chert (Fig. 4b). Sooty grey limestone/marble is also a minor constituent.

Chloritic calc-schist/calc-silicate (SMSMcp)

The dark, graphitic phyllite is in gradational contact with a widely, but discontinuously distributed unit that includes a mix of calcareous and siliciclastic rocks in varying ratios. The most distinctive rock type is a finely layered calc-schist that comprises folia of green, chlorite-rich phyllite/schist interlayered with tan to orange weathering dolomitic siliceous layers (Fig. 4c,d). This rock type commonly hosts abundant carbonate and quartz-carbonate veins. Other varieties include similar calc-schist in which the phyllitic layers are mostly grey rather than green, and intervals that are dominated by grey phyllite with sparse green and tan calcareous/dolomitic layers. Locally, the unit includes relatively pure grey weathering, white to buff marble within calc-schist/silicate intervals. Similar rocks were reported by Colpron (2006) and Westberg (2010) in the Dycer Creek succession north of Mendocino Creek (NTS 105E/8 and 105F/5).

Near the Quiet Lake batholith, this unit was metamorphosed to higher grade and is represented by green, splintery calc-silicate/skarn. The rock is medium to coarse grained, pale to medium green and is compositionally banded (Fig. 4e,f). It is dominated by quartz, plagioclase and green amphibole and/or pyroxene; it also contains K-feldspar and locally pale pink garnet.

Quartzite/micaceous quartzite (SMSMq)

This unit is dominated by micaceous quartzite, with lesser, relatively pure quartzite. Micaceous quartzite weathers beige to pale brown and is mostly grey on fresh surfaces (Fig. 4g). It contains abundant closely spaced, wispy and discontinuous to continuous micaceous folia, and is sometimes characterized by subtle cm-scale colour banding (mostly tones of grey, cream, beige and pale brown). Relatively pure quartzite forms resistant ribs that weather white (Fig. 4h). Micaceous folia are thin and widely spaced (~1 cm); fresh surfaces are pale grey and glassy. Other rock types in this unit include minor pale grey calc-silicate and rare decimetre to metre-scale marble and calc-silicate bands. Pebble conglomerate was also observed in a single locality. Outcrops on slopes above the Boswell River, near the contact with phyllite/calc-schist unit, include intervals of tan weathering metasandstone with thin grey or green (chlorite-rich) folia. This suggests a gradational boundary between the quartzite (SMSMq) and calc-schist (SMSMcp) units. Farther northeast, the quartzite includes thin bands of biotite-bearing greenschist. It is unclear whether this represents part of a stratigraphic transition into the Wiley succession, or is the result of tight infolding. The contact with the Wiley succession is otherwise discrete and is commonly marked by a discontinuous band of white marble and impure calc-silicate marble. The marble is grey weathering, white on fresh surfaces, and commonly 5 to 10 m thick.

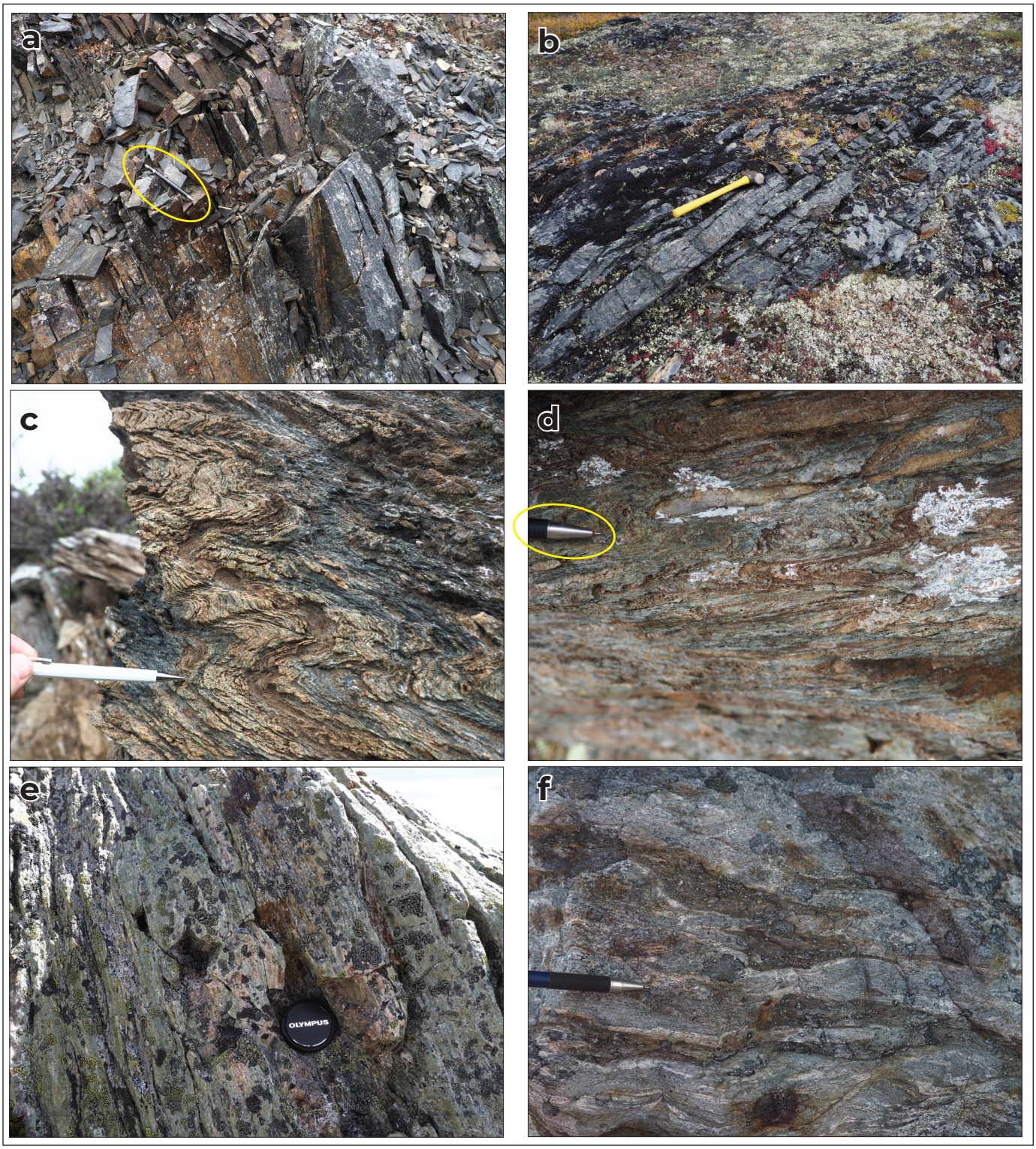


Figure 4. *Slate Mountain succession field photographs.* ***(a)*** *Dark grey, rusty weathering argillite; pencil for scale.* ***(b)*** *Thinly layered dark grey to black, thinly banded quartzite, possibly metachert; hammer for scale.* ***(c and d)*** *Chloritic calc-schist, composed of alternating layers of tan coloured, dolomitic cemented metasandstone, and green or grey, chlorite-rich phyllite; pencil for scale.* ***(e)*** *Banded green calc-silicate with pale pink garnet near the boundary of the Quiet Lake batholith; lens cap for scale.* ***(f)*** *Folded calc-silicate with irregular compositional domains; pencil for scale.* *Figure continued on next page.*

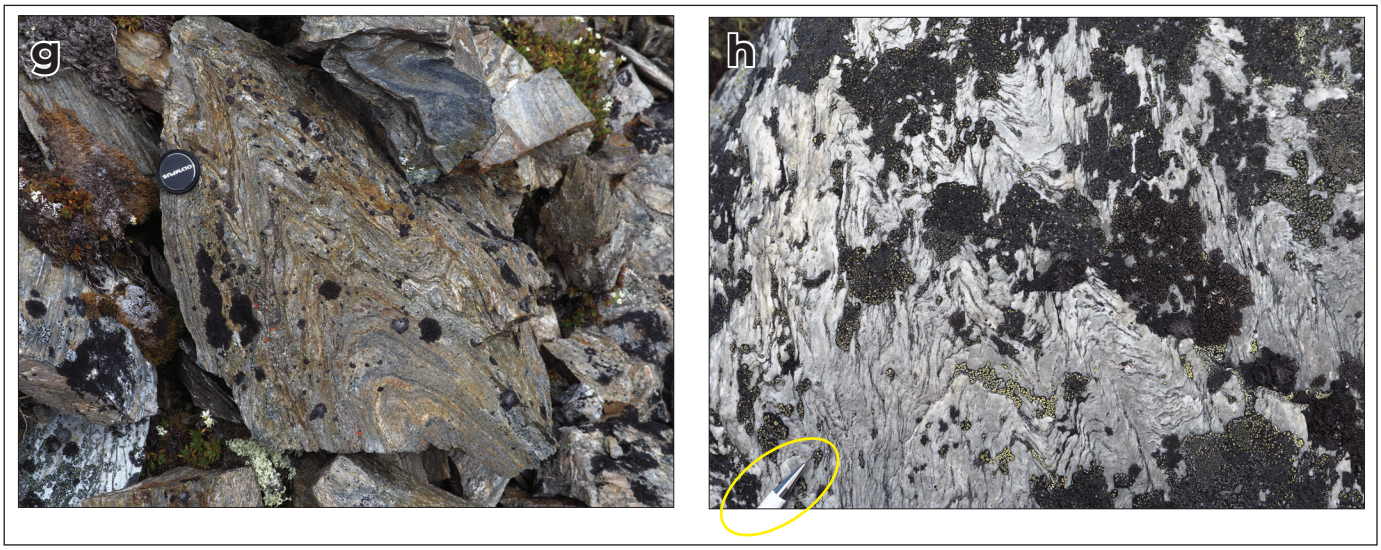


***Figure 4** continued.* ***(g)** Folded micaceous quartzite; lens cap for scale.* ***(h)** White weathering quartzite with widely spaced micaceous folia; pencil tip in lower left corner for scale.*

Age constraints and correlation

The Slate Mountain succession is along strike from, and apparently continuous with similar units in the Livingstone Creek area. The dark phyllite, calc-schist and quartzite units are correlated with PDSp, PDSv and PDSq (Colpron, 2017), respectively. SMSMq is physically continuous with, and therefore correlative with the "Loon Lake" succession of Barresi (2004).

There are few direct constraints on the age of the Slate Mountain succession. The quartzite is intruded by tonalite-granodiorite of the Early Mississippian Simpson Range suite, and small dikes of similar composition were observed in each of the other two units. There is no evidence concerning the relative age of the units, but based on regional patterns, it is likely that PMSMp is the oldest unit, and SMSMq, which is in direct contact with greenschist of the Wiley succession, is younger.

The black phyllite and calc-schist units are interpreted to form part of the Snowcap assemblage, while the quartzite could form part of the Snowcap or Finlayson assemblages. A possible along-strike correlative to the southeast is the Swift River Group of northern British Columbia/southernmost Yukon (Gleeson *et al.*, 2000; Roots *et al.*, 2006).

Wiley succession (DMWv)

There is extensive exposure of greenschist in the northern part of the map area, around the margins of the Livingstone pluton (Fig. 2). Another band of greenschist runs close to the margin of the Quite Lake batholith, in the Boswell River drainage. Each of these belts of greenschist is in contact with rocks of the Slate Mountain succession (quartzite unit) and are assigned to the Wiley succession. The greenschist is mostly medium to dark green (weathered) and dark green fresh. It is commonly banded, with millimetric alternations of dark green layers (rich in chlorite and amphibole) and pale layers rich in plagioclase or its replacement products (epidote, clinozoisite; Fig. 5a). The plagioclase rich layers can be relatively continuous or discontinuous lensoidal streaks. This banding is interpreted to result from solid state segregation during metamorphism and deformation. Hematite-stained surfaces are common, and malachite staining is locally developed.

Greenschist on the west side of the d'Abbadie fault (between the fault and the Livingstone pluton) is more varied, and exhibits abundant evidence for reworking of volcanic rocks (Fig. 5b,c). It includes lapilli tuff and finely banded epiclastic metasandstone. It also includes a 2–3 m band of dusty grey, amphibole rich marble near the top of the unit (Fig. 5d).

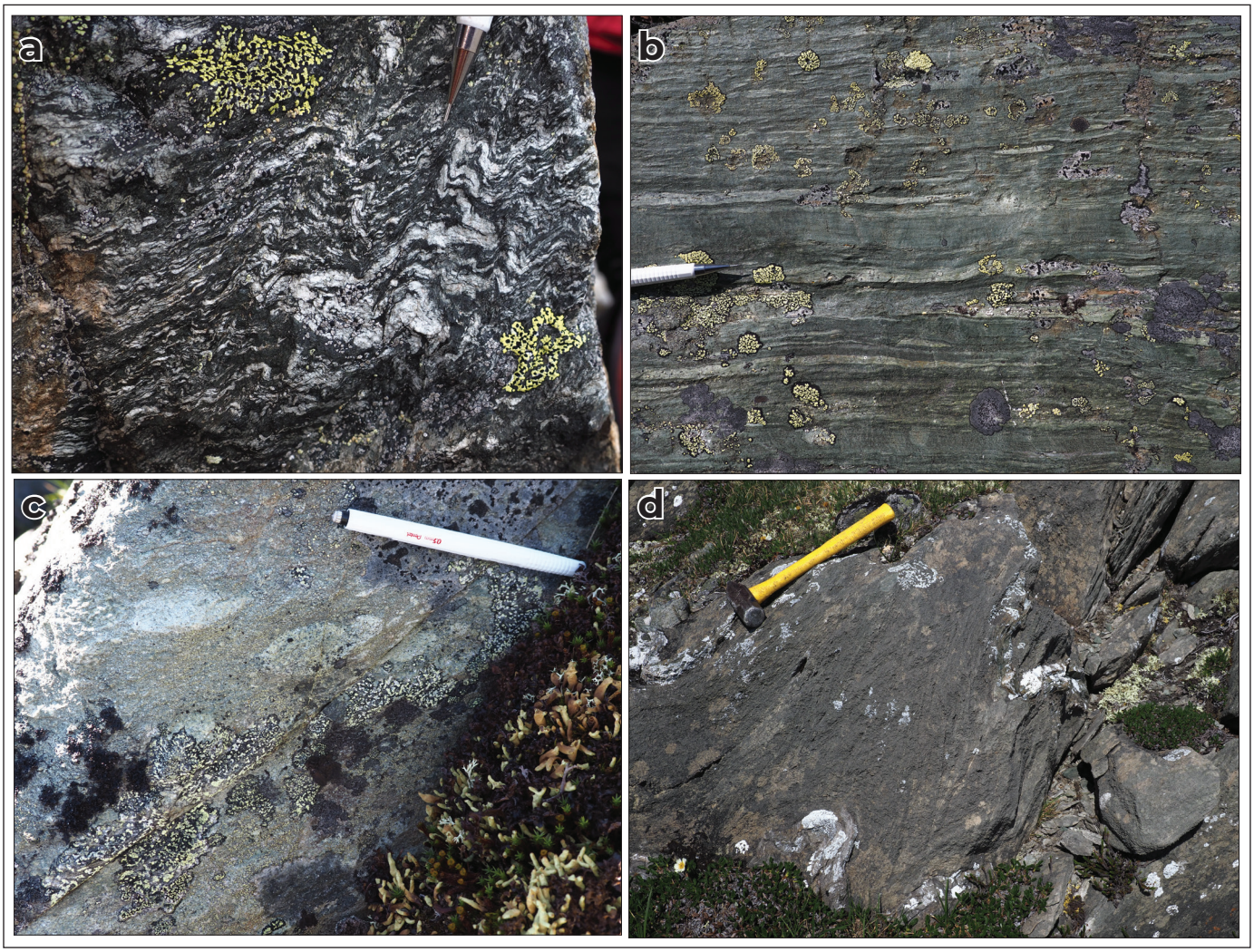


Figure 5. *Wiley succession field photographs.* ***(a)*** *Coarse-grained, segregated amphibolite with refolded folds of plagioclase-rich layers; pencil tip for scale.* ***(b)*** *Layered greenschist with stretched clasts visible in some layers; pencil for scale.* ***(c)*** *Lapilli tuff with centimetre-scale clasts in a matrix of finer grained mafic volcanic detritus; pencil for scale.* ***(d)*** *Folded grey amphibole-rich calc-silicate/marble; hammer for scale.*

Age constraints and correlation

The Wiley succession is interpreted to be intruded by rocks assigned to the Simpson Range suite and is therefore considered to be Early Mississippian or older. It is tentatively interpreted to form part of the Finlayson assemblage of Yukon-Tanana terrane.

Livingstone Creek succession (DMLC)

West of the d'Abbadie fault, greenschist of the Wiley succession is in contact with a distinctive marker unit, approximately 5–10 m thick, which is composed of calcareous (dolomitic) metasandstone and calc-silicate (Fig. 6). The rock weathers white, tan, creamy brown and pale orange and contains abundant coarse carbonate veins. The rock exhibits centimetre-scale layering and has a pitted appearance, caused by the weathering out of recessive carbonate around quartz-rich domains. This passes westward (with contact not exposed) into pale green, amphibole-rich schist.

On the west side of the Livingstone pluton, the Wiley succession is in contact with a mixed package of rocks that includes thin intervals (metres to tens of metres) of



Figure 6. *Basal unit of the Livingstone Creek succession. Layered dolomitic quartzite has a pitted texture caused by preferential weathering out of carbonate in some horizons; pencil for scale.*

many rock types. Lithological units include calc-schist and calcareous quartzite, greenschist, biotite-bearing greenschist with distinctive plagioclase spots, chlorite-muscovite schist, calc-schist and amphibole (chlorite-muscovite) schist.

These rocks are assigned to the Livingstone succession, which was defined by Harvey et *al.* (1997) on the north side of the South Big Salmon River. It is cut by the Livingstone pluton and otherwise only in contact with the Wiley succession. The limited and fragmented nature of its outcrop in the study area inhibits understanding of the distribution of rock types within this unit.

The Livingstone Creek succession is Early Mississippian or older, and was correlated with the Little Kalzas formation of the Finlayson assemblage (Colpron et *al.*, 2006b) by Colpron (2006).

Falls Creek and Red Mountain greenschist (SJv)

There are two regions of greenschist on the east side of the Little Bear fault that have an anomalous relationship to surrounding units; rather than being in contact with quartzite or separated from it by a thin marble, they are in direct contact with graphitic phyllite. The first of these is west of Falls Creek (Fig. 2).

Sulphide-rich greenschist includes intervals of finely banded rock, with mm to cm-scale, sharp to gradational alternations between chlorite-rich schist and siliceous layers. This is interpreted as depositional layering and rules out an intrusive origin for the rock. The Falls Creek greenschist is interpreted to be either 1) unconformable on the Slate Mountain succession, or 2) a local volcanic facies in the approximate stratigraphic position of the calc-schist unit. This greenschist is in contact with Permian augen schist and is therefore older than *ca.* 262 Ma (see below).

Another variety of greenschist in contact with graphitic phyllite was mapped by Taylor (1975) southwest of the Red Mountain deposit, close to the trace of the Little Bear fault; these rocks were described as chlorite schist, chlorite + graphite schist, talc-chlorite schist and talc-sericite schist. Only one outcrop in this area was visited, where graphitic phyllite is intercalated with pale green chloritic phyllite. Faint, thinly layered banding in the chloritic phyllite suggests a volcaniclastic origin for the rock, but further study is needed to better characterize the unit.

Fossiliferous limestone (CKcP)

A thick limestone/marble unit is preserved in a synformal keel directly northeast of the Little Bear fault, near the northwestern boundary of the Iron Creek stock. It overlies graphitic phyllite, and there is some interlayering of phyllite and calc-silicate near the base of the unit. A distinctive layer in the transition zone includes lenses/pods of yellow and orange carbonate in a phyllitic matrix. Most of the carbonate is relatively pure, fully recrystallized cream coloured calcite or dolomite marble, but patches of dark grey limestone are preserved (Fig. 7a). These darker grey regions contain chert bands and are highly fossiliferous, with abundant boundstone (Fig. 7b). Fossils include colonial corals, but formal analysis and identification has not yet been carried out.

The fossiliferous limestone is interpreted to be unconformable on the dark phyllite unit, and may be correlative with the Carboniferous, fossiliferous English Creek/Screw Creek limestone of the Klinkit assemblage (Simard et *al.* 2003; Roots et *al.*, 2006), which is widely distributed along strike to the southeast.

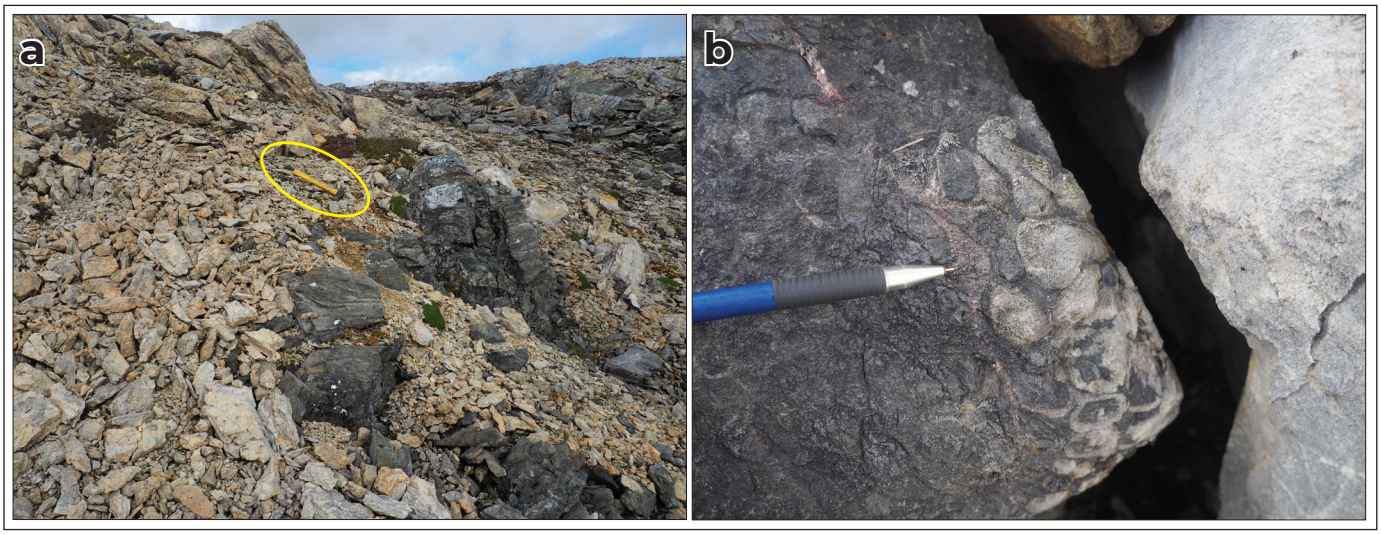


Figure 7. *Fossiliferous limestone field photographs.* ***(a)*** *Enclave of dark grey fossiliferous limestone surrounded by talus and outcrop of fully recrystallized, dolomitic marble.* ***(b)*** *Cross sectional view through coral boundstone; pencil for scale.*

Metasedimentary, metavolcanic and mafic metaplutonic rocks between the Little Bear and Sidney Creek faults (Semenof block)

Sawtooth succession (DMSv, DMSg)

The northeastern flanks of the Sawtooth Range are underlain by greenschist (metabasalt) and metagabbro. The greenschist is medium to dark green and weathers rusty brown. It is chlorite rich (Fig. 8a), phyllitic to schistose, and in some locations exhibits compositional banding, with pale layers/lenses composed of plagioclase and/or its replacement products (e.g., clinozoisite) that alternate with dark green, chlorite, epidote and amphibole-rich domains (Fig. 8b). It locally includes porphyritic tuffaceous layers (Fig. 8c). The greenschist has high to very high magnetic susceptibility (locally up to 80 SI units). Hematite-stained surfaces are common in the greenschist, and malachite staining was locally observed. Greenschist is foliated throughout, but is particularly strongly foliated and banded near boundaries with marble of the overlying Rosy succession. Locally, at or near the top of the greenschist (near its contact with the Rosy succession), there is a white to orange brown weathering, more plagioclase-rich, strongly banded unit that is interpreted as a metamorphosed and deformed interval of volcaniclastic rock (Fig. 8d). This interval also includes some siliceous chlorite-muscovite schist and thin impure marble layers.

Metagabbro is typically medium to very coarse (Fig. 8e), texturally highly variable (Fig. 8f), and commonly weathers white. Local varieties include metagabbroic pegmatite (Fig. 8g) and leucogabbro. It is mostly foliated but variably deformed, with relatively weakly deformed pods surrounded by anastomosing arrays of more highly foliated domains. Typically, metagabbro retains its igneous texture, with plagioclase and pyroxene crystals pseudomorphed by clinozoisite and amphibole-rich domains, respectively. Locally, Cr-rich mica is also developed. In regions of high strain, including some contacts with the Rosy succession, there is a progressive reduction in grain size and metagabbro is transformed to a pale green, chlorite-rich schist.

The boundaries between greenschist and gabbro-dominated regions are commonly gradational, and each contains a minor proportion of the other lithology; gabbroic domains locally include abundant thin screens of metabasalt (Fig. 8h), while there are numerous small gabbro plugs within greenschist-dominated regions. Nevertheless, they form separate map units, and their folded contact defines structures, e.g., the upright antiform north of Sidney Creek.



Figure 8. *Sawtooth succession field photographs.* ***(a)*** *Crenulated chlorite-rich greenschist; pencil for scale.* ***(b)*** *Banded greenschist with tightly folded, plagioclase-rich and poor layers; pencil tip for scale.* ***(c)*** *Plagioclase phenocrysts in a tuffaceous horizon within the Sawtooth succession greenschist unit.* ***(d)*** *Fine-grained, strongly banded interval, interpreted as a volcaniclastic horizon near the top of the Sawtooth succession; pencil for scale.* ***(e)*** *Coarse-grained, foliated metagabbro. Igneous minerals have been replaced but the primary texture is preserved; pencil for scale.* ***(f)*** *Medium to coarse-grained foliated metagabbro with varying grain size and degrees of strain; hammer for scale.* *Figure continued on next page.*

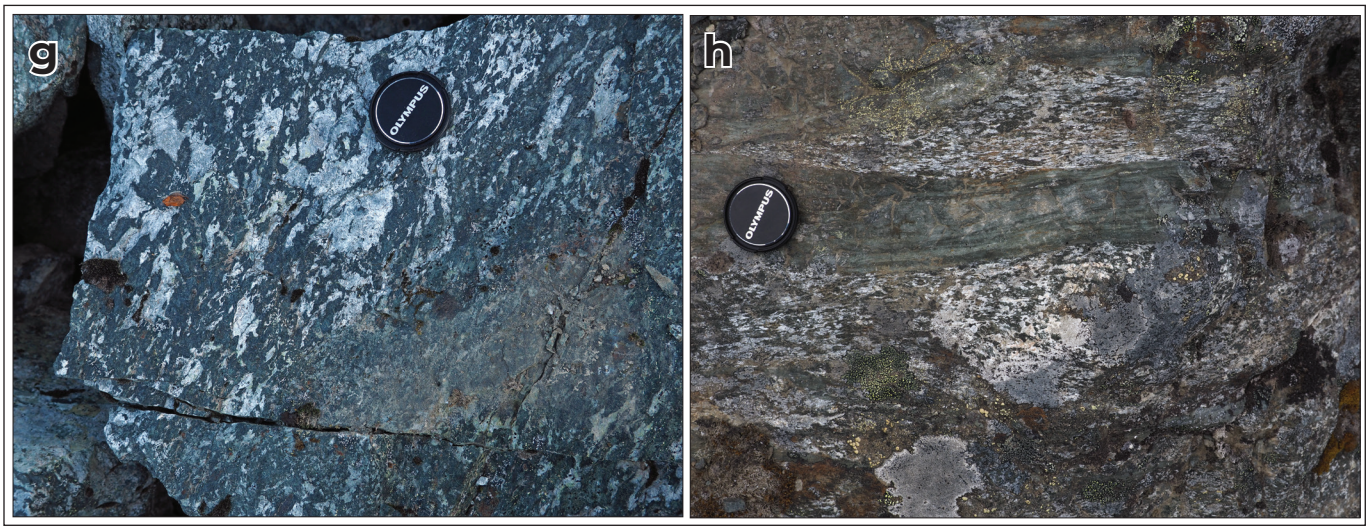


***Figure 8** continued.**(g)** Greenschist enclave in metagabbro, with apparent truncation of the compositional layering; lens cap for scale. **(h)** Metagabbroic pegmatite with cm-scale crystals; lens cap for scale.*

Ultramafic rocks form a negligible proportion of the Sawtooth succession; metre-scale serpentinite pods after metagabbro were observed near the Iron Creek pluton/Little Bear fault, and a few metres of carbonate-altered (?) ultramafic rock is developed along a fault that cuts the greenschist unit south of the Boswell River.

Correlation of the Sawtooth assemblage with the Moose formation

Metavolcanic rocks on the southwestern side of the Little Bear fault have relatively high magnetic susceptibility, whereas metasedimentary rocks on its northeastern side are mostly non-magnetic (Fig. 9). This gives rise to a prominent linear aeromagnetic boundary, which is a geophysical proxy for the fault trace. The fault and its associated aeromagnetic feature extend northwestward from the mapped area into a region, approximately 6 km wide, which is underlain by Late Cretaceous volcanic rocks (80 ± 2.3 Ma; Stevens *et al.*, 1982).

A similar arrangement is evident on the northwestern side of the Late Cretaceous volcanic belt. Here, mafic volcanic rocks of the Moose and Semenof formations are juxtaposed, across the trace of the Big Salmon fault (*sensu* Stevens, 1994; Simard *et al.* 2003; Colpron, 2006a), with non-magnetic metasedimentary rocks of the Loon Lake succession, resulting in a similar aeromagnetic contrast.

The fault and lithological boundaries on either side are collinear, and are interpreted to be continuous under the unconformably overlying Late Cretaceous volcanic rocks. This interpretation is supported by linear aeromagnetic features that pass into and out of the Cretaceous volcanic rocks without deflection. The Slate Mountain succession can be traced continuously on the eastern side of the Little Bear fault into rocks, on the eastern side of the Big Salmon fault, that were assigned to the Loon Lake succession by Barresi (2004). Based on these relationships, the Moose formation and Sawtooth succession are provisionally interpreted to be adjacent parts of the same metavolcanic unit.

There are no direct constraints on the age of the Sawtooth succession, but three U-Pb dates constrain the age of the Moose formation. A quartz-feldspar porphyritic rhyolite at the top of the formation yielded a date of approximately 359 ± 3 Ma (based on 2 concordant fractions out of 5; Yukon Geological Survey (YGS), 2021). Another sample from the same rhyolite member produced a date of 352.1 ± 1 Ma, with one of three fractions concordant. Southwest of Loon Lakes, the Moose formation is intruded by hornblende diorite and by pink and green, locally quartz-porphyritic granite. The granitic phase, which is the later of the two phases yielded a date of 347.0 ± 1.2 Ma, with three of six fractions concordant. Farther north, near Little Salmon Lake, a fine-grained quartz diorite that was interpreted to be comagmatic with basalt, yielded a slightly younger date of 342.8 ± 2.2 Ma (YGS, 2021).

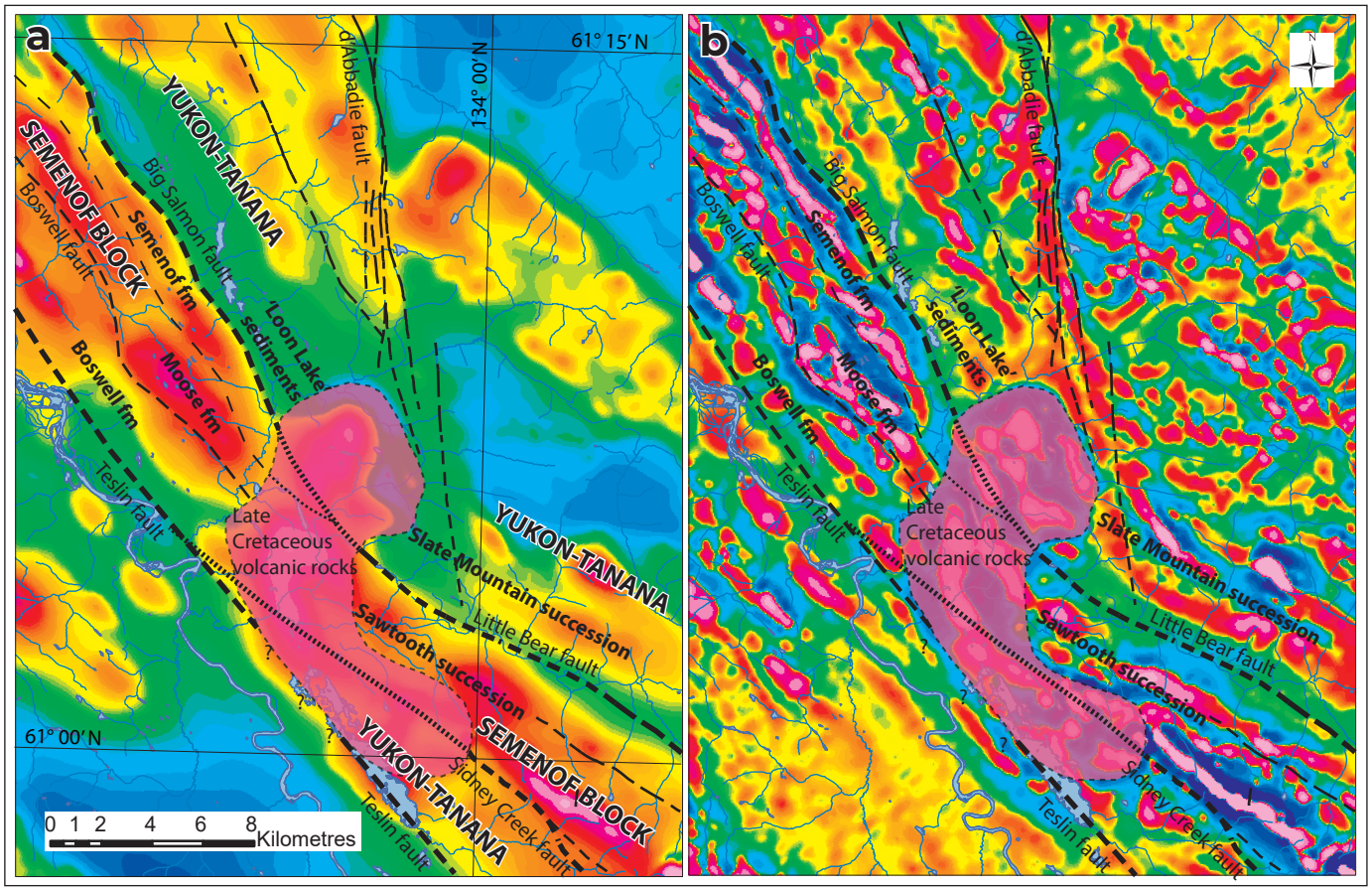


Figure 9. *Residual* ***(a)*** *and second derivative* ***(b)*** *results from the Marsh Lake aeromagnetic survey (Kiss and Boulanger, 2018), covering the northwestern part of the study area and the southern Semenof Hills. Interpreted faults and contacts are shown. The Sawtooth succession is interpreted to be correlative with the Early Mississippian Moose formation, which lies along strike to the northwest. The southern tip zone of the d'Abbadie fault is in the region N-NE of the Late Cretaceous rocks. The southwestern boundary of the Late Cretaceous volcanic belt may coincide with the Teslin fault. Geology of the area NW of the Cretaceous volcanic rocks is from Simard (2003) and Colpron (2017).*

Rosy succession (DMRc, DMRt, DMR)

Gabbro and greenschist of the Sawtooth succession are each in contact with a pale marble/calc-silicate unit that forms the base of the Rosy succession. Marble is mostly white or cream and pale grey weathering (Fig. 10a). Impure parts of the unit are white, cream or tan, with abundant brown weathering micaceous folia between marble bands, or pods of white, columnar tremolite/wollastonite.

In some places, a relatively pure marble/calc-silicate is up to 20 m thick, but elsewhere, the basal Rosy succession consists of thin (metre-scale) alternations of pale marble, quartz-rich white or green calc-silicate (Fig. 10b), and calc-schist. In part of the Sawtooth Range an orange-brown dolomitic breccia forms a thin band surrounded by greenschist. This likely represents an isoclinal infold of the basal Rosy succession, rather than a unit that is stratigraphically within the Sawtooth succession.

Although a basal marble/calc-silicate unit is ubiquitous, the overlying Rosy succession is variable. On the east flank of the Sawtooth Range, basal marble and calc-silicate pass upward through a thin interval (10–15 m) of greenschist and striped siliceous rock (metachert?) into tens of metres of dark graphitic phyllite. Locally, the phyllite contains thin sooty limestone/marble layers (Fig. 10c).

On the western flank of the Sawtooth Range (NW of the Sawtooth stock), marble becomes impure upsection, with abundant thin grey siliceous layers alternating with white to tan marble/calc-silicate (Fig. 10d). The mixed siliceous/carbonate is overlain by thinly layered siliceous rock that is interpreted as metachert (Fig. 10e). The chert ranges from white to brown, is thinly layered, forms platy outcrops, and mostly composed of silica, with some very fine mica crystals on foliation planes. Some thin intervals of greenschist were locally observed near the base of this unit, but rocks above the metachert are not exposed.

Southeast of the Sawtooth stock, the lower parts of the Rosy succession includes massive marble, but contains a greater proportion of mixed marble with siliceous layers. Marble-dominated rock passes into a characteristic stripy unit that contains cm-scale, alternating bands of siliceous rock (metachert?) and recessive weathering, calcareous bands (Fig. 10f). Graphitic phyllite is also locally exposed in this region.

Calcareous layers in the banded unit are mostly grey, but locally buff coloured. The calcareous bands die out into an interval of thinly layered metachert (Fig. 10g). In close proximity to a hornblendite intrusion, (tuffaceous?) calcareous layers within the banded interval are transformed into recessive-weathering, green amphibole schist (Fig. 10f), and siliceous layers are green or pink (Fig. 10h). The pink colouration is



Figure 10. *Rosy succession field photographs.* ***(a)*** *Pure white, grey weathering marble; pencil-sized eraser for scale.* ***(b)*** *Pale green quartzite and calc-silicate near the base of the Rosy succession; hammer for scale.* ***(c)*** *Dusty grey limestone forms thin layers in graphitic phyllite of the Rosy succession northwest of the Sawtooth stock; pencil for scale.* ***(d)*** *Grey marble with numerous thin (1-5 cm thick) siliceous layers. Pencil for scale.* *Figure continued on next page.*

caused by the presence of pink/fuchsia epidote, which may reflect a high Mn content. In this area, the thin-banded chert, which is mostly white, grey (Fig. 10g) or pale green elsewhere, is pink/mauve (not illustrated).

The lower, calcareous part of the Rosy succession is intruded by Mississippian metagranodiorite (ca. 336 Ma; see below). Contact of the basal carbonate unit with both metagabbro and metabasalt of the Sawtooth succession is suggestive of a primary unconformable relationship, but the nature of the relationship is obscured by high strain.

Gunsight succession (MJGv)

Mafic volcanic and volcaniclastic rocks underlie the region immediately northeast of the Sidney Creek fault, from the southeastern margin of the Sawtooth pluton to the edge of the mapped area. The contact with the Rosy succession is tightly constrained on the ridge immediately northeast of the Red Mountain road but is not exposed. Grey metachert of the Rosy succession is in close proximity to an interval of fine to medium grained volcaniclastic metasediments. Grey-green metasiltstone and metasandstone display internal laminations and cm-scale, locally graded layering. This interval also includes some coarser-

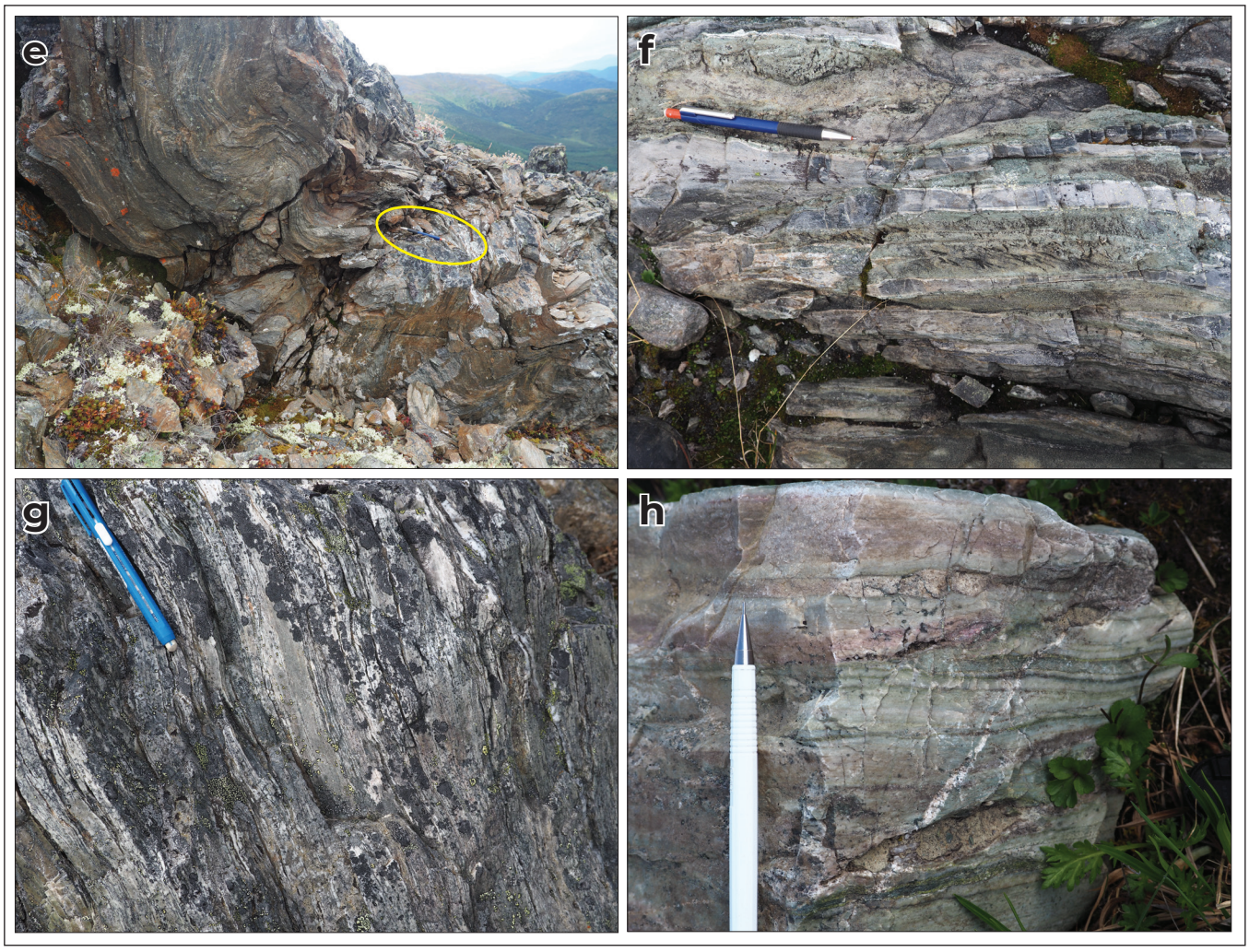


***Figure 10** continued.* ***(e)** Folded brown quartzite, interpreted as metachert, from the northwestern side of the Sawtooth stock; pencil for scale.* ***(f)** Centimetre-scale alternation between grey siliceous layers and green, slightly calcareous (tuffaceous?) amphibole schist; pencil for scale.* ***(g)** Thinly layered interval of white and grey weathering siliceous rock, interpreted as metachert; pencil-sized eraser for scale.* ***(h)** Green chert with some thin calcareous (recessive) layers; pencil for scale.*

grained layers of amphibole-plagioclase schist. This relatively fine-grained interval passes westward into coarser mafic volcaniclastic rocks. Lapilli tuff at the base of the coarse interval includes cm-scale clasts of grey marble in addition to mafic volcanic clasts and sparsely distributed grey chert (Fig. 11a). Recessive weathering of carbonate gives rise to a pitted texture in some layers within this rock. The overlying green-grey to dark grey tuffaceous layers contain lapilli to block clasts, and include discontinuous, wispy layers of ash tuff (Fig. 11b), along with intraclasts of grey to green volcanic metasiltstone/sandstone. The outline of stubby black pseudomorphed (?)pyroxene and plagioclase phenocrysts are preserved, and angular clast outlines are discernable in some of the coarser grained, less foliated horizons (Fig. 11c).

Near the margins (within hundreds of metres) of the hornblendite that intrudes the Gunsight succession, many rocks are massive, black weathering, and grey on fresh surfaces. Elsewhere, the most common rock types include mint green chlorite schist with relic black phenocrysts, green plagioclase-rich metasandstone, and mint green, well foliated lapilli tuff (Fig. 11d).

The Gunsight succession is interpreted to stratigraphically overlie the Rosy succession; It is therefore Mississippian or younger, and could be as young as early Jurassic – the interpreted age of the crosscutting hornblendite body (see below).

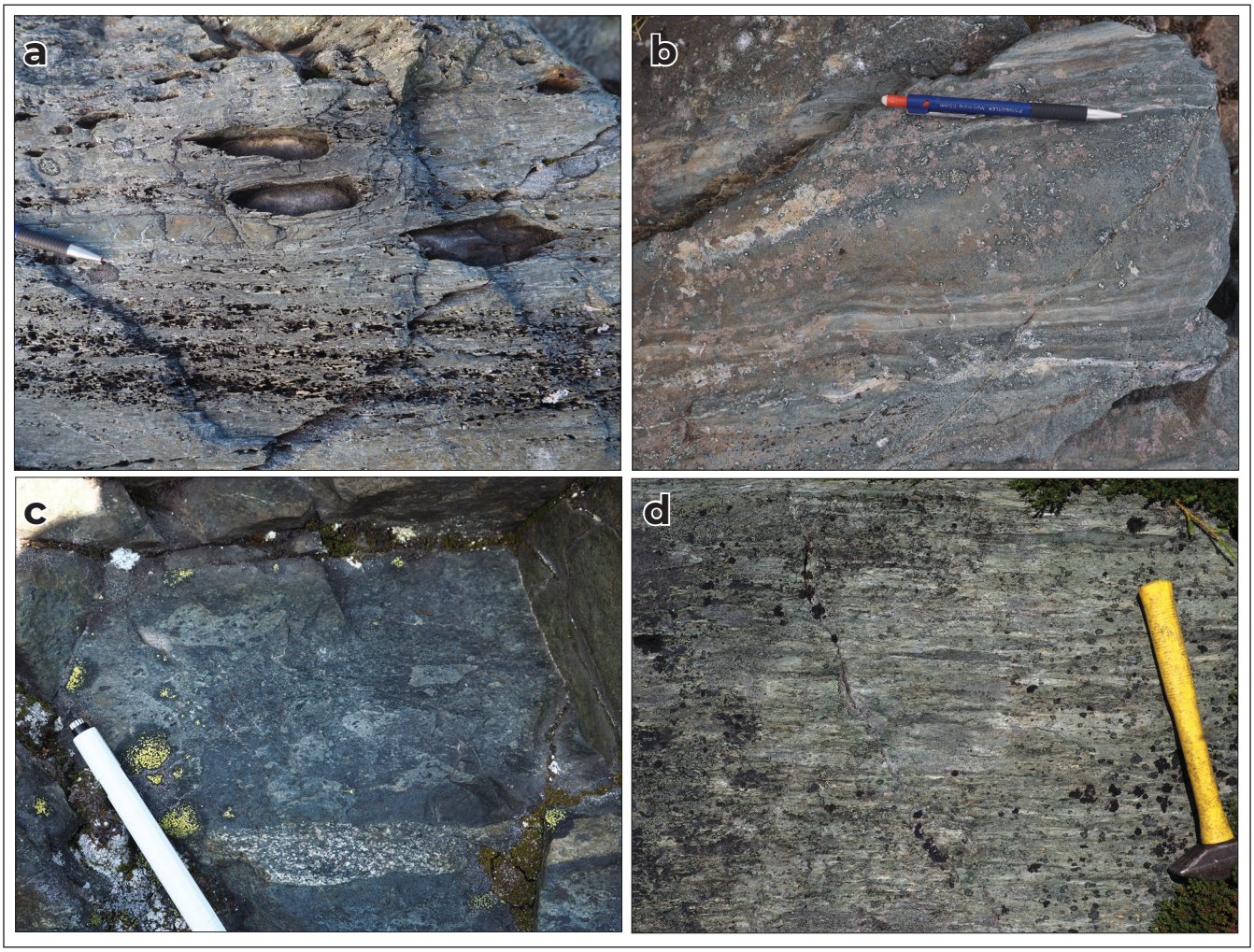


Figure 11. *Gunsight succession field photographs.* ***(a)*** *Lapilli tuff with recessive grey carbonate clasts; pencil for scale.* ***(b)*** *Wispy ash mafic layers near the base of the Gunsight succession; pencil for scale.* ***(c)*** *Angular clasts of clinopyroxene(?) porphyry in a lapilli tuff. The tuff is cut by an undeformed plagioclase-hornblende porphyritic dike, which is interpreted to form part of the Jurassic Lokken suite; pencil for scale.* ***(d)*** *Stretched clasts in green, chloritic lapilli tuff; hammer for scale.*

Metasedimentary and metavolcanic rocks southwest of the Sidney Creek fault (Yukon-Tanana terrane)

Flat Creek succession (PMFCq, PMFCg, PMFCp, PMFCv)

The southern part of the mapped area is dominated by exposures of metaplutonic rocks of the Simpson Range suite (Swift River pluton; Fig. 2). Metasedimentary rocks are exposed around the fringes of the pluton and as a screen within. The most extensive belt of metasedimentary rocks is between the northern margin of the pluton and the Sidney Creek fault. This region is dominated by micaceous quartzite (Fig. 12a), with lesser marble and calc-silicate. The micaceous quartzite is pale shades of beige, grey, green, tan and white, and is grey and glassy on fresh broken surfaces. It contains abundant micaceous foliation surfaces and is locally garnet-bearing. Talus generated from this unit is blocky, has smooth surfaces, and is commonly associated with yellow-orange staining. Foliated 'grit' that is exposed southeast of the Sawtooth stock is also included in the Flat Creek succession (Fig. 12b). The grit comprises thick, homogeneous layers, is cream to tan coloured, poorly sorted, and contains abundant quartz granules.

Marble and calc-silicate (Fig. 12c) form layers and pods that are mostly metres thick, but locally up to 20 m. Marble is white and pale grey weathering, with sparse silicate folia. It is also commonly mixed with white or cream calc-silicate/calc-schist and calcareous quartzite.

The region between the Sidney Creek fault and the batholith also includes two significant regions of amphibolite and garnet amphibolite (Fig. 12d), interpreted as metabasite, with strike lengths >1 km. The (garnet) amphibolite is black, and commonly contains thin (mm to cm-scale) lenses and layers of felsic intrusive rock with sparsely distributed amphibole. The amphibolite is in contact with micaceous quartzite, but the primary relationship (intrusive *vs.* stratigraphic) is unknown.

Metabasite is also exposed on the southwestern flanks of the batholith, near the margin of the mapped area. Here, green, rusty weathering metabasalt forms resistant slabby outcrops with abundant hematite staining. It is in contact with quartz-rich steely grey schist that grades into graphitic phyllite (locally garnet-bearing schist). Outcrops of graphitic phyllite include thin intervals of calc-schist and greenschist.

Varied rocks on the poorly exposed slopes west of the Sawtooth pluton, which host a Triassic metagabbro (described below) include quartz-rich paragneiss with abundant quartzo-feldspathic segregations, garnet amphibolite and deformed felsic-intermediate intrusions. There is also banded (metavolcaniclastic?) rock composed of cm-scale alternations between grey siliceous layers and pale green and grey amphibole/biotite schist, which is intruded by metamorphosed hornblende tonalite/diorite. This amphibole-biotite schist was not observed elsewhere in the Flat Creek succession.

Micaceous quartzite south of the Sidney Creek fault, and graphitic phyllite and greenschist in the southwestern part of the map area are cut by small intrusions of amphibole-bearing metatonalite, possibly of the Simpson Range suite; they are therefore likely to be Early Mississippian or older. The relationship between the graphitic phyllite and the micaceous quartzite/marble unit is not known, nor is the nature of the contacts with greenschist/amphibolite/garnet amphibolite.

Mafic volcanic/volcaniclastic rocks (MJv)

A small region of foliated mafic volcaniclastic rock is in contact with metatonalite of the Simpson Range suite near the southeastern boundary of the map area. This includes mafic lapilli tuff with rare clasts of fibrous serpentinite and quartz clasts. The unit also includes thinly layered amphibole-biotite-plagioclase schist. The mafic unit was either deposited unconformably on the Simpson Range suite prior to deformation that affects both units, or represents a screen within the Swift River pluton.



Figure 12. *Flat Creek succession field photographs.* ***(a)*** *Grey and green quartzite and micaceous quartzite; hammer for scale.* ***(b)*** *Tan weathering 'grit' with prominent quartz grains and granules; pencil for scale.* ***(c)*** *Grey weathering, white marble with resistant-weathering micaceous folia; hammer for scale.* ***(d)*** *Small garnet crystals in black weathering garnet amphibolite; pencil tip for scale.*

Plutonic and metaplutonic rocks

Grass Lakes suite (DMg)

The summit of Mount Black and the ridge leading north from it are underlain by deformed porphyritic two-mica granitic orthogneiss (Figs. 2 and 13a,b). The rock has a spotted appearance, with phenocrysts/porphyroclasts of creamy-yellow weathering K-feldspar in a brown to grey matrix. This is correlated with the Late Devonian-Early Mississippian Grass Lakes suite, which forms extensive sill-like bodies in parts of Yukon-Tanana (Murphy et *al*., 2006). Exposures of this unit north of the mapped area returned latest Devonian U-Pb dates (Hansen et al., 1989; Westberg, 2010; Colpron et *al*. 2017). The Grass Lake suite is cut by Cretaceous granite of the Quiet Lake batholith. As these units form similar topography and rocks are heavily lichen covered, the contact shown on the map is an approximation.

Simpson Range suite (EMt)

Deformed metatonalite and associated rocks are volumetrically significant in two parts of the map area: 1) north of the Indian River, on the northeastern side of the Little Bear fault (Livingstone pluton), and 2) south of the Sidney Creek fault (Swift River pluton). The dominant rock types in these regions are texturally

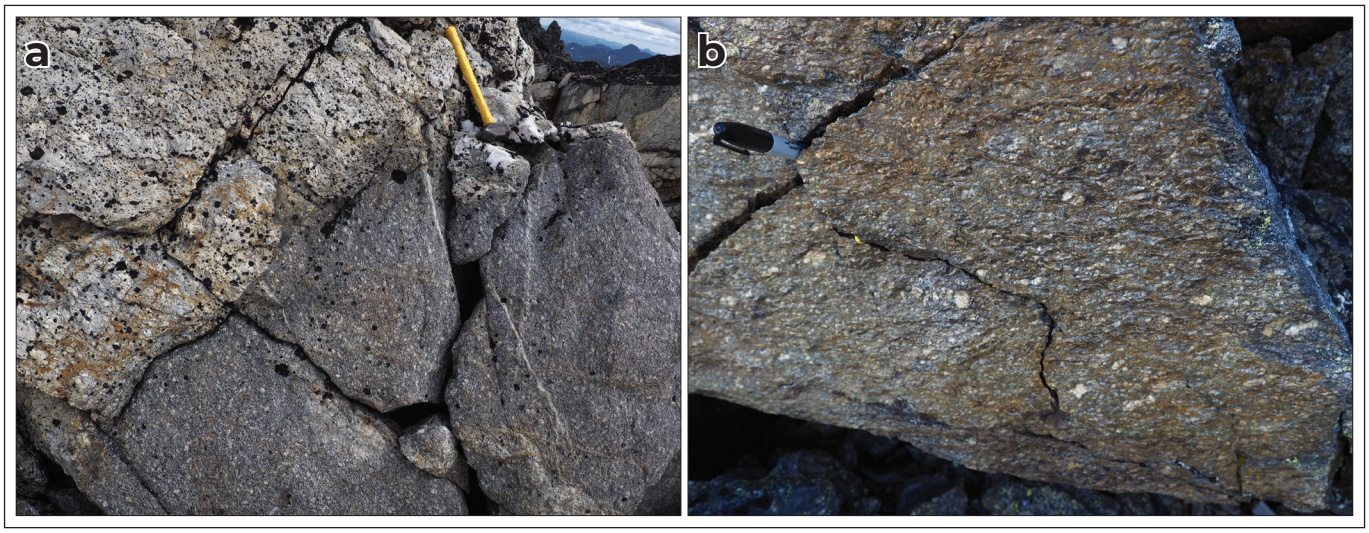


Figure 13. *Grass Lakes suite field photographs.* ***(a)*** *Porphyritic granitic orthogneiss of the Grass Lakes suite cut by undeformed pale yellow Cretaceous granite; hammer for scale.* ***(b)*** *Close-up view of orthogneiss with ~1 cm long K-feldspar crystals wrapped by the foliation; pen for scale visible on extreme left of photograph. Diameter of the pen is ~1 cm.*

and compositionally heterogeneous hornblende metatonalite, metagranodiorite and meta-quartz diorite. Varieties include strained rocks with intact igneous textures, thoroughly recrystallized schists whose protoliths are inferred to be meta-igneous, and intermediate gradations.

Hornblende metatonalite (Fig. 14a) to granodiorite is coarse grained and equigranular or, less commonly porphyritic (Fig. 14b). It is grey-green and weathers white, orange-brown and white, grey or greenish grey. The rock is generally foliated, though non-foliated pods are locally preserved, and is dominated by plagioclase and pseudomorphs of hornblende (now mostly chlorite). Metatonalite is commonly banded or streaky (Fig. 14c,d), characterized by centimetre to decimetre-scale layers or lenses of differing grain size, colour and composition.

Micaceous schists derived from metatonalite-metagranodiorite share the same grey-green colouration and are commonly strongly compositionally banded; they are finer grained, locally weather pale yellow and have a fully recrystallized, metamorphic texture. They have more abundant foliation-parallel quartz veins, and locally include garnet, in addition to plagioclase, quartz, micas and amphibole/chlorite.

The body of metatonalite-granodiorite that underlies the northern part of the area is interpreted to be continuous with the Livingstone pluton, a deformed pluton that underlies a large region in the central part of the Livingstone Creek area to the north (Colpron, 2017). Colpron *et al.* (2017) reported a U-Pb zircon date of 351 ± 1 Ma from metagranodiorite in this pluton. A poorly constrained U-Pb zircon date of 341 +5/-17 Ma was reported by Stevens (1994) for metatonalite of the Swift River pluton. Based on these ages, and characteristics of the rocks, the dominant rock types in these plutons are assigned to the Simpson Range suite. Small intrusions (dikes) of similar rocks were noted in rocks of the Slate Mountain succession and the Flat Creek succession. A single dike of hornblende-bearing diorite crosscuts the Gunsight succession, but it is not known whether this belongs to the Simpson Range, or another, younger plutonic suite.

Part of the eastern flank of the Livingstone pluton comprises banded metadiorite and amphibolite with hornblendite boudins. Outcrops also locally contain abundant deformed pegmatite lenses/layers. This portion of the pluton is broadly coincident with an aeromagnetic high. It is provisionally interpreted as a mafic phase of the Simpson Range suite.

Distinctive leucocratic hornblende metatonalite ('birdfoot leucotonalite') and leucotonalite forms a slender body east of the Livingstone pluton and also forms dikes in its vicinity. Indistinguishable dikes are exposed on the western flanks of the Swift River pluton and leucotonalite forms larger bodies within the Swift River pluton. The characteristic feature of the hornblende leucotonalite (Fig. 14e) is the presence of cm-scale elongate hornblende crystals (now replaced by chlorite) that are sparsely distributed through the rock. Leucotonalite (Fig. 14f) has a medium grained quartzo-feldspathic matrix. It weathers white and is grey-white on fresh surfaces; locally it has a pink/mauve tint and in rare cases contains small (1–2 mm scale) quartz augen. Leucocratic tonalite in the Swift River pluton crosscuts more mafic, hornblende-bearing metatonalite and is therefore, at least locally, a younger phase. In the absence of information to the contrary, the (hornblende) leucotonalite is tentatively interpreted to form part of the Simpson Range suite.

Tatlmain or Kelly suite(?) (EMgd)

A very small (approximately 200 m^2) foliated metagranodiorite intrusion crosscuts the lower, calcareous part of the Rosy succession northwest of the Sawtooth stock. The rock is medium to coarse-grained, weakly porphyritic metagranodiorite with a distinctive pink and green colouration (Fig. 14g).

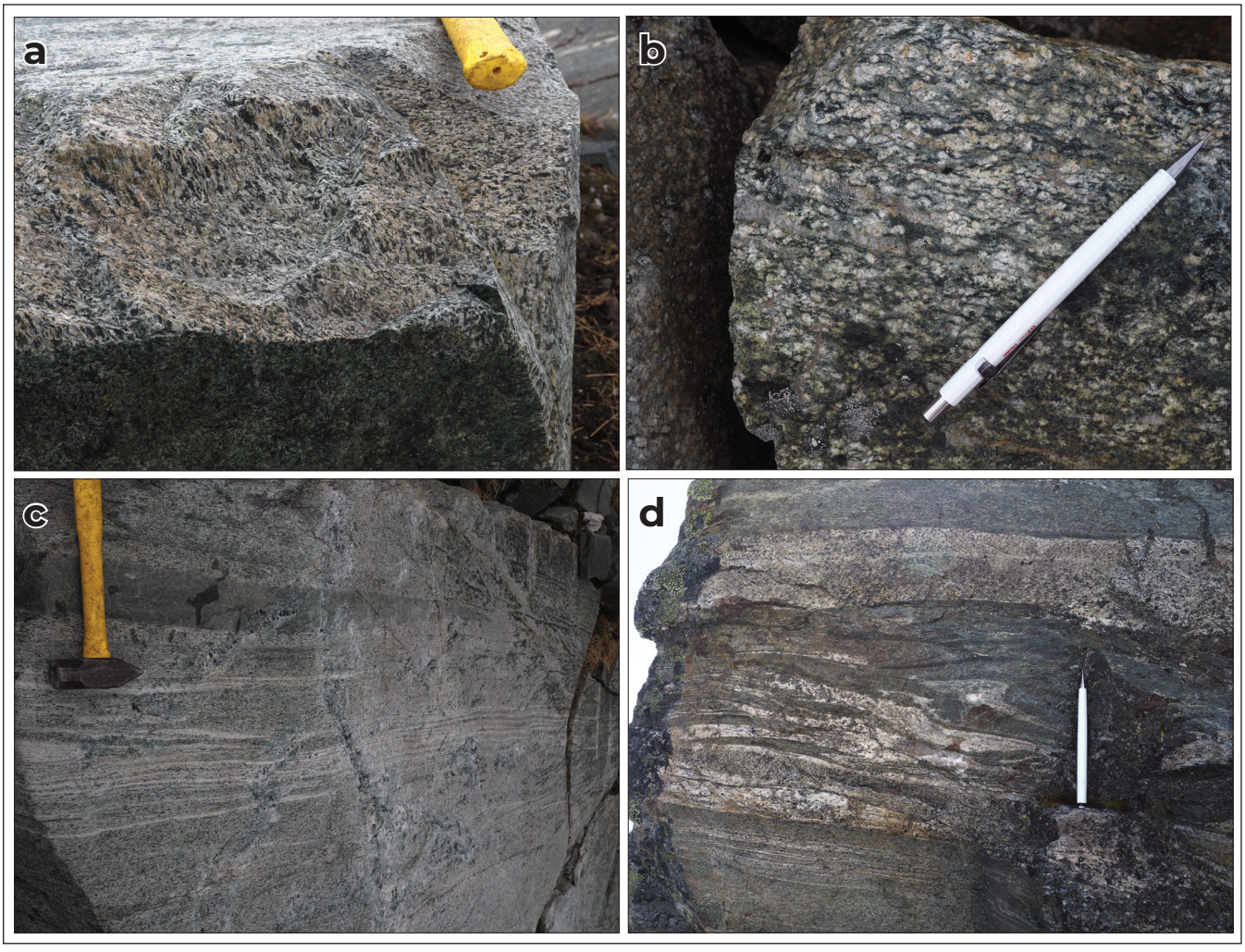


Figure 14. *Simpson Range suite field photographs.* ***(a)*** *Homogeneous, coarse-grained hornblende-bearing metatonalite; hammer for scale.* ***(b)*** *Porphyritic hornblende granodiorite; pencil for scale.* ***(c)*** *Compositionally layered, foliated metatonalite; hammer for scale.* ***(d)*** *Heterogeneous banded metatonalite composed of intrusive sheets of varying composition and grain size; pencil for scale. Figure continued on next page.*

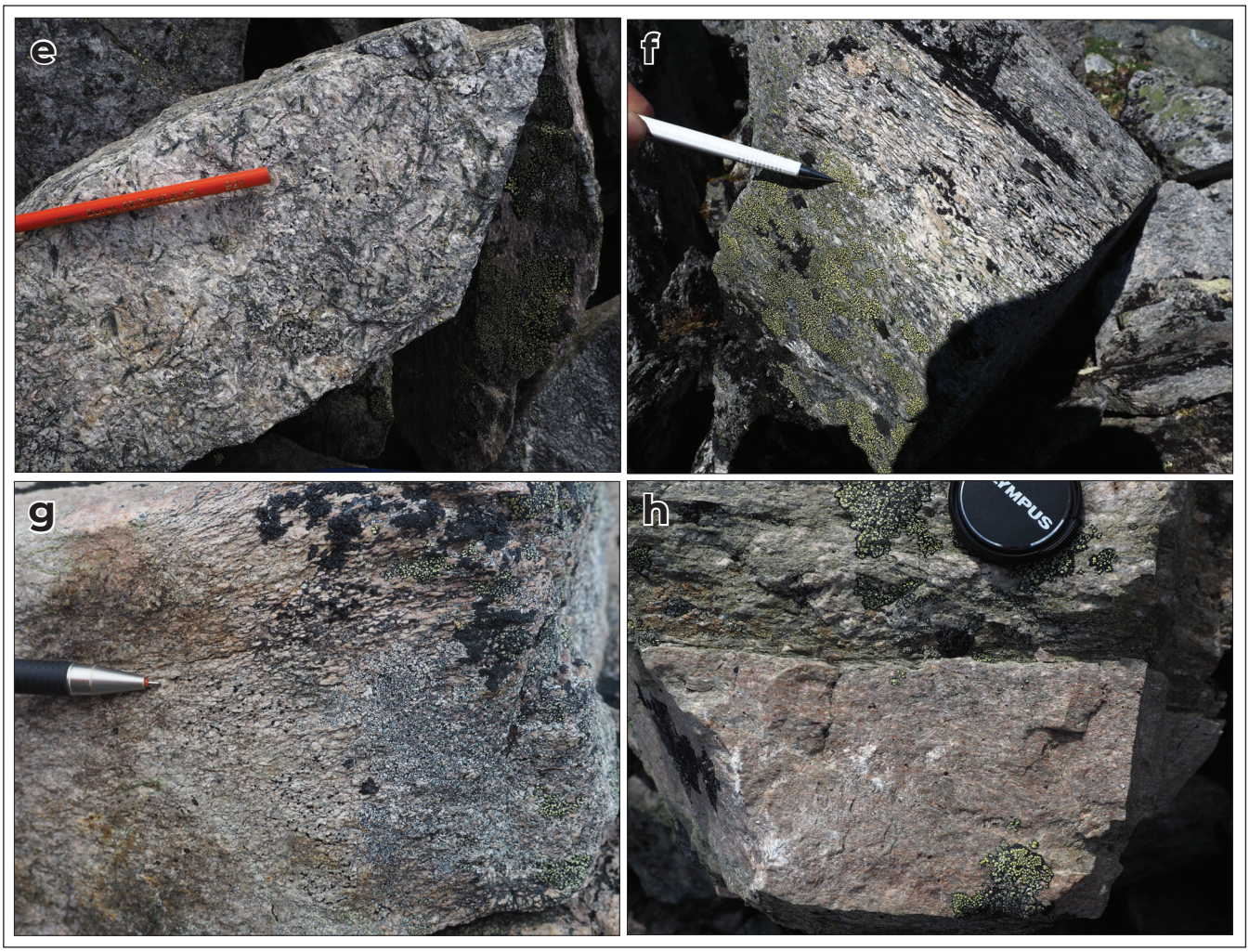


***Figure 14** continued. **(e)** Elongate pseudomorphs of hornblende in leucotonalite; pencil for scale. **(f)** Scaly weathered surface of white weathering leucotonalite; pencil for scale. **(g)** Outcrop photograph of Mississippian metagranodiorite outcrop, from which geochronology sample 20DMO-043 was obtained; pencil for scale. **(h)** Pink-weathering, epidote-rich (metagranodiorite?) dike in metatonalite; lens cap for scale.*

The rock exhibits a penetrative to semi-penetrative foliation that is defined by abundant, preferentially aligned white mica and epidote. The foliation anastomoses around ovoid, rounded crystals of twinned plagioclase. The rocks also includes polycrystalline quartz, accessory phases, and minor retrograde chlorite (Fig. 15).

A sample of this intrusion (20DMO-043; Fig. 15) was separated for U-Pb geochronology. Details on the methods used for this and other geochronology samples are included in the digital Appendix. Two zircon populations were identified in this sample. The first comprises relatively large, elongate crystals that commonly exhibit oscillatory and/or sector zoning. Some of these crystals have thin bright (CL) rims. These crystals have Eu/Eu* values in the range 0.11–0.63, ΣREE values in the range of 385–4403, (Gd/Yb)cn ratios of 0.02–0.06 and Th/U ratios of 0.26–0.91 (Appendix). Calculated Ti in zircon temperatures are in the range of 631–809°C. The second population consists of zircons that are mostly small, equidimensional crystals with complex zoning patterns. These crystals, which have very little U, very low Th/U and ΣREE, are interpreted as metamorphic crystals. It is likely that the bright (CL) rims on the igneous zircon crystals are related to this episode of metamorphic zircon growth.

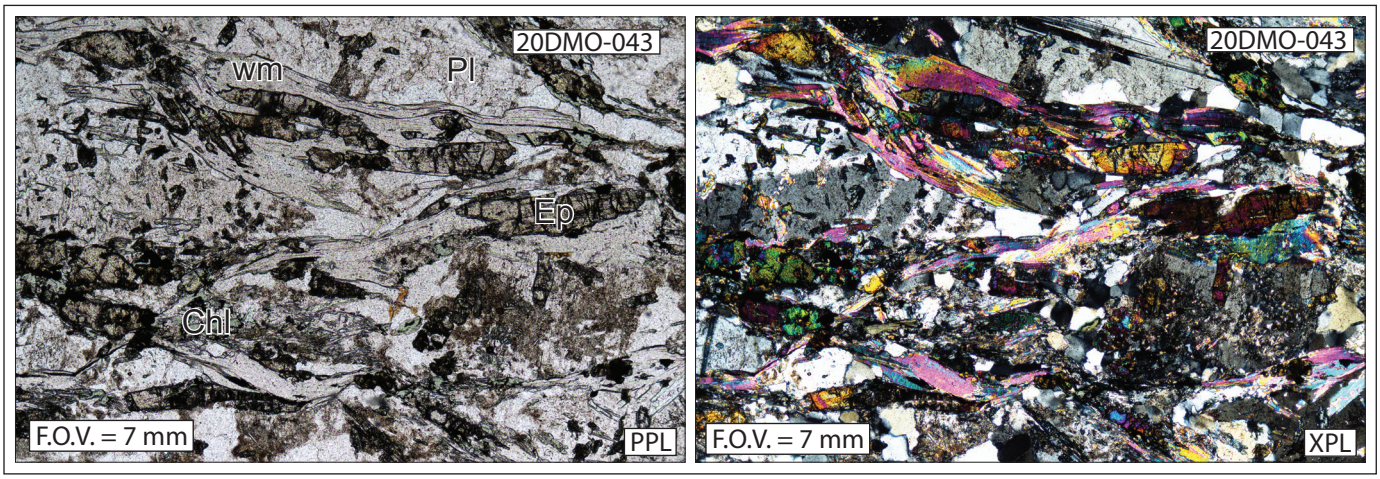


Figure 15. *Thin section photographs of metagranodiorite sample 20DMO-043. The foliation is mostly defined by abundant white mica and epidote. PPL – plane polarized light; XPL- cross-polarized light.*

The igneous population yielded a LA-ICPMS weighted mean $^{206}Pb/^{238}U$ date of 335.2 ± 4.0 Ma (MSWD = 1.5), based on 11 of the 15 analyzed spots, none of which sampled rim material (Fig. 16 a,b; Appendix). Four of these grains were selected for CA-TIMS analysis and all plot along the concordia, with a range in $^{206}Pb/^{238}U$ dates from 330.23 ± 0.24 to 336.09 ± 0.23 Ma (Fig. 16c; Table 1). The scatter in the data is attributed to incorporation of small amounts of metamorphic rim material and/or lead loss, while the oldest date is interpreted as a close approximation to the age of crystallization. This date is within the range of the Tatlmain and Kelly suites. The Tatlmain suite includes at least part of the Mt. Hazel orthogneiss, which underlies parts of the Teslin (105C), Jennings River (104O) and Atlin (104N) map areas (Mihalynuk *et al.* 2006) and crosscuts the 'Jennings Marker succession'.

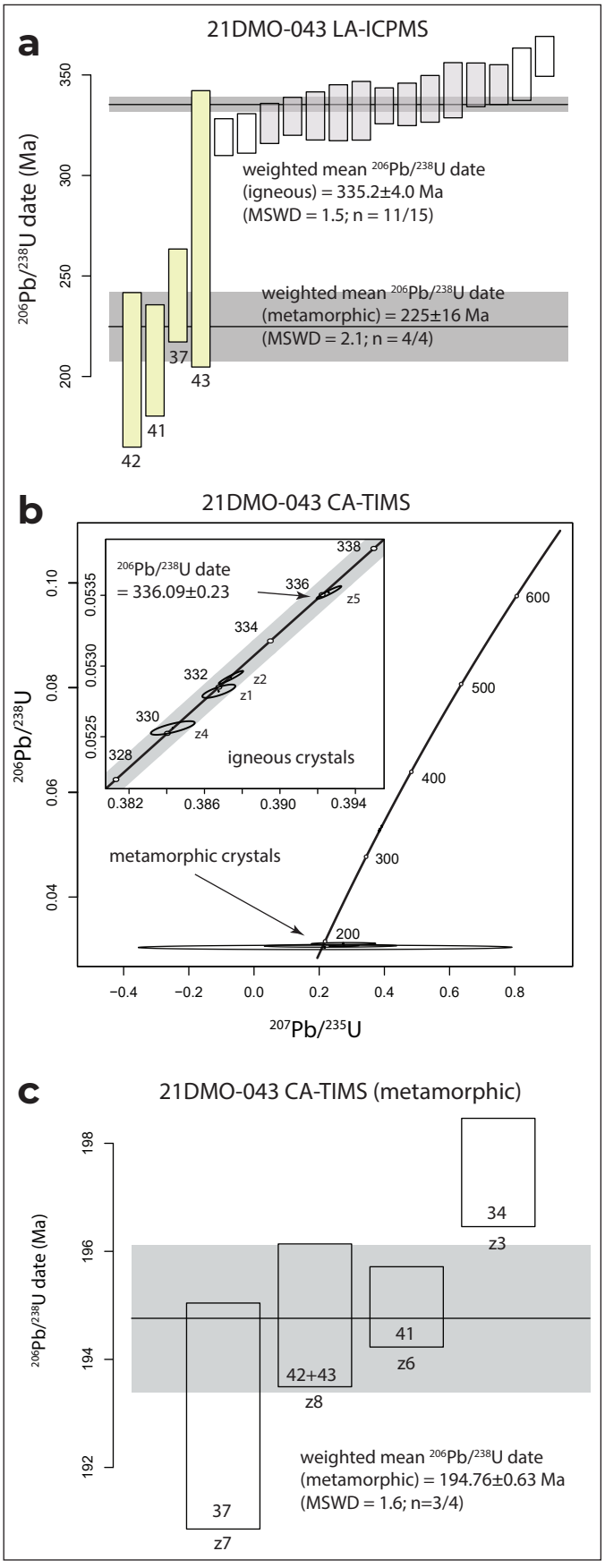
Due to the extremely low levels of U present in the metamorphic crystals, only four LA-ICPMS spot analyses yielded acceptable data. The weighted mean $^{206}Pb/^{238}U$ date of the four analyses is 225 ± 16 Ma (MSWD = 2.2). Five metamorphic crystals were selected for CA-TIMS analysis. Three were single crystals while the fourth fraction included two small grains. All fractions returned similar Early Jurassic dates, and the three youngest yielded a weighted mean $^{206}Pb/^{238}U$ date of 194.76 ± 0.63 Ma (MSWD = 1.6; Fig. 16c; Table 1). This is interpreted as the age of metamorphic zircon growth.

The Livingstone pluton and Wiley succession host numerous thin (mostly centimetre to decimetre thick) dikes and plugs that appear pink and also contain abundant green epidote (Fig. 14h). These dikes could be related to the Mississippian (ca. 336 Ma) metagranodiorite of the Sawtooth Range.

Permian

Late Permian quartz augen schist

Quartz-feldspar augen schist is exposed east of the Little Bear fault, on either side of the Boswell River. A narrow band, approximately 200–400 m wide, can be traced >10 km northwestward from the boundary of the Iron Creek pluton to the slopes above the Boswell River. The band is locally discordant to lithological contacts. There is further exposure of the unit along strike, west of Falls Creek on the north side of the Boswell River. This is interpreted as a separate body on the map (Fig. 2), but it is possible that the augen schist forms a single, continuous belt. The schist is well foliated, commonly chlorite-rich, is mostly fine grained, weathers grey to green, and typically contains distinctive, commonly blue, quartz augen several mm in diameter (Fig. 17a).



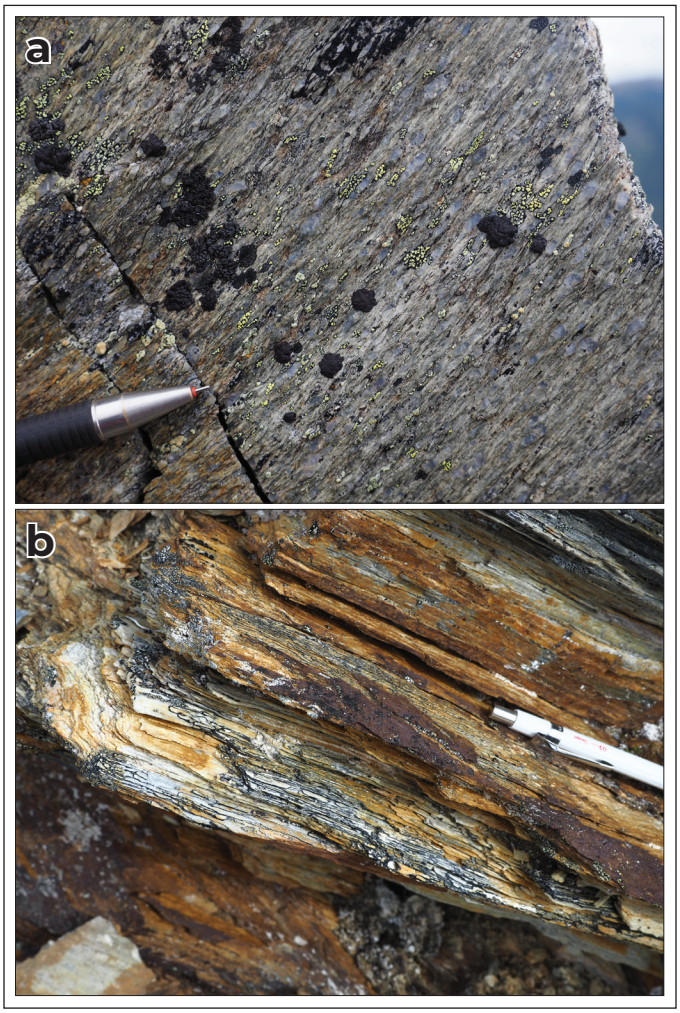


Figure 17. *Field photographs of Permian rocks.* ***(a)*** *Augen schist with abundant blue-grey quartz augen; pencil for scale.* ***(b)*** *Scaly, rusty weathering white felsic schist; pencil for scale*

Figure 16. *U-Pb geochronology results from sample 20DMO-043.* ***(a)*** *LA-ICPMS results for igneous (shaded grey/hollow fill) and metamorphic (pale yellow fill) zircon crystals. The shaded grey analyses contribute to the weighted mean date for the igneous crystals.* ***(b)*** *Results of CA-TIMS analysis of four igneous and four metamorphic crystals.* ***(c)*** *The metamorphic crystals yield a precise, Early Jurassic weighted mean $^{206}Pb/^{238}U$ date. Numbers adjacent to dates on weighted mean plots refer to LA-ICPMS spots analyses (see Appendix). Zircon crystals analyzed by CA-TIMS are labelled z1, z2 etc. (see Table 1). Images of all zircons are included in the Appendix.*

Table 1. *CA-TIMS zircon U-Pb isotopic data. Continued on next page.*

									Radiogenic Isotope Ratios							
Sample	LA-ICPMS	Th/U	$^{206}Pb^*$ x10^{-13} mol	mol % $^{206}Pb^*$	Pb* (pg)	Pb_c (pg)	Pb*/Pb_c	$^{206}Pb/^{204}Pb$	$^{208}Pb/^{206}Pb$	$^{207}Pb/^{206}Pb$	% err	$^{207}Pb/^{235}U$	% err	$^{206}Pb/^{238}U$	% err	corr. coef.
(a)	spot label	(b)	(c)	(c)	(c)	(c)	(c)	(d)	(e)	(e)	(f)	(e)	(f)	(e)	(f)	
18EB052																
z1	46	0.338	7.0377	99.97%	168.15	0.19	883	55341	0.107	0.051468	0.065	0.292984	0.129	0.041305	0.069	0.967
z2	45	0.351	13.2695	99.98%	318.20	0.17	1925	120228	0.111	0.051481	0.062	0.293062	0.127	0.041306	0.069	0.969
z4	51	0.379	4.9831	99.96%	120.38	0.18	666	41309	0.120	0.051461	0.061	0.292846	0.128	0.041291	0.069	0.985
z5	47	0.335	4.6788	99.96%	111.70	0.15	735	46131	0.106	0.051498	0.067	0.292947	0.130	0.041276	0.069	0.963
z6	52	0.497	1.9809	99.91%	49.40	0.14	349	20949	0.157	0.051442	0.077	0.292754	0.138	0.041293	0.071	0.928
20DMO043																
z5	53	0.786	1.5677	99.92%	42.11	0.11	388	21624	0.248	0.053227	0.074	0.392597	0.137	0.053520	0.070	0.950
z2	38	0.474	1.4768	99.90%	36.64	0.12	311	18813	0.150	0.053118	0.073	0.387404	0.137	0.052920	0.071	0.956
z1	39	0.406	1.1740	99.61%	28.61	0.38	75	4600	0.128	0.053128	0.137	0.386760	0.185	0.052822	0.073	0.769
z4	35	0.380	0.3144	99.51%	7.61	0.13	59	3673	0.120	0.053053	0.197	0.384321	0.248	0.052562	0.075	0.757
z3	34	0.120	0.0083	86.08%	0.19	0.11	2	130	0.038	0.064017	29.418	0.274431	29.482	0.031105	0.526	0.131
z6	37	0.057	0.0115	88.96%	0.26	0.12	2	163	0.018	0.065278	13.533	0.276257	13.609	0.030707	0.395	0.206
z8	42 + 43	0.000	0.0065	81.32%	0.14	0.12	1	97	0.000	0.055476	70.831	0.234584	70.903	0.030682	0.703	0.107
z7	41	0.027	0.0037	76.05%	0.08	0.10	1	75	0.009	0.052032	215.151	0.217879	215.200	0.030384	1.123	0.046
20DMO070B																
z1	60	0.308	1.3675	99.87%	32.44	0.15	223	14104	0.098	0.052870	0.079	0.308412	0.143	0.042327	0.073	0.934
z2	59	0.353	1.5732	99.87%	37.74	0.17	225	14072	0.112	0.051540	0.081	0.294976	0.142	0.041528	0.070	0.936
z3	56	0.351	1.3390	99.89%	32.11	0.13	254	15909	0.111	0.051534	0.078	0.294811	0.140	0.041509	0.069	0.946
z4	61	0.450	1.5988	99.88%	39.38	0.15	256	15600	0.143	0.051550	0.077	0.295006	0.139	0.041523	0.069	0.946
z5	89	0.373	0.9333	99.36%	22.52	0.50	45	2810	0.118	0.051578	0.193	0.294943	0.238	0.041493	0.073	0.719
z6	65	0.325	0.9304	99.73%	22.15	0.21	105	6637	0.103	0.051594	0.120	0.295461	0.173	0.041552	0.073	0.828
20DMO124A																
z2	200	0.760	2.8706	99.94%	76.56	0.15	496	27844	0.241	0.051180	0.067	0.274385	0.131	0.038901	0.069	0.965
z3	197	0.896	2.4781	99.93%	68.31	0.15	458	24921	0.284	0.051139	0.071	0.274169	0.134	0.038901	0.069	0.953
z4	202	0.511	1.6997	99.90%	42.54	0.14	311	18629	0.162	0.051184	0.078	0.274295	0.139	0.038884	0.069	0.937
z1	194	0.485	4.6130	99.96%	114.67	0.15	747	45017	0.154	0.051122	0.069	0.273956	0.131	0.038883	0.070	0.945
z5	204	0.673	4.5777	99.96%	119.46	0.15	806	46250	0.213	0.051166	0.064	0.274140	0.129	0.038876	0.070	0.964
z6	212	0.869	1.9348	99.87%	52.99	0.20	262	14361	0.276	0.051142	0.077	0.273991	0.139	0.038873	0.069	0.947

(a) z1, z2, *etc.* are labels for analyses composed of single zircon grains that were annealed and chemically abraded (Mattinson, 2005).

(b) Model Th/U ratio calculated from radiogenic $^{208}Pb/^{206}Pb$ ratio and $^{207}Pb/^{235}U$ date.

(c) Pb* and Pbc are radiogenic and common Pb, respectively. mol % $^{206}Pb^*$ is with respect to radiogenic and blank Pb.

(d) Measured ratio corrected for spike and fractionation only. Fractionation correction for analyses done with tracer solution BSU1B is 0.16 ± 0.03 (1 sigma) %/amu (atomic mass unit) for single-collector Daly analyses, based on analysis of EARTHTIME ^{202}Pb-^{205}Pb ET2535 tracer solution. Fractionation correction for analyses done with tracer solution ET2535 is based on measurement of $^{202}Pb/^{205}Pb$ in the tracer solution.

(e) Corrected for fractionation and spike. Common Pb in zircon analyses is assigned to procedural blank with composition of $^{206}Pb/^{204}Pb$ = 18.04 ± 0.61%; $^{207}Pb/^{204}Pb$ = 15.54 ± 0.52%; $^{208}Pb/^{204}Pb$ = 37.69 ± 0.63% (1 sigma). $^{206}Pb/^{238}U$ and $^{207}Pb/^{206}Pb$ ratios corrected for initial disequilibrium in $^{230}Th/^{238}U$ using a D(Th/U) of 0.20 ± 0.05 (1 sigma).

(f) Errors are 2 sigma, propagated using algorithms of Schmitz and Schoene (2007) and Crowley et al. (2007).

(g) Calculations based on the decay constants of Jaffey et al. (1971). $^{206}Pb/^{238}U$ and $^{207}Pb/^{206}Pb$ dates corrected for initial disequilibrium in $^{230}Th/^{238}U$ using a D(Th/U) of 0.20 ± 0.05 (1 sigma).

***Table 1** continued. CA-TIMS zircon U-Pb isotopic data.*

		Isotopic Dates							
Sample	LA-ICPMS	$^{207}Pb/^{206}Pb$	±	$^{207}Pb/^{235}U$	±	$^{206}Pb/^{238}U$	±	include in weighted mean?	
(a)	spot label	(g)	(f)	(g)	(f)	(g)	(f)		***Weighted Mean Calculations***
18EB052									
z1	46	260.83	1.49	260.91	0.30	260.91	0.18	x	$^{206}Pb/^{238}U$ ± random (+tracer) [+decay constant] **260.85 ± 0.08** (0.15) [0.31] MSWD = 0.7 pof = 0.57 n = 5
z2	45	261.38	1.42	260.97	0.29	260.92	0.18	x	
z4	51	260.52	1.41	260.80	0.29	260.83	0.18	x	
z5	47	262.14	1.54	260.88	0.30	260.74	0.18	x	
z6	52	259.66	1.77	260.73	0.32	260.84	0.18	x	
20DMO043									
z5	53	337.45	1.68	336.26	0.39	336.09	0.23		$^{206}Pb/^{238}U$ ± random (+tracer) [+decay constant] **194.76 ± 0.63** (0.63) [0.67] MSWD = 1.6 pof = 0.20 n = 3
z2	38	332.82	1.65	332.47	0.39	332.42	0.23		
z1	39	333.23	3.10	332.00	0.52	331.82	0.24		
z4	35	330.06	4.47	330.21	0.70	330.23	0.24		
z3	34	741.23	622.16	246.23	64.46	197.46	1.02		
z6	37	782.37	284.31	247.68	29.91	194.97	0.76	x	
z8	42 + 43	430.47	1578.34	213.98	136.80	194.82	1.35	x	
z7	41	285.77	4918.46	200.14	390.92	192.95	2.14	x	
20DMO070B									
z1	60	322.21	1.80	272.95	0.34	267.24	0.19		$^{206}Pb/^{238}U$ ± random (+tracer) [+decay constant] **262.25 ± 0.08** (0.11) [0.30] MSWD = 2.2 pof = 0.07 n = 5
z2	59	264.00	1.86	262.47	0.33	262.30	0.18	x	
z3	56	263.74	1.79	262.34	0.32	262.18	0.18	x	
z4	61	264.48	1.77	262.49	0.32	262.27	0.18	x	
z5	89	265.70	4.42	262.44	0.55	262.08	0.19	x	
z6	65	266.44	2.75	262.85	0.40	262.45	0.19	x	
20DMO124A									
z2	200	247.90	1.55	246.19	0.29	246.02	0.17	x	$^{206}Pb/^{238}U$ ± random (+tracer) [+decay constant] **245.93 ± 0.07** (0.10) [0.28] MSWD = 0.8 pof = 0.58 n = 6
z3	197	246.08	1.64	246.02	0.29	246.01	0.17	x	
z4	202	248.10	1.80	246.12	0.30	245.91	0.17	x	
z1	194	245.31	1.60	245.85	0.29	245.91	0.17	x	
z5	204	247.30	1.48	246.00	0.28	245.86	0.17	x	
z6	212	246.20	1.77	245.88	0.30	245.85	0.17	x	

(a) z1, z2, etc. are labels for analyses composed of single zircon grains that were annealed and chemically abraded (Mattinson, 2005).

(b) Model Th/U ratio calculated from radiogenic $^{208}Pb/^{206}Pb$ ratio and $^{207}Pb/^{235}U$ date.

(c) Pb* and Pbc are radiogenic and common Pb, respectively. mol % $^{206}Pb^*$ is with respect to radiogenic and blank Pb

(d) Measured ratio corrected for spike and fractionation only. Fractionation correction for analyses done with tracer solution BSU1B is 0.16 ± 0.03 (1 sigma) %/amu (atomic mass unit) for single-collector Daly analyses, based on analysis of EARTHTIME ^{202}Pb-^{205}Pb ET2535 tracer solution. Fractionation correction for analyses done with tracer solution ET2535 is based on measurement of $^{202}Pb/^{205}Pb$ in the tracer solution

(e) Corrected for fractionation and spike. Common Pb in zircon analyses is assigned to procedural blank with composition of $^{206}Pb/^{204}Pb$ = 18.04 ± 0.61%; $^{207}Pb/^{204}Pb$ = 15.54 ± 0.52%; $^{208}Pb/^{204}Pb$ = 37.69 ± 0.63% (1 sigma). $^{206}Pb/^{238}U$ and $^{207}Pb/^{206}Pb$ ratios corrected for initial disequilibrium in $^{230}Th/^{238}U$ using a D(Th/U) of 0.20 ± 0.05 (1 sigma).

(f) Errors are 2 sigma, propagated using algorithms of Schmitz and Schoene (2007) and Crowley et al. (2007).

(g) Calculations based on the decay constants of Jaffey et al. (1971). $^{206}Pb/^{238}U$ and $^{207}Pb/^{206}Pb$ dates corrected for initial disequilibrium in $^{230}Th/^{238}U$ using a D(Th/U) of 0.20 ± 0.05 (1 sigma).

The rock is locally sulphide-rich and in these areas is rusty weathering. Compositional banding is also locally apparent. The quartz augen are round and are variably strained/recrystallized. Although quartz augen are characteristic they are not ubiquitous; some rocks contain plagioclase phenocrysts in addition to, or instead of quartz, and non-porphyritic varieties are locally developed. Northeast of the Red Mountain deposit, the unit includes a thin interval of coarser grained, bright green weathering, chloritic, non-porphyritic schist (metatonalite). The matrix of the quartz augen schist is typically composed of recrystallized quartz, plagioclase, epidote, chlorite and white mica. Locally, flakes of biotite are also developed. The augen schist could represent a shallow level subvolcanic intrusion; alternatively, its apparent crosscutting nature could be a result of extrusion onto an unconformable surface.

A sample of dacitic quartz augen schist was selected for geochronology (20DMO-70B; Fig. 18). Zircon crystals are faceted and columnar (Appendix). Many exhibit oscillatory zoning, while some crystals include more complex, patchy CL characteristics. LA-ICPMS analysis was carried out on 54 crystals (Fig. 19a). Forty-one analyses contribute to a weighted mean $^{206}Pb/^{238}U$ date of 263.7 ± 2.1 Ma (MSWD = 1.2; Fig. 19b). Six crystals were selected for analysis by CA-TIMS (Fig. 19c). Five of these give equivalent results, with a weighted mean $^{206}Pb/^{238}U$ date of 262.25 ± 0.08 Ma (MSWD = 2.2; Table 1). This is interpreted as the crystallization age of the rock. The sixth zircon crystal produced an older ($^{206}Pb/^{238}U$), discordant date.

Late Permian felsic schist

A number of thin (1 m to several metres thick) bands of rusty weathering fine-grained felsic schist were encountered on either side of the Little Bear fault. The schist is white on fresh surfaces (Fig. 17b). It is scaly and friable, typically breaking along rusty brown to yellow (limonitic) foliation planes. Small quartz phenocrysts are locally visible. The boundaries of these felsic schist bands are generally parallel to the foliation/compositional banding, but they are interpreted as small deformed intrusions (sills/dikes), based on their scattered occurrence in contact with a variety of other rock types, some of which are demonstrably older.

A sample of this rock type (18EB-052) was collected by E. Bordet in 2018 from the lower part of the Rosy succession and separated for U-Pb geochronology. The zircon crystals are faceted, and exhibit fine oscillatory zoning in CL (Appendix). Thirteen LA-ICPMS spots were analyzed on 11 grains (Fig. 20a). The weighted mean $^{206}Pb/^{238}U$ date for all thirteen spots is 251.4 ± 2.1 Ma. Five crystals were selected for CA-TIMS dating, and these yielded equivalent dates, with a weighted mean $^{206}Pb/^{238}U$ date of 260.85±0.08 Ma (MSWD = 0.7; Fig. 20b,c; Table 1). This is interpreted as the crystallization age of the rock. A ca. 260 Ma date was reported by Colpron et *al.* (2017) from a similar felsic schist in the southern Livingstone Creek area (105E/8).

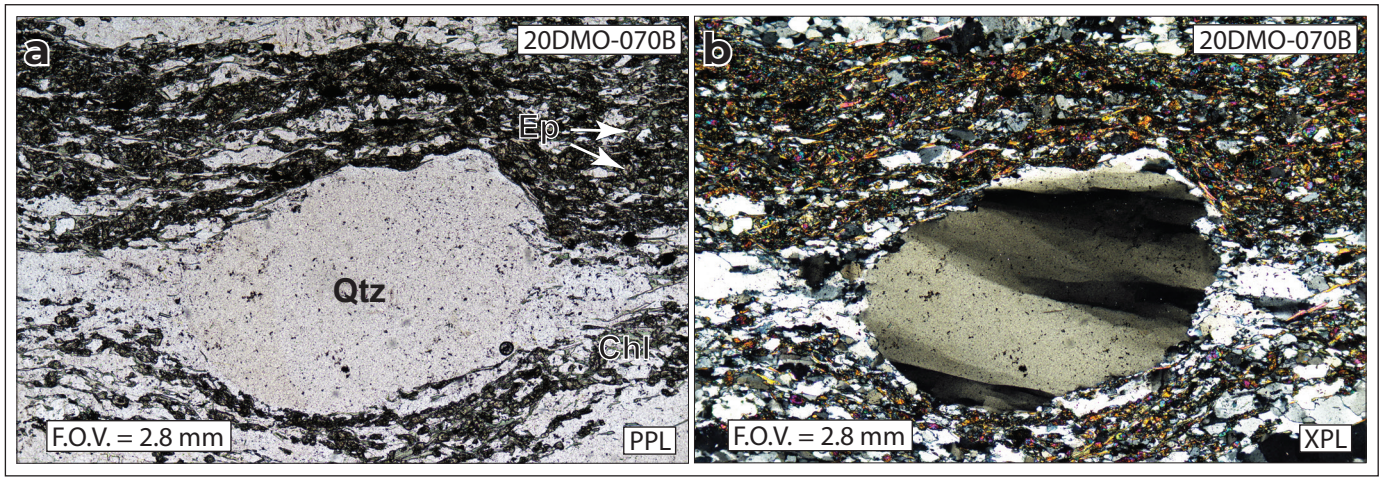
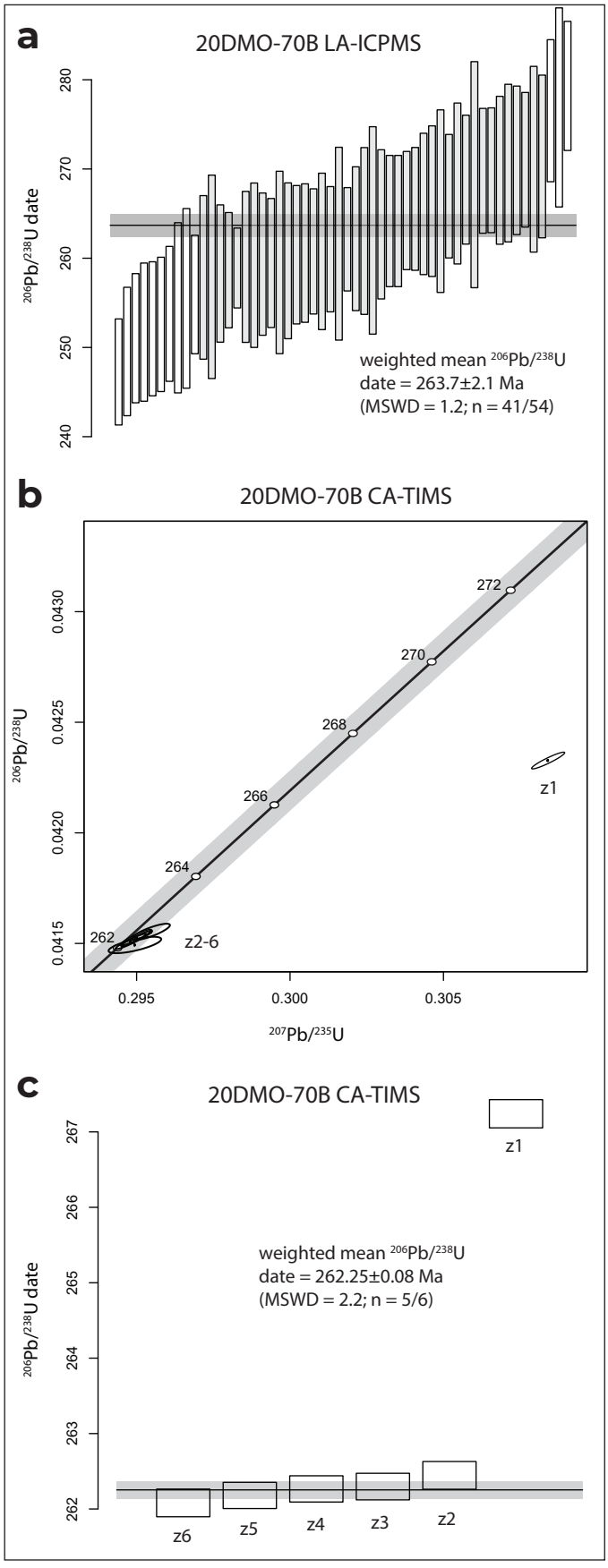


Figure 18. *Photomicrographs of strained quartz augen in geochronology sample 20DMO-070B. The matrix of the rock includes fine grained crystals of epidote, chlorite, quartz and plagioclase (a) PPL; (b) XPL.*



Middle Triassic

Rosy Lake metagabbro

A small (~6 km^2) body of foliated metagabbro or metadiorite is exposed on the west flank of the Sawtooth Range. This metagabbro, which was first recognized by Stevens (1994) coincides with an aeromagnetic high (Kiss and Boulanger, 2018). It is interpreted to intrude rocks on the west side of the Sidney Creek fault and is crosscut by the Early Jurassic Sawtooth stock (Fig. 2). The rock is generally medium to coarse-grained. It is generally well foliated (Fig. 21a), but parts of it are only weakly foliated (Fig. 21b). The metagabbro is dominated by interlocking regions of pseudomorphed plagioclase (mostly clinozoisite) and black (locally dark green) regions, which are clusters of green amphibole that are interpreted to have replaced igneous pyroxene (Fig. 22). The rock also contains quartz, magnetite, biotite and other accessory phases; biotite is restricted to secondary clusters around magnetite. The foliation in and around the intrusion is commonly at a high angle to the regional trend and is folded at the outcrop scale. The metagabbro is intruded by anastomosing weakly deformed, white, sugary textured leucocratic quartz-feldspar dikes and by dikes of porphyritic hornblende-bearing granodiorite.

A sample of coarse-grained, foliated gabbro (20DMO-124A; Fig. 22) was selected for U-Pb geochronology. Zircon from this rock is stubby to elongate and is faceted. It exhibits concentric oscillatory zoning, and in some cases, sector zoning (Appendix).

Figure 19. *U-Pb geochronology results for augen schist sample 20DMO-070B.* ***(a)*** *LA-ICPMS results from 54 spot analyses. CA-TIMS results are presented in* ***(b)*** *and* ***(c)****. Five of the six zircons contribute to the 262.25 ± 0.08 Ma weighted mean $^{206}U/^{238}Pb$ date. Zircon crystals analyzed by CA-TIMS are labelled z1, z2 etc. (see Table 1). Images of all zircons are included in the Appendix.*

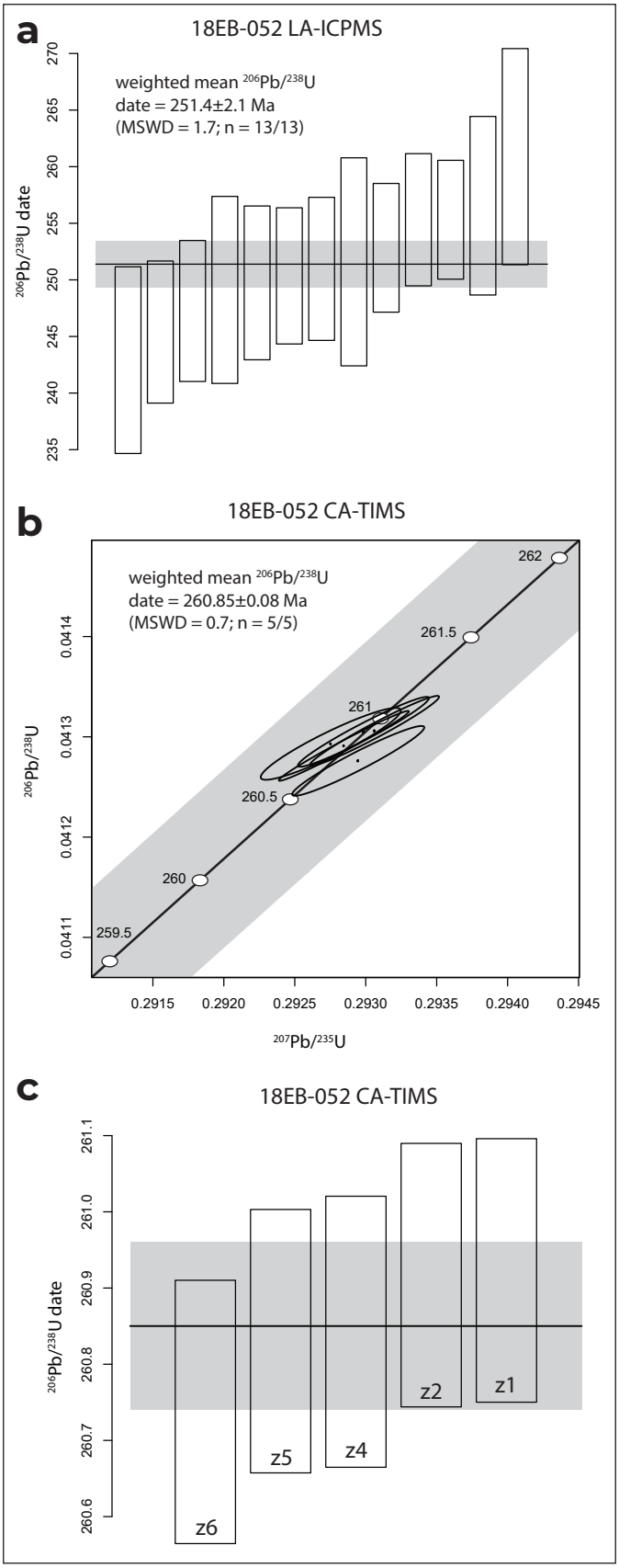


Figure 20. *U-Pb zircon geochronology results from 18EB-052.* **(a)** *LA-ICPMS results from 18EB-052. CA-TIMS results are plotted on Concordia* **(b)** *and weighted mean* **(c)** *diagrams. Zircon crystals analyzed by CA-TIMS are labelled z1, z2 etc. (see Table 1). Images of all zircons are included in the Appendix.*

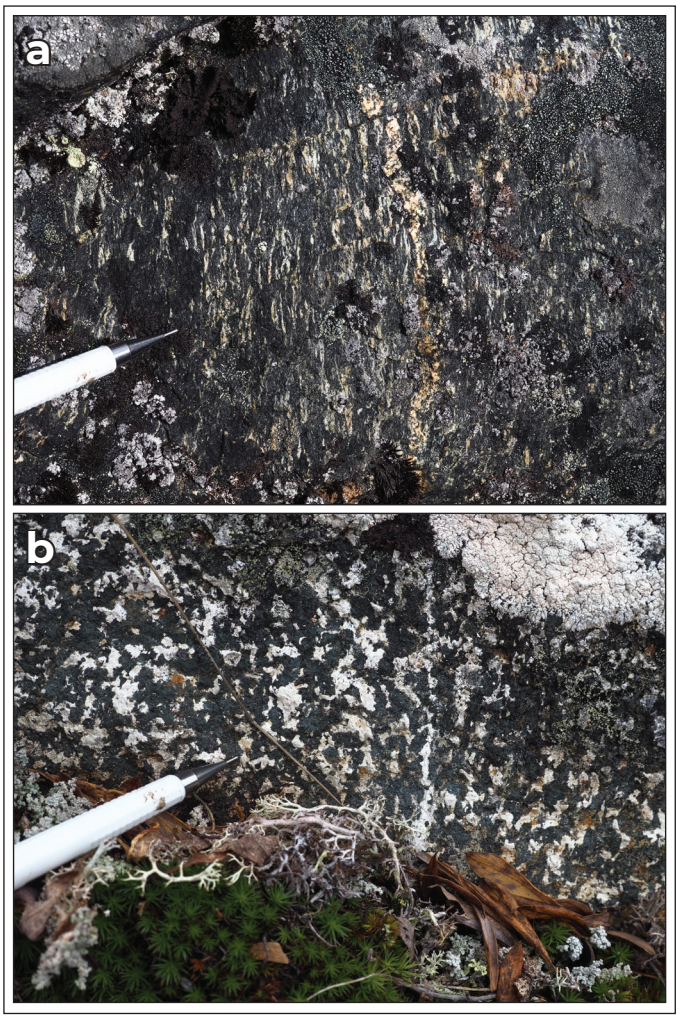


Figure 21. *Field photographs of Middle Triassic metagabbro. Most of the intrusion is well foliated* **(a)**, *but some relatively weakly enclaves are preserved* **(b)**. *Pencil for scale.*

Thirty-six LA-ICPMS spot analyses revealed a single population, and thirty of these spots contribute to the weighted mean $^{206}Pb/^{238}U$ LA-ICPMS date of 243.1 ± 2.0 Ma (MSWD = 1.07; Fig. 23a; Appendix). Six grains were selected for analysis by CA-TIMS, and all six produced equivalent results with a weighted mean $^{206}Pb/^{238}U$ date of 245.93 ± 0.07 Ma (MSWD = 0.8; Fig. 23c; Table 1). This is interpreted as the crystallization age of the metagabbro.

The crystallization age of the Rosy Lake metagabbro is the same as that of zircon that was recovered

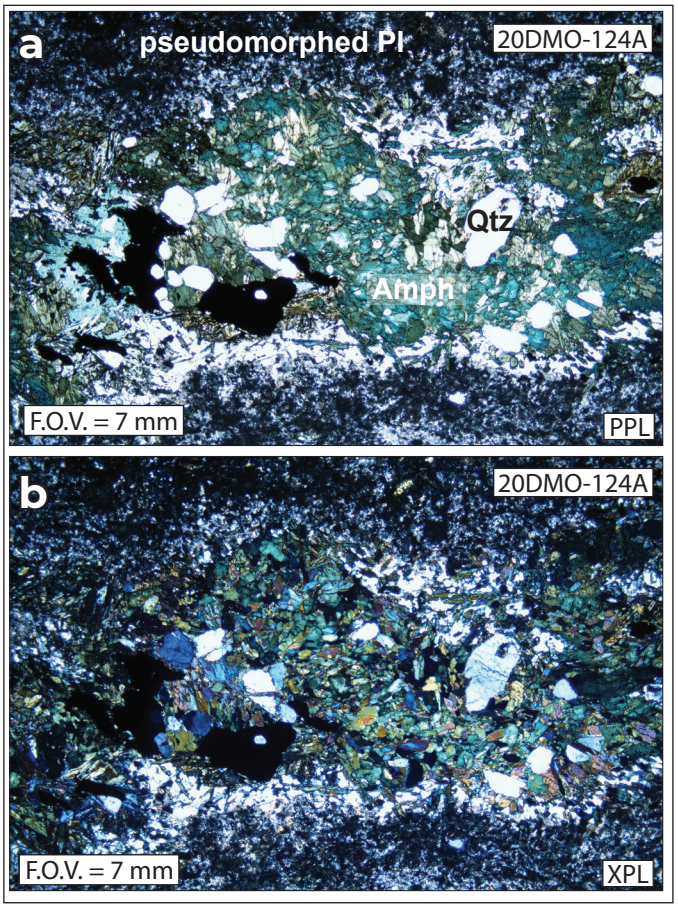


Figure 22. *Photomicrographs of U-Pb geochronology metagabbro sample 20DMO-124,* ***(a)*** *plane polarized (PPL) and* ***(b)*** *cross-polarized (XPL). Amphibole clusters are interpreted as pseudomorphs of igneous pyroxene crystals.*

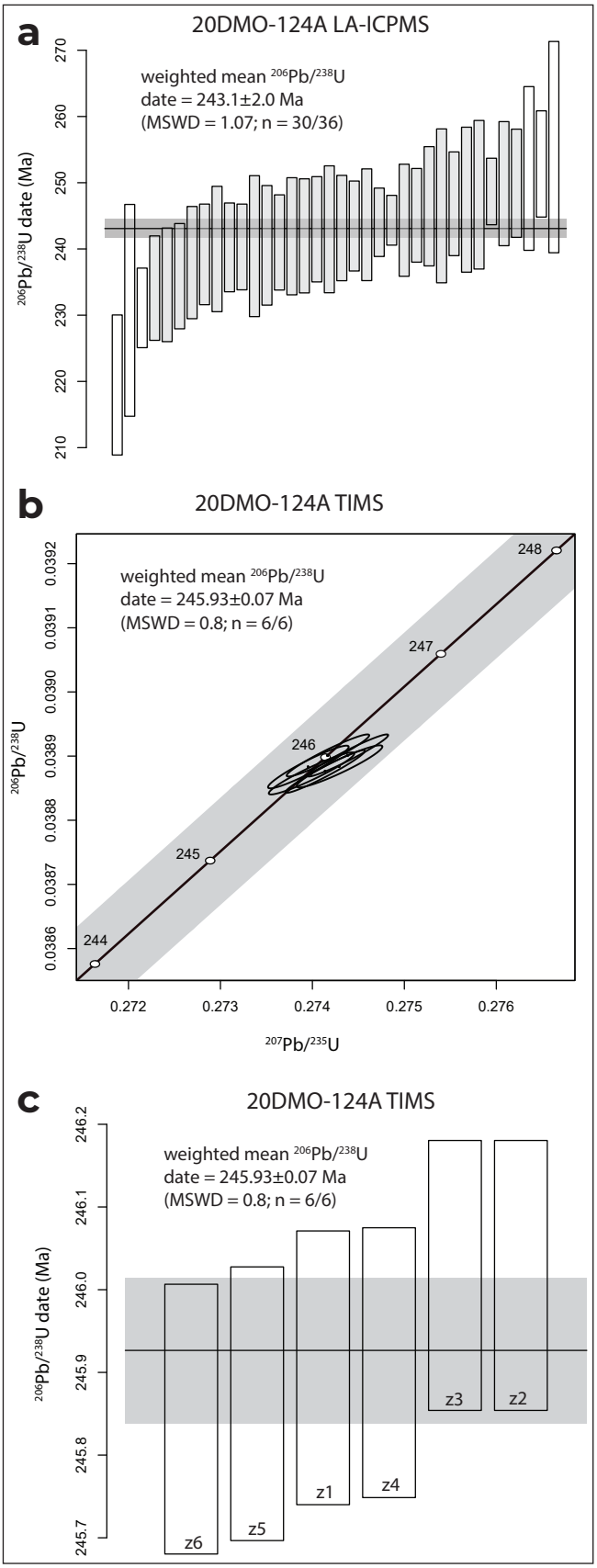


Figure 23. *U-Pb data from 20DMO-124A.* ***(a)*** *LA-ICPMS data derived from single spots analyses on 36 crystals. CA-ID-TIMS results are illustrated in* ***(b)*** *and* ***(c)****. All six crystals that were analyzed overlap to produce a tightly constrained weighted mean Middle Triassic date. Zircon crystals analyzed by CA-TIMS are labelled z1,z2 etc. (see Table 1). Images of all zircons are included in the Appendix.*

from volcaniclastic rocks of the Michie formation (244.64 ± 0.08 Ma; 245.85 ± 0.07 Ma; Bickerton *et al.* 2020), and also overlaps with the age of the Streak Mountain peridotite (245.4 ± 0.8 Ma; Gordey *et al.* 1998). These are located southwest of the Teslin fault in part of the northern Cordillera that has traditionally been referred to as Cache Creek terrane, but recently assigned to the Atlin terrane (Zagorevski *et al.* 2021). A near identical age (244.71 ± 0.09 Ma) was reported by Bordet et al., (2019) from arc rocks of the Joe Mountain formation, which is exposed at a similar latitude to the study area on the west side of the Teslin fault. Middle Triassic gabbro/diorite and arc volcanic rocks also form part of the Tsaybahe Group, which is in stratigraphic contact with the Paleozoic Stikine assemblage and Late Triassic volcanic rocks of the Stikine terrane (Stuhini Group) in the Stikine Canyon-Dease Lake area of northern British Columbia (Read, 1983; van Straten and Wearmouth, 2019).

Lokken suite (EJL)

The Sawtooth stock crosscuts the Sidney Creek fault in the western part of the map area. It is composed of equigranular Hb-Bt granodiorite, monzodiorite, quartz diorite and hornblendite (Stevens, 1994; Sack *et al.* 2020). A central region is dominated by intermediate varieties (Fig. 24a), while parts of the margin are more mafic (Fig. 24b). Textural evidence suggests incorporation and partial dissolution of the marginal mafic phases by granodiorite (Fig. 24 c,d).

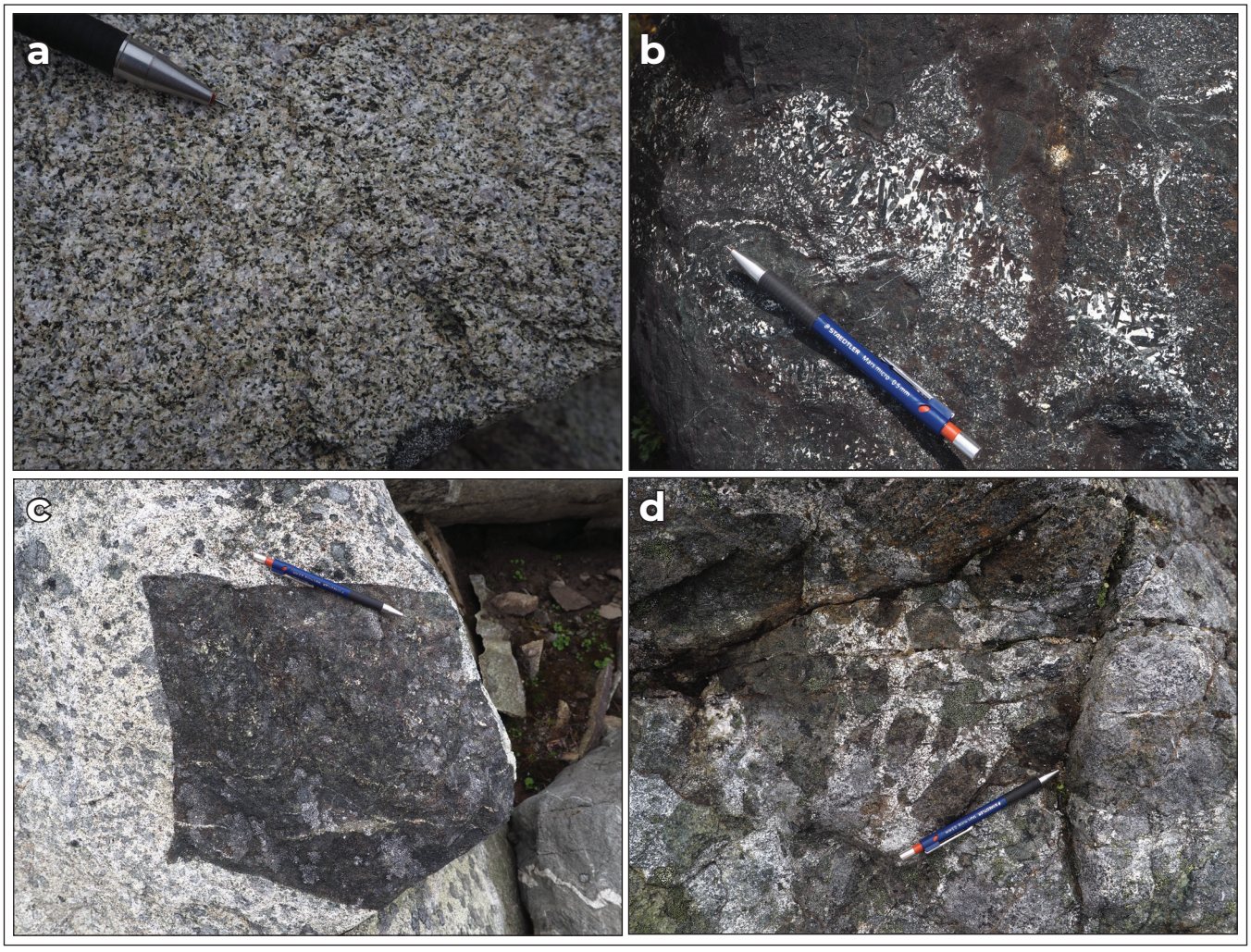


Figure 24. *Sawtooth stock field photographs.* ***(a)*** *Equigranular hornblende-bearing granodiorite from the relatively felsic, central part of the intrusion.* ***(b)*** *Black hornblendite with pegmatitic hornblende-plagioclase enclaves; pencil for scale. Angular* ***(c)*** *to rounded* ***(d)*** *xenoliths of hornblendite are included in the granodioritic phase of the stock.*

The Sawtooth stock forms part of the Lokken suite (Sack *et al.*, 2020), a characteristic feature of which is the presence of clinopyroxene cores inside hornblende crystals. Stevens (1994) reported a U-Pb titanite date of 193.2 ± 4.2 Ma from quartz-diorite to hornblendite of the Sawtooth stock, while Sack *et al.* (2020) produced a zircon U-Pb CA-TIMS date of 184.28 ± 0.07 Ma from monzodiorite of the same body.

Satellite intrusions of the Sawtooth stock include a small, lozenge-shaped body, composed of coarse equigranular granodiorite to diorite that crosscuts the Flat Creek succession southeast of the Sawtooth stock, and small hornblendite intrusions on its northern flank. Hornblendite is black to green, and is dominated by densely intergrown amphibole crystals several mm to 2 cm long, with interstitial plagioclase.

The Loon Lake stock intrudes the quartzite unit of the Slate Mountain succession north of Indian River. The northern part of the pluton is mostly equigranular granodiorite to diorite with local hornblendite, while the southern part is more felsic (granodiorite) and mildly porphyritic, with slender 5–7 mm amphibole crystals and K-feldspar phenocrysts.

The Rosy and Gunsight successions are intruded by a pair of narrow elongate intrusions composed of coarse-grained hornblendite and hornblende-biotite pegmatite southeast of the Sawtooth pluton (Fig. 25 a,b). Hornblendite locally includes small lenses/veins of quartz and epidote. These intrusions crosscut the dominant foliation in the area, but minor post-crystallization deformation/hydration is indicated by kinking of some biotite aggregates (Fig. 25b) and chloritization of hornblende. Some outcrops near the margin of the body include patches of unfoliated hornblende diorite. These localized patches have highly irregular boundaries with the hornblendite, and include numerous angular to rounded (partially digested) hornblendite inclusions (xenoliths).

Both hornblende and biotite from this intrusion yielded Early Jurassic K-Ar dates (ca. 188–185 Ma; Hunt and Roddick, 1992). Hornblendite and minor gabbro also form another small intrusion in the Swift River pluton southeast of the Red Mountain access road.

Small (centimetres to metres thick), hornblende-bearing, dacitic or andesitic dikes are common in parts of the Sawtooth Range. These dikes typically crosscut the penetrative foliation and are generally undeformed or weakly deformed. Varieties include dikes with abundant delicate acicular hornblende crystals in a white weathering dacitic/andesitic matrix (Fig. 25c), dikes with densely arranged, blocky plagioclase crystals in a fine-grained matrix (Fig. 25d) and porphyritic dikes with cm-scale K-feldspar crystals in a fine, hornblende-bearing matrix (Fig. 25e).

Green dikes and xenolithic dikes

Forest green dikes dominated by matted chlorite crystals intrude part of the Swift River pluton in the southern part of the area. The dikes form swarms, range from several cm to >1 m thick and crosscut the penetrative foliation. Many are homogeneous, but some are rich in xenoliths. The xenoliths are mostly angular clasts of the country rock (foliated metatonalite). A similar xenolithic dike or diatreme, approximately 20 m in diameter, was observed in the Livingstone pluton; here the foliated clasts form a clast-supported array, and the chlorite-rich dike-rock is restricted to angular gaps between clasts (Fig. 25f). Locally, patches of coarse-grained, unfoliated intermediate-mafic rocks along the margins of some clasts suggest melting and formation of modified magma during intrusion of the dike.

There are no direct age estimates for the green/xenolithic dikes but they are the same relative age as the pegmatitic hornblendite of the Sawtooth Range; it is possible that they represent fine-grained equivalents and form part of the Lokken suite, or alternatively could form part of a younger magmatic suite.

Felsic dikes and pegmatite

White, coarse-grained, deformed pegmatite forms foliation-parallel sheets and pods in several locations near the eastern boundary of the Livingstone Creek pluton. The sheets are generally centimetres to >1 m thick, and contain abundant folia of country rock. Colpron *et al.* (2017) reported a Middle Triassic U-Pb zircon date (243 ± 1.5 Ma) from deformed pegmatite along strike to the North in the Livingstone Creek area, but no data exist for examples in the study area.



Figure 25. *Minor Jurassic intrusions field photographs.* ***(a)*** *Pegmatitic hornblendite that intrudes the Gunsight succession; lens cap for scale.* ***(b)*** *The hornblendite includes cm-scale, kinked biotite crystal aggregated; pencil for scale.* ***(c)*** *Xenolith-rich, hornblende-bearing dacitic dike, interpreted as part of the Lokken suite; pencil for scale.* ***(d)*** *Thin crowded, hornblende-bearing, plagioclase porphyritic dike that crosscuts deformed metagabbro of the Sawtooth succession. Pencil-sized eraser for scale.* ***(e)*** *Porphyritic granodiorite dike in the Rosy Lake metagabbro; pencil for scale.* ***(f)*** *Xenolith-rich intrusion/breccia that is dominated by rotated clasts of metatonalite with spaces filled by fine-grained, dark green, chlorite-rich intrusive rock; lens cap for scale.*

Garnet amphibolite on the eastern margin of the Livingstone Creek pluton, and similar rocks southwest of the Sidney Creek fault commonly contain thin (millimetres to centimetres thick), foliation-parallel felsic to intermediate (plagioclase-rich) layers. These are commonly lensoidal or anastomosing, weather white to green and in some cases contain sparse amphibole. An outcrop of amphibolite/garnet amphibolite adjacent to the Red Mountain road contains numerous leucocratic layers that exhibit a variety of relationships to the dominant foliation. The least deformed/most highly crosscutting parts of these intrusions grade into white weathering felsic pegmatite.

Deformed, homogeneous felsic dikes crosscut metagabbro of the Sawtooth succession north of Sidney Creek Lakes. These are white (fresh), white weathering and equigranular.

Weakly deformed, porphyritic hornblende-bearing dikes (Lokken suite) that crosscut the Rosy Lake metagabbro are themselves cut by white to pale pink weathering aplite. Curved apophyses and deflection of the foliation along its margins indicates that their emplacement overlapped with the final stages of penetrative deformation.

Cretaceous

Quiet Lake batholith and Iron Creek stock

The Quiet Lake batholith occupies much of the eastern fringe of the study area. The southwestern part of the batholith comprises coarse-grained porphyritic biotite and granitic pegmatite. Biotite granite is porphyritic and commonly crowded, with abundant cm-scale cream to pink K-feldspar crystals, grey to black smoky quartz, biotite books and white plagioclase (Fig. 26a). In places, a weak foliation/preferred alignment is discernable. Pegmatite contains pink K-feldspar and the same mineralogy as the granite. Biotite-muscovite granite forms marginal phases near the southern part of the d'Abbadie fault (Figs. 2 and 26b). U-Pb zircon dates from the Quiet Lake batholith are ca. 100–114 Ma but there are no data from the study area.

The Iron Creek stock is coincident with a circular aeromagnetic anomaly (Kiss and Boulanger, 2018) and may be separate from the main Quiet Lake batholith. The parts that were examined are lithologically distinct from the Quiet Lake batholith, being dominated by white weathering muscovite-biotite granite, leucogranite aplite and pegmatite. There are no geochronological constraints on the age of the Iron Creek stock but a Cretaceous age is likely based on its composition, lack of penetrative deformation, and low-pressure contact metamorphic aureole (see below).

Granitic orthogneiss of the Grass Lakes suite is intruded by undeformed to weakly deformed, medium-grained, pale yellow weathering, equigranular biotite granite and aplite (e.g., Fig. 13a). This does not resemble rocks observed in the Quite Lake batholith and may instead be part of the Late Cretaceous (ca. 103–96 Ma) Seagull suite that intrudes the d'Abbadie fault zone farther north (e.g., Colpron *et al.* 2017).

Red Mountain intrusions and porphyry deposit

A distinctive set of dikes are concentrated around the Red Mountain deposit (Fig. 26c), but are found throughout the area, from the Wiley succession east of the Livingstone pluton to the Swift River pluton. These dikes of rhyolite/dacite are cream-yellow, fine grained and porphyritic, with phenocrysts of rounded quartz and/or plagioclase, typically ~1 mm in diameter (Fig. 26d). Flow-banding textures are locally developed (Fig. 26e). The dikes are blocky, resistant, and often have pyrolusite-coated surfaces. Two main sets of dike are developed in the vicinity of the Red Mountain porphyry deposit: 1) a set that strikes northwest-southeast, parallel to the regional strike, and 2) a set that strikes approximately north-south.

The Red Mountain porphyry deposit is located approximately 2 km northeast of the Little Bear fault (Fig. 2). It is surrounded by a spectacular zone of red-weathering pyritic hornfels (Fig. 26c) that was first reported by Lees (1936). The deposit is primarily hosted in quartz monzonite that intruded graphitic phyllite of the Slate Mountain succession. Several overlapping intrusive phases and breccias have been identified, including a post-mineralization, pyritic quartz-eye diorite that is also exposed at surface (Brown and Kahlert, 1986). The mineralization is concentrated at depth and consists of fine-grained selvages and

disseminations within thin quartz veins that cut the quartz monzonite and hornfels. The calculated reserve is 187 270 000 tonnes grading 0.167% MoS_2 (Brown and Kahlert, 1986). Existing K-Ar data suggest the Red Mountain deposit formed in the Late Cretaceous (*ca.* 81–87 Ma; Yukon Geological Survey geochronology database), but new U-Pb and Re-O dating is underway to establish an accurate date. The age and style of the Red Mountain deposit appear to be similar to the Adanak Mo porphyry (Smith and Arehart, 2010) near Atlin, British Columbia.

Other minor Cretaceous intrusions

Volumetrically minor, small (centimetres to ~2 m thick), undeformed dikes are scattered sporadically through the area. Varieties include: green, non-vesicular porphyritic dacitic dikes with prominent mica (phlogopite?) and plagioclase phenocrysts (Fig. 26f); green (fresh), beige-brown weathering, feather-textured dacite dikes with sparsely distributed quartz eyes and cream, partially filled amygdules; brown weathering, vesicular dikes with abundant phlogopite(?) crystals, and equigranular biotite monzonite with felted texture. A larger (1 km long) porphyritic dacite(?) plug straddles the southwestern boundary of the Quiet Lake batholith north of the Boswell River.

Deformation and metamorphism

The study area is located in a region characterized by mostly steeply-dipping planar structures, which has previously been referred to as the Teslin suture zone (Tempelman-Kluit, 1979), or Teslin tectonic zone (Stevens *et al.*, 1995). This elongate, strike-parallel zone was interpreted as a subduction/imbricate complex by Tempelman-Kluit (1979) and Hansen (1989, 1992) but more detailed work led to recognition of coherent stratigraphy (Stevens *et al.*, 1995) and regional scale folds (Gallagher, 1999; de Keijzer *et al.*, 1999).

The results described here support the contention that, rather than represent a melange or imbricate zone (as initially proposed by Tempelman-Kluit, 1979), the area is underlain by coherent, albeit highly deformed stratigraphic successions that have experienced several generations of folding. Three main phases of folding are recognized, and the general geometry and sequence of deformation observed in the study area is comparable to that described by de Keijzer *et al.* (1999) in the Last Peak area to the north.

Folds and penetrative structures

Pre-Jurassic metavolcanic and metasedimentary rocks of the area are penetratively deformed and tightly folded. The fold axial planes and their axial planar foliation(s) are mostly steeply or moderately steeply dipping and fold axial traces are approximately parallel to the overall trend of the orogen. There is a small but a systematic change in the orientation of structures from NNW-SSE north of Indian River, to NW-SE around the Boswell River and areas to the southeast (Fig. 2).

Map-scale folding is responsible for interdigitation of the Wiley and Slate Mountain successions in the northern part of the area, and of component parts of the Sawtooth succession along strike to the southeast. Map-scale folds are well developed in the Sawtooth Range, where they are defined by marker carbonate of the Rosy succession, and by folding of the metabasalt/metagabbro contact. Map-scale folds were not documented southwest of the Sidney Creek fault, an area that is dominated by the Swift River pluton.

Most outcrops contain evidence for two or three phases of deformation (Figs. 27 and 28). Typically, the cleavage along which rocks break most easily is a second generation, spaced to penetrative foliation (S_2; Fig. 27a) that overprints an earlier, penetrative foliation. The early foliation (S_1) is almost invariably parallel to compositional layering and the axial plane of rare F_1 folds. In regions where S_2 is most intensely developed, S_1 may not be discernable (except around some fold hinges) and layering is transposed. F_2 folds are close to isoclinal (Fig. 27b), and are responsible for folding and reorientation of early intersection (L^1_0) and mineral lineations on S_1 (Fig. 27c). The S_2 foliation is axial planar to the map scale folds described above. The foliation (S_2) and fold axial planes are mostly steeply dipping, but lineation orientations are more variable. Stretching lineations developed in metatonalite are mostly moderately steeply to steeply pitching, while intersection lineations in layered rocks range from shallow to steeply pitching.



Figure 26. *Field photographs of Cretaceous intrusions.* **(a)** *Coarse-grained biotite granite of the Quiet Lake batholith includes cm-scale K-feldspar phenocrysts; pencil for scale.* **(b)** *Foliated pegmatite along the eastern strand of the d'Abbadie fault south of Fish Creek; lens cap for scale.* **(c)** *Red and yellow gossan surrounds the Red Mountain Mo porphyry deposit, which is hosted in rocks of the Slate Mountain succession, south of the Boswell River. The elevation difference between the valley floor and the top of the gossanous hill is approximately 400 m.* **(d)** *Sulphide-rich, porphyritic rhyolite of the Red Mountain suite. Small (1–2 mm) plagioclase phenocrysts are visible in the fine-grained matrix.* **(e)** *Banded texture formed by elongated filled vesicles in rhyolite of the Red Mountain suite.* **(f)** *Pale brown phlogopite(?) and plagioclase crystals form phenocrysts in a green, fine-grained dacite dike. Pencil tip for scale.*

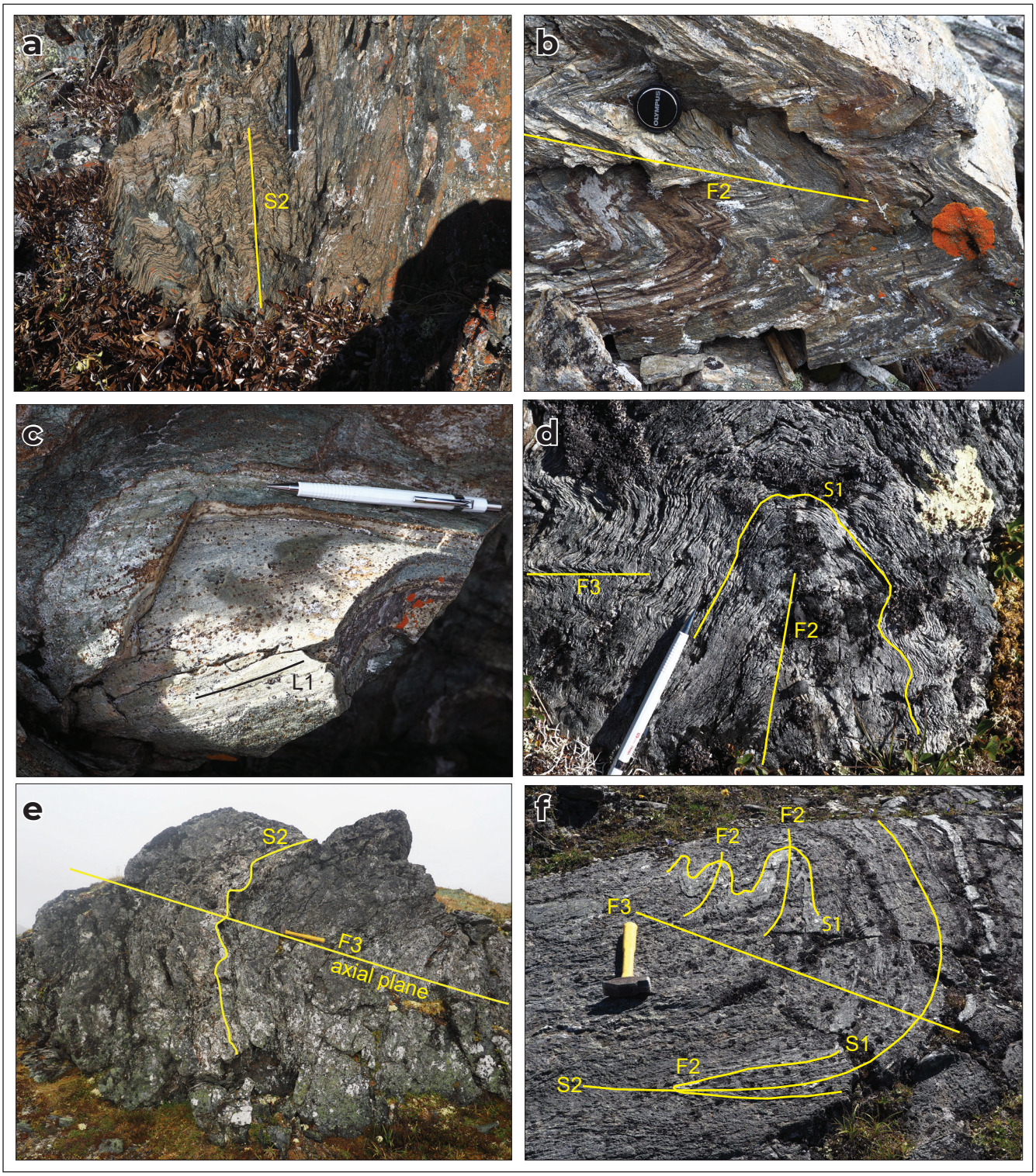


Figure 27. *Fold and deformation styles.* ***(a)*** *Chevron folding of micaceous quartzite; lens cap for scale.* ***(b)*** *Spaced S_2 cleavage at high angle to S_0/S_1 in metasandstone with abundant phyllitic partings; pencil for scale.* ***(c)*** *Polished surface of deformed metatonalite showing reorientation of D_1/$_2$ structures across the trace of an F_3 fold; hammer for scale.* ***(d)*** *Tight F_2 fold whose limbs are overprinted by F_3 chevron folds/crenulations; pencil for scale.* ***(e)*** *Outcrop scale F_3 fold with shallow-dipping axial plane; central Sawtooth Range; hammer for scale.* ***(f)*** *L_1 intersection lineations folded around the axis of a F_2 fold; pencil for scale.*

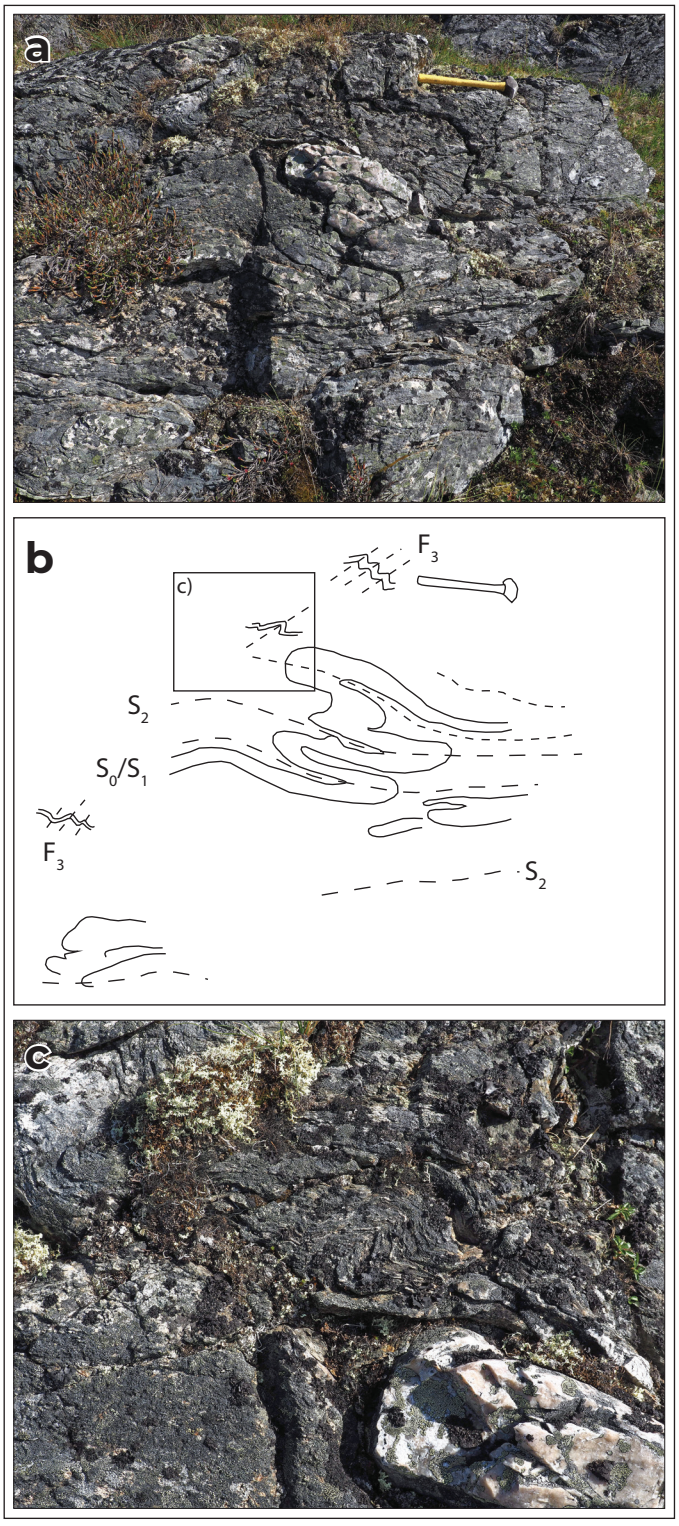


Figure 28. *Photographs and sketch of polyphase structures in an outcrop of metatonalite (Swift River pluton).* ***(a)*** *and* ***(b)*** *are images of the entire outcrop, while* ***(c)*** *is a close-up photographs of the regions marked on* ***(b)****.*

In parts of the area, S_2 and earlier structures are overprinted by another phase of widespread folding (F_3; Figs. 27d–f and 28). These structures are particularly well developed in the western part of the Sawtooth Range and in parts of the Swift River pluton (Fig. 28a–c), and are less conspicuous in the northeastern part of the map area. Chevron folds and crenulations (F_3) are widely developed at a variety of scales from mm to cm-scale crinkles and crenulations to map scale folds. These are open to tight, but only locally exhibit an axial planar cleavage. Axial planes of F_3 folds generally dip at shallow to moderate angles, have mostly shallow to moderate-plunging axes, and are responsible for widespread reorientation of earlier structures. The shallow dip of the lithological enveloping surface immediately northwest of the Sawtooth stock is attributed to its position on the shallow limb of an F_3 fold (Fig. 29).

Major Faults

Little Bear fault

The Little Bear fault separates mafic volcanic and plutonic rocks of the Sawtooth succession from metasedimentary units of the Slate Mountain succession (Fig. 2). It runs approximately parallel to the Boswell River valley in the central part of the map area. To the southeast, it crosses low vegetated spurs and, in the vicinity of the Iron Creek stock, higher mountain ridges. The fault is plugged by the Iron Creek stock (Fig. 30a).

The area around the southwestern flank of the Iron Creek stock is well exposed and the fault is located to within a few metres (the contact is covered by talus), between outcrops of 1) hornfelsed (contact metamorphosed) graphitic phyllite and 2) a thin sliver of calc-schist (Rosy succession) in contact with skarn-altered metabasalt (Sawtooth succession). The orientation of foliations and lineations in rocks on either side of the fault is similar to elsewhere in the surrounding area, and no evidence for high intensity brittle deformation was observed near the fault. Similar observations were made northwest of the Iron Creek stock where the Little Bear fault bifurcates around a lozenge of

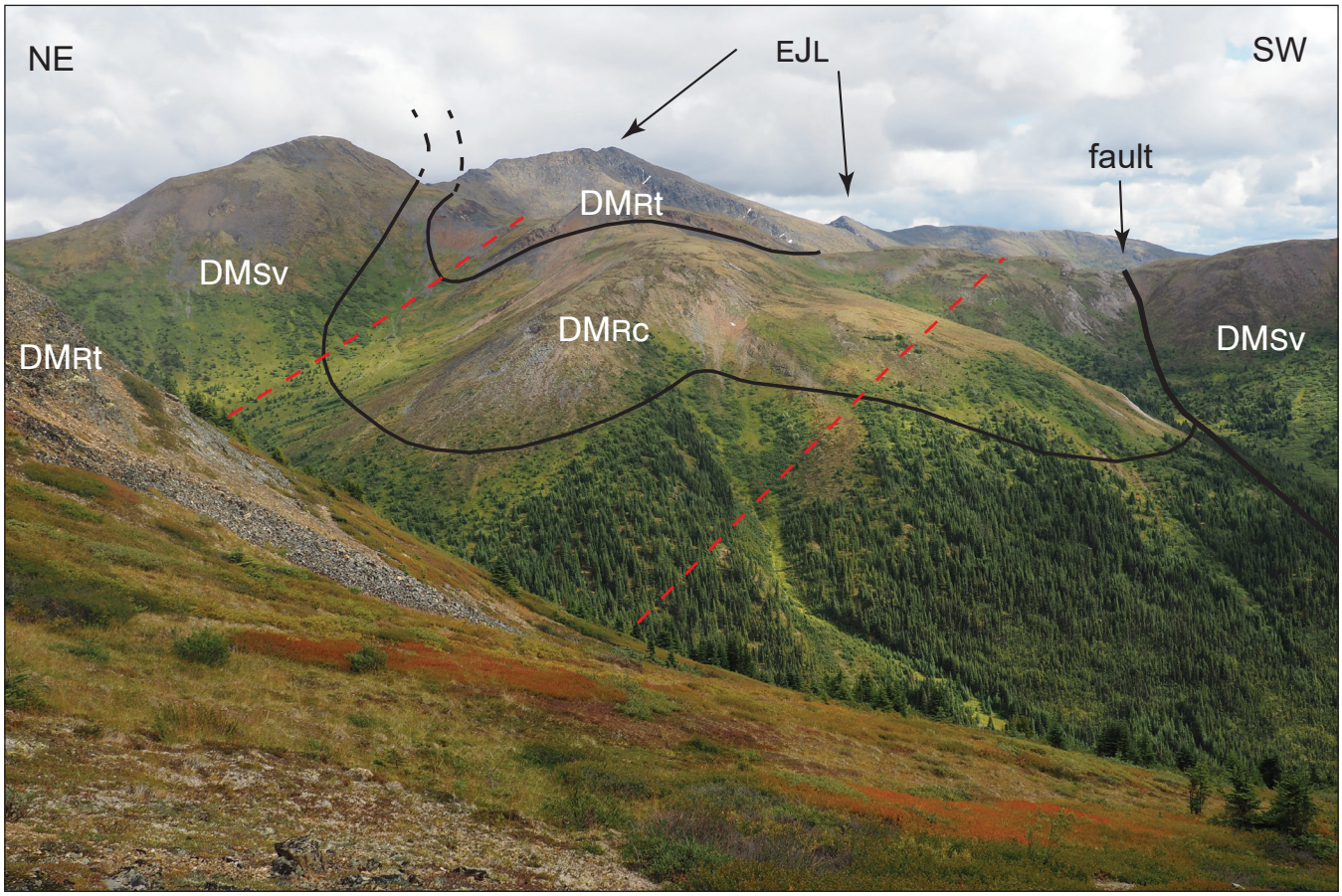


Figure 29. *Shallow-dipping, folded panel of Sawtooth and Rosy successions on the west flank of the Sawtooth Range. The overall shallow dip of the units contrasts with most of the area and is interpreted to reflect its position on the flat limb of a large F_3 fold. The cross-strike distance between the fold axial traces (dashed red lines) is approximately 1 km.*

Rosy succession/Gunsight succession and crosses two gullies. Penetratively deformed metabasalt of the Sawtooth succession that is in fault contact with the Rosy succession has a finely banded, stripy appearance, and lacks evidence for significant brittle deformation. These observations suggest that juxtaposition of units across the Little Bear fault preceded or accompanied the regional deformation and epidote-amphibolite facies metamorphism.

Sidney Creek fault

The Sidney Creek fault separates metavolcanic and metasedimentary rocks of the Gunsight and Rosy successions from the Flat Creek succession. A fault contact is supported by juxtaposition of different units along its trace and the metamorphic contrast between garnet amphibolite of the Flat Creek succession and greenschist-facies metavolcanic rocks on its northeastern side. Exposures of the fault were not encountered but it is interpreted to be folded and have variable, but mostly steep dip, based on the geometry of its trace. Shallow-dipping foliation in the Gunsight succession changes to subvertical adjacent to the fault, with identical strike. The Sidney Creek fault is crosscut by the Early Jurassic Sawtooth stock. The fault is interpreted to emerge on the NW side of the stock, where it may form part of the margin of the Rosy Lake metagabbro (Fig. 2).

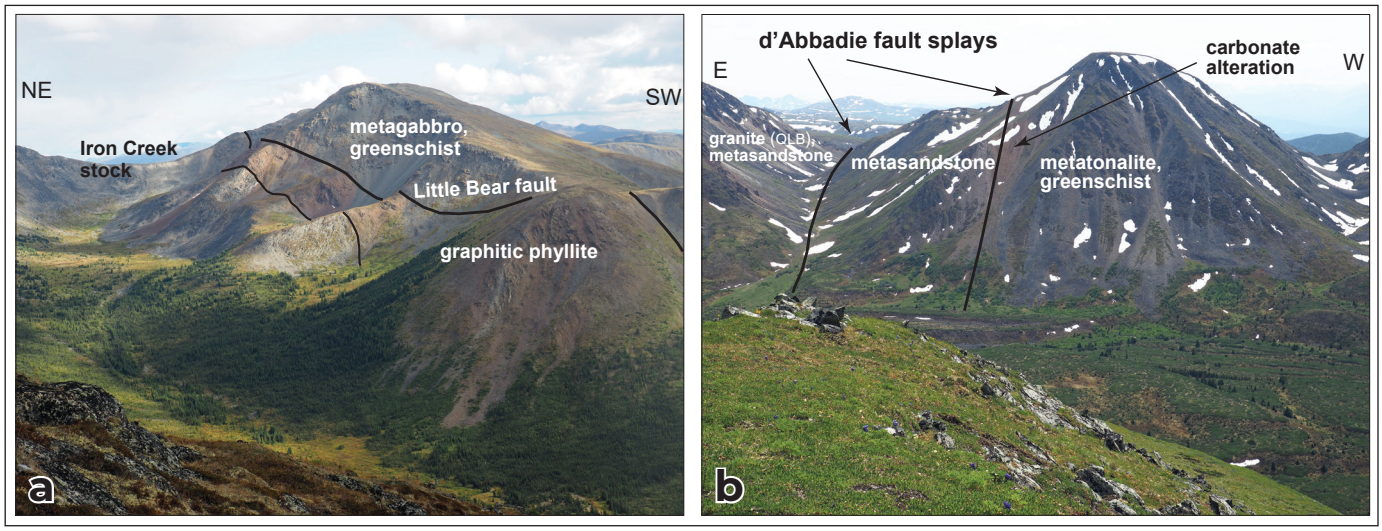


Figure 30. *Landscape photographs of the Little Bear and d'Abbadie faults.* ***(a)*** *The Little Bear fault, which separates graphitic phyllite/argillite (Slate Mountain succession) from metagabbro and greenschist of the Sawtooth succession is plugged by the Iron Creek stock. The distance from the spur in the right foreground to the peak in the centre is approximately 1.6 km.* ***(b)*** *View across Fish Creek, towards two splays of the d'Abbadie fault. The western splay is marked by a zone of orange talus due to carbonate alteration along the fault. The eastern splay occupies the valley and is coincident with subvertical layering/foliation in quartzite and granitic rocks.*

D'Abbadie fault

The d'Abbadie fault is a north-south striking steep fault/shear zone that crosscuts the regional trend and has clear geophysical expression on aeromagnetic maps of the region (Gallagher, 1999; Colpron et *al.*, 2017). The fault zone includes steep brittle structures that are superimposed on a zone of mylonite, which formed during dextral shearing. The mylonite is largely restricted to the immediate vicinity of elongate Late Cretaceous granitic intrusions that are parallel to the trace of the fault zone. Harvey et *al.* (1997) estimated dextral offset of approximately 4 km across the d'Abbadie fault, while a larger offset was inferred by Gabrielse et *al.* (2006), who interpreted the d'Abbadie fault as a splay of the Teslin fault.

The d'Abbadie fault extends into the northern part of the study area. Two main splays cross the ridges on either side of Fish Creek, and bound an orange weathering zone of abundant brittle deformation and pervasive carbonate alteration (Fig. 30b). The faults are steeply dipping, layering in metasandstone is steeply dipping and granite/pegmatite within this zone has a steeply dipping foliation. This brittle deformation is superimposed on a wider region of penetrative strain. Outcrops of Grass Lakes suite orthogneiss adjacent to the eastern strand of the d'Abbadie fault on the western flanks of Mount Black are affected by shear bands (S-C' fabrics) that indicate dextral shearing. These die out to the east over the course of several hundred metres and the rock transitions to deformed orthogneiss with mostly symmetrical strain shadows on phenocrysts, which lacks significant arrays of shear bands. Mineral elongation lineations pitch steeply in the region affected by dextral shear bands and beyond, and therefore appear to predate formation of the shear bands. Splays of the d'Abbadie fault are interpreted to extend across Indian River, but die out before meeting the Boswell River. An eastern splay is in contact with the Quiet Lake batholith; the granite contains abundant scaly fractures and coarse muscovite. Subvertical "sills" of garnet-bearing pegmatite along the trace of this fault are also foliated (Fig. 26b).

The change in the orientation of regional structures from NW-SW to ~N-S around the Indian River is coincident with the tip zone of the d'Abbadie fault and is interpreted to result from late, fault-related deflection of structures towards parallelism with the fault zone.

Metamorphism

Most of the area was affected by epidote amphibolite-facies regional metamorphism during D_1-$_2$ deformation. This resulted in crystallization of chlorite, epidote, plagioclase series feldspar and green amphibole in metabasic rocks, and conversion of mudstone rich in organic material to graphitic phyllite. Many fine-grained metabasites were thoroughly recrystallized, but some coarse-grained rocks, such as metagabbro of the Sawtooth succession, retain their igneous texture and were pseudomorphed by metamorphic minerals (e.g., clinozoisite after plagioclase and green amphibole after pyroxene).

Slightly higher grade metamorphism affected the area southwest of the Sidney Creek fault, and at least part of the area in/around the Livingstone pluton. In these areas, metabasite is black rather than green, lacks chlorite, and amphibolite commonly contains garnet in addition to amphibole, white mica, quartz and accessory minerals. Garnet is sporadically developed in micaceous quartzite of the Flat Creek succession, and also forms part of schistose rocks within the Swift River and Livingstone plutons (Fig. 31a).

Hansen (1992) studied regional metamorphism in the area immediately north of the study area and obtained a wide spread of intermediate to high-pressure, moderate temperature estimates based on amphibole chemistry and application of a number of thermobarometers to metaplutonic, metavolcanic and metasedimentary rocks.

The age of metamorphic recrystallization of the Rosy succession is indicated by the $^{206}Pb/^{238}U$ date of 194.76 ± 0.63Ma from zircon rims on metagranodiorite in the Sawtooth Range. Hansen *et al.* (1991) also obtained Early Jurassic $^{40}Ar/^{39}Ar$ dates from the Livingstone pluton and adjacent schists. The Early Jurassic date is similar to the age of regional metamorphism in other parts of the Yukon-Tanana terrane (Berman *et al.* 2007; Clarke, 2017; Gaidies *et al.*, 2020).

Contact metamorphism of the graphitic phyllite unit (Slate Mountain succession) around the margin of the Iron Creek stock produced cordierite and andalusite-bearing hornfels, which indicates emplacement at low pressure (approximately 3.5–4 Kbar; Pattison and Vogl, 2005; Fig. 31b). Green, garnet-bearing calc-silicate adjacent to the Quiet Lake batholith is also interpreted to have formed during contact metamorphism.



Figure 31. (a) *Regional metamorphic garnet schist derived from metatonalite of the Swift River pluton; pencil for scale.* ***(b)*** *Slender pale pink andalusite crystals in graphitic metapelite adjacent to the Iron Creek pluton; pencil tip for scale.*

Discussion

Are the Slate Mountain and Flat Creek successions the same?

The Slate Mountain and Flat Creek successions contain similar rock types and are each pre-Early Mississippian. However, most of the shared rock types (graphitic phyllite, quartzite, metabasalt) are common throughout Yukon-Tanana terrane and are not diagnostic of specific rock assemblages. The most distinctive unit in the Slate Mountain succession – the green chloritic calc-schist/calc-silicate has not been recognized in the Flat Creek succession; however, only relatively small regions of the succession are preserved around the fringes of the Swift River pluton, and the boundary between the quartzite and phyllite units has not yet been observed. The garnet-bearing amphibolite of the Flat Creek succession is texturally dissimilar to banded greenschist of the Wiley succession, but is similar to thin layers of garnet amphibolite in the Mount Black area, and may be analogous to a larger garnet amphibolite body in the Slate Mountain succession east of the Livingstone pluton (Colpron, 2006; Colpron *et al.* 2017). Whatever their original stratigraphic relationships, the Slate Mountain and Flat Creek successions host similar to indistinguishable (based on field observations) metaplutonic rocks.

Significance of the Little Bear and Sidney Creek faults?

The Little Bear and Sidney Creek faults each separate rocks that are interpreted to form part of the Semenof block from those of the Yukon-Tanana terrane. The Sidney Creek fault is no younger than Early Jurassic as it is crosscut by the Sawtoooth stock. The Little Bear fault is crosscut by the Cretaceous(?) Iron Creek stock but as this pluton is undated this constraint is not definitive. The Little Bear fault lacks evidence for extensive brittle deformation and appears to have been active during or before greenschist to epidote-amphibolite-facies metamorphism and deformation; an Early Jurassic or older age is therefore likely. The Little Bear and Sidney Creek faults converge towards the eastern boundary of the area, but the nature of their interaction is unresolved. Given the apparent stratigraphic similarities and common plutonic rocks on either side of the central panel, it is possible that the Little Bear and Sidney Creek faults are parts of a single, folded detachment. This could be analogous to the Needlerock thrust of the Glenlyon area, which is a Triassic-Jurassic structure (Colpron *et al*., 2003) that marks the boundary between Yukon-Tanana terrane and the Semenof block, is associated with penetrative strain of surrounding units and lacks evidence for extensive brittle deformation.

Termination of the d'Abbadie fault

Continuity of the Slate Mountain succession across southern strands of the d'Abbadie fault suggests it accounts for little discrete offset in this area. The fault is interpreted to terminate in the northern part of the map area, with residual displacement transferred to 1) multiple splays that are associated with brittle deformation and alteration, but which accommodate relatively minor discrete offsets, and 2) deflection of regional structures into a north-south orientation around its tip zone. This interpretation is incompatible with the hypothesis (Gabrielse *et al*., 2006) that the d'Abbadie fault is a splay of the Teslin fault.

Relationship of Rosy Lake metagabbro to coeval arc successions?

The age of the Rosy Lake metagabbro is identical to that of primitive arc successions in southern Yukon and northern/central British Columbia. Bordet *et al*., (2019) suggested the Joe Mountain and Michie formations of southern Yukon, along with the Kutcho and Sitlika assemblages of British Columbia, represented parts of a primitive intra-oceanic arc that subsequently amalgamated with Cache Creek terrane. Zagorevski *et al.* (2021) included Middle Triassic arc rocks (Joe Mountain Formation, Michie formation, Kutcho assemblage, Tsaybahe Group) with Middle Permian to Middle Triassic suprasubduction zone ophiolites in the Atlin terrane and interpreted them as constituent parts of an extensional arc system.

Further geochemical and geological investigation is needed to establish the significance of the Rosy Lake metagabbro, but the overlapping ages and lithological similarities raise a question as to whether and/or how this part of Yukon-Tanana interacted with the Middle

Triassic arc. The only other direct evidence for Middle Triassic magmatism in Yukon-Tanana is pegmatite from the Livingstone Creek area (Colpron *et al.* 2017). Gaidies *et al.* (2020) presented a Lu-Hf date of 245.3 ± 0.8 Ma from garnet within the Snowcap assemblage of western Yukon-Tanana terrane. The composition of the garnet core indicates that it grew during heating at low-pressure, but the cause of this heating is uncertain. One possibility is that Middle Triassic mafic magmatism affected other parts of Yukon Tanana and the low-pressure metamorphism documented by Gaidies *et al.*, (2020) is the result of contact metamorphism adjacent to an unrecognized intrusion.

Acknowledgements

Thanks to Kim Hatcher (2020) and Cassis Lindsay (2021) for their dedication and perseverance during field work, to Maurice Colpron for providing helpful feedback on an earlier version of the manuscript, and to Karen MacFarlane for technical editing and production.

References

Barresi, T., 2004. Sedimentology, structure, and depositional setting of the Loon Lake sedimentary rock unit, southern Semenof Hills, central Yukon. Unpublished BSc Honours thesis, Saint Mary's University, Halifax, Nova Scotia, 85 p.

Berman, R.G., Ryan, J.J., Gordey, S.P. and Villeneuve, M. 2007. Permian to Cretaceous polymetamorphic evolution of the Stewart River region, Yukon-Tanana terrane, Yukon, Canada: P-T evolution linked with in situ SHRIMP monazite geochronology. Journal of Metamorphic Geology, vol. 25, p. 803–827.

Bickerton, L., Colpron, M., Gibson, H.D., Thorkelson, D. and Crowley, J.L., 2020. The northern termination of the Cache Creek terrane in Yukon: Middle Triassic arc activity and Jurassic-Cretaceous structural imbrication. Canadian Journal of Earth Sciences, vol. 57, p. 227–248.

Bordet, E., Crowley, J.L. and Piercey, S.J., 2019. Geology of the eastern Lake Laberge area (105E), south-central Yukon. Yukon Geological Survey, Open File 2019-1, 120 p.

Brown, P. and Kahlert, B., 1986. Geology and mineralization of the Red Mountain porphyry molybdenum deposit south-central Yukon. *In*: Mineral deposits of Northern Cordillera, J.A. Morin (ed.), Canadian Institute of Mining and Metallurgy, Special Volume 37. p. 288–297.

Clarke, A.D., 2017. Tectonometamorphic history of mid-crustal rocks at Aishihik Lake, southwest Yukon. Unpublished MSc thesis, Simon Fraser University, Vancouver, British Columbia.

Cockfield, W.E., Lees, E.J. and Bostock, H.S. 1936. Laberge sheet, Yukon Territory. Geological Survey of Canada, "A" series map 372A, scale 1: 253,440.

Colpron, M., Murphy, D.C., Nelson, J.L., Roots, C.F., Gladwin, K., Gordey, S.P., Abbott, G. and Lipovsky, P., 2002. Preliminary geological map of Glenlyon (105L/1-7, 11-14) and northeast Carmacks (115I/9,16) areas, Yukon Territory (1:125 000 scale). Exploration and Geological Services Division, Yukon Region, Indian and Northern Affairs Canada, Open File 2002-9, also Geological Survey of Canada Open File 1457.

Colpron, M., Murphy, D.C., Nelson, J.L., Roots, C.F., Gladwin, K., Gordey, S.P. and Abbott, J.G., 2003. Yukon Targeted Geoscience Initiative, Part 1: Results of accelerated bedrock mapping in Glenlyon (105L/1-7, 11-14) and northeast Carmacks (115I/9,16) areas, central Yukon. *In:* Yukon Exploration and Geology 2002, D.S. Emond and L.L. Lewis (eds.), Exploration and Geological Services Division, Yukon Region, Indian and Northern Affairs Canada, p. 85–108.

Colpron, M., 2005a. Geological map of Livingstone Creek area (NTS 105E/8), Yukon (1:50 000 scale). Yukon Geological Survey, Open File 2005-9.

Colpron, M. 2005b. Preliminary investigation of the bedrock geology of the Livingstone Creek area (NTS 105E/8), south-central Yukon. *In:* Yukon Exploration and Geology 2004, D.S. Emond, L.L. Lewis and G.D. Bradshaw (eds.), Yukon Geological Survey, p. 95–107.

Colpron, M., 2006. Geology and mineral potential of Yukon-Tanana Terrane in the Livingstone Creek area (NTS 105E/8), south-central Yukon. *In:* Yukon Exploration and Geology 2005, D.S. Emond, G.D. Bradshaw, L.L. Lewis and L.H. Weston (eds.), Yukon Geological Survey, p. 93–107.

Colpron, M., Nelson, J.L. and Murphy, D.C., 2006a. A tectonostratigraphic framework for the pericratonic terranes of the northern Cordillera. *In:* Paleozoic Evolution and Metallogeny of Pericratonic Terranes at the Ancient Pacific Margin of North America, Canadian and Alaskan Cordillera, Colpron, M. and Nelson, J.L. (eds.), Geological Association of Canada, Special Paper 45, p. 1–23.

Colpron, M., Mortensen, J.K., Gehrels, G.E. and Villeneuve, M., 2006b. Basement complex, Carboniferous magmatism and Paleozoic deformation in Yukon-Tanana terrane of central Yukon: Field, geochemical and geochronological constraints from Glenlyon map area. *In:* Paleozoic Evolution and Metallogeny of Pericratonic Terranes at the Ancient Pacific Margin of North America, Canadian and Alaskan Cordillera, Colpron, M. and Nelson, J.L. (eds.), Geological Association of Canada, Special Paper 45, p. 131–151.

Colpron, M. and Nelson, J.L. 2011. A digital atlas of terranes for the Northern Cordillera. British Columbia Geological Survey and Yukon Geological Survey, 7 p.

Colpron, M., Israel, S., Murphy, D., Pigage, L. and Moynihan, D., 2016. Yukon bedrock geology map, 1:1 000 000. Yukon Geological Survey, Open File 2016-1.

Colpron, M., 2017. Revised geological map of Livingstone Creek area (NTS 105E/8), 1:50 000. Yukon Geological Survey, Open File 2017-1.

Colpron, M., Carr, S., Hildes, D. and Piercey, S., 2017. Geophysical, geochemical and geochronological constraints on the geology and mineral potential of the Livingstone Creek area, south-central Yukon (NTS 105E/8). *In:* Yukon Exploration and Geology 2016, K.E. MacFarlane and L.H. Weston (eds.), Yukon Geological Survey, p. 47–86.

Crowley, J.L., Schoene, B. and Bowring, S.A., 2007. U-Pb dating of zircon in the Bishop Tuff at the millennial scale. Geology, vol. 35, p. 1123–1126.

Gabrielse, H., Murphy, D.C. and Mortensen, J.K., 2006, Cretaceous and Cenozoic dextral orogen-parallel displacements, magmatism, and paleogeography, north-central Canadian Cordillera. *In:* Paleogeography of the North American Cordillera: Evidence For and Against Large-Scale Displacements, J.W. Haggart, R.J. Enkin and J.W.H. Monger (eds.), Geological Association of Canada, Special Paper 46, p. 255–276.

Gaidies, F., Morneau, Y.E., Petts, D.C., Jackson, S.E., Zagorevski, A. and Ryan, J., 2021. Major and trace element mapping of garnet: Unravelling the conditions, timing and rates of metamorphism of the Snowcap assemblage, west-central Yukon. Journal of Metamorphic Geology, 32 p., https://onlinelibrary.wiley.com/doi/10.1111/jmg.12562.

Gallagher, 1999. Regional-scale transposition and late large-scale folding in the Teslin Zone, Pelly Mountains, Yukon. Unpublished MSc thesis, Carleton University, Ottawa, Ontario, 199 p.

Gleeson, T.P., Friedman, R.M. and Wahl, K., 2000. Stratigraphy, structure, geochronology and provenance of the Logjam area, northwestern British Columbia (NTS 104O/14W). *In:* British Columbia Geological Survey, Geological Fieldwork 1999, Paper 2000-1, p. 297–306.

Gordey, S.P. and Makepeace, A.J., 2001. Bedrock Geology, Yukon Territory. Geological Survey of Canada, Open File 3754, scale 1:1 000 000.

Gordey, S.P. and Stevens, R.A., 1994. Preliminary interpretation of bedrock geology of the Teslin area (105C), southern Yukon. Geological Survey of Canada, Open File 2886 (1:250 000).

Gordey, S.P., McNicoll, V.J. and Mortensen, J.K., 1998. New U-Pb ages from the Teslin area, southern Yukon, and their bearing on terrane evolution in the northern Cordillera. *In:* Radiogenic age and isotopic studies, report 11. Geological Survey of Canada, Current Research 1998-F, p. 129–148.

Hansen, V.L., 1989. Structural and kinematic evolution of the Teslin suture zone, Yukon: record of an ancient transpressional margin. Journal of Structural Geology, vol. 11, p. 717–733.

Hansen, V.L., Mortensen, J.K. and Armstrong, R.L., 1989. U-Pb, Rb-Sr, and K-Ar isotopic constraints for ductile deformation and related metamorphism in the Teslin suture zone, Yukon Tanana terrane, south-central Yukon. Canadian Journal of Earth Sciences, vol. 26, p. 2224–2235.

Hansen, V.L., Heizler, M.T. and Harrison, T.M., 1991. Mesozoic thermal evolution of the Yukon-Tanana composite terrane: new evidence from $^{40}Ar/^{39}Ar$ data. Tectonics, vol. 10, p. 51–76.

Hansen, V.L., 1992. P-T evolution of the Teslin suture zone and Cassiar tectonites, Yukon, Canada: evidence for A- and B-type subduction. Journal of Metamorphic Geology, vol. 10, p. 239–263.

Hunt, P.A. and Roddick, J.C. 1992. A compliation of K-Ar and $^{40}Ar/^{39}Ar$ ages: report 22. *In:* Radiogenic Age and Isotopic studies: Report 6. Geological Survey of Canada, Paper 92-2, p. 179–226.

Harvey, J.L., Brown, R.L. and Carr, S.D., 1996. Progress in structural mapping in the Teslin suture zone, Big Salmon Range, central Yukon Territory. *In*: Slave-Northern Cordillera Lithospheric Evolution (SNORCLE) Transect and Cordilleran Tectonics Workshop Meeting, F. Cook and P. Erdmer (eds.), Lithoprobe Report No. 50, p. 33–34.

Harvey, J.L., Carr, S.D., Brown, R.L. and Gallagher, C., 1997. Deformation history and geochronology of plutonic rocks near the d'Abbadie fault, Big Salmon Range, Yukon. *In*: Slave-Northern Cordillera Lithospheric Evolution (SNORCLE) Transect and Cordilleran Tectonics Worksghop Meeting, F. Cook and P. Erdmer (eds.), Lithoprobe Report No. 56, p. 103–114.

Jaffey, A.H., Flynn, K.F., Glendenin, L.E., Bentley, W.C. and Essling, A.M., 1971. Precision measurements of half-lives and specific activities of ^{235}U and ^{238}U. Physical Review C, vol. 4, p. 1889–1906.

de Keijzer, M., Williams, P.F. and Brown, R.L., 1999. Kilometre-scale folding in the Teslin zone, northern Canadian Cordillera, and its tectonic implications for the accretion of the Yukon-Tanana terrane to North America. Canadian Journal of Earth Sciences, vol. 36, p. 479–494.

Kiss, F. and Boulanger, O., 2018. Residual Total Magnetic Field, Aeromagnetic Survey of the Marsh Lake Area, Yukon, Part of NTS 105F/North. Yukon Geological Survey, Open File 2018-17, also Geological Survey of Canada, Open File 8426, https://doi.org/10.4095/308237.

Lees, E.J., 1936. Geology of the Teslin-Quiet Lake area, Yukon. Geological Survey of Canada, Memoir 203, 30 p.

Mattinson, J.M., 2005. Zircon U-Pb chemical abrasion ("CA-TIMS") method: combined annealing and multi-step partial dissolution analysis for improved precision and accuracy of zircon ages. Chemical Geology, vol. 220, p. 47–66.

Mihalynuk, M.G., Friedman, R.M., Devine, F. and Heaman, L.M., 2006. Protolith age and deformation history of the Big Salmon Complex, relics of a Paleozoic continental arc in northern British Columbia. *In:* Paleozoic Evolution and Metallogeny of Pericratonic Terranes at the Ancient Pacific Margin of North America, Canadian and Alaskan Cordillera, M. Colpron and J.L. Nelson (eds.), Geological Association of Canada, Special Paper 45, p. 179–200.

Moynihan, D., 2022. Preliminary geological map of the Boswell River area (Parts of NTS 105C/13, 105C/14, 105F/4 and 105E/1). Yukon Geological Survey, Open File 2022-3, scale 1:50 000.

Mulligan, R. 1963. Geology of the Teslin map-area, Yukon Territory. Geological Survey of Canada, Memoir 326, 96 p.

Murphy, D.C., Mortensen, J.K., Piercey, S.J., Orchard, M.J. and Gehrels, G.E., 2006, Mid-Paleozoic to early Mesozoic tectonostratigraphic evolution of Yukon-Tanana and Slide Mountain terranes and affiliated overlap assemblages, Finlayson Lake massive sulphide district, southeastern Yukon. *In:* Paleozoic Evolution and Metallogeny of Pericratonic Terranes at the Ancient Pacific Margin of North America, Canadian and Alaskan Cordillera, M. Colpron and J.L. Nelson (eds.), Geological Association of Canada, Special Paper 45, p. 75–105.

Pattison, D.R.M, and Vogl, J.J., 2005. Contrasting sequences of metapelitic mineral-assemblages in the aureole of the tilted Nelson batholith, British Columbia: implications for phase equilibria and pressure determination in andalusite-sillimanite-type settings. The Canadian Mineralogist, vol. 43, p. 51–88.

Read, P.B., 1983. Geology, Classy Creek (104J/2E) and Stikine Canyon (104J/1W), British Columbia. Geological Survey of Canada, Open File 940, 1:50 000 scale.

Roots, C.F., Nelson, J.L., Simard, R.-L. and Harms, T.A., 2006. Continental fragments, mid-Paleozoic arcs and overlapping late Paleozoic arc and Triassic sedimentary strata in the Yukon-Tanana terrane of northern British Columbia and southern Yukon. *In:* Paleozoic Evolution and Metallogeny of Pericratonic Terranes at the Ancient Pacific Margin of North America, Canadian and Alaskan Cordillera, M. Colpron and J.L. Nelson (eds.), Geological Association of Canada, Special Paper 45, p. 153–177.

Sack, P.J, Colpron, M., Crowley, J., Ryan, J., Allan, M.M., Beranek, L.P. and Joyce, N.L., 2020. An atlas of Late Triassic to Jurassic plutons in the Intermontane terranes of Yukon. Yukon Geological Survey, Open File 2020-1.

Schmitz, M.D. and Schoene, B., 2007. Derivation of isotope ratios, errors and error correlations for U-Pb geochronology using ^{205}Pb-^{235}U-(^{233}U)-spiked isotope dilution thermal ionization mass spectrometric data. Geochemistry, Geophysics, Geosystems (G^3), vol. 8, Q08006, doi:10.1029/2006GC001492.

Simard, R.-L. 2003. Geological map of Southern Semenof Hills (part of NTS 105E/1,7,8), south-central Yukon (1:50 000 scale). Yukon Geological Survey, Open File 2003-12.

Simard, R.-L. and Devine, F., 2003. Preliminary geology of the southern Semenof Hills, central Yukon (105E/1,7,8). *In:* Yukon Exploration and Geology 2002, D.S. Emond and L.L. Lewis (eds.), Exploration and Geological Services Division, Yukon Region, Indian and Northern Affairs Canada, p. 213–222.

Simard, R.-L., Dostal, J. and Roots, C., 2003. Development of late Paleozoic volcanic arcs in the Canadian Cordillera: an example from the Klinkit Group, northern British Columbia and southern Yukon. Canadian Journal of Earth Sciences, vol. 40, p. 907–924.

Smith, J.L. and Arehart, G.B., 2010. Isotopic investigation of the Adanac porphyry molybdenum deposit in northwestern British Columbia (NTS 104N/11): final project report. *In:* Geoscience BC Summary of Activities 2009, Geoscience BC, Report 2010-1, p. 115–126.

Stevens, R.A., 1994. Structural and tectonic evolution of the Teslin tectonic zone, Yukon: a double vergent transpressive shear zone. Unpublished PhD thesis, University of Alberta, Edmonton, Alberta, 208 p.

Stevens, R.A., Erdmer, P., Creaser, R.A. and Grant, S.L., 1995. Mississippian assembly of the Nisutlin assemblage: evidence from primary contact relationships and Mississippian magmatism in the Teslin tectonic zone, part of the Yukon-Tanana terrane of south-central Yukon. Canadian Journal of Earth Sciences, vol 33, p. 103–116.

Stevens, R.D., Lachance, G.R. and DeLabio., 1982. Age determinations and geological studies K-Ar isotopic ages, report 16. Geological Survey of Canada, Paper 82-2, 56 p.

Taylor, B., 1975. Geological, geochemical and geophysical report on the SM claims, 41 p. Yukon Department of Energy, Mines and Resources, Assessment Report 090005.

Tempelman-Kluit, D.J., 1979. Transported cataclasite, ophiolite and granodiorite in the Yukon: evidence of arc-continent collision. Geological Survey of Canada, Paper 79-14, 27 p.

Tempelman-Kluit, D.J., 1984. Geology, Laberge and Carmacks, Yukon Territory. Geological Survey of Canada, Open File 1101, 10 p.

Tempelman-Kluit, D.J., 2009. Geology of Carmacks and Laberge map areas, central Yukon: Incomplete draft manuscript on stratigraphy, structure and its early interpretation (*ca.* 1986). Geological Survey of Canada, Open File 5982, 399 p.

Westberg, 2010. The tectonometamorphic and structural evolution of the Yukon-Tanana and Cassiar terranes in the Mendocina Creek area: implications for the tectonic framework of south-central Yukon. Unpublished MSc thesis, Simon Fraser University, Vancouver, British Columbia.

van Straaten, B.I. and Wearmouth, C., 2019. Geology of the Latham and Pallen Creek area, northwestern British Columbia: Distinguishing the Tsaybahe group, Stuhini Group, and Hazelton Group, and the onset of Triassic arc volcanism in northern Stikinia. *In:* Geological Fieldwork 2018, British Columbia Ministry of Energy, Mines and Petroleum Resources, British Columbia Geological Survey, Paper 2019-01, p. 79–96.

Yukon Geological Survey, 2021. Yukon Geochronology – A database of Yukon isotopic age determinations. Yukon Geological Survey, http://data.geology.gov.yk.ca/Compilation/22, [accessed December, 2021].

Zagorevski, A., van Staal, C.R., Bedard, J.H., Bogatu, A., Canil, D., Coleman, M., Golding, M., Joyce, N.L., Lawley, C., McGoldrick, S., Mihalynuk, M.G., Milidragovic, D., Parson, A., Schiarizza, P., 2021. *In:* Northern Cordillera geology: a synthesis of research from the Geo-mapping for Energy and Minerals program, British Columbia and Yukon, J.J. Ryan and A. Zagorevski (eds.), Geological Survey of Canada, Bulletin 610, p. 21–65.

Appendix

The appendix includes three folders—CL zircon images, LA-ICPMS_tables, and U-Pb geochronology methods—and is only available digitally. The .zip file that accompanies this document and can be downloaded from https://data.geology.gov.yk.ca.

Yukon Geological Survey

Yukon Geological Survey staff are located in two buildings in Whitehorse: the Elijah Smith Building at 300 Main Street, room 102, and the H.S. Bostock Core Library at Mile 918 on the Alaska Highway.

Branch Director

H.S. Bostock Core Library

Relf, Carolyn – Director, (867) 667–8892 carolyn.relf@yukon.ca

Operations

H.S. Bostock Core Library

Minor, Julie – Manager, Finance & Operations, (867) 667–8508 julie.minor@yukon.ca

Outreach

H.S. Bostock Core Library

Weston, Leyla – Outreach Geologist, (867) 393–7187 leyla.weston@yukon.ca

Regional Geology

H.S. Bostock Core Library

Colpron, Maurice – Head, Regional Geology, (867) 667–8235 maurice.colpron@yukon.ca
Ambrose, Tyler – Project Geologist, (867) 667–5175 tyler.ambrose@yukon.ca
Cobbett, Rosie – Project Geologist, (867) 455–2802 rosie.cobbett@yukon.ca
Moynihan, David – Project Geologist, (867) 455–2805 david.moynihan@yukon.ca
Skipton, Diane – Project Geologist, (867) 667–5175 diane.skipton@yukon.ca
Sternbergh, Sarah – Project Geologist, (867) 332-2122 sarah.sternbergh@yukon.ca

Surficial Geology

Elijah Smith Building

Bond, Jeffrey – Head, Surficial Geology, (867) 667–8514 jeff.bond@yukon.ca
van Loon, Sydney – Placer Geologist, (867) 667–3408 sydney.vanloon@yukon.ca

H.S. Bostock Core Library

Kennedy, Kristen – Surficial Geologist, (867) 393–7188 kristen.kennedy@yukon.ca
Lipovsky, Panya – Surficial Geologist, (867) 667–8520 panya.lipovsky@yukon.ca

Minerals Geology

Elijah Smith Building

Casselman, Scott – Head, Minerals Geology, (867) 667–8192 scott.casselman@yukon.ca
Lewis, Lara – Economic Geologist, (867) 667–8518 lara.lewis@yukon.ca
Torgerson, Derek – Yukon Mineral Exploration Program, (867) 456–3828 derek.torgerson@yukon.ca
Bullen, Warwick – Mineral Assessment Geologist, (867) 667-3205 warwick.bullen@yukon.ca

H.S. Bostock Core Library

Emberley, Justin – Core Library Manager, (867) 393–6492 justin.emberley@yukon.ca
Sack, Patrick – Metallogenist, (867) 667–3203 patrick.sack@yukon.ca

Editorial & Technical Services

Elijah Smith Building

MacFarlane, Karen – Head, Technical Services, (867) 667–8519 karen.macfarlane@yukon.ca
Elliot, Brett – Geological Spatial Database Administrator, (867) 667–8481 brett.elliot@yukon.ca
Staffen, Bailey – GIS Technician/Web Manager, (867) 456–6801 bailey.staffen@yukon.ca

Yukon Geological Survey
Energy, Mines and Resources
Government of Yukon

